

DYNAMIC ANALYSIS OF VISCOELASTIC SERPENTINE BELT DRIVE SYSTEMS

By

Lixin Zhang

A thesis submitted in conformity with the requirements
for the degree of

DOCTOR OF PHILOSOPHY

Department of Mechanical and Industrial Engineering
University of Toronto

© Copyright by Lixin Zhang 1999



National Library
of Canada

Acquisitions and
Bibliographic Services

395 Wellington Street
Ottawa ON K1A 0N4
Canada

Bibliothèque nationale
du Canada

Acquisitions et
services bibliographiques

395, rue Wellington
Ottawa ON K1A 0N4
Canada

Your file Votre référence

Our file Notre référence

The author has granted a non-exclusive licence allowing the National Library of Canada to reproduce, loan, distribute or sell copies of this thesis in microform, paper or electronic formats.

The author retains ownership of the copyright in this thesis. Neither the thesis nor substantial extracts from it may be printed or otherwise reproduced without the author's permission.

L'auteur a accordé une licence non exclusive permettant à la Bibliothèque nationale du Canada de reproduire, prêter, distribuer ou vendre des copies de cette thèse sous la forme de microfiche/film, de reproduction sur papier ou sur format électronique.

L'auteur conserve la propriété du droit d'auteur qui protège cette thèse. Ni la thèse ni des extraits substantiels de celle-ci ne doivent être imprimés ou autrement reproduits sans son autorisation.

0-612-45747-8

Canadä

DYNAMIC ANALYSIS OF VISCOELASTIC SERPENTINE BELT DRIVE SYSTEMS

DOCTOR OF PHILOSOPHY 1999

LIXIN ZHANG

DEPARTMENT OF MECHANICAL AND INDUSTRIAL ENGINEERING

UNIVERSITY OF TORONTO

ABSTRACT

This thesis is devoted to accurately modeling and analyzing the dynamic behavior of damped serpentine belt drive systems. A viscoelastic moving material model is proposed to describe the transverse vibration of belt spans and a hybrid (continuous/discrete components) viscoelastic system is proposed to represent the dynamics of the entire serpentine belt drive.

The direct multiple scales method is applied to the nonlinear vibration analysis of free, forced and parametric vibration of viscoelastic moving belts. Nonlinear natural frequencies and near-modal nonlinear response of free vibration of viscoelastic moving belts are obtained in closed-form. The amplitude of near- and exact-resonant response is predicted for viscoelastic moving belts excited by the eccentricity of pulleys. Closed-form solutions of response amplitudes, existence conditions, and stability conditions of limit cycles are derived for parametrically excited viscoelastic moving belts. Block-by-block numerical integration method together with a Galerkin discretization using travelling eigenfunctions is proposed to calculate the transient response of moving belts with general viscoelasticity.

An explicit exact characteristic equation of eigenvalues for undamped hybrid serpentine belt drives is derived, which could provide insight into effects of design parameters on the frequency spectrum of the system. A complex modal analysis method is developed for linear vibration analysis of non-self-adjoint hybrid serpentine belt drive systems for the first time. The adjoint eigenfunction can be conveniently determined from the proposed auxiliary system.

Nonlinear vibrations of viscoelastic and elastic hybrid serpentine belt drive systems are analyzed using the discretization multiple scales method for the first time. This provides a basic understanding of parametric excitation threshold levels and the existence of multiple limit cycles. The direct multiple scales method is developed for the nonlinear analysis of elastic hybrid serpentine belt drive systems. Comparisons between the direct multiple scale method and the discretization multiple scales help better understand the relationship between the two approaches.

ACKNOWLEDGEMENTS

A great deal of credit for this thesis belongs to my supervisor, Professor Jean W. Zu. I would like to take this opportunity to thank her for her invaluable guidance and constant encouragement throughout this investigation.

Thanks to members of my Ph.D. committee, Professor J.K. Spelt and Professor R. Ben Mrad for their helpful advice and constructive criticism.

Thanks to Brenda Fung and everyone else in the Department of Mechanical and Industrial Engineering for their help.

Thanks to my daughter, Chuchu and my wife, Xiurong for their understanding and sacrifice.

Most importantly, I would like to thank my father, my mother, my brothers and sister for their great support. My father and mother have been taking care of my daughter during my Ph.D. candidacy. Sadly, my father was not able to see the fruits he would have loved to see.

Finally, I wish to acknowledge the financial support for this research provided by Materials and Manufacturing Ontario.

TABLE of CONTENTS

ABSTRACT	ii
ACKNOWLEDGEMENTS.....	iv
TABLE OF CONTENTS.....	v
LIST OF TABLES.....	xii
LIST OF FIGURES.....	xiii
LIST OF APPENDICES.....	xix
NOMENCLATURE	xx
1 INTRODUCTION.....	1
1.1 MOTIVATION.....	1
1.2 LITERATURE REVIEW.....	5
1.2.1 Transverse Vibration of Serpentine Belt Drive Systems.....	6
1.2.2 Rotational Vibration of Serpentine Belt Drive Systems.....	9
1.2.3 Coupling of Transverse and Rotational Vibrations	9
1.2.4 Vibration Analysis of Viscoelastic Materials.....	10
1.2.5 Multiple Scales Method.....	11
1.3 OUTLINE OF THE THESIS	13
1.4 CONTRIBUTIONS OF THE THESIS.....	15
PART I VIBRATION ANALYSIS OF VISCOELASTIC MOVING BELTS	17
2 FREE VIBRATION OF VISCOELASTIC MOVING BELTS	18
2.1 CONSTITUTIVE RELATION OF VISCOELASTIC MATERIALS	18
2.1.1 Differential Viscoelastic Constitutive Law	19
2.1.2 Integral Viscoelastic Constitutive Law	21

2.2 EQUATION OF MOTION.....	21
2.3 MODAL ANALYSIS OF LINEAR MOVING MATERIALS	25
2.4 NONLINEAR VIBRATION ANALYSIS.....	27
2.4.1 Multiple Scales Method.....	28
2.4.2 The Zeroth Order Solution	31
2.4.3 The First Order Solution.....	34
2.5 NUMERICAL RESULTS AND DISCUSSIONS.....	35
2.5.1 Material Properties of Belts.....	35
2.5.2 Numerical Results and Discussions.....	36
2.6 SUMMARY AND CONCLUSIONS	40
3 FORCED VIBRATION OF VISCOELASTIC MOVING BELTS	46
3.1 EQUATION OF MOTION.....	46
3.1.1 Non-homogenous Boundary Conditions	47
3.1.2 Equation of Motion in Standard Symbolic Form	48
3.2 NONLINEAR FORCED VIBRATION ANALYSIS.....	50
3.2.1 Multiple Scales Method.....	50
3.2.2 Steady State Solutions	53
3.2.3 The First Order Solution.....	55
3.3 STABILITY ANALYSIS OF STEADY STATE SOLUTIONS	56
3.4 NUMERICAL RESULTS AND DISCUSSIONS.....	58
3.5 SUMMARY AND CONCLUSIONS	60
4 DYNAMIC RESPONSE OF PARAMETRICALLY EXCITED VISCOELASTIC MOVING BELTS	65
4.1 EQUATION OF MOTION.....	66
4.2 DIRECT MULTIPLE SCALES METHOD	68
4.3 DISCRETIZATION MULTIPLE SCALES METHOD.....	71
4.3.1 Galerkin Discretization.....	71
4.3.2 Multiple Scales Method.....	73
4.3.3 Solvability Condition	74

4.4	LIMIT CYCLES AND EXISTENCE CONDITIONS.....	78
4.4.1	Equations of Response Amplitudes and Phases	78
4.4.2	Limit Cycles of Elastic Moving Belts	80
4.4.3	Limit Cycles of Viscoelastic Moving Belts.....	81
4.5	NUMERICAL RESULTS AND DISCUSSIONS.....	84
4.6	SUMMARY AND CONCLUSIONS	87
5	STABILITY OF PARAMETRICALLY EXCITED VISCOELASTIC MOVING BELTS	98
5.1	STABILITY OF TRIVIAL LIMIT CYCLES	99
5.1.1	Stability Boundary of Summation Resonance.....	99
5.1.2	Stability Boundary of Difference Resonance	103
5.2	STABILITY OF NON-TRIVIAL LIMIT CYCLES	105
5.2.1	Jacobian Matrix	105
5.2.2	Routh-Hurwitz Criterion	108
5.2.3	Simplification of h_1 , h_2 , h_3 and h_4	109
5.2.4	Parametric Resonance of Viscoelastic Moving Belts.....	114
5.2.5	Parametric Resonance of Elastic Moving Belts	115
5.3	NUMERICAL RESULTS AND DISCUSSIONS.....	116
5.4	SUMMARY AND CONCLUSIONS	117
6	TRANSIENT RESPONSE OF MOVING BELTS WITH INTEGRAL VISCOELASTIC CONSTITUTIVE LAW	122
6.1	EQUATION OF MOTION.....	123
6.2	DISCRETIZATION APPROACH.....	126
6.2.1	Canonical Form of Equation of Motion	126
6.2.2	Galerkin Discretization Using Translating Eigenfunctions.....	127
6.3	BLOCK-BY-BLOCK METHOD.....	131
6.4	NUMERICAL RESULTS AND DISCUSSIONS.....	134
6.4.1	Three-element Viscoelastic Model.....	134
6.4.2	One Mode Expansion	135

6.4.3 Transient Response of Viscoelastic Moving Belts	136
6.5 SUMMARY AND CONCLUSIONS	137

PART II VIBRATION ANALYSIS OF SERPENTINE BELT DRIVE SYSTEMS

143

7 HYBRID MODEL OF VISCOELASTIC SERPENTINE BELT DRIVE SYSTEMS	144
7.1 NONLINEAR EQUATIONS OF MOTION FOR GENERAL VISCOELASTIC MODEL	144
7.2 EQUATIONS OF MOTION FOR KELVIN VISCOELASTIC MODEL	150
7.2.1 Linear Equations of Motion for Kelvin Viscoelastic Model	151
7.2.2 Nonlinear Equations of Motion for Kelvin Viscoelastic Model	153
8 MODAL ANALYSIS OF UNDAMPED SERPENTINE BELT DRIVE SYSTEMS	155
8.1 CANONICAL FORM OF EQUATIONS OF MOTION.....	156
8.2 EIGENVALUES AND EIGENFUNCTIONS.....	161
8.2.1 Orthogonality of Eigenfunctions	161
8.2.2 Characteristic Equation of Eigenvalues.....	162
8.3 RESPONSE TO ARBITRARY EXCITATIONS	166
8.4 STEADY STATE RESPONSE SUBJECTED TO HARMONIC EXCITATIONS	168
8.5 NUMERICAL RESULTS AND DISCUSSIONS.....	171
8.6 SUMMARY AND CONCLUSIONS	176
9 COMPLEX MODAL ANALYSIS OF NON-SELF-ADJOINT SERPENTINE BELT DRIVE SYSTEMS	183
9.1 CANONICAL FORM OF EQUATIONS OF MOTION.....	184
9.2 THE ADJOINT EIGENVALUE PROBLEMS.....	186
9.2.1 Formulation of the Adjoint Eigenvalue Problem	186
9.2.2 Physical Meaning of Adjoint Eigenfunctions.....	188
9.3 ORTHOGONALITY OF STATE SPACE EIGENFUNCTIONS	190

9.4 COMPLEX MODAL ANALYSIS OF SERPENTINE BELT DRIVE SYSTEMS.....	192
9.4.1 Eigenvalues and Eigenfunctions of the Serpentine Belt Drive System.....	192
9.4.2 Eigenfunctions of the Adjoint System.....	195
9.5 MODAL EXPANSION REPRESENTATION FOR THE DYNAMIC RESPONSE	197
9.6 SUMMARY AND CONCLUSIONS	198
10 NONLINEAR VIBRATION ANALYSIS OF ELASTIC SERPENTINE BELT DRIVE SYSTEMS: DISCRETIZATION MULTIPLE SCALES METHOD.....	199
10.1 DISCRETIZATION	200
10.1.1 Symbolic Form of Equations of Motion for Subsystem 1 and Subsystem 2.....	200
10.1.2 Modal Expansion.....	202
10.1.3 The Two Mode Expansion	203
10.2 MULTIPLE SCALES METHOD	207
10.3 ONE-TO-ONE INTERNAL RESONANCE.....	210
10.3.1 Solvability Condition of the Second Order Equations	211
10.3.2 The Second Order Solution	211
10.3.3 Solvability Condition of the Third Order Equations	213
10.3.4 Modulation Equations and Steady State Solutions.....	214
10.4 TWO-TO-ONE INTERNAL RESONANCE	216
10.4.1 The Second Order Solution	217
10.4.2 Solvability Condition of the Third Order Equations	218
10.4.3 Modulation Equations and Steady State Solutions.....	219
10.5 STABILITY ANALYSIS.....	221
10.6 PSEUDO-ARCLENGTH CONTINUATION	222
10.7 NUMERICAL RESULTS AND DISCUSSIONS.....	224
10.7.1 One-to-one Internal Resonance	224
10.7.2 Two-to-one Internal Resonance	229
10.8 SUMMARY AND CONCLUSIONS	233
11 NONLINEAR VIBRATION ANALYSIS OF ELASTIC SERPENTINE BELT DRIVE SYSTEMS: DIRECT MULTIPLE SCALES METHOD.....	260

11.1 DIRECT MULTIPLE SCALES METHOD	261
11.1.1 Direct Approach	262
11.1.2 The First Order Solutions and Nonlinear Terms of the Second Order Equations.....	264
11.2 ONE-TO-ONE INTERNAL RESONANCE.....	266
11.2.1 Solvability Condition of the Second Order Equations	267
11.2.2 Spatial Distribution Functions Using Modal Expansions	267
11.2.3 Spatial Distribution Functions Using the Exact Method.....	270
11.2.4 Solvability Condition of the Third Order Equations	274
11.2.5 Modulation Equations and Steady State Solutions.....	277
11.3 TWO-TO-ONE INTERNAL RESONANCE	279
11.3.1 The Second Order Solutions.....	279
11.3.2 Solvability Condition of the Third Order Equations	281
11.3.3 Modulation Equations and Steady State Solutions.....	283
11.4 NUMERICAL RESULTS AND DISCUSSIONS.....	285
11.4.1 One-to-one Internal Resonance	285
11.4.2 Two-to-one Internal Resonance	288
11.5 SUMMARY AND CONCLUSIONS	290
 12 NONLINEAR VIBRATION ANALYSIS OF VISCOELASTIC SERPENTINE BELT DRIVE SYSTEMS	306
12.1 EQUATIONS OF MOTION.....	306
12.2 DISCRETIZATION MULTIPLE SCALES METHOD.....	308
12.3 NUMERICAL RESULTS AND DISCUSSIONS.....	310
12.3.1 One-to-one Internal Resonance	310
12.3.2 Two-to-one Internal Resonance	312
12.4 SUMMARY AND CONCLUSIONS	313
 13 SUMMARY, CONCLUSIONS, RECOMMENDATIONS FOR DESIGN WORK, AND FUTURE WORK	326
13.1 SUMMARY AND CONCLUSIONS	326

13.2 RECOMMENDATIONS FOR DESIGN WORK.....	331
13.3 FUTURE WORK	332
REFERENCES	334

LIST OF TABLES

Table 2.1	Basic linear viscoelastic models.....	20
Table 8.1	The physical properties of the prototypical system.....	172
Table 8.2	Comparison of the natural frequency of the baseline system at zero speed.....	173
Table 8.3	Comparison of the natural frequency of the modified system at zero speed.....	173
Table 8.4	Effect of the tensioner arm orientation on the natural frequency (Hz) of the base line system at zero speed	174

LIST OF FIGURES

Figure 1.1	A typical serpentine belt drive system	1
Figure 1.2	Rotational vibration of pulleys and the tensioner arm	2
Figure 1.3	Transverse vibration of each belt span.....	2
Figure 1.4	Principal changes in belt tension T and belt length L with time of service.....	4
Figure 1.5	Stress-strain curves of the treated polyester cord 1100×2×5 by repeated deformations	5
Figure 2.1	A prototypical model of a viscoelastic moving belt.....	22
Figure 2.2	A comparison of nonlinear fundamental frequencies of an elastic moving belt.....	42
Figure 2.3A	Waveform of the generalized coordinate ζ_1^R for $E_e=400$	42
Figure 2.3B	The discrete Fourier transform of the wave ζ_1^R for $E_e=400$	43
Figure 2.4A	Waveform of the generalized coordinate ζ_1' for $E_e=400$	43
Figure 2.4B	The discrete Fourier transform of the wave ζ_1' for $E_e=400$	44
Figure 2.5	The influence of viscoelasticity on response amplitude for $E_e=400$	44
Figure 2.6	The influence of viscoelasticity on response amplitude for $\gamma=0.5$, $E_e=400$ at time instant 500	45
Figure 2.7	The influence of nonlinearity on response amplitude for $E_v=1$, $\gamma=0.5$	45
Figure 3.1	A prototypical model of a viscoelastic moving belt driven by eccentrically-mounted pulleys.....	46
Figure 3.2	Comparison of response amplitudes predicated by the method of multiple scales and those given by Moon and Wickert (1997)	62
Figure 3.3	Comparison of response amplitudes without the quasi-static assumption and those with the quasi-static assumption	62

Figure 3.4	Comparison of responses for different E_v ($E_\epsilon=400$)	63
Figure 3.5	Comparison of responses for different E_v ($E_\epsilon=800$)	63
Figure 3.6	Comparison of responses for different E_v ($E_\epsilon=1000$)	64
Figure 4.1	The nontrivial limit cycles that bifurcate from the boundary of the first principal parameter instability region ($\gamma=0.2$, $n=l=1$, $E_\epsilon=400$, $E_v=0$)	89
Figure 4.2	The nontrivial limit cycles that bifurcate from the boundary of the second principal parameter instability region ($\gamma=0.2$, $n=l=2$, $E_\epsilon=400$, $E_v=0$)	90
Figure 4.3	The nontrivial limit cycles that bifurcate from the boundary of the first summation parameter instability region ($\gamma=0.2$, $n=1$, $l=2$, $E_\epsilon=400$, $E_v=0$)	91
Figure 4.4	The response amplitude of non-trivial limit cycles for the summation parametric resonance of a viscoelastic moving belt ($n=1$, $l=2$, $E_\epsilon = 400$, $E_v = 10$, $\gamma = 0.2$)	92
Figure 4.5	Effects of E_v on the nontrivial limit cycles for the first summation parametric resonance ($n=1$, $l=2$, $E_\epsilon = 400$, $\gamma = 0.25$, $a=0.5$)	93
Figure 4.6	Effects of the transport speed on non-trivial limit cycles of the first principal parametric resonance ($E_\epsilon = 400$, $E_v = 10$, $a=0.5$, $n=l=1$)	94
Figure 4.7	Effects of the transport speed on non-trivial limit cycles of the first summation parametric resonance ($E_\epsilon = 400$, $E_v = 10$, $a=0.5$, $n=1$, $l=2$)	95
Figure 4.8	Effects of the transport speed on the existence boundary of nontrivial limit cycles for the first summation parametric resonance ($n=1$, $l=2$, $E_\epsilon = 400$, $a=0.5$, $E_v = 10$)	96
Figure 4.9	Relations of μ and E_v on the upper existence boundary of non-trivial limit cycles for summation parametric resonance ($n=1$, $l=2$, $E_\epsilon = 400$, $\gamma = 0.25$, $a=0.5$)	97
Figure 5.1	Stability boundaries of the trivial limit cycle for the first principal parametric resonance ($n=1$, $l=1$, $E_\epsilon = 400$)	119
Figure 5.2	Stability boundaries of the trivial limit cycle for the second principal parametric resonance ($n=2$, $l=2$, $E_\epsilon = 400$)	119
Figure 5.3	Stability boundaries of the trivial limit cycle for the summation	

parametric resonance ($n=1$, $l=2$, $E_c = 400$)	120
Figure 5.4 Stability boundaries of the trivial limit cycle for the summation parametric resonance ($n=1$, $l=3$, $E_c = 400$)	120
Figure 5.5 Effect of E_v on the stability boundary of nontrivial limit cycles for the first summation parametric resonance ($n=1$, $l=2$, $E_c = 400$, $\gamma = 0.25$)	121
Figure 6.1 Three-element model of the viscoelastic belt material.....	134
Figure 6.2 The relaxation modulus of the three-element model.....	134
Figure 6.3 A comparison of responses for different values of k_3	139
Figure 6.4 A comparison of the amplitudes for different values of k_3 in the case of parametric resonance with a constant travelling speed	140
Figure 6.5 The effect of the axial perturbation velocity γ_1 on the transient amplitude for $\omega_0 = \pi(1 - \gamma_0^2)$ ($\gamma_0 = 0.5$, $k_3 = 10$)	141
Figure 6.6 The effect of the axial perturbation velocity γ_1 on the transient amplitude for $\omega_0 = 2\pi(1 - \gamma_0^2)$ ($\gamma_0 = 0.5$, $k_3 = 10$)	142
Figure 7.1 A prototypical serpentine belt drive system.....	145
Figure 7.2 Coulomb tensioner characteristic	147
Figure 8.1 The three-pulley serpentine belt drive system.....	171
Figure 8.2 Error function of the characteristic equation for eigenvalues	178
Figure 8.3 Transverse vibration mode of span 2 of the baseline system (50.53Hz).....	179
Figure 8.4 Rotational vibration mode of the baseline system (62.18 Hz)	179
Figure 8.5 Relations between natural frequencies and the engine speed	180
Figure 8.6 The steady state response of span 1	181
Figure 8.7 The steady state response of span 2	181
Figure 8.8 The steady state responses of discrete components	182
Figure 10.1 Response-frequency curves of system 1 for $\alpha_m=0$	235

Figure 10.2	Multi-valued region of system 1 for $\alpha_m = 0.0$	235
Figure 10.3	Response-frequency curves of system 1 for $\zeta_n = 1\%, \zeta_m = 0.3\%$	236
Figure 10.4	Periodic solutions of system 1	237
Figure 10.5	Phase plane curves of system 1	238
Figure 10.6	Relation between frequencies of periodic solutions and σ_2 for system 1	239
Figure 10.7	Region of nontrivial limit cycles of system 1	239
Figure 10.8	Response-excitation curves of system 1 for $\zeta_n = 1\%, \zeta_m = 0.3\%$	240
Figure 10.9	Relation between responses of system 1 and internal detuning parameter σ_1	241
Figure 10.10	Response-frequency curves of system 2 for $\alpha_m=0$	242
Figure 10.11	Multi-valued region of system 2 for $\alpha_m = 0.0$	242
Figure 10.12	Response-frequency curves of system 2 for $\zeta_n = 1\%, \zeta_m = 0.3\%$	243
Figure 10.13	Relation between frequencies of periodic solutions and σ_2 for system 2	244
Figure 10.14	Region of nontrivial limit cycles of system 2	244
Figure 10.15	Response-excitation curves of system 2 for $\zeta_n = 1\%, \zeta_m = 0.3\%$	245
Figure 10.16	Relation between responses of system 2 and internal detuning parameter σ_1	246
Figure 10.17	Response-frequency curves of system 3 for $\zeta_n = 1\%, \zeta_m = 0.3\%$	247
Figure 10.18	Relation between frequencies of periodic solutions and σ_2 for system 3	248
Figure 10.19	Region of nontrivial limit cycles of system 3	248
Figure 10.20	Free responses of rotationally dominant mode and transversely dominant mode for system 4 in the case of no internal resonance	249
Figure 10.21	Free responses of rotationally dominant mode and transversely dominant mode for system 4 in the case of internal resonance	250

Figure 10.22	Free responses of rotationally dominant mode and transversely dominant mode for system 4 in the case of internal resonance (3.1% detuning).....	251
Figure 10.23	Forced, damped responses of rotationally dominant mode and transversely dominant mode ($\zeta_n = 1\%$, $\zeta_m = 0.1\%$) for system 4	252
Figure 10.24	Response-frequency curves of system 5 for $\alpha_m=0.0$.....	253
Figure 10.25	Multiple-valued region of system 5 for $\alpha_m=0.0$.....	253
Figure 10.26	Response-frequency curves of system 5 for $\zeta_n = 1\%$, $\zeta_m = 0.3\%$	254
Figure 10.27	Periodic solutions of the amplitude α_n for system 5	255
Figure 10.28	Relation between frequencies of periodic solutions and σ_2 for system 5	255
Figure 10.29	Periodic solutions of system 5.....	256
Figure 10.30	Phase plane curves of system 5	257
Figure 10.31	Response-excitation curves of system 5 for $\zeta_n = 1\%$, $\zeta_m = 0.3\%$	258
Figure 10.32	Relation between responses of system 5 and internal detuning parameter σ_1	259
Figure 11.1	Response-frequency curves of system 2 for $\alpha_m=0$	292
Figure 11.2	Multi-valued region of system 2 for $\alpha_m = 0.0$	292
Figure 11.3	Response-frequency curves of system 2 for $\zeta_n = 1\%$, $\zeta_m = 0.3\%$	293
Figure 11.4	Relation between frequencies of periodic solutions and σ_2 for system 2	294
Figure 11.5	Periodic solutions of system 2.....	295
Figure 11.6	Phase plane curves of system 2	296
Figure 11.7	Response-excitation curves of system 2 for $\zeta_n = 1\%$, $\zeta_m = 0.3\%$	297
Figure 11.8	Relation between responses of system 2 and internal detuning parameter σ_1	298
Figure 11.9	Response-frequency curves of system 5 for $\alpha_m=0$	299
Figure 11.10	Multi-valued region of system 5 for $\alpha_m = 0.0$	299

Figure 11.11 Response-frequency curves of system 5 for $\zeta_n = 1\%, \zeta_m = 0.3\%$	300
Figure 11.12 Relation between frequencies of periodic solutions and σ_2 for system 5.....	301
Figure 11.13 Periodic solutions of system 5.....	302
Figure 11.14 Phase plane curves of system 5	303
Figure 11.15 Response-excitation curves of system 5 for $\zeta_n = 1\%, \zeta_m = 0.3\%$	304
Figure 11.16 Relation between responses of system 5 and internal detuning parameter σ_1	305
Figure 12.1 Response-frequency curves of system 2 for $\delta = 0.0001$	314
Figure 12.2 Relation between responses of system 2 and parameter σ_1 for $\delta=0.0001$	315
Figure 12.3 Response-excitation curves of system 2 for $\delta = 0.0001$	316
Figure 12.4 Response-frequency curves of system 2 for $\delta = 0.0005$	317
Figure 12.5 Relation between responses of system 2 and parameter σ_1 for $\delta=0.0005$	318
Figure 12.6 Response-excitation curves of system 2 for $\delta = 0.0005$	319
Figure 12.7 Response-frequency curves of system 5 for $\delta = 0.00005$	320
Figure 12.8 Relation between responses of system 5 and parameter σ_1 for $\delta=0.00005$	321
Figure 12.9 Response-excitation curves of system 5 for $\delta = 0.00005$	322
Figure 12.10 Response-frequency curves of system 5 for $\delta = 0.0001$	323
Figure 12.11 Relation between responses of system 5 and parameter σ_1 for $\delta=0.0001$	324
Figure 12.12 Response-excitation curves of system 5 for $\delta = 0.0001$	325

LIST OF APPENDICES

APPENDIX A	Expressions of g_i for Viscoelastic Systems	341
APPENDIX B	Expressions of h_i for Viscoelastic Systems	345
APPENDIX C	Expressions of s_i and t_i for Viscoelastic Systems.....	347
APPENDIX D	Expressions of $\hat{\Theta}_i$ and $\tilde{\Theta}_i$ for Viscoelastic Systems.....	349

NOMENCLATURE

Roman Characters

a	Non-dimensional amplitude of perturbation tension
A	Cross-sectional area of belt
A_k	Complex amplitude of the k th mode response
\mathbf{A}	Matrix operator for canonical equations of motion
\mathbf{A}^*	Adjoint matrix of \mathbf{A}
B_m	Complex amplitude of the m th mode response for subsystem 1
\mathbf{B}	Matrix operator for canonical equations of motion
\mathbf{B}^*	Adjoint matrix of \mathbf{B}
c	Axial velocity of belt
c'_i	Transverse wave velocity of span i
c'_a, c'_b, c'_c	Phase velocity of span 1, span 2, and span 3
d_i	Damping coefficient of span i , $d_i = \eta A / l_i$
D_c	Equivalent damping coefficient of coulomb damping
D_v	Viscous damping coefficient
\mathbf{D}	Damping matrix
e_0, e_1	Eccentricities of pulleys
E	Non-dimensional equivalent Young's modulus
$E(t)$	Relaxation modulus of belt materials
E^*	Equivalent Young's modulus
E_0	Initial Young's modulus

E_1, E_2	Stiffness constant of the three-parameter viscoelastic model
E_ϵ	Non-dimensional Young's modulus
E_v	Non-dimensional viscoelastic parameter
$\bar{E}(t)$	Non-dimensional relaxation modulus of belt materials
f	Non-dimensional external force
$F(x, t)$	External force transferred from the boundary excitation
\mathbf{F}	Vector of non-homogeneous and nonlinear terms
\mathbf{F}_{pi}	Spatial distribution function vector of the second order solution
g_s	Coefficients of nonlinear terms for subsystem 2
G	Gyroscopic operator
\mathbf{G}	Gyroscopic operator matrix
h_s	Coefficients of nonlinear terms for subsystem 1
\mathbf{H}	Jacobian matrix
\mathbf{I}	Identity matrix
J_i	Mass moment of inertia of the i th discrete element
k_s	Translation tensioner arm stiffness due to belt elongation
k_i	Stiffness coefficient of span i , EA/l_i
k_r	Rotational spring stiffness of tensioner spring
K	Stiffness operator
\mathbf{K}	Stiffness operator matrix
\mathbf{K}_{DD}	Stiffness matrix of discrete elements
l_i	Length of belt span i
L	Length of moving belts

m	Belt mass per unit length
m_i	$m_i = J_i / r_i^2$
M	Mass operator of moving belts
M_i	External moment applied to i th discrete element
M_{1k}, M_{2k}	Nonlinear spatial operators
\mathbf{M}	Mass operator matrix
\mathbf{M}_{DD}	Mass matrix of the discrete elements
N	Nonlinear terms
N_c	Cubic nonlinear terms
N_q	Quadratic nonlinear terms
\mathbf{N}_c	Cubic nonlinear vector
\mathbf{N}_q	Quadratic nonlinear vector
P_{di}	Dynamic tension in belt span i
P_{diL}, P_{diNL}	Linear and nonlinear components of P_{di}
P_{oi}	Total operating tension in span i
P_n	Tractive tension in belt span i
q_n^R, q_n^I	Non-homogeneous terms for modal coordinates
\mathbf{Q}	Excitation vector in state space
r_i	Radius of i th discrete element. For tensioner arm, r_3 is the distance from tensioner arm pivot to pulley center
T	Initial tension of moving belts
T_0	Steady state tension
T_1	Perturbation tension

T_0, T_1, T_2	Different time scales
\mathbf{U}	State space vector
\mathbf{U}_0	Initial state space vector
$v(\xi, \tau)$	Non-dimensional transverse displacement of moving belts
v_0, v_1	The zeroth and first order solution of moving belts
$V(x, t)$	Transverse displacement of moving belts
\mathbf{V}	State space vector
$w_i(x, t)$	Transverse displacement in i th belt span
\mathbf{w}	State space vector for moving belts
\mathbf{W}	Displacement vector
$\mathbf{W}_1, \mathbf{W}_2, \mathbf{W}_3$	The first, second and the third order approximation of \mathbf{W}
$\tilde{\mathbf{W}}$	Displacement vector of the auxiliary system
x	Local coordinate in longitudinal direction

Greek Characters

α_n, α_m	Response amplitude of the n th and m th mode
β_n, β_m	Phase of the n th and m th mode
$\chi_i(t)$	Perimeter displacement along pulley arc, $\chi_i(t) = r_i \theta_i(t)$
$\hat{\chi}_i$	Mode shape of pulley i
δ	Damping ratio
ε	Non-dimensional small parameter
ε_{α_n}	Variation of α_{n0}

$\phi_n(\xi)$	The n th eigenfunction of moving belts
ϕ_{1n}, ϕ_{2n}	The n th eigenfunctions of span 1 and span 2
Φ_i	Displacement eigenfunctions
γ	Non-dimensional translating speed
γ_0	Non-dimensional mean translating speed
γ_1	Non-dimensional perturbed translating speed
η	Viscosity of the dashpot
η_n^R, η_n^I	Real and imaginary components of modal coordinate
γ_i	Spatial distribution function vector of the third order solution
Γ_i	Adjoint state eigenfunction vector
φ_m	The m th eigenfunction of span 3
φ_i	Adjoint displacement eigenfunction
$\hat{\varphi}_i$	$\hat{\varphi}_i = -K\varphi_i / \bar{\lambda}_i$
$\tilde{\varphi}_i$	Displacement eigenfunction of the auxiliary system
λ_n	Eigenvalue of mode n
θ	Phase of autonomous systems
μ	Detuning parameter
σ_1	Internal detuning parameter
σ_2	External detuning parameter
τ	Non-dimensional time
ω	Excitation frequency
ω_n	Natural frequency for mode n
Ω	Excitation frequency

ξ	Non-dimensional coordinate in longitudinal direction
ξ_k^R, ξ_k^I	Real component and imaginary component of modal coordinates
ψ_1, ψ_2	Alignment angles between the adjacent belt spans and the direction of the tensioner pulley center
Ψ_i	State space eigenfunction vector
ζ_k^R, ζ_k^I	Real component and imaginary component of modal coordinates
ζ_1, ζ_2	Phase of autonomous system
ξ_n, ξ_m	Modal damping of mode n and m

CHAPTER 1

INTRODUCTION

1.1 MOTIVATION

The trend in automotive accessory drives has been to replace multiple V-belt drives with a single multi-rib belt drive to power all the accessories including a crankshaft, an alternator, a power steering pump, a tensioner pulley and so on. Such systems are termed “serpentine belt drives”, as shown in Figure 1.1.



Figure 1.1: A typical serpentine belt drive system

The advantage of the serpentine belt drives over the conventional two- or three-point drives using V-belt is the space savings in regard to drive width. Accessory drive width contributes to the overall engine length, which is a very critical dimension on the transverse mounted engines commonly used on later models of front-wheel-drive cars. Another important advantage of the serpentine belt drives is the high reliability and low maintenance requirements due to less heat generation, lower stress, and lower sensitivity of tension to operating conditions (Beikmann *et al.*, 1996). However, the additional compliance renders belts more susceptible to large amplitude vibrations, which may possibly lead to various noise problems and belt fatigue failures. Therefore, it is very important to conduct research on the dynamic characteristics of serpentine belt drive systems.

Serpentine belt drives can exhibit complex dynamic behavior, including rotational vibrations and transverse belt motions. In rotational motions shown in Figure 1.2, the accessory pulleys and tensioner arm oscillate about their spin axes with the belt spans serving as coupling springs. In

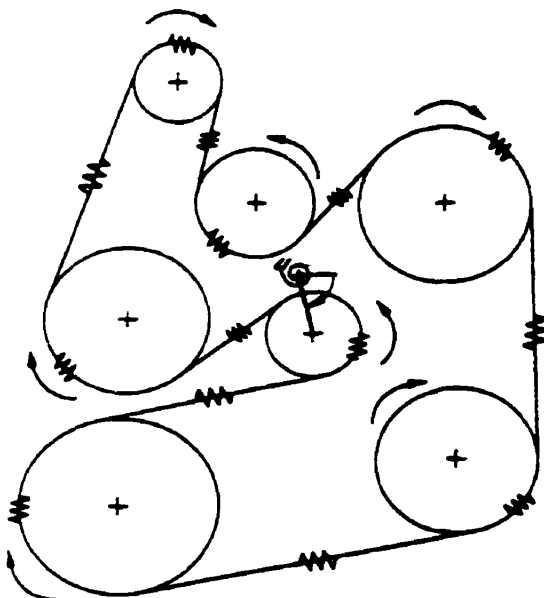


Figure 1.2: Rotational vibration of pulleys and the tensioner arm

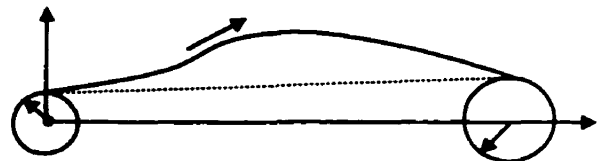


Figure 1.3: Transverse vibration of each belt span

transverse motions shown in Figure 1.3, the belt spans vibrate transversely in a manner similar to a taut string. Both types of vibration may be excited by applied moments from the crankshaft, driven accessories, pulley eccentricities, or motion of the pulley supports. The rotational motion provides a means by which torque fluctuations may parametrically induce transverse belt vibrations. The transverse belt vibration may also induce dynamic tension variations, which may directly radiate noise and induce rotational motions.

Proper modelling of serpentine belt drive systems is especially important in predicting the system's dynamic behavior. Currently, there exist three models to describe serpentine belt drive systems: 1) axially moving continua (Mote, 1966), 2) discrete spring-mass system (Kraver *et al.*, 1996), and 3) hybrid discrete-continuous element model (Beikmann *et al.*, 1996). The first model is used to characterize the transverse motion of belt spans and the second model is used to predict the rotational vibration of discrete components. The first two models assume that the rotational and transverse motions are uncoupled, which is an approximation for accessory drives containing a dynamic tensioner. The third model, proposed by Beikmann *et al.* (1996), captures the coupling between the rotational motion of each discrete component and the transverse motion of each belt span. In serpentine belt drives, as shown by Beikmann *et al.* (1996), there is a linear mechanism that couples the rotational motion of the pulleys and tensioner arm, and transverse motion of the belt spans adjacent to the tensioner arm. Therefore, the third model can represent dynamic behavior of serpentine belt drives more accurately. Moreover, there is a high possibility for two modes to have commensurable natural frequencies. In this case, nonlinear interactions between the rotational vibration and transverse vibrations will produce higher vibration levels than either would alone. Since the coupling between rotational vibration and transverse vibration

seriously impacts vibration performance of the vehicle and the durability of the drive system, it is desirable to capture it when modeling serpentine belt drive systems.

Material damping has long been known to play an important role in determining the dynamic response of serpentine belt drive systems. With exception for some metallic or ceramic reinforcement materials, like steel-cord or glass-cord, serpentine belts are usually composed of polymeric materials such as rubber. Most of these materials exert viscoelastic behavior; i.e. they flow when subjected to stress or strain. Such flow is accompanied by the dissipation of energy due to some internal loss mechanism (for example, bond breakage and bond formation reaction, dislocation). Figure 1.4 illustrates the creep of a practical belt during the operation (Palmgren, 1986). Dynamic loading in operation will not only lead to creep, but also to orientation of the material, by which its stiffness increases. Figure 1.5 shows relaxation and creep effect by repeated deformations of treated polyester cord 1100×2×5 (Palmgren, 1986). A viscoelastic characteristic generally leads to reduced noise and vibrations in the accessory systems. However, it can also cause excessive slip of the belt. In order to model the mechanical characteristics of belt materials accurately, it is necessary to adopt the viscoelastic theory of materials for belts.

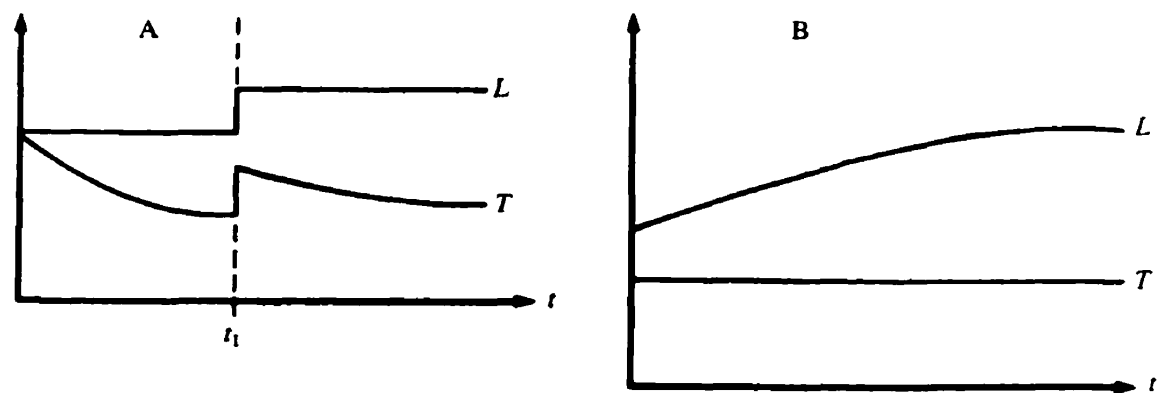


Figure 1.4: Principal changes in belt tension T and belt length L with time of service
 A: Pre-tensioning with constant elongation B: Pre-tensioning with constant force

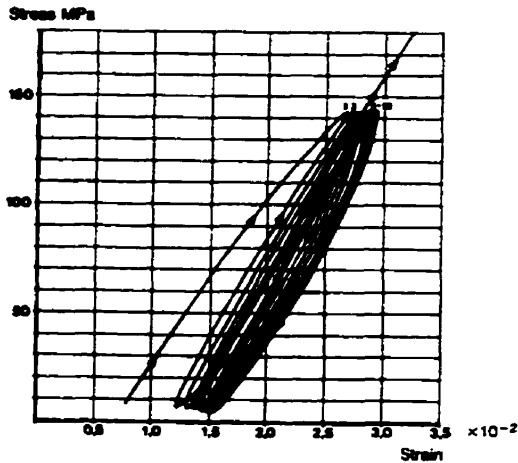


Figure 1.5: Stress-strain curves of the treated polyester cord 1100x2x5 by repeated deformations

Unfortunately, in the three models discussed above, the belt material is assumed to be linear elastic and damping is either ignored or introduced simply as linearly viscous without reference to any damping mechanism. This modeling usually leads to physically unreasonable results (Abrate, 1992), such as unreasonable bifurcations and stability boundaries, due to inaccurate representation of damping. In fact, for serpentine belts, damping is expected to be much higher and to result from different mechanisms. One important damping mechanism is that the viscoelastic behavior of belt materials leads to the dissipation of energy.

In view of the importance of dynamic behavior of the serpentine drive and the lack of research in the analysis of the entire drive accounting for damping and the coupling vibrations, it is therefore the objective of this thesis to set up a new viscoelastic dynamic model for the serpentine belt drive and to develop an efficient approach for the dynamic analysis of the proposed model.

1.2 LITERATURE REVIEW

In this section, a literature survey was undertaken to identify the research related to serpentine

belt drive systems, analytical and numerical methods in viscoelasticity, and multiple scales method for nonlinear vibration analysis.

1.2.1 Transverse Vibration of Serpentine Belt Drive Systems

Automotive serpentine belts are an example of a class of mechanical systems commonly called axially moving continua (Mote, 1972). Aiken (1878) is the first one to study the dynamics of moving continua. This system shares several common characteristics. One important characteristic is that the axial velocity of the moving material introduces two convective acceleration terms, which are not present in the equivalent stationary system. Another characteristic of these systems is that the eigenfunctions governing free vibration response are complex and speed-dependent resulting from the Coriolis and centripetal acceleration terms (Wickert and Mote, 1990).

The bending rigidity of the belt may often be neglected with small errors in the analysis for multi-rib serpentine belts. In the absence of bending stiffness, the belt can be modelled as an axially moving string. Skutch (1897) first determined natural frequencies of a moving string by superposition of two waves propagating in opposite direction. Archibald and Emslie (1958) considered the same problem but derived the equations using a variational approach.

The classical modal analysis and Green's function method, which are applied to the linear non-translating string model, are not directly applicable to linear axially moving string since the generalized coordinates in an eigenfunction expansion remain coupled. Wickert and Mote (1990)

modified the classical modal analysis method by casting the equation of motion for the traveling string into a canonical, first order form that is defined by one symmetric and one skew-symmetric matrix differential operators. When the equation of motion is represented in this form, the eigenfunctions are orthogonal with respect to each other. The response of axially moving materials to arbitrary excitations and initial conditions can be represented in closed-forms.

The earliest calculation on the fundamental period of autonomous nonlinear transverse vibration of an axially moving, elastic, tensioned string was given by Mote (1966). Computation difficulties in the integration of the equation restricted the solution to speeds below 40% of critical speed. In the work done by Thurman and Mote (1969), a hybrid discretization and perturbation method were employed to quantify the speed dependence of the deviation between the linear and nonlinear fundamental periods for a broad range of amplitude and speed parameters. This method was limited because secular excitation terms in the perturbation analysis were not eliminated. Other analyses in this vein, such as those by Bapat and Srinivasan (1967) and by Korde (1985) were performed to derive closed-form approximations to the nonlinear period. The adopted approach required discarding a convective acceleration component from the equation of motion, an approximation that becomes increasingly inaccurate as the transport speed grows. In Wickert's study (1992), the governing equation of motion was cast in the standard form of continuous gyroscopic systems. A second-order perturbation solution was derived through the asymptotic methods of Krylov, Bogoliubov, and Mitropolsky for the near-modal response of a general gyroscopic system with weakly nonlinear stiffness. More recently, Moon and Wickert (1997) extended Wickert's development for weakly nonlinear autonomous systems to non-autonomous systems and developed an averaging solution through

the asymptotic method of KBM for the dynamic response both near and at the exact-resonance regions.

The vibration analysis of a parametrically excited, axially moving system has been studied extensively. Mahalingam (1957) was the first one to notice the possibility of parametric resonance due to the tension fluctuation in a translating string. Later, Mote (1968) evaluated Mahalingam's problem using Hsu's method and obtained the stable–unstable boundaries. Instead of seeking an exact solution, Naguleswaran and Williams (1968) developed a numerical solution by employing Galerkin approximation in the basis of stationary string eigenfunctions. Their theoretical conclusions were verified experimentally. Mockensturm *et al.* (1996) used eigenfunctions of a translating string as the basis for a Galerkin discretization and obtained an analytical expression for the amplitudes and stability boundaries of non-trivial limit cycles that exist around the n th mode principal parametric instability regions.

In the investigations above, the belt material is assumed to be linear elastic and damping is either ignored or introduced simply as linearly viscous without reference to any damping mechanism. The literature that is specially related to viscoelastic moving continuum is very limited. Fung *et al.* (1997) calculated the dynamic response of a viscoelastic moving string using finite difference method. The author (Zhang and Zu, 1998) has studied the free and forced vibrations of viscoelastic moving belts by the use of the direct multiple scales method. The nonlinear natural frequencies and free response amplitude for autonomous systems are predicted. The amplitude of near- and exact-resonant steady state response for non-autonomous systems is obtained. The parametric resonance of viscoelastic moving belts was also investigated by the author (Zhang

and Zu, 1998). The closed-form expressions for amplitude, existence conditions and stability boundary of limit cycles are derived.

1.2.2 Rotational Vibration of Serpentine Belt Drive Systems

The rotational vibration of a serpentine belt drive system has been studied in recent research. Hawker (1991) investigated natural frequencies of damped drive systems with a dynamic tensioner. Barker *et al.* (1991) used a Runge-Kutta method to solve a rapid acceleration-deceleration case involving a movable coulomb-damped tensioner arm. Hwang *et al.* (1994) modeled the rotational vibrations of a serpentine drive and applied the results to predict the onset of belt slip. For linear viscous damping, Kraver *et al.* (1996) developed a complex procedure to solve both underdamped and overdamped cases.

Ulsoy *et al.* (1985) studied the transverse belt vibrations in a two-span subsystem coupled to a dynamic tensioner. Dynamic tensions in the spans were prescribed by torque variations in an adjacent driven accessory. The dynamic tensions parametrically excite transverse vibrations, leading to Mathieu-type instabilities. Mockensturm *et al.* (1996) evaluated the large amplitude limit cycle oscillations that may occur near the instability regions.

1.2.3 Coupling of Transverse and Rotational Vibrations

The above investigations assume that the rotational and transverse motions are uncoupled for linear response. This is true for fixed center band-wheel systems provided that the band

equilibrium is trivial. For serpentine belt drives, Beikmann *et al.* (1996) showed that there exists a linear mechanism coupling rotational motion and transverse motion of the belt spans adjacent to the tensioner. The natural frequencies and mode shapes of an operating serpentine belt drive system were determined using analytical and experimental methods.

Beikmann *et al.* (1996) demonstrated that finite belt stretching created a nonlinear mechanism that may lead to string coupling between pulley/tensioner rotation and transverse belt vibration. Using the eigensolutions obtained from linear analysis, the nonlinear vibration model was discretized and the coupled vibration response was evaluated numerically.

The author (Zhang and Zu, 1998) derived an explicit exact characteristic equation for natural frequencies of the self-adjoint prototypical system instead of using iteration method. Exact closed-form expressions are obtained for responses to arbitrary excitation and initial conditions. For nonlinear vibration of serpentine belt drive systems, the author (Zhang and Zu, 1998) used the direct and discretization multiple scales method to investigate the two-to-one and one-to-one internal resonances. It is shown that while the nonlinear coupling is often small, it can become greatly magnified under conditions leading to an internal or autoparametric resonance. Since the frequency of the transverse models is strongly dependent on translating speed of belt spans, the system may enter regimes, which initiate this highly coupled belt response. The closed-form equations for steady state response and periodic solution are given.

1.2.4 Vibration Analysis of Viscoelastic Materials

The literature specially related to viscoelastic moving continuum is limited. No studies on

vibration of viscoelastic serpentine belt drive systems have been reported. However various methods have been presented for the vibration analysis of structures composed of viscoelastic materials.

Lee and Rogers (1963) studied the stress analysis for linear viscoelastic materials using integral type of stress-strain relation and a simple finite difference numerical procedure. The application of Laplace transform to viscoelastic beams was presented by Flügge (1975). Findley *et al.* (1976) used the correspondence and superposition principles to solve the governing equations of the viscoelastic beams. Christensen (1982) used Fourier transform to solve the transient response of viscoelastic beams. Chen (1995) used Laplace transform and the resulting equation was solved by the finite element method. Fung *et al.* (1996) employed Galerkin approximation to reduce the governing equation to a third order nonlinear ordinary differential equation. The Stevens method was followed to analyze the stability of the linear system. The method of variation of parameters and the method of averaging were used to analyze the dynamic response of nonlinear systems. The Routh-Hurwitz criterion (Chen, 1971) was adopted to investigate the stability of steady solutions of the parametric resonance and the nonlinear effects.

1.2.5 Multiple Scales Method

The multiple scales method is a very efficient perturbation technique for nonlinear dynamic analysis (Nayfeh and Balachandran, 1995). In the analysis of nonlinear vibrations of continuous systems, there are two different approaches: one is the discretization multiple scales method and the other is the direct multiple scales method.

In the discretization multiple scales method, the governing partial differential equations are reduced to ordinary differential equations by assuming the eigenfunctions of the linear problem to be the spatial solutions at all levels of approximations. The discretized equations are then solved by applying the multiple scales method. Little or no attempt is made to verify that the behavior of the discretized system corresponds to that of the original continuous system. Huang *et al.* (1995) used this method to study the dynamic stability of a moving string undergoing three-dimensional Vibration. Rao and Iyengar (1991) solved the coupled nonlinear equations of motion of a sagged cable by the method of multiple scales.

In the direct approach, the multiple scales method is applied directly to the partial differential equations. This approach does not require the selection of an orthogonal basis. Recently, comparisons of these two methods for specific and more general problems have appeared in the literature. Nayfeh *et al.* (1992) were the first to show that direct perturbation yield better results for finite mode truncations and for systems having quadratic and cubic nonlinearities. Pakdemirli *et al.* (1995) further proved Nayfeh's conclusion by investigating a nonlinear cable vibration problem. Pakdemirli and Ulsoy (1997) also found that in some cases, the two approach yield the same results.

In an important work, Rahman and Burton (1989) suggested an improvement for the multiple scales method. They showed that the usual ordering of damping and external excitation produces extra non-physical results for some cases. They proposed a different expansion and ordering in which those results can be eliminated.

1.3 OUTLINE OF THE THESIS

The objective of this thesis is to accurately model and analyze the vibration problems of serpentine belt drive systems. The primary concern is the role of the belt material damping and the nonlinear coupling behavior of entire belt drive systems. To this end, this task is divided in two subtasks which are 1) dynamic analysis of the viscoelastic moving belt model; and 2) dynamic analysis of the hybrid serpentine belt drive model. Accordingly, this thesis is also divided in two parts. Part 1, including Chapter 2 to Chapter 6, is devoted to the formulation and solution of transverse vibration of belt spans. Part 2, including Chapter 7 to Chapter 12, is devoted to the formulation and solution of coupling between the transverse vibration and the rotational vibration for entire belt drive systems. A chapter-by-chapter review is as follows:

Chapter 1 presents the historical perspective and the state of the art of the research on dynamics of serpentine belt drives. The outline and contributions of this thesis are summarized.

Chapter 2 is devoted to the free vibration of viscoelastic moving belts. Kelvin viscoelastic model is employed to characterize the damping mechanism of belt materials. The direct multiple scales method is proposed for the treatment of autonomous gyroscopic systems.

Chapter 3 presents results of forced vibration analysis of viscoelastic moving belts. The amplitude of near- and exact-resonant steady state response for non-autonomous gyroscopic systems is predicted and the stability condition of the steady state solution is given.

Chapter 4 discusses the dynamic response of parametrically excited viscoelastic moving belts.

Comparison is made between the direct multiple scales method and the discretization multiple scales method. Closed-form solutions for the amplitude and the existence conditions of non-trivial limit cycles of the summation resonance are obtained.

Chapter 5 investigates the stability of parametrically excited viscoelastic moving belts. Stability boundaries of the trivial limit cycle for general summation and difference parametric resonances are predicated. The Routh-Hurwitz criterion is used to investigate the stability of non-trivial limit cycles.

Chapter 6 presents a numerical method to calculate transient response of moving belts with viscoelasticity in integral representation. The transient amplitudes of parametrically excited viscoelastic moving belts with uniform and non-uniform travelling speed are given.

Chapter 7 is concerned with the modelling of serpentine belt drives. Viscoelastic constitutive relation is used to represent the material property. A hybrid model is used to capture the linear and nonlinear coupling between the transverse vibration and the rotational vibration.

Chapter 8 is devoted to the modal analysis of self-adjoint hybrid serpentine belt drive systems. An explicit exact characteristic equation of eigenvalues is derived. Solutions of linear response are obtained based on modal expansion.

Chapter 9 presents a new complex modal analysis method for non-self-adjoint hybrid serpentine belt drive systems. The physical meaning of adjoint eigenfunctions and the bi-orthogonality of state space eigenfunctions are discussed in this chapter. An auxiliary system is proposed to

determine the adjoint eigenfunctions.

Chapter 10 presents the discretization multiple scales method for nonlinear vibration analysis of entire hybrid elastic serpentine belt drive systems. The cases of both one-to-one and two-to-one internal resonances are considered. Solutions for the amplitudes of non-trivial limit cycles are obtained.

Chapter 11 is devoted to the direct multiple scales method for nonlinear vibration analysis of entire hybrid elastic serpentine belt drive systems. Comparison is made between the direct approach and the discretization approach for the complicated systems involving quadratic and cubic nonlinearities.

Chapter 12 presents results of nonlinear vibration analysis of hybrid viscoelastic serpentine belt drive systems. The steady state responses under different belt damping ratio are compared.

Chapter 13 provides concluding remarks and offers suggestions for future work.

1.4 CONTRIBUTIONS OF THE THESIS

The contributions of this thesis are summarized as follows:

- 1) Identification of the damping mechanism of belt materials using the viscoelastic models.
- 2) Application of the direct multiple scales method in the dynamic analysis of free, forced and parametric vibration of viscoelastic moving belts for the first time. This analysis provides an

indication of the effect of viscoelastic property.

- 3) Closed-form solutions of response amplitudes, existence conditions, and stability conditions for free, forced and parametric vibration of viscoelastic moving belts.
- 4) Development of a numerical method for the transient response of moving belts with general viscoelasticity. The convergence of travelling eigenfunctions suggested is superior to the stationary string eigenfunctions that are commonly used.
- 5) Development of a viscoelastic hybrid model for the dynamic analysis of serpentine belt drives. This model could describe the damping mechanism of belt material and capture the coupling between the rotational vibration and transverse vibration.
- 6) Exact (closed-form) and explicit characteristic equation of eigenvalues for self-adjoint hybrid serpentine belt drive systems. This characteristic equation provides insight concerning the effect of design parameters on natural frequencies of the system
- 7) Development of a new complex modal analysis method for linear vibration analysis of non-self-adjoint hybrid serpentine belt drives. The adjoint eigenfunction can be conveniently determined from the proposed auxiliary system.
- 8) Development of the discretization multiple scales method for nonlinear dynamic analysis of hybrid nonlinear serpentine belt drive systems. This provides a basic understanding of parametric excitation threshold levels and the existence of multiple limit cycles.
- 9) Development of the direct multiple scales method for the nonlinear dynamic analysis of hybrid serpentine belt drive systems. The comparison between the direct multiple scales method and the discretization multiple scales helps better understand the relationship between the two approaches.

PART I

VIBRATION ANALYSIS OF VISCOELASTIC MOVING BELTS

In Part I (Chapters 2 – 6), an axially moving continua model is used to describe the transverse vibration of each belt span when the coupling between the rotational vibration of accessory components and the transverse vibration of the belt is negligible. Belt materials are considered to satisfy the viscoelastic constitutive law. Free, forced, and parametric vibration analyses are performed to determine the dynamic response of serpentine belts under different load conditions. Although the axially moving continua model is an approximation of an entire serpentine belt drive, it is widely used by accessory drive engineers. The uncoupled analysis is computationally much more efficient than the coupled analysis, and is preferred for preliminary design work. Therefore, the analysis in Part I could help accessory drive engineers better understand the transverse vibration behavior of serpentine belt drives and provide general recommendations for design. In the meantime, this part of the research lays the theory foundation for the further study of more complicated viscoelastic hybrid serpentine belt drive models.

CHAPTER 2

FREE VIBRATION OF VISCOELASTIC MOVING BELTS

In this chapter, as a first step to tackle the problem, free vibration analysis of viscoelastic moving belts is performed. The linear differential viscoelastic constitutive law is adopted to characterize the internal damping mechanism of belt materials. The equation of motion is derived for a viscoelastic moving belt with geometric nonlinearities. A modal perturbation solution is developed in the context of the asymptotic multiple scales method for a general continuous autonomous gyroscopic system. The near-modal nonlinear response for autonomous systems is predicted by the perturbation method. The results obtained with the quasi-static assumption are compared with those without this assumption. Effects of elastic and viscoelastic parameters, the axial moving speed and the nonlinear term on the response are also investigated from numerical examples.

2.1 CONSTITUTIVE RELATION OF VISCOELASTIC MATERIALS

Viscoelasticity theory is a natural extension of the classical theory of elasticity to take into account the energy absorption in continuous systems. In this section, a brief review of viscoelastic constitutive relation is presented. Section 2.1.1 deals with linear differential constitutive relation. Several commonly used models are discussed. Section 2.1.2 is concerned with the linear integral constitutive law and the relation between differential and integral constitutive laws.

2.1.1 Differential Viscoelastic Constitutive Law

The standard linear differential viscoelastic constitutive equation connecting the stress to the strain is

$$P\sigma(t) = Q\varepsilon(t) \quad (2.1)$$

where P and Q are linear differential operators with respect to the time, which account for the complicated rate-dependent behavior including instantaneous elasticity, delayed elasticity, and viscous flow. In a general form, P and Q are expressed as

$$P = \sum_{i=0}^p a_i \frac{\partial^i}{\partial t^i} \quad (2.2)$$

$$Q = \sum_{i=0}^q b_i \frac{\partial^i}{\partial t^i} \quad (2.3)$$

where a_i and b_i are material constants. The number of the constants a_i and b_i will depend on the viscoelastic property of the particular material under consideration.

The linear differential viscoelastic relationship (2.1) may also be rewritten in the symbolic forms as:

$$\sigma(t) = E^* \varepsilon(t) \quad (2.4)$$

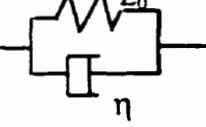
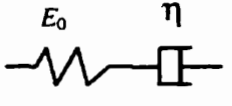
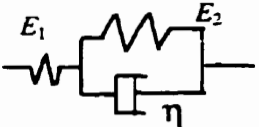
where E^* is the equivalent Young's modulus. Equation (2.4) has to be interpreted simply as an alternative notation. As the linear differential operator E^* may be handled formally as an algebraic quantity, this notation simplifies the formulations of the problem.

The relationship between the equivalent Young's modulus E^* and differential operator P and Q is as follows:

$$E^* = \frac{P}{Q} \quad (2.5)$$

It might be sufficient to represent the viscoelastic response over a limited time scale by considering only one or two terms on each side of equation (2.1). This would be equivalent to describing the linear viscoelastic behavior by mechanical models constructed of linear elastic elements, which obey Hooke's law, and viscous dashpots, which obey Newton's law of viscosity. Thus the viscoelastic behavior of materials, in general, may be investigated by the use of mechanical models, which consist of finite networks of springs and dashpots. Table 2.1 shows four basic viscoelastic models that are commonly used.

Table 2.1: Basic Linear Viscoelastic Models

	Name	Differential equation	E^*
	Kelvin	$\sigma = E_0 \epsilon + \eta \dot{\epsilon}$	$E_0 (1 + \frac{\eta}{E_0} \frac{\partial}{\partial t})$
	Maxwell	$\frac{\dot{\sigma}}{E_0} + \frac{\sigma}{\eta} = \dot{\epsilon}$	$\frac{\eta \frac{\partial}{\partial t}}{1 + \frac{\eta}{E_0} \frac{\partial}{\partial t}}$
	Standard	$\sigma(E_1 + E_2) + \dot{\sigma}\eta = E_1 E_2 \epsilon + E_1 \eta \dot{\epsilon}$	$\frac{E_1 E_2}{E_1 + E_2} \frac{1 + \frac{\eta}{E_2} \frac{\partial}{\partial t}}{1 + \frac{\eta}{E_1 + E_2} \frac{\partial}{\partial t}}$
	Maxwell-Kelvin	$\sigma + \dot{\sigma} \left(\frac{\eta_1}{E_1} + \frac{\eta_2}{E_2} + \frac{\eta_1}{E_2} \right) + \ddot{\sigma} \frac{\eta_1 \eta_2}{E_1 E_2} = \dot{\epsilon} \eta_1 + \ddot{\epsilon} \frac{\eta_1 \eta_2}{E_2}$	$\frac{\eta_1 \frac{\partial}{\partial t} + \frac{\eta_1 \eta_2}{E_2} \frac{\partial^2}{\partial t^2}}{1 + \left(\frac{\eta_1}{E_1} + \frac{\eta_2}{E_2} + \frac{\eta_1}{E_2} \right) \frac{\partial}{\partial t} + \frac{\eta_1 \eta_2}{E_1 E_2} \frac{\partial^2}{\partial t^2}}$

2.1.2 Integral Viscoelastic Constitutive Law

The standard linear integral viscoelastic model, which is an alternative form of equation (2.1), is given in the following

$$\sigma(t) = \int_0^t E(t-\tau) \frac{d\varepsilon}{d\tau} d\tau \quad (2.6)$$

$$\varepsilon(t) = \int_0^t k(t-\tau) \frac{d\sigma}{d\tau} d\tau \quad (2.7)$$

where $E(t)$ is the relaxation modulus and $k(t)$ is the creep compliance. The energy loss in this formulation is attributed to the elastic delay by which the deformation lags behind the applied stress.

The integral constitutive relations (2.6) and (2.7) were first introduced by Boltzmann in 1874 with limitation to isotropic materials and were later generalized to anisotropic materials by Volterra in 1909. Integral constitutive models can represent more complicated mechanical property of materials compared to differential models. However, using integral constitutive relations leads to differential-integral equations of motion, which is difficult to be solved analytically. For some materials, a particularly convenient differential form of viscoelastic constitutive relation can be obtained from a given integral representation by means of state variables.

2.2 EQUATION OF MOTION

A prototypical model of a viscoelastic moving belt is shown in Figure 2.1, where c is the

transport speed of the belt, L is the length of the belt span, V is the displacement in the transverse direction. Several assumptions are made in modeling moving belts as follows:

- 1) Only transverse vibration in the y direction is taken into consideration
- 2) Transport speed of belts, c , is constant
- 3) Lagrangian strain for belt extension is employed as a finite measure of the strain
- 4) The viscoelastic string is in a state of uniform initial stress

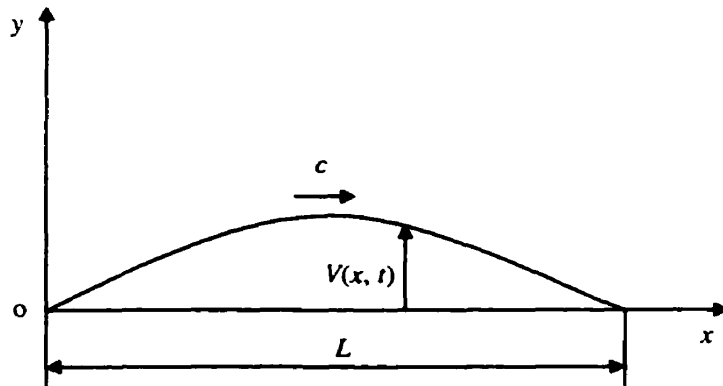


Figure 2.1: A prototypical model of a viscoelastic moving belt.

Based on the above assumptions, the equation of motion in the y direction can be obtained by Newton's second law (Fung *et al.*, 1997)

$$\left(\frac{T}{A} + \sigma \right) V_{xx} + V_x \sigma_x = \rho V_{tt} \quad (2.8)$$

where the subscript notation x and t denote partial differentiation with respect to spatial Cartesian coordinate x and time t , σ is the perturbed stress, A is the area of cross-section of the belt, ρ is the mass per unit volume, and T is the initial force.

For free vibration analysis, the system is subjected to the homogeneous boundary conditions (Wickert, 1992)

$$V = 0 \quad \text{at } x=0 \text{ and } x=L \quad (2.9)$$

For moving belts, the transverse acceleration is given by (Mote, 1966)

$$\frac{d^2V}{dt^2} = \frac{\partial^2V}{\partial t^2} + 2c \frac{\partial^2V}{\partial x \partial t} + c^2 \frac{\partial^2V}{\partial x^2} \quad (2.10)$$

Note that in equation (2.10), the first term on the right hand side represents the local acceleration component, the second term represents the Coriolis acceleration component, and the last term represents the centripetal acceleration component.

In this research, only geometric nonlinearity due to finite stretching is considered. For moving belts with large amplitude, the perturbed Lagrangian strain component in the x direction in relation to the displacement is given by

$$\varepsilon(x,t) = \frac{1}{2} V_x^2 \quad (2.11)$$

Applying the linear differential viscoelastic constitutive law equation (2.4), the perturbed stress is in the form

$$\sigma = E^* \left(\frac{1}{2} V_x^2 \right) \quad (2.12)$$

Substituting equations (2.10) and (2.12) into equation (2.8) yields

$$\rho \frac{\partial^2V}{\partial t^2} + 2\rho c \frac{\partial^2V}{\partial t \partial x} + \left(\rho c^2 - \frac{T}{A} \right) \frac{\partial^2V}{\partial x^2} = E^* \left(\frac{1}{2} V_x^2 \right) V_{xx} + V_x \left\{ E^* \left(\frac{1}{2} V_x^2 \right) \right\}_x \quad (2.13)$$

Equation (2.13) has the same form as the equation of motion for elastic moving materials proposed by Thurman and Mote (1969). The difference is that the usual modulus of elasticity E is replaced by E^* , which is a linear differential operator characterizing the viscoelastic property of the belt material. The differential operator E^* determined from viscoelastic models complicates the equations substantially.

Introducing the following non-dimensional parameters

$$\nu = \frac{V}{L} \quad \xi = \frac{x}{L} \quad \tau = t \left(\frac{T}{\rho A L^2} \right)^{\frac{1}{2}} \quad \gamma = c \left(\frac{\rho A}{T} \right)^{\frac{1}{2}} \quad E' = \frac{E' A}{T} \quad (2.14)$$

the following non-dimensional equation of transverse motion can be obtained

$$\frac{\partial^2 \nu}{\partial \tau^2} + 2\gamma \frac{\partial^2 \nu}{\partial \tau \partial \xi} + (\gamma^2 - 1) \frac{\partial^2 \nu}{\partial \xi^2} = N(\nu) \quad (2.15)$$

where the nonlinear operator $N(\nu)$ is defined as

$$N(\nu) = E \left(\frac{1}{2} \nu_{\xi\xi}^2 \right) \nu_{\xi\xi} + \nu_{\xi} \left\{ E \left(\frac{1}{2} \nu_{\xi\xi}^2 \right) \right\}_{\xi} \quad (2.16)$$

Equation (2.15) is the generalized equations of motion valid for all kinds of viscoelastic model.

Introduce the mass, gyroscopic, and linear stiffness operators as follows

$$M = I, \quad G = 2\gamma \frac{\partial}{\partial \xi}, \quad K = (\gamma^2 - 1) \frac{\partial^2}{\partial \xi^2} \quad (2.17)$$

where operators M and K are symmetric and positive definite for sub-critical transport speeds; G is skew-symmetric and represents a convective Coriolis acceleration component. Thus, equation (2.15) can be written in a standard symbolic form

$$M \nu_{\tau\tau} + G \nu_{\tau\xi} + K \nu_{\xi\xi} = N(\nu) \quad (2.18)$$

As a first step, the most frequently used Kelvin viscoelastic model is chosen to describe the viscoelastic property of the belt material. This model is composed of a linear spring and a linear dashpot connected in parallel. The corresponding equivalent Young's modulus E' for Kelvin viscoelastic model is given below

$$E^* = E_0 + \eta \frac{\partial}{\partial t} \quad (2.19)$$

where E_0 is the stiffness constant of the spring and η is the dynamic viscosity of the dashpot. According to the definition of non-dimensional parameters, the dimensionless operator E can be expressed as

$$E = E_e + E_v \frac{\partial}{\partial \tau} \quad (2.20)$$

where

$$E_e = \frac{E_0 A}{T} \quad (2.21)$$

$$E_v = \eta \sqrt{\frac{A}{\rho T L^2}} \quad (2.22)$$

Substituting equation (2.20) into (2.16) and with some manipulations, the nonlinear operator $N(v)$ for the Kelvin viscoelastic model becomes

$$N(v) = \frac{3}{2} E_e v_\xi^2 v_{\xi\xi} + E_v \frac{\partial}{\partial \tau} \left(\frac{1}{2} v_\xi^2 \right) v_{\xi\xi} + v_\xi E_v \frac{\partial}{\partial \tau} (v_\xi v_{\xi\xi}) \quad (2.23)$$

It should be mentioned that the nonlinear operators in equation (2.23) for Kelvin model are due to the geometric nonlinearity.

2.3 MODAL ANALYSIS OF LINEAR MOVING MATERIALS

As the base solution to be used in the multiple scales method for the nonlinear moving belts in the next section, the modal analysis for the dynamic response of linear moving materials is presented in this Section. The classical modal analysis is not directly applicable to linear axially

moving strings since the generalized coordinates in an eigenfunction expansion remain coupled. Wickert and Mote (1990) modified the classical modal analysis method by casting the equations of motion for a traveling string into a canonical, first order form that is defined by one symmetric and one skew-symmetric matrix differential operators. The response of axially moving materials to arbitrary excitation and initial conditions can be represented in closed-forms.

Introduce the state vector and the excitation vectors

$$\mathbf{w} = \begin{Bmatrix} \dot{v} \\ v \end{Bmatrix} \quad \mathbf{Q} = \begin{Bmatrix} f \\ 0 \end{Bmatrix} \quad (2.24)$$

and the matrix differential operators

$$\mathbf{A} = \begin{bmatrix} M & 0 \\ 0 & K \end{bmatrix} \quad \mathbf{B} = \begin{bmatrix} G & K \\ -K & 0 \end{bmatrix} \quad (2.25)$$

Equation (2.18) without the nonlinear term becomes

$$\mathbf{A}\dot{\mathbf{w}} + \mathbf{B}\mathbf{w} = \mathbf{Q} \quad (2.26)$$

Equation (2.26) is a canonical form of the equation of motion and its solution satisfies the initial condition v_0 and the corresponding boundary condition. The general solution of the linear response for equation (2.26) is

$$\mathbf{w}(\xi, \tau) = \sum_{n=1, \pm 2, \dots} \zeta_n(\tau) \psi_n(\xi) \quad (2.27)$$

where

$$\zeta_n(\tau) = \zeta_n(0) e^{\lambda_n \tau} + \int_0^\tau e^{\lambda_n (\tau-t)} Q_n(t) dt \quad (2.28)$$

$$Q_n(\tau) = \langle \mathbf{Q}, \psi_n \rangle \quad (2.29)$$

$$\zeta_n(0) = \langle \mathbf{A}\mathbf{w}_0, \psi_n \rangle \quad (2.30)$$

and the eigenvalues $\lambda_n = i\omega_n$ are imaginary with natural frequencies ω_n being positive for $n \geq 1$; $\psi_n(\xi)$ is the state eigenfunction that has the representation $\psi_n = \{\lambda_n \phi_n, \phi_n\}^T$ in terms of the complex scalar eigenfunction ϕ_n of the displacement field. $\psi_n(\xi)$ satisfies the orthogonal relations

$$\langle \mathbf{A}\psi_n, \psi_m \rangle = \delta_{mn} \quad \langle \mathbf{B}\psi_n, \psi_m \rangle = -\lambda_n \delta_{mn}, \quad \text{for } n, m = \pm 1, \pm 2, \dots \quad (2.31)$$

In particular, the closed-form steady-state displacement response for the non-resonance harmonic excitation $\mathbf{Q} = \{f(x)e^{i\omega t} \quad 0\}^T$ is

$$v(\xi, t) = e^{i\omega t} \sum_{n=\pm 1, \pm 2, \dots} \frac{\langle f, \psi_n \rangle}{1 - \frac{\omega}{\omega_n}} \phi_n(\xi) \quad (2.32)$$

2.4 NONLINEAR VIBRATION ANALYSIS

In this section, nonlinear vibration analysis will be performed to obtain free response and natural frequencies of viscoelastic moving belts. The method of multiple scales (A.H. Nayfeh and S.A. Nayfeh, 1994) is applied directly to the governing equations of motion without a priori assumption regarding the spatial solutions.

Introducing a small dimensionless parameter ϵ as a bookkeeping device, equation (2.18) can be rewritten as follows

$$Mv_{tt} + Gv_t + Kv = \epsilon N(v) \quad (2.33)$$

2.4.1 Multiple Scales Method

A first order uniform approximation is sought in the form

$$v(\xi, \tau, \epsilon) = v_0(\xi, T_0, T_1) + \epsilon v_1(\xi, T_0, T_1) + \dots \quad (2.34)$$

where $T_0 = \tau$ is a fast scale characterizing motions occurring at one of the natural frequencies ω_k of the system, and $T_1 = \epsilon\tau$ is a slow scale characterizing the shift in the natural frequencies due to the nonlinearity.

Using the chain rule, the time derivatives in terms of T_0 and T_1 become

$$\frac{\partial}{\partial \tau} = \frac{\partial}{\partial T_0} + \epsilon \frac{\partial}{\partial T_1} + \dots \quad (2.35)$$

$$\frac{\partial^2}{\partial \tau^2} = \frac{\partial^2}{\partial T_0^2} + 2\epsilon \frac{\partial^2}{\partial T_0 \partial T_1} + \dots \quad (2.36)$$

Substituting equations (2.34) - (2.36) into (2.33) and equating coefficients of like powers of ϵ gives

$$M \frac{\partial^2 v_0}{\partial T_0^2} + G \frac{\partial v_0}{\partial T_0} + K v_0 = 0 \quad (2.37)$$

$$v_0 = 0 \quad \text{at } \xi = 0 \text{ and } 1 \quad (2.38)$$

$$M \frac{\partial^2 v_1}{\partial T_0^2} + G \frac{\partial v_1}{\partial T_0} + K v_1 = -2M \frac{\partial^2 v_0}{\partial T_0 \partial T_1} - G \frac{\partial v_0}{\partial T_1} + N(v_0) \quad (2.39)$$

$$v_1 = 0 \quad \text{at } \xi = 0 \text{ and } 1 \quad (2.40)$$

The excitation components on the right hand side of equation (2.39) are evaluated at the first order solution v_0 and are known at each level of approximation. The nonlinear operator $N(v_0)$ in

equation (2.39) acts on the first order correction to the displacement and velocity fields.

Equation (2.37) is satisfied by

$$v_0 = \phi_k(\xi) A_k(T_1) e^{i\omega_k T_0} + \bar{\phi}_k(\xi) \bar{A}_k(T_1) e^{-i\omega_k T_0} \quad (2.41)$$

where the overbar denotes complex conjugate. Function A_k will be determined by eliminating the secular terms from v_1 . The zeroth order solution corresponds to the free response of the unperturbed system, equation (2.37), in the k th mode.

Substituting equation (2.41) into (2.39) leads to

$$\begin{aligned} M \frac{\partial^2 v_1}{\partial T_0^2} + G \frac{\partial v_1}{\partial T_0} + K v_1 &= M_{1k}(E_e + 2i\omega_k E_v) A_k^3 e^{3i\omega_k T_0} \\ &+ [M_{2k}(3E_e + 2i\omega_k E_v) A_k^2 \bar{A}_k - 2i\omega_k A'_k M \phi_k - A'_k G \phi_k] e^{i\omega_k T_0} + cc \end{aligned} \quad (2.42)$$

where cc denotes the complex conjugate of all preceding terms on the right side of equation (2.42), the prime indicates the derivative with respect to T_1 , and M_{1k} and M_{2k} are nonlinear spatial operators which are defined as follows

$$M_{1k} = \frac{3}{2} \left(\frac{\partial \phi_k}{\partial \xi} \right)^2 \frac{\partial^2 \phi_k}{\partial \xi^2} \quad (2.43)$$

$$M_{2k} = \frac{1}{2} \left[\left(\frac{\partial \phi_k}{\partial \xi} \right)^2 \frac{\partial^2 \bar{\phi}_k}{\partial \xi^2} + 2 \frac{\partial \phi_k}{\partial \xi} \frac{\partial \bar{\phi}_k}{\partial \xi} \frac{\partial^2 \phi_k}{\partial \xi^2} \right] \quad (2.44)$$

Equation (2.42) has a solution only if a solvability condition is satisfied. This solvability condition demands that the right side of equation (2.42) be orthogonal to every solution of the homogeneous problem. For the case where internal resonance does not exist, the solvability condition can be determined as

$$-2i\omega_k A'_k m_k - A'_k g_k i + (3E_\epsilon + 2i\omega_k E_\nu) A_k^2 \bar{A}_k m_{2k} = 0 \quad (2.45)$$

in which

$$m_k = \langle M\phi_k, \phi_k \rangle \quad (2.46)$$

$$g_k = -i \langle G\phi_k, \phi_k \rangle \quad (2.47)$$

$$m_{2k} = \langle M_{2k}, \phi_k \rangle \quad (2.48)$$

and the notation $\langle \cdot, \cdot \rangle$ represents the standard inner product of two complex functions over $\xi \in (0,1)$

Referring to Wickert and Mote (1990), the k th natural frequency and eigenfunction which has been normalized such that $m_k=1$ for linear moving belts are

$$\omega_k = k\pi(1-\gamma^2) \quad (2.49)$$

$$\phi_k = \sqrt{2} \sin(k\pi\xi) e^{(ik\pi\xi)} \quad (2.50)$$

The complex eigenfunctions indicate that unlike non-gyroscopic linear systems, the material particles comprising axially moving continua do not pass through equilibrium simultaneously.

Substituting the eigenvalues and eigenfunctions given by equations (2.49) and (2.50) into equations (2.47) and (2.48) leads to

$$g_k = 2k\pi\gamma^2 \quad (2.51)$$

$$m_{2k} = -\frac{1}{4}\pi^4 k^4 (3 + 2\gamma^2 + 3\gamma^4) \quad (2.52)$$

It can be seen that both g_k and m_{2k} are real.

Express A_k in the polar form

$$A_k = \frac{1}{2} \alpha_k e^{i\beta_k} \quad (2.53)$$

Note that α_k and β_k represent the amplitude and the phase of the response, respectively.

Substituting equation (2.53) into (2.45) and separating the resulting equation into real and imaginary parts yield

$$\frac{1}{2} \alpha_k \beta'_k (2\omega_k + g_k) + \frac{\alpha_k^3}{8} (3E_\epsilon \operatorname{Re}(m_{2k}) - 2\omega_k E_v \operatorname{Im}(m_{2k})) = 0 \quad (2.54)$$

$$-\frac{1}{2} \alpha'_k (2\omega_k + g_k) + \frac{\alpha_k^3}{8} (3E_\epsilon \operatorname{Im}(m_{2k}) + 2\omega_k E_v \operatorname{Re}(m_{2k})) = 0 \quad (2.55)$$

where $\operatorname{Re}(m_{2k})$ and $\operatorname{Im}(m_{2k})$ denote the real and imaginary components of m_{2k} . Since m_{2k} is real, $\operatorname{Im}(m_{2k})$ should be zero for Kelvin viscoelastic moving belts.

2.4.2 The Zeroth Order Solution

Equation (2.55) is an ordinary differential equation involving one variable α_k only. After some manipulations, equation (2.55) can be rewritten as

$$\frac{d\alpha_k}{dT_1} = C_k \alpha_k^3 \quad (2.56)$$

where

$$C_k = \frac{3E_\epsilon \operatorname{Im}(m_{2k}) + 2\omega_k E_v \operatorname{Re}(m_{2k})}{4(2\omega_k + g_k)} \quad (2.57)$$

For Kelvin viscoelastic moving belts, substituting equations (2.51) and (2.52) into (2.57) leads to

$$C_k = -\frac{1}{16} \pi^4 k^4 (1 - \gamma^2) (3 + 2\gamma^2 + 3\gamma^4) E_v \quad (2.58)$$

Therefore, α_k can be obtained from equation (2.56) in the form

$$\alpha_k = \frac{\alpha_0}{\sqrt{1 - 2C_k\alpha_0^2 T_1}} \quad (2.59)$$

where α_0 is the initial amplitude.

Substituting equation (2.58) into (2.59), the response amplitude of viscoelastic moving belts with geometric nonlinearity can be written in the form

$$\alpha_k = \frac{\alpha_0}{\sqrt{1 + \frac{k^4 \pi^4 E_v (1 - \gamma^2)(3 + 2\gamma^2 + 3\gamma^4) \alpha_0^2 \varepsilon \tau}{8}}} \quad (2.60)$$

It should be noted that for the linear elastic constitutive law, which does not account for damping, the amplitude α_k is a constant. However for a viscoelastic model which takes into account the damping of belt materials, the amplitude α_k should decrease with time and thus $\alpha'_k \neq 0$.

Substituting equation (2.59) into (2.54) gives

$$\frac{d\beta_k}{dT_1} = -\frac{D_k \alpha_0^2}{1 - 2C_k \alpha_0^2 T_1} \quad (2.61)$$

where

$$D_k = \frac{3E_\epsilon \operatorname{Re}(m_{2k}) - 2\omega_k E_v \operatorname{Im}(m_{2k})}{4(2\omega_k + g_k)} \quad (2.62)$$

For viscoelastic moving belts, substitution of equations (2.51) and (2.52) into (2.62) yields

$$D_k = -\frac{3}{32} E_\epsilon \pi^3 k^3 (3 + 2\gamma^2 + 3\gamma^4) \quad (2.63)$$

Solving equation (2.61), the solution can be expressed as

$$\beta_k = \frac{D_k}{2C_k} \ln(1 - 2C_k \alpha_0^2 T_1) + \beta_{k0} \quad (C_k \neq 0) \quad (2.64)$$

$$\beta_k = -D_k \alpha_0^2 T_1 + \beta_{k0} \quad (C_k = 0) \quad (2.65)$$

where β_{k0} is a constant.

Now that α_k , β_k and thus A_k are obtained, the zeroth order asymptotic solution for the free vibration of moving viscoelastic belts can be obtained

$$v_0 = \frac{1}{2} \phi_k(\xi) \frac{\alpha_0}{\sqrt{1 - 2C_k \alpha_0^2 \epsilon \tau}} e^{i \left(\omega_k \tau + \frac{D_k}{2C_k} \ln(1 - 2C_k \alpha_0^2 \epsilon \tau) + \beta_{k0} \right)} + cc \quad (C_k \neq 0) \quad (2.66)$$

$$v_0 = \frac{1}{2} \phi_k(\xi) \alpha_0 e^{i \left((\omega_k - D_k \alpha_0^2 \epsilon) \tau + \beta_{k0} \right)} + cc \quad (C_k = 0) \quad (2.67)$$

Note that equation (2.67) for $C_k = 0$ is corresponding to the linear elastic model.

Equation (2.66) shows clearly that the zeroth order asymptotic solution is not a simple harmonic motion due to existence of material damping introduced by the viscoelastic model. If the material has light damping, the value of $2C_k \alpha_0^2$ is very small. In this case, the nonlinear frequency ω_{nk} can be approximated as

$$\omega_{nk} = \omega_k - D_k \alpha_0^2 \epsilon \quad (2.68)$$

Using equation (2.63), for light damping, the natural frequency of the viscoelastic geometric nonlinear moving string is derived from equation (2.68) as

$$\omega_{nk} = k\pi(1 - \gamma^2) + \frac{3E_\epsilon \alpha_0^2 (k\pi)^3}{32} (3 + 2\gamma^2 + 3\gamma^4) \quad (2.69)$$

It can be seen that the nonlinear natural frequency of the system for the first order approximation is independent of the viscoelastic characteristic of the material when Kelvin model is adopted. This is not surprising, as the frequencies of lightly damped viscoelastic materials should approach to that of the elastic materials.

2.4.3 The First Order Solution

It follows from equation (2.45) that

$$A'_k = \frac{(3E_e + 2i\omega_k E_v)m_{2k}}{2i\omega_k m_k + ig_k} A_k^2 \bar{A}_k \quad (2.70)$$

Substituting equation (2.70) into (2.42), the resulting equation can be rewritten as

$$M \frac{\partial^2 v_1}{\partial T_0^2} + G \frac{\partial v_1}{\partial T_0} + Kv_1 = f_1(\xi) A_k^3 e^{3i\omega_k T_0} + f_2(\xi) A_k^2 \bar{A}_k e^{i\omega_k T_0} + cc \quad (2.71)$$

where

$$f_1(\xi) = M_{1k} (E_e + 2i\omega_k E_v) \quad (2.72)$$

$$f_2(\xi) = M_{2k} (3E_e + 2i\omega_k E_v) - (2i\omega_k M\phi_k + G\phi_k) \frac{(3E_e + 2i\omega_k E_v)m_{2k}}{2i\omega_k m_k + ig_k} \quad (2.73)$$

The solution of equation (2.71), which is the corresponding response correction of v_0 , can be

obtained using separation of variables

$$v_1 = h_1(\xi) A_k^3 e^{3i\omega_k \tau} + h_2(\xi) A_k^2 \bar{A}_k e^{i\omega_k \tau} + cc \quad (2.74)$$

where

$$h_1(\xi) = \sum_{n=\pm 1, \pm 2, \dots} \frac{\langle f_1(\xi), \phi_n(\xi) \rangle}{1 - \frac{3\omega_k}{\omega_n}} \phi_n(\xi) \quad (2.75)$$

$$h_2(\xi) = \sum_{\substack{n=\pm 1, \pm 2, \dots \\ n \neq k}} \frac{\langle f_2(\xi), \phi_n(\xi) \rangle}{1 - \frac{\omega_k}{\omega_n}} \phi_n(\xi) \quad (2.76)$$

The specification of no internal resonance requires that ω_k/ω_n and $3\omega_k/\omega_n$ be away from unity. Examining equation (2.74) - (2.76), it can be seen that the spatial variations of the first order solutions are different from those of the linear solutions. Hence, the validity of the assumption that the spatial variation can be represented in terms of linear eigenfunctions is questionable. However, this assumption is the basis for the usual perturbation approach in which the partial differential equation is discretized first using linear eigenfunctions.

2.5 NUMERICAL RESULTS AND DISCUSSIONS

Numerical results for the free vibration of viscoelastic moving belts are presented in this section. Effects of moving speed, nonlinearity and viscoelasticity are investigated.

2.5.1 Material Properties of Belts

Belts are composed of cord reinforcement materials and the outer layer of rubber materials, which can be considered as a spring (reinforcement materials) and a dashpot (rubber materials) connected in parallel. Thus, Kelvin viscoelastic model is a natural representation of the mechanical properties of belt materials. The modulus of elasticity of belt material, E_0 , varies from 4000 MPa to 150000 MPa (Palmgren, 1986), mainly depending on the reinforcement material. For instance, E_0 for the commonly used polyester is around 8000 MPa. The

recommended strain at pre-tension is less than 1.5% (Palmgren, 1986), that is, $T/E_0A < 1.5\%$. Therefore, the non-dimensional Young's modulus, $E_e = E_0A/T$, should be greater than 67 in value. In this study, different values of E_e , which are more than 400 in value, are chosen to investigate the influence of the nonlinearity.

The dynamic viscosity η of the dashpot for Kelvin model is related to Young's modulus by $\eta = \delta E_0$, where δ is around 0.00001 to 0.01 (Kraver *et al.*, 1996). The relation between non-dimensional viscoelastic parameter E_v and non-dimensional Young's modulus E_e can then be obtained from equations (2.21) and (2.22) as

$$\frac{E_v}{E_e} = \delta \sqrt{\frac{T}{\rho A}} \frac{1}{L} \quad (2.77)$$

where $\sqrt{T/\rho A}$, which is the speed of the transverse wave, is near 100 m/s. Therefore, the value of E_v should be approximately around $(0.001-1)E_e$. For example, a typical production belt has a δ near 0.0012, thus E_v is about $0.12E_e$. In this study, all the values of E_v chosen to investigate the influence of viscoelasticity are within the region of $0.001E_e$ to $0.125E_e$.

2.5.2 Numerical Results and Discussions

In the vibration analysis of moving belts, many people (Wickert, 1992, Huang *et al.*, 1995, and Mockensturm *et al.*, 1996) adopted the “quasi-static stretch” assumption under which dynamic tensions in the belt are uniform throughout the span. When $T \ll EA$, the quasi-static stretch assumption is valid. In this case, the axial wave spreads much faster than the transverse wave.

Thus, the variation of axial stress can been approximated to spread instantly from one end to the other. Using the method of multiple scales, free responses under this assumption are obtained to compare with those given in previous sections. Redefining M_{1k} , M_{2k} , m_{2k} , C_k , and D_k in equations (2.43), (2.44), (2.48), (2.57) and (2.62) for the case with quasi-static assumption as

$$M_{1k} = \frac{\partial^2 \phi_k}{2\partial \xi^2} \int_0^1 \left(\frac{\partial \phi_k}{\partial \xi} \right)^2 d\xi \quad (2.78)$$

$$M_{2k} = \frac{\partial^2 \phi_k}{3\partial \xi^2} \int_0^1 \left(\frac{\partial \phi_k}{\partial \xi} \right) \left(\frac{\partial \bar{\phi}_k}{\partial \xi} \right) d\xi + \frac{\partial^2 \bar{\phi}_k}{6\partial \xi^2} \int_0^1 \left(\frac{\partial \phi_k}{\partial \xi} \right)^2 d\xi \quad (2.79)$$

$$m_{2k} = -\frac{k^2 \pi^2}{6\xi^2} \left(2k^2 \pi^2 \gamma^2 (\gamma^2 + 1)^2 + \sin^2(k\pi\gamma) \right) \quad (2.80)$$

$$C_k = -\frac{E_v \pi^2 k^2 (1 - \gamma^2) \left(2\pi^2 k^2 \gamma^2 (1 + \gamma^2)^2 + \sin^2(k\pi\gamma) \right)}{24\gamma^2} \quad (2.81)$$

$$D_k = -\frac{E_v \pi k \left(2\pi^2 k^2 \gamma^2 (1 + \gamma^2)^2 + \sin^2(k\pi\gamma) \right)}{16\gamma^2} \quad (2.82)$$

Applying equations (2.59) and (2.68), the natural frequency and response amplitude of viscoelastic moving belts with geometric nonlinearity under the quasi-static assumption are derived as

$$\omega_{Nk} = k\pi(1 - \gamma^2) + \frac{E_v \alpha_0^2 (k\pi)^3}{8} \left[(1 + \gamma^2)^2 + \frac{1}{2} \left(\frac{\sin(k\pi\gamma)}{k\pi\gamma} \right)^2 \right] \quad (2.83)$$

$$\alpha_k = \frac{\alpha_0}{\sqrt{1 + \frac{E_v \pi^2 k^2 \alpha_0^2 (1 - \gamma^2) \left(2\pi^2 k^2 \gamma^2 (1 + \gamma^2)^2 + \sin^2(k\pi\gamma) \right) \xi \tau}{12\gamma^2}}} \quad (2.84)$$

It can be seen that for viscoelastic materials, the natural frequencies given by equation (2.83) are

identical to those of elastic systems (Wickert, 1992). However, the response amplitudes depend on the viscoelastic property of the material. When the linear elastic model is considered, in which $E_v = 0$, the response amplitude remains constant. This conclusion agrees with that in Wickert (1992).

Figure 2.2 compares the fundamental natural frequencies without the quasi-static assumption and those with the quasi-static assumption for moving belts. The nonlinear natural frequency is plotted against the non-dimensional transport speed. The material is assumed to be linear elastic, i.e., $E_v = 0$. Different values of E_v are chosen to show the influence of nonlinearity. The higher the value of E_v is, the stronger the nonlinearity of the system has. It is observed that the natural frequency decreases as the transport speed increases. This is because a larger moving speed leads to smaller linear stiffness of the belt, resulting in lower frequencies. Note that with the increase of the nonlinearity, the natural frequency increases. It can be seen that the results with the quasi-static assumption and those without such an assumption are close to each other at the lower speed range. The difference, however, grows with the moving speed. This is because at higher moving speed, the contribution of the nonlinearity to the natural frequencies is larger. Since the quasi-static assumption only involves the nonlinear terms, the difference between nonlinear terms with the quasi-static assumption and those without quasi-static assumption leads to larger difference of natural frequencies.

To show the influence of viscoelastic parameter E_v on nonlinear natural frequencies, the displacement v_0 in equation (2.27) is rewritten in the near- and exact-resonance conditions as

$$v_0 = \zeta_k^R \phi_k^R + \zeta_k' \phi_k' \quad (2.85)$$

where ζ_k^R and ζ_k' are generalized coordinates governing the evolution of the real and imaginary components of the eigenfunction ϕ_k . ζ_k^R and ζ_k' can be derived as

$$\zeta_k^R = \frac{\alpha_0}{\sqrt{1-2C_k\alpha_0^2\varepsilon\tau}} \cos\left(\omega_k\tau + \frac{D_k}{2C_k} \ln(1-2C_k\alpha_0^2\varepsilon\tau) + \beta_{k0}\right) \quad (2.86)$$

$$\zeta_k' = \frac{\alpha_0}{\sqrt{1-2C_k\alpha_0^2\varepsilon\tau}} \sin\left(\omega_k\tau + \frac{D_k}{2C_k} \ln(1-2C_k\alpha_0^2\varepsilon\tau) + \beta_{k0}\right) \quad (2.87)$$

ζ_k^R and ζ_k' on the time domain and the frequency domain for different values of E_v are displayed in Figure 2.3 and Figure 2.4, respectively, to show effects of viscoelasticity on natural frequencies. The viscoelastic parameters E_v are chosen as 0.1, 1, and 10, respectively. Since ζ_k^R and ζ_k' are not a simple harmonic motion, it is difficult to show the influence of E_v on natural frequencies during a short time scale. Thus, in Figure 2.3 and Figure 2.4, the starting point of the non-dimensional time is chosen as 500. It can be seen that even after a longer time, the difference of natural frequencies among different values of E_v is still small. Therefore, for the first order approximation, the viscoelasticity does not have significant effect on the natural frequency of viscoelastic moving belts. Materials with strong damping that do not suffer from greatly reduced natural frequencies are conceivable.

The effect of the viscoelastic parameter E_v on the response amplitude α_k is illustrated in Figure 2.5 and Figure 2.6. In Figure 2.5, the response amplitude is plotted over the non-dimensional time range 0 to 500. E_v and the non-dimensional transport speed γ are set to be 400 and 0.5, respectively. Three different values of viscoelastic parameter E_v are considered. At the time

instant $\tau = 500$, the amplitude decrease is 2% for $E_v=0.1$, 16.2% for $E_v=1$ and 56.2% for $E_v=10$. As expected, the response amplitude decreases with time and the amplitude is strongly dependent on the viscoelastic coefficient E_v . In Figure 2.6, the response amplitude is plotted over the viscoelastic parameter E_v ranging from 0 to 50 at the time instant $\tau = 500$ while other parameters remains the same as those in Figure 2.5. It can be seen that the larger E_v is, the smaller the amplitude is. Since higher E_v corresponds to higher damping, the viscoelastic nature of the material can be effective in reducing the vibration of moving belts.

Figure 2.7 shows the effect of nonlinearity, reflected by E_c , on response amplitudes for viscoelastic moving belts. Three viscoelastic systems having identical E_v and γ but having different E_c are compared. $E_v=1$ and $\gamma=0.5$. For system 1, $E_c=400$; for system 2, $E_c=2500$; for system 3, $E_c=10000$. It is clear that the amplitudes are identical for three different systems over the non-dimensional time range 0 to 500. Hence, it is concluded that nonlinear parameter E_c has no influence on the amplitude of response while E_c affects the nonlinear natural frequencies of viscoelastic moving belts as shown in Figure 2.2.

2.6 SUMMARY AND CONCLUSIONS

In this chapter, the nonlinear natural frequencies and near-modal nonlinear response for free vibration of viscoelastic elastic moving belts are obtained by using the method of multiple scales. The Kelvin model is adopted to describe the viscoelastic characteristic of belt materials. The

governing equation of motion is derived and cast in a first order form. The method of multiple scales is applied directly to the governing partial differential equation. Effects of the axial moving speed, geometric nonlinearity and viscoelastic property on the natural frequencies and amplitude of free response are investigated from the numerical examples. The following conclusions are made in this study:

- 1) The damping introduced by the viscoelastic model has no significant effect on nonlinear natural frequencies while it has an important influence on the amplitude of response for viscoelastic moving belts. The response amplitude decreases with time more quickly as the increase of the viscoelastic parameter E_v . Thus, materials with strong viscoelastic property can effectively reduce the vibration of moving belts without suffering from greatly reduced natural frequencies.
- 2) The nonlinear natural frequencies decrease as the moving speed increases.
- 3) The natural frequencies grow with the nonlinear parameter E_e , but the free response amplitude does not change with E_e .
- 4) No assumptions about the spatial dependence of the motion are made in the method of solution. This is more appropriate than usual perturbation approaches in which the linear spatial solutions are assumed a priori to describe the spatial solution of the nonlinear problem.

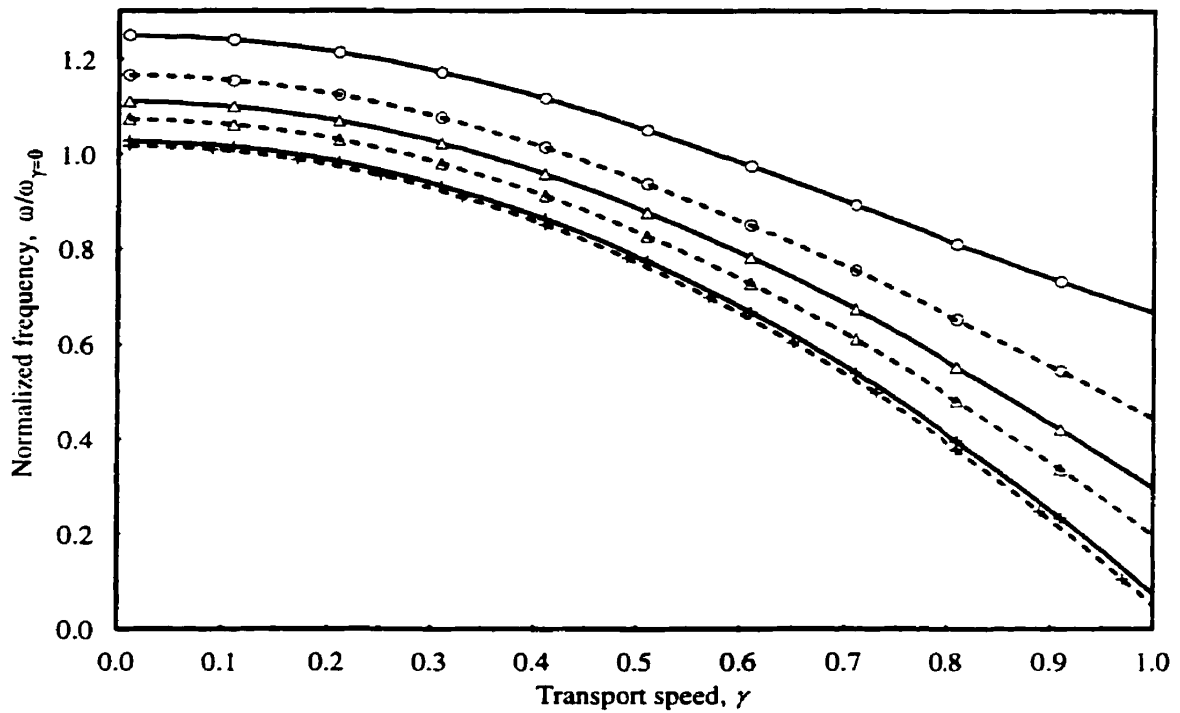


Figure 2.2: A comparison of nonlinear fundamental frequencies of an elastic moving belt

$+$: $E_e=400$	Δ : $E_e=1600$	\circ : $E_e=2500$
— : without quasi-static assumption	--- : With quasi-static assumption	

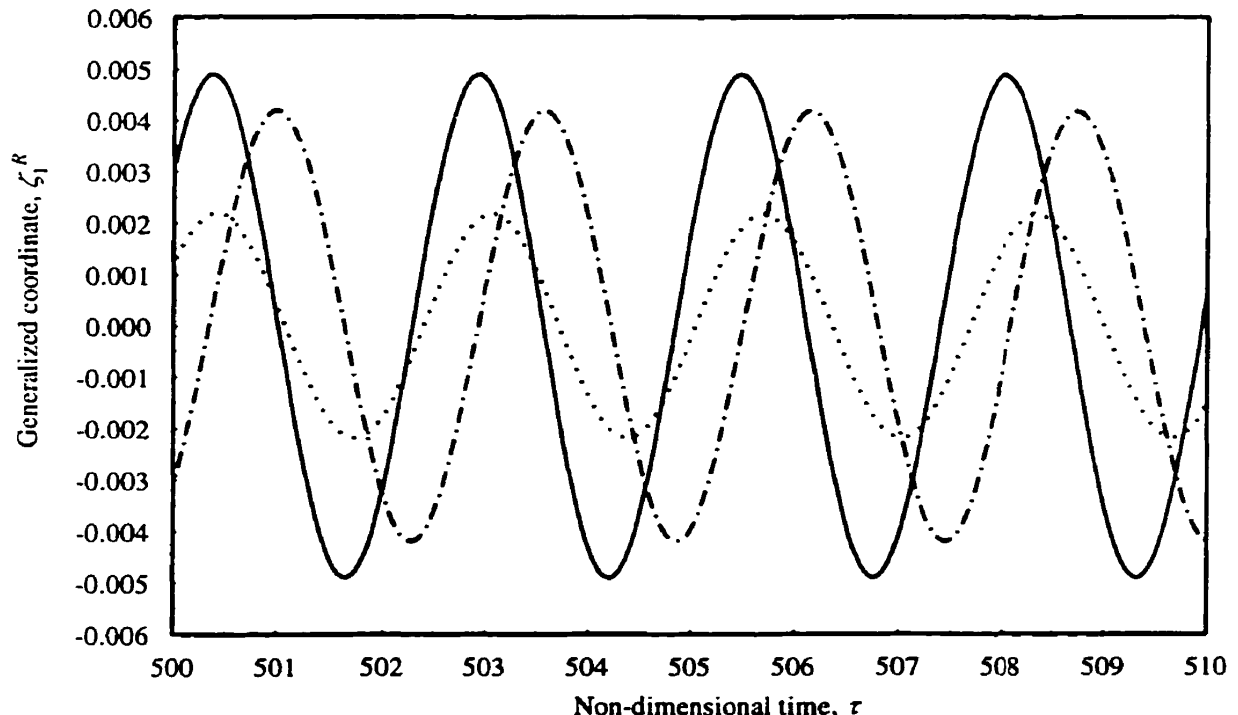


Figure 2.3A: Waveform of the generalized coordinate ζ_1^R for $E_e=400$

— : $E_v=0.1$	--- : $E_v=1$... : $E_v=10$
---------------	---------------	----------------

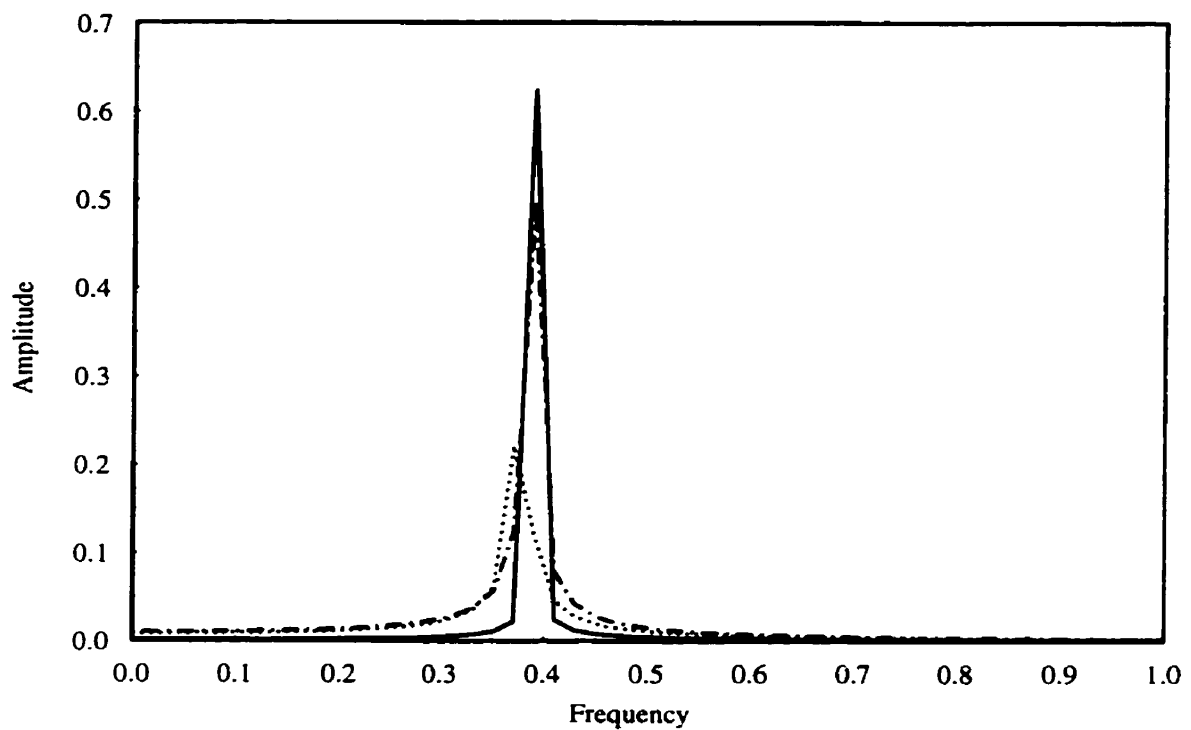


Figure 2.3B: The discrete Fourier transform of the wave ζ_1^R for $E_\epsilon=400$

— : $E_\nu=0.1$ - - - : $E_\nu=1$ - · - : $E_\nu=10$

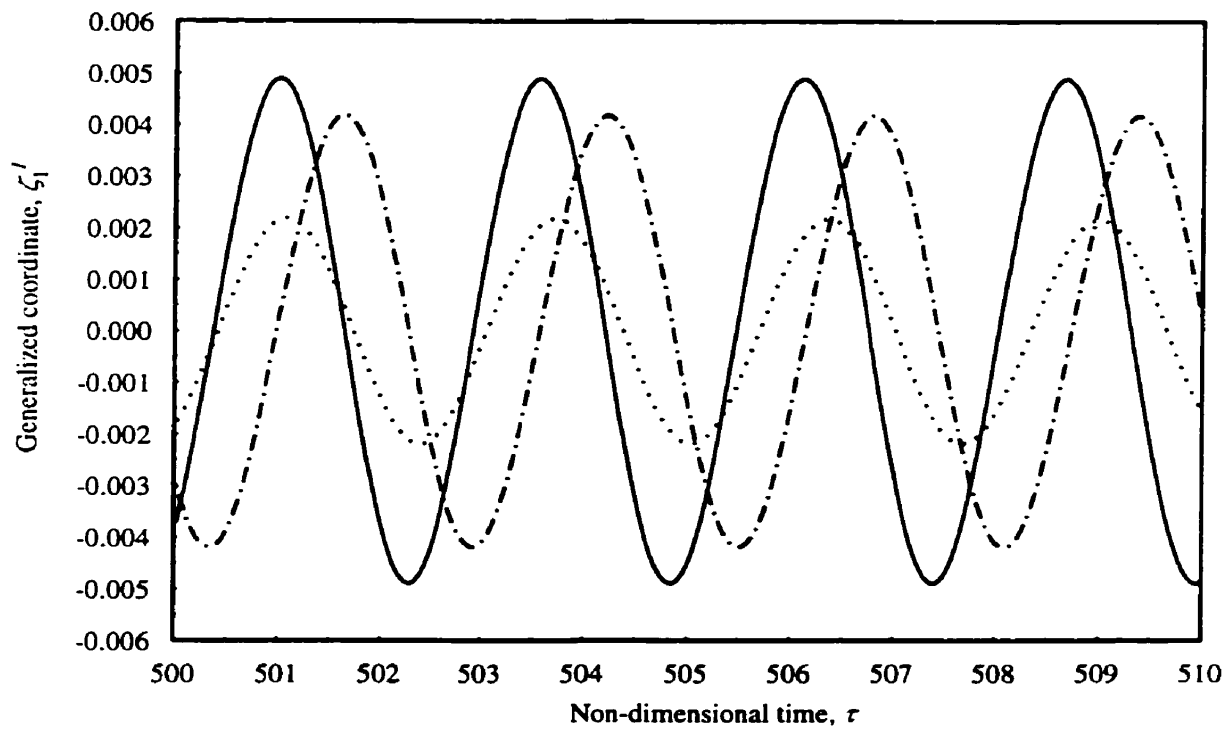


Figure 2.4A: Waveform of the generalized coordinate ζ_1' for $E_\epsilon=400$

— : $E_\nu=0.1$ - - - : $E_\nu=1$ - · - : $E_\nu=10$

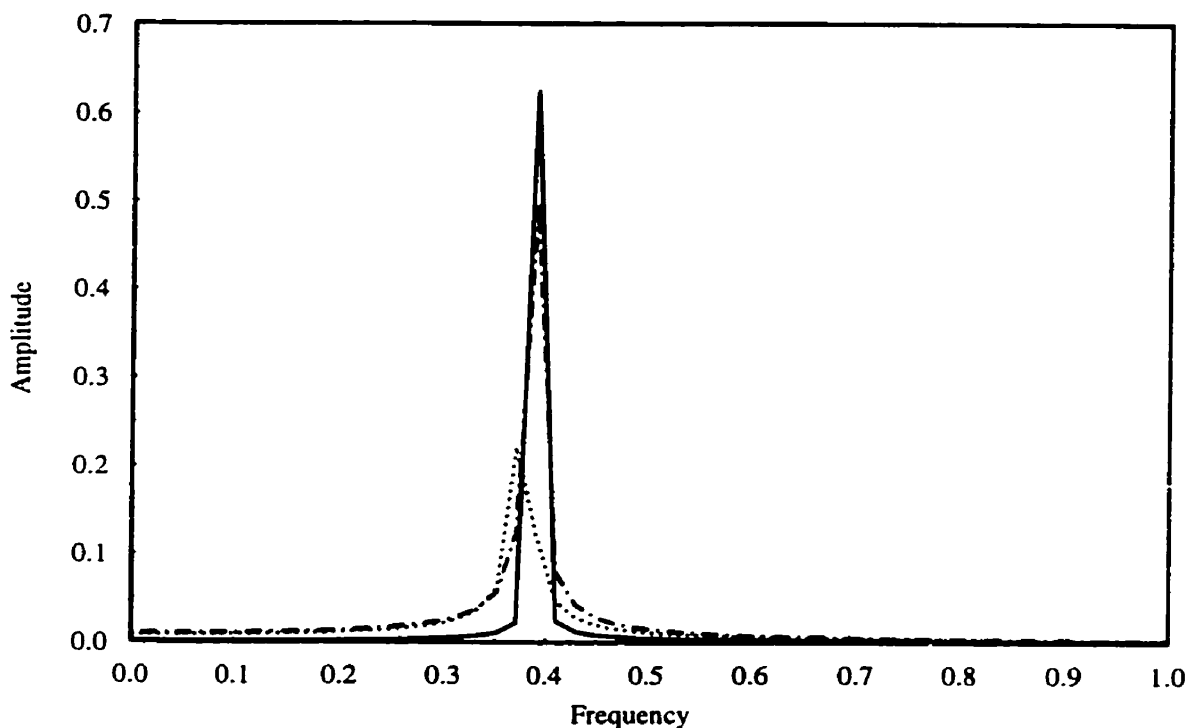


Figure 2.4B: The discrete Fourier transform of the wave ζ'_1 for $E_\epsilon=400$

— : $E_\nu=0.1$ - - - : $E_\nu=1$ - · - : $E_\nu=10$

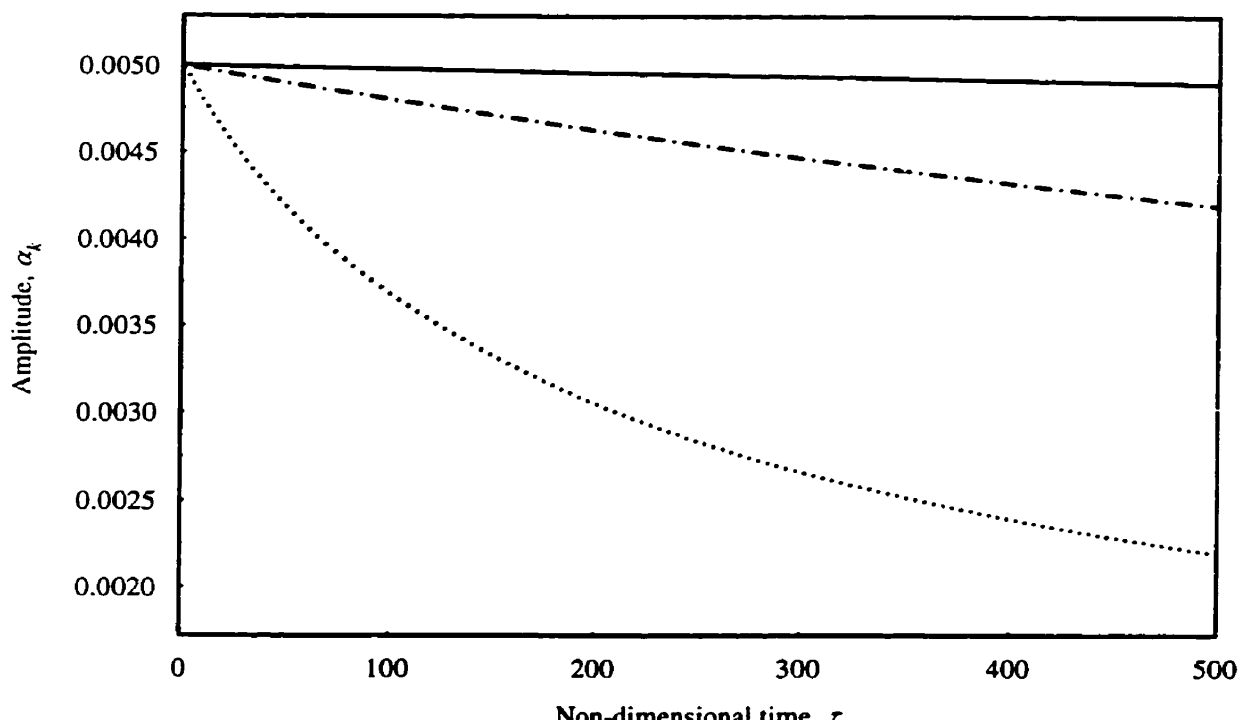


Figure 2.5: The influence of viscoelasticity on response amplitude for $E_\epsilon=400$

— : $E_\nu=0.1$ - - - : $E_\nu=1$ - · - : $E_\nu=10$

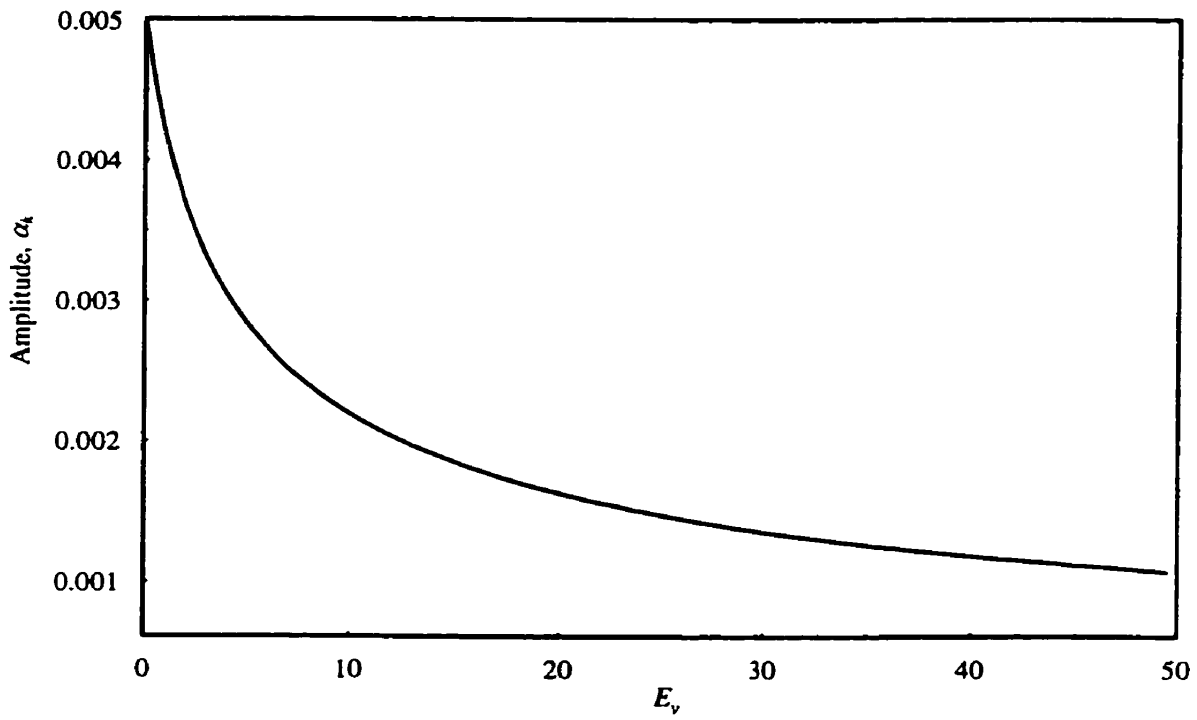


Figure 2.6: The influence of viscoelasticity on response amplitude for $\gamma=0.5$, $E_c=400$ at time instant 500

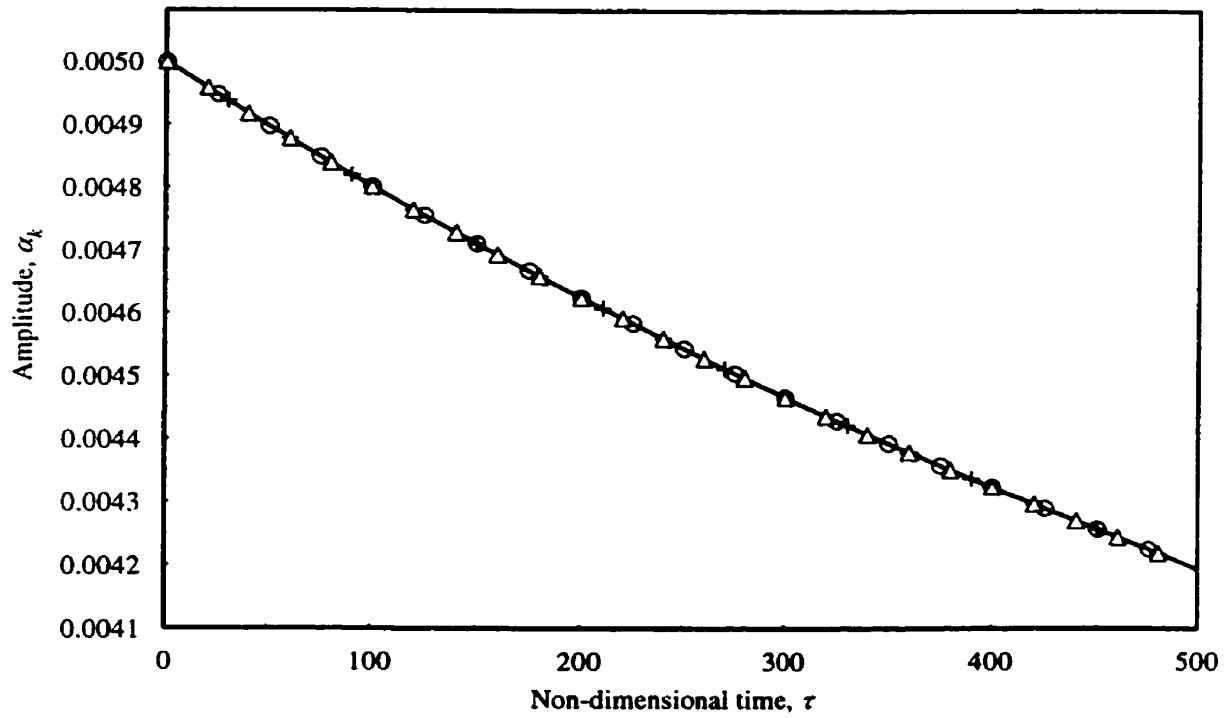


Figure 2.7: The influence of nonlinearity on response amplitude for $E_v=1$, $\gamma=0.5$
 $+ : E_c=400$ $\Delta : E_c=1600$ $\circ : E_c=3600$.

CHAPTER 3

FORCED VIBRATION OF VISCOELASTIC MOVING BELTS

The transverse vibration of each belt span of serpentine belt drives may be excited by applied moments from the crankshaft, pulley eccentricities, and irregular pulley radii. This kind of forced vibration induces dynamic tension variations and directly radiates noise. In the present chapter, the forced vibration of nonlinear viscoelastic moving belts excited by the eccentricity of pulleys is investigated. The results obtained here can be readily extended to other types of excitations. The method of multiple scales is applied directly to the governing equations of a viscoelastic moving belt. This direct treatment does not involve a prior assumption regarding the spatial solutions. The amplitude of near- and exact-resonant steady state response for non-autonomous systems is predicted. The stability of the steady state solutions is studied.

3.1 EQUATION OF MOTION

Figure 3.1 shows a prototypical system of a moving belt driven by eccentrically-mounted pulleys. c is the moving speed of the belt and r_0 , r_1 , e_0 and e_1 denote radii and eccentricities of pulleys.

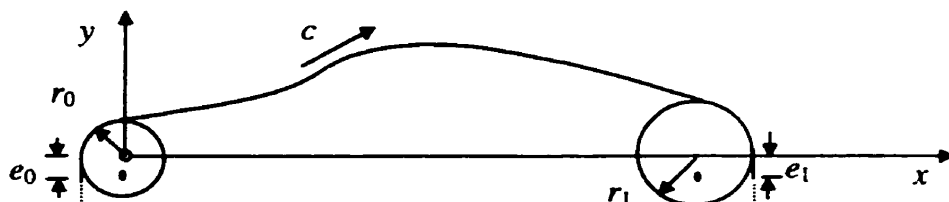


Figure 3.1: A prototypical model of a viscoelastic moving belt driven by eccentrically-mounted pulleys

The equation of motion in the y direction can be obtained by Newton's second law

$$\left(\frac{T}{A} + \sigma\right)V_{xx} + V_x\sigma_x = \rho\left(\frac{\partial^2 V}{\partial t^2} + 2c\frac{\partial^2 V}{\partial x \partial t} + c^2\frac{\partial^2 V}{\partial x^2}\right) \quad (3.1)$$

where all the quantities are defined in Chapter 2. The difference between the prototypical system studied here and that discussed in Chapter 2 is that pulleys in the current model are eccentric. The eccentricities of the pulleys would lead to non-homogenous boundary conditions.

3.1.1 Non-homogenous Boundary Conditions

The system is subjected to the following non-homogenous boundary conditions,

$$V(0, t) = e_0 \sin(\Omega_0 t) \quad V(L, t) = e_1 \sin(\Omega_1 t) \quad (3.2)$$

where Ω_0 and Ω_1 are rotational frequencies of the pulleys.

In practice, the pulleys can have different radii r_0 and r_1 , and so the excitations could be at distinct frequencies Ω_0 and Ω_1 . The substitution of transverse displacement V with $V + e_0 \sin(\Omega_0 t) + (e_1 \sin(\Omega_1 t) - e_0 \sin(\Omega_0 t)) \frac{x}{L}$ renders the boundary condition (3.2) homogeneous.

and the excitation is transferred from the boundary to the domain (Moon and Wickert, 1997).

Correspondingly, equations (3.1) and (3.2) are changed into the following form

$$\left(\frac{T}{A} + \sigma\right)V_{xx} + V_x\sigma_x + \frac{F(x, t)}{A} = \rho\left(\frac{\partial^2 V}{\partial t^2} + 2c\frac{\partial^2 V}{\partial x \partial t} + c^2\frac{\partial^2 V}{\partial x^2}\right) \quad (3.3)$$

$$V(0, t) = 0 \quad V(L, t) = 0 \quad (3.4)$$

Note that $F(x, t)$ is the external force per unit length, which is transferred from the boundary

support excitation.

In this study, only the eccentricity of the right pulley is considered, and thus the external force $F(x, t)$ can be expressed as

$$F(x, t) = (x - 2ir_1)e_i \Omega^2 e^{i\Omega t} + cc \quad (3.5)$$

where Ω is the rotational frequency of the right pulley, cc denotes the complex conjugate of all preceding terms on the right side of equation (3.5). Under the assumption of no slip, the relation between the excitation frequency and the transport speed is in the form

$$\Omega = \frac{c}{r_1} \quad (3.6)$$

The same prototypical model was investigated recently by Moon and Wickert (1997) using asymptotic method of Krylov, Bogoliubov, and Mitropolsky. Near- and exact-resonant responses amplitudes were predicated. In their study, the belt is assumed to be linear elastic and damping is ignored. However, most of belt materials exert inherently viscoelastic behavior. To accurately describe the material property of moving belts, viscoelastic constitutive relation should be employed

3.1.2 Equation of Motion in Standard Symbolic Form

The one-dimensional linear differential viscoelastic constitutive law can be written as

$$\sigma(t) = E^* \varepsilon(t) \quad (3.7)$$

where the equivalent Young's modulus E^* is determined by the viscoelastic property of belt

materials and may be handled formally as an algebraic quantity.

Applying the linear differential viscoelastic constitutive law and considering the Lagrangian strain component, the perturbed stress is in the form

$$\sigma = E^* \left(\frac{1}{2} V_x^2 \right) \quad (3.8)$$

Substituting equation (3.8) into equation (3.3) yields

$$\rho \frac{\partial^2 V}{\partial t^2} + 2\rho c \frac{\partial^2 V}{\partial t \partial x} + \left(\rho c^2 - \frac{T}{A} \right) \frac{\partial^2 V}{\partial x^2} = E^* \left(\frac{1}{2} V_x^2 \right) V_{xx} + V_x \left\{ E^* \left(\frac{1}{2} V_x^2 \right) \right\}_x + \frac{F(x,t)}{A} \quad (3.9)$$

Introducing the following non-dimensional parameters

$$v = \frac{V}{L} \quad \xi = \frac{x}{L} \quad \tau = t \left(\frac{T}{\rho A L^2} \right)^{\frac{1}{2}} \quad \gamma = c \left(\frac{\rho A}{T} \right)^{\frac{1}{2}} \quad E = \frac{E^* A}{T} \quad f(x,t) = \frac{F(x,t)L}{T} \quad (3.10)$$

The following non-dimensional equation for the transverse motion can be obtained

$$\frac{\partial^2 v}{\partial \tau^2} + 2\gamma \frac{\partial^2 v}{\partial \tau \partial \xi} + (\gamma^2 - 1) \frac{\partial^2 v}{\partial \xi^2} = N(v) + f(x,t) \quad (3.11)$$

where the nonlinear operator $N(v)$ is defined by equation (2.16) in Chapter 2.

Equation (3.11) is the generalized equation of motion valid for all kinds of viscoelastic model. In this study, the most frequently used Kelvin viscoelastic model is chosen to describe the viscoelastic property of the belt material. The linear dimensionless differential operator E for Kelvin viscoelastic model is given by equation (2.20) in Chapter 2. In a same way as in Chapter 2, equation (3.11) can be written in a standard symbolic form

$$Mv_{\xi\xi} + Gv_{\xi} + Kv = N(v) + f(x,t) \quad (3.12)$$

where M , G and K are given by equation (2.17). Moving belts are one example of gyroscopic

dynamic systems to the degree that their deformation involves small amplitude vibration, which is superimposed on the mean rigid body motion. Mechanical structures that can vibrate about a state of mean rotation or translation are related by the mathematical similarity of their governing equation (3.12). In what follows, the direct multiple scales method is applied to any such gyroscopic dynamics system, and to moving belts in particular.

3.2 NONLINEAR FORCED VIBRATION ANALYSIS

In this section, the amplitude of near- and exact-resonant steady state response for non-autonomous systems is predicted. The method of multiple scales is applied directly to the equation, which is in the form of continuous non-autonomous gyroscopic systems.

3.2.1 Multiple Scales Method

Introducing a small dimensionless parameter ϵ as a bookkeeping device, equation (3.12) can be rewritten as

$$Mv_{\pi\pi} + Gv_{\tau} + Kv = \epsilon N(v) + \epsilon f(\xi, \tau) \quad (3.13)$$

A first order uniform approximation is sought in the form

$$v(\xi, \tau, \epsilon) = v_0(\xi, T_0, T_1) + \epsilon v_1(\xi, T_0, T_1) + \dots \quad (3.14)$$

Substituting equation (3.14) and the time derivatives in terms of T_0 and T_1 into (3.13) and equating coefficients of like powers of ϵ ,

$$M \frac{\partial^2 v_0}{\partial T_0^2} + G \frac{\partial v_0}{\partial T_0} + Kv_0 = 0 \quad (3.15)$$

$$M \frac{\partial^2 v_1}{\partial T_0^2} + G \frac{\partial v_1}{\partial T_0} + K v_1 = -2M \frac{\partial^2 v_0}{\partial T_0 \partial T_1} - G \frac{\partial v_0}{\partial T_1} + N(v_0) + f(\xi, \tau) \quad (3.16)$$

All the excitation components on the right side of equation (3.16) except for $f(\xi, \tau)$ are evaluated from first order solution v_0 .

The solution of equation (3.15) is in the form

$$v_0 = \phi_k(\xi) A_k(T_1) e^{i\omega_k T_0} + \bar{\phi}_k(\xi) \bar{A}_k(T_1) e^{-i\omega_k T_0} \quad (3.17)$$

where the overbar denotes complex conjugate, ω_k is the k th natural frequency, and ϕ_k is the k th eigenfunction. Function A_k in equation (3.17) will be determined by eliminating the secular terms from v_1 . Substituting equation (3.17) into (3.16) leads to

$$\begin{aligned} M \frac{\partial^2 v_1}{\partial T_0^2} + G \frac{\partial v_1}{\partial T_0} + K v_1 &= M_{1k}(E_e + 2i\omega_k E_v) A_k^3 e^{3i\omega_k T_0} \\ &+ [M_{2k}(3E_e + 2i\omega_k E_v) A_k^2 \bar{A}_k - 2i\omega_k A'_k M \phi_k - A'_k G \phi_k] e^{i\omega_k T_0} + f_0(\xi) e^{i\Omega T_0} + cc \end{aligned} \quad (3.18)$$

The solvability condition requires that the right side of equation (3.18) be orthogonal to every solution of the homogeneous problem. For the case where internal resonance does not exist, the solvability condition can be determined as

$$-2i\omega_k A'_k m_k - A'_k g_k i + (3E_e + 2i\omega_k E_v) A_k^2 \bar{A}_k m_{2k} + f_k e^{i(\Omega - \omega_k) T_0} = 0 \quad (3.19)$$

in which

$$f_k = \langle f_0, \psi_k \rangle \quad (3.20)$$

In the near and exact-resonance cases, introduce a detuning parameter $\mu = o(1)$ defined by

$$\Omega = \omega_k + \epsilon \mu \quad (3.21)$$

Substituting equation (3.21) into (3.19) leads to

$$-2i\omega_k A'_k m_k - A'_k g_k i + (3E_\epsilon + 2i\omega_k E_v) A_k^2 \bar{A}_k m_{2k} + f_k e^{i\mu T_1} = 0 \quad (3.22)$$

For convenience, express A_k in the polar form

$$A_k = \frac{1}{2} \alpha_k e^{i\beta_k} \quad (3.23)$$

Note that α_k and β_k represent the amplitude and the phase of the response, respectively.

Substituting equation (3.23) into (3.22) and separating the resulting equation into real and imaginary parts yields

$$\frac{1}{2} \alpha_k \beta'_k (2\omega_k m_k + g_k) + \frac{3\alpha_k^3 E_\epsilon m_{2k}}{8} = -\operatorname{Re}(f_k) \cos(\mu T_1 - \beta_k) + \operatorname{Im}(f_k) \sin(\mu T_1 - \beta_k) \quad (3.24)$$

$$-\frac{1}{2} \alpha'_k (2\omega_k m_k + g_k) + \frac{\alpha_k^3 \omega_k E_v m_{2k}}{4} = -\operatorname{Re}(f_k) \sin(\mu T_1 - \beta_k) - \operatorname{Im}(f_k) \cos(\mu T_1 - \beta_k) \quad (3.25)$$

Since T_1 appears explicitly in equations (3.24) and (3.25), the equations are referred as a non-autonomous system. It is convenient to eliminate the explicit dependence on T_1 , thereby transforming these equations into an autonomous system. This can be accomplished by introducing a new dependent variable θ_k defined by

$$\theta_k = \mu T_1 - \beta_k \quad (3.26)$$

Using equation (3.26), equations (3.24) and (3.25) can be rewritten as

$$\frac{1}{2} \alpha_k (\mu - \theta'_k) (2\omega_k m_k + g_k) + \frac{3\alpha_k^3 E_\epsilon m_{2k}}{8} = -\operatorname{Re}(f_k) \cos(\theta_k) + \operatorname{Im}(f_k) \sin(\theta_k) \quad (3.27)$$

$$-\frac{1}{2} \alpha'_k (2\omega_k m_k + g_k) + \frac{\alpha_k^3 \omega_k E_v m_{2k}}{4} = -\operatorname{Re}(f_k) \sin(\theta_k) - \operatorname{Im}(f_k) \cos(\theta_k) \quad (3.28)$$

3.2.2 Steady State Solutions

For the steady-state response, the amplitude α_k and the new phase angle θ_k in equations (3.27) and (3.28) should be constant. Thus, setting $\alpha'_k = 0$ and $\theta'_k = 0$ and with some manipulations, the amplitude and phase of the response can be determined from the following algebraic equations

$$c_3(\alpha_k^2)^3 + c_2(\alpha_k^2)^2 + c_1(\alpha_k^2) + c_0 = 0 \quad (3.29)$$

$$\theta_k = \tan^{-1} \left(\frac{C_k \operatorname{Re}(f_k) - (1 + D_k) \operatorname{Im}(f_k)}{(1 + D_k) \operatorname{Re}(f_k) + C_k \operatorname{Im}(f_k)} \right) \quad (3.30)$$

where

$$C_k = \frac{\omega_k E_v m_{2k}}{2(2\omega_k m_k + g_k)} \quad (3.31)$$

$$D_k = \frac{3E_\epsilon m_{2k}}{4(2\omega_k m_k + g_k)} \quad (3.32)$$

$$c_0 = -((\operatorname{Re}(f_k))^2 + (\operatorname{Im}(f_k))^2) \quad (3.33)$$

$$c_1 = \frac{1}{4} (2\omega_k m_k + g_k)^2 \mu^2 \quad (3.34)$$

$$c_2 = \frac{3E_\epsilon m_{2k} (2\omega_k m_k + g_k) \mu}{8} \quad (3.35)$$

$$c_3 = \frac{1}{64} ((3E_\epsilon m_{2k})^2 + (2\omega_k E_v m_{2k})^2) \quad (3.36)$$

Note that c_0 , c_1 and c_2 are independent of the viscoelastic property of the belt material. Only c_3 changes with E_v , which is a measure of the degree of viscoelastic behavior of the belt. Equation (3.29) has one real and two complex conjugate roots for moving speeds below a critical fold

velocity, and three real roots above that point.

Substituting equations (2.51) and (2.52) in Chapter 2 into equations (3.31) - (3.36) yields

$$C_k = -\frac{1}{16}\pi^4 k^4 (1-\gamma^2)(3+2\gamma^2+3\gamma^4) E_v \quad (3.37)$$

$$D_k = -\frac{3}{32} E_e \pi^3 k^3 (3+2\gamma^2+3\gamma^4) \quad (3.38)$$

$$c_1 = k^2 \pi^2 \mu^2 \quad (3.39)$$

$$c_2 = -\frac{3E_e k^5 \pi^5}{16} (3+2\gamma^2+3\gamma^4) \mu \quad (3.40)$$

$$c_3 = \frac{9E_e^2 k^8 \pi^8}{1024} (3+2\gamma^2+3\gamma^4)^2 + \frac{E_v^2 k^{10} \pi^{10} (1-\gamma^2)^2 (3+2\gamma^2+3\gamma^4)^2}{256} \quad (3.41)$$

If the “quasi-static stretch” is assumed, the steady response amplitude can also be obtained using the same equation (3.29) and (3.30) by simply redefining coefficients c_1 , c_2 , and c_3 as

$$c_1 = k^2 \pi^2 \mu^2 \quad (3.42)$$

$$c_2 = -\frac{E_e k^3 \pi^3 (2k^2 \pi^2 \gamma^2 (1+\gamma^2)^2 + \sin^2(k\pi\gamma)) \mu}{8} \quad (3.43)$$

$$c_3 = \frac{(9E_e^2 + 4\omega_k^2 E_v^2) k^4 \pi^4 (2k^2 \pi^2 \gamma^2 (1+\gamma^2)^2 + \sin^2(k\pi\gamma))^2}{2304 \gamma^4} \quad (3.44)$$

The response of the zeroth order solution is obtained by substituting the root of equations (3.29) and (3.30) into equation (3.17) as

$$v_0 = \phi_k(\xi) \frac{1}{2} \alpha_k e^{i(\Omega t - \theta_k)} + cc \quad (3.45)$$

3.2.3 The First Order Solution

Using equation (3.19), the following relation can be obtained

$$A'_k = \frac{(3E_e + 2i\omega_k E_v) m_{2k} A_k^2 \bar{A}_k + f_k e^{i\mu T_1}}{2i\omega_k m_k + ig_k} \quad (3.46)$$

Substituting equation (3.46) into (3.18) yields

$$M \frac{\partial^2 v_1}{\partial T_0^2} + G \frac{\partial v_1}{\partial T_0} + K v_1 = f_1(\xi) A_k^3 e^{3i\omega_k T_0} + f_2(\xi, T_1) e^{i\omega_k T_0} + cc \quad (3.47)$$

where

$$f_1(\xi) = M_{1k} (E_e + 2i\omega_k E_v) \quad (3.48)$$

$$f_2(\xi, T_1) = f_k(\xi) e^{i\mu T_1} + M_{2k} (3E_e + 2i\omega_k E_v) A_k^2 \bar{A}_k - \\ (2i\omega_k M \phi_k + G \phi_k) \frac{(3E_e + 2i\omega_k E_v) m_{2k} A_k^2 \bar{A}_k + f_k e^{i\mu T_1}}{2i\omega_k m_k + ig_k} \quad (3.49)$$

The solution of equation (3.47), which is the corresponding response correction of v_0 , can be obtained using separation of variables,

$$v_1(T_0, T_1) = h_1(\xi) A_k^3 e^{3i\omega_k T_0} + h_2(\xi, T_1) A_k^2 \bar{A}_k e^{i\omega_k T_0} + cc \quad (3.50)$$

where

$$h_1(\xi) = \sum_{n=\pm 1, \pm 2, \dots} \frac{\langle f_1(\xi), \phi_n(\xi) \rangle}{1 - \frac{3\omega_k}{\omega_n}} \phi_n(\xi) \quad (3.51)$$

$$h_2(\xi, T_1) = \sum_{\substack{n=\pm 1, \pm 2, \dots \\ n \neq k}} \frac{\langle f_2(\xi, T_1), \phi_n(\xi) \rangle}{1 - \frac{\omega_k}{\omega_n}} \phi_n(\xi) \quad (3.52)$$

From equations (3.50) - (3.52), it is evident that the spatial variations of the first order solutions are different from those of the linear solutions.

3.3 STABILITY ANALYSIS OF STEADY STATE SOLUTIONS

The stability of the steady state solutions is determined by the Jacobian Matrix of the system. If all of the eigenvalues of the Jacobian Matrix have negative real parts, then the steady state solution is asymptotically stable. If one or more of the eigenvalues of Jacobian have positive real parts, the steady state is unstable.

In order to analyze the stability of steady state solutions, Jacobian Matrix should be obtained first. In this section, α_{k0} and θ_{k0} are used to denote the steady state responses. Introduce small variations ε_{α_t} and ε_{θ_t} as

$$\alpha_t = \alpha_{k0} + \varepsilon_{\alpha_t} \quad (3.53)$$

$$\theta_t = \theta_{k0} + \varepsilon_{\theta_t} \quad (3.54)$$

Noting that $\alpha'_{k0} = 0$ and $\theta'_{k0} = 0$ for steady state solutions.

Substituting expressions (3.53) and (3.54) into equations (3.27) and (3.28) and linearizing the resulting equations, the following relations are obtained

$$\varepsilon'_{\alpha_t} = \frac{3E_v \omega_k m_{2k} \alpha_{k0}^2}{4k\pi} \varepsilon_{\alpha_t} + \frac{\cos \theta_{k0} \operatorname{Re}(f_k) - \sin \theta_{k0} \operatorname{Im}(f_k)}{k\pi} \varepsilon_{\theta_t} \quad (3.55)$$

$$\begin{aligned} \varepsilon'_{\theta_t} = & \left(\frac{3E_v m_{2k} \alpha_{k0}}{4k\pi} - \frac{\cos \theta_{k0} \operatorname{Re}(f_k) - \sin \theta_{k0} \operatorname{Im}(f_k)}{k\pi \alpha_{k0}^2} \right) \varepsilon_{\alpha_t} \\ & - \frac{\sin \theta_{k0} \operatorname{Re}(f_k) + \cos \theta_{k0} \operatorname{Im}(f_k)}{k\pi \alpha_{k0}} \varepsilon_{\theta_t} \end{aligned} \quad (3.56)$$

Therefore, the Jacobian Matrix \mathbf{H} can be expressed as

$$\mathbf{H} = \begin{bmatrix} \frac{3E_v\omega_k m_{2k}\alpha_{k0}^2}{4k\pi} & \frac{\cos\theta_{k0} \operatorname{Re}(f_k) - \sin\theta_{k0} \operatorname{Im}(f_k)}{k\pi} \\ \frac{3E_e\omega_k m_{2k}\alpha_{k0}}{4k\pi} - \frac{\cos\theta_{k0} \operatorname{Re}(f_k) - \sin\theta_{k0} \operatorname{Im}(f_k)}{k\pi\alpha_{k0}^2} & -\frac{\sin\theta_{k0} \operatorname{Re}(f_k) + \cos\theta_{k0} \operatorname{Im}(f_k)}{k\pi\alpha_{k0}} \end{bmatrix} \quad (3.57)$$

To avoid the complexity of evaluating θ_{k0} , it is necessary to express those terms relating to θ_{k0} in terms of α_{k0} from equations (3.55) and (3.56) by letting $\alpha'_{k0} = 0$ and $\theta'_{k0} = 0$:

$$\frac{\cos\theta_{k0} \operatorname{Im}(f_k) + \sin\theta_{k0} \operatorname{Re}(f_k)}{k\pi\alpha_{k0}} = -\frac{E_v\omega_k m_{2k}\alpha_{k0}^2}{4k\pi} \quad (3.58)$$

$$\frac{\cos\theta_{k0} \operatorname{Re}(f_k) - \sin\theta_{k0} \operatorname{Im}(f_k)}{k\pi} = -\frac{3E_e m_{2k}\alpha_{k0}^3}{8k\pi} - \mu\alpha_{k0} \quad (3.59)$$

Using equations (3.58) and (3.59), the Jacobian matrix \mathbf{H} can be simplified as

$$\mathbf{H} = \begin{bmatrix} \frac{3E_v\omega_k m_{2k}\alpha_{k0}^2}{4k\pi} & -\frac{3E_e m_{2k}\alpha_{k0}^3}{8k\pi} - \mu\alpha_{k0} \\ \frac{9E_e m_{2k}\alpha_{k0}}{8k\pi} + \frac{\mu}{\alpha_{k0}} & \frac{E_v\omega_k m_{2k}\alpha_{k0}^2}{4k\pi} \end{bmatrix} \quad (3.60)$$

The corresponding eigenvalues λ are the root of

$$\lambda^2 - \frac{E_v\omega_k m_{2k}\alpha_{k0}^2}{k\pi} \lambda + 3\left(\frac{E_v\omega_k m_{2k}\alpha_{k0}^2}{4k\pi}\right)^2 + 3\left(\frac{3E_e m_{2k}\alpha_{k0}^2}{8k\pi}\right)^2 + \frac{3E_e \mu m_{2k}\alpha_{k0}^2}{2k\pi} + \mu^2 = 0 \quad (3.61)$$

From equation (3.61), it is found that the sum of the eigenvalues is $\frac{E_v\omega_k m_{2k}\alpha_{k0}^2}{k\pi}$, which is negative because $m_{2k} < 0$. This fact eliminates the possibility of a pair of purely imaginary eigenvalues and, hence, a Hopf bifurcation. With some manipulations, the product of the eigenvalues, which is the third term in equation (3.61), can be simplified as

$$\lambda_1 \lambda_2 = -\frac{c_2}{k^2 \pi^2 \alpha_{k0}^2} \left(\alpha_{k0}^2 - \frac{-c_1 + \sqrt{c_1^2 - 3c_0 c_2}}{c_2} \right) \left(\alpha_{k0}^2 - \frac{-c_1 - \sqrt{c_1^2 - 3c_0 c_2}}{c_2} \right) \quad (3.62)$$

Considering $c_2 < 0$, from equation (3.62), it is found that the product of the eigenvalues is always minus for the intermediate real root while the product of the eigenvalues is always positive for the other two real roots. This shows that the intermediate steady state solution is unstable and the other two steady state solutions are always stable. The interval where there are two stable and one unstable steady state solutions for each value of μ is referred to an interval of bistability.

3.4 NUMERICAL RESULTS AND DISCUSSIONS

In this section, numerical results of steady response amplitudes near and at exact resonance for moving belts are presented. Effects of the transport speed, nonlinearity and the viscoelastic parameter on the steady state response are discussed.

To compare the results obtained in this study with those given by Moon and Wickert (1997). linear elastic constitutive law is first employed. Figure 3.2 shows the response amplitudes predicated by the method of multiple scales under the quasi-static assumption and those given by Moon and Wickert (1997). The non-dimensional transport speed γ ranges from 0.1 to 0.4, which includes the resonant region. Three different values of the nonlinear parameter E_ϵ are chosen to investigate the nonlinear effect. The system parameters are $e_1 = 0.00083$, $r_1 = 0.0733$. It is clear that the results obtained in this study are identical to those given by Moon and Wickert (1997). This shows the validation of the proposed method. It can be seen that the effect of the moving

speed on the response amplitude is significant. This is because both the linear natural frequencies of the system and the excitation frequencies depend on the moving speed. For moving speeds below a critical speed, the response amplitude is single valued; for moving speed above that critical speed, the response amplitude has three values corresponding to the same transport speed γ . Thus, the system shows a typical multi-valued nonlinear phenomenon. When the excitation frequencies determined by the moving speed is near or at exact natural frequencies, the response amplitude becomes very large. In addition, it is observed that the bending of the curves is responsible for the jump phenomenon. The maximum amplitude is attainable only when approached from a lower moving speed. In the multi-valued response, the intermediate response is unstable and hence, cannot be produced both numerically and experimentally. However, the other two amplitudes are stable. Note that E_ϵ is a measure of nonlinearity. The higher the value of E_ϵ is, the stronger the nonlinearity of the system is. It can be seen that E_ϵ has a significant effect on the steady response amplitude of the system. With the increase of E_ϵ , response amplitudes under the same transport speed decreases.

The response amplitudes obtained using the method of multiple scales under the quasi-static assumption are compared with those without this assumption in Figure 3.3. The same system parameters as those in Figure 3.2 are adopted. It is clear that the results without the quasi-static assumption and those with such an assumption are close to each other over the non-resonance region. The difference, however, grows within the resonant region. This shows that the quasi-static assumption is accurate at most time span. However, since the near- and exact-resonant response is very larger, the differences between the results with the quasi-static assumption and those without quasi-static become significant.

Effects of the viscoelastic parameter E_v on the response amplitude are illustrated in Figure 3.4 to Figure 3.6. The non-dimensional radius r_1 and eccentricity of pulley e_1 are 0.00083 and 0.0733. In Figure 3.4, $E_e=400$. Three different values of E_v are chosen as 0.1, 25, 50, respectively. From Figure 3.4, it is evident that the damping introduced by the viscoelastic model reduces the amplitude of response, especially at near- and exact-resonant region. The amplitude of the response decreases as the damping increases. The maximum amplitude reduction for $E_v = 25$ is 40.3% while for $E_v = 50$, the maximum amplitude reduction is 55.6%. The degree of vibration reduction also depends on the nonlinear parameter E_e . Figure 3.5 and Figure 3.6 show the response amplitudes corresponding to higher values of E_e , i.e., $E_e=800$ and $E_e=1000$, respectively. It is seen that under the same E_v , the amplitude increases as E_e increases. Therefore, the degree of vibration reduction depends on the ratio E_v / E_e . When the ratio E_v / E_e is very small, the influence of viscoelasticity on vibration reduction is not significant.

3.5 SUMMARY AND CONCLUSIONS

The amplitude of near- and exact-resonant response is predicted for forced vibrations of viscoelastic moving belts excited by the eccentricity of pulleys. Based on the linear viscoelastic differential constitutive law, the generalized equations of motion are derived for a viscoelastic moving belt with geometric nonlinearities. The method of multiple scales is applied directly to the governing equations, which are in the form of continuous non-autonomous gyroscopic systems. From the above study, the following conclusions can be drawn:

- 1) The moving speed of belts has a significant effect on the steady state response since both the

linear natural frequencies and the excitation frequencies depend on the moving speed. For moving speeds below a critical speed, the response amplitude is single valued; for moving speed above that critical speed, the response amplitude has three values corresponding to the same transport speed.

- 2) Viscoelastic model can be used to accurately describe the damping mechanism of belt materials. The damping introduced by the viscoelastic model determines the vibration reduction. Therefore, it is possible to predict a desirable damping value that can significantly reduce the transverse vibration of moving belts.
- 3) The method of multiple scales is applied directly to the governing equations. No assumptions regarding the spatial dependence of the motion are made while commonly used perturbation approach assumes that the motion of the nonlinear system has the same spatial dependence as the linear system. Discrepancy between the direct approach proposed in this study and the discretization approach commonly used exists at the first order approximation.

It should be mentioned that viscoelastic property not only reduces the vibration, but also shifts stability boundaries significantly in the parametric vibration of moving belts, which will be shown in Chapter 4 and Chapter 5. Furthermore, viscoelastic model can also be used to predict the belt creep which leads to the excessive slip of the belt drive system. More work needs to be done to get deep insight on the effects of the viscoelastic property of belts.

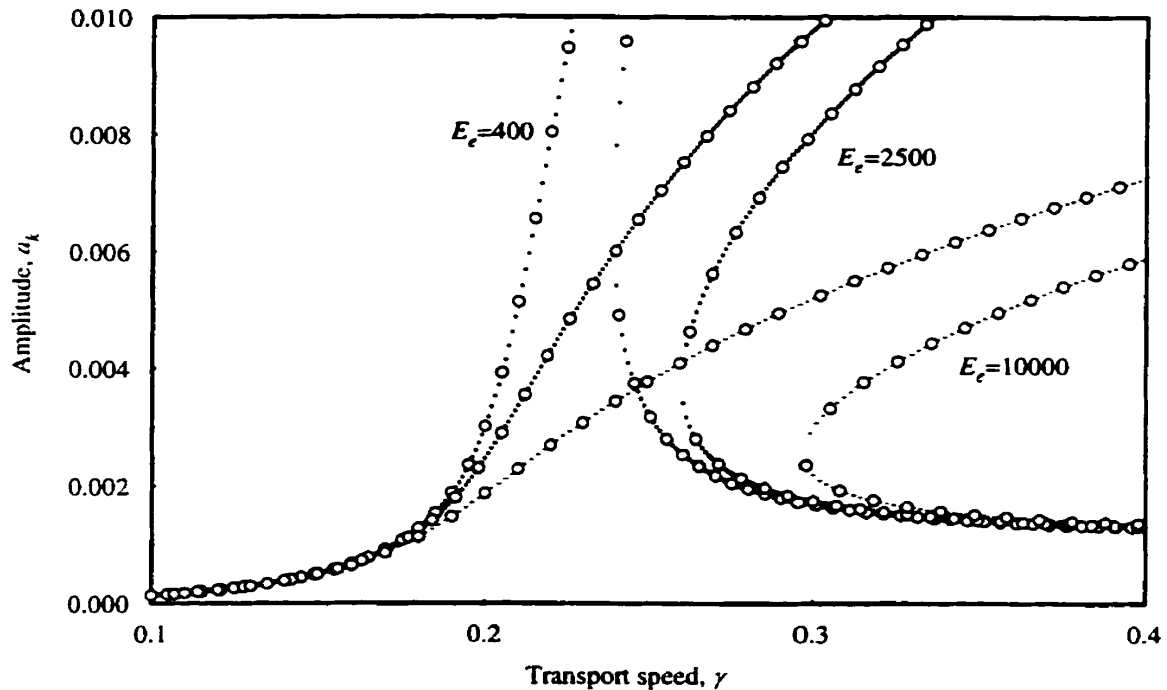


Figure 3.2: Comparison of response amplitudes predicated by the method of multiple scales and those given by Moon and Wickert (1997)

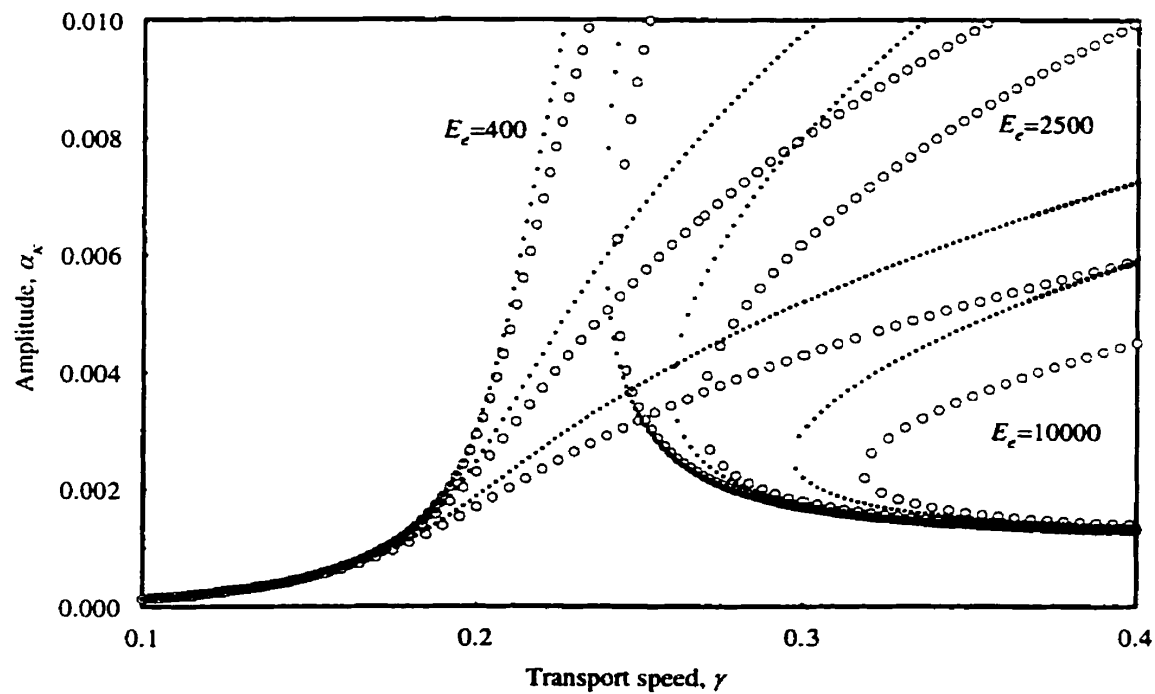


Figure 3.3: Comparison of response amplitudes without the quasi-static assumption and those with the quasi-static assumption

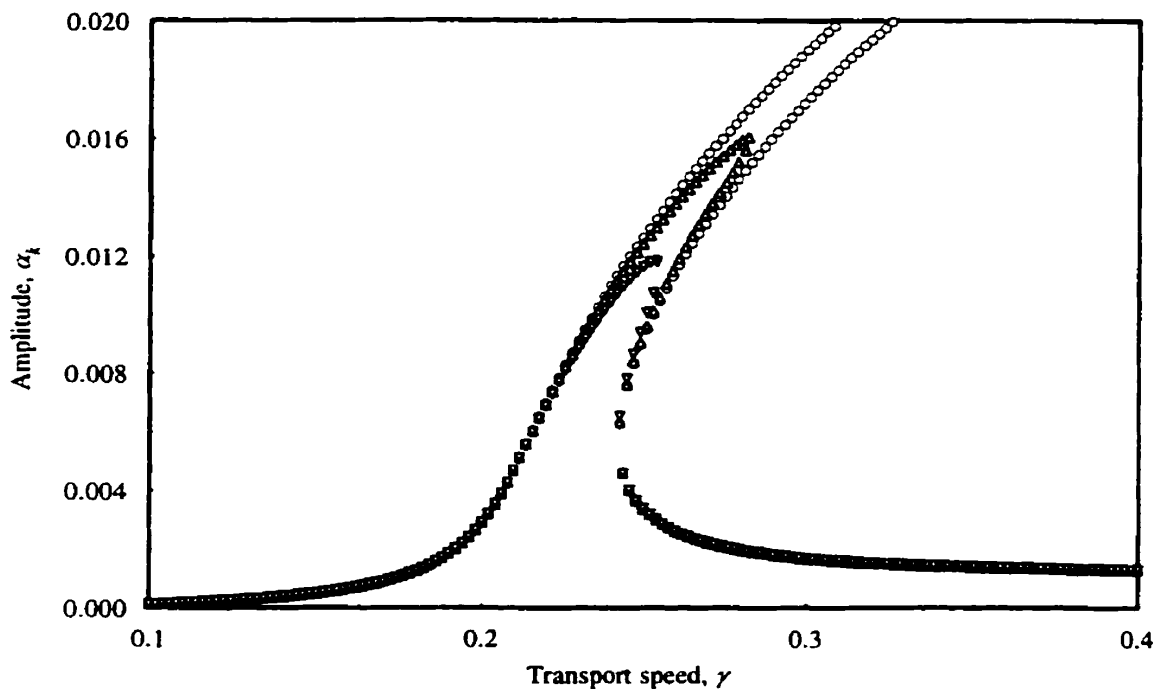


Figure 3.4: Comparison of responses for different E_v ($E_e=400$)

○: $E_v=0.1$ Δ: $E_v=25$ ▽: $E_v=50$

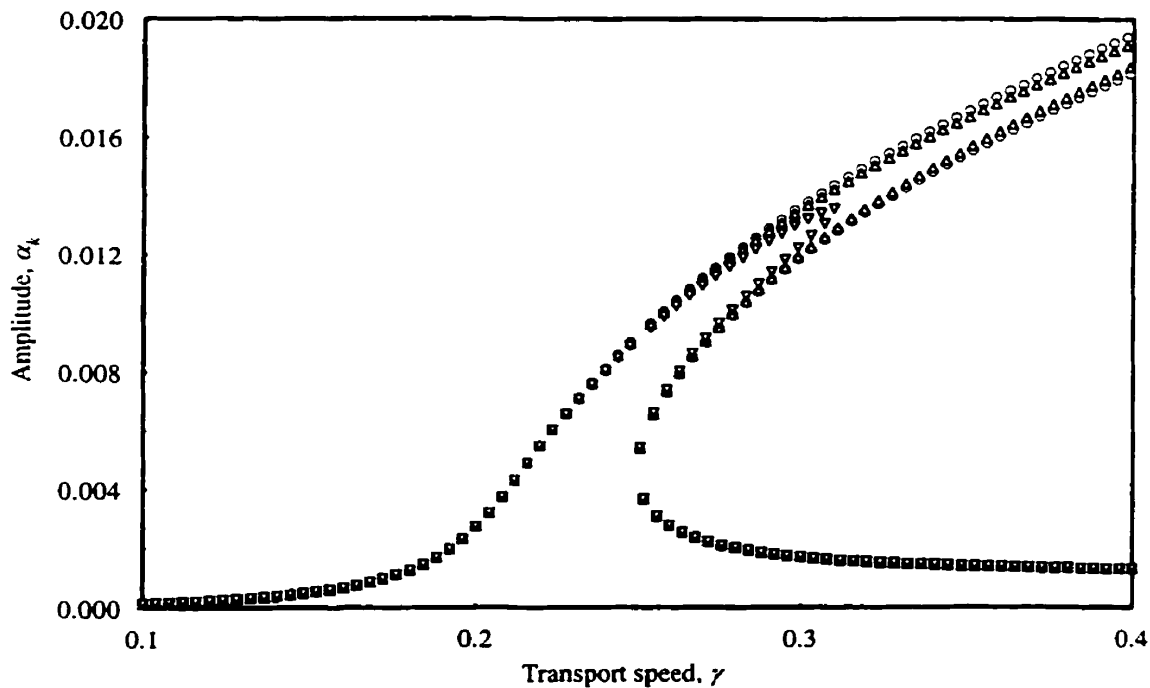


Figure 3.5: Comparison of responses for different E_v ($E_e=800$)

○: $E_v=0.1$ Δ: $E_v=25$ ▽: $E_v=50$

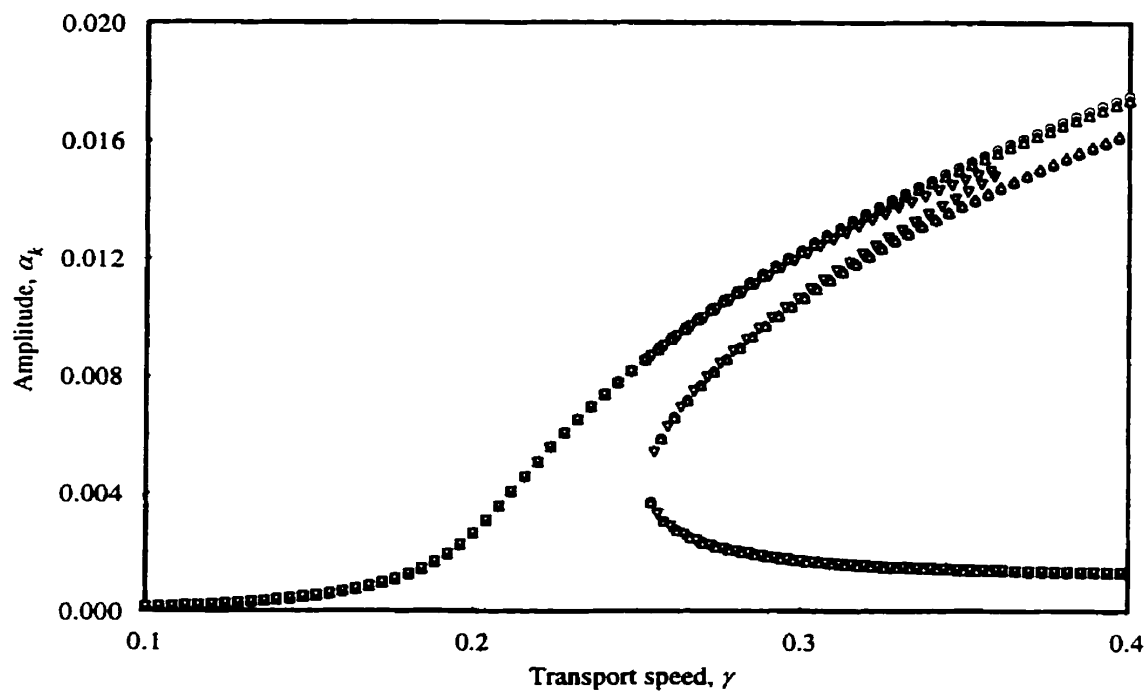


Figure 3.6: Comparison of responses for different E_v ($E_c=1000$)

○: $E_v=0.1$ Δ: $E_v=25$ ▽: $E_v=50$

CHAPTER 4

DYNAMIC RESPONSE OF PARAMETRICALLY EXCITED VISCOELASTIC MOVING BELTS

In Chapter 2 and Chapter 3, the free and forced vibrations of viscoelastic moving belts are studied where a prior assumption in modelling prototypical systems is that the initial tension is constant. However, one major problem in belt drive systems is that crankshaft-driven belt tension actually fluctuates, which leads to the occurrence of large transverse belt vibrations. Such a system with fluctuation tension as a source of excitation is called a parametrically excited moving belt system. With reliability, wear, and noise of utmost concern, it is of great interest to recognize and understand this important source of dynamic response.

The dynamic response and stability of parametrically excited viscoelastic belts are investigated in the current and the next chapters. In this chapter, the generalized equation of motion is obtained for a viscoelastic moving belt with geometric nonlinearity. Approximate solutions are obtained by two different approaches. In the first approach, the method of multiple scales is applied directly to the governing equation, which is in the form of continuous gyroscopic systems with weakly nonlinearity. In the second approach, the equation of motion is first discretized by using translating string eigenfunctions as a basis for a Galerkin discretization, and then the method of multiple scales is applied to the resulting discretized gyroscopic equation. It is demonstrated that the results given by the two approaches are identical for the zeroth order

approximation. There are discrepancies between solutions at the higher level of approximation. Closed-form solutions for the amplitude and the existence conditions of non-trivial limit cycles of the summation resonance are obtained. It is shown that there exists an upper boundary for the existence condition of the summation parametric resonance due to the existence of viscoelasticity. Effects of viscoelastic parameters, excitation frequencies, excitation amplitudes, and the axial moving speed on dynamic responses and existence boundaries are investigated.

4.1 EQUATION OF MOTION

The prototypical model of a viscoelastic moving belt used in this chapter is the same as that in Chapter 2. Consider that the viscoelastic string is in a state of uniform initial stress, and only the transverse vibration in the y direction is taken into consideration. The Lagrangian strain component in the x direction related to the transverse displacement is $\varepsilon(x,t) = V_x^2(x,t)/2$. Thus, the equation of motion in the y direction can be obtained by rearranging equation (3.3)

$$\rho \frac{\partial^2 V}{\partial t^2} + 2\rho c \frac{\partial^2 V}{\partial t \partial x} + \left(\rho c^2 - \frac{T}{A} \right) \frac{\partial^2 V}{\partial x^2} = E^* \left(\frac{1}{2} V_x^2 \right) V_{xx} + V_x \left\{ E^* \left(\frac{1}{2} V_x^2 \right) \right\}_x \quad (4.1)$$

with boundary conditions

$$V(0,t) = 0 \quad V(L,t) = 0 \quad (4.2)$$

where the subscript notation x denotes partial differentiation with respect to the spatial Cartesian coordinate x , A is the area of cross-section of the string, ρ is the mass per unit volume, T is the tension in the belt, and E^* is the equivalent Young's modulus determined by the viscoelastic property of belt materials.

It is assumed that the tension T is characterized as a small periodic perturbation $T_1 \cos \Omega t$ on the steady state tension T_0 , i.e.

$$T = T_0 + T_1 \cos \Omega t \quad (4.3)$$

where Ω is the frequency of excitation. These belt tension variations arise from the loading of the pulley by the belt-drive accessories (e.g., air conditioning compressor). They may also arise from pulley eccentricities. The rotational modes may also induce tension variations, which will be shown in Chapter 10.

The Kelvin viscoelastic model is chosen to describe the viscoelastic property of the belt material. The linear differential operator E^* for the Kelvin viscoelastic model is given below

$$E^* = E_0 + \eta \frac{\partial}{\partial t} \quad (4.4)$$

where E_0 is the stiffness constant of the spring and η is the dynamic viscosity of the dashpot.

Introducing the following non-dimensional parameters

$$\begin{aligned} v &= \frac{x}{L} & \xi &= \frac{x}{L} & \tau &= t \sqrt{\frac{T_0}{\rho A L^2}} & \gamma &= c \sqrt{\frac{\rho A}{T_0}} \\ a &= \frac{T_1}{T_0} & \omega &= \Omega \sqrt{\frac{\rho A L^2}{T_0}} & E_e &= \frac{E_0 A}{T_0} & E_v &= \eta \sqrt{\frac{A}{\rho T_0 L^2}} \end{aligned} \quad (4.5)$$

the corresponding non-dimensional equation of the transverse motion is given by

$$\frac{\partial^2 v}{\partial \tau^2} + 2\gamma \frac{\partial^2 v}{\partial \tau \partial \xi} + (\gamma^2 - 1 - a \cos \omega \tau) \frac{\partial^2 v}{\partial \xi^2} = N(v) \quad (4.6)$$

where the nonlinear operator $N(v)$ is defined in Chapter 2.

Introduce the mass, gyroscopic, and linear stiffness operators as follows

$$M = I, \quad G = 2\gamma \frac{\partial}{\partial \xi}, \quad K = (\gamma^2 - 1) \frac{\partial^2}{\partial \xi^2} \quad (4.7)$$

where operators M and K are symmetric and positive definite and G is skew-symmetric for sub-critical transport speeds. Employing a small dimensionless parameter ϵ as a bookkeeping device, equation (4.6) can be rewritten in a standard symbolic form

$$Mv_{\pi} + Gv_{\tau} + Kv = \epsilon N(v) + \epsilon a \cos \omega \tau \frac{\partial^2 v}{\partial \xi^2} \quad (4.8)$$

Equation (4.8) is in the form of a continuous gyroscopic system with weakly nonlinearity and parameter excitation term. The direct multiple scales method and the discretization multiple scales method will be employed to solve equation (4.8) in the following.

4.2 DIRECT MULTIPLE SCALES METHOD

In this section, the method of multiple scales is applied directly to the governing partial differential equation, which is in the form of a continuous gyroscopic system. No assumptions regarding the spatial dependence of the motion are made. A first order uniform approximation is sought in the form

$$v(\xi, \tau, \epsilon) = v_0(\xi, T_0, T_1) + \epsilon v_1(\xi, T_0, T_1) + \dots \quad (4.9)$$

where $T_0 = \tau$ is a fast scale characterizing motions occurring at one of the natural frequencies ω_k of the system or ω ; $T_1 = \epsilon \tau$ is a slow scale characterizing the modulation of the amplitudes and phases due to the nonlinearity, viscoelasticity and possible resonance.

Substituting equation (4.9) into (4.8), using the chain rule of time derivatives and equating coefficients of like powers of ϵ give

$$M \frac{\partial^2 v_0}{\partial T_0^2} + G \frac{\partial v_0}{\partial T_0} + Kv_0 = 0 \quad (4.10)$$

$$M \frac{\partial^2 v_1}{\partial T_0^2} + G \frac{\partial v_1}{\partial T_0} + Kv_1 = -2M \frac{\partial^2 v_0}{\partial T_0 \partial T_1} - G \frac{\partial v_0}{\partial T_1} + N(v_0) + a \cos \omega T_0 \frac{\partial^2 v_0}{\partial \xi^2} \quad (4.11)$$

When the perturbation frequency ω approaches the sum of any two natural frequencies of the system, summation parametric resonance can occur. As a special case of the summation parametric resonance, the principal parametric resonance will also be presented when ω approaches $2\omega_i$. A detuning parameter μ is introduced to quantify the deviation of ω from $\omega_n + \omega_l$, and is described by

$$\omega = \omega_n + \omega_l + \epsilon \mu \quad (4.12)$$

in which, ω_n and ω_l are the n th and l th natural frequencies of the corresponding linear system.

To investigate the summation parametric response and stability, solution of equation (4.10) can be expressed as

$$v_0 = \phi_n(\xi) A_n(T_1) e^{i\omega_n T_0} + \phi_l(\xi) A_l(T_1) e^{i\omega_l T_0} + cc \quad (4.13)$$

where $\phi_n(\xi)$ and $\phi_l(\xi)$ are the n th and l th complex eigenfunction of the displacement field, and cc denotes the complex conjugate of all preceding terms on the right side of equation (4.13). Functions A_n and A_l will be determined by eliminating the secular terms from v_1 .

Substituting equations (4.12) and (4.13) into (4.11) and expressing the trigonometric functions in exponential form result in

$$M \frac{\partial^2 v_1}{\partial T_0^2} + G \frac{\partial v_1}{\partial T_0} + K v_1 = NST +$$

$$\left[-2i\omega_n A'_n M \phi_n - A'_n G \phi_n + \frac{a\bar{A}_l}{2} \frac{\partial^2 \bar{\phi}_l}{\partial \xi^2} e^{i\mu T_1} + M_{2n} (3E_e + 2i\omega_n E_v) A_n^2 \bar{A}_n \right] e^{i\omega_n T_0} \quad (4.14)$$

$$\left[-2i\phi_l A'_l M \phi_l - A'_l G \phi_l + \frac{a\bar{A}_n}{2} \frac{\partial^2 \bar{\phi}_n}{\partial \xi^2} e^{i\mu T_1} + M_{2l} (3E_e + 2i\omega_l E_v) A_l^2 \bar{A}_l \right] e^{i\omega_l T_0} + cc$$

where

$$M_{2k} = \frac{1}{2} \left[\left(\frac{\partial \phi_k}{\partial \xi} \right)^2 \frac{\partial^2 \bar{\phi}_k}{\partial \xi^2} + 2 \frac{\partial \phi_k}{\partial \xi} \frac{\partial \bar{\phi}_k}{\partial \xi} \frac{\partial^2 \phi_k}{\partial \xi^2} \right] \quad \text{for } k = n, l \quad (4.15)$$

NST in equation (4.14) represents all the non-secular terms and overbar denotes complex conjugate. Due to the nonlinearity and viscoelasticity, *NST* involves some complicated spatial distribution functions. Thus, the spatial variations of the first order solution v_1 is different from that of linear solution v_0 .

Equation (4.14) has a solution only if a solvability condition is satisfied. For cases where internal resonance does not exist, the solvability condition can be determined as

$$-2i\omega_n A'_n m_n - A'_n g_n i + (3E_e + 2i\omega_n E_v) A_n^2 \bar{A}_n m_{2n} + \frac{a\bar{A}_l}{2} m_{ln} e^{i\mu T_1} = 0 \quad (4.16)$$

$$-2i\omega_l A'_l m_l - A'_l g_l i + (3E_e + 2i\omega_l E_v) A_l^2 \bar{A}_l m_{2l} + \frac{a\bar{A}_n}{2} m_{nl} e^{i\mu T_1} = 0 \quad (4.17)$$

in which

$$m_{nl} = \left\langle \frac{\partial^2 \bar{\phi}_n}{\partial \xi^2}, \phi_l \right\rangle \quad (4.18)$$

$$m_{ln} = \left\langle \frac{\partial^2 \bar{\phi}_l}{\partial \xi^2}, \phi_n \right\rangle \quad (4.19)$$

Referring to Wickert and Mote (1990), the k th natural frequency and eigenfunction normalized for $m_k = 1$ of linear moving belts are $\omega_k = k\pi(1 - \gamma^2)$ and $\phi_k = \sqrt{2} \sin(k\pi\xi) e^{(ik\pi\xi)}$, respectively.

Substituting these eigenvalues and eigenfunctions into equations (4.18) and (4.19) leads to

$$m_{nl} = m_{ln} = \frac{4\pi n^2 l^2 v [-\sin(n+l)\pi v + i(1-\cos(n+l)\pi v)]}{(n+l)[(n+l)^2 v^2 - (n-l)^2]} \quad (4.20)$$

4.3 DISCRETIZATION MULTIPLE SCALES METHOD

In this section, the governing partial differential equation is discretized first using Galerkin procedure. By assuming the translating eigenfunctions of the linear problem to be the spatial solutions at all levels of approximation, the governing equation is reduced to an ordinary differential equation in time. Then the method of multiple scales is applied to the resulting ordinary differential equation.

4.3.1 Galerkin Discretization

The nonlinear differential equation (4.8) can be cast in the canonical form

$$\mathbf{A}\dot{\mathbf{w}} + \mathbf{B}\mathbf{w} = \begin{bmatrix} \varepsilon N(v) \\ 0 \end{bmatrix} + \begin{bmatrix} \varepsilon a \cos \omega t \frac{\partial^2 v}{\partial \xi^2} \\ 0 \end{bmatrix} \quad (4.21)$$

where

$$\mathbf{w} = \begin{bmatrix} \dot{v} \\ v \end{bmatrix} \quad \mathbf{A} = \begin{bmatrix} M & 0 \\ 0 & K \end{bmatrix} \quad \mathbf{B} = \begin{bmatrix} G & K \\ -K & 0 \end{bmatrix} \quad (4.22)$$

The corresponding translating complex eigenfunctions ψ_t have the structure

$$\Psi_k = \Psi_k^R + i\Psi_k^I \quad \Psi_k^R = \begin{Bmatrix} -\omega_k \phi_k' \\ \phi_k^R \end{Bmatrix} \quad \Psi_k^I = \begin{Bmatrix} -\omega_k \phi_k^R \\ \phi_k' \end{Bmatrix} \quad (4.23)$$

It has been shown that the translating complex eigenfunction is a superior basis for the solution of linear response problems under free and externally excited conditions. Presently, the translating eigenfunctions will be used in a Galerkin discretization of nonlinear parametrically excited response problems.

Consider the expansion

$$\mathbf{w} = \zeta_n^R \Psi_n^R + \zeta_n^I \Psi_n^I + \zeta_l^R \Psi_l^R + \zeta_l^I \Psi_l^I \quad (4.24)$$

as the solution of equation (4.21). ζ_k^R and ζ_k^I ($k = n, l$) are the real and imaginary components of the generalized coordinates. Substituting equation (4.24) into the governing equation (4.21) and using the orthogonality conditions from equation (2.31) yield the following equations of modal coordinates

$$\dot{\zeta}_n^R - \omega_n \zeta_n^I = -\frac{\int_0^1 \phi_n' N(v) d\xi}{n\pi} - \frac{\int_0^1 \phi_n' \frac{\partial^2 v}{\partial \xi^2} d\xi}{n\pi} a \cos \omega t \quad (4.25)$$

$$\dot{\zeta}_n^I + \omega_n \zeta_n^R = \frac{\int_0^1 \phi_n^R N(v) d\xi}{n\pi} + \frac{\int_0^1 \phi_n^R \frac{\partial^2 v}{\partial \xi^2} d\xi}{n\pi} a \cos \omega t \quad (4.26)$$

$$\dot{\zeta}_l^R - \omega_l \zeta_l^I = -\frac{\int_0^1 \phi_l' N(v) d\xi}{l\pi} - \frac{\int_0^1 \phi_l' \frac{\partial^2 v}{\partial \xi^2} d\xi}{l\pi} a \cos \omega t \quad (4.27)$$

$$\dot{\zeta}_l^I + \omega_l \zeta_l^R = \frac{\int_0^1 \phi_l^R N(v) d\xi}{l\pi} + \frac{\int_0^1 \phi_l^R \frac{\partial^2 v}{\partial \xi^2} d\xi}{l\pi} a \cos \omega t \quad (4.28)$$

4.3.2 Multiple Scales Method

After the partial differential equation is reduced to the ordinary differential equations, the method of multiple scales can be applied to the resulting equations (4.25) to (4.28). ζ_k^R and ζ_k^I are assumed to be of the form

$$\zeta_k^R = \zeta_{k0}^R(T_0, T_1) + \varepsilon \zeta_{k1}^R(T_0, T_1) + \dots \quad (4.29)$$

$$\zeta_k^I = \zeta_{k0}^I(T_0, T_1) + \varepsilon \zeta_{k1}^I(T_0, T_1) + \dots \quad (4.30)$$

for $k = n, l$

Upon substitution of equations (4.29) and (4.30) into (4.25) - (4.28), gathering coefficients of like powers of ε yields the following equations:

Order 0 (ε^0),

$$\frac{\partial \zeta_{k0}^R}{\partial T_0} - \omega_k \zeta_{k0}^I = 0 \quad (4.31)$$

$$\frac{\partial \zeta_{k0}^I}{\partial T_0} + \omega_k \zeta_{k0}^R = 0 \quad (4.32)$$

for $k = n, l$

Order 1 (ε^1),

$$\frac{\partial \zeta_{k1}^R}{\partial T_0} - \omega_k \zeta_{k1}^I = -\frac{\int_0^l \phi_k^I N(v_0) d\xi}{k\pi} - \frac{\int_0^l \phi_k^I \frac{\partial^2 v_0}{\partial \xi^2} d\xi}{k\pi} \alpha \cos \omega T_0 - \frac{\partial \zeta_{k0}^R}{\partial T_1} \quad (4.33)$$

$$\frac{\partial \zeta_{k1}^I}{\partial T_0} + \omega_k \zeta_{k1}^R = \frac{\int_0^l \phi_k^R N(v_0) d\xi}{k\pi} + \frac{\int_0^l \phi_k^R \frac{\partial^2 v_0}{\partial \xi^2} d\xi}{k\pi} \alpha \cos \omega T_0 - \frac{\partial \zeta_{k0}^I}{\partial T_1} \quad (4.34)$$

for $k = n, l$

where

$$\nu_0 = \zeta_{n0}^R \phi_n^R + \zeta_{n0}' \phi_n' + \zeta_{l0}^R \phi_l^R + \zeta_{l0}' \phi_l' \quad (4.35)$$

Solving equation (4.31) and (4.32) yields a pair of general solutions, given by

$$\zeta_{k0}^R = A_k(T_1) e^{i\omega_k T_0} + \bar{A}_k(T_1) e^{-i\omega_k T_0} \quad (4.36)$$

$$\zeta_{k0}' = iA_k(T_1) e^{i\omega_k T_0} - i\bar{A}_k(T_1) e^{-i\omega_k T_0} \quad (4.37)$$

for $k = n, l$

Each of the above solutions comprises two terms, in which the second term is the complex conjugate of the first. Coefficients A_k and \bar{A}_k are functions of T_1 and will be determined by eliminating secular terms from ζ_{k1}^R and ζ_{k1}' . Substituting equations (4.36) and (4.37) into (4.35) results in

$$\nu_0 = \phi_n(\xi) A_n(T_1) e^{i\omega_n T_0} + \phi_l(\xi) A_l(T_1) e^{i\omega_l T_0} + cc \quad (4.38)$$

It can be seen that the spatial distribution of the zeroth order solution used in discretization approach is the same as that of the zeroth order solution used in the direct approach.

4.3.3 Solvability Condition

Attention will be focused on the summation parametric resonance in which a detuning parameter is defined through equation (4.12). Substituting equations (4.12), (4.36), and (4.37) into (4.33) and (4.34) with the trigonometric functions re-expressed in exponential form results in the occurrence of the undesirable secular term $e^{i\omega_k T_0}$ or $e^{i\omega_l T_0}$. To determine the solvability conditions, particular solutions, which are free of secular terms, are sought in the form

$$\zeta_{k1}^R = \rho_{k1}(T_1) e^{i\omega_k T_0} \quad (4.39)$$

$$\zeta'_{k1} = \rho_{k2}(T_1) e^{i\omega_k T_0} \quad (4.40)$$

Substitution of equation (4.39) and (4.40) into equations (4.33) and (4.34), and equating the coefficient of $e^{i\omega_k T_0}$ to zero ($k=n$), the following pair of equations with a singular coefficient matrix is obtained:

$$i\omega_n \rho_{n1} - \omega_n \rho_{n2} = -A'_n - \frac{ae^{i\mu T_1} \bar{A}_l}{2n\pi} \left(\int_0^1 \phi_n' \frac{\partial^2 \phi_l^R}{\partial \xi^2} d\xi - i \int_0^1 \phi_n' \frac{\partial^2 \phi_l'}{\partial \xi^2} d\xi \right) \\ - \frac{1}{n\pi} \int_0^1 \phi_n' M_{2n} d\xi (3E_e + 2i\omega_n E_v) A_n^2 \bar{A}_n \quad (4.41)$$

$$\omega_n \rho_{n1} + i\omega_n \rho_{n2} = -iA'_n + \frac{ae^{i\mu T_1} \bar{A}_l}{2n\pi} \left(\int_0^1 \phi_n^R \frac{\partial^2 \phi_l^R}{\partial \xi^2} d\xi - i \int_0^1 \phi_n^R \frac{\partial^2 \phi_l'}{\partial \xi^2} d\xi \right) \\ + \frac{1}{n\pi} \int_0^1 \phi_n^R M_{2n} d\xi (3E_e + 2i\omega_n E_v) A_n^2 \bar{A}_n \quad (4.42)$$

Since the homogeneous equations of (4.41) and (4.42) have a non-trivial solution, the inhomogeneous equation of ρ_{n1} and ρ_{n2} will only exist if and only if the following solvability condition is satisfied

$$\begin{vmatrix} -A'_n - \frac{ae^{i\mu T_1} \bar{A}_l}{2n\pi} \left(\int_0^1 \phi_n' \frac{\partial^2 \phi_l^R}{\partial \xi^2} d\xi - i \int_0^1 \phi_n' \frac{\partial^2 \phi_l'}{\partial \xi^2} d\xi \right) \\ i\omega_n - \frac{1}{n\pi} \int_0^1 \phi_n' M_{2n} d\xi (3E_e + 2i\omega_n E_v) A_n^2 \bar{A}_n \\ \omega_n - iA'_n + \frac{ae^{i\mu T_1} \bar{A}_l}{2n\pi} \left(\int_0^1 \phi_n^R \frac{\partial^2 \phi_l^R}{\partial \xi^2} d\xi - i \int_0^1 \phi_n^R \frac{\partial^2 \phi_l'}{\partial \xi^2} d\xi \right) \\ + \frac{1}{n\pi} \int_0^1 \phi_n^R M_{2n} d\xi (3E_e + 2i\omega_n E_v) A_n^2 \bar{A}_n \end{vmatrix} = 0 \quad (4.43)$$

This solvability condition can be simplified as

$$2in\pi A'_n - m_{2n} (3E_e + 2i\omega_n E_v) A_n^2 \bar{A}_n - \frac{ae^{i\mu T_1} \bar{A}_l}{2} \int_0^1 \left(\frac{\partial^2 \phi_l^R}{\partial \xi^2} - i \frac{\partial^2 \phi_l'}{\partial \xi^2} \right) (\phi_n^R - i\phi_n') d\xi = 0 \quad (4.44)$$

Using the following relation

$$m_n = \int_0^1 \frac{\partial^2 \bar{\phi}_l}{\partial \xi^2} \bar{\phi}_n d\xi = \int_0^1 \left(\frac{\partial^2 \phi_l^R}{\partial \xi^2} - i \frac{\partial^2 \phi_l'}{\partial \xi^2} \right) (\phi_n^R - i \phi_n') d\xi \quad (4.45)$$

Equation (4.44) can be simplified further as

$$-2i\omega_n A'_n m_n - A'_n g_n i + (3E_e + 2i\omega_n E_v) A_n^2 \bar{A}_n m_{2n} + \frac{a\bar{A}_l}{2} m_{ln} e^{i\mu T_1} = 0 \quad (4.46)$$

Note that the above equation is the same as equation (4.16).

Similarly, when $k=l$, equating the coefficient of $e^{i\omega_l T_0}$ to zero yields

$$\begin{aligned} i\omega_l \rho_{ll} - \omega_l \rho_{l2} &= -A'_l - \frac{ae^{i\mu T_1} \bar{A}_n}{2l\pi} \left(\int_0^1 \phi_l' \frac{\partial^2 \phi_n^R}{\partial \xi^2} d\xi - i \int_0^1 \phi_l' \frac{\partial^2 \phi_n'}{\partial \xi^2} d\xi \right) \\ &\quad - \frac{1}{l\pi} \int_0^1 \phi_l' M_{2l} d\xi (3E_e + 2i\omega_l E_v) A_l^2 \bar{A}_l \end{aligned} \quad (4.47)$$

$$\begin{aligned} \omega_l \rho_{ll} + i\omega_l \rho_{l2} &= -iA'_l + \frac{ae^{i\mu T_1} \bar{A}_n}{2l\pi} \left(\int_0^1 \phi_l^R \frac{\partial^2 \phi_n^R}{\partial \xi^2} d\xi - i \int_0^1 \phi_l^R \frac{\partial^2 \phi_n'}{\partial \xi^2} d\xi \right) \\ &\quad + \frac{1}{l\pi} \int_0^1 \phi_l^R M_{2l} d\xi (3E_e + 2i\omega_l E_v) A_l^2 \bar{A}_l \end{aligned} \quad (4.48)$$

The solutions for ρ_{ll} and ρ_{l2} will exist if and only if the following solvability condition is satisfied

$$\begin{vmatrix} -A'_l - \frac{ae^{i\mu T_1} \bar{A}_n}{2l\pi} \left(\int_0^1 \phi_l' \frac{\partial^2 \phi_n^R}{\partial \xi^2} d\xi - i \int_0^1 \phi_l' \frac{\partial^2 \phi_n'}{\partial \xi^2} d\xi \right) \\ - \frac{1}{l\pi} \int_0^1 \phi_l' M_{2l} d\xi (3E_e + 2i\omega_l E_v) A_l^2 \bar{A}_l \\ -iA'_l + \frac{ae^{i\mu T_1} \bar{A}_n}{2l\pi} \left(\int_0^1 \phi_l^R \frac{\partial^2 \phi_n^R}{\partial \xi^2} d\xi - i \int_0^1 \phi_l^R \frac{\partial^2 \phi_n'}{\partial \xi^2} d\xi \right) \\ + \frac{1}{l\pi} \int_0^1 \phi_l^R M_{2l} d\xi (3E_e + 2i\omega_l E_v) A_l^2 \bar{A}_l \end{vmatrix} = 0 \quad (4.49)$$

With some algebraic manipulations, the solvability condition (4.49) can be rewritten as

$$-2i\omega_l A'_l m_l - A'_l g_l i + (3E_\epsilon + 2i\omega_l E_v) A_l^2 \bar{A}_l m_{2l} + \frac{a\bar{A}_n}{2} m_{nl} e^{i\mu T_1} = 0 \quad (4.50)$$

Note that the above equation is also the same as equation (4.17).

The modulation equations (4.46) and (450) obtained in this section are in full agreement with those obtained using the direct multiple scales approach. This is because the equation of motion for moving belts only involves the cubic nonlinearities. In this case, the modulation equations are determined only by the spatial variations of the zeroth order solutions, which are identical for both approaches. This is valid only when the first order approximation is sought. It should be mentioned that though the zeroth order solutions for both approaches are the same, the first order solutions from the two approaches are different.

If the second order approximation is sought, where the expansion for the displacement is in the form

$$v = v_0(\xi, T_0, T_1, T_2) + \epsilon v_1(\xi, T_0, T_1, T_2) + \epsilon^2 v_2(\xi, T_0, T_1, T_2) + \dots \quad (4.51)$$

the modulation equations governing the zeroth order amplitude and phase of the motion will be determined by the first order and second order equations. The spatial distributions of both the zeroth order and the first order solutions have influence on the modulation equations. Since the spatial distributions of the first order solution for the two approaches are different, discrepancy exists between the modulation equations obtained from the two approaches. Therefore, even the zeroth order solutions of the two approaches are different.

4.4 LIMIT CYCLES AND EXISTENCE CONDITIONS

For nonlinear systems, limit cycles may exist in the vicinity of a parametric instability region. In this section, the interest is focused on the behavior of limit cycles around the parametric instability regions for elastic and viscoelastic nonlinear systems.

4.4.1 Equations of Response Amplitudes and Phases

To solve the nonlinear equations (4.16) and (4.17), express A_n and A_l in polar form

$$A_n = \frac{1}{2} \alpha_n e^{i\beta_n} \quad (4.52)$$

$$A_l = \frac{1}{2} \alpha_l e^{i\beta_l} \quad (4.53)$$

Note that α_k and β_k ($k = n, l$) represent the amplitude and the phase angle of the response, respectively.

Substituting equations (4.52) and (4.53) into (4.16) and (4.17) and separating the resulting equation into real and imaginary parts yield

$$\begin{aligned} & \frac{1}{2} \alpha_n \beta'_n (2\omega_n m_n + g_n) + \frac{\alpha_n^3}{8} (3E_e \operatorname{Re}(m_{2n}) - 2\omega_n E_v \operatorname{Im}(m_{2n})) + \\ & \frac{a\alpha_l}{4} [\cos(\mu T_l - \beta_n - \beta_l) \operatorname{Re}(m_{nl}) - \sin(\mu T_l - \beta_n - \beta_l) \operatorname{Im}(m_{nl})] = 0 \end{aligned} \quad (4.54)$$

$$\begin{aligned} & -\frac{1}{2} \alpha'_n (2\omega_n m_n + g_n) + \frac{\alpha_n^3}{8} (3E_e \operatorname{Im}(m_{2n}) + 2\omega_n E_v \operatorname{Re}(m_{2n})) + \\ & \frac{a\alpha_l}{4} [\cos(\mu T_l - \beta_n - \beta_l) \operatorname{Im}(m_{nl}) + \sin(\mu T_l - \beta_n - \beta_l) \operatorname{Re}(m_{nl})] = 0 \end{aligned} \quad (4.55)$$

$$\begin{aligned} & \frac{1}{2}\alpha_l\beta'_l(2\omega_l m_l + g_l) + \frac{\alpha_l^3}{8}(3E_\epsilon \operatorname{Re}(m_{2l}) - 2\omega_l E_v \operatorname{Im}(m_{2l})) + \\ & \frac{a\alpha_n}{4}[\cos(\mu T_1 - \beta_n - \beta_l)\operatorname{Re}(m_{nl}) - \sin(\mu T_1 - \beta_n - \beta_l)\operatorname{Im}(m_{nl})] = 0 \end{aligned} \quad (4.56)$$

$$\begin{aligned} & -\frac{1}{2}\alpha'_l(2\omega_l m_l + g_l) + \frac{\alpha_l^3}{8}(3E_\epsilon \operatorname{Im}(m_{2l}) + 2\omega_l E_v \operatorname{Re}(m_{2l})) + \\ & \frac{a\alpha_n}{4}[\cos(\mu T_1 - \beta_n - \beta_l)\operatorname{Im}(m_{nl}) + \sin(\mu T_1 - \beta_n - \beta_l)\operatorname{Re}(m_{nl})] = 0 \end{aligned} \quad (4.57)$$

where $\operatorname{Re}(m_{nl})$ and $\operatorname{Im}(m_{nl})$ indicate the real and imaginary components of m_{nl} .

It is convenient to eliminate the explicit dependence on T_1 from the above equations, thereby transform these non-autonomous equations into autonomous equations. This can be accomplished by introducing a new dependent variable θ defined as

$$\theta = \mu T_1 - \beta_n - \beta_l \quad (4.58)$$

Differentiating equation (4.58) with respect to T_1 yields

$$\theta' = \mu - \beta'_n - \beta'_l \quad (4.59)$$

Using equations (4.58) and (4.59) with some algebraic manipulations, the amplitude modulation equations (4.54) - (4.57) can be rewritten after combining equations as

$$\alpha'_n = \frac{E_v \omega_n m_{2n}}{4n\pi} \alpha_n^3 + \frac{a\alpha_l}{4n\pi} [\cos \theta \operatorname{Im}(m_{nl}) + \sin \theta \operatorname{Re}(m_{nl})] \quad (4.60)$$

$$\alpha'_l = \frac{E_v \omega_l m_{2l}}{4l\pi} \alpha_l^3 + \frac{a\alpha_n}{4l\pi} [\cos \theta \operatorname{Im}(m_{nl}) + \sin \theta \operatorname{Re}(m_{nl})] \quad (4.61)$$

$$\theta' = \mu + \frac{3E_\epsilon m_{2n} \alpha_n^2}{8n\pi} + \frac{3E_\epsilon m_{2l} \alpha_l^2}{8l\pi} + (\cos \theta \operatorname{Re}(m_{nl}) - \sin \theta \operatorname{Im}(m_{nl})) \left(\frac{a\alpha_l}{4n\pi \alpha_n} + \frac{a\alpha_n}{4l\pi \alpha_l} \right) \quad (4.62)$$

4.4.2 Limit Cycles of Elastic Moving Belts

For the steady state response of elastic moving belts, the amplitudes α_{n0} and α_{l0} , and the phase angle θ_0 in equations (4.60) - (4.62) should be constant. Thus, for elastic systems, setting $\alpha'_{n0} = 0$, $\alpha'_{l0} = 0$, and $E_v = 0$ in equations (4.60) and (4.61) and eliminating terms involving θ_0 yield

$$\alpha_{l0}^2 = \frac{n}{l} \alpha_{n0}^2 \quad (4.63)$$

For steady state analysis, eliminating θ_0 from equations (4.60) and (4.62) with $\alpha'_{n0} = 0$ and $\theta'_0 = 0$ and substituting equation (4.63) into the resulting equation, the amplitudes of steady state response of summation parametric resonance for elastic systems are obtained

$$\alpha_{n0}^2 = \frac{\mu \pm \frac{a}{2\sqrt{nl}\pi} \sqrt{\operatorname{Re}(m_{nl})^2 + \operatorname{Im}(m_{nl})^2}}{-\left(\frac{3E_e m_{2n}}{8n\pi} + \frac{3E_e m_{2l} n}{8l^2\pi}\right)} \quad (4.64)$$

$$\alpha_{l0}^2 = \frac{n}{l} \frac{\mu \pm \frac{a}{2\sqrt{nl}\pi} \sqrt{\operatorname{Re}(m_{nl})^2 + \operatorname{Im}(m_{nl})^2}}{-\left(\frac{3E_e m_{2n}}{8n\pi} + \frac{3E_e m_{2l} n}{8l^2\pi}\right)} \quad (4.65)$$

From the amplitude expressions (4.64) and (4.65) of elastic problems, it can be seen that the first limit cycle exists if

$$\mu \geq -\frac{\sqrt{\operatorname{Re}(m_{nl})^2 + \operatorname{Im}(m_{nl})^2}}{2\sqrt{nl}\pi} a \quad (4.66)$$

and the second limit cycle exists if

$$\mu \geq \frac{\sqrt{\operatorname{Re}(m_{nl})^2 + \operatorname{Im}(m_{nl})^2}}{2\sqrt{nl}\pi} a \quad (4.67)$$

As a special case, the response amplitude of principal parametric resonance ($n = l$) for elastic belts is given in the following

$$\alpha_{n0}^2 = \frac{4n\pi\mu \pm \frac{2n\pi|\sin n\pi\gamma|a}{\gamma}}{3E_e(-m_{2n})} \quad (4.68)$$

where $| |$ denotes absolute value. The first limit cycle (select plus sign in equation (4.68)) exists

if the translation speed is subcritical ($\gamma < 1$) and $\mu + \frac{|\sin n\pi\gamma|a}{2\gamma} > 0$. The second limit cycle

(select negative sign in equation (4.68)) exists if the translation speed is subcritical ($\gamma < 1$) and

$$\mu - \frac{|\sin n\pi\gamma|a}{2\gamma} > 0.$$

It should be mentioned that existence conditions of non-trivial limit cycles are the same as the stability conditions of the trivial solution for elastic systems (Zhang and Zu, 1998). Thus, it is concluded that the non-trivial limit cycles bifurcate from the trivial limit cycle at the stability boundary of the trivial limit cycle for elastic summation parametric resonance.

4.4.3 Limit Cycles of Viscoelastic Moving Belts

For the steady state response of viscoelastic moving belts, setting $\alpha'_{n0} = 0$, $\alpha'_{l0} = 0$, and $\theta'_0 = 0$. and eliminating the term $\cos\theta_0 \operatorname{Im}(m_{nl}) + \sin\theta_0 \operatorname{Re}(m_{nl})$ from equations (4.60) and (4.61) lead to the following relationship between α_{n0} and α_{l0}

$$\alpha_{l0}^2 = \frac{n^2}{l^2} \sqrt{\frac{n}{l}} \alpha_{n0}^2 \quad (4.69)$$

It is seen that the relation between α_{n0} and α_{l0} of viscoelastic systems is different from that of elastic systems.

Eliminating θ_0 from equations (4.60) and (4.62) with $\alpha'_{n0} = 0$ and $\theta'_0 = 0$, and substituting equation (4.69) into the resulting equation, the following amplitude modulation equation for steady state response is obtained

$$c_1 \alpha_{n0}^6 + c_2 \alpha_{n0}^4 + c_3 \alpha_{n0}^2 = 0 \quad (4.70)$$

where

$$c_1 = \left(\frac{3E_e m_{2n}}{2n} + \frac{3E_e m_{2l}}{2l} \frac{n^2}{l^2} \sqrt{\frac{n}{l}} \right)^2 \frac{\sqrt{\frac{n}{l}}}{\left(\frac{1}{l} \sqrt{\frac{n}{l}} + \frac{1}{n} \right)^2} + (E_v \omega_n m_{2n})^2 \frac{l^2}{n^2} \sqrt{\frac{l}{n}} \quad (4.71)$$

$$c_2 = 12\pi\mu E_e \left(\frac{m_{2n}}{n} + \frac{m_{2l}}{l} \frac{n^2}{l^2} \sqrt{\frac{n}{l}} \right) \frac{\sqrt{\frac{n}{l}}}{\left(\frac{1}{l} \sqrt{\frac{n}{l}} + \frac{1}{n} \right)^2} \quad (4.72)$$

$$c_3 = 16\pi^2 \mu^2 \frac{\sqrt{\frac{n}{l}}}{\left(\frac{1}{l} \sqrt{\frac{n}{l}} + \frac{1}{n} \right)^2} - a^2 (\text{Im}(m_{nl})^2 + \text{Re}(m_{nl})^2) \quad (4.73)$$

It is obvious that equation (4.70) possesses a singular point at the origin (trivial periodic solution). In addition, two non-trivial singular points may exist describing limit cycles with amplitudes

$$\alpha_{n0}^2 = \frac{-c_2 \pm \sqrt{c_2^2 - 4c_1c_3}}{2c_1} \quad (4.74)$$

$$\alpha_{l0}^2 = \frac{n^2}{l^2} \sqrt{\frac{n}{l}} \frac{-c_2 \pm \sqrt{c_2^2 - 4c_1c_3}}{2c_1} \quad (4.75)$$

Equations (4.74) and (4.75) represent the amplitudes of the steady state response of the summation parametric resonance for viscoelastic systems. From the amplitude equations (4.74) and (4.75) of viscoelastic systems, it can be seen that the two non-trivial steady state solutions exist only when the following conditions are satisfied:

$$c_2^2 - 4c_1c_3 \geq 0 \quad (4.76)$$

$$-c_2 \pm \sqrt{c_2^2 - 4c_1c_3} \geq 0 \quad (4.77)$$

Substituting the expressions of c_1 , c_2 , and c_3 into equations (4.76) and (4.77) leads to the following conclusions that the first limit cycle of viscoelastic systems exists if

$$-\frac{\left(\frac{1}{l}\sqrt{\frac{n}{l}} + \frac{1}{n}\sqrt{\frac{l}{n}}\right)\sqrt{\text{Re}(m_{nl})^2 + \text{Im}(m_{nl})^2}}{4\pi} a \leq \mu \leq \frac{\left(\frac{n}{l^2}\sqrt{\frac{n}{l}} + \frac{1}{l}\right)\sqrt{(\text{Re}(m_{nl})^2 + \text{Im}(m_{nl})^2)c_1}}{-4\pi E_v \omega_n m_{2n}} a \quad (4.78)$$

and the second limit cycle exists if

$$\frac{\left(\frac{1}{l}\sqrt{\frac{n}{l}} + \frac{1}{n}\sqrt{\frac{l}{n}}\right)\sqrt{\text{Re}(m_{nl})^2 + \text{Im}(m_{nl})^2}}{4\pi} a \leq \mu \leq \frac{\left(\frac{n}{l^2}\sqrt{\frac{n}{l}} + \frac{1}{l}\right)\sqrt{(\text{Re}(m_{nl})^2 + \text{Im}(m_{nl})^2)c_1}}{-4\pi E_v \omega_n m_{2n}} a \quad (4.79)$$

As a special case, the response amplitude of principal parametric resonance ($n = l$) for viscoelastic belts is given in the following

$$\alpha_{n0}^2 = \frac{\frac{3E_e n \pi \mu}{8} \pm \sqrt{\frac{n^2 \pi^2 a^2 \sin^2 n\pi\gamma}{4\gamma^2} \left(\frac{3E_e}{8}\right)^2 - \left(n^2 \pi^2 \mu^2 - \frac{n^2 \pi^2 a^2 \sin^2 n\pi\gamma}{4\gamma^2}\right) \left(\frac{E_v \omega_n}{4}\right)^2}}{2 \left[\left(\frac{3E_e}{8}\right)^2 + \left(\frac{E_v \omega_n}{4}\right)^2 \right] (-m_{2n})} \quad (4.80)$$

The first limit cycle (select plus sign in equation (4.80)) exists if the translation speed is

subcritical ($\gamma < 1$), and $\frac{3E_e \mu}{8} + \sqrt{\frac{a^2 \sin^2 n\pi\gamma}{4\gamma^2} \left(\frac{3E_e}{8}\right)^2 - \left(\mu^2 - \frac{a^2 \sin^2 n\pi\gamma}{4\gamma^2}\right) \left(\frac{E_v \omega_n}{4}\right)^2} > 0$. The

second limit cycle (select negative sign in equation (4.80)) exists if the translation speed is

subcritical, and $\frac{3E_e \mu}{8} - \sqrt{\frac{a^2 \sin^2 n\pi\gamma}{4\gamma^2} \left(\frac{3E_e}{8}\right)^2 - \left(\mu^2 - \frac{n^2 \pi^2 a^2 \sin^2 n\pi\gamma}{4\gamma^2}\right) \left(\frac{E_v \omega_n}{4}\right)^2} > 0$.

It can be seen from equations (4.78) and (4.79) that the existence conditions of non-trivial limit cycles have an upper boundary for viscoelastic models, which is different from the conclusion of the corresponding elastic systems. The upper boundaries of existence conditions for the first limit cycle and the second limit cycle are identical and are determined by the viscoelastic parameter E_v . The lower boundaries of existence conditions have no relation with the nonlinear parameter E_e and the viscoelastic parameter E_v , and are different from those of the corresponding elastic systems.

4.5 NUMERICAL RESULTS AND DISCUSSIONS

In this section, numerical results of steady state responses and existence boundaries for the summation parametric resonance of moving belts are presented. Effects of the viscoelastic

parameter, the amplitude of excitation, the frequency of excitation and the transport speed on the response of non-trivial limit cycles are investigated.

The amplitudes of non-trivial limit cycles of the first principal parametric resonance ($n=1$, $l=1$) are plotted in Figure 4.1 as a function of excitation frequency (detuning), μ and excitation amplitude, a , for an elastic system. The non-dimensional transport speed γ is 0.2 and the nonlinear parameter E_e is 400. Figure 4.2 and Figure 4.3 show the analogous results for the second principal parametric resonance ($n=2$, $l=2$) and the first summation parametric resonance ($n=1$, $l=2$), respectively. From Figures 4.1 – 4.3, it can be seen that the amplitude increases without bound as μ increases. When the excitation amplitude grows, the response amplitude of the first limit cycle increases while the second limit cycle decreases. Only the trivial solution exists if the existence conditions of non-trivial solutions are not satisfied. The results obtained here are identical to those given by Mockensturm *et al.* (1996).

The non-trivial limit cycles of the first summation parametric resonance ($n=1$, $l=2$) for a viscoelastic moving belt are shown Figure 4.4. The non-dimensional transport speed γ is 0.2, the nonlinear parameter E_e is 400, and the viscoelastic parameter E_v is 10. It is evident that though the amplitude increases with the growth of frequency μ , there exists an upper bound. The non-trivial limit cycle will vanish when a and μ approach this bound, which indicates that damping introduced by the viscoelasticity enlarges the region of the trivial limit cycles. This phenomenon for viscoelastic moving belts is quite different from the corresponding elastic systems.

The effect of viscoelastic parameter E_v on the amplitude and the existence boundary of non-

trivial limit cycles is illustrated in Figure 4.5. The system parameters are $E_e = 400$, $a = 0.5$ and $\gamma = 0.25$. Three different values of E_v are chosen as 0, 25, and 50. It is clear that the amplitude decreases with the increase of E_v for the first limit cycle while the amplitude increases with the growth of E_v for the second limit cycle. The most important phenomenon is that the existence condition has an upper boundary for viscoelastic system. The larger the viscoelastic parameter E_v is, the narrower the region of non-trivial limit cycles is.

Translation speeds not only influence the amplitude of the non-trivial limit cycles, but also influence the existence region of non-trivial limit cycles significantly. Figure 4.6 and Figure 4.7 illustrate the effect of the translating speed on non-trivial limit cycles of the first principal ($n = l = 1$) and the first summation ($n = 1, l = 2$) parametric resonance, respectively. The excitation amplitude a is chosen as 0.5 and the nonlinear parameter E_e is 400. From Figure 4.6, for the principal parametric resonance, it is seen that the amplitude of limit cycles decreases with the increase of transport speeds. The non-trivial amplitude grows more slowly with μ when translation speeds is larger. Moreover, for the translation speed unsatisfying equation (4.78) and (4.79), the non-trivial limit cycles no longer exist. These results indicate that by increasing the transport speed while keeping other parameters constant, an unstable belt can be stabilized. For the summation parametric resonance, the relation between the response and the transport speed is much more complicated. There exists a maximum value of response for the first limit cycle and a minimum value of response for the second limit cycle when γ is around 0.2.

The relation between the excitation frequency μ and the transport speed on the boundaries of

existence condition for the non-trivial limit cycles is plotted in Figure 4.8. The system parameters are $E_v = 10$, $E_e = 400$, and $a=0.5$. It is clear that the transport speed has a significant effect on the boundary of existence.

The excitation frequency (detuning) μ on the upper boundary of existence is plotted against viscoelastic property E_v in Figure 4.9. In this example, $\gamma = 0.25$, $E_e = 400$, and $a=0.5$. It is much clearer that when E_v increases, μ decreases. Since the lower boundary has no relation with E_v , the region of existence will narrow with the increase of E_v . Especially when E_v approach zero, the upper boundary of μ will approach infinite. This agrees with the conclusion obtained by Mockensturm *et al.* (1996) that there is no upper boundary of existence for elastic problems.

4.6 SUMMARY AND CONCLUSIONS

In this chapter, the dynamic response of parametrically excited viscoelastic moving belts is investigated. The Kelvin viscoelastic model is employed to characterize the property of belt materials. The method of multiple scales is applied directly to the governing equation of motion, which is in the form of continuous gyroscopic systems. No assumptions about the spatial dependence of the motion are made in this approach. Closed-form expressions are found for the response and existence conditions of the summation parametric resonance. The following conclusions can be drawn from the above study:

- 1) The amplitude of the first limit cycle decreases with the increase of the viscoelastic

parameter E_v , while the amplitude of the second limit cycle increases with E_v .

- 2) The amplitude of the limit cycles decreases with increasing transport speeds for principal parametric resonance. There is no such a simple relation for the summation parametric resonance.
- 3) There exists an upper existence boundary for the viscoelastic model and this upper boundary of existence for limit cycles is determined by the viscoelastic property E_v .
- 4) The lower boundary of existence for limit cycles of elastic systems is identical to the stability boundary of the trivial solution. This suggests that non-trivial limit cycles of the summation parametric resonance bifurcate from the trivial limit cycle at the boundary of the trivial limit cycle.
- 5) The boundaries of existence have no relation with the nonlinear parameter E_c .

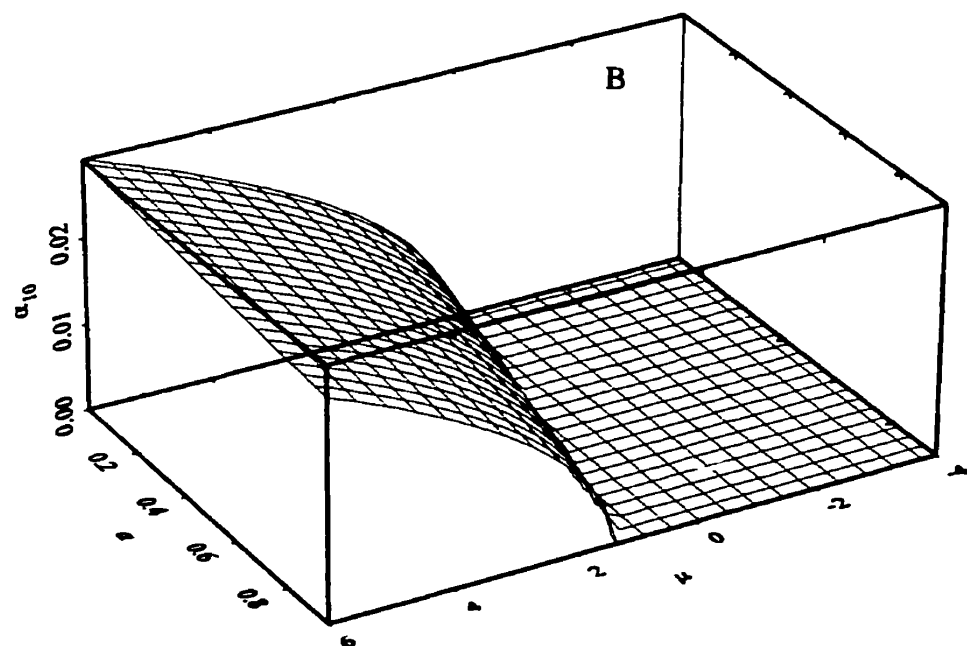
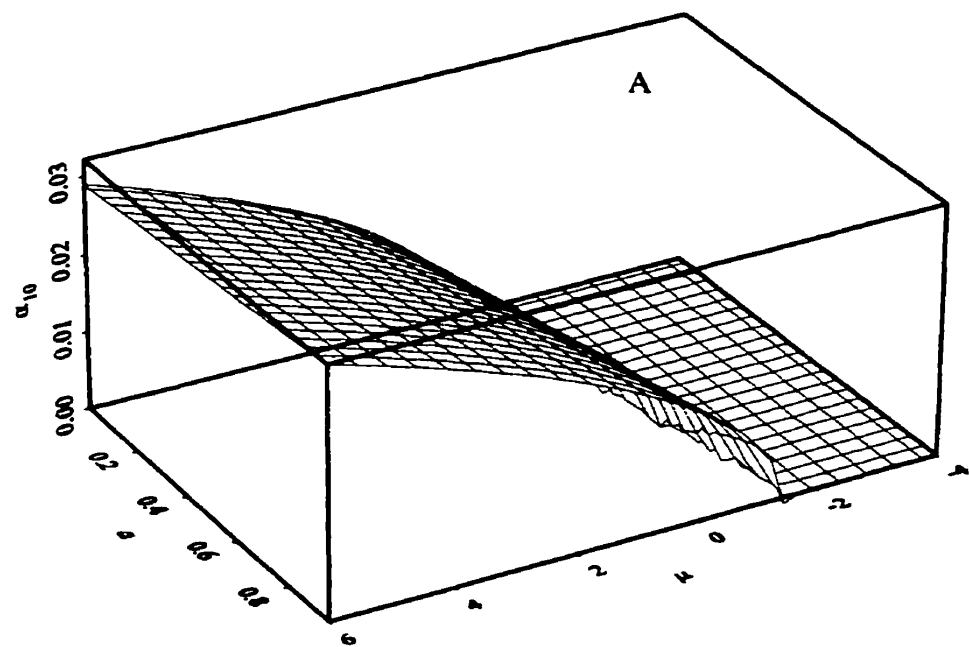


Figure 4.1: The nontrivial limit cycles that bifurcate from the boundary of the first principal parameter instability region ($\gamma=0.2$, $n=l=1$, $E_c=400$, $E_v=0$)

A: the first limit cycle

B: the second limit cycle

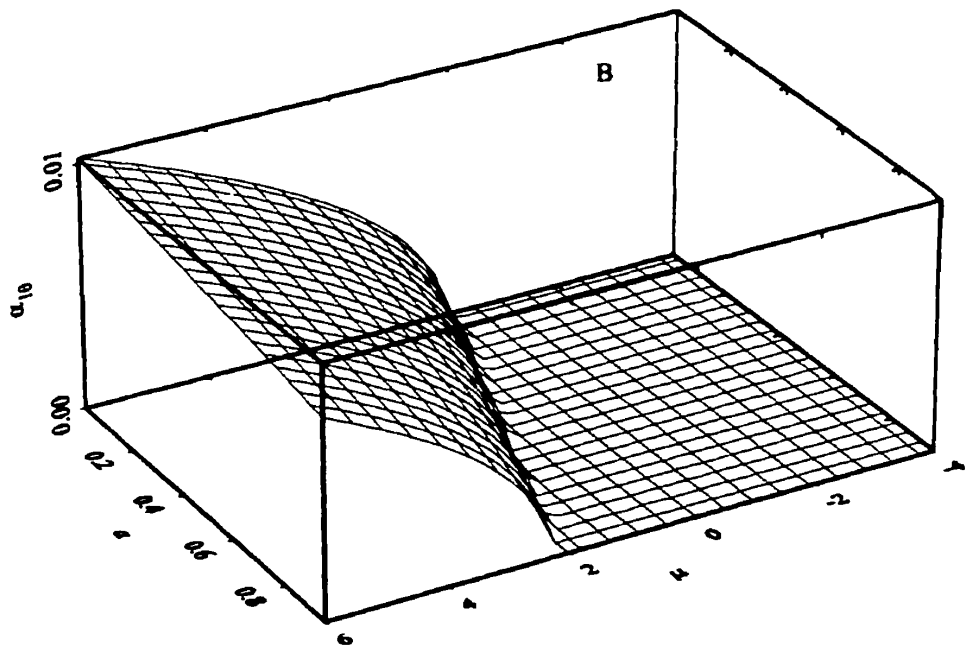
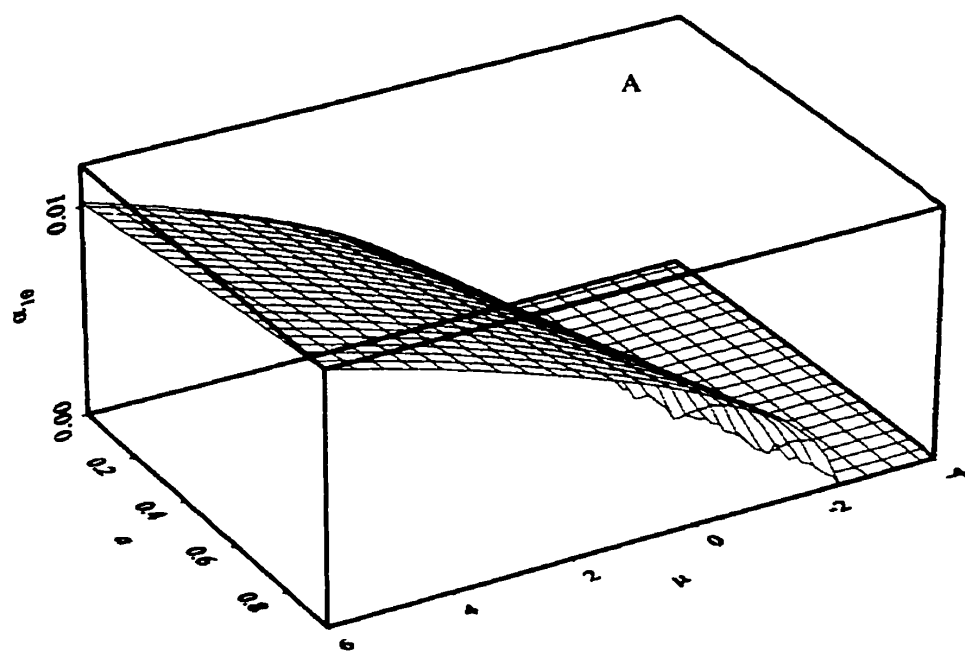


Figure 4.2: The nontrivial limit cycles that bifurcate from the boundary of the second principal parameter instability region ($\gamma=0.2$, $n=l=2$, $E_c=400$, $E_v=0$)

A: the first limit cycle

B: the second limit cycle

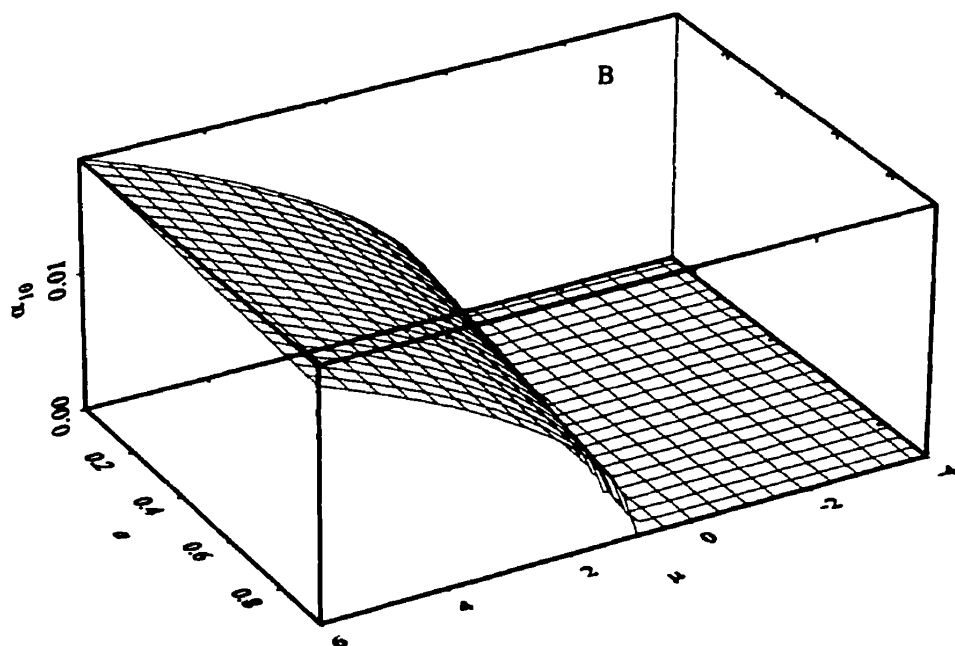
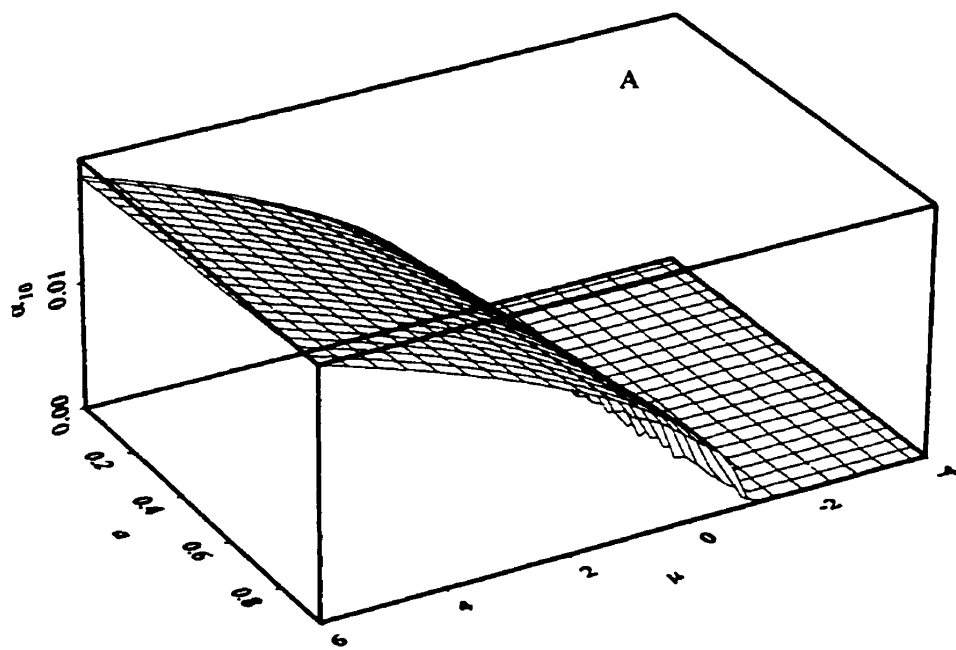


Figure 4.3: The nontrivial limit cycles that bifurcate from the boundary of the first summation parameter instability region ($\gamma=0.2$, $n=1$, $l=2$, $E_c=400$, $E_v=0$)

A: the first limit cycle

B: the second limit cycle

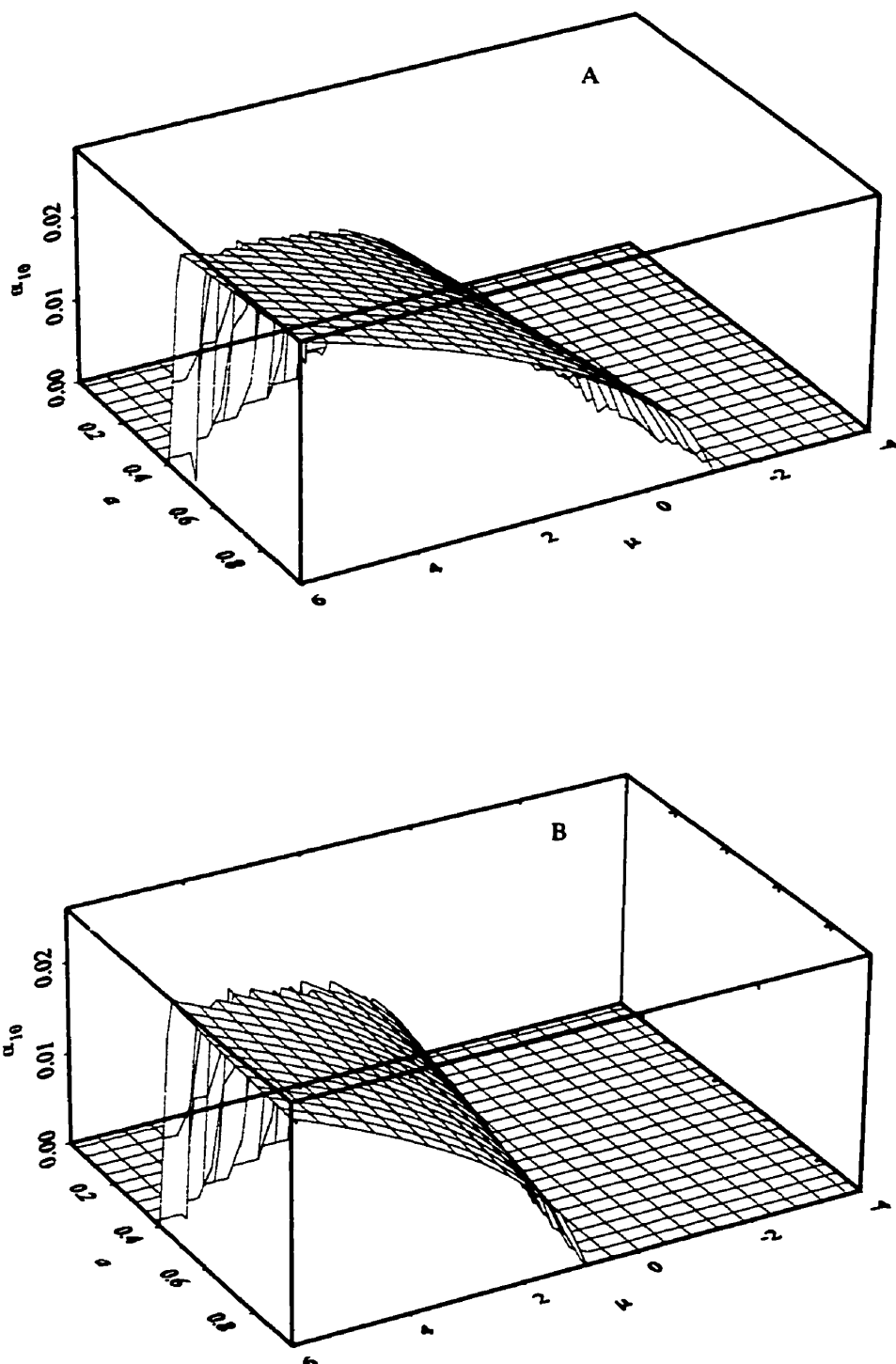


Figure 4.4: The response amplitude of non-trivial limit cycles for the summation parametric resonance of a viscoelastic moving belt ($n=1$, $l=2$, $E_e = 400$, $E_v = 10$, $\gamma = 0.2$)

A: the first limit cycle

B: the second limit cycle

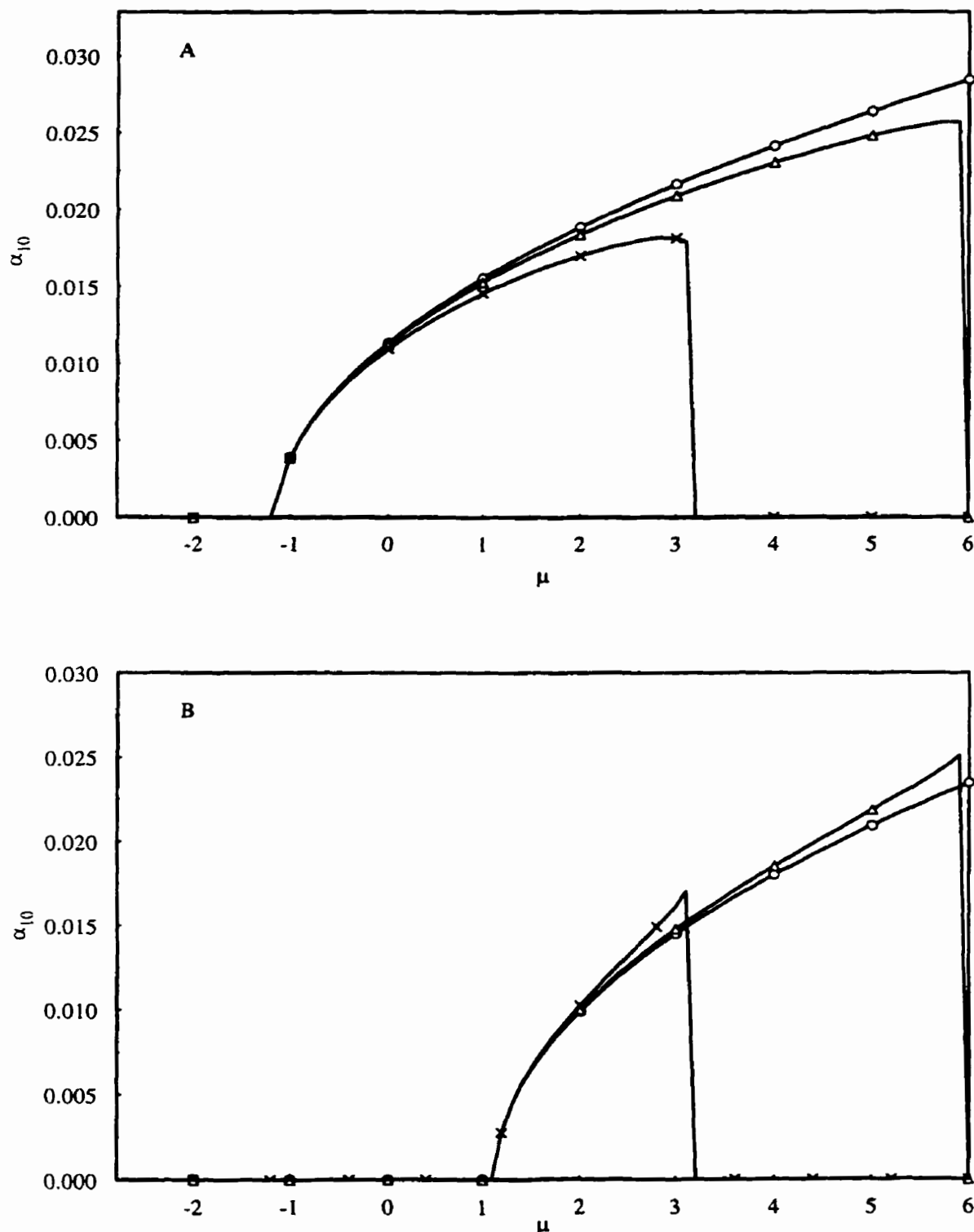


Figure 4.5: Effects of E_v on the nontrivial limit cycles for the first summation parametric resonance ($n=1$, $l=2$, $E_\epsilon = 400$, $\gamma = 0.25$, $a=0.5$)

A: the first limit cycle B: the second limit cycle $\circ: E_v=0$ $\Delta: E_v=25$ $\times: E_v=50$

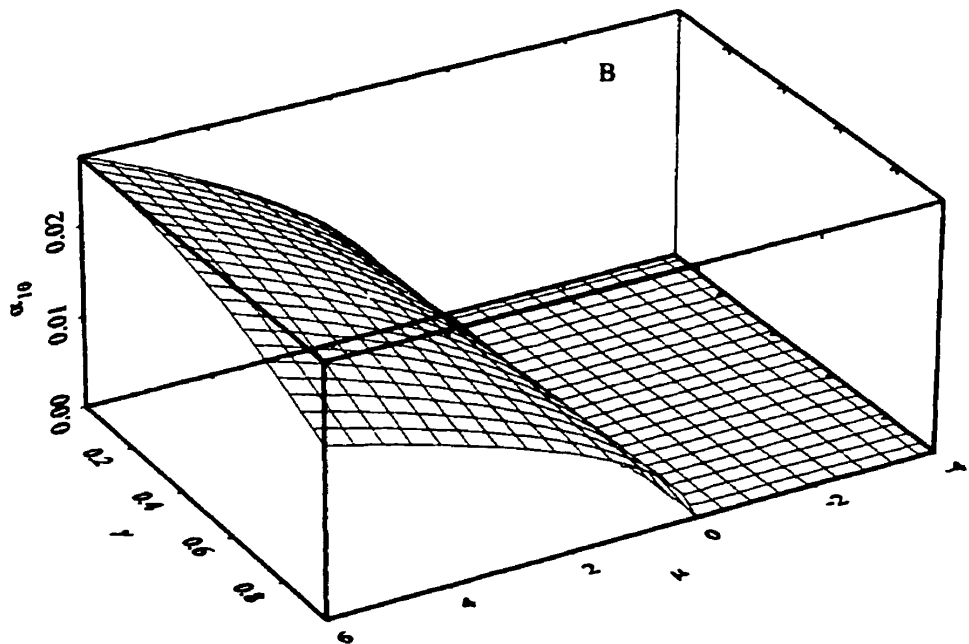
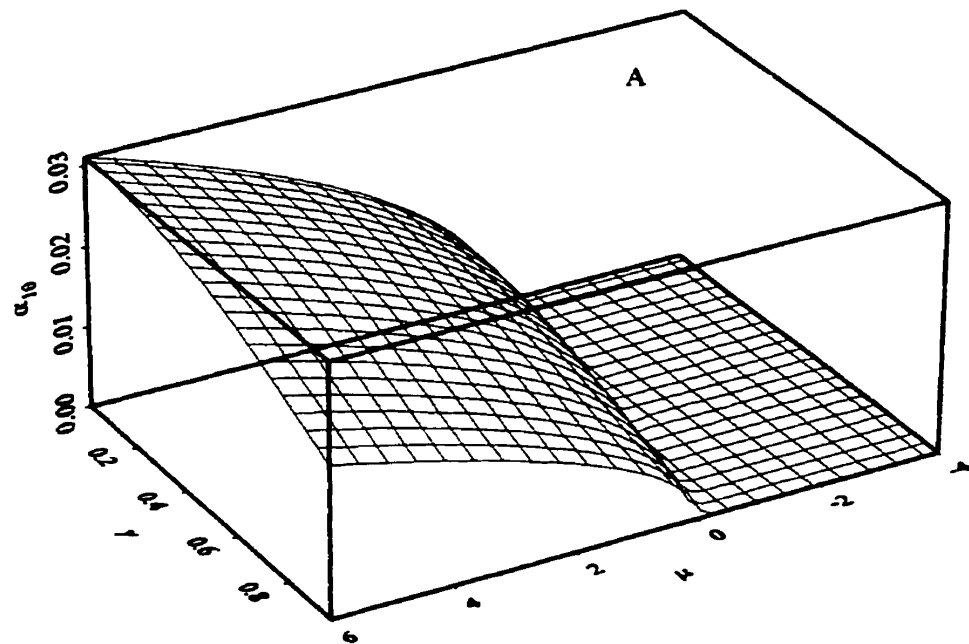


Figure 4.6: Effects of the transport speed on non-trivial limit cycles of the first principal parametric resonance ($E_c = 400$, $E_v = 10$, $a=0.5$, $n=l=1$)

A: the first limit cycle

B: the second limit cycle

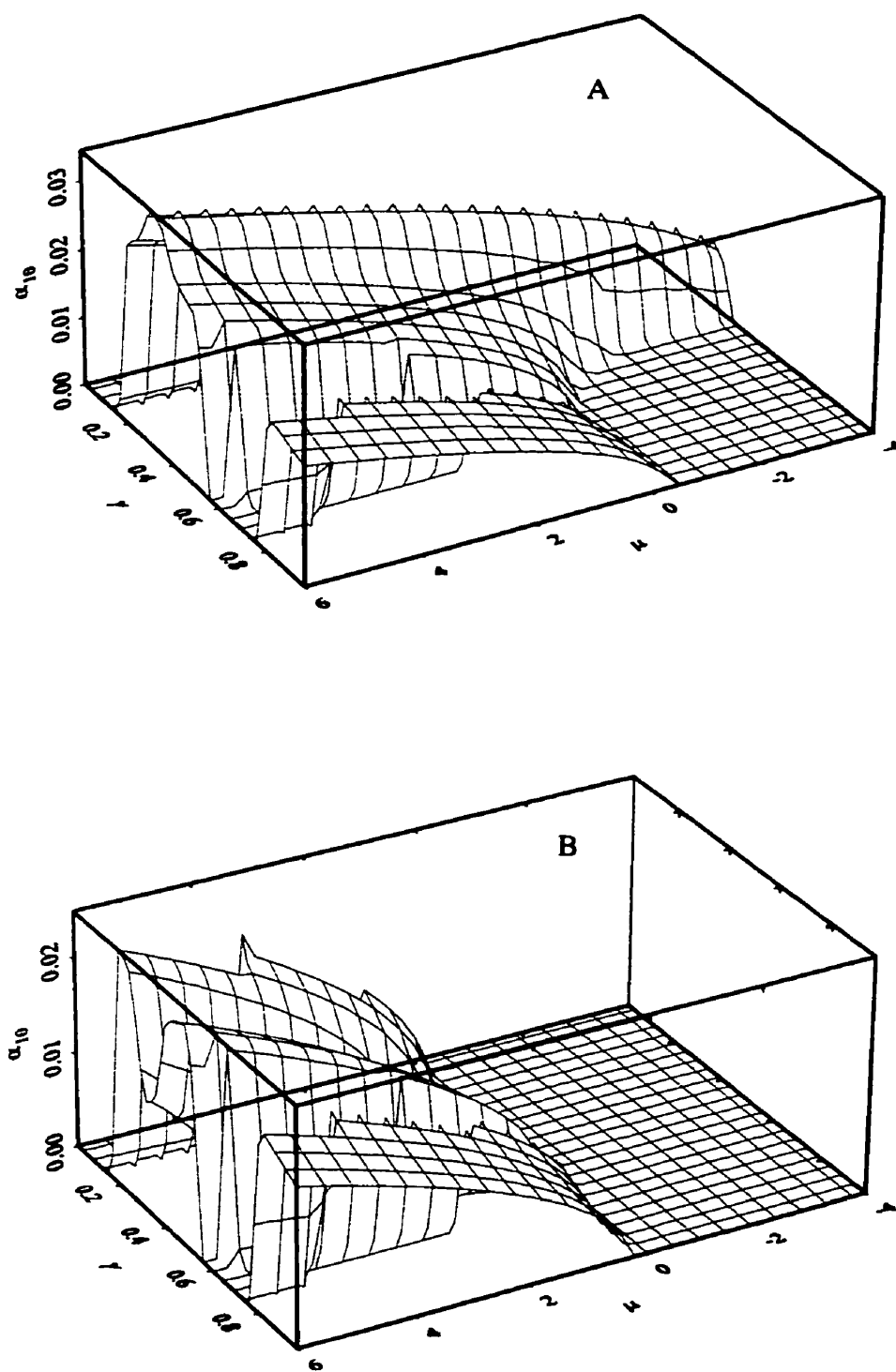


Figure 4.7: Effects of the transport speed on non-trivial limit cycles of the first summation parametric resonance ($E_c = 400$, $E_v = 10$, $a=0.5$, $n=1$, $l=2$)

A: the first limit cycle

B: the second limit cycle

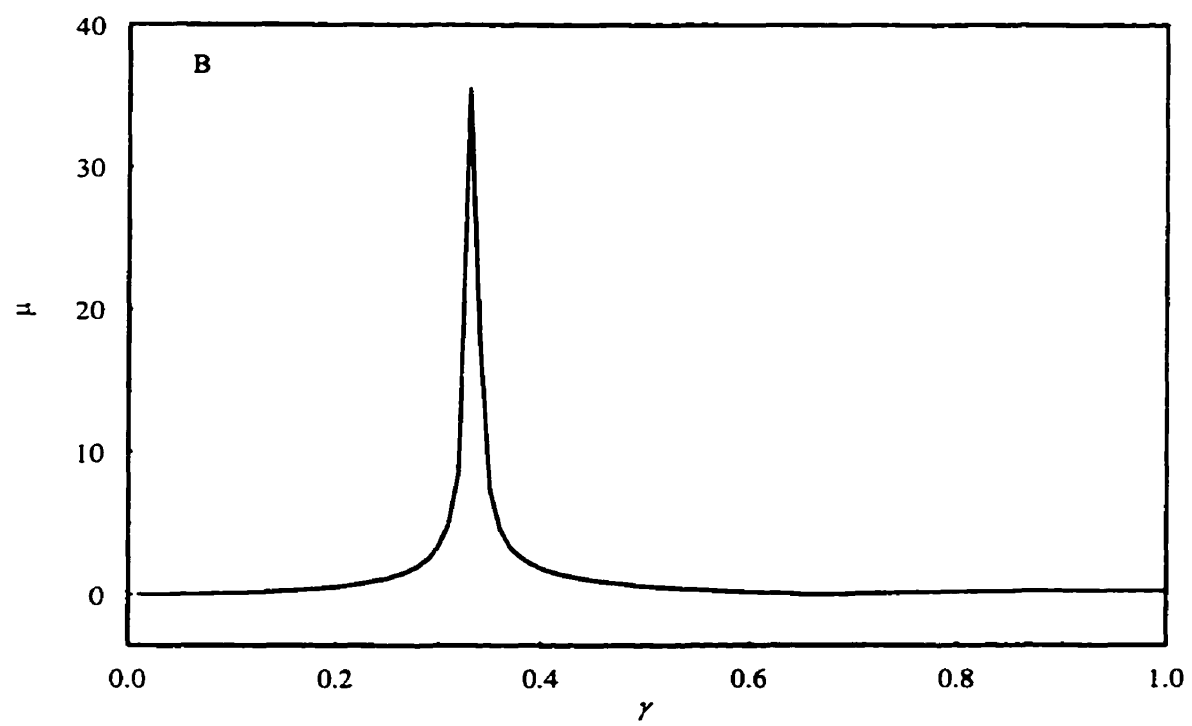
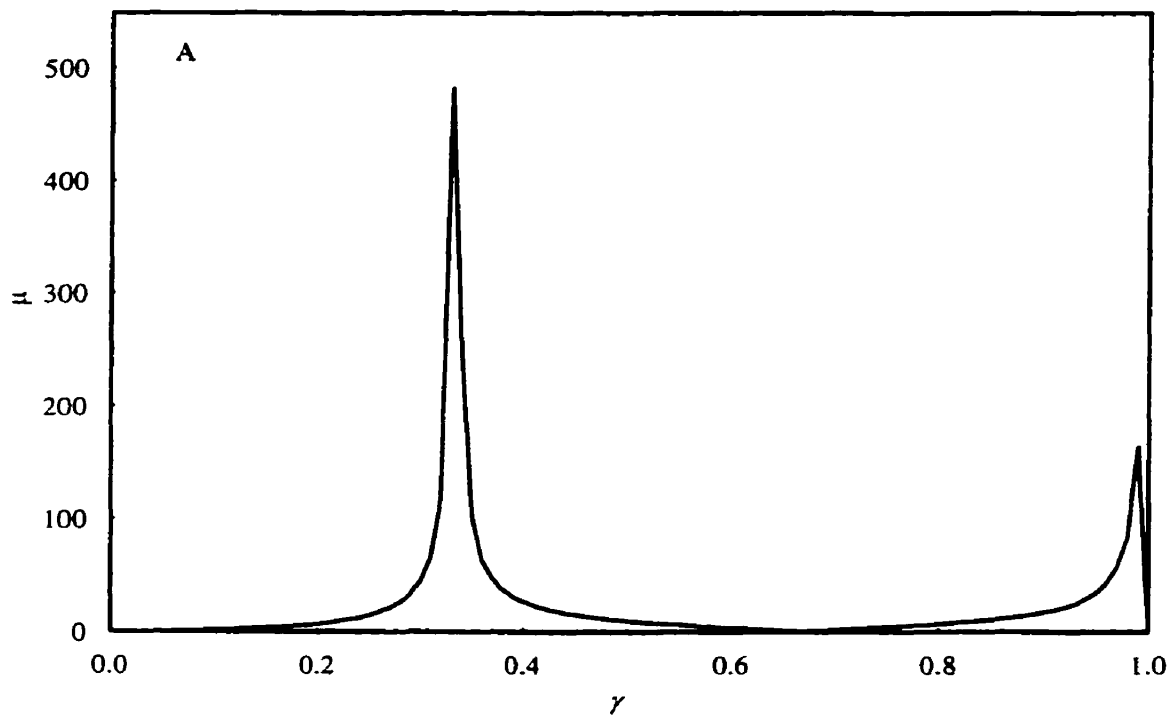


Figure 4.8: Effects of the transport speed on the existence boundary of nontrivial limit cycles for the first summation parametric resonance ($n=1$, $l=2$, $E_r = 400$, $a=0.5$, $E_v = 10$)

A: Upper boundary

B: Lower boundary

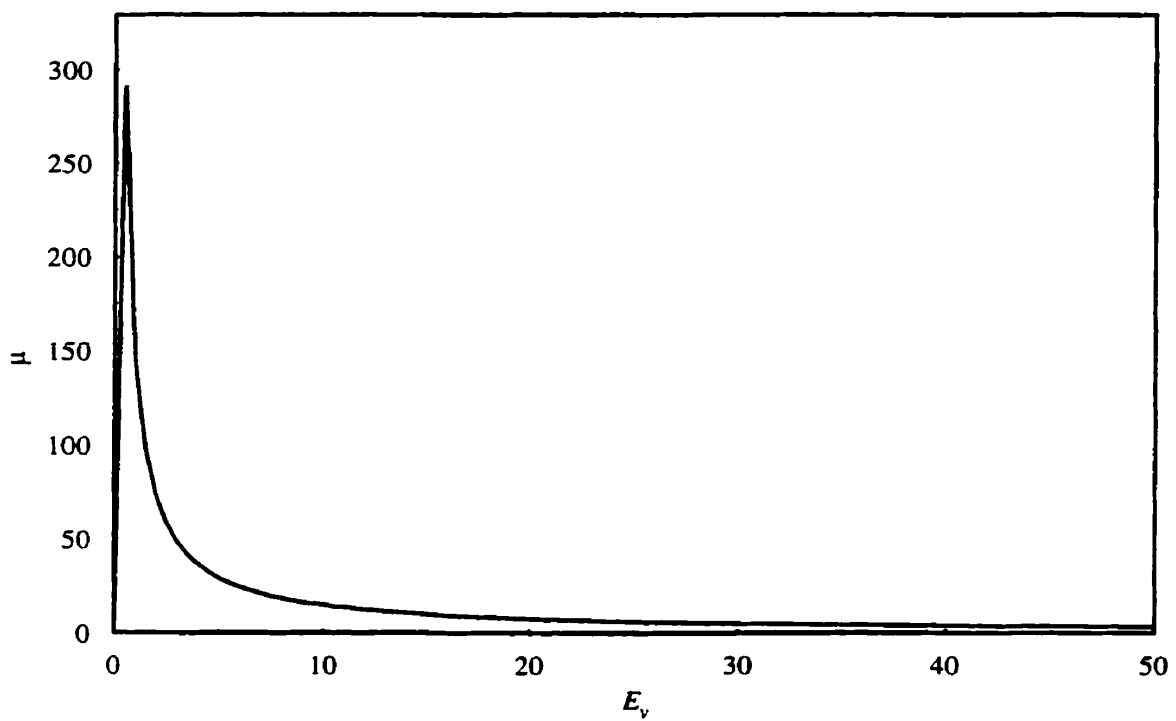


Figure 4.9: Relations of μ and E_v on the upper existence boundary of non-trivial limit cycles for summation parametric resonance ($n=1$, $l=2$, $E_\epsilon = 400$, $\gamma = 0.25$, $a=0.5$)

CHAPTER 5

STABILITY ANALYSIS OF PARAMETRICALLY EXCITED VISCOELASTIC MOVING BELTS

The amplitude and existence conditions of non-trivial limit cycles are derived in Chapter 4. The stability of these limit cycles is of great concern by automobile manufacturers since an unstable belt could lead to large amplitude vibration and adversely impact belt life. To better understand the effect of design parameters on the stability of belt drives and to stabilize an unstable belt drives are an important topic.

In this chapter, the stability of parametrically excited viscoelastic moving belts is studied. Stability boundaries of the trivial limit cycle for general summation and difference parametric resonance are obtained. The Routh-Hurwitz criterion is used to investigate the stability of non-trivial limit cycles. Closed-form expressions are found for the stability of non-trivial limit cycles of general summation parametric resonance. It is shown that the first limit cycle is always stable while the second limit cycle is always unstable for the viscoelastic moving belts. Examples highlight the important effects of viscoelastic parameters, excitation frequencies, excitation amplitudes and axial moving speeds on stability boundaries.

5.1 STABILITY OF TRIVIAL LIMIT CYCLES

It has been shown (Wanda, 1990) that the stability of the trivial limit cycle of nonlinear systems coincides with the stability of the equilibrium point of the corresponding linear systems. Thus, it is convenient to perform the stability analysis of linear systems to obtain the stability boundary of the trivial limit cycle of nonlinear systems. Mockensturm *et al.* (1996) derived the closed-form expressions for the stability boundaries of the principal and the first summation resonance of linear systems using KBM method. In this section, the stability boundaries of the trivial solution of summation and difference parametric resonance are obtained based on the amplitude modulation equations derived in Chapter 4.

5.1.1 Stability Boundary of Summation Resonance

The amplitude modulation equations of the linear system are given from equations (4.16) and (4.17) by removing the nonlinear terms as

$$-2i\omega_n m_n A'_n - g_n A'_n i + \frac{a\bar{A}_l}{2} m_{nl} e^{i\mu T_l} = 0 \quad (5.1)$$

$$-2i\omega_l m_l A'_l - g_l A'_l i + \frac{a\bar{A}_n}{2} m_{nl} e^{i\mu T_l} = 0 \quad (5.2)$$

Note that the nonlinear terms have been taken out from the original equations. In order to transform equations (5.1) and (5.2) into equations with constant coefficients, introduce the following transformation

$$A_n = A_l e^{\frac{i\mu T_l}{2}} \quad (5.3)$$

$$A_1 = A_2 e^{\frac{i\mu T_1}{2}} \quad (5.4)$$

Substitution of equations (5.3) and (5.4) into equations (5.1) and (5.2) yields

$$-2n\pi i \left(\frac{A_1}{2} i\mu + A'_1 \right) + \frac{a\bar{A}_2}{2} m_{nl} = 0 \quad (5.5)$$

$$-2l\pi i \left(\frac{A_2}{2} i\mu + A'_2 \right) + \frac{a\bar{A}_1}{2} m_{nl} = 0 \quad (5.6)$$

Express A_1 and A_2 into real and imaginary parts

$$A_1 = A_{1r} + iA_{1i} \quad (5.7)$$

$$A_2 = A_{2r} + iA_{2i} \quad (5.8)$$

Substituting equations (5.7) and (5.8) into (5.5) and (5.6) and separating the real and imaginary parts from the resulting equations lead to

$$2n\pi \left(\frac{\mu A_{1r}}{2} + A'_{1i} \right) + \frac{a[A_{2r} \operatorname{Re}(m_{nl}) + A_{2i} \operatorname{Im}(m_{nl})]}{2} = 0 \quad (5.9)$$

$$-2n\pi \left(-\frac{\mu A_{1i}}{2} + A'_{1r} \right) + \frac{a[A_{2r} \operatorname{Im}(m_{nl}) - A_{2i} \operatorname{Re}(m_{nl})]}{2} = 0 \quad (5.10)$$

$$2l\pi \left(\frac{\mu A_{2r}}{2} + A'_{2i} \right) + \frac{a[A_{1r} \operatorname{Re}(m_{nl}) + A_{1i} \operatorname{Im}(m_{nl})]}{2} = 0 \quad (5.11)$$

$$-2l\pi \left(-\frac{\mu A_{2i}}{2} + A'_{2r} \right) + \frac{a[A_{1r} \operatorname{Re}(m_{nl}) - A_{1i} \operatorname{Re}(m_{nl})]}{2} = 0 \quad (5.12)$$

Since equations (5.9) to (5.12) have constant coefficients, the general solutions can be sought in the form

$$A_{1r} = a_{1r} e^{\beta T_1} \quad (5.13)$$

$$A_{1i} = a_{1i} e^{\beta T_1} \quad (5.14)$$

$$A_{2r} = a_{2r} e^{\beta T_1} \quad (5.15)$$

$$A_{2i} = a_{2i} e^{\beta T_1} \quad (5.16)$$

Inserting equations (5.13) – (5.16) into equations (5.9) - (5.12) results in

$$n\pi\mu a_{1r} + 2n\pi\beta a_{1i} + \frac{a}{2} a_{2r} \operatorname{Re}(m_{nl}) + \frac{a}{2} a_{2i} \operatorname{Im}(m_{nl}) = 0 \quad (5.17)$$

$$-2n\pi\beta a_{1r} + n\pi\mu a_{1i} + \frac{a}{2} a_{2r} \operatorname{Im}(m_{nl}) - \frac{a}{2} a_{2i} \operatorname{Re}(m_{nl}) = 0 \quad (5.18)$$

$$l\pi\mu a_{2r} + 2l\pi\beta a_{2i} + \frac{a}{2} a_{1r} \operatorname{Re}(m_{nl}) + \frac{a}{2} a_{1i} \operatorname{Im}(m_{nl}) = 0 \quad (5.19)$$

$$-2l\pi\beta a_{2r} + l\pi\mu a_{2i} + \frac{a}{2} a_{1r} \operatorname{Im}(m_{nl}) - \frac{a}{2} a_{1i} \operatorname{Re}(m_{nl}) = 0 \quad (5.20)$$

Express a_{2r} and a_{2i} in terms of a_{1r} and a_{1i} from equations (5.17) and (5.18) as

$$a_{2r} = -\frac{n\pi a_{1r} (\mu \operatorname{Re}(m_{nl}) - 2\beta \operatorname{Im}(m_{nl})) + n\pi a_{1i} (2\beta \operatorname{Re}(m_{nl}) + \mu \operatorname{Im}(m_{nl}))}{\frac{a}{2} (\operatorname{Re}(m_{nl})^2 + \operatorname{Im}(m_{nl})^2)} \quad (5.21)$$

$$a_{2i} = -\frac{n\pi a_{1r} (\mu \operatorname{Im}(m_{nl}) + 2\beta \operatorname{Re}(m_{nl})) + n\pi a_{1i} (2\beta \operatorname{Im}(m_{nl}) - \mu \operatorname{Re}(m_{nl}))}{\frac{a}{2} (\operatorname{Re}(m_{nl})^2 + \operatorname{Im}(m_{nl})^2)} \quad (5.22)$$

Substitution of equations (5.21) and (5.22) into equations (5.19) and (5.20) yields

$$\left[\frac{a \operatorname{Re}(m_{nl})}{2} - \frac{n! \pi^2 \operatorname{Re}(m_{nl}) (\mu^2 + 4\beta^2)}{2} \right] a_{1r} + \left[\frac{a \operatorname{Im}(m_{nl})}{2} - \frac{n! \pi^2 \operatorname{Im}(m_{nl}) (\mu^2 + 4\beta^2)}{2} \right] a_{1i} = 0 \quad (5.23)$$

$$\left[\frac{a \operatorname{Im}(m_{nl})}{2} - \frac{n! \pi^2 \operatorname{Im}(m_{nl}) (\mu^2 + 4\beta^2)}{2} \right] a_{1r} + \left[-\frac{a \operatorname{Re}(m_{nl})}{2} + \frac{n! \pi^2 \operatorname{Re}(m_{nl}) (\mu^2 + 4\beta^2)}{2} \right] a_{1i} = 0 \quad (5.24)$$

For non-trivial a_{1r} and a_{1i} , the determinant of the coefficient matrix in equations (5.23) and (5.24) must vanish, i.e.,

$$\left[\frac{a \operatorname{Re}(m_{nl})}{2} - \frac{nl\pi^2 \operatorname{Re}(m_{nl})(\mu^2 + 4\beta^2)}{2(\operatorname{Re}(m_{nl})^2 + \operatorname{Im}(m_{nl})^2)} \right]^2 + \left[\frac{a \operatorname{Im}(m_{nl})}{2} - \frac{nl\pi^2 \operatorname{Im}(m_{nl})(\mu^2 + 4\beta^2)}{2(\operatorname{Re}(m_{nl})^2 + \operatorname{Im}(m_{nl})^2)} \right]^2 = 0 \quad (5.25)$$

Since the system is stable only when β has a negative real component, the transition at which $\beta = 0$ is where the stability boundaries are located. Therefore, the stability condition for the general summation resonance of linear moving belts is obtained as

$$\mu^2 > \frac{a^2 (\operatorname{Re}(m_{nl})^2 + \operatorname{Im}(m_{nl})^2)}{4nl\pi^2} \quad (5.26)$$

Substituting the expression of m_{nl} given in Chapter 4 into equation (5.26) yields

$$\mu^2 > \frac{8n^3 l^3 \gamma^2 (1 - \cos((n+l)\pi\gamma)) a^2}{(n+l)^2 [(n+l)\gamma + n - l][(n+l)\gamma - n + l]} \quad (5.27)$$

It is seen that equation (5.27) is the same as the existence condition of non-trivial limit cycles of nonlinear elastic systems given by equations (4.66) and (4.67) in Chapter 4. This suggests that the non-trivial limit cycle of summation parametric resonance of elastic systems bifurcates from the instability boundary of trivial solution.

Equation (5.27) represents the stability boundary of summation resonance for the linear belt system. Two special cases are discussed here. The first case is the primary parametric instability. When $n = l$ in equation (5.1), primary parametric instability occurs. Upon substituting $n = l$ into equation (5.27), the stability boundary condition of trivial solution is

$$\mu = \pm \frac{\sin n\pi\gamma a}{2\gamma} \quad (5.28)$$

which leads to the stability boundaries for the first order approximation

$$\omega^2 = [n\pi(1-\gamma^2)]^2 \left[4 \pm \frac{2a \sin n\pi\gamma}{n\pi\gamma(1-\gamma^2)} \right] \quad (5.29)$$

The above solution is identical to the results given by Mockensturm *et al.* (1996)

The second case is the fundamental summation resonance. When the excitation frequency is equal to the sum of frequencies of the first and second mode, the fundamental summation resonance occurs. Upon substitution of $n=1, l=2$ into equation (5.27), the stability boundary condition of trivial solutions is

$$\mu = \pm \frac{4\sqrt{2}\gamma \sin \frac{3\pi\gamma}{2} a}{3\pi^2(1-\gamma^2)(3\gamma+1)(3\gamma-1)} \quad (5.30)$$

which leads to the following stability boundaries for the excitation frequency

$$\omega^2 = [3\pi(1-\gamma^2)]^2 \pm \frac{8\sqrt{2}a\gamma \sin \frac{3\pi}{2}\gamma}{\pi(3\gamma+1)(3\gamma-1)} \quad (5.31)$$

5.1.2 Stability Boundary of Difference Resonance

Following the same procedure as that in the analysis of summation resonance, the difference resonance is examined by introducing a detuning parameter μ defined as

$$\omega = \omega_n - \omega_l + \varepsilon\mu \quad (5.32)$$

The elimination of secular terms yields the corresponding solvability condition. The first order approximation equation for difference resonance is of the same form as equations (5.1) and (5.2) except that the terms involving parametric excitation are different

$$-2i\omega_n A'_n m_n - g_n A'_n i + \frac{aA_l}{2} \hat{m}_{nl} e^{i\mu T_l} = 0 \quad (5.33)$$

$$-2i\omega_l A'_l m_l - g_l A'_l i + \frac{aA_n}{2} \hat{m}_{ln} e^{i\mu T_l} = 0 \quad (5.34)$$

where

$$\hat{m}_{nl} = \left\langle \frac{\partial^2 \phi_n}{\partial \xi^2}, \phi_l \right\rangle \quad (5.35)$$

$$\hat{m}_{ln} = \left\langle \frac{\partial^2 \phi_l}{\partial \xi^2}, \phi_n \right\rangle \quad (5.36)$$

It can be proved that \hat{m}_{nl} and \hat{m}_{ln} are conjugate pair for difference resonance while $m_{nl} = m_{ln}$ for summation resonance.

The equations of a_{lr} and a_{li} for the difference resonance can then be obtained in a same way as in the summation resonance:

$$\left[\frac{a \operatorname{Re}(m_{nl})}{2} + \frac{nl\pi^2 \operatorname{Re}(m_{nl})(\mu^2 + 4\beta^2)}{2} \right] a_{lr} + \left[\frac{a \operatorname{Im}(m_{nl})}{2} + \frac{nl\pi^2 \operatorname{Im}(m_{nl})(\mu^2 + 4\beta^2)}{2} \right] a_{li} = 0 \quad (5.37)$$

$$\left[-\frac{a \operatorname{Im}(m_{nl})}{2} - \frac{nl\pi^2 \operatorname{Im}(m_{nl})(\mu^2 + 4\beta^2)}{2} \right] a_{lr} + \left[\frac{a \operatorname{Re}(m_{nl})}{2} + \frac{nl\pi^2 \operatorname{Re}(m_{nl})(\mu^2 + 4\beta^2)}{2} \right] a_{li} = 0 \quad (5.38)$$

For a non-trivial a_{lr} and a_{li} , the determinant of the coefficient matrix in equations (5.37) and (5.38) must vanish, i.e.,

$$\left[\frac{a \operatorname{Re}(m_{nl})}{2} + \frac{nl\pi^2 \operatorname{Re}(m_{nl})(\mu^2 + 4\beta^2)}{2} \right]^2 + \left[\frac{a \operatorname{Im}(m_{nl})}{2} + \frac{nl\pi^2 \operatorname{Im}(m_{nl})(\mu^2 + 4\beta^2)}{2} \right]^2 = 0 \quad (5.39)$$

For linear problems, β which is the parameter determining if the solution is stable, should satisfy the following equation

$$\frac{a}{2} + \frac{n l \pi^2 (\mu^2 + 4\beta^2)}{\frac{a}{2} (\operatorname{Re}(m_{nl})^2 + \operatorname{Im}(m_{nl})^2)} = 0 \quad (5.40)$$

It follows from equation (5.40) that β must be pure imaginary. Therefore, for difference resonance of linear system, the trivial solution is always stable.

5.2 STABILITY OF NON-TRIVIAL LIMIT CYCLES

The stability of the non-trivial limit cycles is determined by the corresponding Jacobian Matrix of the system. For nonlinear elastic systems, Mockensturm *et al.* (1996) used KBM approximation to obtain a closed-form expression for stability boundary of non-trivial limit cycles that exist around the principal parametric instability regions. In this study, the stability boundary of resonances of any arbitrary two modes is derived for viscoelastic systems.

5.2.1 Jacobian Matrix

As given in Chapter 4, the equations of amplitudes α_n and α_l for non-trivial limit cycles and the corresponding phase angle θ are obtained using the method of multiple scales as

$$\alpha'_n = \frac{E_v \omega_n m_{2n}}{4n\pi} \alpha_n^3 + \frac{a\alpha_l}{4n\pi} [\cos\theta \operatorname{Im}(m_{nl}) + \sin\theta \operatorname{Re}(m_{nl})] \quad (5.41)$$

$$\alpha'_l = \frac{E_v \omega_l m_{2l}}{4l\pi} \alpha_l^3 + \frac{a\alpha_n}{4l\pi} [\cos\theta \operatorname{Im}(m_{nl}) + \sin\theta \operatorname{Re}(m_{nl})] \quad (5.42)$$

$$\theta' = \mu + \frac{3E_e m_{2n} \alpha_n^2}{8n\pi} + \frac{3E_e m_{2l} \alpha_l^2}{8l\pi} + (\cos \theta \operatorname{Re}(m_{nl}) - \sin \theta \operatorname{Im}(m_{nl})) \left(\frac{a\alpha_l}{4n\pi\alpha_n} + \frac{a\alpha_n}{4l\pi\alpha_l} \right) \quad (5.43)$$

In order to analyze the stability of steady state solutions of α_{n0} , α_{l0} , and θ_0 , introduce small variations ε_{α_n} , ε_{α_l} , and ε_θ as

$$\alpha_n = \alpha_{n0} + \varepsilon_{\alpha_n} \quad (5.44)$$

$$\alpha_l = \alpha_{l0} + \varepsilon_{\alpha_l} \quad (5.45)$$

$$\theta = \theta_0 + \varepsilon_\theta \quad (5.46)$$

Note that $\alpha'_{n0} = 0$, $\alpha'_{l0} = 0$, and $\theta'_0 = 0$ for steady state solutions.

Substituting expressions (5.44) – (5.46) into equations (5.41) – (5.43) and linearizing the resulting equations, the following relations are obtained

$$\begin{aligned} \varepsilon'_{\alpha_n} &= \frac{3E_v \omega_n m_{2n} \alpha_{n0}^2}{4n\pi} \varepsilon_{\alpha_n} + \frac{a[\cos \theta_0 \operatorname{Im}(m_{nl}) + \sin \theta_0 \operatorname{Re}(m_{nl})]}{4n\pi} \varepsilon_\theta, \\ &\quad + \frac{a\alpha_{l0}[-\sin \theta_0 \operatorname{Im}(m_{nl}) + \cos \theta_0 \operatorname{Re}(m_{nl})]}{4n\pi} \varepsilon_\theta \end{aligned} \quad (5.47)$$

$$\begin{aligned} \varepsilon'_{\alpha_l} &= \frac{a[\cos \theta_0 \operatorname{Im}(m_{nl}) + \sin \theta_0 \operatorname{Re}(m_{nl})]}{4l\pi} \varepsilon_{\alpha_n} + \frac{3E_v \omega_l m_{2l} \alpha_{l0}^2}{4l\pi} \varepsilon_{\alpha_l}, \\ &\quad + \frac{a\alpha_{n0}[-\sin \theta_0 \operatorname{Im}(m_{nl}) + \cos \theta_0 \operatorname{Re}(m_{nl})]}{4l\pi} \varepsilon_\theta \end{aligned} \quad (5.48)$$

$$\begin{aligned} \varepsilon'_\theta &= \left[\frac{3E_e m_{2n} \alpha_{n0}}{4n\pi} + (\cos \theta_0 \operatorname{Re}(m_{nl}) - \sin \theta_0 \operatorname{Im}(m_{nl})) \left(\frac{a}{4l\pi\alpha_{l0}} - \frac{a\alpha_{l0}}{4n\pi\alpha_{n0}^2} \right) \right] \varepsilon_{\alpha_n} \\ &\quad + \left[\frac{3E_e m_{2l} \alpha_{l0}}{4l\pi} + (\cos \theta_0 \operatorname{Re}(m_{nl}) - \sin \theta_0 \operatorname{Im}(m_{nl})) \left(\frac{a}{4n\pi\alpha_{n0}} - \frac{a\alpha_{n0}}{4l\pi\alpha_{l0}^2} \right) \right] \varepsilon_{\alpha_l} \\ &\quad - (\sin \theta_0 \operatorname{Re}(m_{nl}) + \cos \theta_0 \operatorname{Im}(m_{nl})) \left(\frac{a\alpha_{l0}}{4n\pi\alpha_{n0}} + \frac{a\alpha_{n0}}{4l\pi\alpha_{l0}} \right) \varepsilon_\theta \end{aligned} \quad (5.49)$$

To avoid the complexity of evaluating θ_0 , it is necessary to express those terms relating to θ_0 in terms of α_{n0} and α_{l0} . This can be accomplished by setting $\alpha'_{n0} = 0$, $\alpha'_{l0} = 0$, and $\theta'_0 = 0$ in equations (5.41) - (5.43) and rearranging the resulting equations as

$$\frac{a[\cos\theta_0 \operatorname{Im}(m_{nl}) + \sin\theta_0 \operatorname{Re}(m_{nl})]}{4n\pi} = -\frac{E_v \omega_n m_{2n} \alpha_{n0}^3}{4n\pi \alpha_{l0}} \quad (5.50)$$

$$\frac{a[\cos\theta_0 \operatorname{Im}(m_{nl}) + \sin\theta_0 \operatorname{Re}(m_{nl})]}{4l\pi} = -\frac{E_v \omega_l m_{2l} \alpha_{l0}^3}{4l\pi \alpha_{n0}} \quad (5.51)$$

$$\begin{aligned} g &= \cos\theta_0 \operatorname{Re}(m_{nl}) - \sin\theta_0 \operatorname{Im}(m_{nl}) \\ &= -\frac{4nl\pi\alpha_{l0}\alpha_{n0} \left(\mu + \frac{3E_e m_{2n} \alpha_{n0}^2}{8n\pi} + \frac{3E_e m_{2l} \alpha_{l0}^2}{8l\pi} \right)}{al\alpha_{l0}^2 + an\alpha_{n0}^2} \end{aligned} \quad (5.52)$$

Substitution of equations (5.50) - (5.52) into (5.47) - (5.49) results in equations for perturbed motions with coefficients matrix expressed in terms of α_{n0} and α_{l0} as

$$\begin{bmatrix} \varepsilon'_{a_n} \\ \varepsilon'_{a_l} \\ \varepsilon'_{\theta} \end{bmatrix} = \mathbf{H} \begin{bmatrix} \varepsilon_{a_n} \\ \varepsilon_{a_l} \\ \varepsilon_{\theta} \end{bmatrix} \quad (5.53)$$

where

$$\mathbf{H} = \begin{bmatrix} \frac{3E_v \omega_n m_{2n} \alpha_{n0}^2}{4n\pi} & -\frac{E_v \omega_n m_{2n} \alpha_{n0}^3}{4n\pi \alpha_{l0}} & \frac{a\alpha_{l0}g}{4n\pi} \\ -\frac{E_v \omega_l m_{2l} \alpha_{l0}^3}{4l\pi \alpha_{n0}} & \frac{3E_v \omega_l m_{2l} \alpha_{l0}^2}{4l\pi} & \frac{a\alpha_{n0}g}{4l\pi} \\ \frac{3E_e m_{2n} \alpha_{n0}}{4n\pi} + g \left(\frac{a}{4l\pi \alpha_{l0}} - \frac{a\alpha_{l0}}{4n\pi \alpha_{n0}^2} \right) & \frac{3E_e m_{2l} \alpha_{l0}}{4l\pi} + g \left(\frac{a}{4n\pi \alpha_{n0}} - \frac{a\alpha_{n0}}{4l\pi \alpha_{l0}^2} \right) & \frac{E_v \omega_n m_{2n} \alpha_{n0}^2}{4n\pi} + \frac{E_v \omega_l m_{2l} \alpha_{l0}^2}{4l\pi} \end{bmatrix} \quad (5.54)$$

5.2.2 Routh-Hurwitz Criterion

Stability of the non-trivial limit cycles is now decided by the nature of the eigenvalues of Jacobian matrix \mathbf{H} . If all the eigenvalues have negative real parts, the steady state solutions are stable. On the other hand, if the real part of at least one of the eigenvalues is positive, the corresponding steady state solution is unstable. By the use of Routh-Hurwitz criterion the stability conditions can be determined as

$$h_1 < 0 \quad (5.55)$$

$$h_2 > 0 \quad (5.56)$$

$$h_3 < 0 \quad (5.57)$$

$$h_4 < 0 \quad (5.58)$$

where

$$h_1 = H(1,1) + H(2,2) + H(3,3) \quad (5.59)$$

$$h_2 = \begin{vmatrix} H(1,1) & H(1,2) \\ H(2,1) & H(2,2) \end{vmatrix} + \begin{vmatrix} H(1,1) & H(1,3) \\ H(3,1) & H(3,3) \end{vmatrix} + \begin{vmatrix} H(2,2) & H(2,3) \\ H(3,2) & H(3,3) \end{vmatrix} \quad (5.60)$$

$$h_3 = |\mathbf{H}| \quad (5.61)$$

$$h_4 = h_1 h_2 - h_3 \quad (5.62)$$

and $| |$ denotes the determinant of a matrix.

It should be noted that if $h_1 < 0$, $h_3 < 0$ and $h_4 < 0$, then h_2 is always greater than zero. Thus, $h_1 < 0$, $h_3 < 0$ and $h_4 < 0$ are the sufficient conditions that the steady state is stable. However, if $h_1 = 0$, then $h_2 > 0$ must be considered for the stability analysis.

5.2.3 Simplification of h_1 , h_2 , h_3 and h_4

Substituting the expression of matrix \mathbf{H} in equation (5.54) into equations (5.59) and (5.60), and performing algebraic manipulations result in

$$h_1 = \frac{E_v \omega_n m_{2n} \alpha_{n0}^2}{n\pi} + \frac{E_v \omega_l m_{2l} \alpha_{l0}^2}{l\pi} \quad (5.63)$$

$$\begin{aligned} h_2 &= \frac{E_v^2 \omega_n \omega_l m_{2n} m_{2l} \alpha_{n0}^2 \alpha_{l0}^2}{2nl\pi^2} + 3 \left(\frac{E_v \omega_n m_{2n} \alpha_{n0}^2}{4n\pi} + \frac{E_v \omega_l m_{2l} \alpha_{l0}^2}{4l\pi} \right)^2 \\ &\quad + a^2 g^2 \left(\frac{\alpha_{n0}}{4l\pi\alpha_{l0}} - \frac{\alpha_{l0}}{4n\pi\alpha_{n0}} \right)^2 - \frac{3E_e m_{2l} \alpha_{n0} \alpha_{l0} ag}{16l^2\pi^2} - \frac{3E_e m_{2n} \alpha_{n0} \alpha_{l0} ag}{16n^2\pi^2} \end{aligned} \quad (5.64)$$

The main difficulty in the stability analysis of non-trivial limit cycles lies on how to evaluate h_3 and h_4 . In this section, the main procedure in evaluating h_3 and h_4 is shown in the following.

Substituting equation (5.54) into (5.61), the determinant h_3 of matrix \mathbf{H} can be obtained as follows

$$\begin{aligned} h_3 &= \left(\frac{E_v \omega_n m_{2n} \alpha_{n0}^2}{4n\pi} + \frac{E_v \omega_l m_{2l} \alpha_{l0}^2}{4l\pi} \right) \frac{E_v^2 \omega_n \omega_l m_{2n} m_{2l} \alpha_{n0}^2 \alpha_{l0}^2}{2nl\pi^2} \\ &\quad - \frac{a\alpha_{n0}g}{4l\pi} \left\{ \frac{3E_v \omega_n m_{2n} \alpha_{n0}^2}{4n\pi} \left[\frac{3E_e m_{2l} \alpha_{l0}}{4l\pi} + g \left(\frac{a}{4n\pi\alpha_{n0}} - \frac{a\alpha_{n0}}{4l\pi\alpha_{l0}^2} \right) \right] \right. \\ &\quad \left. + \frac{E_v \omega_n m_{2n} \alpha_{n0}^3}{4n\pi\alpha_{l0}} \left[\frac{3E_e m_{2n} \alpha_{n0}}{4n\pi} + g \left(\frac{a}{4l\pi\alpha_{l0}} - \frac{a\alpha_{l0}}{4n\pi\alpha_{n0}^2} \right) \right] \right\} \\ &\quad + \frac{a\alpha_{l0}g}{4n\pi} \left\{ \frac{-E_v \omega_l m_{2l} \alpha_{l0}^3}{4l\pi\alpha_{n0}} \left[\frac{3E_e m_{2l} \alpha_{l0}}{4l\pi} + g \left(\frac{a}{4n\pi\alpha_{n0}} - \frac{a\alpha_{n0}}{4l\pi\alpha_{l0}^2} \right) \right] \right. \\ &\quad \left. - \frac{3E_v \omega_l m_{2l} \alpha_{l0}^2}{4l\pi} \left[\frac{3E_e m_{2n} \alpha_{n0}}{4n\pi} + g \left(\frac{a}{4l\pi\alpha_{l0}} - \frac{a\alpha_{l0}}{4n\pi\alpha_{n0}^2} \right) \right] \right\} \end{aligned} \quad (5.65)$$

Using the relation between α_{n0} and α_{l0} , i.e., $\frac{\omega_n m_{2n} \alpha_{n0}^3}{\omega_l m_{2l} \alpha_{l0}^3} = \frac{\alpha_{l0}}{\alpha_{n0}}$, and performing algebraic manipulations, the following relation can be obtained

$$\begin{aligned} & -\frac{a\alpha_{n0}}{4l\pi} \left[\frac{3E_v \omega_n m_{2n} \alpha_{n0}^2}{4n\pi} \left(\frac{a}{4n\pi\alpha_{n0}} - \frac{a\alpha_{n0}}{4l\pi\alpha_{l0}^2} \right) + \frac{E_v \omega_n m_{2n} \alpha_{n0}^3}{4n\pi\alpha_{l0}} \left(\frac{a}{4l\pi\alpha_{l0}} - \frac{a\alpha_{l0}}{4n\pi\alpha_{n0}^2} \right) \right] g^2 \\ & -\frac{a\alpha_{l0}}{4n\pi} \left[\frac{3E_v \omega_l m_{2l} \alpha_{l0}^2}{4l\pi} \left(\frac{a}{4l\pi\alpha_{l0}} - \frac{a\alpha_{l0}}{4n\pi\alpha_{n0}^2} \right) + \frac{E_v \omega_l m_{2l} \alpha_{l0}^3}{4l\pi\alpha_{n0}} \left(\frac{a}{4n\pi\alpha_{n0}} - \frac{a\alpha_{n0}}{4l\pi\alpha_{l0}^2} \right) \right] g^2 = 0 \end{aligned} \quad (5.66)$$

Substituting equation (5.66) into (5.65), h_3 can be rewritten as

$$\begin{aligned} h_3 = & \left(\frac{E_v \omega_n m_{2n} \alpha_{n0}^2}{4n\pi} + \frac{E_v \omega_l m_{2l} \alpha_{l0}^2}{4l\pi} \right) \frac{E_v^2 \omega_n \omega_l m_{2n} m_{2l} \alpha_{n0}^2 \alpha_{l0}^2}{2nl\pi^2} \\ & - \frac{3agE_c E_v \omega_n m_{2n} m_{2l} \alpha_{n0}^3 \alpha_{l0}}{16nl^2\pi^3} - \frac{3agE_c E_v \omega_l m_{2n} m_{2l} \alpha_{l0}^3 \alpha_{n0}}{16n^2l\pi^3} \end{aligned} \quad (5.67)$$

It is difficult to determine if h_3 is greater than zero from equation (5.67) directly. The expression of g in terms of the specific steady solution (the first limit cycle or the second limit cycle) must be obtained first. However, it would be too complicate to evaluate h_3 if substituting the expressions of α_{n0} and α_{l0} directly into the expression of g in equation (5.52) as well as equation (5.67). This difficulty can be overcome by using the following relation derived from equation (4.64) in Chapter 4

$$2c_1\alpha_{n0}^2 + c_2 = \pm\sqrt{c_2^2 - 4c_1c_3} \quad (5.68)$$

Inserting equations (4.71) and (4.72) into (5.68) yields

$$3aE_c g = -\frac{\left(\pm\sqrt{c_2^2 - 4c_1c_3} - 2E_v^2 \omega_n^2 m_{2n}^2 \alpha_{n0}^2 \frac{l^2}{n^2} \sqrt{\frac{l}{n}} \right) \left(\frac{\alpha_{l0}}{4n\pi\alpha_{n0}} + \frac{\alpha_{n0}}{4l\pi\alpha_{l0}} \right)}{\left(\frac{m_{2n}}{4n\pi} + \frac{m_{2l}n^2}{4l^3\pi} \sqrt{\frac{n}{l}} \right)} \quad (5.69)$$

Note that plus sign is selected for the first limit cycle and the minus sign is selected for the second limit cycle.

Substituting equation (5.69) into equation (5.67) results in

$$h_3 = \pm \frac{E_v m_{2n} m_{2l} \alpha_{n0}^2 \alpha_{l0}^2 \left(\frac{\alpha_{l0}}{4n\pi\alpha_{n0}} + \frac{\alpha_{n0}}{4l\pi\alpha_{l0}} \right) \left(\frac{\omega_n \alpha_{n0}}{l\alpha_{l0}} + \frac{\omega_l \alpha_{l0}}{n\alpha_{n0}} \right)}{4 \left(m_{2n} l + m_{2l} \frac{n^3}{l^2} \sqrt{\frac{n}{l}} \right) \pi^2} \sqrt{c_2^2 - 4c_1 c_3} \\ + \frac{E_v m_{2n} m_{2l} \alpha_{n0}^2 \alpha_{l0}^2}{4 \left(m_{2n} l + m_{2l} \frac{n^3}{l^2} \sqrt{\frac{n}{l}} \right) \pi} (a_1 + a_2) \quad (5.70)$$

where

$$a_1 = E_v \omega_n \omega_l \left(\frac{E_v \omega_n m_{2n} \alpha_{n0}^2}{4n\pi} + \frac{E_v \omega_l m_{2l} \alpha_{l0}^2}{4l\pi} \right) \left(\frac{2m_{2n}}{n} + \frac{2m_{2l} n^2}{l^3} \sqrt{\frac{n}{l}} \right) \quad (5.71)$$

$$a_2 = -2E_v \omega_n^2 m_{2n}^2 \alpha_{n0}^2 \frac{l^2}{n^2} \sqrt{\frac{l}{n}} \left(\frac{\alpha_{l0}}{4n\pi\alpha_{n0}} + \frac{\alpha_{n0}}{4l\pi\alpha_{l0}} \right) \left(\frac{\omega_n \alpha_{n0}}{l\alpha_{l0}} + \frac{\omega_l \alpha_{l0}}{n\alpha_{n0}} \right) \quad (5.72)$$

Substituting the relation between α_{n0} and α_{l0} into equation (5.71) leads to

$$a_1 = 2E_v^2 m_{2n}^2 \omega_n^2 \omega_l \alpha_{n0}^2 \left(\frac{1}{4n^2\pi} + \frac{1}{4n^2\pi} \sqrt{\frac{l}{n}} + \frac{l}{4n^3\pi} \sqrt{\frac{l}{n}} + \frac{l^2}{4n^4\pi} \right) \quad (5.73)$$

Inserting the relation between α_{n0} and α_{l0} into equation (5.72) and performing complicate algebraic manipulation yields

$$a_2 = -2E_v^2 m_{2n}^2 \omega_n^2 \omega_l \alpha_{n0}^2 \left(\frac{1}{4n^2\pi} + \frac{1}{4n^2\pi} \sqrt{\frac{l}{n}} + \frac{l}{4n^3\pi} \sqrt{\frac{l}{n}} + \frac{l^2}{4n^4\pi} \right) \quad (5.74)$$

From equations (5.73) and (5.74), it is evident that $a_1 + a_2 = 0$. Therefore, the expression of h ,

can be simplified as

$$h_3 = \pm \frac{E_v m_{2n} m_{2l} \left(\frac{\alpha_{l0}}{4n\pi\alpha_{n0}} + \frac{\alpha_{n0}}{4l\pi\alpha_{l0}} \right) \left(\frac{\omega_n \alpha_{n0}}{l\alpha_{l0}} + \frac{\omega_l \alpha_{l0}}{n\alpha_{n0}} \right) \alpha_{n0}^2 \alpha_{l0}^2}{4 \left(m_{2n} l + m_{2l} \frac{n^3}{l^2} \sqrt{\frac{n}{l}} \right) \pi^2} \sqrt{c_2^2 - 4c_1 c_3} \quad (5.75)$$

where plus sign h_3 is selected for the first limit cycle and minus sign in h_3 is selected for the second limit cycle.

Substituting the expressions of h_1 , h_2 , and h_3 into equation (5.62), h_4 can be obtained as follows

$$\begin{aligned} h_4 &= 3 \left(\frac{E_v \omega_n m_{2n} \alpha_{n0}^2}{4n\pi} + \frac{E_v \omega_l m_{2l} \alpha_{l0}^2}{4l\pi} \right) \frac{E_v^2 \omega_n \omega_l m_{2n} m_{2l} \alpha_{n0}^2 \alpha_{l0}^2}{2nl\pi^2} \\ &\quad + 12 \left(\frac{E_v \omega_n m_{2n} \alpha_{n0}^2}{4n\pi} + \frac{E_v \omega_l m_{2l} \alpha_{l0}^2}{4l\pi} \right)^3 + \frac{3agE_v E_\epsilon \omega_n m_{2n}^2 \alpha_{n0}^3 \alpha_{l0}}{16n^3\pi^3} + \frac{3agE_v E_\epsilon \omega_l m_{2l}^2 \alpha_{l0}^3 \alpha_{n0}}{16l^3\pi^3} \\ &\quad + \left(\frac{E_v \omega_n m_{2n} \alpha_{n0}^2}{n\pi} + \frac{E_v \omega_l m_{2l} \alpha_{l0}^2}{l\pi} \right) a^2 g^2 \left(\frac{a}{4n\pi\alpha_{n0}} - \frac{a\alpha_{n0}}{4l\pi\alpha_{l0}^2} \right)^2 \end{aligned} \quad (5.76)$$

Substituting equation (5.69) into (5.76) results in

$$\begin{aligned} h_4 &= \frac{a_3}{\left(\frac{m_{2n}}{4n\pi} + \frac{m_{2l}}{4l\pi} \frac{n^2}{l^2} \sqrt{\frac{n}{l}} \right)} + \left(\frac{E_v \omega_n m_{2n} \alpha_{n0}^2}{n\pi} + \frac{E_v \omega_l m_{2l} \alpha_{l0}^2}{l\pi} \right) a^2 g^2 \left(\frac{\alpha_{n0}}{4l\pi\alpha_{l0}} - \frac{\alpha_{l0}}{4n\pi\alpha_{n0}} \right)^2 \\ &\quad \pm \frac{E_v \alpha_{n0}^2 \alpha_{l0}^2 m_{2n}^2 \omega_n}{16\pi^3 \left(\frac{m_{2n}}{4n\pi} + \frac{m_{2l}}{4l\pi} \frac{n^2}{l^2} \sqrt{\frac{n}{l}} \right)} \left(\frac{\alpha_{n0}}{n^3\alpha_{l0}} + \frac{\omega_l m_{2l}^2 \alpha_{l0}}{l^3 \omega_n m_{2n}^2 \alpha_{n0}} \right) \left(\frac{\alpha_{l0}}{4n\pi\alpha_{n0}} + \frac{\alpha_{n0}}{4l\pi\alpha_{l0}} \right) \sqrt{c_2^2 - 4c_1 c_3} \end{aligned} \quad (5.77)$$

where

$$\begin{aligned}
a_3 = & 3 \left(\frac{m_{2n}}{4n\pi} + \frac{m_{2l}}{4l\pi} \frac{n^2}{l^2} \sqrt{\frac{n}{l}} \right) \left(\frac{E_v \omega_n m_{2n} \alpha_{n0}^2}{4n\pi} + \frac{E_v \omega_l m_{2l} \alpha_{l0}^2}{4l\pi} \right) \frac{E_v^2 \omega_n \omega_l m_{2n} m_{2l} \alpha_{n0}^2 \alpha_{l0}^2}{2nl\pi^2} \\
& + 12 \left(\frac{m_{2n}}{4n\pi} + \frac{m_{2l}}{4l\pi} \frac{n^2}{l^2} \sqrt{\frac{n}{l}} \right) \left(\frac{E_v \omega_n m_{2n} \alpha_{n0}^2}{4n\pi} + \frac{E_v \omega_l m_{2l} \alpha_{l0}^2}{4l\pi} \right)^3 \\
& + \frac{E_v^3 \omega_n^3 m_{2n}^4 \alpha_{n0}^4 \alpha_{l0}^2}{32\pi^4} \left(\frac{\alpha_{n0}}{n^3 \alpha_{l0}} + \frac{l^6 \alpha_{l0}}{n^9 \alpha_{n0}} \right) \frac{l^2}{n^2} \sqrt{\frac{l}{n}} \left(\frac{\alpha_{l0}}{n \alpha_{n0}} + \frac{\alpha_{n0}}{l \alpha_{l0}} \right)
\end{aligned} \tag{5.78}$$

Using the relation between α_{n0} and α_{l0} , and performing complicate algebraic manipulation, a_3 can be rewritten as

$$a_3 = \frac{l^3 E_v^3 \omega_n^3 m_{2n}^4 \alpha_{n0}^4 \alpha_{l0}^2}{64n^7 \pi^4} \left(3 + \sqrt{\frac{n}{l}} + 15 \frac{l}{n} + 13 \frac{l^2}{n^2} \sqrt{\frac{n}{l}} + 13 \frac{l^3}{n^3} + 15 \frac{l^3}{n^3} \sqrt{\frac{n}{l}} + \frac{3l^4}{n^4} + \frac{l^5}{n^5} \sqrt{\frac{n}{l}} \right) \tag{5.79}$$

Substituting equation (5.79) into (5.77), the final form of h_3 can be obtained as

$$\begin{aligned}
h_3 = & \frac{\frac{l^3 E_v^3 \omega_n^3 m_{2n}^4 \alpha_{n0}^4 \alpha_{l0}^2}{64n^7 \pi^4} \left(3 + \sqrt{\frac{n}{l}} + 15 \frac{l}{n} + 13 \frac{l^2}{n^2} \sqrt{\frac{n}{l}} + 13 \frac{l^3}{n^3} + 15 \frac{l^3}{n^3} \sqrt{\frac{n}{l}} + \frac{3l^4}{n^4} + \frac{l^5}{n^5} \sqrt{\frac{n}{l}} \right)}{\left(\frac{m_{2n}}{4n\pi} + \frac{m_{2l}}{4l\pi} \frac{n^2}{l^2} \sqrt{\frac{n}{l}} \right)} \\
& + \left(\frac{E_v \omega_n m_{2n} \alpha_{n0}^2}{n\pi} + \frac{E_v \omega_l m_{2l} \alpha_{l0}^2}{l\pi} \right) a^2 g^2 \left(\frac{\alpha_{n0}}{4l\pi\alpha_{l0}} - \frac{\alpha_{l0}}{4n\pi\alpha_{n0}} \right)^2 \\
& \pm \frac{E_v \alpha_{n0}^2 \alpha_{l0}^2 m_{2n}^2 \omega_n}{16\pi^3} \left(\frac{\alpha_{n0}}{n^3 \alpha_{l0}} + \frac{\omega_l m_{2l}^2 \alpha_{l0}}{l^3 \omega_n m_{2n}^2 \alpha_{n0}} \right) \left(\frac{\alpha_{l0}}{4n\pi\alpha_{n0}} + \frac{\alpha_{n0}}{4l\pi\alpha_{l0}} \right) \sqrt{c_2^2 - 4c_1 c_3}
\end{aligned} \tag{5.80}$$

where plus sign is selected for the first limit cycle and minus sign is selected for the second limit cycle.

Based on equations (5.63), (5.64), (5.75), and (5.80) and the Routh-Hurwitz criterion, the stability of viscoelastic moving belts and elastic moving belts are examined, respectively, in the following.

5.2.4 Parametric Resonance of Viscoelastic Moving Belts

For viscoelastic moving belts, Since $m_{2n} < 0$ and $m_{2l} < 0$, it can be seen from equations (5.63), (5.75) and (5.80) that h_1 , h_3 and h_4 are always less than zero for the first limit cycle. Thus, the first limit cycle is always stable. It is also evident that h_3 is always greater than zero for the second limit cycle. Thus, the second amplitude limit cycle is always unstable.

Considering the existence condition of limit cycles given in Chapter 4, the following conclusions can be drawn for parametric resonance of viscoelastic moving belts

$$1) \text{ If } -\frac{\left(\frac{1}{l}\sqrt{\frac{n}{l}} + \frac{1}{n}\sqrt{\frac{l}{n}}\right)\sqrt{\operatorname{Im}(m_{nl})^2 + \operatorname{Re}(m_{nl})^2}}{4\pi} \leq \mu \leq \frac{\left(\frac{n}{l^2}\sqrt{\frac{n}{l}} + \frac{1}{l}\right)\sqrt{\operatorname{Im}(m_{nl})^2 + \operatorname{Re}(m_{nl})^2}c_1}{4\pi E_v \omega_n m_{2n}} a,$$

the first limit cycle exists and it is always stable.

$$2) \text{ If } \frac{\left(\frac{1}{l}\sqrt{\frac{n}{l}} + \frac{1}{n}\sqrt{\frac{l}{n}}\right)\sqrt{\operatorname{Im}(m_{nl})^2 + \operatorname{Re}(m_{nl})^2}}{4\pi} \leq \mu \leq \frac{\left(\frac{n}{l^2}\sqrt{\frac{n}{l}} + \frac{1}{l}\right)\sqrt{\operatorname{Im}(m_{nl})^2 + \operatorname{Re}(m_{nl})^2}c_1}{4\pi E_v \omega_n m_{2n}} a, \text{ the}$$

second limit cycle exists and it is always unstable.

It is noted that the lower boundaries of limit cycles do not coincide with the stability boundary of linear systems, which is quite different from corresponding elastic systems. The possible reason is that the viscoelastic model introduces material damping which will lead to vanish of limit cycles in some region. Therefore, for viscoelastic model, there exists an upper boundary and a lower boundary. In other words, viscoelasticity narrows the stable region for the first limit cycle and also narrows the unstable region for the second limit cycle. Since the second limit cycle is

always unstable, this corresponds to saddle point and therefore a motion which is unrealizable in either numerical or laboratory experiments.

5.2.5 Parametric Resonance of Elastic Moving Belts

For elastic moving belts, since $E_v = 0$, h_1 , h_3 , and h_4 are equal to zero. In this case, the limit cycles are stable if and only if $h_2 > 0$. Setting $E_v = 0$, h_2 can be rewritten as

$$h_2 = a^2 g^2 \left(\frac{\alpha_{n0}}{4l\pi\alpha_{l0}} - \frac{\alpha_{l0}}{4n\pi\alpha_{n0}} \right)^2 - \frac{3E_e m_{2l} \alpha_{n0} \alpha_{l0} a g}{16l^2 \pi^2} - \frac{3E_e m_{2n} \alpha_{n0} \alpha_{l0} a g}{16n^2 \pi^2} \quad (5.81)$$

For elastic parametric resonance, there exist the following relations

$$\alpha_l^2 = \frac{n}{l} \alpha_n^2 \quad (5.82)$$

$$g = \pm \sqrt{\operatorname{Re}(m_{nl})^2 + \operatorname{Im}(m_{nl})^2} \quad (5.83)$$

where plus sign is selected for the first limit cycle and minus sign is selected for the second limit cycle. Substituting equations (5.82) and (5.83) into (5.81) yields

$$h_2 = \pm \left(\frac{-3E_e m_{2l} \alpha_{n0} \alpha_{l0} a}{16l^2 \pi^2} - \frac{3E_e m_{2n} \alpha_{n0} \alpha_{l0} a}{16n^2 \pi^2} \right) \sqrt{\operatorname{Re}(m_{nl})^2 + \operatorname{Im}(m_{nl})^2} \quad (5.84)$$

It can be seen that $h_2 > 0$ for the first limit cycle while $h_2 < 0$ for the second limit cycle. This leads to the conclusion that the first limit cycle is always stable and the second limit cycle is always unstable for the parametric resonance of elastic moving belts.

Considering the existence condition of non-trivial limit cycles, the following conclusions can be drawn for parametric resonance of elastic moving belts:

1) If $\mu \geq -\frac{\sqrt{\text{Im}(m_{nl})^2 + \text{Re}(m_{nl})^2}}{2\sqrt{nl}\pi} a$, the first limit cycle exists and it is always stable.

2) If $\mu \geq \frac{\sqrt{\text{Im}(m_{nl})^2 + \text{Re}(m_{nl})^2}}{2\sqrt{nl}\pi} a$, the second limit cycle exists and it is always unstable.

Comparing with equation (5.26), it is suggested that the non-trivial limit cycle of summation parametric resonance of elastic systems bifurcates from the instability boundary of the trivial solution.

5.3 NUMERICAL RESULTS AND DISCUSSIONS

In this section, numerical results for the stability analysis of summation parametric resonance of moving belts are presented. Effects of the viscoelastic parameter, the amplitude of excitation, the frequency of excitation and the transport speed on stability boundaries of non-trivial limit cycles are discussed.

The stability boundaries of the trivial solution for the principal parametric resonances ($n=1, l=1$ and $n=2, l=2$) and the summation parametric resonance ($n=1, l=2$ and $n=1, l=3$) are plotted in Figure 5.1 to Figure 5.4 as a function of the transport speed, excitation amplitude and frequency (detuning). From Figure 5.2, it is seen that for the second mode principal parametric resonance, there are two translating speeds where the slopes are unbounded and the instability region closes altogether. The instability region reaches maximum when the transport speed γ approaches zero. As the translating speed grows, the instability region begins to close. The instability region widens with the increase of the excitation amplitude. From Figure 5.3 ($n=1, l=2$) and Figure 5.4

($n=1, l=3$), it is evident that the instability region almost closes when the transport speed is very small. As the transport speed γ increases, the instability becomes wider, reaches a maximum and closes as the translation speed increases to the critical speed.

The stability regions of the first non-trivial limit cycle and the second non-trivial limit cycle are illustrated in Figure 5.5 for summation parametric resonance ($n = 1, l = 2$) of a viscoelastic moving belt. Three different values of E_v , i.e. 10, 25, and 50, are chosen to show the effect of the viscoelastic property on the stability and instability regions. Since the first limit cycle is always stable while the second limit cycle is always unstable for viscoelastic materials, the stable (unstable) region of the first (second) limit cycle should be the same as the corresponding region of existence. It can be seen that the lower boundaries for different E_v are identical, while the upper boundaries are different for different E_v . The lower boundaries for the first and the second limit cycle have the same absolute value but opposite sign. The upper boundaries for the first and the second limit cycle with the same E_v are identical.

5.4 SUMMARY AND CONCLUSIONS

In this chapter, the dynamic stability of parametrically excited viscoelastic belts is investigated. The Routh-Hurwitz criterion is employed to investigate the stability of limit cycles. Closed-form expressions are found for the stability of limit cycles of the general summation parametric resonance of viscoelastic moving belts. The following conclusions are drawn in this study:

- 1) The first limit cycle is always stable for both viscoelastic and elastic parametric resonance.

- 2) The second limit cycle is unstable for both viscoelastic parametric resonance and for elastic parametric resonance.
- 3) The existence boundary of non-trivial limit cycles of elastic systems coincides with that of the stability boundary of the trivial limit cycle. For viscoelastic systems, however, the existence boundary of non-trivial limit cycles is different from the stability boundary of the trivial limit cycle.
- 4) Viscoelasticity leads to the upper boundary of existence for non-trivial limit cycles. This suggests that viscoelasticity narrows the stable region of the first limit cycle and the unstable region of the second limit cycle.
- 5) The translating speed, excitation frequency and excitation amplitude have significant influence on the stable and unstable region of limit cycles.

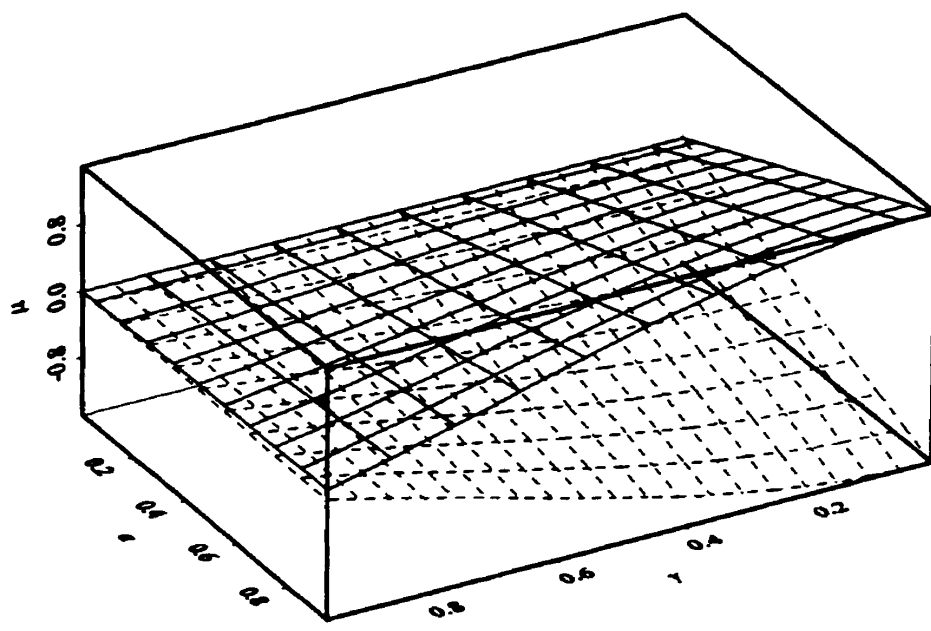


Figure 5.1: Stability boundaries of the trivial limit cycle for the first principal parametric resonance ($n=1, l=1, E_\epsilon = 400$)

— The upper boundary ----- The lower boundary

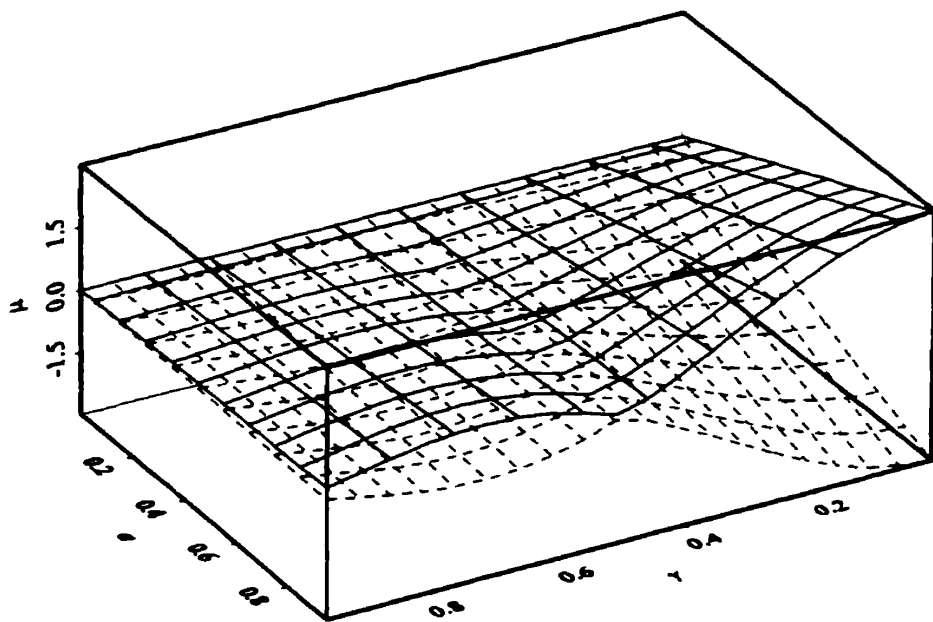


Figure 5.2: Stability boundaries of the trivial limit cycle for the second principal parametric resonance ($n=2, l=2, E_\epsilon = 400$)

— The upper boundary ----- The lower boundary

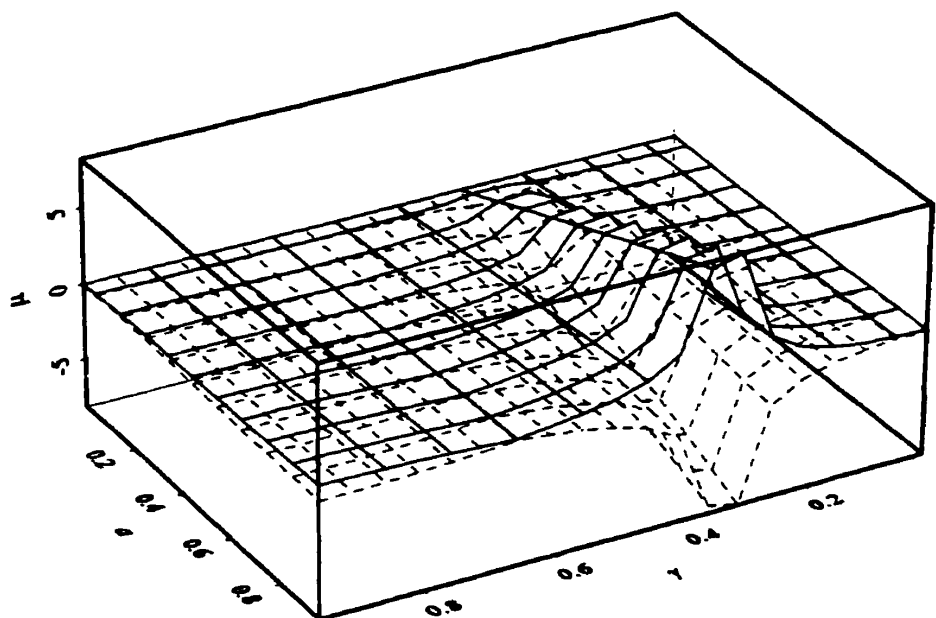


Figure 5.3: Stability boundaries of the trivial limit cycle for the summation parametric resonance ($n=1, l=2, E_c = 400$)

— The upper boundary ----- The lower boundary

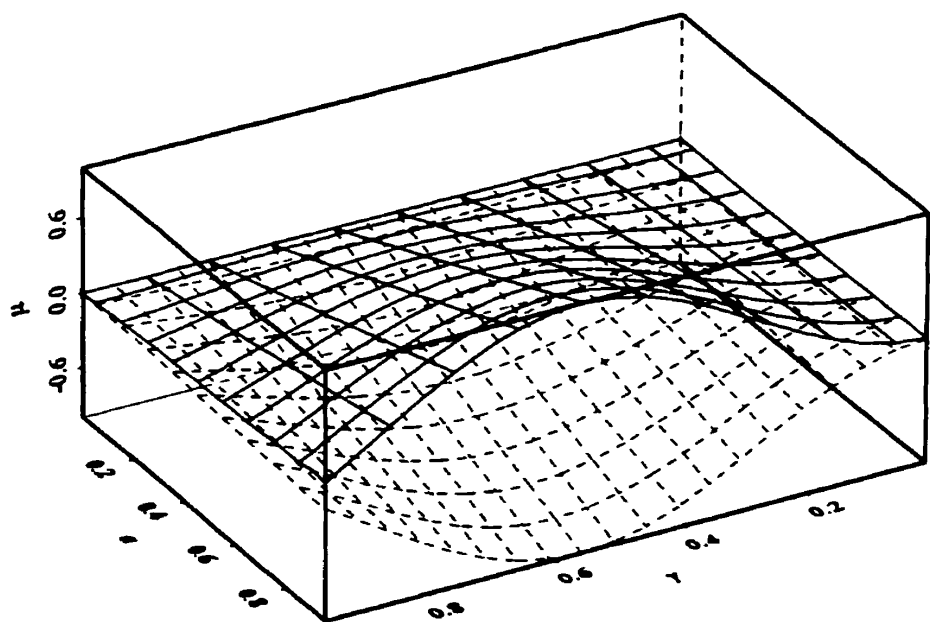


Figure 5.4: Stability boundaries of the trivial limit cycle for the summation parametric resonance ($n=1, l=3, E_c = 400$)

— The upper boundary ----- The lower boundary

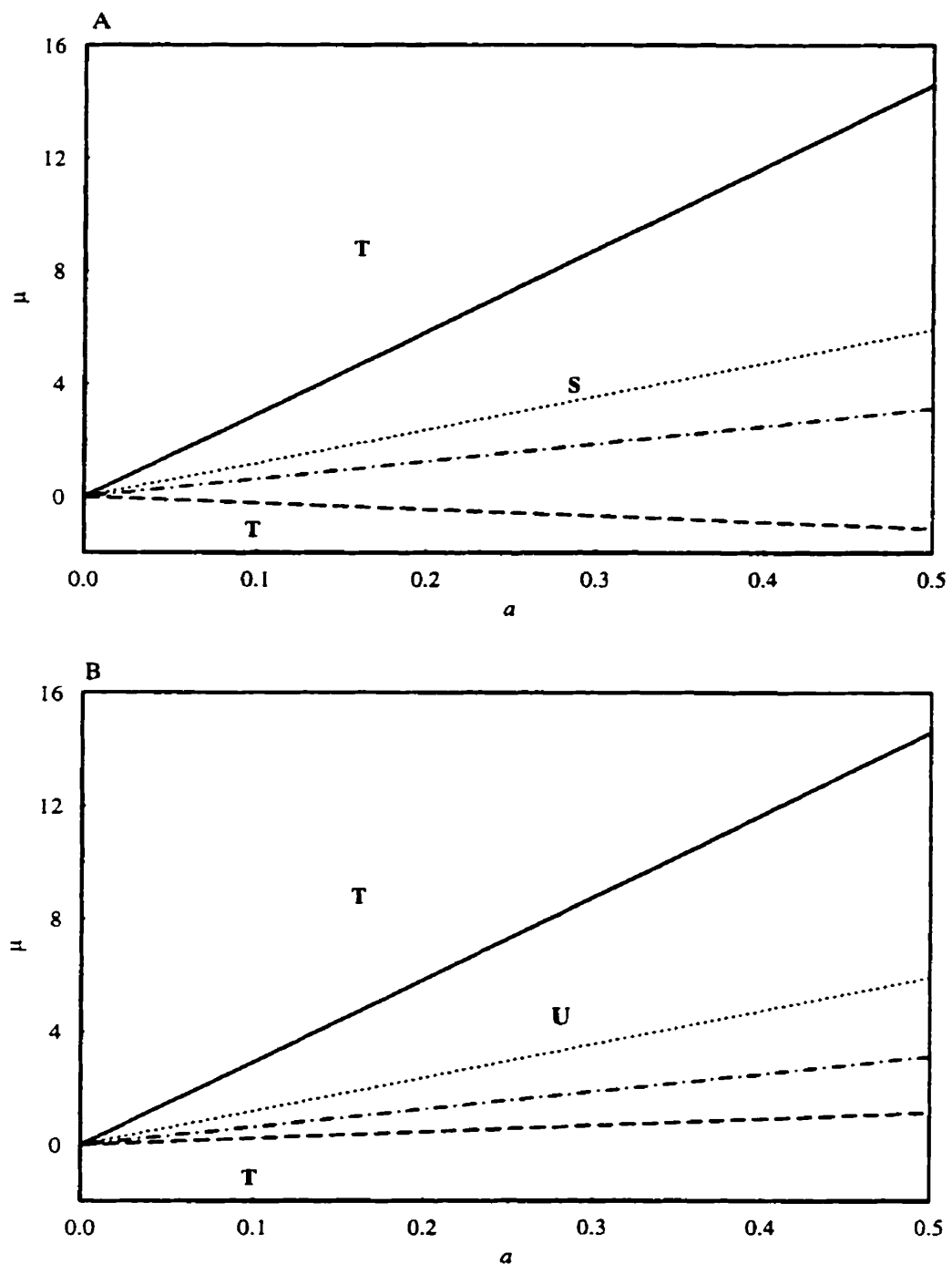


Figure 5.5: Effect of E_v on the stability boundary of nontrivial limit cycles for the first summation parametric resonance ($n=1, l=2, E_c = 400, \gamma = 0.25$)

A: First limit cycle B: Second limit cycle
 S: Stable region U: Unstable region T: Trivial Solution region
 — Upper boundary, $E_v = 10$ — Upper boundary, $E_v = 25$
 - - - Upper boundary, $E_v = 50$ - - - Lower boundary

CHAPTER 6

TRANSIENT RESPONSE OF MOVING BELTS WITH INTEGRAL VISCOELASTIC CONSTITUTIVE LAW

In Chapter 2 to Chapter 5, the free, forced and parametrical vibrations of Kelvin viscoelastic moving belts with the constant translating speed have been analyzed. For most of the belt materials, Kelvin viscoelastic model is accurate enough to describe the material property. However, for some materials such as plastics and composite materials, more sophisticated constitutive relations are needed to characterize the material properties. Furthermore, serpentine belt drives are often subject to accelerations and decelerations, during which the travelling speed is not constant but time dependent. Transient dynamic response must be considered in these cases. Thus, the objective of this chapter is to study the transient response of moving belts having more complicated viscoelastic property.

Coleman and Noll (1960) proved that simple isotropic material under small deformation can be represented by linear integral viscoelastic constitutive law. The integral types of viscoelastic relations are more widely used in recent years since they can represent more complicated material properties. Fung *et al.* (1997) investigated the dynamic response of an integral type of viscoelastic moving string. In their paper, the string material was assumed to be constituted by the hereditary integral type. The governing partial differential-integral equation of motion was reduced to a set of second order nonlinear differential-integral equations by applying Galerkin's

method. The stationary string eigenfunctions was chosen as the spatial distribution functions. The resulting equations were solved by the finite difference numerical integration procedure.

Wickert and Mote (1991), and Pakdemirli (1994) demonstrated that the usual choice of stationary string eigenfunctions has poorer convergence properties than travelling string eigenfunctions. Taking only one mode of travelling string eigenfunction yields comparable results with those of four modes of stationary string eigenfunctions. The convergence of travelling eigenfunctions is superior since the physics of the problem involves motion, which can be captured better through travelling eigenfunctions.

The current chapter employs the linear viscoelastic integral constitutive law to model the viscoelastic characteristic of belt materials. By assuming the translating eigenfunctions instead of stationary eigenfunctions to be the spatial solutions, the governing equation is reduced to differential-integral equations in time, which are then solved by the block-by-block method. The transient amplitudes of parametrically excited viscoelastic moving belts with uniform and non-uniform travelling speed are obtained. The effects of viscoelastic parameters and perturbed axial velocity on the system response are also investigated.

6.1 EQUATION OF MOTION

Consider that the viscoelastic string is in a state of uniform initial stress, and only the transverse vibration in the y direction is taken into consideration. The Lagrangian strain component in the x direction related to the transverse displacement is $\epsilon(x,t)=V_x^2(x,t)/2$. Thus, the equation of

motion in the y direction can be obtained by Newton's second law as

$$\left(\frac{T}{A} + \sigma\right)V_{xx} + V_x \sigma_x = \rho \left(\frac{\partial^2 V}{\partial t^2} + 2x_t \frac{\partial^2 V}{\partial x \partial t} + x_t^2 \frac{\partial^2 V}{\partial x^2} + x_{tt} \frac{\partial V}{\partial x} \right) \quad (6.1)$$

with boundary condition

$$V(0, t) = 0 \quad V(L, t) = 0 \quad (6.2)$$

where x_t and x_{tt} denote the translating velocity and acceleration of the moving belt and all the other quantities are defined in Chapter 2. Note that an extra term that related to the translating acceleration is added to the right side of equation (6.1) due to variation of the travelling speed.

For viscoelastic material, the stress-strain relation is given by the Boltzmann superposition principle

$$\sigma(x, t) = E_0 \epsilon(x, t) + \int_0^t \dot{E}(t - t') \epsilon(x, t') dt' \quad (6.3)$$

where $E(t)$ is the stress relaxation function while E_0 is its value at $t = 0$, i.e., the initial Young's modulus of the material.

Substituting equation (6.3) into equation (6.1) yields

$$\begin{aligned} \rho \frac{\partial^2 V}{\partial t^2} + 2\rho x_t \frac{\partial^2 V}{\partial t \partial x} + \left(\rho x_t^2 - \frac{T}{A} \right) \frac{\partial^2 V}{\partial x^2} &= -\rho x_{tt} \frac{\partial V}{\partial x} + \frac{3}{2} E_0 V_x^2 V_{xx} \\ &\quad + \frac{1}{2} V_{xx} \int_0^t \dot{E}(t - t') V_x^2 dt' + V_x \int_0^t \dot{E}(t - t') V_x V_{xx} dt' \end{aligned} \quad (6.4)$$

The nonlinear partial differential-integral equation (6.4) governs the dynamic behavior of the viscoelastic travelling belts. In the present study, it is assumed that the initial tension T is characterized as a small period perturbation $T_1 \cos \Omega t$ superimposed on the steady state tension

T_0 , i.e.,

$$T = T_0 + T_1 \cos \Omega t \quad (6.5)$$

Introduce the following non-dimensional parameters

$$\begin{aligned} v &= \frac{V}{L} & \xi &= \frac{x}{L} & \tau &= t \left(\frac{T}{\rho A L^2} \right)^{\frac{1}{2}} & \bar{E}(t-\tau) &= E(t-\tau)A/T_0 \\ a &= \frac{T_1}{T_0} & \omega &= \Omega \sqrt{\frac{\rho A L^2}{T_0}} & k_1 &= \sqrt{\frac{E_0 T_0}{A}} \end{aligned} \quad (6.6)$$

The non-dimensional equation of transverse motion can be obtained

$$\frac{\partial^2 v}{\partial \tau^2} + 2\xi \tau \frac{\partial^2 v}{\partial \tau \partial \xi} + (\xi^2 - 1) \frac{\partial^2 v}{\partial \xi^2} = \frac{\partial^2 v}{\partial \xi^2} a \cos \omega \tau - \xi \pi \frac{\partial v}{\partial \xi} + N(v) \quad (6.7)$$

where the nonlinear operator $N(v)$ is defined as

$$N(v) = \frac{3}{2} k_1^2 v_\xi^2 v_{\xi\xi} - \frac{1}{2} v_{\xi\xi} \int_0^\tau \frac{\partial \bar{E}(\tau - \tau')}{\partial \tau'} v_\xi^2 d\tau' - v_\xi \int_0^\tau \frac{\partial \bar{E}(\tau - \tau')}{\partial \tau'} v_\xi v_{\xi\xi} d\tau' \quad (6.8)$$

In many studies of axial moving materials, the axial velocity is considered to be constant. However, when a system is subjected to acceleration, the dynamics of the system may be changed. Pakdemirli *et al.* (1994) analyzed the stability of an axial accelerating linear elastic string using multiple scales method. In this study, the transient response of non-uniform travelling viscoelastic belts is calculated numerically. Assume the velocity of moving belts to have a small harmonic variation about a non-dimensional mean velocity γ_0 as follows:

$$\xi_\tau = \gamma_0 + \gamma_1 \sin \omega_0 \tau \quad (6.9)$$

where γ_1 is the amplitude of the perturbed axial velocity and ω_0 is the frequency of the perturbed velocity. This model better represents many real systems, since small variations in the

velocity are likely occur in many applications.

Using the following relations derived from equation (6.9)

$$\xi_\pi = \gamma_1 \omega_0 \cos \omega_0 \tau \quad (6.10)$$

$$\xi_\tau^2 = \gamma_0^2 + 2\gamma_0 \gamma_1 \sin \omega_0 \tau + \frac{\gamma_1^2 (1 - \cos 2\omega_0 \tau)}{2} \quad (6.11)$$

and substituting equations (6.9) – (6.11) into equation (6.7) result in

$$\begin{aligned} \frac{\partial^2 v}{\partial \tau^2} + 2\gamma_0 \frac{\partial^2 v}{\partial \tau \partial \xi} + (\gamma_0^2 - 1) \frac{\partial^2 v}{\partial \xi^2} &= \frac{\partial^2 v}{\partial \xi^2} a \cos \omega \tau - \gamma_1 \omega_0 \cos \omega_0 \tau \frac{\partial v}{\partial \xi} \\ &\quad - 2\gamma_1 \sin \omega_0 \tau \frac{\partial^2 v}{\partial \tau \partial \xi} - \left(2\gamma_0 \gamma_1 \sin \omega_0 \tau + \frac{\gamma_1^2 (1 - \cos 2\omega_0 \tau)}{2} \right) \frac{\partial^2 v}{\partial \xi^2} + N(v) \end{aligned} \quad (6.12)$$

It is noted that the time-dependent coefficients of equation (6.12) include $\sin \omega \tau$, $\sin \omega_0 \tau$, $\cos \omega_0 \tau$, and $\cos 2\omega_0 \tau$. Thus, the parametric excitation may occur at frequencies ω , ω_0 , or $2\omega_0$.

6.2 DISCRETIZATION APPROACH

In this section, the governing partial differential-integral equation is discretized using Galerkin procedure. By assuming the translating eigenfunctions of the linear problem to be the spatial solutions, the governing equation is reduced to an ordinary differential equation in time.

6.2.1 Canonical Form of Equation of Motion

Following Wickert and Mote (1990), the nonlinear differential equation (6.12) can be cast in the

canonical form

$$\mathbf{A}\dot{\mathbf{w}} + \mathbf{B}\mathbf{w} = \begin{bmatrix} N(v) \\ 0 \end{bmatrix} + a \cos \omega_0 \tau \begin{bmatrix} \frac{\partial^2 v}{\partial \xi^2} \\ 0 \end{bmatrix} - \gamma_1 \omega_0 \cos \omega_0 \tau \begin{bmatrix} \frac{\partial v}{\partial \xi} \\ 0 \end{bmatrix} - 2\gamma_1 \sin \omega_0 \tau \begin{bmatrix} \frac{\partial^2 v}{\partial \tau \partial \xi} \\ 0 \end{bmatrix} - \left(2\gamma_0 \gamma_1 \sin \omega_0 \tau + \frac{\gamma_1^2 (1 - \cos 2\omega_0 \tau)}{2} \right) \begin{bmatrix} \frac{\partial^2 v}{\partial \xi^2} \\ 0 \end{bmatrix} \quad (6.13)$$

where

$$\mathbf{w} = \begin{bmatrix} \dot{v} \\ v \end{bmatrix} \quad \mathbf{A} = \begin{bmatrix} 1 & 0 \\ 0 & (\gamma^2 - 1) \frac{\partial^2}{\partial \xi^2} \end{bmatrix} \quad \mathbf{B} = \begin{bmatrix} 2\gamma \frac{\partial}{\partial \xi} & (\gamma^2 - 1) \frac{\partial^2}{\partial \xi^2} \\ -(\gamma^2 - 1) \frac{\partial^2}{\partial \xi^2} & 0 \end{bmatrix} \quad (6.14)$$

The corresponding translating complex eigenfunctions have the structure

$$\Psi_k = \Psi_k^R + i\Psi_k^I \quad \Psi_k^R = \begin{Bmatrix} -\omega_k \phi_k' \\ \phi_k^R \end{Bmatrix} \quad \Psi_k^I = \begin{Bmatrix} \omega_k \phi_k^R \\ \phi_k' \end{Bmatrix} \quad (6.15)$$

6.2.2 Galerkin Discretization Using Translating Eigenfunctions

Consider the expansion

$$v = \sum_{n=1}^{\infty} (\eta_n^R \phi_n^R + \eta_n^I \phi_n^I) \quad \dot{v} = \sum_{n=1}^{\infty} (-\eta_n^R \omega_n \phi_n^I + \eta_n^I \omega_n \phi_n^R) \quad (6.16)$$

as the solution of equation (6.13). η_n^R and η_n^I are the real and imaginary components of the generalized coordinates. Substituting equation (6.16) into the equation (6.13) and using the orthogonality conditions yield the following equations of modal coordinates

$$\dot{\eta}_n^R - \omega_n \eta_n^R = q_n^R \quad (n = 1, 2, \dots) \quad (6.17)$$

$$\dot{\eta}_n^I + \omega_n \eta_n^R = q_n^I \quad (n = 1, 2, \dots) \quad (6.18)$$

where

$$q_n^R = -\omega_n \int_0^1 N(\nu) \phi_n' d\xi - \omega_n \int_0^1 \frac{\partial^2 \nu}{\partial \xi^2} \phi_n' d\xi a \cos \omega_0 \tau + \omega_n \gamma_1 \omega_0 \int_0^1 \frac{\partial \nu}{\partial \xi} \phi_n' d\xi \cos \omega_0 \tau \\ + 2\omega_n \gamma_1 \sin \omega_0 \tau \int_0^1 \frac{\partial \nu}{\partial \xi} \phi_n' d\xi + \omega_n \left(2\gamma_0 \gamma_1 \sin \omega_0 \tau + \frac{\gamma_1^2 (1 - \cos 2\omega_0 \tau)}{2} \right) \int_0^1 \frac{\partial^2 \nu}{\partial \xi^2} \phi_n' d\xi \quad (6.19)$$

$$q_n^R = \omega_n \int_0^1 N(\nu) \phi_n^R d\xi + \omega_n \int_0^1 \frac{\partial^2 \nu}{\partial \xi^2} \phi_n^R d\xi a \cos \omega_0 \tau - \omega_n \gamma_1 \omega_0 \int_0^1 \frac{\partial \nu}{\partial \xi} \phi_n^R d\xi \cos \omega_0 \tau \\ - 2\omega_n \gamma_1 \sin \omega_0 \tau \int_0^1 \frac{\partial \nu}{\partial \xi} \phi_n^R d\xi - \omega_n \left(2\gamma_0 \gamma_1 \sin \omega_0 \tau + \frac{\gamma_1^2 (1 - \cos 2\omega_0 \tau)}{2} \right) \int_0^1 \frac{\partial^2 \nu}{\partial \xi^2} \phi_n^R d\xi \quad (6.20)$$

Substituting equation (6.16) into equation (6.19) and performing algebraic manipulations yield

$$q_n^R = \left(a \cos \omega_0 \tau - 2\gamma_0 \gamma_1 \sin \omega_0 \tau - \frac{\gamma_1^2 (1 - \cos 2\omega_0 \tau)}{2} \right) \sum_{m=1}^{\infty} (A_{mn}^1 \eta_m^R + A_{mn}^2 \eta_m') \\ - \gamma_1 \omega_0 \cos \omega_0 \tau \sum_{m=1}^{\infty} (B_{mn}^1 \eta_m^R + B_{mn}^2 \eta_m') - 2\gamma_1 \sin \omega_0 \tau \sum_{m=1}^{\infty} \omega_m (-B_{mn}^2 \eta_m^R + B_{mn}^1 \eta_m') \\ + \frac{3}{2} k_1^2 \sum_{k=1}^{\infty} \sum_{l=1}^{\infty} \sum_{m=1}^{\infty} \left(C_{klmn}^1 \eta_k^R \eta_l^R \eta_m^R + C_{klmn}^2 \eta_k^R \eta_l^R \eta_m' + C_{klmn}^3 \eta_k^R \eta_l' \eta_m^R + \right. \\ \left. C_{klmn}^4 \eta_k^R \eta_l' \eta_m' + C_{klmn}^5 \eta_k' \eta_l' \eta_m^R + C_{klmn}^6 \eta_k' \eta_l' \eta_m' \right) \\ - \sum_{k=1}^{\infty} \sum_{l=1}^{\infty} \sum_{m=1}^{\infty} \left(D_{klmn}^1 \eta_k^R \int_0^{\tau} \frac{\partial}{\partial \tau'} \bar{E}(\tau - \tau') \eta_l^R \eta_m^R d\tau' + D_{klmn}^2 \eta_k' \int_0^{\tau} \frac{\partial}{\partial \tau'} \bar{E}(\tau - \tau') \eta_l^R \eta_m^R d\tau' \right) \\ - \sum_{k=1}^{\infty} \sum_{l=1}^{\infty} \sum_{m=1}^{\infty} \left(D_{klmn}^3 \eta_k^R \int_0^{\tau} \frac{\partial}{\partial \tau'} \bar{E}(\tau - \tau') \eta_l^R \eta_m' d\tau' + D_{klmn}^4 \eta_k' \int_0^{\tau} \frac{\partial}{\partial \tau'} \bar{E}(\tau - \tau') \eta_l^R \eta_m' d\tau' \right) \\ - \sum_{k=1}^{\infty} \sum_{l=1}^{\infty} \sum_{m=1}^{\infty} \left(D_{klmn}^5 \eta_k^R \int_0^{\tau} \frac{\partial}{\partial \tau'} \bar{E}(\tau - \tau') \eta_l' \eta_m' d\tau' + D_{klmn}^6 \eta_k' \int_0^{\tau} \frac{\partial}{\partial \tau'} \bar{E}(\tau - \tau') \eta_l' \eta_m' d\tau' \right) \quad (6.21)$$

where

$$A_{mn}^1 = -\omega_n \int_0^1 \frac{\partial^2 \phi_m^R}{\partial \xi^2} \phi_n' d\xi \quad (6.22)$$

$$A_{mn}^2 = -\omega_n \int_0^1 \frac{\partial^2 \phi_m'}{\partial \xi^2} \phi_n' d\xi \quad (6.23)$$

$$B_{mn}^1 = -\omega_n \int_0^1 \frac{\partial \phi_m^R}{\partial \xi} \phi'_n d\xi \quad (6.24)$$

$$B_{mn}^2 = -\omega_n \int_0^1 \frac{\partial \phi_m'}{\partial \xi} \phi'_n d\xi \quad (6.25)$$

$$C_{klmn}^1 = -\omega_n \int_0^1 \frac{\partial \phi_k^R}{\partial \xi} \frac{\partial \phi_l^R}{\partial \xi} \frac{\partial^2 \phi_m^R}{\partial \xi^2} \phi'_n d\xi \quad (6.26)$$

$$C_{klmn}^2 = -\omega_n \int_0^1 \frac{\partial \phi_k^R}{\partial \xi} \frac{\partial \phi_l^R}{\partial \xi} \frac{\partial^2 \phi_m'}{\partial \xi^2} \phi'_n d\xi \quad (6.27)$$

$$C_{klmn}^3 = -2\omega_n \int_0^1 \frac{\partial \phi_k^R}{\partial \xi} \frac{\partial \phi_l'}{\partial \xi} \frac{\partial^2 \phi_m^R}{\partial \xi^2} \phi'_n d\xi \quad (6.28)$$

$$C_{klmn}^4 = -2\omega_n \int_0^1 \frac{\partial \phi_k^R}{\partial \xi} \frac{\partial \phi_l'}{\partial \xi} \frac{\partial^2 \phi_m'}{\partial \xi^2} \phi'_n d\xi \quad (6.29)$$

$$C_{klmn}^5 = -\omega_n \int_0^1 \frac{\partial \phi_k'}{\partial \xi} \frac{\partial \phi_l'}{\partial \xi} \frac{\partial^2 \phi_m^R}{\partial \xi^2} \phi'_n d\xi \quad (6.30)$$

$$C_{klmn}^6 = -\omega_n \int_0^1 \frac{\partial \phi_k'}{\partial \xi} \frac{\partial \phi_l'}{\partial \xi} \frac{\partial^2 \phi_m'}{\partial \xi^2} \phi'_n d\xi \quad (6.31)$$

$$D_{klmn}^1 = \frac{C_{mlkn}^1}{2} + C_{klmn}^1 \quad (6.32)$$

$$D_{klmn}^2 = \frac{C_{mlkn}^2}{2} + \frac{C_{lkmn}^3}{2} \quad (6.33)$$

$$D_{klmn}^3 = \frac{C_{mlkn}^3}{2} + C_{klmn}^2 + \frac{C_{km\ln}^3}{2} \quad (6.34)$$

$$D_{klmn}^4 = \frac{C_{mlkn}^4}{2} + \frac{C_{lkmn}^4}{2} + C_{km\ln}^5 \quad (6.35)$$

$$D_{klmn}^5 = \frac{C_{mlkn}^5}{2} + C_{klmn}^4 \quad (6.36)$$

$$D_{klmn}^6 = \frac{C_{mlkn}^6}{2} + C_{klmn}^6 \quad (6.37)$$

Similarly, substituting equation (6.16) into equation (6.20) and performing algebraic manipulations yield

$$\begin{aligned} q_n' = & \left(a \cos \omega \tau - 2\gamma_0 \gamma_1 \sin \omega_0 \tau - \frac{\gamma_1^2 (1 - \cos 2\omega_0 \tau)}{2} \right) \sum_{m=1}^{\infty} (\bar{A}_{mn}^1 \eta_m^R + \bar{A}_{mn}^2 \eta_m^I) \\ & - \gamma_1 \omega_0 \cos \omega_0 \tau \sum_{m=1}^{\infty} (\bar{B}_{mn}^1 \eta_m^R + \bar{B}_{mn}^2 \eta_m^I) - 2\gamma_1 \sin \omega_0 \tau \sum_{m=1}^{\infty} \omega_m (-\bar{B}_{mn}^2 \eta_m^R + \bar{B}_{mn}^1 \eta_m^I) \\ & + \frac{3}{2} k_1^2 \sum_{k=1}^{\infty} \sum_{l=1}^{\infty} \sum_{m=1}^{\infty} \left(\bar{C}_{klmn}^1 \eta_k^R \eta_l^R \eta_m^R + \bar{C}_{klmn}^2 \eta_k^R \eta_l^R \eta_m^I + \bar{C}_{klmn}^3 \eta_k^R \eta_l^I \eta_m^R + \right. \\ & \left. \bar{C}_{klmn}^4 \eta_k^R \eta_l^I \eta_m^I + \bar{C}_{klmn}^5 \eta_k^I \eta_l^I \eta_m^R + \bar{C}_{klmn}^6 \eta_k^I \eta_l^I \eta_m^I \right) \\ & - \sum_{k=1}^{\infty} \sum_{l=1}^{\infty} \sum_{m=1}^{\infty} \left(\bar{D}_{klmn}^1 \eta_k^R \int_0^{\tau} \frac{\partial}{\partial \tau'} \bar{E}(\tau - \tau') \eta_l^R \eta_m^R d\tau' + \bar{D}_{klmn}^2 \eta_k^I \int_0^{\tau} \frac{\partial}{\partial \tau'} \bar{E}(\tau - \tau') \eta_l^R \eta_m^R d\tau' \right) \\ & - \sum_{k=1}^{\infty} \sum_{l=1}^{\infty} \sum_{m=1}^{\infty} \left(\bar{D}_{klmn}^3 \eta_k^R \int_0^{\tau} \frac{\partial}{\partial \tau'} \bar{E}(\tau - \tau') \eta_l^R \eta_m^I d\tau' + \bar{D}_{klmn}^4 \eta_k^I \int_0^{\tau} \frac{\partial}{\partial \tau'} \bar{E}(\tau - \tau') \eta_l^R \eta_m^I d\tau' \right) \\ & - \sum_{k=1}^{\infty} \sum_{l=1}^{\infty} \sum_{m=1}^{\infty} \left(\bar{D}_{klmn}^5 \eta_k^R \int_0^{\tau} \frac{\partial}{\partial \tau'} \bar{E}(\tau - \tau') \eta_l^I \eta_m^R d\tau' + \bar{D}_{klmn}^6 \eta_k^I \int_0^{\tau} \frac{\partial}{\partial \tau'} \bar{E}(\tau - \tau') \eta_l^I \eta_m^R d\tau' \right) \end{aligned} \quad (6.38)$$

where

$$\bar{A}_{mn}^1 = \omega_n \int_0^1 \frac{\partial^2 \phi_m^R}{\partial \xi^2} \phi_n^R d\xi \quad (6.39)$$

$$\bar{A}_{mn}^2 = \omega_n \int_0^1 \frac{\partial^2 \phi_m^I}{\partial \xi^2} \phi_n^R d\xi \quad (6.40)$$

$$\bar{B}_{mn}^1 = \omega_n \int_0^1 \frac{\partial \phi_m^R}{\partial \xi} \phi_n^R d\xi \quad (6.41)$$

$$\bar{B}_{mn}^2 = \omega_n \int_0^1 \frac{\partial \phi_m^I}{\partial \xi} \phi_n^R d\xi \quad (6.42)$$

$$\bar{C}_{klmn}^1 = \omega_n \int_0^1 \frac{\partial \phi_k^R}{\partial \xi} \frac{\partial \phi_l^R}{\partial \xi} \frac{\partial^2 \phi_m^R}{\partial \xi^2} \phi_n^R d\xi \quad (6.43)$$

$$\bar{C}_{klmn}^2 = \omega_n \int_0^1 \frac{\partial \phi_k^R}{\partial \xi} \frac{\partial \phi_l^R}{\partial \xi} \frac{\partial^2 \phi_m'}{\partial \xi^2} \phi_n^R d\xi \quad (6.44)$$

$$\bar{C}_{klmn}^3 = 2\omega_n \int_0^1 \frac{\partial \phi_k^R}{\partial \xi} \frac{\partial \phi_l'}{\partial \xi} \frac{\partial^2 \phi_m^R}{\partial \xi^2} \phi_n^R d\xi \quad (6.45)$$

$$\bar{C}_{klmn}^4 = 2\omega_n \int_0^1 \frac{\partial \phi_k^R}{\partial \xi} \frac{\partial \phi_l'}{\partial \xi} \frac{\partial^2 \phi_m'}{\partial \xi^2} \phi_n^R d\xi \quad (6.46)$$

$$\bar{C}_{klmn}^5 = \omega_n \int_0^1 \frac{\partial \phi_k'}{\partial \xi} \frac{\partial \phi_l'}{\partial \xi} \frac{\partial^2 \phi_m^R}{\partial \xi^2} \phi_n^R d\xi \quad (6.47)$$

$$\bar{C}_{klmn}^6 = \omega_n \int_0^1 \frac{\partial \phi_k'}{\partial \xi} \frac{\partial \phi_l'}{\partial \xi} \frac{\partial^2 \phi_m'}{\partial \xi^2} \phi_n^R d\xi \quad (6.48)$$

$$\bar{D}_{klmn}^1 = \frac{\bar{C}_{mlkn}^1}{2} + \bar{C}_{klmn}^1 \quad (6.49)$$

$$\bar{D}_{klmn}^2 = \frac{\bar{C}_{mlkn}^2}{2} + \frac{\bar{C}_{lknn}^3}{2} \quad (6.50)$$

$$\bar{D}_{klmn}^3 = \frac{\bar{C}_{mlkn}^3}{2} + \bar{C}_{klmn}^2 + \frac{\bar{C}_{km\ln}^3}{2} \quad (6.51)$$

$$\bar{D}_{klmn}^4 = \frac{\bar{C}_{mlkn}^4}{2} + \frac{\bar{C}_{lknn}^4}{2} + \bar{C}_{km\ln}^5 \quad (6.52)$$

$$\bar{D}_{klmn}^5 = \frac{\bar{C}_{mlkn}^5}{2} + \bar{C}_{klmn}^4 \quad (6.53)$$

$$\bar{D}_{klmn}^6 = \frac{\bar{C}_{mlkn}^6}{2} + \bar{C}_{klmn}^6 \quad (6.54)$$

6.3 BLOCK-BY-BLOCK METHOD

There exists great difficulty to solve the nonlinear differential-integral equations (6.17) and

(6.18) analytically. Thus, it is necessary to resort to numerical techniques. There are many alternative methods available such as finite difference integration, linear multistep method and block-by-block method.

Except for some relatively low order methods such as the trapezoidal method, most of the schemes require more starting values, which must be found in some other way. The block-by-block method (Linz, 1985) used in this study not only gives starting values but also provides a convenient and efficient way for solving the equations over the whole interval. The block-by-block method is a generalization of the well-known implicit Runge-Kutta method for ordinary differential equations.

To construct the block-by-block method, equations (6.17) and (6.18) are rewritten in general standard form of the differential-integral equations:

$$\eta'(t) = \mathbf{F}\left(t, \eta(t), \int_0^t \mathbf{K}(t, s, \eta(s))ds\right) \quad (6.55)$$

where

$$\eta(t) = \{\eta_1^R \quad \eta_1' \quad \dots \quad \eta_m^R \quad \eta_m'\} \quad (6.56)$$

and m is the numbers of mode used in the mode expansion.

For the time step $p > 1$, integrating equation (6.55) yields

$$\eta(t_{n+p}) = \eta(t_n) + \int_{t_n}^{t_{n+p}} \mathbf{F}(t, \eta(s), \mathbf{z}(s))ds \quad (6.57)$$

$$\mathbf{z}(t) = \int_0^t \mathbf{K}(t, s, \eta(s))ds \quad (6.58)$$

The block-by-block method is then formulated by appropriate combinations of numerical integration and interpolation. Using $p=1$ and $p=2$ in equation (6.57) and replacing the integral by appropriate Simpson's rule result in

$$\eta_{2n+1} = \eta_{2n} + \frac{h}{6} \{ \mathbf{F}(t_{2n}, \eta_{2n}, \mathbf{z}_{2n}) + 4\mathbf{F}(t_{2n+1/2}, \eta_{2n+1/2}, \mathbf{z}_{2n+1/2}) + \mathbf{F}(t_{2n+1}, \eta_{2n+1}, \mathbf{z}_{2n+1}) \} \quad (6.59)$$

$$\eta_{2n+2} = \eta_{2n} + \frac{h}{3} \{ \mathbf{F}(t_{2n}, \eta_{2n}, \mathbf{z}_{2n}) + 4\mathbf{F}(t_{2n+1}, \eta_{2n+1}, \mathbf{z}_{2n+1}) + \mathbf{F}(t_{2n+2}, \eta_{2n+2}, \mathbf{z}_{2n+2}) \} \quad (6.60)$$

where h is the time step of the integration and $t_{2n+1/2} = t_{2n} + h/2$.

\mathbf{z}_i is computed by applying Simpson's rule to equation (6.58)

$$\begin{aligned} \mathbf{z}_{2n+1} &= \frac{h}{3} \sum_{i=0}^{2n} w_i \mathbf{K}(t_{2n+1}, t_i, \eta_i) \\ &\quad + \frac{h}{6} \{ \mathbf{K}(t_{2n+1}, t_{2n}, \mathbf{z}_{2n}) + 4\mathbf{K}(t_{2n+1}, t_{2n+1/2}, \mathbf{z}_{2n+1/2}) + \mathbf{K}(t_{2n+1}, t_{2n+1}, \mathbf{z}_{2n+1}) \} \end{aligned} \quad (6.61)$$

$$\mathbf{z}_{2n+2} = \frac{h}{3} \sum_{i=0}^{2n+2} w_i \mathbf{K}(t_{2n+2}, t_i, \eta_i) \quad (6.62)$$

Here $\{w_i\}$ is the set of Simpson's rule weighs $\{1 \quad 4 \quad 2 \quad 4 \quad \dots \quad 4 \quad 2 \quad 4 \quad 1\}$. The extraneous values $\eta_{2n+1/2}$ and $\mathbf{z}_{2n+1/2}$ are approximated by quadratic interpolation as

$$\eta_{2n+1/2} = \frac{3}{8} \eta_{2n} + \frac{3}{4} \eta_{2n+1} - \frac{1}{8} \eta_{2n+2} \quad (6.63)$$

$$\mathbf{z}_{2n+1/2} = \frac{3}{8} \mathbf{z}_{2n} + \frac{3}{4} \mathbf{z}_{2n+1} - \frac{1}{8} \mathbf{z}_{2n+2} \quad (6.64)$$

Equations (6.59) – (6.64) constitute an implicit set of equations for η_{2n+1} and η_{2n+2} . Starting from the initial conditions, a block of two values η_{2n+1} and η_{2n+2} at each time step can be obtained. It

is proved that the block-by-block method has fourth order accuracy.

6.4 NUMERICAL RESULTS AND DISCUSSIONS

6.4.1 Three-element Viscoelastic Model

In order to study the trends of the nonlinear response, the belt material is considered as a three-element viscoelastic model shown in Figure 6.1. The constitutive law of the model is

$$\dot{\sigma} + \frac{E_1 + E_2}{\eta_2} \sigma = E_1 \dot{\epsilon} + \frac{E_1 E_2}{\eta_2} \epsilon \quad (6.65)$$

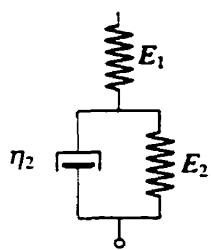


Figure 6.1: Three-element model of the viscoelastic belt material

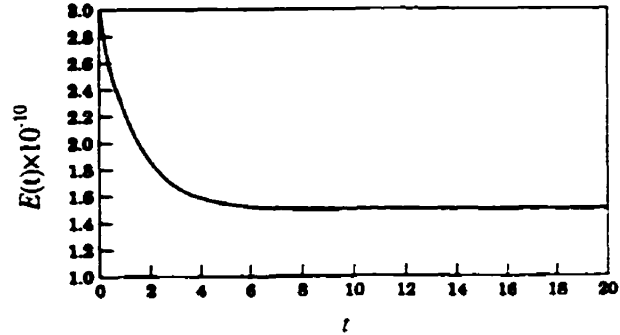


Figure 6.2: The relaxation modulus of the three-element model

This kind of model is the simplest spring-dashpot model that can simulate the behavior of linear viscoelastic materials of the solid type with limited creep deformations when E_2 is nonzero, and of the fluid type with unlimited viscous deformations for $E_2 = 0$. The stress relaxation function of the three-element model can be found from the constitutive law by applying Laplace transform and the inverse Laplace transform as

$$E(t) = \frac{E_1 E_2}{E_1 + E_2} + \frac{E_1^2}{E_1 + E_2} e^{-(E_1 + E_2)t/\eta_2} \quad (6.66)$$

and $E(0) = E_0 = E_1$. The value of $E_1 = E_2 = 3.0 \times 10^{10}$ Pa and $\eta_2 = 3 \times 10^8$ Pa days used here are from Fung *et al.* (1997). The plot of $E(t)$ is shown in Figure 6.2. The transient curve approaches a steady state value of $E_1/2$.

6.4.2 One Mode Expansion

Taking the one-mode shape approximation in equations (6.21) and (6.38) and using the definition of the non-dimensional parameter \bar{E} , q_n^R and q_n' can be reduced to

$$q_n^R = \left(a \cos \omega \tau - 2\gamma_0 \gamma_1 \sin \omega_0 \tau - \frac{\gamma_1^2 (1 - \cos 2\omega_0 \tau)}{2} \right) (A_n^1 \eta_n^R + A_n^2 \eta_n') + \\ - \gamma_1 \omega_0 \cos \omega_0 \tau (B_n^1 \eta_n^R + B_n^2 \eta_n') - 2\gamma_1 \sin \omega_0 \tau \omega_n (-B_n^2 \eta_n^R + B_n^1 \eta_n') \\ + \frac{3}{2} k_1^2 (C_n^1 (\eta_n^R)^3 + C_n^2 (\eta_n^R)^2 \eta_n' + C_n^3 \eta_n^R (\eta_n')^2 + C_n^4 (\eta_n')^3) \\ - (D_n^1 \eta_n^R + D_n^2 \eta_n') k_1^2 k_2 k_3 \int_0^\tau e^{-k_3(\tau-\tau')} (\eta_n^R)^2 d\tau' \\ - (D_n^3 \eta_n^R + D_n^4 \eta_n') k_1^2 k_2 k_3 \int_0^\tau e^{-k_3(\tau-\tau')} \eta_n^R \eta_n' d\tau' \\ - (D_n^5 \eta_n^R + D_n^6 \eta_n') k_1^2 k_2 k_3 \int_0^\tau e^{-k_3(\tau-\tau')} (\eta_n')^2 d\tau' \quad (6.67)$$

$$q_n^R = \left(a \cos \omega \tau - 2\gamma_0 \gamma_1 \sin \omega_0 \tau - \frac{\gamma_1^2 (1 - \cos 2\omega_0 \tau)}{2} \right) (\bar{A}_n^1 \eta_n^R + \bar{A}_n^2 \eta_n') + \\ - \gamma_1 \omega_0 \cos \omega_0 \tau (\bar{B}_n^1 \eta_n^R + \bar{B}_n^2 \eta_n') - 2\gamma_1 \sin \omega_0 \tau \omega_n (-\bar{B}_n^2 \eta_n^R + \bar{B}_n^1 \eta_n') \\ + \frac{3}{2} k_1^2 (\bar{C}_n^1 (\eta_n^R)^3 + \bar{C}_n^2 (\eta_n^R)^2 \eta_n' + \bar{C}_n^3 \eta_n^R (\eta_n')^2 + \bar{C}_n^4 (\eta_n')^3) \\ - (\bar{D}_n^1 \eta_n^R + \bar{D}_n^2 \eta_n') k_1^2 k_2 k_3 \int_0^\tau e^{-k_3(\tau-\tau')} (\eta_n^R)^2 d\tau' \\ - (\bar{D}_n^3 \eta_n^R + \bar{D}_n^4 \eta_n') k_1^2 k_2 k_3 \int_0^\tau e^{-k_3(\tau-\tau')} \eta_n^R \eta_n' d\tau' \\ - (\bar{D}_n^5 \eta_n^R + \bar{D}_n^6 \eta_n') k_1^2 k_2 k_3 \int_0^\tau e^{-k_3(\tau-\tau')} (\eta_n')^2 d\tau' \quad (6.68)$$

where

$$k_2 = \frac{E_1}{E_1 + E_2} \quad (6.69)$$

$$k_3 = \frac{E_1 + E_2}{\eta_2} \sqrt{\frac{\rho A}{T_0}} L \quad (6.70)$$

and all other coefficients can be calculated using equations (6.22) - (6.37) and equations (6.39) - (6.54). The parameter k_3 is a measure of the degree of viscoelasticity of the moving belts. The viscoelasticity increases while k_3 decreases. The case for k_3 approaching infinity corresponds to the elastic string system.

6.4.3 Transient Response of Viscoelastic Moving Belts

The influence of the material parameter k_3 on the transient amplitudes of free vibrations is shown in Figure 6.3. For the convenience of verifying the numerical results, all the parameters used here are from Fung *et al.* (1997). The initial tension T_0 is 100 N, the density of the material ρ is 7860 kg/m³, and the length of the span L is 1 m. The initial condition $\eta_i^R = 0.01$ and $\eta_i' = 0.0$ is used to integrate equations (6.17) and (6.18). It can be seen that the vibration frequency of the corresponding elastic moving belts is greater than that of the viscoelastic belts. This is because the damping introduced by viscoelasticity of the material generally leads to lower vibration frequency. It is observed that the vibration frequency decreases as the value of parameter k_3 increases. This conclusion agrees with the results by Fung *et al.* (1997).

The transient amplitudes of parametrically excited moving belt with constant travelling velocity are shown in Figure 6.4. The amplitude of excitation a is equal to 0.5 and the excitation frequency ω is equal to 6.0. Three different values of material parameter k_3 are considered here.

It is seen that the modal responses exhibit a typical beat phenomenon since the excitation frequency is near $2\omega_1$. Comparing the responses of different values of k_3 shows that the increase in k_3 leads to the increase in motion.

The transverse vibrations of an axial accelerating viscoelastic parameter are illustrated in Figure 6.5 and Figure 6.6. The steady state velocity γ_0 is equal to 0.5 and initial tension T_0 remains constant. In order to diverge rapidly in the transient amplitude, γ_1 is set to be the same order as γ_0 . In Figure 6.5, the frequency of the perturbed velocity is equal to $\pi(1 - \gamma_0^2)$. In Figure 6.6, the frequency of the perturbed velocity is equal to $2\pi(1 - \gamma_0^2)$. It is noted that the transient amplitudes increase with the growth of the amplitude of the perturbed axial velocity γ_1 . The parametric excitation occurs at both the frequencies ω_1 and $2\omega_1$. No beat phenomenon occurs when γ_1 is small. The critical γ_1 when parametrical resonance occurs for $\omega_0 = \pi(1 - \gamma_0^2)$ is greater than that for $\omega_0 = 2\pi(1 - \gamma_0^2)$.

6.5 SUMMARY AND CONCLUSIONS

The viscoelastic integral constitutive law can be used to characterize the complicated physical properties of some belt materials. Travelling eigenfunctions instead of stationary eigenfunctions are used to discretize the partial differential-integral equation governing the motion of moving belts. The resulting differential-integral equations are solved by the block-by-block method. The transient response of a viscoelastic moving belt with the constant and non-uniform axial velocities is calculated. The major conclusions of this study include:

- 1) The convergence of travelling eigenfunctions is superior to that of stationary eigenfunctions.
Usually, taking only one mode of travelling eigenfunctions yields very accurate results.
- 2) The block-by-block method is more accurate, convenient, and efficient to solve differential-integral equations than the finite difference method. This method can be applied to a wide range of problems with more complicated integral kernel.
- 3) The parametric resonance occurs at both frequencies ω_n and $2\omega_n$ for harmonic variation of the axially moving velocity. The critical γ_1 when parametrical resonance occurs at ω_n is greater than that at $2\omega_n$.
- 4) The damping introduced by the viscoelasticity of belt materials leads to the decrease of vibration frequencies. However, the vibration frequency does not decrease with an increasing viscoelasticity.

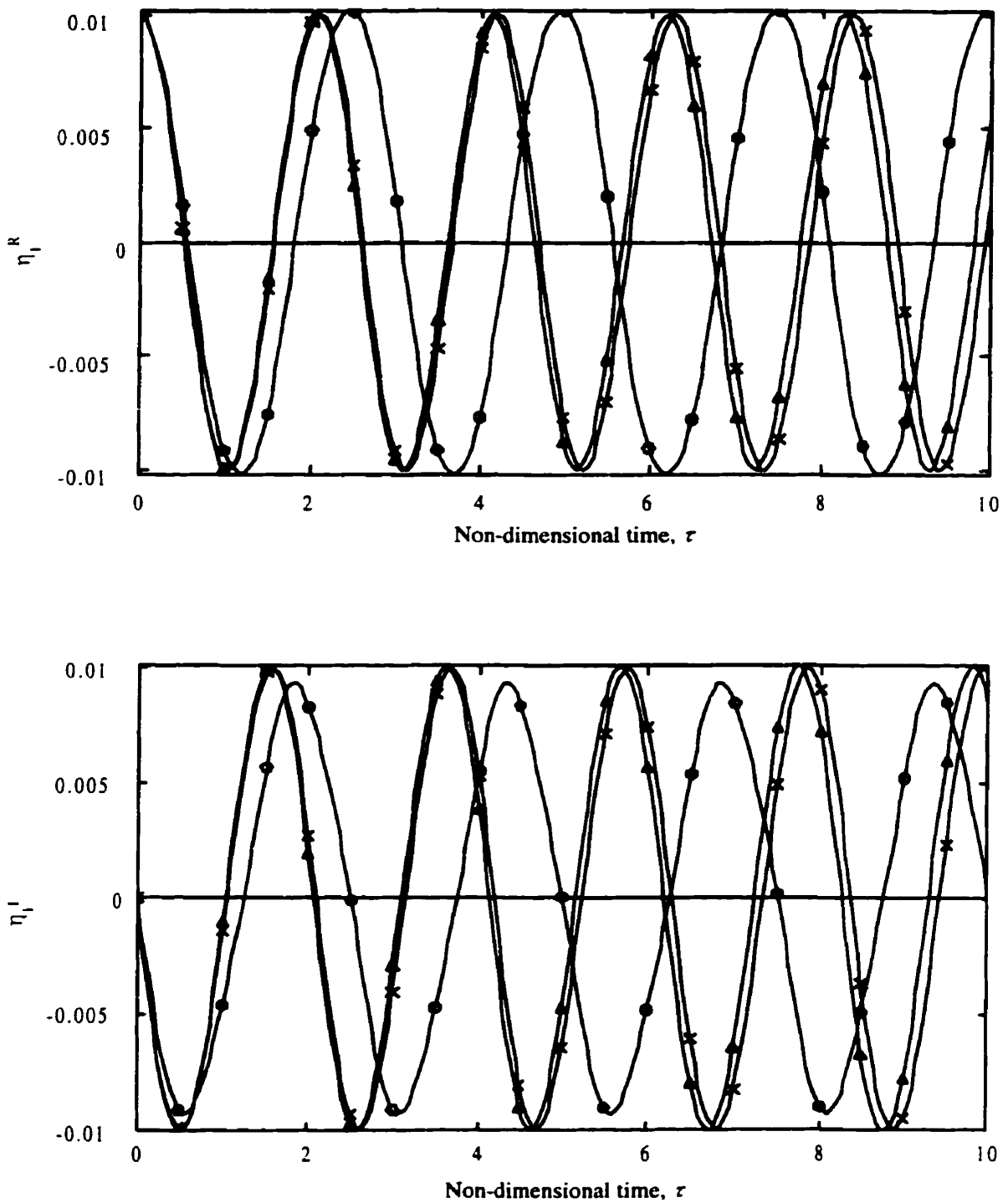


Figure 6.3: A comparison of responses for different values of k_3

○: $k_3=1000$

×: $k_3=100$

Δ: $k_3=10$

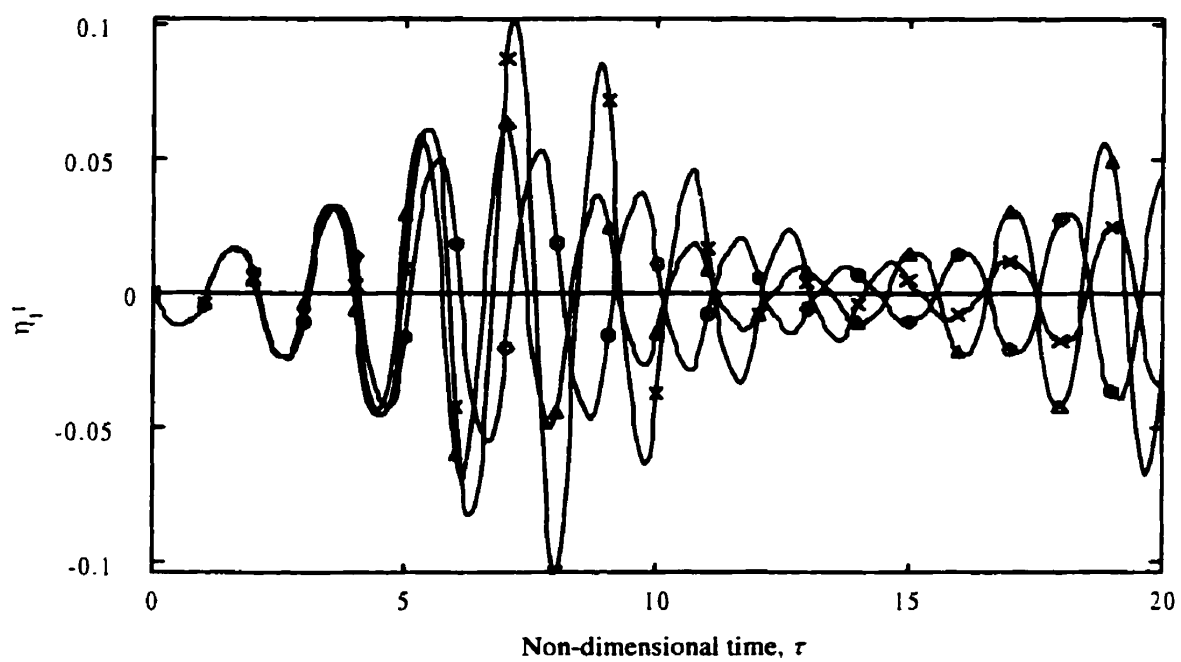
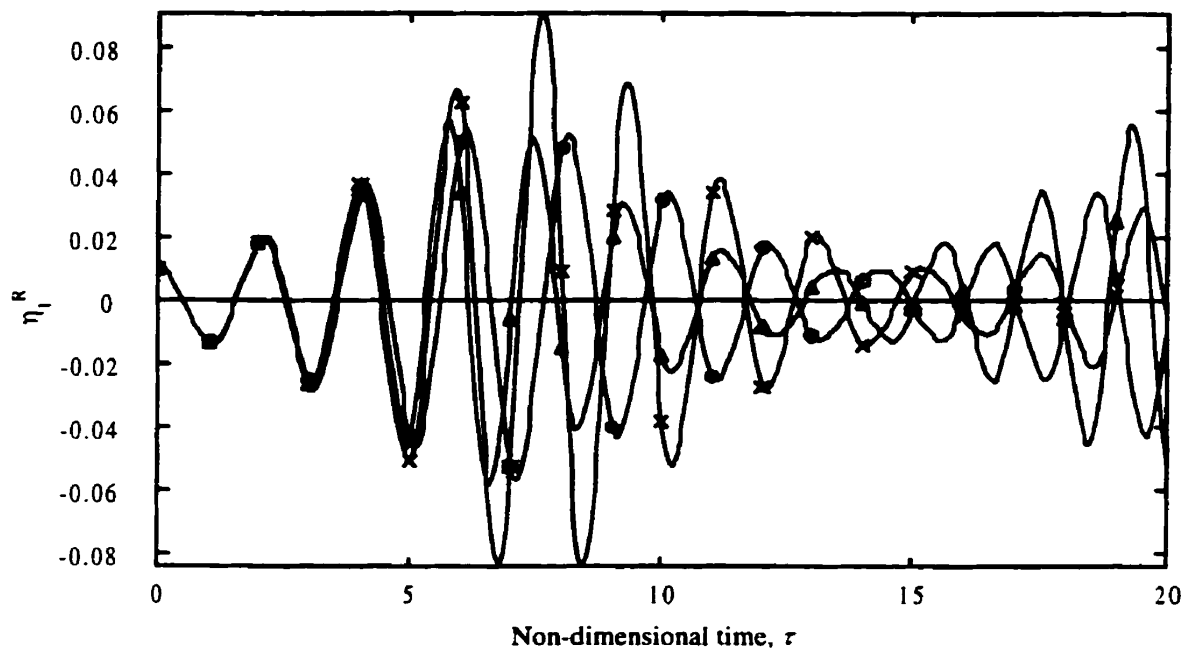


Figure 6.4: A comparison of the amplitudes for different values of k_3 in the case of parametric resonance with a constant travelling speed.

\circ : $k_3=100$ \times : $k_3=50$ Δ : $k_3=10$

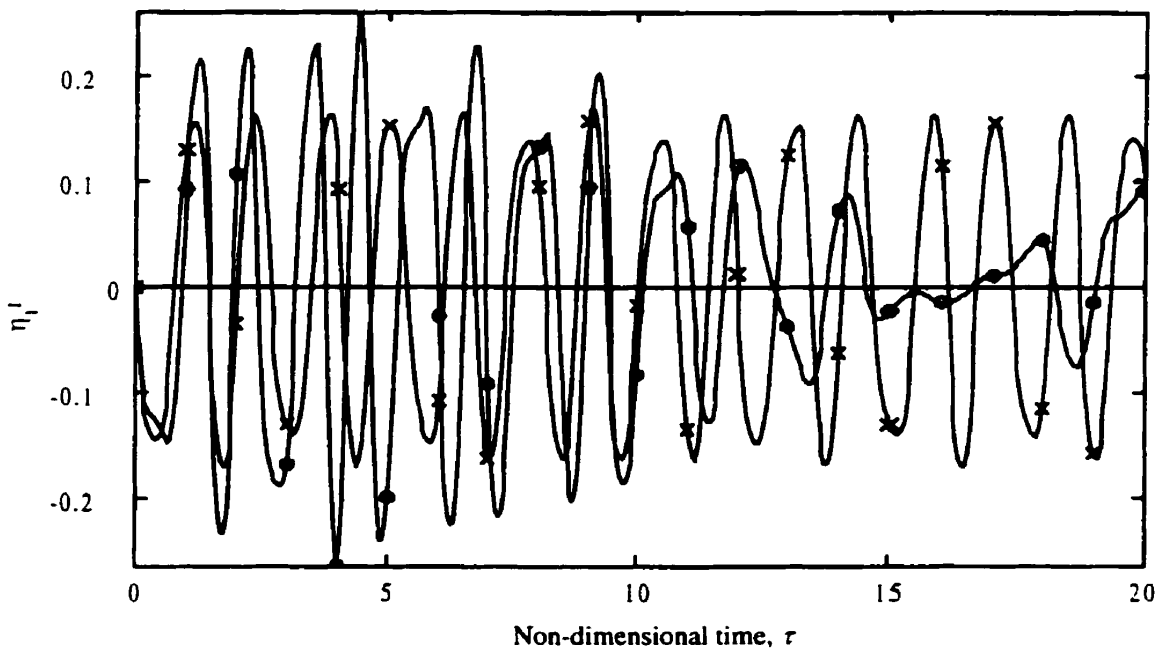
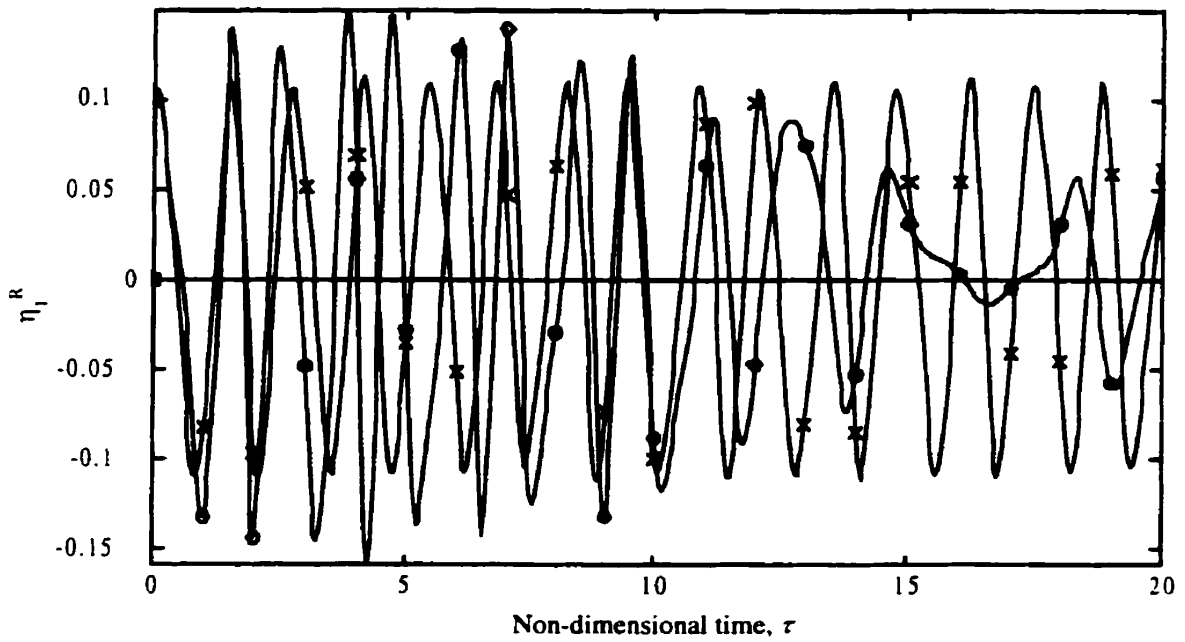


Figure 6.5: The effect of the axial perturbation velocity γ_1 on the transient amplitude for $\omega_0 = \pi(1 - \gamma_0^2)$ ($\gamma_0 = 0.5$, $k_3 = 10$)

o: $\gamma_1=1$ x: $\gamma_1=0.5$

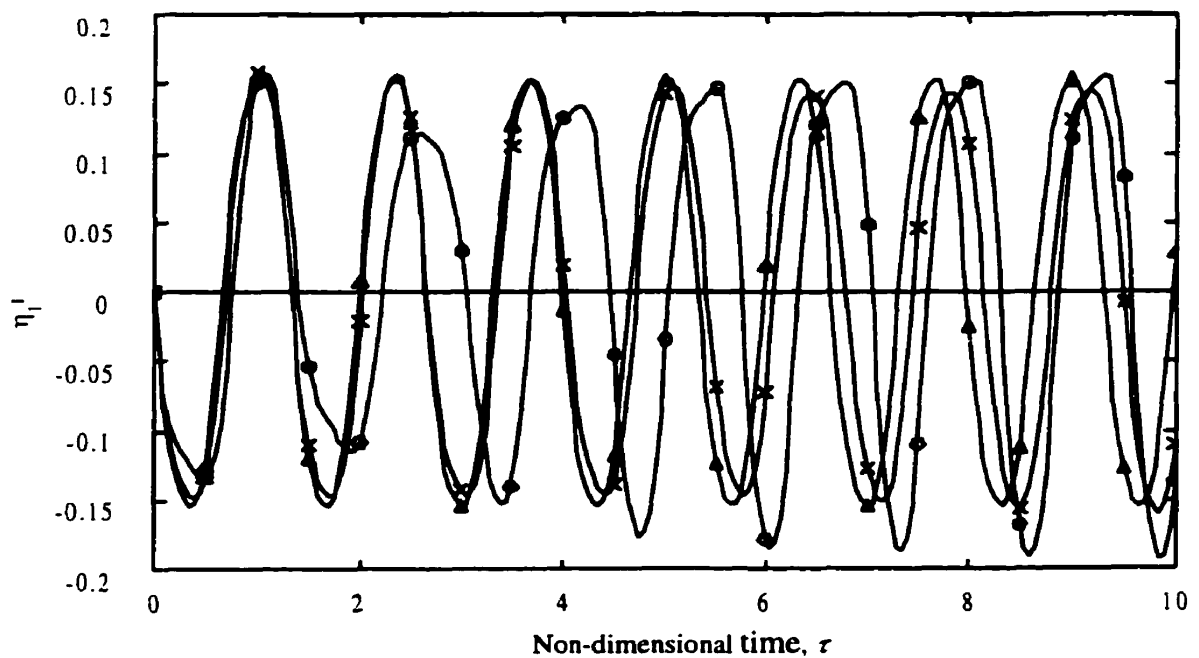
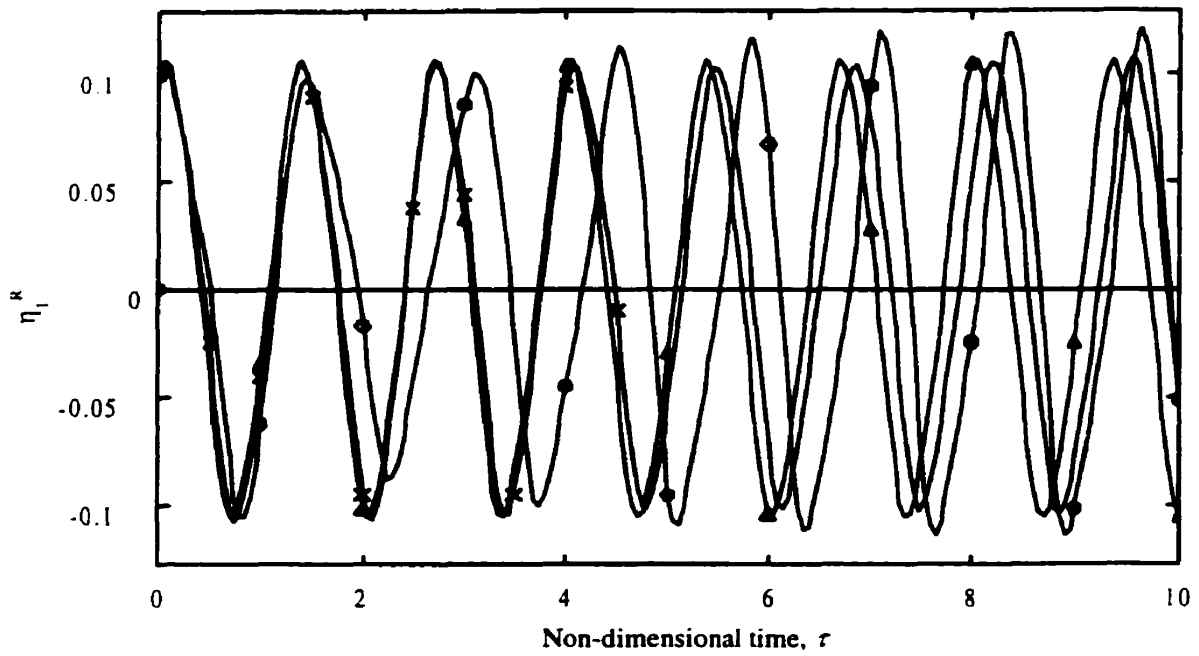


Figure 6.6: The effect of the axial perturbation velocity γ_1 on the transient amplitude for $\omega_0 = 2\pi(1 - \gamma_0^2)$ ($\gamma_0 = 0.5$, $k_3 = 10$)

$\circ: \gamma_1=0.6$ $\times: \gamma_1=0.2$ $\Delta: \gamma_1=0.0$

PART II

VIBRATION ANALYSIS OF SERPENTINE BELT DRIVE SYSTEMS

In Part I, only the transverse vibration of belt spans is considered as an axially moving material while the rotational vibration of serpentine belt drive systems is ignored. However, Beikmann *et al.* (1996) demonstrated that there exists a coupling mechanism between the rotational vibration and the transverse vibration. In Beikmann's model, the belt material is elastic and damping is not considered. As pointed out in Chapter 1, most of belt materials exert inherently viscoelastic behavior. In order to model damping characteristics of belt materials accurately, it is necessary to turn to the viscoelastic theory of materials.

In Part II (Chapters 7 – 12), a viscoelastic hybrid model is developed to represent the entire serpentine belt drives. The coupled model could give a more complete picture of the dynamic behavior of the system since the belt tension variation and the belt damping can be directly accounted for. Modal analysis of linear self-adjoint and non-self-adjoint hybrid model is performed to determine natural frequencies, modal shapes, and dynamic responses of linear systems. The discretization multiple scales method and the direct multiple scales method are employed to derive the steady state responses of nonlinear systems analytically. The results of coupled analysis could explain the existence of multiple limit cycles and the large amplitude vibration regions, which are greatly concerned by accessory drive engineers.

CHAPTER 7

HYBRID MODEL OF VISCOELASTIC SERPENTINE BELT DRIVE SYSTEMS

In this chapter, the nonlinear equations of motion will be derived for viscoelastic serpentine belt drive systems. This prototypical system contains all the essential components present in automotive serpentine drives: 1) a driving pulley 2) a driven pulley 3) a dynamic tensioner and 4) a serpentine belt span. The material properties of belts are characterized by the linear viscoelastic constitutive law and Hamilton's Principle will be used to derive the governing equations of motion and boundary conditions.

7.1 NONLINEAR EQUATIONS OF MOTION FOR GENERAL VISCOELASTIC MODEL

The prototypical system proposed by Beikmann *et al.* (1996) is shown in Figure 7.1. Several assumptions are made to simplify modeling of the serpentine belt drive:

- 1) Longitudinal vibrations of belt spans are not taken into consideration
- 2) Lagrangian strain for belt extension is employed as a finite measure of the strain
- 3) The stress-strain relation satisfies linear differential viscoelastic constitutive law
- 4) Belt bending stiffness is negligible

- 5) Axial translation speed of the belt, c , is constant
- 6) Belt slippage is negligible
- 7) Belt/pulley contact points do no change from those defined at the equilibrium state

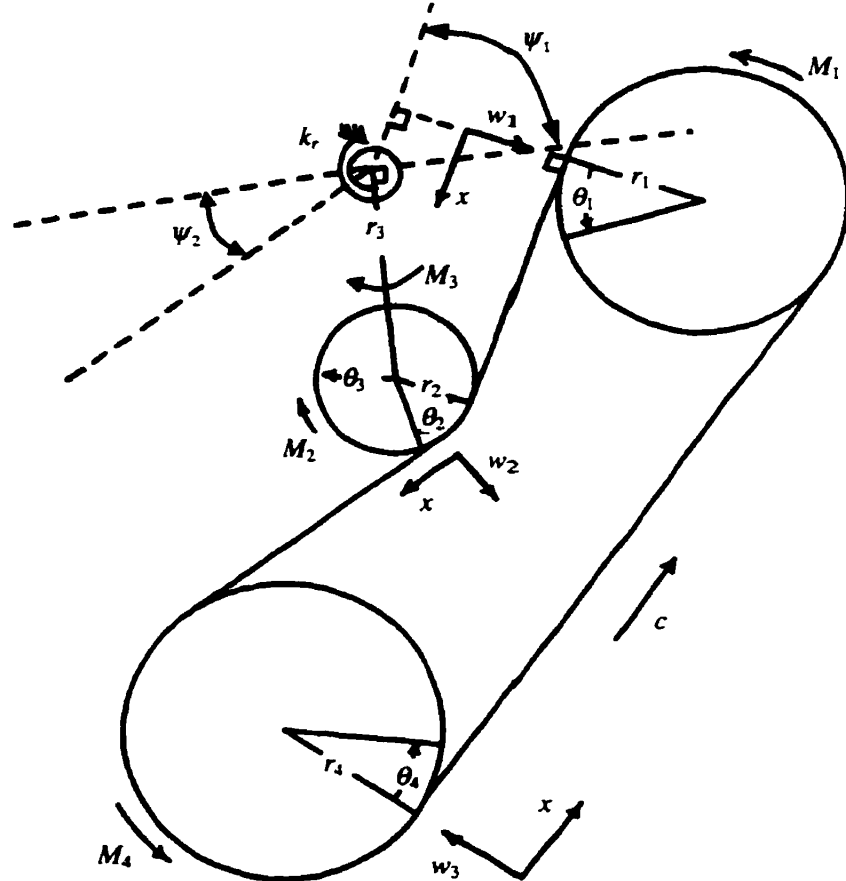


Figure 7.1: A prototypical serpentine belt drive system

Based on the above assumptions, the system kinetic energy T is obtained as

$$T = \frac{1}{2} J_1 \left(\frac{c}{r_1} + \theta_{1,x} \right)^2 + \frac{1}{2} J_2 \left(\frac{c}{r_2} + \theta_{2,x} \right)^2 + \frac{1}{2} J_3 \theta_{3,x}^2 + \frac{1}{2} J_4 \left(\frac{c}{r_4} + \theta_{4,x} \right)^2 + \int_0^{l_1} \frac{1}{2} m (w_{1,x} + cw_{1,x})^2 dx + \int_0^{l_2} \frac{1}{2} m (w_{2,x} + cw_{2,x})^2 dx + \int_0^{l_3} \frac{1}{2} m (w_{3,x} + cw_{3,x})^2 dx \quad (7.1)$$

where θ_i ($i=1, 4$) is the rotation from equilibrium of the i th discrete element (pulleys or tensioner

arm), w_i ($i=1, 3$) is the transverse deflection of span i from equilibrium, J_i and r_i are the mass moment of inertial and radius of the i th discrete element, and l_i is the length of belt span i .

The linear differential viscoelastic model is employed to characterize the damping and elastic behavior of belt materials:

$$\sigma(t) = E^* \varepsilon(t) \quad (7.2)$$

where $\sigma(t)$ and $\varepsilon(t)$ are the stress and strain in belt spans, and E^* is the equivalent Young's modulus.

Using kinematics constrains, the strain in the x direction for span i ($i=1, 3$) related to the displacement can be expressed as

$$\varepsilon_1(t) = \frac{P_{01}}{E^* A} + \frac{r_3 \theta_3 \cos \psi_1 + r_2 \theta_2 - r_1 \theta_1}{l_1} + \frac{1}{2} w_{1,x}^2 \quad (7.3)$$

$$\varepsilon_2(t) = \frac{P_{02}}{E^* A} + \frac{r_3 \theta_3 \cos \psi_2 + r_4 \theta_4 - r_2 \theta_2}{l_2} + \frac{1}{2} w_{2,x}^2 \quad (7.4)$$

$$\varepsilon_3(t) = \frac{P_{03}}{E^* A} + \frac{r_1 \theta_1 - r_4 \theta_4}{l_3} + \frac{1}{2} w_{3,x}^2 \quad (7.5)$$

where ψ_1 and ψ_2 are the alignment angles between the tensioner arm motion and the adjacent belt spans at equilibrium, P_{oi} is the total equilibrium operating tension for the i th span, and A is the cross sectional area of the belt.

Considering equations (7.2) - (7.5), the potential energy of the prototypical system is

$$\begin{aligned}
U = & \frac{E^* A}{2} \int_0^{l_1} \left(\frac{P_{01}}{E^* A} + \frac{r_3 \theta_3 \cos \psi_1 + r_2 \theta_2 - r_1 \theta_1}{l_1} + \frac{1}{2} w_{1,x}^2 \right)^2 dx \\
& + \frac{E^* A}{2} \int_0^{l_2} \left(\frac{P_{02}}{E^* A} + \frac{r_3 \theta_3 \cos \psi_2 + r_4 \theta_4 - r_2 \theta_2}{l_2} + \frac{1}{2} w_{2,x}^2 \right)^2 dx \\
& + \frac{E^* A}{2} \int_0^{l_3} \left(\frac{P_{03}}{E^* A} + \frac{r_1 \theta_1 - r_4 \theta_4}{l_3} + \frac{1}{2} w_{3,x}^2 \right)^2 dx + \frac{1}{2} k_r (\theta_3 + \theta_{3r})^2
\end{aligned} \tag{7.6}$$

where θ_{3r} is the tensioner spring deflection in the reference position, and k_r is the rotational spring stiffness of the tensioner spring.

The external tensioner arm damping considered here includes viscous damping and coulomb damping. The viscous damping force T_v is given by

$$T_v = -D_v \dot{\theta}_3 \tag{7.7}$$

where D_v is the viscous damping coefficient. Spring coulomb-damped tensioner has a slip-stick characteristic (Kraver *et al.*, 1996). A viscous equivalent for the coulomb vibration damping is defined as

$$T_c = -D_c \dot{\theta}_3 \tag{7.8}$$

where T_c is the coulomb damping force and D_c is the equivalent viscous damping coefficient.

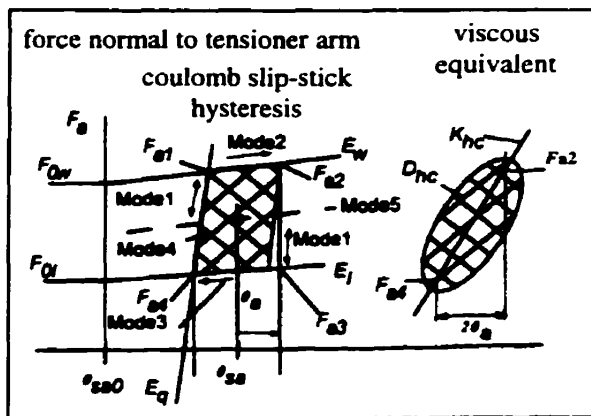


Figure 7.2: Coulomb tensioner characteristic

Rao (1986) proposed a method to determine the equivalent viscous damping coefficient. The basic idea is that the energy loss in a hysteresis cycle is set equal to the energy loss in a viscously damped cycle. Thus, the equivalent viscous damping coefficient can be obtained as

$$D_c = r_3 \sqrt{J_3 / k_r} (F_{a1} + F_{a2} - F_{a3} - F_{a4}) / (\pi \theta_a) \quad (7.9)$$

where F_{a1} , F_{a2} , F_{a3} , F_{a4} , and θ_a are defined in Figure 7.2.

For viscous damping and equivalent viscous damping, the Rayleigh dissipation function Φ can be expressed as

$$\Phi = \frac{1}{2} (D_v + D_c) \dot{\theta}_3^2 \quad (7.10)$$

As shown in Figure 7.1, the work done by external forces including the work done by accessory drive and engine torque M_i is

$$W = M_1 \theta_1 + M_2 \theta_2 + M_3 \theta_3 + M_4 \theta_4 \quad (7.11)$$

As pointed out by Rao (1992), Hamilton's Principle is applicable to any material. Hence, Hamilton's Principle can be used to derive the equation of motion for viscoelastic serpentine belt drive systems

$$\int_{t_1}^{t_2} \delta(T - U + W + \Phi) dt = 0 \quad (7.12)$$

Upon integrating by parts when needed, the equations of motion for the belt spans are

$$m(w_{i,tt} + 2cw_{i,xt} + c^2w_{i,xx}) - (P_{di} + P_{oi})w_{i,xx} = 0 \quad i = 1, 2, 3 \quad (7.13)$$

where P_{di} ($i=1, 3$) is the dynamic tension in each belt span. Note that the form of equations of

motion for viscoelastic belts is the same as that of corresponding elastic systems except that Young's modulus E for elastic belts is replaced by the equivalent Young's modulus E^* for viscoelastic belts.

For elastic belt drive systems, the longitudinal waves propagate much more rapidly than transverse waves since $P_o/EA \ll 1$. Therefore, belt tension can be assumed as being spatially constant. This assumption is often referred to as "quasi-static stretching". For viscoelastic belt drive systems, this assumption is still valid. Under this assumption the dynamic tensions P_{di} ($i=1, 3$) in the belt span can be expressed as

$$P_{d1} = \frac{E^* A}{l_1} \left(r_3 \theta_3 \cos \psi_1 + r_2 \theta_2 - r_1 \theta_1 + \frac{1}{2} \int_0^{l_1} (w_{1,x}(x,t))^2 dx \right) \quad (7.14)$$

$$P_{d2} = \frac{E^* A}{l_2} \left(r_3 \theta_3 \cos \psi_2 + r_4 \theta_4 - r_2 \theta_2 + \frac{1}{2} \int_0^{l_2} (w_{2,x}(x,t))^2 dx \right) \quad (7.15)$$

$$P_{d3} = \frac{E^* A}{l_3} \left(r_1 \theta_1 - r_4 \theta_4 + \frac{1}{2} \int_0^{l_3} (w_{3,x}(x,t))^2 dx \right) \quad (7.16)$$

Using kinematic constraints, the boundary terms can be expressed as functions of the discrete element rotations as

$$w_1(l_1, t) = r_3 \theta_3 \sin \psi_1 \quad (7.17)$$

$$w_2(0, t) = r_3 \theta_3 \sin \psi_2 \quad (7.18)$$

Substituting equations (7.14) - (7.18) into (7.12) and integrating by parts yield the equations of motion for the discrete elements

For pulley #1,

$$J_1 \theta_{1,n} = (P_{d1} + P_{o1})r_1 - (P_{d3} + P_{o3})r_1 + M_1 \quad (7.19)$$

For pulley #2,

$$J_2 \theta_{2,n} = -(P_{d1} + P_{o1})r_2 + (P_{d2} + P_{o2})r_2 + M_2 \quad (7.20)$$

For the tensioner arm,

$$\begin{aligned} J_3 \theta_{3,n} = & [mcw_{1,x}(l_1) + (mc^2 - (P_{d1} + P_{o1}))w_{1,x}(l_1)]r_3 \sin \psi_1 \\ & + (mc^2 - (P_{d1} + P_{o1}))r_3 \cos \psi_1 + (mc^2 - (P_{d2} + P_{o2}))r_3 \cos \psi_2 \\ & - [mcw_{2,x}(0) + (mc^2 - (P_{d2} + P_{o2}))w_{2,x}(0)]r_3 \sin \psi_2 \\ & - k_r(\theta_3 + \theta_{3r}) - (D_v + D_c)\dot{\theta}_3 + M_3 \end{aligned} \quad (7.21)$$

For pulley #4,

$$J_4 \theta_{4,n} = -(P_{d2} + P_{o2})r_4 + (P_{d3} + P_{o3})r_4 + M_4 \quad (7.22)$$

The equations of motion of serpentine belt drive systems are composed of a set of ordinary and partial differential equations. This kind of model is called a hybrid model since it describes the motions of both discrete elements and distributed elements.

7.2 EQUATIONS OF MOTION FOR KELVIN VISCOELASTIC MODEL

In the above section, the governing equations of serpentine belt drive systems with general differential viscoelastic constitutive relations are derived in the symbolic form. In this section, the most frequently used Kelvin viscoelastic model is adopted to characterize the constitutive relation of belt materials. The resulting linear and nonlinear equations are the basis for the modal analysis and nonlinear analysis described in Chapters 8 - 12.

7.2.1 Linear Equations of Motion for Kelvin Viscoelastic Model

Substituting the constitutive equation (2.19) of Kelvin model into equations (7.13), (7.19) – (7.22) and linearizing resulting equations for small oscillations about the equilibrium state, the linear equations of motion for Kelvin viscoelastic model are obtained.

The linear equations of motion for belt spans are

$$m(w_{i,\alpha} + 2cw_{i,\alpha}) - P_i w_{i,\alpha} = 0 \quad i = 1, 2, 3 \quad (7.23)$$

where $P_i = P_{oi} - mc^2$. Note that the linear equation of motion (7.23) for viscoelastic moving belt is the same as that for elastic moving belt.

For pulley #1, the linear equation of motion is

$$\begin{aligned} m_1 \ddot{\chi}_{1,\alpha} + (k_1 + k_3) \dot{\chi}_1 - k_1 \dot{\chi}_2 - k_1 \cos \psi_1 \dot{\chi}_3 - k_3 \dot{\chi}_4 \\ + (d_1 + d_3) \ddot{\chi}_1 - d_1 \dot{\chi}_2 - d_1 \cos \psi_1 \dot{\chi}_3 - d_3 \dot{\chi}_4 = F_{d1} \end{aligned} \quad (7.24)$$

where

$$\chi_i = r_i \theta_i \quad (i = 1, 4) \quad (7.25)$$

$$m_i = J_i / r_i^2 \quad (i = 1, 4) \quad (7.26)$$

$$k_i = EA / l_i \quad (i = 1, 3) \quad (7.27)$$

$$d_i = \eta A / l_i \quad (i = 1, 3) \quad (7.28)$$

$$F_{di} = M_{di} / r_i \quad (i = 1, 4) \quad (7.29)$$

and M_{di} is the dynamic component of the applied moment on pulley i . It is noted that damping terms, which have the same formulation as that of viscous damping, occur in equation (7.24).

This shows that viscoelastic constitutive relation not only can describe the elastic behavior of materials but also can characterize the dissipation behavior of materials.

Similar treatment of pulley #2 and pulley #4 yields

$$m_2 \ddot{\chi}_{2,n} - k_1 \chi_1 + (k_1 + k_2) \chi_2 + (k_1 \cos \psi_1 - k_2 \cos \psi_2) \chi_3 - k_2 \chi_4 - d_1 \dot{\chi}_1 + (d_1 + d_2) \dot{\chi}_2 + (d_1 \cos \psi_1 - d_2 \cos \psi_2) \dot{\chi}_3 - d_2 \dot{\chi}_4 = F_{d2} \quad (7.30)$$

and

$$m_4 \ddot{\chi}_{4,n} - k_3 \chi_1 - k_2 \chi_2 + k_2 \cos \psi_2 \chi_3 + (k_2 + k_3) \chi_4 - d_3 \dot{\chi}_1 - d_2 \dot{\chi}_2 + d_2 \cos \psi_2 \dot{\chi}_3 + (d_2 + d_3) \dot{\chi}_4 = F_{d4} \quad (7.31)$$

Equations (7.23), (7.24), (7.30), and (7.31) show that linear transverse belt vibration and pulley vibration are decoupled. However, linear coupling does exist between the transverse vibration of the belt spans and that of the tensioner arm. Neglecting nonlinear terms in equation (7.21) and using trigonometric relations leads to the equation of motion for the tensioner arm

$$m_3 \ddot{\chi}_{3,n} + (P_{t1} w_{1,x}(l_1) - mcw_{1,t}(l_1)) \sin \psi_1 + (-P_{t2} w_{2,x}(0) + mcw_{2,t}(0)) \sin \psi_2 - k_1 \cos \psi_1 \chi_1 + (k_1 \cos \psi_1 - k_2 \cos \psi_2) \chi_2 + (k_1 \cos^2 \psi_1 + k_2 \cos^2 \psi_2 + k_4) \chi_3 + k_2 \cos \psi_2 \chi_4 - d_1 \cos \psi_1 \dot{\chi}_1 + (d_1 \cos \psi_1 - d_2 \cos \psi_2) \dot{\chi}_2 + (d_1 \cos^2 \psi_1 + d_2 \cos^2 \psi_2 + d_4) \dot{\chi}_3 + d_2 \cos \psi_2 \dot{\chi}_4 = F_{d3} \quad (7.32)$$

where

$$k_4 = k_s + k_{gr} \quad (7.33)$$

$$k_s = k_r / r_3^2 \quad (7.34)$$

$$k_{gr} = \frac{P_{t1} \sin \psi_1 - P_{t2} \sin \psi_2}{r_3} \quad (7.35)$$

$$d_4 = (D_v + D_c) / r_3^2 \quad (7.36)$$

Equations (7.23), (7.24), (7.30) - (7.32) constitute the linear equations of motion for the serpentine belt drive system. Since both damping terms and gyroscopic terms exist in the equations and the system includes discrete and distributed elements, this system is a hybrid non-self-adjoint system. In Chapter 8, the eigenvalue problem governing free vibrations of the coupled system is formulated by neglecting the damping terms. In Chapter 9, complex modal analysis is performed and closed-form solutions are obtained for this hybrid non-self-adjoint system for the first time.

7.2.2 Nonlinear Equations of Motion for Kelvin Viscoelastic Model

Substituting the constitutive relation of Kelvin model into equations (7.13), (7.19) – (7.22) and omitting nonlinear terms higher than the third order, the nonlinear equations of motion for the Kelvin viscoelastic model are derived.

For belt spans, the nonlinear equations of motion are

$$m(w_{i,xx} + 2cw_{i,xx}) - P_n w_{i,xx} = P_{di} w_{i,xx} \quad i = 1, 2, 3 \quad (7.37)$$

where P_{di} can be separated into the linear component P_{diL} and the nonlinear component P_{diNL}

$$P_{di} = P_{diL} + P_{diNL} \quad (7.38)$$

$$P_{d1L} = k_1(\chi_3 \cos \psi_1 + \chi_2 - \chi_1) + d_1(\dot{\chi}_3 \cos \psi_1 + \dot{\chi}_2 - \dot{\chi}_1) \quad (7.39)$$

$$P_{d2L} = k_2(\chi_3 \cos \psi_2 + \chi_4 - \chi_2) + d_2(\dot{\chi}_3 \cos \psi_2 + \dot{\chi}_4 - \dot{\chi}_2) \quad (7.40)$$

$$P_{d3L} = k_3(\chi_1 - \chi_4) + d_3(\dot{\chi}_1 - \dot{\chi}_4) \quad (7.41)$$

$$P_{dNL} = \frac{EA}{2l_i} \int_0^{l_i} w_{i,x}^2 dx + \frac{\eta A}{l_i} \int_0^{l_i} w_{i,x} \dot{w}_{i,x} dx \quad (7.42)$$

The nonlinear equations of motion for the discrete elements are

For pulley#1

$$\begin{aligned} m_1 \ddot{\chi}_{1,n} + (k_1 + k_3) \chi_1 - k_1 \chi_2 - k_1 \cos \psi_1 \chi_3 - k_3 \chi_4 \\ + (d_1 + d_3) \dot{\chi}_1 - d_1 \dot{\chi}_2 - d_1 \cos \psi_1 \dot{\chi}_3 - d_3 \dot{\chi}_4 = P_{d1NL} - P_{d3NL} + F_{d1} \end{aligned} \quad (7.43)$$

For pulley #2

$$\begin{aligned} m_2 \ddot{\chi}_{2,n} - k_1 \chi_1 + (k_1 + k_2) \chi_2 + (k_1 \cos \psi_1 - k_2 \cos \psi_2) \chi_3 - k_2 \chi_4 \\ - d_1 \dot{\chi}_1 + (d_1 + d_2) \dot{\chi}_2 + (d_1 \cos \psi_1 - d_2 \cos \psi_2) \dot{\chi}_3 - d_2 \dot{\chi}_4 = P_{d2NL} - P_{d1NL} + F_{d2} \end{aligned} \quad (7.44)$$

For the tensioner arm,

$$\begin{aligned} m_3 \ddot{\chi}_{3,n} + (P_{r1} w_{1,x}(l_1) - mc w_{1,x}(l_1)) \sin \psi_1 + (-P_{r2} w_{2,x}(0) + mc w_{2,x}(0)) \sin \psi_2 \\ - k_1 \cos \psi_1 \chi_1 + (k_1 \cos \psi_1 - k_2 \cos \psi_2) \chi_2 + (k_1 \cos^2 \psi_1 + k_2 \cos^2 \psi_2 + k_4) \chi_3 \\ + k_2 \cos \psi_2 \chi_4 - d_1 \cos \psi_1 \dot{\chi}_1 + (d_1 \cos \psi_1 - d_2 \cos \psi_2) \dot{\chi}_2 \\ + (d_1 \cos^2 \psi_1 + d_2 \cos^2 \psi_2 + d_4) \dot{\chi}_3 + d_2 \cos \psi_2 \dot{\chi}_4 = -P_{d1NL} \cos \psi_1 - P_{d2NL} \cos \psi_2 + F_{d3} \end{aligned} \quad (7.45)$$

For pulley #4

$$\begin{aligned} m_4 \ddot{\chi}_{4,n} - k_3 \chi_1 - k_2 \chi_2 + k_2 \cos \psi_2 \chi_3 + (k_2 + k_3) \chi_4 \\ - d_3 \dot{\chi}_1 - d_2 \dot{\chi}_2 + d_2 \cos \psi_2 \dot{\chi}_3 + (d_2 + d_3) \dot{\chi}_4 = P_{d3NL} - P_{d2NL} + F_{d4} \end{aligned} \quad (7.46)$$

The nonlinear equation (7.37) for the belt spans couples to equations (7.43) - (7.46) governing the four discrete elements (three pulleys and the tensioner arm). This set of nonlinear equations provides the basis for the nonlinear analysis described in Chapters 10 - 12.

CHAPTER 8

MODAL ANALYSIS OF UNDAMPED SERPENTINE BELT DRIVE SYSTEMS

In Chapter 7, the nonlinear equations of motion for serpentine belt drive systems are derived. The damping is introduced through viscoelasticity of belt materials. In this chapter, as a first step to tackle the original problem, the modal analysis of linear undamped serpentine belt drive system is performed to identify the natural frequency spectrum and to calculate the corresponding mode shapes. The eigenfunctions obtained here will be used in Chapters 10 – 12 for the nonlinear vibration analysis of damped serpentine drive systems.

The eigenvalues and eigenfunctions of the linear undamped prototypical system were calculated by Beikmann *et al.* (1996). A two-level iteration based on Holzer's method is employed to solve the eigenvalue problem. However, this numerical approach lacks the ability to provide an indication of the effect of design parameters on natural frequencies.

In this study, the entire system is divided into two subsystems: one with a single belt and its motion is not coupled with the rest of the system in the linear analysis, and the other with the remaining components. Instead of using the iteration method, an explicit exact characteristic equation for natural frequencies of the prototypical system is obtained. This characteristic equation can provide insight concerning the effect of design parameters on natural frequencies of

the system. The response of serpentine belt drive systems to arbitrary excitations is obtained as a superposition of orthogonal eigenfunctions. The exact solution without using eigenfunction expansion is derived when the excitations are non-resonance harmonic.

8.1 CANONICAL FORM OF EQUATIONS OF MOTION

From equations (7.23), (7.24), and (7.30) – (7.32), it is seen that for the linear analysis, the transverse vibration of span 3 and vibration of other components are decoupled. Thus, it is desirable to divide the entire system into two subsystems: subsystem 1 which includes span 3 only and subsystem 2 which includes all the other parts of the system.

For subsystem 1, the equation of motion can be rewritten in operator form

$$M_3 \ddot{w}_3 + G_3 \dot{w}_3 + K_3 w_3 = F_3 \quad (8.1)$$

where

$$M_3 = m \quad (8.2)$$

$$G_3 = 2mc \frac{\partial}{\partial x} \quad (8.3)$$

$$K_3 = -P_{t3} \frac{\partial^2}{\partial x^2} \quad (8.4)$$

For subsystem 2, the equations of motion can be rewritten in matrix operator form

$$\mathbf{M}\ddot{\mathbf{W}} + \mathbf{G}\dot{\mathbf{W}} + \mathbf{K}\mathbf{W} = \mathbf{F} \quad (8.5)$$

where

$$\mathbf{F} = \{f_1(x,t) f_2(x,t) f_3(x,t) f_4(x,t) f_5(x,t) f_6(x,t)\}^T \quad (8.6)$$

and the displacement vector \mathbf{W} is composed of the displacement of belt span 1, belt span 2, three pulleys and the tensioner arm

$$\mathbf{W} = \{w_1(x,t) w_2(x,t) \chi_1(t) \chi_2(t) \chi_3(t) \chi_4(t)\}^T \quad (8.7)$$

The mass matrix operator \mathbf{M} , stiffness matrix operator \mathbf{K} , and gyroscopic matrix operator \mathbf{G} are defined, respectively, as follows

$$\mathbf{M} = \begin{bmatrix} m & 0 & 0 & 0 & 0 & 0 \\ 0 & m & 0 & 0 & 0 & 0 \\ 0 & 0 & m_1 & 0 & 0 & 0 \\ 0 & 0 & 0 & m_2 & 0 & 0 \\ 0 & 0 & 0 & 0 & m_3 & 0 \\ 0 & 0 & 0 & 0 & 0 & m_4 \end{bmatrix} \quad (8.8)$$

$$\mathbf{K} = \begin{bmatrix} -P_{11} \frac{\partial^2}{\partial x^2} & 0 & 0 & 0 & 0 & 0 \\ 0 & -P_{22} \frac{\partial^2}{\partial x^2} & 0 & 0 & 0 & 0 \\ 0 & 0 & k_1 + k_3 & -k_1 & -k_1 \cos \psi_1 & -k_3 \\ 0 & 0 & -k_1 & k_1 + k_2 & k_1 \cos \psi_1 - k_2 \cos \psi_2 & -k_2 \\ P_{11} \sin \psi_1 \frac{\partial}{\partial x} \Big|_{l_1} & -P_{22} \sin \psi_2 \frac{\partial}{\partial x} \Big|_{l_2} & -k_1 \cos \psi_1 & k_1 \cos \psi_1 - k_2 \cos \psi_2 & k_1 \cos^2 \psi_1 + k_2 \cos^2 \psi_2 + k_4 & k_2 \cos \psi_2 \\ 0 & 0 & -k_3 & -k_2 & k_2 \cos \psi_2 & k_2 + k_3 \end{bmatrix} \quad (8.9)$$

$$\mathbf{G} = \begin{bmatrix} 2mc \frac{\partial}{\partial x} & 0 & 0 & 0 & 0 & 0 \\ 0 & 2mc \frac{\partial}{\partial x} & 0 & 0 & 0 & 0 \\ 0 & 0 & 0 & 0 & 0 & 0 \\ 0 & 0 & 0 & 0 & 0 & 0 \\ -mc \sin \psi_1|_{l_1} & mc \sin \psi_2|_0 & 0 & 0 & 0 & 0 \\ 0 & 0 & 0 & 0 & 0 & 0 \end{bmatrix} \quad (8.10)$$

The presence of boundary terms in \mathbf{G} and \mathbf{K} appears to break skew or symmetry. However, this is not true and the following will demonstrate that matrix operator \mathbf{G} is skew symmetric and matrix operator \mathbf{K} is symmetric.

$$\langle \mathbf{G}\mathbf{W}, \tilde{\mathbf{W}} \rangle = \int_0^{l_1} 2mc \frac{\partial w_1}{\partial x} \bar{w}_1 dx + \int_0^{l_2} 2mc \frac{\partial w_2}{\partial x} \bar{w}_2 dx - mc \sin \psi_1 w_1(l_1) \bar{\chi}_3 + mc \sin \psi_2 w_2(0) \bar{\chi}_3 \quad (8.11)$$

$$\begin{aligned} \langle \mathbf{K}\mathbf{W}, \tilde{\mathbf{W}} \rangle &= \int_0^{l_1} -P_{11} \frac{\partial^2 w_1}{\partial x^2} \bar{w}_1 dx + \int_0^{l_2} -P_{22} \frac{\partial^2 w_2}{\partial x^2} \bar{w}_2 dx + \boldsymbol{\chi}^T \mathbf{K}_{DD} \tilde{\boldsymbol{\chi}} \\ &\quad + P_{11} \sin \psi_1 \left. \frac{\partial w_1}{\partial x} \right|_{l_1} \tilde{\chi}_3 - P_{22} \sin \psi_2 \left. \frac{\partial w_2}{\partial x} \right|_0 \tilde{\chi}_3 \end{aligned} \quad (8.12)$$

where

$$\mathbf{K}_{DD} = \begin{bmatrix} k_1 + k_3 & -k_1 & -k_1 \cos \psi_1 & -k_3 \\ -k_1 & k_1 + k_2 & k_1 \cos \psi_1 - k_2 \cos \psi_2 & -k_2 \\ -k_1 \cos \psi_1 & k_1 \cos \psi_1 - k_2 \cos \psi_2 & k_1 \cos^2 \psi_1 + k_2 \cos^2 \psi_2 + k_4 & k_2 \cos \psi_2 \\ -k_3 & -k_2 & k_2 \cos \psi_2 & k_2 + k_3 \end{bmatrix} \quad (8.13)$$

$$\boldsymbol{\chi} = \{\chi_1(t) \ \chi_2(t) \ \chi_3(t) \ \chi_4(t)\}^T \quad (8.14)$$

Equations (8.11) and (8.12) become, after integrating by parts,

$$\begin{aligned} \langle \mathbf{G}\mathbf{W}, \tilde{\mathbf{W}} \rangle &= - \int_0^{l_1} 2mc \frac{\partial \bar{w}_1}{\partial x} w_1 dx - \int_0^{l_2} 2mc \frac{\partial \bar{w}_2}{\partial x} w_2 dx \\ &\quad + mc \sin \psi_1 \bar{w}_1(l_1) \chi_3 - mc \sin \psi_2 \bar{w}_2(0) \chi_3 \\ &= - \langle \mathbf{W}, \mathbf{G}\tilde{\mathbf{W}} \rangle \end{aligned} \quad (8.15)$$

$$\begin{aligned}
\langle \mathbf{K}\mathbf{W}, \tilde{\mathbf{W}} \rangle &= \int_0^{l_1} -P_{r1} \frac{\partial^2 \tilde{w}_1}{\partial x^2} w_1 dx + \int_0^{l_2} -P_{r2} \frac{\partial^2 \tilde{w}_2}{\partial x^2} w_2 dx + \chi^T \mathbf{K}_{DD} \tilde{\chi} \\
&\quad P_{r1} \sin \psi_1 \left. \frac{\partial \tilde{w}_1}{\partial x} \right|_{l_1} \chi_3 - P_{r2} \sin \psi_2 \left. \frac{\partial \tilde{w}_2}{\partial x} \right|_0 \chi_3 \\
&= \langle \mathbf{W}, \mathbf{K}\tilde{\mathbf{W}} \rangle
\end{aligned} \tag{8.16}$$

From equations (8.15) and (8.16), it is concluded that matrix operator \mathbf{G} is skew symmetric and matrix operator \mathbf{K} is symmetric in the inner product definition. Therefore, the serpentine belt drive system operating at non-zero axial belt speed constitutes a conservative gyroscopic system.

The modal analysis of discrete gyroscopic systems was studied extensively (Meirovitch, 1974, 1975). A similar study of a single axially moving span was conducted by Wickert and Mote (1990) and their analysis can be applied directly to subsystem 1. Thus, the modal analysis of subsystem 1 will no longer be discussed in this study. Instead, focus of the present study will be on subsystem 2. Since the serpentine belt drive system is a hybrid system consisting of both discrete and continuous elements, a combination of both Meirovitch's and Wickert's methods suggested by Beikmann *et al.* (1996) is employed to formulate the eigenvalue problem and to evaluate the properties of the eigensolutions.

To apply the methods of Meirovitch (1974) and Wickert and Mote (1990) to the present continuous/discrete system, equation (8.5) should be cast in the first order form. Defining the state vector and the excitation vector

$$\mathbf{U} = \begin{Bmatrix} \dot{\mathbf{W}} \\ \mathbf{W} \end{Bmatrix} \tag{8.17}$$

$$\mathbf{Q}(x,t) = \begin{Bmatrix} \mathbf{F}(x,t) \\ \mathbf{0} \end{Bmatrix} \quad (8.18)$$

and matrix differential operators

$$\mathbf{A} = \begin{bmatrix} \mathbf{M} & \mathbf{0} \\ \mathbf{0} & \mathbf{K} \end{bmatrix} \quad (8.19)$$

$$\mathbf{B} = \begin{bmatrix} \mathbf{G} & \mathbf{K} \\ -\mathbf{K} & \mathbf{0} \end{bmatrix} \quad (8.20)$$

equation (8.5) becomes

$$\mathbf{A}\dot{\mathbf{U}} + \mathbf{B}\mathbf{U} = \mathbf{Q} \quad (8.21)$$

Equation (8.21) is the canonical form of the equation of motion and its solution satisfies the appropriate boundary conditions and initial conditions.

The inner product of two state space vectors \mathbf{U}_n and \mathbf{U}_r is defined as

$$\langle \mathbf{U}_n, \mathbf{U}_r \rangle = \int_0^{l_1} (\bar{w}_{1n} \bar{w}_{1r} + w_{1n} \bar{w}_{1r}) dx + \int_0^{l_2} (\bar{w}_{2n} \bar{w}_{2r} + w_{2n} \bar{w}_{2r}) dx + \bar{\chi}_n^T \bar{\chi}_r + \chi_n^T \bar{\chi}_r \quad (8.22)$$

where the overbar denotes complex conjugate. With respect to this inner product, the operator \mathbf{A} and \mathbf{B} satisfy several properties, which are the cornerstones of the subsequent analysis. First, operator \mathbf{A} is symmetric, and operator \mathbf{B} is skew symmetric; namely,

$$\langle \mathbf{A}\mathbf{U}_n, \mathbf{U}_r \rangle = \langle \mathbf{U}_n, \mathbf{A}\mathbf{U}_r \rangle \quad (8.23)$$

$$\langle \mathbf{B}\mathbf{U}_n, \mathbf{U}_r \rangle = -\langle \mathbf{U}_n, \mathbf{B}\mathbf{U}_r \rangle \quad (8.24)$$

Second, operator \mathbf{A} is positive definite for sufficiently low transport speed. Dynamic systems described by one symmetric and one skew-symmetric operator are termed gyroscopic systems.

8.2 EIGENVALUES AND EIGENFUNCTIONS

The eigenvalue problem of the subsystem 2 can be studied in the context of gyroscopic dynamic systems when the equation of motion is cast in the operator form.

8.2.1 Orthogonality of Eigenfunctions

The separable solution

$$\mathbf{U}(x,t) = \operatorname{Re}\{\Psi_n e^{i\lambda_n t}\} \quad (8.25)$$

leads to the eigenvalue problem

$$\lambda_n \mathbf{A} \Psi_n + \mathbf{B} \Psi_n = 0 \quad (8.26)$$

in which λ_n and Ψ_n are complex. The eigensolutions satisfy several properties. The eigenvalues are imaginary; namely, $\lambda_n = i\omega_n$, where ω_n is the real oscillation frequency. Furthermore, the eigenfunctions Ψ_n have the structure

$$\Psi_n = \Psi_n^R + i\Psi_n^I \quad (8.27)$$

$$\Psi_n^R = \begin{Bmatrix} -\omega_n \phi_n'(x) \\ \phi_n^R \end{Bmatrix} \quad (8.28)$$

$$\Psi_n^I(x) = \begin{Bmatrix} \omega_n \phi_n^R(x) \\ \phi_n'(x) \end{Bmatrix} \quad (8.29)$$

Here, $\phi_n(x)$ is the normalized eigenfunction associated with the displacement field, which can be expressed as

$$\phi_n(x) = \{\phi_{1n}(x) \ \phi_{2n}(x) \ \hat{x}_{1n} \ \hat{x}_{2n} \ \hat{x}_{3n} \ \hat{x}_{4n}\}^T \quad (8.30)$$

where ϕ_{1n} and ϕ_{2n} are the normalized eigenfunctions of transverse displacements $w_1(x,t)$ and $w_2(x,t)$, $\hat{\chi}_{1n}$, $\hat{\chi}_{2n}$, $\hat{\chi}_{3n}$ and $\hat{\chi}_{4n}$ are normalized eigenfunctions associated with the displacement of discrete components. The eigenfunctions ψ_n satisfy the orthonormality relations

$$\langle \mathbf{A}\psi_n^R, \psi_m^R \rangle = \delta_{nm} \quad (8.31)$$

$$\langle \mathbf{A}\psi_n^I, \psi_m^I \rangle = \delta_{nm} \quad (8.32)$$

$$\langle \mathbf{A}\psi_n^R, \psi_m^I \rangle = 0 \quad (8.33)$$

$$\langle \mathbf{B}\psi_n^R, \psi_m^R \rangle = 0 \quad (8.34)$$

$$\langle \mathbf{B}\psi_n^I, \psi_m^I \rangle = 0 \quad (8.35)$$

$$\langle \mathbf{B}\psi_n^R, \psi_m^I \rangle = \omega_n \delta_{nm} \quad (8.36)$$

8.2.2 Characteristic Equation of Eigenvalues

Since the serpentine belt drive system is a hybrid system (part continuous and part discrete), the usual approaches to solve the corresponding eigenvalue problem are not applicable to this systems. Beikmann *et al.* (1996) used Holzer's method to solve the free vibration problems. Holzer's method (Meirovitch, 1986) involves two iteration loops: 1) an "inner loop" for the cyclic belt span/pulleys, and 2) an "outer loop" for the tensioner arm. The iteration solution was employed in both the inner loop and the outer loop and thus provide little indication of the effect of design parameters on natural frequencies. In the following study, instead of using the iteration solution, the direct solution method is used to derive the explicit exact characteristic equation.

It is assumed that the motion is harmonic, that is

$$w_i(x, t) = \phi_{in}(x)e^{i\omega t} \quad (i = 1, 2) \quad (8.37)$$

$$\chi_i = \hat{\chi}_{in} e^{i\omega t} \quad (i = 1, 4) \quad (8.38)$$

Substituting equations (8.37) and (8.38) into equation of motion for pulleys, eliminating $e^{i\omega t}$, and putting those terms including $\hat{\chi}_{3n}$ on the right side of equations yield

$$(k_1 + k_3 - m_1 \omega^2) \hat{\chi}_{1n} - k_1 \hat{\chi}_{2n} - k_3 \hat{\chi}_{4n} = k_1 \cos \psi_1 \hat{\chi}_{3n} \quad (8.39)$$

$$-k_1 \hat{\chi}_{1n} + (k_1 + k_2 - m_2 \omega^2) \hat{\chi}_{2n} - k_2 \hat{\chi}_{4n} = (k_2 \cos \psi_2 - k_1 \cos \psi_1) \hat{\chi}_{3n} \quad (8.40)$$

$$-k_3 \hat{\chi}_{1n} - k_2 \hat{\chi}_{2n} + (k_2 + k_3 - m_4 \omega^2) \hat{\chi}_{4n} = -k_2 \cos \psi_2 \hat{\chi}_{3n} \quad (8.41)$$

Sum of equations (8.39) – (8.41) leads to

$$m_1 \hat{\chi}_{1n} + m_2 \hat{\chi}_{2n} + m_4 \hat{\chi}_{4n} = 0 \quad (8.42)$$

Inserting equation (8.42) into (8.39) and (8.41) and solving the resulting equations lead to

$$\hat{\chi}_{1n} = \frac{\left[\left(1 + \frac{m_4}{m_2} \right) k_2 + k_3 - m_4 \omega^2 \right] k_1 \cos \psi_1 + \left(\frac{m_4}{m_2} k_1 - k_3 \right) k_2 \cos \psi_2}{\Delta} \hat{\chi}_{3n} \quad (8.43)$$

$$\hat{\chi}_{2n} = \frac{\left(-\frac{m_1}{m_2} k_2 - \frac{m_1 + m_4}{m_2} k_3 + \frac{m_1 m_4}{m_2} \omega^2 \right) k_1 \cos \psi_1}{\Delta} \hat{\chi}_{3n} \quad (8.44)$$

$$+ \frac{\left(\frac{m_4}{m_2} k_1 + \frac{m_1 + m_4}{m_2} k_3 - \frac{m_1 m_4}{m_2} \omega^2 \right) k_2 \cos \psi_2}{\Delta} \hat{\chi}_{3n}$$

$$\hat{\chi}_{4n} = \frac{-\left(\frac{m_1}{m_2} k_2 - k_3 \right) k_1 \cos \psi_1 - \left[\left(1 + \frac{m_1}{m_2} \right) k_1 + k_3 - m_1 \omega^2 \right] k_2 \cos \psi_2}{\Delta} \hat{\chi}_{3n} \quad (8.45)$$

where

$$\Delta = \left[\left(1 + \frac{m_1}{m_2} \right) k_1 + k_3 - m_1 \omega^2 \right] \left[\left(1 + \frac{m_4}{m_2} \right) k_2 + k_3 - m_4 \omega^2 \right] - \left(\frac{m_1}{m_2} k_2 - k_3 \right) \left(\frac{m_4}{m_2} k_1 - k_3 \right) \quad (8.46)$$

To capture the coupling between the transverse belt motion and the tensioner arm rotation, general solutions for the transverse response of the belt spans must be obtained. The solution form used here is the one presented by Sack (1954). For belt span 1, the eigenfunction $\phi_{1n}(x)$ can be expressed as

$$\phi_{1n}(x) = e^{i\alpha x/c'_1} [a_1 \sin(\alpha x/c'_1) + b_1 \cos(\alpha x/c'_1)] \quad (8.47)$$

where the effective wave velocity c'_1 , the propagation speed c_1 of transverse wave, and the phase propagation velocity c'_a for span 1 are defined as

$$c_1 = \sqrt{\frac{P_{ol}}{m}} \quad (8.48)$$

$$c'_1 = \frac{c_1^2 - c^2}{c_1} \quad (8.49)$$

$$c'_a = \frac{c_1^2 - c^2}{c} \quad (8.50)$$

Using boundary conditions $\phi_{1n}(0) = 0$ and $\phi_{1n}(l_1) = \hat{\chi}_{3n} \sin \psi_1$ to determine the integration constants in the eigenfunction expression (8.47) leads to

$$a_1 = \frac{e^{-i\alpha l_1/c'_a} \sin \psi_1}{\sin(\alpha l_1/c'_1)} \hat{\chi}_{3n} \quad (8.51)$$

$$b_1 = 0 \quad (8.52)$$

Similarly, for span 2, the eigenfunction can be expressed as

$$\phi_{2n}(x) = e^{i\alpha x/c'_2} [a_2 \sin(\alpha x/c'_2) + b_2 \cos(\alpha x/c'_2)] \quad (8.53)$$

where the effective wave velocity c'_2 , the propagation speed c_2 of transverse wave, and the phase propagation velocity c'_b for span 2 are defined as

$$c_2 = \sqrt{\frac{P_{o2}}{m}} \quad (8.54)$$

$$c'_2 = \frac{c_2^2 - c^2}{c_2} \quad (8.55)$$

$$c'_b = \frac{c_2^2 - c^2}{c} \quad (8.56)$$

Applying the boundary condition that $\phi_{2n}(0) = \hat{x}_{3n} \sin \psi_2$ and $\phi_{2n}(l_2) = 0$, the integration constants in equation (8.53) can be obtained as follows

$$a_2 = -\sin \psi_2 \cot(\omega l_2 / c'_2) \hat{x}_{3n} \quad (8.57)$$

$$b_2 = \sin \psi_2 \hat{x}_{3n} \quad (8.58)$$

Substituting equations (8.43) - (8.45), (8.47) and (8.53) into the equation of motion for tensioner arm yields the characteristic equation for eigenvalues of the system

$$\begin{aligned} & P_{r1} \sin^2 \psi_1 \cot(\omega l_1 / c'_1) \omega / c'_1 + P_{r2} \sin^2 \psi_2 \cot(\omega l_2 / c'_2) \omega / c'_2 + k_1 \cos^2 \psi_1 + k_2 \cos^2 \psi_2 + k_4 - m_3 \omega^2 \\ & + \frac{(k_1 \cos \psi_1 - k_2 \cos \psi_2)^2 \left(-\frac{m_1 + m_2 + m_4}{m_2} k_3 + \frac{m_1 m_4}{m_2} \omega^2 \right)}{\Delta} \\ & + \frac{k_1^2 \cos^2 \psi_1 \left(-\frac{m_1 + m_2 + m_4}{m_2} k_2 + m_4 \omega^2 \right) + k_2^2 \cos^2 \psi_2 \left(-\frac{m_1 + m_2 + m_4}{m_2} k_1 + m_1 \omega^2 \right)}{\Delta} = 0 \end{aligned} \quad (8.59)$$

From equation (8.59), it is not difficult to study effects of different parameters on eigenvalues of the system. For the rotationally dominant modes, since the first two terms on the left side of the

characteristic equations are much smaller than the remaining terms, the natural frequencies are mainly determined by the axial stiffness, masses and the tensioner arm orientation. Therefore, the natural frequency should be weak functions of the translating speed. For transversely dominant modes, since $\cot(\omega_1/c'_1)$ or $\cot(\omega_2/c'_2)$ is very large, the natural frequencies are mainly determined by the span tension and the translating speed. Thus, the natural frequencies are expected to decrease significantly with the speed. For the lower order transversely dominant modes, the axial stiffness, masses and the tensioner arm orientation have some effect on the natural frequencies while for the higher order modes, the natural frequencies are almost independent on masses of the discrete components and the tensioner arm orientation.

The characteristic equation (8.59) is a nonlinear equation which can be solved numerically. The approach proposed for the analysis of the three-pulley system is readily extended to more complex belt drive systems involving multiple accessories. After having eigenvalues of the system, the corresponding eigenfunctions can be obtained by substituting these eigenvalues into equations (8.43) - (8.45), (8.47) and (8.53). It is noted that both the amplitudes of the complex eigenfunctions of the belt spans and the amplitudes of the real eigenvectors of the discrete components depend on the normalization.

8.3 RESPONSE TO ARBITRARY EXCITATIONS

The response of a single belt subjected to general excitations and initial conditions was obtained by Wickert and Mote (1990). In this study, modal analysis method for a single belt is extended to

the hybrid subsystem 2 while the response of subsystem 1 can be directly calculated using the results given by Wickert and Mote (1990).

Consider the expansion

$$\mathbf{U} = \sum_{n=1}^{\infty} \xi_n^R \psi_n^R + \xi_n' \psi_n' \quad (8.60)$$

as the solution of equation (8.21). The components $\xi_n^R(t)$ and $\xi_n'(t)$ of the generalized coordinates are real, and it is assumed that the expansion is complete. Substituting equation (8.60) into (8.21), forming an inner product with $(\psi_n^R \quad \psi_n')$ and using the orthonormality conditions lead to the following equations of motion for modal coordinates

$$\dot{\xi}_n^R - \omega_n \xi_n' = q_n^R(t) \quad (8.61)$$

$$\dot{\xi}_n' + \omega_n \xi_n^R = q_n'(t) \quad (8.62)$$

where

$$q_n^R(t) = -\omega_n \int_0^{t_1} \phi_{1n}' f_1(x, t) dx - \omega_n \int_0^{t_2} \phi_{2n}' f_2(x, t) dx \quad (8.63)$$

$$\begin{aligned} q_n'(t) = & \omega_n \int_0^{t_1} \phi_{1n}^R f_1(x, t) dx + \omega_n \int_0^{t_2} \phi_{2n}^R f_2(x, t) dx \\ & + \omega_n \hat{\chi}_{1n} f_3(t) + \omega_n \hat{\chi}_{2n} f_4(t) + \omega_n \hat{\chi}_{3n} f_5(t) + \omega_n \hat{\chi}_{4n} f_6(t) \end{aligned} \quad (8.64)$$

The solutions of equations (8.61) and (8.62) are given as follows

$$\begin{aligned} \xi_n^R(t) = & \int_0^t [q_n^R(s) \cos(\omega_n(t-s)) + q_n'(s) \sin(\omega_n(t-s))] ds + \\ & \xi_n^R(0) \cos(\omega_n t) + \xi_n'(0) \sin(\omega_n t) \end{aligned} \quad (8.65)$$

$$\begin{aligned} \xi_n'(t) = & \int_0^t [q_n'(s) \cos(\omega_n(t-s)) - q_n^R(s) \sin(\omega_n(t-s))] ds + \\ & \xi_n'(0) \cos(\omega_n t) - \xi_n^R(0) \sin(\omega_n t) \end{aligned} \quad (8.66)$$

where the initial values of the modal coordinates are

$$\xi_n^R(0) = \langle \mathbf{A}\mathbf{U}_0, \Psi_n^R \rangle \quad (8.67)$$

$$\xi_n'(0) = \langle \mathbf{A}\mathbf{U}_0, \Psi_n' \rangle \quad (8.68)$$

Following equation (8.60), the field variable expansion becomes

$$\mathbf{W} = \sum_{n=1}^{\infty} \xi_n^R \phi_n^R + \xi_n' \phi_n' \quad (8.69)$$

8.4 STEADY STATE RESPONSE SUBJECTED TO HARMONIC EXCITATIONS

In the previous section, the response of serpentine belt drive systems to arbitrary excitation is obtained using the eigenfunction expansion method. This result is obviously applicable to the steady state response of the system subjected to non-resonance harmonic excitations. However, since the expression is in terms of the linear mode shapes, it is not easy to use in the direct perturbation analysis for nonlinear systems. Explicit exact expression for the steady state response is still preferred.

Assume that the harmonic excitations are in the form

$$\mathbf{F} = \{f_1(x, t) \ f_2(x, t) \ f_3(x, t) \ f_4(x, t) \ f_5(x, t) \ f_6(x, t)\}^T e^{i\omega t} \quad (8.70)$$

where ω is the excitation frequency. The steady state response of the system is also harmonic with the same oscillation frequency

$$\mathbf{W} = \{\Phi_1(x) \ \Phi_2(x) \ \tilde{x}_1 \ \tilde{x}_2 \ \tilde{x}_3 \ \tilde{x}_4\}^T e^{i\omega t} \quad (8.71)$$

Substituting equations (8.70) and (8.71) into equation of motion of belt span 1 from equation (8.5) and eliminating $e^{i\omega t}$ yield the following two-point boundary-value problem

$$-m\omega^2\Phi_1(x) + 2i\omega mc \frac{d\Phi_1(x)}{dx} - P_{l_1} \frac{d^2\Phi_1(x)}{dx^2} = f_1(x) \quad (8.72)$$

$$\Phi_1(0) = 0 \quad (8.73)$$

$$\Phi_1(l_1) = \tilde{\chi}_3 \sin \psi_1 \quad (8.74)$$

The general solution of equation (8.72) is

$$\Phi_1(x) = e^{i\omega x/c'_1} [a_1 \sin(\omega x/c'_1) + b_1 \cos(\omega x/c'_1)] + \hat{\Phi}_1(x) \quad (8.75)$$

where $\hat{\Phi}_1(x)$ is the particular solution of equation (8.72). Applying boundary conditions, the integration constants in equation (8.75) can be obtained as

$$a_1 = \frac{[\tilde{\chi}_3 \sin \psi_1 - \hat{\Phi}_1(l_1)]e^{-i\omega l_1/c'_1} + \hat{\Phi}_1(0)\cos(\omega l_1/c'_1)}{\sin(\omega l_1/c'_1)} \quad (8.76)$$

$$b_1 = -\hat{\Phi}_1(0) \quad (8.77)$$

Similarly, for span 2, the spatial dependence function is given as follows

$$\Phi_2(x) = e^{i\omega x/c'_2} [a_2 \sin(\omega x/c'_2) + b_2 \cos(\omega x/c'_2)] + \hat{\Phi}_2(x) \quad (8.78)$$

with boundary conditions

$$\Phi_2(0) = \tilde{\chi}_3 \sin \psi_2 \quad (8.79)$$

$$\Phi_2(l_2) = 0 \quad (8.80)$$

where $\hat{\Phi}_2(x)$ is the particular solution. The integration constants a_2 and b_2 are obtained by using the boundary conditions:

$$a_2 = \frac{-\hat{\Phi}_2(l_2)e^{-i\omega l_2/c'_2}}{\sin(\omega l_2/c'_2)} - (\tilde{\chi}_3 \sin \psi_2 - \hat{\Phi}_2(0))\cot(\omega l_2/c'_2) \quad (8.81)$$

$$b_2 = \hat{\chi}_3 \sin \psi_2 - \hat{\Phi}_2(0) \quad (8.82)$$

Inserting equations (8.75) and (8.78) for belt spans into the equation of motion (8.5) for the tensioner arm, the terms involving w_1 and w_2 can be simplified as

$$-P_{t1}w_{1,x}\Big|_{l_1} + mcw_{1,t}\Big|_{l_1} = \left(-P_{t1}\sin\psi_1 \cot(\omega l_1/c'_1) \frac{\omega}{c'_1} \tilde{\chi}_3 + f_7 \right) e^{i\omega t} \quad (8.83)$$

$$-P_{t2}w_{2,x}\Big|_0 + mcw_{2,t}\Big|_0 = \left(P_{t2}\sin\psi_2 \cot(\omega l_2/c'_2) \frac{\omega}{c'_2} \tilde{\chi}_3 + f_8 \right) e^{i\omega t} \quad (8.84)$$

where

$$f_7 = -\frac{P_{t1}\omega e^{i\omega l_1/c'_1} \hat{\Phi}_1(0)}{c'_1 \sin(\omega l_1/c'_1)} + \left(i\omega mc + P_{t1} \cot(\omega l_1/c'_1) \frac{\omega}{c'_1} \right) \hat{\Phi}_1(l_1) - P_{t1} \hat{\Phi}'_1(l_1) \quad (8.85)$$

$$f_8 = \frac{P_{t2}\omega e^{-i\omega l_2/c'_2} \hat{\Phi}_2(l_2)}{c'_2 \sin(\omega l_2/c'_2)} + \left(i\omega mc - P_{t2} \cot(\omega l_2/c'_2) \frac{\omega}{c'_2} \right) \hat{\Phi}_2(0) - P_{t2} \hat{\Phi}'_2(0) \quad (8.86)$$

Substituting equations (8.83) and (8.84) into the equation of motion of the tensioner arm, rewriting the resulting equation and the three equations of motion for pulleys into matrix form, and eliminating $e^{i\omega t}$ lead to the following algebraic equation

$$(\mathbf{K}_{DD} - \mathbf{M}_{DD}\omega^2) \begin{Bmatrix} \tilde{\chi}_1 \\ \tilde{\chi}_2 \\ \tilde{\chi}_3 \\ \tilde{\chi}_4 \end{Bmatrix} = \begin{Bmatrix} f_3 \\ f_4 \\ f_5 + f_7 \sin\psi_1 - f_8 \sin\psi_2 \\ f_6 \end{Bmatrix} \quad (8.87)$$

where

$$\mathbf{K}_{DD} = \begin{bmatrix} k_1 + k_3 & -k_1 & -k_1 \cos\psi_1 & -k_3 \\ -k_1 & k_1 + k_2 & k_1 \cos\psi_1 - k_2 \cos\psi_2 & -k_2 \\ -k_1 \cos\psi_1 & k_1 \cos\psi_1 - k_2 \cos\psi_2 & k_{33} & k_2 \cos\psi_2 \\ -k_3 & -k_2 & k_2 \cos\psi_2 & k_2 + k_3 \end{bmatrix} \quad (8.88)$$

$$k_{33} = k_1 \cos^2\psi_1 + k_2 \cos^2\psi_2 + k_4 + P_{t1} \sin^2\psi_1 \cot(\omega l_1/c'_1) \frac{\omega}{c'_1} + P_{t2} \sin^2\psi_2 \cot(\omega l_2/c'_2) \frac{\omega}{c'_2} \quad (8.89)$$

$$\mathbf{M}_{DD} = \begin{bmatrix} m_1 & 0 & 0 & 0 \\ 0 & m_2 & 0 & 0 \\ 0 & 0 & m_3 & 0 \\ 0 & 0 & 0 & m_4 \end{bmatrix} \quad (8.90)$$

Substituting the solution of equation (8.87) into (8.75) and (8.78), the explicit exact expression for the response of the serpentine belt drive system is derived. It is noted that the solution procedure does not involve eigenfunction expansion. The solution in this form is very convenient to be used in the direct perturbation analysis of the corresponding nonlinear problem.

8.5 NUMERICAL RESULTS AND DISCUSSIONS

In this section, numerical results of natural frequencies and linear forced vibration response of serpentine belt drive systems are presented. Effects of the transport speed and the tensioner arm orientation on natural frequencies are discussed.

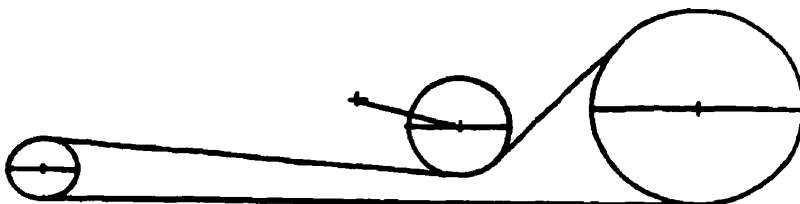


Figure 8.1: The three-pulley serpentine belt drive system

Two prototypical systems simulated are identical to those proposed by Beikmann *et al.* (1996) where natural frequencies of the two systems were calculated using the iteration approach. In this study, natural frequencies are obtained directly from the characteristic equation and the response is calculated from the exact closed-form expressions. The physical properties are shown in Table

8.1. The baseline system shown in Figure 8.1 has a first rotationally dominant mode frequency nearly twice that of the first transverse mode of span 3. The modified system is identical to the first, except for the addition of a 0.076kg mass to the tensioner arm.

Table 8.1: The physical properties of the prototypical system

	Pulley 1	Pulley 2	Tensioner arm	Pulley 4
Spin Axis Coordinates	(0.5525,0.0556)	(0.3477,0.05715)	(0.2508,0.0635)	(0.0, 0.0)
Radii (m)	0.0889	0.0452	0.097	0.02697
Rotational Inertia ($\text{kg}\cdot\text{m}^2$)	0.07248	0.00293	0.001165	0.000293
Other Physical Properties	Belt modulus: $EA=170000 \text{ N}$, $m=0.1029 \text{ kg/m}$, Tensioner Spring Constant: $k_s = 54.37 \text{ N-m/rad}$, Tensioner Pulley Mass: 0.302 kg (baseline) 0.378 kg (modified)			

The error function of the characteristic equation (8.59) is plotted against the frequency in Figure 8.2. It is seen that the transversely dominant natural frequencies are nearly equal to those of the fixed-fixed span. This is because the belt mass is small compared to the discrete masses. In this case, numerical problems occur for the iteration method due to the singularity. Analysis in clockwise and counter-clockwise is needed to ensure that no natural frequency is missed. However, from the explicit characteristic equation, all the eigenvalues can be obtained without any numerical difficulties.

Comparison of natural frequencies among those obtained from experiment (Beikmann *et al.*, 1996), Holzer's method (Beikmann *et al.*, 1996) and the approach proposed in this study is shown in Table 8.2 and Table 8.3. It can be seen that correlation among three methods is quite good. The first mode, for both systems, is dominated by span 3 vibration. Since there is no

coupling between the transverse vibration of span 3 and pulley rotations, the change of properties of subsystem 2 does not alter the natural frequency of span 3. This is demonstrated by the negligible difference in the fundamental natural frequency of span 3 between the baseline and modified systems. The second mode is the vibration dominated by span 2. It has a frequency of 50.53Hz in the baseline system and 50.27 Hz in the modified system.

Table 8.2: Comparison of the natural frequency of the baseline system at zero speed

Mode #	Experimental (Hz)	Holzer's Method (Hz)	Characteristic equation (Hz)	Dominant mode
1	33.0	32.03	32.03	1 st Mode, Span 3
2	51.75	50.52	50.53	1 st Mode, Span 2
3	62.5	62.22	62.18	1 st Rotational
4	N/A	N/A	102.50	2 nd mode , Span 2
5	N/A	N/A	114.19	1 st Mode, Span 1
6	N/A	N/A	153.75	3 rd Mode, Span 2
7	N/A	N/A	218.51	2 nd Mode, Rotational

Table 8.3: Comparison of the natural frequency of the modified system at zero speed

Mode #	Experimental (Hz)	Holzer's Method (Hz)	Characteristic equation (Hz)	Dominant mode
1	33.0	32.03	32.03	1 st Mode, Span 3
2	51.5	50.25	50.27	1 st Mode, Span 2
3	58.0	58.81	58.57	1 st Rotational
4	N/A	N/A	102.50	2 nd mode , Span 2
5	N/A	N/A	114.19	1 st Mode, Span 1
6	N/A	N/A	153.75	3 rd Mode, Span 2
7	N/A	N/A	203.19	2 nd Mode, Rotational

The third mode is dominated by the tensioner arm rotation. It has a natural frequency of 62.18 Hz in the baseline system and 58.27 Hz in the modified system. This demonstrates the significant effect of the mass on the natural frequency of this mode. The vibration mode shapes of the baseline system are shown in Figure 8.3 and Figure 8.4. As predicated in the modal analysis, there is a significant coupling between the span's transverse vibration and the tensioner arm rotational vibration as shown in Figures 8.3 and 8.4.

Table 8.4: Effect of the tensioner arm orientation on the natural frequency (Hz) of the baseline system at zero speed

Mode #	(ψ_1, ψ_2)			
	$(45.78^\circ, 91.26^\circ)$	$(49.54^\circ, 87.51^\circ)$	$(53.29^\circ, 83.76^\circ)$	$(60.79^\circ, 76.26^\circ)$
1	32.03	32.03	32.03	32.03
2	50.53	50.63	50.70	50.80
3	62.18	63.81	65.25	67.43
4	102.50	102.50	102.50	102.50
5	114.19	114.19	114.19	114.19
6	153.75	153.75	153.75	153.75
7	218.51	219.54	219.41	219.67

The effect of the tensioner arm orientation on natural frequencies is shown in Table 4. It can be seen that the tensioner arm orientation has a significant effect on the rotationally dominant mode while it has less effect on the transversely dominant mode for zero speed. From the characteristic equation, it is seen that the tensioner arm orientation affects the tensioner stiffness and the coupling between the tensioner arm and the transverse span motion. Therefore, the tensioner arm orientation influences rotationally dominant modes significantly. With the increase of the translating speed, the tensioner arm orientation will change the span tensions and thus will significantly affect the natural frequency of transversely dominant modes.

The effect of the translating speed on the natural frequencies of single moving belt has been studied extensively (Beikmann *et al.*, 1996, Moon and Wickert, 1997). However, for the whole serpentine belt drive system where the coupling between pulleys and belt spans exists, this effect need further considered. Beikmann *et al.* (1996) investigated this effect using experimental and numerical method. In this study, the relation between the translating speed and natural frequencies are obtained directly from the characteristic equation (8.59). Figure 8.5 illustrates the relation between natural frequencies and the engine speed for the baseline system and the modified system, respectively. Higher order transversely dominant mode frequencies are not shown in Figure 8.5 since they are simply integer times of the first transversely dominant mode frequency of span1 or span2. It is evident that the natural frequencies of rotationally dominant modes remain nearly constant while those of transversely dominant modes decrease with the speed. These results agree very well with the conclusions by Beikmann *et al.* (1996). It is noted that there are some irregularities for the second rotationally dominant mode. This is because at some operating speeds, a higher order transversely dominant mode frequency which is not shown in Figure 8.5 approaches that of the second rotationally dominant mode. This is termed "curve veering" and indicates large and complementary changes in the associated modes. From the characteristic equation (8.59), it can be seen that one of the first two terms on the left side of equation (8.59) becomes not negligible at curve veering, which result in some irregularities at some speeds.

The steady state responses of the serpentine belt system subjected to a harmonic excitation are shown in Figure 8.6 to Figure 8.8. The excitation is imposed on pulley 4 with the amplitude of excitation 2.697 N·m and the excitation frequency 124.36 Hz. Figure 8.6 and Figure 8.7 show 3-

D diagrams for the response of span 1 and span 2 with respect to time t and space x and Figure 8.8 shows the response of discrete components. It is seen that the response of span 1 at $x=0$ is zero while it is not equal to zero at the other end due to the coupling with the tensioner arm. The response of span 2 at $x=0$ is not equal to zero. The response of the tensioner arm is the largest compared with that of other pulleys. It is noted that for the linear model, when the excitation frequency is not equal to the natural frequency of the system, the dynamic response is very small. However, for the nonlinear model, under the condition of the internal resonance, the response may be very large.

8.6 SUMMARY AND CONCLUSIONS

The modal analysis of the linear prototypical serpentine belt drive system is performed in this study. The entire system is divided into two subsystems: subsystem 1 with belt span 3 only and subsystem 2 with other components. In the linear analysis, the equations of motion of these two subsystems are uncoupled. Therefore, it is convenient to deal with these two systems separately.

Although the eigenvalues and eigenfunctions of the prototypical system were calculated in previous study (Beikmann *et al.*, 1996), it is not convenient to investigate the effects of different parameters on eigenvalues since an iteration approach is employed. In this study, the explicit exact characteristic equation for eigenvalue is derived without using the iteration approach. From the characteristic equation, the following two conclusions about the effect of the design parameters on natural frequencies can be drawn:

- 1) The translating speed has a significant effect on natural frequencies of transversely dominant

modes while it has less effect on those of rotationally dominant modes. The natural frequencies of transversely dominant modes decrease with the increase of translating speed.

- 2) The tensioner arm orientation influences natural frequency of rotationally dominant modes greatly. At lower translating speed, the effect of the tensioner arm on transversely dominant modes is small. With the increase of the translating speed, this effect also increases.

The response of serpentine belt drive system subjected to arbitrary excitations is represented as a superposition of orthogonal eigenfunctions. When the excitations are non-resonance harmonic, the explicit exact solution without using eigenfunction expansion is derived. This kind of expression is particularly useful in the direct perturbation analysis of the corresponding nonlinear problems.

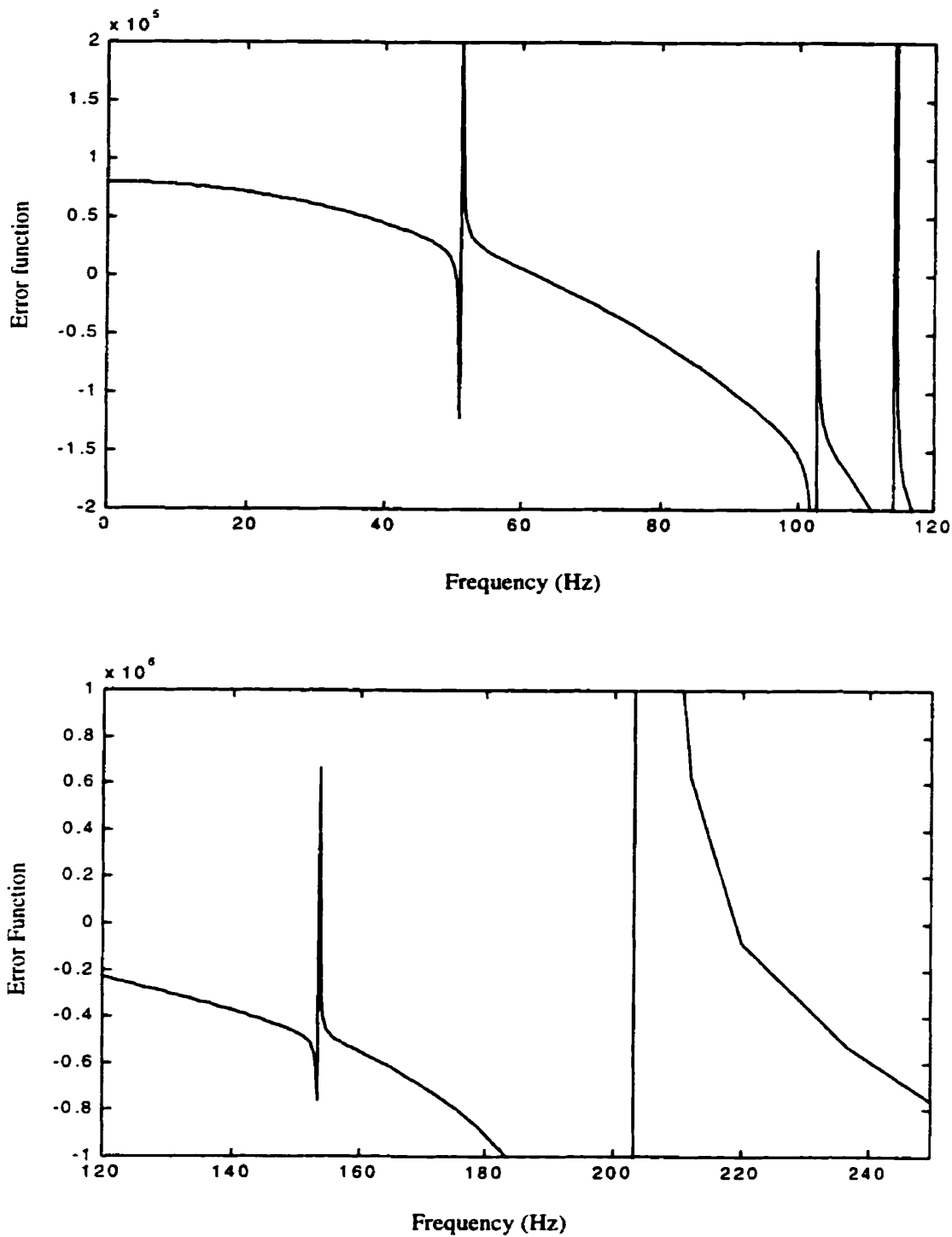


Figure 8.2: Error function of the characteristic equation for eigenvalues

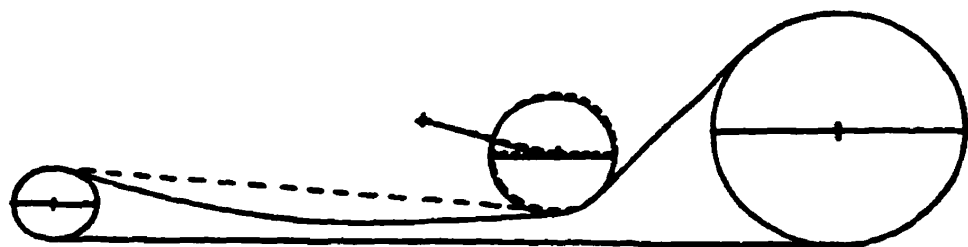


Figure 8.3: Transverse vibration mode of span 2 of the baseline system (50.53Hz)

— mode shape - - - baseline system

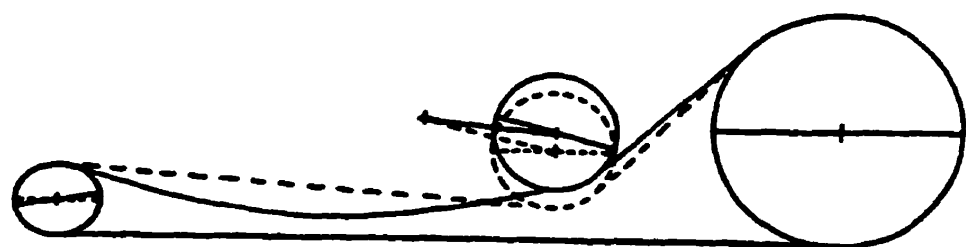


Figure 8.4: Rotational vibration mode of the baseline system (62.18 Hz)

— mode shape - - - baseline system

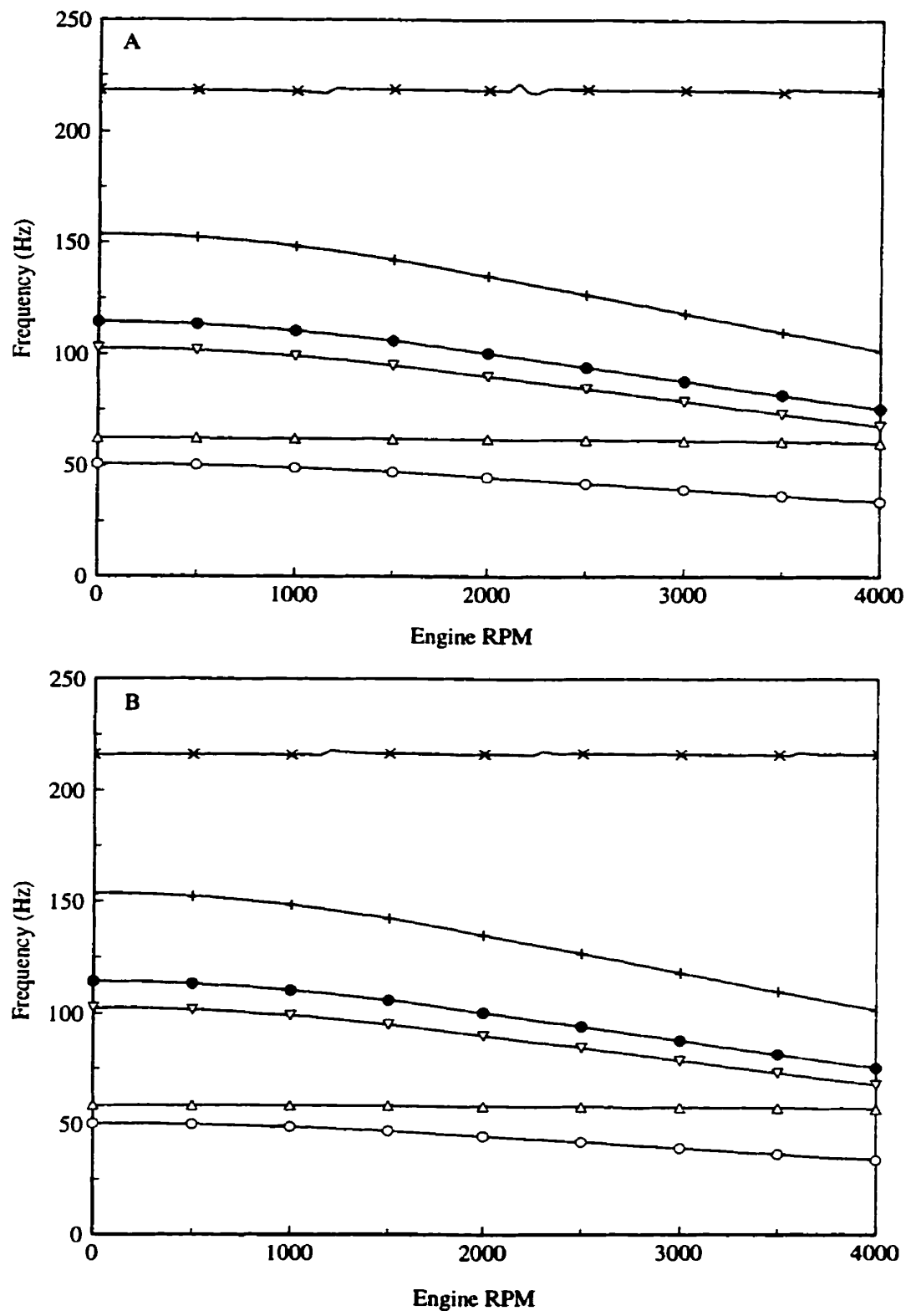


Figure 8.5: Relations between natural frequencies and the engine speed

A: the baseline system **B: the modified system**
 o: mode 2 Δ: mode 3 ▽: mode 4 ●: mode 5 +: mode 6 ×: mode 7

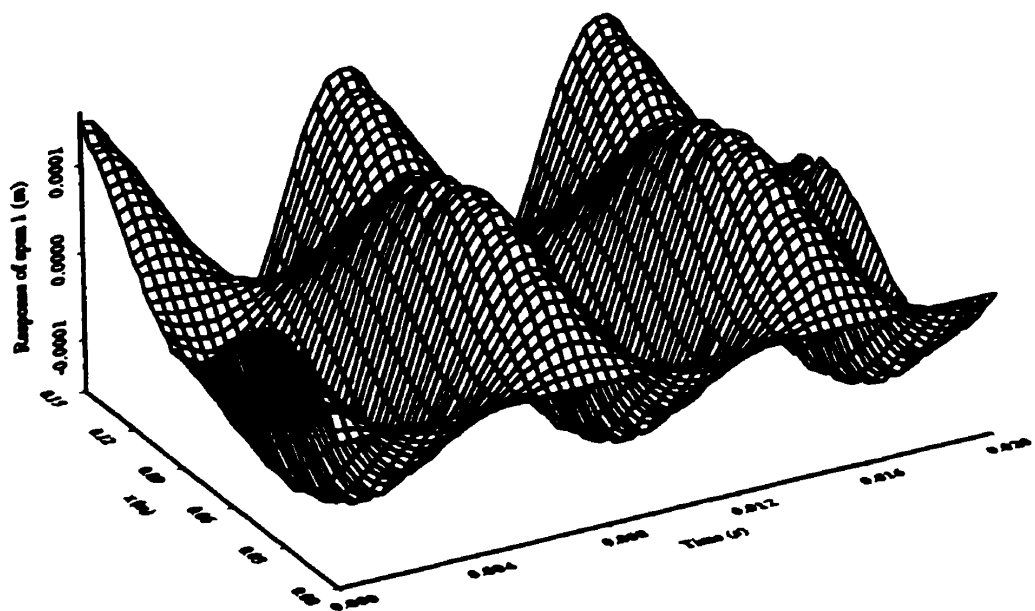


Figure 8.6: The steady state response of span 1

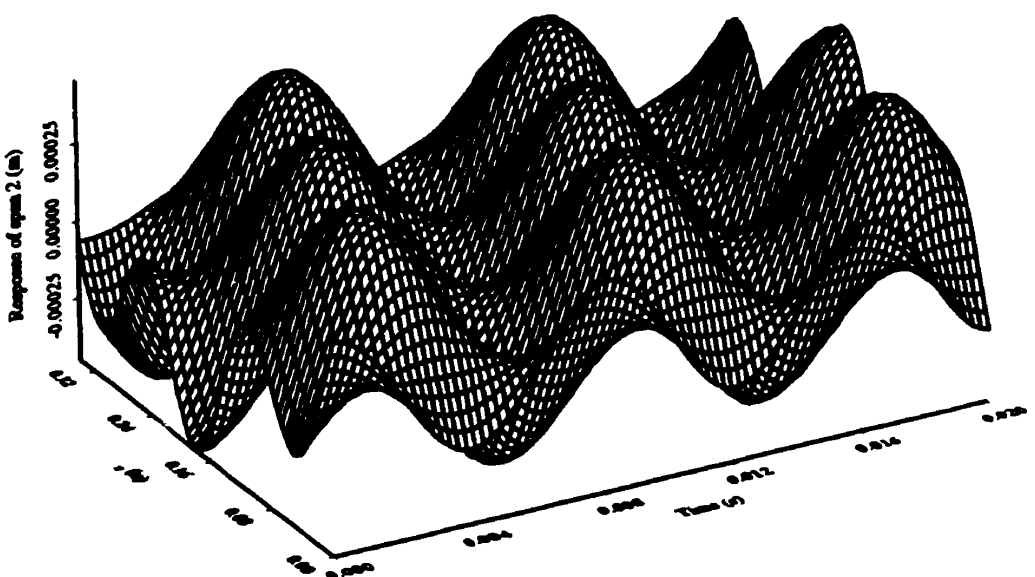


Figure 8.7: The steady state response of span 2

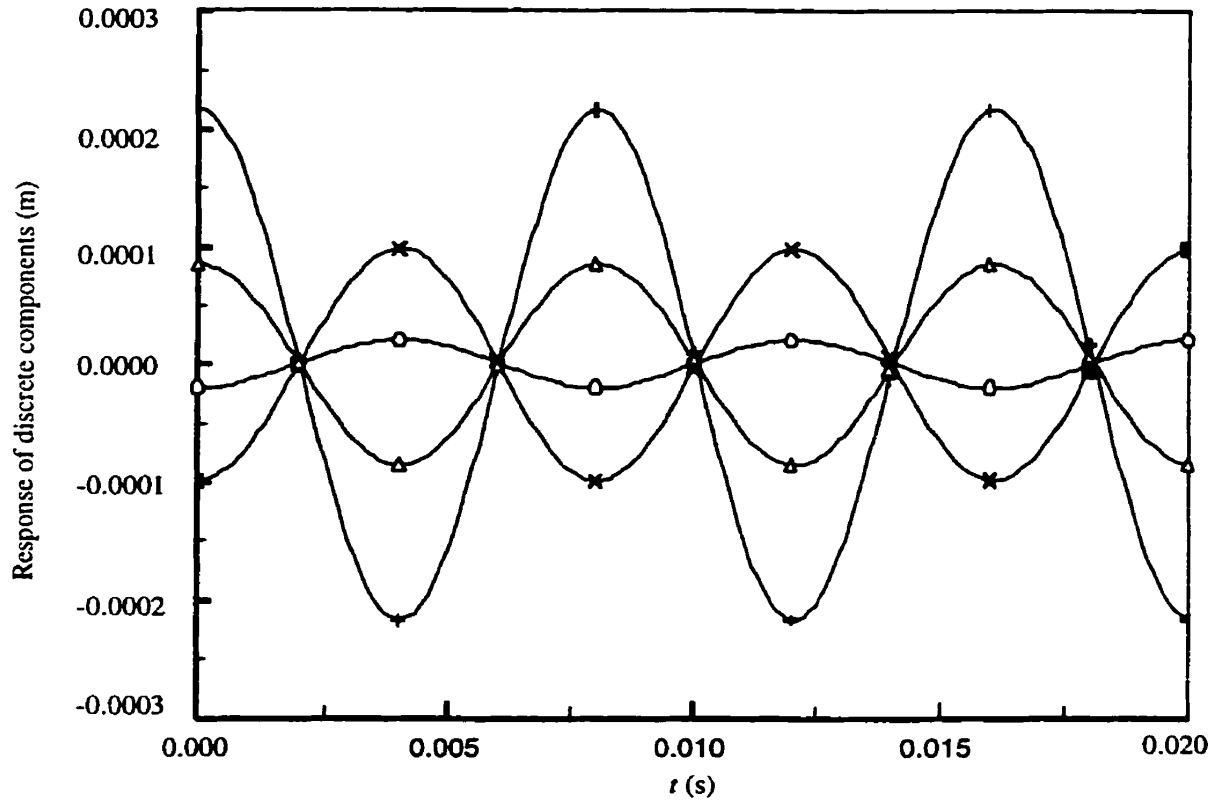


Figure 8.8: The steady state responses of discrete components

O Pulley 1 × Pulley 2 + Tensioner arm Δ Pulley 4

CHAPTER 9

COMPLEX MODAL ANALYSIS OF NON-SELF-ADJOINT SERPENTINE BELT DRIVE SYSTEMS

In Chapter 8, the modal analysis is performed for linear undamped serpentine belt drives. In this chapter, the damping introduced by viscoelasticity of belt materials is considered. In this case, the serpentine belt drive of interest is a hybrid, gyroscopic and damped system. Any system with combined effects of damping and gyroscopic forces belongs to a class of non-self-adjoint systems. The modal analysis proposed in Chapter 8 is not valid for a non-self-adjoint belt drive system since the eigenfunctions are not orthogonal to the operators. An approach to solve this problem is to use the bi-orthogonal state space eigenfunctions, which has to estimate the adjoint state space eigenfunctions whose physical meaning has not been well classified (Pesterev and Bergman, 1998). Only in a few special cases, the closed-form eigenfunctions of the adjoint system can be obtained.

In the present chapter, the complex modal analysis method is extended to the hybrid linear non-self-adjoint model of serpentine belt drive systems for the first time. The adjoint eigenfunctions are acquired in terms of the mode shapes of an auxiliary hybrid system. The explicit closed-form characteristic equation for eigenvalues and exact closed-form solution for dynamic response of non-self-adjoint hybrid serpentine belt drive systems are given.

9.1 CANONICAL FORM OF EQUATIONS OF MOTION

The equations of motion of a linear viscoelastic serpentine belt drive system are derived in Chapter 7. The damping terms introduced by Kelvin viscoelastic model have the same formulation as that of viscous damping. As in Chapter 8, the entire hybrid serpentine belt drive system is divided into two subsystems: subsystem 1 which includes span 3 only and subsystem 2 which includes all the other parts of the system. Since the linear vibration of subsystem 1 and subsystem 2 is decoupled, only subsystem 2 is considered here.

For subsystem 2, the equations of motion can be rewritten in matrix operator form

$$\mathbf{M}\ddot{\mathbf{W}} + (\mathbf{D} + \mathbf{G})\dot{\mathbf{W}} + \mathbf{K}\mathbf{W} = \mathbf{F} \quad (9.1)$$

with boundary condition

$$w_1(0, t) = 0 \quad w_1(l_1, t) = \chi_3(t) \sin \psi_1 \quad (9.2)$$

$$w_2(0, t) = \chi_3(t) \sin \psi_2 \quad w_2(l_2, t) = 0 \quad (9.3)$$

where matrix \mathbf{M} , \mathbf{G} , and \mathbf{K} , and vectors \mathbf{W} and \mathbf{F} are defined in Chapter 8. Damping matrix \mathbf{D} is defined as follows

$$\mathbf{D} = \begin{bmatrix} 0 & 0 & 0 & 0 & 0 \\ 0 & 0 & 0 & 0 & 0 \\ 0 & 0 & d_1 + d_3 & -d_1 & -d_1 \cos \psi_1 & -d_3 \\ 0 & 0 & -d_1 & d_1 + d_2 & d_1 \cos \psi_1 - d_2 \cos \psi_2 & -d_2 \\ 0 & 0 & -d_1 \cos \psi_1 & d_1 \cos \psi_1 - d_2 \cos \psi_2 & d_1 \cos^2 \psi_1 + d_2 \cos^2 \psi_2 + d_4 & d_2 \cos \psi_2 \\ 0 & 0 & -d_3 & -d_2 & d_2 \cos \psi_2 & d_2 + d_3 \end{bmatrix} \quad (9.4)$$

To apply the complex modal analysis method to the present non-conservative continuous-discrete system, equation (9.1) should be cast in the first order form:

$$\mathbf{A}\dot{\mathbf{U}} = \mathbf{B}\mathbf{U} + \mathbf{Q} \quad (9.5)$$

where the state vector and the excitation vector are defined as

$$\mathbf{U} = \begin{Bmatrix} \dot{\mathbf{W}} \\ \mathbf{W} \end{Bmatrix} \quad (9.6)$$

$$\mathbf{Q}(x,t) = \begin{Bmatrix} \mathbf{F}(x,t) \\ \mathbf{0} \end{Bmatrix} \quad (9.7)$$

and matrix differential operators \mathbf{A} and \mathbf{B} are defined as

$$\mathbf{A} = \begin{bmatrix} \mathbf{M} & \mathbf{0} \\ \mathbf{0} & \mathbf{I} \end{bmatrix} \quad (9.8)$$

$$\mathbf{B} = \begin{bmatrix} -(\mathbf{D} + \mathbf{G}) & -\mathbf{K} \\ \mathbf{I} & \mathbf{0} \end{bmatrix} \quad (9.9)$$

Equation (9.5) is the canonical form of the equations of motion and its solution satisfies the appropriate boundary conditions and initial conditions.

For the two arbitrary vectors

$$\mathbf{U} = \{u_1(x) \ u_2(x) \ u_3 \ u_4 \ u_5 \ u_6 \ u_7(x) \ u_8(x) \ u_9 \ u_{10} \ u_{11} \ u_{12}\} \quad (9.10)$$

and

$$\mathbf{V} = \{v_1(x) \ v_2(x) \ v_3 \ v_4 \ v_5 \ v_6 \ v_7(x) \ v_8(x) \ v_9 \ v_{10} \ v_{11} \ v_{12}\} \quad (9.11)$$

the inner product is defined as

$$\langle \mathbf{U}, \mathbf{V} \rangle = \int_0^{l_1} (u_1(x)\bar{v}_1(x) + u_7(x)\bar{v}_7(x))dx + \int_0^{l_2} (u_2(x)\bar{v}_2(x) + u_8(x)\bar{v}_8(x))dx + \sum_{i=3}^6 u_i \bar{v}_i + \sum_{i=9}^{12} u_i \bar{v}_i \quad (9.12)$$

With respect to this inner product, the matrix operator \mathbf{B} is non-self-adjoint since both damping and gyroscopic terms exist in the equations of motion. Therefore, the adjoint eigenvalue problem has to be solved.

9.2 THE ADJOINT EIGENVALUE PROBLEMS

For the distributed system, Yang (1996) showed that the adjoint eigenfunctions is related to the mode shapes of the original system. In this study, the relation between the eigenvalue problem of the adjoint system and that of the original system is studied for the hybrid serpentine belt drive system.

9.2.1 Formulation of the Adjoint Eigenvalue Problem

The eigenvalue problem associated with equation (9.5) is

$$\mathbf{B}\Psi_n = \lambda_n \mathbf{A}\Psi_n \quad (9.13)$$

where $\lambda_n \in C$ is the n th the eigenvalue and Ψ_n is the n th state space eigenfunction. Note that λ_n is not pure imaginary due to the presence of damping while λ_n is pure imaginary for undamped gyroscopic system. In light of equation (9.6), the complex eigenfunctions Ψ_n have the structure

$$\Psi_n = \{\lambda_n \phi_n \quad \Phi_n\}^T \quad (9.14)$$

$$\Phi_i = \{\phi_{1n}(x) \quad \phi_{2n}(x) \quad \hat{x}_{1n} \quad \hat{x}_{2n} \quad \hat{x}_{3n} \quad \hat{x}_{4n}\} \quad (9.15)$$

Here, ϕ_n is the physical space eigenfunction satisfying the following eigenvalue problem

$$[\lambda_n^2 \mathbf{M} + \lambda_n (\mathbf{D} + \mathbf{G}) + \mathbf{K}] \phi_n = 0 \quad (9.16)$$

The adjoint eigenvalue problem to equation (9.13) is defined as

$$\mathbf{B}^* \Gamma_n = \bar{\lambda}_n \mathbf{A}^* \Gamma_n \quad (9.17)$$

where the asterisk * denotes adjoint operator and Γ_n is the n th eigenfunction of the adjoint hybrid system in the state space which is in the form of

$$\Gamma_n = \{\Phi_n \quad \hat{\Phi}_n\}^T \quad (9.18)$$

$$\Phi_n = \{\varphi_{1n}(x) \quad \varphi_{2n}(x) \quad \tilde{\chi}_{1n} \quad \tilde{\chi}_{2n} \quad \tilde{\chi}_{3n} \quad \tilde{\chi}_{4n}\} \quad (9.19)$$

Since \mathbf{A} is a constant symmetric matrix, the adjoint differential operator \mathbf{A}^* is equal to \mathbf{A} . The adjoint differential operator \mathbf{B}^* can be determined from the definition of adjoint problems (Roach, 1982):

$$\langle \Gamma_i, \mathbf{B} \Psi_j \rangle = \langle \mathbf{B}^* \Gamma_i, \Psi_j \rangle \quad (9.20)$$

Substituting equation (9.9) and (9.14) into the left side of equation (9.20) and integrating by parts yield

$$\begin{aligned} \langle \Gamma_i, \mathbf{B} \Psi_j \rangle &= \langle -\bar{\lambda}_j (\mathbf{D} - \mathbf{G}) \varphi_i, \phi_j \rangle + \langle -\mathbf{K} \varphi_i, \phi_j \rangle + \langle \tilde{\varphi}_i, \lambda_j \phi_j \rangle \\ &\quad - 2mc\bar{\lambda}_j \varphi_{1i}(l_1) \bar{\phi}_{1j}(l_1) + 2mc\bar{\lambda}_j \tilde{\chi}_{3i} \sin \psi_1 \bar{\phi}_{1j}(l_1) \\ &\quad + 2mc\bar{\lambda}_j \varphi_{2i}(0) \bar{\phi}_{2j}(0) - 2mc\bar{\lambda}_j \tilde{\chi}_{3i} \sin \psi_2 \bar{\phi}_{2j}(0) \\ &\quad + P_{i1} \varphi_{1i}(l_1) \frac{\partial \bar{\phi}_{1j}(l_1)}{\partial x} - P_{i1} \tilde{\chi}_{3i} \sin \psi_1 \frac{\partial \bar{\phi}_{1j}(l_1)}{\partial x} - P_{i1} \varphi_{1i}(0) \frac{\partial \bar{\phi}_{1j}(0)}{\partial x} \\ &\quad - P_{i2} \varphi_{2i}(0) \frac{\partial \bar{\phi}_{1j}(0)}{\partial x} + P_{i2} \tilde{\chi}_{3i} \sin \psi_2 \frac{\partial \bar{\phi}_{1j}(0)}{\partial x} + P_{i2} \varphi_{2i}(l_2) \frac{\partial \bar{\phi}_{2j}(l_2)}{\partial x} \end{aligned} \quad (9.21)$$

Express \mathbf{B}^* in the following form:

$$\mathbf{B}^* = \begin{bmatrix} \mathbf{B}_{11} & \mathbf{B}_{12} \\ \mathbf{B}_{21} & \mathbf{B}_{22} \end{bmatrix} \quad (9.22)$$

where \mathbf{B}_{11} , \mathbf{B}_{12} , \mathbf{B}_{21} and \mathbf{B}_{22} are spatial operators to be determined. Inserting equation (9.22) into the right side of equation (9.20) leads to

$$\langle \mathbf{B}^* \Gamma_i, \Psi_j \rangle = \bar{\lambda}_j \langle \mathbf{B}_{11} \Phi_i, \phi_j \rangle + \bar{\lambda}_j \langle \mathbf{B}_{12} \tilde{\Phi}_i, \phi_j \rangle + \langle \mathbf{B}_{21} \Phi_i, \phi_j \rangle + \langle \mathbf{B}_{22} \tilde{\Phi}_i, \phi_j \rangle \quad (9.23)$$

Comparing the corresponding terms in equations (9.21) and (9.23), the following relations are derived

$$\mathbf{B}_{11} = -(\mathbf{D} - \mathbf{G}) \quad (9.24)$$

$$\mathbf{B}_{12} = \mathbf{I} \quad (9.25)$$

$$\mathbf{B}_{21} = -\mathbf{K} \quad (9.26)$$

$$\mathbf{B}_{22} = \mathbf{0} \quad (9.27)$$

$$\varphi_{1i}(0) = 0 \quad (9.28)$$

$$\varphi_{1i}(l_1) = \tilde{\chi}_{3i} \sin \psi_1 \quad (9.29)$$

$$\varphi_{2i}(0) = \tilde{\chi}_{3i} \sin \psi_2 \quad (9.30)$$

$$\varphi_{2i}(l_2) = 0 \quad (9.31)$$

Note that adjoint physical space eigenfunction φ_n satisfies the same boundary condition as the eigenfunction ϕ_n for the serpentine belt drive system. From equations (9.24) – (9.27), the adjoint differential operator \mathbf{B}^* is given by

$$\mathbf{B}^* = \begin{bmatrix} -(\mathbf{D}-\mathbf{G}) & \mathbf{I} \\ -\mathbf{K} & \mathbf{0} \end{bmatrix} \quad (9.32)$$

9.2.2 Physical Meaning of Adjoint Eigenfunctions

The physical meaning of adjoint eigenfunctions is not clear for systems with combined effects of damping and gyroscopic force. Extending a recent study on adjoint eigenfunctions of distributed

systems (Yang, 1996), the following discussion shows that the adjoint eigenfunctions can be obtained in terms of the mode shapes of an auxiliary system.

Substituting equation (9.18) into (9.17) yields

$$[\bar{\lambda}_n^2 \mathbf{M} + \bar{\lambda}_n (\mathbf{D} - \mathbf{G}) + \mathbf{K}] \varphi_n = 0 \quad (9.33)$$

$$\hat{\Phi}_n = -\frac{\mathbf{K}\varphi_n}{\bar{\lambda}_n} \quad (9.34)$$

Note that φ_n is the eigenfunction of the adjoint eigenvalue problem to equation (9.16). As defined in Chapter 8, the stiffness and gyroscopic matrix operators are dependent on the translating speed c of belts with the properties

$$\mathbf{K} = \mathbf{K}(c) = \mathbf{K}(-c) \quad (9.35)$$

$$\mathbf{G} = \mathbf{G}(c) = -\mathbf{G}(-c) \quad (9.36)$$

Define an auxiliary system

$$\ddot{\mathbf{M}}\tilde{\mathbf{W}} + (\mathbf{D} + \mathbf{G}(-c))\dot{\tilde{\mathbf{W}}} + \mathbf{K}\tilde{\mathbf{W}} = \mathbf{F} \quad (9.37)$$

with boundary conditions

$$\tilde{w}_1(0, t) = 0 \quad \tilde{w}_1(l_1, t) = \tilde{\chi}_3(t) \sin \psi_1 \quad (9.38)$$

$$\tilde{w}_2(0, t) = \tilde{\chi}_3(t) \sin \psi_2 \quad \tilde{w}_2(l_2, t) = 0 \quad (9.39)$$

where

$$\tilde{\mathbf{W}} = \{\tilde{w}_1(x, t) \ \tilde{w}_2(x, t) \ \tilde{\chi}_1(t) \ \tilde{\chi}_3(t) \ \tilde{\chi}_3(t) \ \tilde{\chi}_4(t)\}^T \quad (9.40)$$

The auxiliary system actually is the same as the original system represented by equation (9.1) except for that its transport speed is in the opposite direction. The eigenvalue problem of the auxiliary system is

$$[\tilde{\lambda}_n^2 \mathbf{M} + \tilde{\lambda}_n (\mathbf{D} \cdot \mathbf{G}) + \mathbf{K}] \tilde{\mathbf{p}}_n = 0 \quad (9.41)$$

where $\tilde{\lambda}_n$ and $\tilde{\mathbf{p}}_n$ are the n th eigenvalue and n th eigenfunction of the auxiliary system. It is seen that solutions of the eigenvalue problem (9.33) and (9.41) are in the relationships

$$\bar{\lambda}_n = \tilde{\lambda}_n \quad (9.42)$$

$$\Phi_n = \tilde{\Phi}_n \quad (9.43)$$

Therefore, the adjoint eigenfunction Φ_n is the mode shape of the auxiliary system (9.37). This conclusion provides an easy way to estimate the adjoint state space eigenfunctions.

9.3 ORTHOGONALITY OF STATE SPACE EIGENFUNCTIONS

The state space eigenfunctions of the original and the adjoint systems are in the bi-orthogonality relations

$$\langle \Gamma_i, \mathbf{B}\Psi_j \rangle = \bar{\lambda}_j \delta_{ij} \quad (9.44)$$

$$\langle \Gamma_i, \mathbf{A}\Psi_j \rangle = \delta_{ij} \quad (9.45)$$

The above equations are proved as follows. The inner product of equation (9.13) with Γ_i is

$$\langle \Gamma_i, \mathbf{B}\Psi_j \rangle = \langle \Gamma_i, \lambda_j \mathbf{A}\Psi_j \rangle \quad (9.46)$$

and the inner product of equation (9.17) with Ψ_j is

$$\langle \mathbf{B}^* \Gamma_i, \Psi_j \rangle = \bar{\lambda}_i \langle \mathbf{A}^* \Gamma_i, \Psi_j \rangle \quad (9.47)$$

According to the definition of adjoint operators equation (9.20), the adjoint operator \mathbf{A}^* and \mathbf{B}^* satisfy the following equations

$$\langle \Gamma_i, \mathbf{A}\Psi_j \rangle = \langle \mathbf{A}^*\Gamma_i, \Psi_j \rangle \quad (9.48)$$

$$\langle \Gamma_i, \mathbf{B}\Psi_j \rangle = \langle \mathbf{B}^*\Gamma_i, \Psi_j \rangle \quad (9.49)$$

Subtracting equation (9.46) from (9.47) and using equations (9.48) and (9.49) lead to

$$(\bar{\lambda}_i - \bar{\lambda}_j) \langle \Gamma_i, \mathbf{A}\Psi_j \rangle = 0 \quad (9.50)$$

By assumption, the eigenvalues $\bar{\lambda}_i$ and $\bar{\lambda}_j$ are distinct. Hence, equation (9.50) can be satisfied if and only if

$$\langle \Gamma_i, \mathbf{A}\Psi_j \rangle = 0 \quad (9.51)$$

Equation (9.51) represents the bi-orthogonality relation of state space eigenfunctions of hybrid serpentine drive systems. Substituting equation (9.51) into (9.46), it can be shown that the state space eigenfunctions satisfy a second bi-orthogonality relation, namely,

$$\langle \Gamma_i, \mathbf{B}\Psi_j \rangle = 0 \quad (9.52)$$

If an eigenvalue has multiplicity m , then there are exactly m eigenfunctions belonging to the repeated eigenvalue, and these eigenfunctions are generally not orthogonal to one another, although they are independent and orthogonal to the remaining eigenfunctions of the hybrid system. However, independent functions can be orthogonalized by using the Schmidt orthogonalization procedure.

Note that the eigenvalue problems, equation (9.13) and (9.17), are homogeneous. Thus only the shape of the eigenfunctions is unique and the amplitude is arbitrary. This arbitrariness can be removed through normalization. A mathematically convenient normalization scheme is given by

$$\langle \Gamma_i, \mathbf{A}\Psi_i \rangle = \bar{\lambda}_i \langle \Phi_i, \mathbf{M}\Phi_i \rangle - \frac{1}{\bar{\lambda}_i} \langle \mathbf{K}\Phi_i, \Phi_i \rangle = 1 \quad (9.53)$$

where

$$\begin{aligned} \langle \Phi_i, \mathbf{M}\Phi_i \rangle &= \int_0^{l_1} m\varphi_{1i}(x)\bar{\psi}_{1i}(x)dx + \int_0^{l_2} m\varphi_{2i}(x)\bar{\psi}_{2i}(x)dx \\ &\quad m_1\tilde{\chi}_{1i}\bar{\tilde{\chi}}_{1i} + m_2\tilde{\chi}_{2i}\bar{\tilde{\chi}}_{2i} + m_3\tilde{\chi}_{3i}\bar{\tilde{\chi}}_{3i} + m_4\tilde{\chi}_{4i}\bar{\tilde{\chi}}_{4i} \end{aligned} \quad (9.54)$$

$$\begin{aligned} \langle \mathbf{K}\Phi_i, \Phi_i \rangle &= \int_0^{l_1} P_{r1} \frac{\partial \varphi_{1i}(x)}{\partial x} \frac{\partial \bar{\psi}_{1i}(x)}{\partial x} dx + \int_0^{l_2} P_{r2} \frac{\partial \varphi_{2i}(x)}{\partial x} \frac{\partial \bar{\psi}_{2i}(x)}{\partial x} dx \\ &\quad + \{\tilde{\chi}_{1i} \quad \tilde{\chi}_{2i} \quad \tilde{\chi}_{3i} \quad \tilde{\chi}_{4i}\} \mathbf{K}_{DD} \{\bar{\tilde{\chi}}_{1i} \quad \bar{\tilde{\chi}}_{2i} \quad \bar{\tilde{\chi}}_{3i} \quad \bar{\tilde{\chi}}_{4i}\}^T \end{aligned} \quad (9.55)$$

$$\mathbf{K}_{DD} = \begin{bmatrix} k_1 + k_3 & -k_1 & -k_1 \cos \psi_1 & -k_3 \\ -k_1 & k_1 + k_2 & k_1 \cos \psi_1 - k_2 \cos \psi_2 & -k_2 \\ -k_1 \cos \psi_1 & k_1 \cos \psi_1 - k_2 \cos \psi_2 & k_1 \cos^2 \psi_1 + k_2 \cos^2 \psi_2 + k_4 & k_2 \cos \psi_2 \\ -k_3 & -k_2 & k_2 \cos \psi_2 & k_2 + k_3 \end{bmatrix} \quad (9.56)$$

9.4 COMPLEX MODAL ANALYSIS OF SERPENTINE BELT DRIVE SYSTEMS

In Chapter 8, the explicit exact characteristic equation of undamped serpentine belt drive systems is derived. In this chapter, the same approach is employed to determine the eigenvalues and eigenfunctions of damped serpentine belt drive systems. The eigenfunctions of the corresponding adjoint system are also derived in terms of the proposed auxiliary system.

9.4.1 Eigenvalues and Eigenfunctions of the Serpentine Belt Drive System

It is assumed that the motion of the serpentine belt drive system is in the form

$$\mathbf{W} = \phi_n e^{\lambda_n t} \quad (9.57)$$

Substituting equation (9.57) into equations of pulleys from equation (9.1) without the force terms, eliminating $e^{\lambda_n t}$, and putting those terms including $\hat{\chi}_{3n}$ on the right of equations yield

$$(k_1 + k_3 + d_1 \lambda_n + d_3 \lambda_n + m_1 \lambda_n^2) \hat{\chi}_{1n} - (k_1 + d_1 \lambda_n) \hat{\chi}_{2n} - (k_3 + d_3 \lambda_n) \hat{\chi}_{4n} = (k_1 + d_1 \lambda_n) \cos \psi_1 \hat{\chi}_{3n} \quad (9.58)$$

$$-(k_1 + d_1 \lambda_n) \hat{\chi}_{1n} + (k_1 + k_2 + d_1 \lambda_n + d_2 \lambda_n + m_2 \lambda_n^2) \hat{\chi}_{2n} - (k_2 + d_2 \lambda_n) \hat{\chi}_{4n} = \\ ((k_2 + d_2 \lambda_n) \cos \psi_2 - (k_1 + d_1 \lambda_n) \cos \psi_1) \hat{\chi}_{3n} \quad (9.59)$$

$$-(k_3 + d_3 \lambda_n) \hat{\chi}_{1n} - (k_2 + d_2 \lambda_n) \hat{\chi}_{2n} + (k_2 + k_3 + d_2 \lambda_n + d_3 \lambda_n + m_4 \lambda_n^2) \hat{\chi}_{4n} = \\ -(k_2 + d_2 \lambda_n) \cos \psi_2 \hat{\chi}_{3n} \quad (9.60)$$

Sum of equations (9.58) – (9.60) leads to

$$m_1 \hat{\chi}_{1n} + m_2 \hat{\chi}_{2n} + m_4 \hat{\chi}_{4n} = 0 \quad (9.61)$$

Inserting equation (9.61) into (9.58) and (9.60) and solving the resulting equations yield

$$\hat{\chi}_{1n} = C_{13} \hat{\chi}_{3n} \quad (9.62)$$

$$\hat{\chi}_{2n} = C_{23} \hat{\chi}_{3n} \quad (9.63)$$

$$\hat{\chi}_{4n} = C_{43} \hat{\chi}_{3n} \quad (9.64)$$

where

$$C_{13} = \frac{\left[\left(1 + \frac{m_4}{m_2} \right) (k_2 + d_2 \lambda_n) + k_3 + d_3 \lambda_n + m_4 \lambda_n^2 \right] (k_1 + d_1 \lambda_n) \cos \psi_1}{\Delta} \quad (9.65)$$

$$+ \frac{\left(\frac{m_4}{m_2} (k_1 + d_1 \lambda_n) - (k_3 + d_3 \lambda_n) \right) (k_2 + d_2 \lambda_n) \cos \psi_2}{\Delta}$$

$$C_{23} = \frac{\left(-\frac{m_1}{m_2} (k_2 + d_2 \lambda_n) - \frac{m_1 + m_4}{m_2} (k_3 + d_3 \lambda_n) - \frac{m_1 m_4}{m_2} \lambda_n^2 \right) (k_1 + d_1 \lambda_n) \cos \psi_1}{\Delta} \quad (9.66)$$

$$+ \frac{\left(\frac{m_4}{m_2} (k_1 + d_1 \lambda_n) + \frac{m_1 + m_4}{m_2} (k_3 + d_3 \lambda_n) + \frac{m_1 m_4}{m_2} \lambda_n^2 \right) (k_2 + d_2 \lambda_n) \cos \psi_2}{\Delta}$$

$$C_{43} = \frac{-\left(\frac{m_1}{m_2}(k_2 + d_2\lambda_n) - (k_3 + d_3\lambda_n)\right)(k_1 + d_1\lambda_n)\cos\psi_1}{\Delta} \\ - \frac{\left[\left(1 + \frac{m_1}{m_2}\right)(k_1 + d_1\lambda_n) + (k_3 + d_3\lambda_n) - m_1\lambda_n^2\right](k_2 + d_2\lambda_n)\cos\psi_2}{\Delta} \quad (9.67)$$

$$\Delta = \left[\left(1 + \frac{m_1}{m_2}\right)(k_1 + d_1\lambda_n) + (k_3 + d_3\lambda_n) + m_1\lambda_n^2 \right] \left(1 + \frac{m_4}{m_2}\right)(k_2 + d_2\lambda_n) + (k_3 + d_3\lambda_n) + m_4\lambda_n^2 \right] \\ - \left(\frac{m_1}{m_2}(k_2 + d_2\lambda_n) - (k_3 + d_3\lambda_n) \right) \left(\frac{m_4}{m_2}(k_1 + d_1\lambda_n) - (k_3 + d_3\lambda_n) \right) \quad (9.68)$$

For belt span 1, the eigenfunction $\phi_{1n}(x)$ can be expressed as

$$\phi_{1n}(x) = a_1 e^{\lambda_n \left(\frac{x+x'}{c_a - c'_1} \right)} + b_1 e^{\lambda_n \left(\frac{x-x'}{c_a - c'_1} \right)} \quad (9.69)$$

Using boundary conditions $\phi_{1n}(0) = 0$ and $\phi_{1n}(l_1) = \hat{\chi}_{3n} \sin\psi_1$ to determine the integration constants in the eigenfunction expression (9.69) leads to

$$a_1 = \frac{\hat{\chi}_{3n} \sin\psi_1 e^{-\lambda_n \left(\frac{l_1 - l_1}{c_a - c'_1} \right)}}{e^{2\lambda_n \frac{l_1}{c'_1}} - 1} \quad (9.70)$$

$$b_1 = -a_1 \quad (9.71)$$

Similarly, for span 2, the eigenfunction can be expressed as

$$\phi_{2n}(x) = a_2 e^{\lambda_n \left(\frac{x+x'}{c_b - c'_2} \right)} + b_2 e^{\lambda_n \left(\frac{x-x'}{c_b - c'_2} \right)} \quad (9.72)$$

Applying the boundary conditions $\phi_{2n}(0) = \hat{\chi}_{3n} \sin\psi_2$ and $\phi_{2n}(l_2) = 0$, the integration constants in equation (9.72) can be obtained as follows

$$a_2 = \frac{\chi_{3n} \sin \psi_2}{e^{2\lambda_n l_2/c_2}} \quad (9.73)$$

$$b_2 = \frac{\chi_{3n} \sin \psi_2}{e^{-2\lambda_n l_2/c_2}} \quad (9.74)$$

Substituting equations (9.62) - (9.64), (9.69) and (9.72) into the equation of motion (9.1) for tensioner arm yields the characteristic equation for eigenvalues of the damped serpentine belt drive system

$$\begin{aligned} & P_{11} \sin^2 \psi_1 \frac{(e^{2\lambda_n/c_1} + 1)\lambda_n}{(e^{2\lambda_n/c_1} - 1)c'_1} + P_{12} \sin^2 \psi_2 \frac{(e^{2\lambda_n/c_2} + 1)\lambda_n}{(e^{2\lambda_n/c_2} - 1)c'_2} \\ & + k_1 \cos^2 \psi_1 + k_2 \cos^2 \psi_2 + k_4 + (d_1 \cos^2 \psi_1 + d_2 \cos^2 \psi_2 + d_4) \lambda_n + m_3 \lambda_n^2 \\ & - (k_1 + d_1 \lambda_n) \cos \psi_1 C_{13} + (k_1 \cos \psi_1 - k_2 \cos \psi_2 + d_1 \cos \psi_1 \lambda_n - d_2 \cos \psi_2 \lambda_n) C_{23} \\ & + (k_2 + d_2 \lambda_n) \cos \psi_2 C_{43} = 0 \end{aligned} \quad (9.75)$$

9.4.2 Eigenfunctions of the Adjoint System

As discussed in Section 9.2, the eigenfunctions of the adjoint system are the mode shapes of the auxiliary system, which is the same as the original system but with its transport speed in the opposite direction.

After calculating the eigenvalue λ_n of the original system, replacing λ_n with $\bar{\lambda}_n$ in equations (9.62) – (9.64) yields the modal shapes of discrete elements,

$$\tilde{\chi}_{1n} = \tilde{C}_{13} \tilde{\chi}_{3n} \quad (9.76)$$

$$\tilde{\chi}_{2n} = \tilde{C}_{23} \tilde{\chi}_{3n} \quad (9.77)$$

$$\tilde{\chi}_{4n} = \tilde{C}_{43} \tilde{\chi}_{3n} \quad (9.78)$$

Since the transport speed of the auxiliary system is in the opposite direction, the eigenfunction $\varphi_{1n}(x)$ can be expressed as

$$\varphi_{1n}(x) = \tilde{a}_1 e^{\bar{\lambda}_n \left(\frac{x - l_1}{c_a - c'_1} \right)} + \tilde{b}_1 e^{\bar{\lambda}_n \left(\frac{x - l_1}{c_a - c'_1} \right)} \quad (9.79)$$

Note that formulation of the eigenfunctions of the auxiliary system is the same as that of the original system except that the phase propagation velocity c'_a is minus. Using boundary conditions $\varphi_{1n}(0) = 0$ and $\varphi_{1n}(l_1) = \tilde{\chi}_{3n} \sin \psi_1$ to determine the integration constants in the eigenfunction expression (9.79) leads to

$$\tilde{a}_1 = \frac{\tilde{\chi}_{3n} \sin \psi_1 e^{-\bar{\lambda}_n \left(\frac{l_1 - l_1}{c_a - c'_1} \right)}}{e^{2\bar{\lambda}_n \frac{l_1}{c'_1}} - 1} \quad (9.80)$$

$$\tilde{b}_1 = -\tilde{a}_1 \quad (9.81)$$

Similarly, for span 2 of the auxiliary system, the eigenfunction can be expressed as

$$\varphi_{2n}(x) = \tilde{a}_2 e^{\bar{\lambda}_n \left(\frac{x - l_2}{c_b - c'_2} \right)} + \tilde{b}_2 e^{\bar{\lambda}_n \left(\frac{x - l_2}{c_b - c'_2} \right)} \quad (9.82)$$

Applying the boundary condition $\varphi_{2n}(0) = \tilde{\chi}_{3n} \sin \psi_2$ and $\varphi_{2n}(l_2) = 0$, the integration constants in equation (9.82) can be obtained as follows

$$\tilde{a}_2 = \frac{\tilde{\chi}_{3n} \sin \psi_2}{e^{-2\bar{\lambda}_n \frac{l_2}{c'_2}} - 1} \quad (9.83)$$

$$\tilde{b}_2 = \frac{\tilde{\chi}_{3n} \sin \psi_2}{1 - e^{-2\bar{\lambda}_n \frac{l_2}{c'_2}}} \quad (9.84)$$

9.5 MODAL EXPANSION REPRESENTATION FOR THE DYNAMIC RESPONSE

The modal expansion theorem lays a foundation for developing series solutions method for hybrid non-self-adjoint systems. Consider the expansion

$$\mathbf{U} = \sum_{i=1}^{\infty} \xi_i \psi_i \quad (9.85)$$

as the solution of equation (9.5) and it is assumed that the expansion is complete. Substituting equation (9.85) into (9.5), forming an inner product with Γ_n and using the bi-orthonormality conditions lead to the following equations of motion for modal coordinates

$$\dot{\xi}_n = \bar{\lambda}_n \xi_n + q_n(t) \quad n = 1, 2, \dots \quad (9.86)$$

where

$$q_n(t) = \int_0^{t_1} \varphi_{1n}(x) f_1(x, t) dx + \int_0^{t_2} \varphi_{2n}(x) f_2(x, t) dx \\ + \tilde{\chi}_{1n} f_3(t) + \tilde{\chi}_{2n} f_4(t) + \tilde{\chi}_{3n} f_5(t) + \tilde{\chi}_{4n} f_6(t) \quad (9.87)$$

Representing complex values in the standard form $\xi_n = \xi_n^R + i\xi_n^I$, $q_n = q_n^R + iq_n^I$, $\Gamma_n = \Gamma_n^R + i\Gamma_n^I$

and denoting $\lambda_n = \alpha_n + i\omega_n$, equation (9.86) can be rewritten as two real equations as

$$\dot{\xi}_n^R = \alpha_n \xi_n^R + \omega_n \xi_n^I + q_n^R(t) \quad (9.88)$$

$$\dot{\xi}_n^I = -\omega_n \xi_n^R + \alpha_n \xi_n^I + q_n^I(t) \quad (9.89)$$

Comparing equations (9.88) and (9.89) for non-self-adjoint systems with equations (8.61) and (8.62) for undamped systems shows that additional terms $\alpha_n \xi_n^R$ and $\alpha_n \xi_n^I$ related to damping occur in the mode equations. The solutions of equation (9.88) and (9.89) are given as follows

$$\xi_n^R(t) = \int_0^t e^{\alpha_n(t-s)} [q_n^R(s) \cos(\omega_n(t-s)) + q_n^I(s) \sin(\omega_n(t-s))] ds \\ + e^{\alpha_n t} (\xi_n^R(0) \cos(\omega_n t) + \xi_n^I(0) \sin(\omega_n t)) \quad (9.90)$$

$$\begin{aligned}\xi_n^I(t) = & \int_0^t e^{\alpha_n(t-s)} [q_n^I(s)\cos(\omega_n(t-s)) - q_n^R(s)\sin(\omega_n(t-s))] ds \\ & + e^{\alpha_n t} (\xi_n^I(0)\cos(\omega_n t) - \xi_n^R(0)\sin(\omega_n t))\end{aligned}\quad (9.91)$$

where the initial values of the modal coordinates are

$$\xi_n^R(0) = \langle \Gamma_n^R, \mathbf{A}\mathbf{U}_0 \rangle \quad (9.92)$$

$$\xi_n^I(0) = \langle \Gamma_n^I, \mathbf{A}\mathbf{U}_0 \rangle \quad (9.93)$$

Following equation (9.85), the field variable expansion becomes

$$\mathbf{W} = 2 \sum_{n=1}^{\infty} (\xi_n^R \phi_n^R - \xi_n^I \phi_n^R) \quad (9.94)$$

9.6 SUMMARY AND CONCLUSIONS

The complex modal method is applied to hybrid non-self-adjoint serpentine belt drive systems. A relationship between the adjoint state space eigenfunctions and the original mode shapes is established. This relationship makes it possible to represent the adjoint eigenfunctions with the equations of motion for an auxiliary system. The dynamic responses of a non-self-adjoint system subjected to arbitrary disturbance and initial conditions are obtained in modal expansion expression. The major conclusions of this study include:

- 1) The eigenvalue of non-self-adjoint system is not pure imaginary, which is different from undamped serpentine belt drive systems.
- 2) The eigenfunctions of the adjoint system are the modal shapes of the auxiliary system, which is the same as the original system but with its transport speed in the opposite direction
- 3) The state space eigenfunctions of original system and the corresponding adjoint system are in the bi-orthogonality relations.

CHAPTER 10

NONLINEAR VIBRATION ANALYSIS OF ELASTIC

SERPENTINE BELT DRIVE SYSTEMS: DISCRETIZATION

MULTIPLE SCALES METHOD

The current chapter deals with the nonlinear vibration of elastic serpentine belt drive systems using discretization multiple scales method. In the serpentine belt drives, nonlinear interactions between rotational and transverse vibrations could cause large parametric resonance, which seriously impacts the noise and vibration performance of vehicles. Therefore, it is very important to predict the excitation threshold levels of parametric resonance and provide recommendations to reduce vibration levels.

Beikmann *et al.* (1996) used Runge-Kutta method to calculate the nonlinear response of serpentine belt drives. Although the numerical integration method can provide the trends of nonlinear responses, it can not provide a basic understanding of parametric resonance and the existence of multiple limit cycles.

In this chapter, belt material is considered to be linear elastic and modal damping is introduced to capture the energy dissipation of the system. The equation of motion is cast into a system of first order equations and suitable orthogonal basis functions are chosen to discretize the equations. The method of multiple scales is then used to treat the resulting ordinary differential equations.

The cases of both one-to-one and two-to-one internal resonances combined with a primary external resonance are considered. Solutions for the amplitude of non-trivial limit cycles are obtained. It is shown that quadratic nonlinearity terms in the equations affect the behavior of the system significantly. Effects of excitation frequencies, excitation amplitudes and modal damping on dynamic responses are investigated. Stability analyses of the amplitude and phase modulation equations are performed.

10.1 DISCRETIZATION

A prototypical serpentine belt drive system developed by Beikmann *et al.* (1996) shown in Figure 7.1 is used in the present study. The complete derivation of equations of motion for this model is given in Chapter 7. However, the viscoelasticity is not included in this chapter to simplify the problem. Instead, modal damping is introduced to capture the energy dissipation of the system. The nonlinear equations of motion for the belt spans couple to those governing the four discrete elements (three pulleys and the tensioner arm). As shown by Beikmann *et al.* (1996), for linear analysis, the transverse vibration of span 3 and the vibration of other components are decoupled. Thus, it is desirable to divide the entire system into two subsystems: subsystem 1 which includes span 3 only and subsystem 2 which includes all the other components of the whole system.

10.1.1 Symbolic Form of Equations of Motion for Subsystem 1 and Subsystem 2

For subsystem 1, the equation of motion is compactly written in the operator form as

$$\mathbf{M}_3 \ddot{\mathbf{w}}_3 + \mathbf{G}_3 \dot{\mathbf{w}}_3 + \mathbf{K}_3 \mathbf{w}_3 = \mathbf{F}_3 \quad (10.1)$$

with boundary conditions

$$w_3(0, t) = 0 \quad w_3(l_3, t) = 0 \quad (10.2)$$

where

$$\mathbf{M}_3 = m \quad \mathbf{G}_3 = 2mc \frac{\partial}{\partial x} \quad \mathbf{K}_3 = -P_{t3} \frac{\partial^2}{\partial x^2} \quad \mathbf{F}_3 = P_{d3} w_{3,xx} \quad (10.3)$$

For subsystem 2, the equations of motion can be rewritten in the operator form as

$$\mathbf{M}\ddot{\mathbf{W}} + \mathbf{G}\dot{\mathbf{W}} + \mathbf{K}\mathbf{W} = \mathbf{F} \quad (10.4)$$

with boundaries

$$w_1(0, t) = 0 \quad w_1(l_1, t) = \chi_3(t) \sin \psi_1 \quad (10.5)$$

$$w_2(0, t) = \chi_3(t) \sin \psi_2 \quad w_2(l_2, t) = 0 \quad (10.6)$$

where the vector \mathbf{F} includes all non-homogeneous and nonlinear terms:

$$\mathbf{F} = \begin{Bmatrix} P_{d1} w_{1,xx} \\ P_{d2} w_{2,xx} \\ P_{d1NL} - P_{d3NL} + F_{d1} \\ P_{d2NL} - P_{d1NL} \\ -P_{d2NL} \cos \psi_2 - P_{d1NL} \cos \psi_1 \\ P_{d3NL} - P_{d2NL} + F_{d4} \end{Bmatrix} \quad (10.7)$$

$F_{di} = M_{di} / r_i$ results from the applied dynamic moment on pulley i , and the total dynamic tension P_{di} in each span can be separated into the linear component P_{diL} and the nonlinear component P_{diNL}

$$P_{di} = P_{diL} + P_{diNL} \quad (10.8)$$

where

$$P_{diL} = k_i [u_i(l_i, t) - u_i(0, t)] \quad (10.9)$$

$$P_{dNL} = \frac{EA}{2l_i} \int_0^{l_i} w_{i,x}^2 dx \quad (10.10)$$

10.1.2 Modal Expansion

Following Beikmann *et al.* (1996), it is assumed that the eigenfunctions are complete, i.e., any arbitrary function in the domain of interest can be written in terms of the infinite sum of those eigenfunctions. Under this assumption, the response of the system can be expressed as

$$w_3 = \sum_{m=1}^{\infty} \eta_m^R \phi_m^R + \eta_m' \phi_m' \quad (10.11)$$

$$\mathbf{W} = \sum_{n=1}^{\infty} \xi_n^R \phi_n^R + \xi_n' \phi_n' \quad (10.12)$$

where $\phi_m(x)$ and $\phi_n(x)$ are the eigenfunctions of subsystem 1 and subsystem 2, ξ_n^R and ξ_n' are the real and imaginary components of the modal coordinate ξ_n , and η_m^R , η_m' are the real and imaginary components of the modal coordinate η_m .

The orthogonal properties (see Chapter 8) of the eigenfunctions are then used to diagonalize the linear terms in the equations of motion. Substituting equations (10.11) and (10.12) into equations (10.1) and (10.4), taking the inner product with vectors $(\phi_m^R, \phi_m')^T$ and $(\phi_n^R, \phi_n')^T$, respectively, and applying the orthogonal conditions yield

$$\dot{\xi}_n^R - \omega_n \xi_n' = q_n^R - 2\zeta_n \omega_n \xi_n^R \quad (10.13)$$

$$\dot{\xi}_n' + \omega_n \xi_n^R = q_n' \quad (10.14)$$

$$\dot{\eta}_m^R - \lambda_m \eta_m' = q_m^R - 2\zeta_m \lambda_m \eta_m^R \quad (10.15)$$

$$\dot{\eta}_m' + \lambda_m \eta_m^R = q_{m3}' \quad (10.16)$$

where ζ_n and ζ_m are modal damping, λ_m is the m th order frequency of the subsystem 1, ω_n is the n th order frequency of the subsystem 2, and

$$q_n^R = -\omega_n P_{d1} \int_0^{l_1} \phi_{1n}' w_{1,xx} dx - \omega_n P_{d2} \int_0^{l_2} \phi_{2n}' w_{2,xx} dx \quad (10.17)$$

$$\begin{aligned} q_n' = & \omega_n P_{d1} \int_0^{l_1} \phi_{1n}^R w_{1,xx} dx + \omega_n P_{d2} \int_0^{l_2} \phi_{2n}^R w_{2,xx} dx + \omega_n \hat{\chi}_{1n} (P_{d1NL} - P_{d3NL}) \\ & + \omega_n \hat{\chi}_{2n} (P_{d2NL} - P_{d1NL}) + \omega_n \hat{\chi}_{3n} (-P_{d2NL} \cos \psi_2 - P_{d1NL} \cos \psi_1) \\ & + \omega_n \hat{\chi}_{4n} (P_{d3NL} - P_{d2NL}) + \omega_n (F_{d1} \hat{\chi}_{1n} + F_{d4} \hat{\chi}_{4n}) \end{aligned} \quad (10.18)$$

$$q_{m3}^R = -\lambda_m P_{d3} \int_0^{l_3} \varphi_m' w_{3,xx} dx \quad (10.19)$$

$$q_{m3}' = \lambda_m P_{d3} \int_0^{l_3} \varphi_m^R w_{3,xx} dx \quad (10.20)$$

Note that each term of q_n^R , q_n' , q_{m3}^R , and q_{m3}' contain different modal coordinates, which appear in the curvature and dynamic tension terms in equation (10.10). These terms provide modal coupling. Furthermore, since the dynamic tensions contain linear and quadratic terms, q_n^R , q_n' , q_{m3}^R , and q_{m3}' will contain quadratic and cubic nonlinearities.

10.1.3 The Two Mode Expansion

In this study, the cases of one-to-one and two-to-one internal resonances combined with a primary external resonance are considered. Thus, only the eigenfunctions of those modes involving internal resonance occur in the expression of solutions. Therefore, q_n^R , q_n' , q_{m3}^R , and q_{m3}' in equations (10.17) – (10.20) can be expressed as follows

$$q_n^R = g_1 (\xi_n^R)^2 + g_2 \xi_n^R \xi_n' + g_3 (\xi_n^R)^3 + g_4 (\xi_n^R)^2 \xi_n' + g_5 \xi_n^R (\xi_n')^2 + g_6 (\xi_n')^3 \quad (10.21)$$

$$\begin{aligned} q_n' &= g_7 (\xi_n^R)^2 + g_8 \xi_n^R \xi_n' + g_9 (\xi_n')^2 + g_{10} (\eta_m^R)^2 + g_{11} \eta_m^R \eta_m' + g_{12} (\eta_m')^2 \\ &\quad g_{13} (\xi_n^R)^3 + g_{14} (\xi_n^R)^2 \xi_n' + g_{15} \xi_n^R (\xi_n')^2 + g_{16} (\xi_n')^3 + \omega_n (F_d \hat{\chi}_{1n} + F_d \hat{\chi}_{4n}) \end{aligned} \quad (10.22)$$

$$q_{m3}^R = h_1 \xi_n^R \eta_m^R + h_2 \xi_n^R \eta_m' + h_3 (\eta_m^R)^3 + h_4 (\eta_m^R)^2 \eta_m' + h_5 \eta_m^R (\eta_m')^2 + h_6 (\eta_m')^3 \quad (10.23)$$

$$q_{m3}' = h_7 \xi_n^R \eta_m^R + h_8 \xi_n^R \eta_m' + h_9 (\eta_m^R)^3 + h_{10} (\eta_m^R)^2 \eta_m' + h_{11} \eta_m^R (\eta_m')^2 + h_{12} (\eta_m')^3 \quad (10.24)$$

where

$$\begin{aligned} g_1 &= -\omega_n k_1 (\hat{\chi}_{3n} \cos \psi_1 + \hat{\chi}_{2n} - \hat{\chi}_{1n}) \int_0^{l_1} \phi_{1n}' \frac{\partial^2 \phi_{1n}^R}{\partial x^2} dx \\ &\quad - \omega_n k_2 (\hat{\chi}_{3n} \cos \psi_2 + \hat{\chi}_{4n} - \hat{\chi}_{2n}) \int_0^{l_2} \phi_{2n}' \frac{\partial^2 \phi_{2n}^R}{\partial x^2} dx \end{aligned} \quad (10.25)$$

$$\begin{aligned} g_2 &= -\omega_n k_1 (\hat{\chi}_{3n} \cos \psi_1 + \hat{\chi}_{2n} - \hat{\chi}_{1n}) \int_0^{l_1} \phi_{1n}' \frac{\partial^2 \phi_{1n}'}{\partial x^2} dx \\ &\quad - \omega_n k_2 (\hat{\chi}_{3n} \cos \psi_2 + \hat{\chi}_{4n} - \hat{\chi}_{2n}) \int_0^{l_2} \phi_{2n}' \frac{\partial^2 \phi_{2n}'}{\partial x^2} dx \end{aligned} \quad (10.26)$$

$$g_3 = -\omega_n \frac{EA}{2l_1} \left(\frac{\partial \phi_{1n}^R}{\partial x} \right)^2 dx \int_0^{l_1} \phi_{1n}' \frac{\partial^2 \phi_{1n}^R}{\partial x^2} dx - \omega_n \frac{EA}{2l_2} \int_0^{l_2} \left(\frac{\partial \phi_{2n}^R}{\partial x} \right)^2 dx \int_0^{l_2} \phi_{2n}' \frac{\partial^2 \phi_{2n}^R}{\partial x^2} dx \quad (10.27)$$

$$\begin{aligned} g_4 &= -\omega_n \frac{EA}{2l_1} \left(\frac{\partial \phi_{1n}^R}{\partial x} \right)^2 dx \int_0^{l_1} \phi_{1n}' \frac{\partial^2 \phi_{1n}'}{\partial x^2} dx - \omega_n \frac{EA}{2l_1} \int_0^{l_1} 2 \frac{\partial \phi_{1n}^R}{\partial x} \frac{\partial \phi_{1n}'}{\partial x} dx \int_0^{l_1} \phi_{1n}' \frac{\partial^2 \phi_{1n}^R}{\partial x^2} dx \\ &\quad - \omega_n \frac{EA}{2l_2} \int_0^{l_2} \left(\frac{\partial \phi_{2n}^R}{\partial x} \right)^2 dx \int_0^{l_2} \phi_{2n}' \frac{\partial^2 \phi_{2n}'}{\partial x^2} dx - \omega_n \frac{EA}{2l_2} \int_0^{l_2} 2 \frac{\partial \phi_{2n}^R}{\partial x} \frac{\partial \phi_{2n}'}{\partial x} dx \int_0^{l_2} \phi_{2n}' \frac{\partial^2 \phi_{2n}^R}{\partial x^2} dx \end{aligned} \quad (10.28)$$

$$\begin{aligned} g_5 &= -\omega_n \frac{EA}{2l_1} \int_0^{l_1} \left(\frac{\partial \phi_{1n}'}{\partial x} \right)^2 dx \int_0^{l_1} \phi_{1n}' \frac{\partial^2 \phi_{1n}^R}{\partial x^2} dx - \omega_n \frac{EA}{2l_1} \int_0^{l_1} 2 \frac{\partial \phi_{1n}^R}{\partial x} \frac{\partial \phi_{1n}'}{\partial x} dx \int_0^{l_1} \phi_{1n}' \frac{\partial^2 \phi_{1n}'}{\partial x^2} dx \\ &\quad - \omega_n \frac{EA}{2l_2} \int_0^{l_2} \left(\frac{\partial \phi_{2n}'}{\partial x} \right)^2 dx \int_0^{l_2} \phi_{2n}' \frac{\partial^2 \phi_{2n}^R}{\partial x^2} dx - \omega_n \frac{EA}{2l_2} \int_0^{l_2} 2 \frac{\partial \phi_{2n}^R}{\partial x} \frac{\partial \phi_{2n}'}{\partial x} dx \int_0^{l_2} \phi_{2n}' \frac{\partial^2 \phi_{2n}'}{\partial x^2} dx \end{aligned} \quad (10.29)$$

$$g_6 = -\omega_n \frac{EA}{2l_1} \int_0^{l_1} \left(\frac{\partial \phi_{1n}'}{\partial x} \right)^2 dx \int_0^{l_1} \phi_{1n}' \frac{\partial^2 \phi_{1n}'}{\partial x^2} dx - \omega_n \frac{EA}{2l_2} \int_0^{l_2} \left(\frac{\partial \phi_{2n}'}{\partial x} \right)^2 dx \int_0^{l_2} \phi_{2n}' \frac{\partial^2 \phi_{2n}'}{\partial x^2} dx \quad (10.30)$$

$$g_7 = \omega_n (\hat{\chi}_{3n} \cos \psi_1 + \hat{\chi}_{2n} - \hat{\chi}_{1n}) \left(k_1 \int_0^{l_1} \phi_{1n}^R \frac{\partial^2 \phi_{1n}^R}{\partial x^2} dx - \frac{EA}{2l_1} \int_0^{l_1} \left(\frac{\partial \phi_{1n}^R}{\partial x} \right)^2 dx \right) \\ + \omega_n (\hat{\chi}_{3n} \cos \psi_2 + \hat{\chi}_{4n} - \hat{\chi}_{2n}) \left(k_2 \int_0^{l_2} \phi_{2n}^R \frac{\partial^2 \phi_{2n}^R}{\partial x^2} dx - \frac{EA}{2l_2} \int_0^{l_2} \left(\frac{\partial \phi_{2n}^R}{\partial x} \right)^2 dx \right) \quad (10.31)$$

$$g_8 = \omega_n (\hat{\chi}_{3n} \cos \psi_1 + \hat{\chi}_{2n} - \hat{\chi}_{1n}) \left(k_1 \int_0^{l_1} \phi_{1n}^R \frac{\partial^2 \phi_{1n}'}{\partial x^2} dx - \frac{EA}{2l_1} \int_0^{l_1} 2 \frac{\partial \phi_{1n}^R}{\partial x} \frac{\partial \phi_{1n}'}{\partial x} dx \right) \\ + \omega_n (\hat{\chi}_{3n} \cos \psi_2 + \hat{\chi}_{4n} - \hat{\chi}_{2n}) \left(k_2 \int_0^{l_2} \phi_{2n}^R \frac{\partial^2 \phi_{2n}'}{\partial x^2} dx - \frac{EA}{2l_2} \int_0^{l_2} 2 \frac{\partial \phi_{2n}^R}{\partial x} \frac{\partial \phi_{2n}'}{\partial x} dx \right) \quad (10.32)$$

$$g_9 = -\omega_n (\hat{\chi}_{3n} \cos \psi_1 + \hat{\chi}_{2n} - \hat{\chi}_{1n}) \frac{EA}{2l_1} \int_0^{l_1} \left(\frac{\partial \phi_{1n}'}{\partial x} \right)^2 dx \\ - \omega_n (\hat{\chi}_{3n} \cos \psi_2 + \hat{\chi}_{4n} - \hat{\chi}_{2n}) \frac{EA}{2l_2} \int_0^{l_2} \left(\frac{\partial \phi_{2n}'}{\partial x} \right)^2 dx \quad (10.33)$$

$$g_{10} = \omega_n (\hat{\chi}_{4n} - \hat{\chi}_{1n}) \frac{EA}{2l_3} \int_0^{l_3} \left(\frac{\partial \phi_m^R}{\partial x} \right)^2 dx \quad (10.34)$$

$$g_{11} = \omega_n (\hat{\chi}_{4n} - \hat{\chi}_{1n}) \frac{EA}{2l_3} \int_0^{l_3} 2 \frac{\partial \phi_m^R}{\partial x} \frac{\partial \phi_m'}{\partial x} dx \quad (10.35)$$

$$g_{12} = \omega_n (\hat{\chi}_{4n} - \hat{\chi}_{1n}) \frac{EA}{2l_3} \int_0^{l_3} \left(\frac{\partial \phi_m'}{\partial x} \right)^2 dx \quad (10.36)$$

$$g_{13} = \omega_n \frac{EA}{2l_1} \int_0^{l_1} \left(\frac{\partial \phi_{1n}^R}{\partial x} \right)^2 dx \int_0^{l_1} \phi_{1n}^R \frac{\partial^2 \phi_{1n}^R}{\partial x^2} dx + \omega_n \frac{EA}{2l_2} \int_0^{l_2} \left(\frac{\partial \phi_{2n}^R}{\partial x} \right)^2 dx \int_0^{l_2} \phi_{2n}^R \frac{\partial^2 \phi_{2n}^R}{\partial x^2} dx \quad (10.37)$$

$$g_{14} = \omega_n \frac{EA}{2l_1} \int_0^{l_1} \left(\frac{\partial \phi_{1n}^R}{\partial x} \right)^2 dx \int_0^{l_1} \phi_{1n}^R \frac{\partial^2 \phi_{1n}'}{\partial x^2} dx + \omega_n \frac{EA}{2l_1} \int_0^{l_1} 2 \frac{\partial \phi_{1n}^R}{\partial x} \frac{\partial \phi_{1n}'}{\partial x} dx \int_0^{l_1} \phi_{1n}^R \frac{\partial^2 \phi_{1n}^R}{\partial x^2} dx \\ + \omega_n \frac{EA}{2l_2} \int_0^{l_2} \left(\frac{\partial \phi_{2n}^R}{\partial x} \right)^2 dx \int_0^{l_2} \phi_{2n}^R \frac{\partial^2 \phi_{2n}'}{\partial x^2} dx + \omega_n \frac{EA}{2l_2} \int_0^{l_2} 2 \frac{\partial \phi_{2n}^R}{\partial x} \frac{\partial \phi_{2n}'}{\partial x} dx \int_0^{l_2} \phi_{2n}^R \frac{\partial^2 \phi_{2n}^R}{\partial x^2} dx \quad (10.38)$$

$$g_{15} = \omega_n \frac{EA}{2l_1} \int_0^{l_1} \left(\frac{\partial \phi'_{1n}}{\partial x} \right)^2 dx \int_0^{l_1} \phi_{1n}^R \frac{\partial^2 \phi_{1n}^R}{\partial x^2} dx + \omega_n \frac{EA}{2l_1} \int_0^{l_1} 2 \frac{\partial \phi_{1n}^R}{\partial x} \frac{\partial \phi'_{1n}}{\partial x} dx \int_0^{l_1} \phi_{1n}^R \frac{\partial^2 \phi_{1n}'}{\partial x^2} dx \\ + \omega_n \frac{EA}{2l_2} \int_0^{l_2} \left(\frac{\partial \phi'_{2n}}{\partial x} \right)^2 dx \int_0^{l_2} \phi_{2n}^R \frac{\partial^2 \phi_{2n}^R}{\partial x^2} dx + \omega_n \frac{EA}{2l_2} \int_0^{l_2} 2 \frac{\partial \phi_{2n}^R}{\partial x} \frac{\partial \phi'_{2n}}{\partial x} dx \int_0^{l_2} \phi_{2n}^R \frac{\partial^2 \phi_{2n}'}{\partial x^2} dx \quad (10.39)$$

$$g_{16} = \omega_n \frac{EA}{2l_1} \int_0^{l_1} \left(\frac{\partial \phi'_{1n}}{\partial x} \right)^2 dx \int_0^{l_1} \phi_{1n}^R \frac{\partial^2 \phi_{1n}'}{\partial x^2} dx + \omega_n \frac{EA}{2l_2} \int_0^{l_2} \left(\frac{\partial \phi'_{2n}}{\partial x} \right)^2 dx \int_0^{l_2} \phi_{2n}^R \frac{\partial^2 \phi_{2n}'}{\partial x^2} dx \quad (10.40)$$

$$h_1 = -\lambda_m k_3 (\hat{\chi}_{1n} - \hat{\chi}_{4n}) \int_0^{l_1} \varphi'_m \frac{\partial^2 \varphi_m^R}{\partial x^2} dx \quad (10.41)$$

$$h_2 = -\lambda_m k_3 (\hat{\chi}_{1n} - \hat{\chi}_{4n}) \int_0^{l_1} \varphi'_m \frac{\partial^2 \varphi'_m}{\partial x^2} dx \quad (10.42)$$

$$h_3 = -\lambda_m \frac{EA}{2l_3} \int_0^{l_3} \left(\frac{\partial \varphi_m^R}{\partial x} \right)^2 dx \int_0^{l_3} \varphi'_m \frac{\partial^2 \varphi_m^R}{\partial x^2} dx \quad (10.43)$$

$$h_4 = -\lambda_m \frac{EA}{2l_3} \int_0^{l_3} \left(\frac{\partial \varphi_m^R}{\partial x} \right)^2 dx \int_0^{l_3} \varphi'_m \frac{\partial^2 \varphi'_m}{\partial x^2} dx - \lambda_m \frac{EA}{2l_3} \int_0^{l_3} 2 \frac{\partial \varphi_m^R}{\partial x} \frac{\partial \varphi'_m}{\partial x} dx \int_0^{l_3} \varphi'_m \frac{\partial^2 \varphi_m^R}{\partial x^2} dx \quad (10.44)$$

$$h_5 = -\lambda_m \frac{EA}{2l_3} \int_0^{l_3} \left(\frac{\partial \varphi'_m}{\partial x} \right)^2 dx \int_0^{l_3} \varphi'_m \frac{\partial^2 \varphi_m^R}{\partial x^2} dx - \lambda_m \frac{EA}{2l_3} \int_0^{l_3} 2 \frac{\partial \varphi_m^R}{\partial x} \frac{\partial \varphi'_m}{\partial x} dx \int_0^{l_3} \varphi'_m \frac{\partial^2 \varphi'_m}{\partial x^2} dx \quad (10.45)$$

$$h_6 = -\lambda_m \frac{EA}{2l_3} \int_0^{l_3} \left(\frac{\partial \varphi'_m}{\partial x} \right)^2 dx \int_0^{l_3} \varphi'_m \frac{\partial^2 \varphi'_m}{\partial x^2} dx \quad (10.46)$$

$$h_7 = \lambda_m k_3 (\hat{\chi}_{1n} - \hat{\chi}_{4n}) \int_0^{l_1} \varphi_m^R \frac{\partial^2 \varphi_m^R}{\partial x^2} dx \quad (10.47)$$

$$h_8 = \lambda_m k_3 (\hat{\chi}_{1n} - \hat{\chi}_{4n}) \int_0^{l_1} \varphi_m^R \frac{\partial^2 \varphi'_m}{\partial x^2} dx \quad (10.48)$$

$$h_9 = \lambda_m \frac{EA}{2l_3} \int_0^{l_3} \left(\frac{\partial \varphi_m^R}{\partial x} \right)^2 dx \int_0^{l_3} \varphi_m^R \frac{\partial^2 \varphi_m^R}{\partial x^2} dx \quad (10.49)$$

$$h_{10} = \lambda_m \frac{EA}{2l_3} \int_0^{l_3} \left(\frac{\partial \varphi_m^R}{\partial x} \right)^2 dx \int_0^{l_3} \varphi_m^R \frac{\partial^2 \varphi_m'}{\partial x^2} dx + \lambda_m \frac{EA}{2l_3} \int_0^{l_3} 2 \frac{\partial \varphi_m^R}{\partial x} \frac{\partial \varphi_m'}{\partial x} dx \int_0^{l_3} \varphi_m^R \frac{\partial^2 \varphi_m^R}{\partial x^2} dx \quad (10.50)$$

$$h_{11} = \lambda_m \frac{EA}{2l_3} \int_0^{l_3} \left(\frac{\partial \varphi_m'}{\partial x} \right)^2 dx \int_0^{l_3} \varphi_m^R \frac{\partial^2 \varphi_m^R}{\partial x^2} dx + \lambda_m \frac{EA}{2l_3} \int_0^{l_3} 2 \frac{\partial \varphi_m^R}{\partial x} \frac{\partial \varphi_m'}{\partial x} dx \int_0^{l_3} \varphi_m^R \frac{\partial^2 \varphi_m'}{\partial x^2} dx \quad (10.51)$$

$$h_{12} = \lambda_m \frac{EA}{2l_3} \int_0^{l_3} \left(\frac{\partial \varphi_m'}{\partial x} \right)^2 dx \int_0^{l_3} \varphi_m^R \frac{\partial^2 \varphi_m'}{\partial x^2} dx \quad (10.52)$$

Inspecting equations (10.21) – (10.24) for the modal coordinates reveals which modal frequency ratios can produce internal resonances. An internal resonance arises for two modes, n and m , when the nonlinear terms q_n^R and q_n' have a dominant frequency ω_n , and the nonlinear terms q_{m3}^R and q_{m3}' have a dominant frequency λ_m . Such a pair of modes can exchange energy and interact strongly. Significant energy exchange between modes may still occur under slight internal detuning. In the following study, the method of multiple scales will be employed to investigate these interactions between different modes due to the nonlinearities.

10.2 MULTIPLE SCALES METHOD

It is evident from equations (10.21) – (10.24) that the discretized equations of motion of serpentine belt drive systems involve quadratic and cubic nonlinearities. Therefore, up to third order approximation is needed for the multiple scales method. The solutions for ξ_n^R , ξ_n' , η_{m3}^R , and η_{m3}' are assumed in the form of

$$\xi_n^R = \varepsilon \xi_{n1}^R(T_0, T_1, T_2) + \varepsilon^2 \xi_{n2}^R(T_0, T_1, T_2) + \varepsilon^3 \xi_{n3}^R(T_0, T_1, T_2) + \dots \quad (10.53)$$

$$\xi'_n = \varepsilon \xi'_{n1}(T_0, T_1, T_2) + \varepsilon^2 \xi'_{n2}(T_0, T_1, T_2) + \varepsilon^3 \xi'_{n3}(T_0, T_1, T_2) + \dots \quad (10.54)$$

$$\eta_m^R = \varepsilon \eta_{m1}^R(T_0, T_1, T_2) + \varepsilon^2 \eta_{m2}^R(T_0, T_1, T_2) + \varepsilon^3 \eta_{m3}^R(T_0, T_1, T_2) + \dots \quad (10.55)$$

$$\eta'_m = \varepsilon \eta'_{m1}(T_0, T_1, T_2) + \varepsilon^2 \eta'_{m2}(T_0, T_1, T_2) + \varepsilon^3 \eta'_{m3}(T_0, T_1, T_2) + \dots \quad (10.56)$$

where ε is a small dimensionless measure of the response amplitude used as a bookkeeping device; $T_0 = t$ is the fast-time scale whereas $T_1 = \varepsilon t$ and $T_2 = \varepsilon^2 t$ are the slow-time scales. The time derivatives can be written in terms of T_n as follows

$$\frac{\partial}{\partial t} = \frac{\partial}{\partial T_0} + \varepsilon \frac{\partial}{\partial T_1} + \varepsilon^2 \frac{\partial}{\partial T_2} + \dots \quad (10.57)$$

The damping and forcing terms are ordered so that they counter the effect of the nonlinear terms; that is

$$\zeta_n = \varepsilon^2 \hat{\zeta}_n \quad \zeta_m = \varepsilon^2 \hat{\zeta}_m \quad (10.58)$$

$$\omega_n(F_{d1}\hat{x}_{1n} + F_{d4}\hat{x}_{4n}) = \varepsilon^2 F_d \quad (10.59)$$

Substituting equations (10.53) – (10.59) into equations (10.21) – (10.24) and equating coefficients of like powers of ε yield

First order

$$\frac{\partial \xi_{n1}^R}{\partial T_0} - \omega_n \xi'_{n1} = 0 \quad \frac{\partial \xi'_{n1}}{\partial T_0} + \omega_n \xi_{n1}^R = 0 \quad (10.60)$$

$$\frac{\partial \eta_{m1}^R}{\partial T_0} - \lambda_m \eta'_{m1} = 0 \quad \frac{\partial \eta'_{m1}}{\partial T_0} + \lambda_m \eta_{m1}^R = 0 \quad (10.61)$$

Second order

$$\frac{\partial \xi_{n2}^R}{\partial T_0} - \omega_n \xi_{n2}' = -\frac{\partial \xi_{n1}^R}{\partial T_1} + N_{Q1} \quad \frac{\partial \xi_{n2}'}{\partial T_0} + \omega_n \xi_{n2}^R = -\frac{\partial \xi_{n1}'}{\partial T_1} + N_{Q2} \quad (10.62)$$

$$\frac{\partial \eta_{m2}^R}{\partial T_0} - \lambda_m \eta_{m2}' = -\frac{\partial \eta_{m1}^R}{\partial T_1} + N_{Q3} \quad \frac{\partial \eta_{m2}'}{\partial T_0} + \lambda_m \eta_{m2}^R = -\frac{\partial \eta_{m1}'}{\partial T_1} + N_{Q4} \quad (10.63)$$

where

$$N_{Q1} = g_1 (\xi_{n1}^R)^2 + g_2 \xi_{n1}^R \xi_{n1}' \quad (10.64)$$

$$N_{Q2} = g_7 (\xi_{n1}^R)^2 + g_8 \xi_{n1}^R \xi_{n1}' + g_9 (\xi_{n1}')^2 + g_{10} (\eta_{m1}^R)^2 + g_{11} \eta_{m1}^R \eta_{m1}' + g_{12} (\eta_{m1}')^2 \quad (10.65)$$

$$N_{Q3} = h_1 \xi_{n1}^R \eta_{m1}^R + h_2 \xi_{n1}^R \eta_{m1}' \quad (10.66)$$

$$N_{Q4} = h_7 \xi_{n1}^R \eta_{m1}^R + h_8 \xi_{n1}^R \eta_{m1}' \quad (10.67)$$

Third order

$$\frac{\partial \xi_{n3}^R}{\partial T_0} - \omega_n \xi_{n3}' = -\frac{\partial \xi_{n1}^R}{\partial T_2} - \frac{\partial \xi_{n2}^R}{\partial T_1} - 2\zeta_n \omega_n \xi_{n3}^R + N_{C1} \quad (10.68)$$

$$\frac{\partial \xi_{n3}'}{\partial T_0} + \omega_n \xi_{n3}^R = -\frac{\partial \xi_{n1}'}{\partial T_2} - \frac{\partial \xi_{n2}'}{\partial T_1} + F_d + N_{C2} \quad (10.69)$$

$$\frac{\partial \eta_{m3}^R}{\partial T_0} - \lambda_m \eta_{m3}' = -\frac{\partial \eta_{m1}^R}{\partial T_2} - \frac{\partial \eta_{m2}^R}{\partial T_1} - 2\zeta_m \lambda_m \eta_{m3}^R + N_{C3} \quad (10.70)$$

$$\frac{\partial \eta_{m3}'}{\partial T_0} + \lambda_m \eta_{m3}^R = -\frac{\partial \eta_{m1}'}{\partial T_2} - \frac{\partial \eta_{m2}'}{\partial T_1} + N_{C4} \quad (10.71)$$

where

$$N_{C1} = 2g_1 \xi_{n1}^R \xi_{n2}^R + g_2 (\xi_{n1}^R \xi_{n2}' + \xi_{n2}^R \xi_{n1}') + g_3 (\xi_{n1}^R)^3 + g_4 (\xi_{n1}^R)^2 \xi_{n1}' + g_5 \xi_{n1}^R (\xi_{n1}')^2 + g_6 (\xi_{n1}')^3 \quad (10.72)$$

$$N_{C2} = 2g_7 \xi_{n1}^R \xi_{n2}^R + g_8 (\xi_{n1}^R \xi_{n2}' + \xi_{n2}^R \xi_{n1}') + 2g_9 \xi_{n1}^R \xi_{n2}' + 2g_{10} \eta_{m1}^R \eta_{m2}^R + g_{11} (\eta_{m1}^R \eta_{m2}' + \eta_{m2}^R \eta_{m1}') + 2g_{12} \eta_{m1}' \eta_{m2}' + g_{13} (\xi_{n1}^R)^3 + g_{14} (\xi_{n1}^R)^2 \xi_{n1}' + g_{15} \xi_{n1}^R (\xi_{n1}')^2 + g_{16} (\xi_{n1}')^3 \quad (10.73)$$

$$N_{C3} = h_1(\xi_{n1}^R \eta_{m2}^R + \xi_{n2}^R \eta_{m1}^R) + h_2(\xi_{n1}^R \eta'_{m2} + \xi_{n2}^R \eta'_{m1}) + h_3(\eta_{m1}^R)^3 + h_4(\eta_{m1}^R)^2 \eta'_{m1} + h_5 \eta_{m1}^R (\eta'_{m1})^2 + h_6(\eta'_{m1})^3 \quad (10.74)$$

$$N_{C4} = h_7(\xi_{n1}^R \eta_{m2}^R + \xi_{n2}^R \eta_{m1}^R) + h_8(\xi_{n1}^R \eta'_{m2} + \xi_{n2}^R \eta'_{m1}) + h_9(\eta_{m1}^R)^3 + h_{10}(\eta_{m1}^R)^2 \eta'_{m1} + h_{11} \eta_{m1}^R (\eta'_{m1})^2 + h_{12}(\eta'_{m1})^3 \quad (10.75)$$

The first order solution is

$$\xi_{n1}^R = A_n(T_1, T_2) e^{i\omega_n T_0} + cc \quad (10.76)$$

$$\xi'_{n1} = iA_n(T_1, T_2) e^{i\omega_n T_0} + cc \quad (10.77)$$

$$\eta_{m1}^R = B_m(T_1, T_2) e^{i\lambda_m T_0} + cc \quad (10.78)$$

$$\eta'_{m1} = iB_m(T_1, T_2) e^{i\lambda_m T_0} + cc \quad (10.79)$$

where *cc* stands for the complex conjugate of the preceding terms and A_n and B_m are complex functions yet to be determined.

10.3 ONE-TO-ONE INTERNAL RESONANCE

When one of the frequencies of subsystem 1 is near one of the frequencies of subsystem 2, a one-to-one internal resonance will occur. To quantitatively describe a primary external resonance and a one-to-one internal resonance, introduce two detuning parameters σ_1 and σ_2 defined by

$$\omega_n = \lambda_m + \varepsilon^2 \sigma_1 \quad (10.80)$$

$$\Omega = \omega_n + \varepsilon^2 \sigma_2 \quad (10.81)$$

where Ω is the frequency of excitation force.

10.3.1 Solvability Condition of the Second Order Equations

For one-to-one internal resonance, since there is no secular term arising from N_{Q1} , N_{Q2} , N_{Q3} and N_{Q4} , the solvability conditions for equations (10.62) and (10.63) are obtained by eliminating the secular terms

$$\begin{vmatrix} i\omega_n & -\frac{\partial A_n}{\partial T_1} \\ \omega_n & -i\frac{\partial A_n}{\partial T_1} \end{vmatrix} = 0 \quad (10.82)$$

$$\begin{vmatrix} i\lambda_m & -\frac{\partial B_m}{\partial T_1} \\ \lambda_m & -i\frac{\partial B_m}{\partial T_1} \end{vmatrix} = 0 \quad (10.83)$$

that is

$$\frac{\partial A_n}{\partial T_1} = 0 \quad (10.84)$$

$$\frac{\partial B_m}{\partial T_1} = 0 \quad (10.85)$$

Therefore, $A_n = A_n(T_2)$ and $B_m = B_m(T_2)$ only. This shows that for one-to-one internal resonance, there is no $T_1 = \epsilon t$ dependence.

10.3.2 The Second Order Solutions

After eliminating the secular terms, the solutions of the second order equations (10.62) and (10.63) can be obtained as

$$\xi_{n2}^R = (s_1 A_n^2 e^{2i\omega_n T_0} + cc) + s_2 A_n \bar{A}_n + (s_3 B_m^2 e^{2i\lambda_m T_0} + cc) + s_4 B_m \bar{B}_m \quad (10.86)$$

$$\xi_{n2}' = (s_5 A_n^2 e^{2i\omega_n T_0} + cc) + s_6 A_n \bar{A}_n + (s_7 B_m^2 e^{2i\lambda_m T_0} + cc) + s_8 B_m \bar{B}_m \quad (10.87)$$

$$\eta_{m2}^R = (t_1 A_n B_m e^{i(\omega_n + \lambda_m) T_0} + cc) + (t_2 A_n \bar{B}_m e^{i(\omega_n - \lambda_m) T_0} + cc) \quad (10.88)$$

$$\eta_{m2}' = (t_3 A_n B_m e^{i(\omega_n + \lambda_m) T_0} + cc) + (t_4 A_n \bar{B}_m e^{i(\omega_n - \lambda_m) T_0} + cc) \quad (10.89)$$

where

$$s_1 = -\frac{2i(g_1 + ig_2) + (g_7 + ig_8 - g_9)}{3\omega_n} \quad (10.90)$$

$$s_2 = \frac{2g_7 + 2g_9}{\omega_n} \quad (10.91)$$

$$s_3 = \frac{(g_{10} + ig_{11} - g_{12})\omega_n}{\omega_n^2 - 4\lambda_m^2} \quad (10.92)$$

$$s_4 = \frac{2g_{10} + 2g_{12}}{\omega_n} \quad (10.93)$$

$$s_5 = \frac{(g_1 + ig_2) - 2i(g_7 + ig_8 - g_9)}{3\omega_n} \quad (10.94)$$

$$s_6 = -\frac{2g_1}{\omega_n} \quad (10.95)$$

$$s_7 = \frac{2i\lambda_m(g_{10} + ig_{11} - g_{12})}{\omega_n^2 - 4\lambda_m^2} \quad (10.96)$$

$$s_8 = 0 \quad (10.97)$$

$$t_1 = \frac{i(\omega_n + \lambda_m)(h_1 + ih_2) + \lambda_m(h_7 + ih_8)}{\lambda_m^2 - (\omega_n + \lambda_m)^2} \quad (10.98)$$

$$t_2 = \frac{i(\omega_n - \lambda_m)(h_1 - ih_2) + \lambda_m(h_7 - ih_8)}{\lambda_m^2 - (\omega_n - \lambda_m)^2} \quad (10.99)$$

$$t_3 = \frac{i(\omega_n + \lambda_m)(h_7 + ih_8) - \lambda_m(h_1 + ih_2)}{\lambda_m^2 - (\omega_n + \lambda_m)^2} \quad (10.100)$$

$$t_4 = \frac{i(\omega_n - \lambda_m)(h_7 - ih_8) - \lambda_m(h_1 - ih_2)}{\lambda_m^2 - (\omega_n - \lambda_m)^2} \quad (10.101)$$

10.3.3 Solvability Conditions of the Third Order Equations

Substituting equations (10.86) – (10.89) into (10.72) – (10.75) yield

$$N_{C1} = \left(A_n^2 \bar{A}_n \hat{\Theta}_1 + A_n B_m \bar{B}_m \hat{\Theta}_2 + e^{-2i\sigma_1 T_2} \bar{A}_n B_m^2 \hat{\Theta}_3 \right) e^{i\omega_n T_0} + NST \quad (10.102)$$

$$N_{C2} = \left(A_n^2 \bar{A}_n \tilde{\Theta}_1 + A_n B_m \bar{B}_m \tilde{\Theta}_2 + e^{-2i\sigma_1 T_2} \bar{A}_n B_m^2 \tilde{\Theta}_3 \right) e^{i\omega_n T_0} + NST \quad (10.103)$$

$$N_{C3} = \left(e^{2i\sigma_1 T_2} A_n^2 \bar{B}_m \hat{\Theta}_4 + A_n \bar{A}_n B_m \hat{\Theta}_5 + B_m^2 \bar{B}_m \hat{\Theta}_6 \right) e^{i\lambda_m T_0} + NST \quad (10.104)$$

$$N_{C4} = \left(e^{2i\sigma_1 T_2} A_n^2 \bar{B}_m \tilde{\Theta}_4 + A_n \bar{A}_n B_m \tilde{\Theta}_5 + B_m^2 \bar{B}_m \tilde{\Theta}_6 \right) e^{i\lambda_m T_0} + NST \quad (10.105)$$

where NST denotes non-secular terms and

$$\hat{\Theta}_1 = 2g_1s_1 + 2g_1s_2 + g_2s_3 + g_2s_6 - ig_2s_1 + ig_2s_2 + 3g_3 + ig_4 + g_5 + 3ig_6 \quad (10.106)$$

$$\hat{\Theta}_2 = 2g_1s_4 + ig_2s_4 \quad (10.107)$$

$$\hat{\Theta}_3 = 2g_1s_3 - ig_2s_3 + g_2s_7 \quad (10.108)$$

$$\tilde{\Theta}_1 = 2g_7s_1 + 2g_7s_2 + g_8s_3 + g_8s_6 - ig_8s_1 + ig_8s_2 + 2ig_9s_6 - 2ig_9s_5 + 3g_{13} + ig_{14} + g_{15} + 3ig_{16} \quad (10.109)$$

$$\tilde{\Theta}_2 = 2g_7s_4 + ig_8s_4 + 2g_{10}s_2 + 2g_{10}t_1 + g_{11}t_4 + g_{11}t_3 + ig_{11}t_2 - ig_{11}s_1 + 2ig_{12}t_4 - 2ig_{12}t_3 \quad (10.110)$$

$$\tilde{\Theta}_3 = 2g_7s_3 - ig_6s_3 + g_8s_7 - 2ig_9s_7 + 2g_{10}\bar{t}_2 + g_{11}\bar{t}_4 + ig_{11}\bar{t}_2 + 2ig_{12}\bar{t}_4 \quad (10.111)$$

$$\hat{\Theta}_4 = h_1(t_2 + s_1) + h_2(t_4 - is_1) \quad (10.112)$$

$$\hat{\Theta}_5 = h_1(t_1 + \bar{t}_2 + s_2) + h_2(t_3 + \bar{t}_4 + is_2) \quad (10.113)$$

$$\hat{\Theta}_6 = 3h_3 + ih_4 + h_5 + 3ih_6 + h_7(s_3 + s_4) + h_8(-is_3 + is_4) \quad (10.114)$$

$$\tilde{\Theta}_4 = h_7(t_2 + s_1) + h_8(t_4 - is_1) \quad (10.115)$$

$$\tilde{\Theta}_5 = h_7(t_1 + \bar{t}_2 + s_2) + h_8(t_3 + \bar{t}_4 + is_2) \quad (10.116)$$

$$\tilde{\Theta}_6 = 3h_9 + ih_{10} + h_{11} + 3ih_{12} + h_7(s_3 + s_4) + h_8(-is_3 + is_4) \quad (10.117)$$

Eliminating the secular terms in equations (10.68) – (10.71) leads to the following solvability conditions:

$$\begin{vmatrix} i\omega_n & -\frac{\partial A_n}{\partial T_2} + A_n^2 \bar{A}_n \hat{\Theta}_1 + A_n B_m \bar{B}_m \hat{\Theta}_2 + e^{-2i\sigma_1 T_2} \bar{A}_n B_m^2 \hat{\Theta}_3 - 2\zeta_n \omega_n A_n \\ \omega_n & -i \frac{\partial A_n}{\partial T_2} + A_n^2 \bar{A}_n \tilde{\Theta}_1 + A_n B_m \bar{B}_m \tilde{\Theta}_2 + e^{-2i\sigma_1 T_2} \bar{A}_n B_m^2 \tilde{\Theta}_3 + F_d e^{i\sigma_2 T_2} \end{vmatrix} = 0 \quad (10.118)$$

$$\begin{vmatrix} i\lambda_m & -\frac{\partial B_m}{\partial T_2} + A_n^2 \bar{B}_m \hat{\Theta}_4 e^{2i\sigma_1 T_2} + A_n \bar{A}_n B_m \hat{\Theta}_5 + B_m^2 \bar{B}_m \hat{\Theta}_6 - 2\zeta_m \lambda_m B_m \\ \lambda_m & -i \frac{\partial B_m}{\partial T_2} + A_n^2 \bar{B}_m \tilde{\Theta}_4 e^{2i\sigma_1 T_2} + A_n \bar{A}_n B_m \tilde{\Theta}_5 + B_m^2 \bar{B}_m \tilde{\Theta}_6 \end{vmatrix} = 0 \quad (10.119)$$

10.3.4 Modulation Equations and Steady State Solutions

From equations (10.118) and (10.119), the modulation equations for the complex amplitudes A_n and B_m are obtained as

$$2 \frac{\partial A_n}{\partial T_2} + A_n^2 \bar{A}_n \Theta_1 + A_n B_m \bar{B}_m \Theta_2 + e^{-2i\sigma_1 T_2} \bar{A}_n B_m^2 \Theta_3 + iF_d e^{i\sigma_2 T_2} + 2\zeta_n \omega_n A_n = 0 \quad (10.120)$$

$$2 \frac{\partial B_m}{\partial T_2} + e^{2i\sigma_1 T_2} A_n^2 \bar{B}_m \Theta_4 + A_n \bar{A}_n B_m \Theta_5 + B_m^2 \bar{B}_m \Theta_6 + 2\zeta_m \lambda_m B_m = 0 \quad (10.121)$$

where

$$\Theta_1 = i\tilde{\Theta}_1 - \hat{\Theta}_1 \quad \Theta_2 = i\tilde{\Theta}_2 - \hat{\Theta}_2 \quad \Theta_3 = i\tilde{\Theta}_3 - \hat{\Theta}_3 \quad (10.122)$$

$$\Theta_4 = i\tilde{\Theta}_4 - \hat{\Theta}_4 \quad \Theta_5 = i\tilde{\Theta}_5 - \hat{\Theta}_5 \quad \Theta_6 = i\tilde{\Theta}_6 - \hat{\Theta}_6 \quad (10.123)$$

Express the complex amplitudes A_n and B_m in the polar form

$$A_n = \frac{1}{2}\alpha_n e^{i\beta_n} \quad B_m = \frac{1}{2}\alpha_m e^{i\beta_m} \quad (10.124)$$

Substituting this polar form into equations (10.120) and (10.121), and separating the resulting equations into real and imaginary parts, the first order differential equations for the amplitudes and phases are obtained as follows

$$\begin{aligned} \frac{\partial \alpha_n}{\partial T_2} + \frac{\operatorname{Re}(\Theta_1)}{8}\alpha_n^3 + \frac{\operatorname{Re}(\Theta_2)}{8}\alpha_n\alpha_m^2 + \frac{\operatorname{Re}(\Theta_3)\cos\zeta_1 + \operatorname{Im}(\Theta_3)\sin\zeta_1}{8}\alpha_n\alpha_m^2 \\ - F_d \sin\zeta_2 + \zeta_n \omega_n \alpha_n = 0 \end{aligned} \quad (10.125)$$

$$\begin{aligned} \alpha_n \left(\sigma_2 - \frac{\partial \zeta_2}{\partial T_2} \right) + \frac{\operatorname{Im}(\Theta_1)}{8}\alpha_n^3 + \frac{\operatorname{Im}(\Theta_2)}{8}\alpha_n\alpha_m^2 + \frac{\operatorname{Im}(\Theta_3)\cos\zeta_1 - \operatorname{Re}(\Theta_3)\sin\zeta_1}{8}\alpha_n\alpha_m^2 \\ + F_d \cos\zeta_2 = 0 \end{aligned} \quad (10.126)$$

$$\frac{\partial \alpha_m}{\partial T_2} + \frac{\operatorname{Re}(\Theta_6)}{8}\alpha_m^3 + \frac{\operatorname{Re}(\Theta_5)}{8}\alpha_n^2\alpha_m + \frac{\operatorname{Re}(\Theta_4)\cos\zeta_1 - \operatorname{Im}(\Theta_4)\sin\zeta_1}{8}\alpha_n^2\alpha_m + \zeta_m \lambda_m \alpha_m = 0 \quad (10.127)$$

$$\begin{aligned} \alpha_m \left(\sigma_1 + \sigma_2 - \frac{1}{2} \frac{\partial \zeta_1}{\partial T_2} - \frac{\partial \zeta_2}{\partial T_2} \right) + \frac{\operatorname{Im}(\Theta_6)}{8}\alpha_m^3 + \frac{\operatorname{Im}(\Theta_5)}{8}\alpha_n^2\alpha_m \\ + \frac{\operatorname{Im}(\Theta_4)\cos\zeta_1 + \operatorname{Re}(\Theta_4)\sin\zeta_1}{8}\alpha_n^2\alpha_m = 0 \end{aligned} \quad (10.128)$$

where

$$\zeta_1 = 2(\beta_n - \beta_m + \sigma_1 T_2) \quad (10.129)$$

$$\zeta_2 = \sigma_2 T_2 - \beta_n \quad (10.130)$$

For the steady-state response, the amplitude α_n and α_m and the new phase angle ζ_1 and ζ_2 in equations (10.125) – (10.128) should be constant. Setting

$$\partial\alpha_n/\partial T_2 = \partial\alpha_m/\partial T_2 = \partial\zeta_1/\partial T_2 = \partial\zeta_2/\partial T_2 = 0 \quad (10.131)$$

and with some manipulations, the amplitude and phase of the response can be determined from the resulting algebraic equations. However, analytical solutions of equations (10.125) – (10.128) are impossible to obtain, thus numerical procedure will be adopted.

It is of great interest to determine how solutions of a system vary with a certain parameter. There are several algorithms pertaining to find the steady state solutions and periodic solutions of continuous-time systems. In this study, an arclength continuation scheme will be employed in Section 10.6 to trace the branches of steady state solutions or periodic solutions in a given state-control space.

10.4 TWO-TO-ONE INTERNAL RESONANCE

When one of the frequencies of subsystem 2 is near two times of one of the frequencies of subsystem 1, secular terms will arise from nonlinear terms. In this case, a two-to-one internal resonance will occur. To quantitatively describe a primary resonance and a two-to-one internal resonance, two detuning parameters σ_1 and σ_2 are introduced as

$$\omega_n = 2\lambda_m + \epsilon\sigma_1 \quad (10.132)$$

$$\Omega = \omega_n + \epsilon^2\sigma_2 \quad (10.133)$$

10.4.1 The Second Order Solution

For two-to-one internal resonance, there are secular terms arising from N_{Q1} , N_{Q2} , N_{Q3} and N_{Q4} . Eliminating the secular terms leads to the following solvability conditions for equations (10.62) and (10.63)

$$\begin{vmatrix} i\omega_n & -\frac{\partial A_n}{\partial T_1} \\ \omega_n & -i\frac{\partial A_n}{\partial T_1} + B_m^2(g_{10} + ig_{11} - g_{12})e^{-i\sigma_1 T_1} \end{vmatrix} = 0 \quad (10.134)$$

$$\begin{vmatrix} i\lambda_m & -\frac{\partial B_m}{\partial T_1} + (h_1 - ih_2)A_n \bar{B}_m e^{i\sigma_1 T_1} \\ \lambda_m & -i\frac{\partial B_m}{\partial T_1} + (h_1 - ih_2)A_n \bar{B}_m e^{i\sigma_1 T_1} \end{vmatrix} = 0 \quad (10.135)$$

Therefore, the explicit expression for $\frac{\partial A_n}{\partial T_1}$ and $\frac{\partial B_m}{\partial T_1}$ are obtained as

$$\frac{\partial A_n}{\partial T_1} = p_1 B_m^2 e^{-i\sigma_1 T_1} \quad (10.136)$$

$$\frac{\partial B_m}{\partial T_1} = p_2 A_n \bar{B}_m e^{i\sigma_1 T_1} \quad (10.137)$$

where

$$p_1 = -\frac{i}{2}(g_{10} + ig_{11} - g_{12}) \quad (10.138)$$

$$p_2 = -\frac{1}{2}(h_3 - h_1 + ih_7 + ih_2) \quad (10.139)$$

Compared with equations (10.84) and (10.85), it is seen that the complex amplitudes A_n and B_m are dependent on T_1 for two-to-one internal resonance while A_n and B_m are independent of T_1

for one-to-one internal resonance. This is because there are secular terms arising from the nonlinear terms at the second order for the two-to-one internal resonance.

After eliminating the secular terms, the solution of equations (10.62) and (10.63) can be expressed as

$$\xi_{n2}^R = (s_1 A_n^2 e^{2i\omega_n T_0} + cc) + s_2 A_n \bar{A}_n + s_4 B_m \bar{B}_m \quad (10.140)$$

$$\xi_{n2}^I = (s_5 A_n^2 e^{2i\omega_n T_0} + cc) + s_6 A_n \bar{A}_n + s_8 B_m \bar{B}_m \quad (10.141)$$

$$\eta_{m2}^R = t_1 A_n B_m e^{i(\omega_n + \lambda_m) T_0} + cc \quad (10.142)$$

$$\eta_{m2}^I = t_3 A_n B_m e^{i(\omega_n + \lambda_m) T_0} + cc \quad (10.143)$$

where *cc* denotes complex conjugate of the preceding terms. It is noted that the solutions at the second order for two-to-one internal resonance can be directly obtained from equations (10.86) – (10.89) by letting those secular terms be zero.

10.4.2 Solvability Condition of the Third Order Equations

Substituting equations (10.140) – (10.143) into (10.72) – (10.75) yields

$$N_{c1} = (A_n^2 \bar{A}_n \hat{\Theta}_1 + A_n B_m \bar{B}_m \hat{\Theta}_2) e^{i\omega_n T_0} + NST \quad (10.144)$$

$$N_{c2} = (A_n^2 \bar{A}_n \tilde{\Theta}_1 + A_n B_m \bar{B}_m \tilde{\Theta}_2) e^{i\omega_n T_0} + NST \quad (10.145)$$

$$N_{c3} = (A_n \bar{A}_n B_m \hat{\Theta}_5 + B_m^2 \bar{B}_m \hat{\Theta}_6) e^{i\lambda_m T_0} + NST \quad (10.146)$$

$$N_{c4} = (A_n \bar{A}_n B_m \tilde{\Theta}_5 + B_m^2 \bar{B}_m \tilde{\Theta}_6) e^{i\lambda_m T_0} + NST \quad (10.147)$$

where *NST* represents non-secular terms.

Eliminating the secular terms, solvability conditions for equations (10.68) – (10.71) are

$$\begin{vmatrix} i\omega_n & -\frac{\partial A_n}{\partial T_2} + A_n^2 \bar{A}_n \hat{\Theta}_1 + A_n B_m \bar{B}_m \hat{\Theta}_2 - 2\zeta_n \omega_n A_n \\ \omega_n & -i \frac{\partial A_n}{\partial T_2} + A_n^2 \bar{A}_n \tilde{\Theta}_1 + A_n B_m \bar{B}_m \tilde{\Theta}_2 + F_d e^{i\sigma_2 T_2} \end{vmatrix} = 0 \quad (10.148)$$

$$\begin{vmatrix} i\lambda_m & -\frac{\partial B_m}{\partial T_2} + A_n \bar{A}_n B_m \hat{\Theta}_5 + B_m^2 \bar{B}_m \hat{\Theta}_6 - 2\zeta_m \lambda_m B_m \\ \lambda_m & -i \frac{\partial B_m}{\partial T_2} + A_n \bar{A}_n B_m \tilde{\Theta}_5 + B_m^2 \bar{B}_m \tilde{\Theta}_6 \end{vmatrix} = 0 \quad (10.149)$$

Therefore, the explicit expression for $\frac{\partial A_n}{\partial T_2}$ and $\frac{\partial B_m}{\partial T_2}$ are obtained as

$$\frac{\partial A_n}{\partial T_2} = -\frac{1}{2} (A_n^2 \bar{A}_n \Theta_1 + A_n B_m \bar{B}_m \Theta_2 + iF_d e^{i\sigma_2 T_2} + 2\zeta_n \omega_n A_n) \quad (10.150)$$

$$\frac{\partial B_m}{\partial T_2} = -\frac{1}{2} (A_n \bar{A}_n B_m \Theta_5 + B_m^2 \bar{B}_m \Theta_6 + 2\zeta_m \lambda_m B_m) \quad (10.151)$$

10.4.3 Modulation Equations and Steady State Solutions

Upon noting that A_n and B_m are independent of T_0 , it follows that

$$\frac{dA_n}{dt} = \epsilon \frac{\partial A_n}{\partial T_1} + \epsilon^2 \frac{\partial A_n}{\partial T_2} + O(\epsilon^3) \quad (10.152)$$

$$\frac{dB_m}{dt} = \epsilon \frac{\partial B_m}{\partial T_1} + \epsilon^2 \frac{\partial B_m}{\partial T_2} + O(\epsilon^3) \quad (10.153)$$

Substituting equations (10.136), (10.137), (10.150), and (10.151) into (10.152) and (10.153) results in the equations of motion for the slow evaluation of A_n and B_m in time t

$$\frac{dA_n}{dt} = \epsilon p_1 B_m^2 e^{-i\sigma_1 T_1} - \frac{\epsilon^2}{2} (A_n^2 \bar{A}_n \Theta_1 + A_n B_m \bar{B}_m \Theta_2 + iF_d e^{i\sigma_2 T_2} 2\zeta_n \omega_n A_n) \quad (10.154)$$

$$\frac{dB_m}{dT_1} = \epsilon p_2 A_n \bar{B}_m e^{i\sigma_1 T_1} - \frac{\epsilon^2}{2} (A_n \bar{A}_n B_m \Theta_5 + B_m^2 \bar{B}_m \Theta_6 + 2\hat{\zeta}_m \lambda_m B_m) \quad (10.155)$$

Inserting the polar form of A_n and B_m into equations (10.154) and (10.155), and separating the result into real and imaginary parts, the first order differential equations for the amplitudes and phases are obtained as follows

$$\begin{aligned} \frac{d\alpha_n}{dt} = & -\epsilon^2 \frac{\operatorname{Re}(\Theta_1)}{8} \alpha_n^3 - \epsilon^2 \frac{\operatorname{Re}(\Theta_2)}{8} \alpha_n \alpha_m^2 - \epsilon^2 F_d \sin \zeta_2 \\ & + \epsilon \frac{\operatorname{Re}(p_1) \cos \zeta_1 - \operatorname{Im}(p_1) \sin \zeta_1}{2} \alpha_m^2 - \hat{\zeta}_n \omega_n \alpha_n \end{aligned} \quad (10.156)$$

$$\begin{aligned} \alpha_n \left(-\frac{d\zeta_2}{dt} + \epsilon^2 \sigma_2 \right) = & -\epsilon^2 \frac{\operatorname{Im}(\Theta_1)}{8} \alpha_n^3 - \epsilon^2 \frac{\operatorname{Im}(\Theta_2)}{8} \alpha_n \alpha_m^2 - F_d \cos \zeta_2 \\ & + \epsilon \frac{\operatorname{Im}(p_1) \cos \zeta_1 + \operatorname{Re}(p_1) \sin \zeta_1}{2} \alpha_m^2 \end{aligned} \quad (10.157)$$

$$\begin{aligned} \frac{d\alpha_m}{dt} = & -\epsilon^2 \frac{\operatorname{Re}(\Theta_6)}{8} \alpha_m^3 - \epsilon^2 \frac{\operatorname{Re}(\Theta_5)}{8} \alpha_n^2 \alpha_m \\ & + \epsilon \frac{\operatorname{Re}(p_2) \cos \zeta_1 + \operatorname{Im}(p_2) \sin \zeta_1}{2} \alpha_n \alpha_m - \hat{\zeta}_m \lambda_m \alpha_m \end{aligned} \quad (10.158)$$

$$\begin{aligned} \alpha_m \frac{\zeta'_1 - \zeta'_2 + \epsilon \sigma_1 + \epsilon^2 \sigma_2}{2} = & -\epsilon^2 \frac{\operatorname{Im}(\Theta_6)}{8} \alpha_m^3 - \epsilon^2 \frac{\operatorname{Im}(\Theta_5)}{8} \alpha_n^2 \alpha_m \\ & + \epsilon \frac{\operatorname{Im}(p_2) \cos \zeta_1 - \operatorname{Re}(p_2) \sin \zeta_1}{2} \alpha_n \alpha_m \end{aligned} \quad (10.159)$$

where

$$\zeta_1 = 2\beta_m - \beta_n - \epsilon \sigma_1 t \quad (10.160)$$

$$\zeta_2 = -\beta_n + \epsilon^2 \sigma_2 t \quad (10.161)$$

For the steady-state response, the amplitude and phase of the response can be determined from the equations (10.156) – (10.159) by setting $d\alpha_n/dt = d\alpha_m/dt = d\zeta_1/dt = d\zeta_2/dt = 0$. The

resulting equations can be solved by the use of continuation method.

10.5 STABILITY ANALYSIS

To determine the stability of a steady state solution of α_{n0} , α_{m0} , ζ_{10} , and ζ_{20} , small variations ε_{α_n} , ε_{α_m} , ε_{ζ_1} , and ε_{ζ_2} , are superimposed on the steady state solution, that is,

$$\alpha_n = \alpha_{n0} + \varepsilon_{\alpha_n} \quad (10.162)$$

$$\alpha_m = \alpha_{m0} + \varepsilon_{\alpha_m} \quad (10.163)$$

$$\zeta_1 = \zeta_{10} + \varepsilon_{\zeta_1} \quad (10.164)$$

$$\zeta_2 = \zeta_{20} + \varepsilon_{\zeta_2} \quad (10.165)$$

Substituting equations (10.162) – (10.165) into equations (10.125) – (10.128) or (10.156) – (10.159) and linearization the resulting equations, the following equations are obtained in matrix form:

$$\dot{\varepsilon}_{err} = \mathbf{H}\varepsilon_{err} \quad (10.166)$$

where $\varepsilon_{err} = \begin{bmatrix} \varepsilon_{\alpha_n} & \varepsilon_{\alpha_m} & \varepsilon_{\zeta_1} & \varepsilon_{\zeta_2} \end{bmatrix}^T$ and \mathbf{H} is the Jacobian matrix. The elements of matrix \mathbf{H} are functions of α_{n0} , α_{m0} , ζ_{10} , and ζ_{20} .

The stability of the steady state solution is decided by the eigenvalues of the matrix \mathbf{H} (Nayfeh and Balachandran, 1995). If all of the eigenvalues of \mathbf{H} have negative real parts, then the steady state solution is asymptotically stable. An asymptotically stable steady state solution is called a

sink. If the matrix \mathbf{H} associated with a sink has complex eigenvalues, the sink is also called a stable focus. On the other hand, if all of the eigenvalues of the matrix \mathbf{H} associated with a sink are real, the sink is also called stable node.

If one or more of the eigenvalues of \mathbf{H} have positive real parts, the steady state is unstable. When all of the eigenvalues of \mathbf{H} have positive real parts, the steady state is said to be a source. If \mathbf{H} associated with a source has complex eigenvalues, the source is also called an unstable focus. On the other hand, if all of the eigenvalues of the matrix \mathbf{H} associated with a source are real, the source is also called an unstable node. When some, but not all, of the eigenvalues have positive real parts while the rest of the eigenvalues have negative real parts, the associated fixed point is called a saddle point.

10.6 PSEUDO-ARCLENGTH CONTINUATION

In this study, program AUTO developed by Doedel (1986) is used to investigate the behavior of nonlinear dynamical systems as a function of parameters. AUTO can compute branches of stable and unstable steady state solutions and periodic solutions, locate Hopf bifurcation points, and locate folds and continue these in two parameters. AUTO uses the pseudo-arclength continuation scheme proposed by Keller (1977) to trace out the branch of fixed points and periodic solutions in the state-control space.

Consider variation of the solution of

$$\mathbf{F}(\mathbf{x}, \alpha) = 0 \quad (10.167)$$

with respect to the scalar parameter α . In the $(n+1)$ dimensional (\mathbf{x}, α) space, there may be many branches of fixed points. It is assumed that at least one solution \mathbf{x}_0 has been calculated at α_0 and that the Jacobian matrix \mathbf{F}_x at (\mathbf{x}_0, α_0) is nonsingular so that the implicit function theorem holds locally.

The arclength s along a branch of solutions is used as the continuation parameter. Thus, \mathbf{x} and α are considered to be functions of s . Near the turning point, at $s = s^*$, the solution (\mathbf{x}^*, α^*) is obtained by using the usual arclength continuation approach. The prediction (\mathbf{x}_1, α_1) is then calculated by using the tangent predictor; that is

$$\alpha_1 = \alpha^* + \alpha^* \cdot \Delta s \quad (10.168)$$

$$\mathbf{x}_1 = \mathbf{x}^* + \mathbf{x}^* \cdot \Delta s \quad (10.169)$$

where Δs is the step length.

At this stage, the usual Newton-Raphson corrector would break down in the vicinity of the turning point because there is no solutions on the vertical line. To overcome this problem, Keller suggested a correction to (\mathbf{x}_1, α_1) along a solution path that is normal to the tangent vector \mathbf{t} at (\mathbf{x}_1, α_1) . On the solution path, (\mathbf{x}, α) satisfies equation (10.167) and the vector

$$\mathbf{X} = \begin{Bmatrix} \mathbf{x} - \mathbf{x}_1 \\ \alpha - \alpha_1 \end{Bmatrix} \quad (10.170)$$

is normal to the tangent vector \mathbf{t} ; that is,

$$\mathbf{X}^T \mathbf{t} = 0 \quad (10.171)$$

Substituting (10.168) and (10.169) into (10.171) and using the definition of \mathbf{t} yield

$$(\mathbf{x} - \mathbf{x}^*)^T \mathbf{x}' + (\alpha - \alpha^*) \alpha' - \Delta s = 0 \quad (10.172)$$

Equations (10.167) and (10.172) constitute the pseudo-arc length continuation scheme. In this scheme, the $n+1$ nonlinear algebraic equations are needed to be solved for the $n+1$ unknowns (\mathbf{x}, α) .

The solutions of equations (10.125) – (10.128) for one-to-one internal resonance and (10.156) – (10.159) for two-to-one internal resonance are calculated using AUTO and numerical results are presented in the following section.

10.7 NUMERICAL RESULTS AND DISCUSSIONS

In this section, the steady state solutions with one-to-one and two-to-one internal resonances are solved using program AUTO. The modal response of two-to-one internal resonance is calculated from direct integration of the original coupled equations (10.13) - (10.16) to show the trends of the nonlinear response. The effects of excitation amplitude, excitation frequency and the internal resonance parameter are investigated.

10.7.1 One-to-one Internal Resonance

Three prototypical systems used in this simulation are identical to that proposed by Beikmann *et al.* (1996) except the amount of additional mass added to the tensioner arm. This added inertia serves to change the frequency of the rotationally dominant mode, but does not alter the frequency of the span 3 mode. The physical properties of the three systems are shown in Table

8.1. An addition of 2.30 kg, 2.15 kg, and 1.65 kg mass is added to the tensioner arm of system 1, system 2, and system 3, respectively, at the tensioner pulley axis. The operating speed for system 1 and system 2 are 2000 RPM and the operating speed for system 3 is zero RPM. The frequency of the first transverse mode of span 3 for system 1 and system 2 is calculated as 28.11 Hz and for system 3 is 32.03 Hz. The natural frequency of the first rotationally dominant mode for system 1, system 2 and system 3 is 28.19 Hz, 29.06 Hz, and 32.71 Hz, respectively.

Examination of equations (10.125) – (10.128) governing the nonlinear response of one-to-one internal resonance reveals that two possibilities arise for the steady state solutions of one-to-one internal resonance, namely 1) $\alpha_m = 0, \alpha_n \neq 0$ and 2) $\alpha_m \neq 0, \alpha_n \neq 0$.

In the case of $\alpha_m = 0$, for steady state solution, equations (10.125) and (10.126) can be rewritten as

$$\frac{\text{Re}(\Theta_1)}{8} \alpha_n^3 - F_d \sin \zeta_2 + \hat{\zeta}_n \omega_n \alpha_n = 0 \quad (10.173)$$

$$\alpha_n \sigma_2 + \frac{\text{Im}(\Theta_1)}{8} \alpha_n^3 + F_d \cos \zeta_2 = 0 \quad (10.174)$$

It is noted that equations (10.173) and (10.174) are the same as that for no internal resonance. The internal detuning parameter σ_1 does not appear in above equations.

Figure 10.1 presents the amplitude curves of α_n versus σ_2 of system 1 for different modal damping. When modal damping is equal to zero, bifurcation occurs. For σ_2 below -0.4356 1/s, the response amplitude is single-valued; for σ_2 within -0.4356 1/s and -0.2022 1/s, the

response amplitude has three values corresponding to the same σ_2 . Thus, the system shows a typical multi-valued nonlinear phenomenon. The dominance of the quadratic nonlinearity is evident from the softening behavior shown in Figure 10.1. It is noted that no bifurcation occurs when damping exists, which indicates that damping has a significant effect on the nonlinear response of serpentine belt drive systems. Figure 10.2 shows the region where there exist multi-valued steady state responses. The two curves represent the two branches of limit points. Within the region bounded by the two curves, there are three rest states and outside of the region there is only one steady state solution.

In the case of $\alpha_m \neq 0$, for steady state solution, equations (10.125) – (10.128) can be rewritten as

$$\frac{\operatorname{Re}(\Theta_1)}{8}\alpha_n^3 + \frac{\operatorname{Re}(\Theta_2)}{8}\alpha_n\alpha_m^2 + \frac{\operatorname{Re}(\Theta_3)\cos\zeta_1 + \operatorname{Im}(\Theta_3)\sin\zeta_1}{8}\alpha_n\alpha_m^2 - F_d \sin\zeta_2 + \zeta_n\omega_n\alpha_n = 0 \quad (10.175)$$

$$\alpha_n\sigma_2 + \frac{\operatorname{Im}(\Theta_1)}{8}\alpha_n^3 + \frac{\operatorname{Im}(\Theta_2)}{8}\alpha_n\alpha_m^2 + \frac{\operatorname{Im}(\Theta_3)\cos\zeta_1 - \operatorname{Re}(\Theta_3)\sin\zeta_1}{8}\alpha_n\alpha_m^2 + F_d \cos\zeta_2 = 0 \quad (10.176)$$

$$\frac{\operatorname{Re}(\Theta_6)}{8}\alpha_m^2 + \frac{\operatorname{Re}(\Theta_5)}{8}\alpha_n^2 + \frac{\operatorname{Re}(\Theta_4)\cos\zeta_1 - \operatorname{Im}(\Theta_4)\sin\zeta_1}{8}\alpha_n^2 + \zeta_m\lambda_m = 0 \quad (10.177)$$

$$\alpha_m(\sigma_1 + \sigma_2) + \frac{\operatorname{Im}(\Theta_6)}{8}\alpha_m^2 + \frac{\operatorname{Im}(\Theta_5)}{8}\alpha_n^2 + \frac{\operatorname{Im}(\Theta_4)\cos\zeta_1 + \operatorname{Re}(\Theta_4)\sin\zeta_1}{8}\alpha_n^2 = 0 \quad (10.178)$$

In Figure 10.3, the solution curves for α_n and α_m of system 1 obtained from equations (10.175) – (10.178) are shown with σ_2 as the parameter on the x -axis. The modal damping for rotational mode is chosen as 1% and for transverse mode is chosen as 0.3%. It is seen that two branch curves exist for α_n and α_m on both sides of $\sigma_2 = 0$ axis. This is typical of a coupled system with quadratic non-linearities. However, the presence of cubic nonlinearity causes distortion and

asymmetry in these curves. The stable and unstable solutions are also marked by thick solid lines and thin solid lines separately. There always exist two steady state solutions for α_n within the range where non-trivial solutions exist. Two steady state solutions are possible for α_m , one being stable and the other unstable within a certain range of σ_2 values. The single possible solution for α_m becomes unstable near $\sigma_2 = 2.647$ 1/s. The instability of the steady state solutions for α_n and α_m is followed by a Hopf bifurcation which leads to oscillating amplitudes and phases. It is seen from Figure 10.3 that there is a branch of periodic orbits emanating from the rest state. Filled circles represent stable periodic orbits and open circles are unstable. The period-doubling bifurcations also occur.

The periodic solutions for α_n , α_m , ζ_1 , and ζ_2 are shown in Figure 10.4 for $\sigma_2 = 2.647$ 1/s at which the amplitudes and phases become periodic. The solutions are obtained by numerically integrating equations (10.125) – (10.128) with the values of α_n , α_m , ζ_1 , and ζ_2 for $\sigma_2 = 2.647$ 1/s being the initial condition.

Phase plane curves of α_n and α_m versus ζ_1 and ζ_2 , shown in Figure 10.5, reflect their limit cycle behavior. The dotted lines represents the nullclines which are curves where $d/dt=0$. The intersection of two nullclines is an equilibrium point.

The frequency of the periodic solutions as a function of detuning parameter σ_2 is presented in Figure 10.6. The frequency initially goes down and then goes up. Note that the minimal frequency is not zero.

Figure 10.7 shows the region where there exist non-trivial steady state solutions. The amplitude of the excitation is the y -axis and the detuning parameter σ_2 is the x -axis. The four curves represent the two branches of limit points, respectively. Within the region bounded by the first curve (from left to right) and the fourth curve (from left to right), there exist non-trivial solutions for both α_n and α_m .

The effect of the amplitude of excitation is illustrated in Figure 10.8. The external detuning parameter σ_2 is set as 5.00 1/s and the internal detuning parameter σ_1 is set as 0.5296 1/s. As the excitation level is increased from low levels, the steady state response is initially zero. When the excitation reaches a certain level, the response jumps to attain high amplitude. The response amplitude of rotational mode grows with the increase of the excitation amplitude. However, one branch of transversely dominant mode decreases with the growth of the excitation amplitude.

Figure 10.9 shows the effect of the internal detuning parameter σ_1 . The external detuning parameter σ_2 chosen as 5.00 1/s and the excitation amplitude is chosen as 0.5. There is no non-trivial solutions when σ_1 is less than -7.217 1/s. With the increase of σ_1 , one steady solution for α_n grows and the other solution decreases. Both steady state solutions for α_m grow with σ_1 .

System 1 has a very small internal detuning parameter σ_1 (0.529594 1/s). For serpentine belt drive system 2 with larger internal detuning parameter $\sigma_1 = 5.95989$ 1/s, the numerical results may be different. The numerical results of system 2 in the case of $\alpha_m = 0$ are shown in Figure

10.10 and Figure 11. Since the internal detuning parameter σ_1 does not appear in the governing equations (10.173) and (10.174), the nonlinear responses of system 2 are similar to those of system 1 in the case of $\alpha_m = 0$. Figures 10.12 – 10.16 show the numerical results of systems 2 in the case of $\alpha_m \neq 0$. It is seen that the steady state solutions of α_m for system 1 and system 2 are different. There exists an additional unstable steady state solution between $\sigma_2 = -5.295$ i/s and $\sigma_2 = -1.41$ i/s. The relation between steady state response and excitation amplitude F_d is also different. Three steady state solutions are possible in a certain range of F_d for system 2 while only two solutions exist for system 1. The plot of the frequency of the periodic solutions vs. σ_2 shows that there exist two frequencies at the same σ_2 .

Figures 10.17 – 10.19 show the nonlinear response of system 3 with zero operating speed. In this case, gyroscopic terms perish in governing equations (10.1) – (10.4). The numerical results are similar to those of systems 2.

10.7.2 Two-to-one Internal Resonance

Two prototypical systems (system 4 and system 5) used in this simulation are the same as that proposed by Beikmann *et al.* (1996). The operating speed for system 4 is zero RPM and the natural frequency of mode 1 of span 3 is 32.03 Hz. The operating speed for system 5 is 2000 RPM. An addition of 0.39 kg mass is added to the tensioner arm of system 5, at the tensioner pulley axis. The frequencies of the first rotationally dominant mode of system 5 and the mode 1 of span 3 are calculated as 57.41 Hz and 28.11 Hz, respectively.

The free responses of system 4 where no internal resonance exists are shown in Figure 10.20. The natural frequency of the first rotationally dominant mode is 55.00 Hz. The initial conditions are as follows: $\xi_n^R = 0.02$, $\eta_m^R = 0.01$, $\xi_n' = 0.0$, and $\eta_m' = 0.0$. It can be seen that each mode appears to vibrate independently at its natural frequency, modified slightly by the nonlinearities. This is qualitatively similar to the linear case.

Figure 10.21 shows the free responses of system 4 with zero detuning parameter. In this example, the first rotationally dominant mode starts with zero initial conditions. The initial conditions for span3 are $\eta_m^R = 0.01$ and $\eta_m' = 0.0$. Comparing the response of rotationally dominant mode and mode 1 of span 3 shows that the increase in the rotational mode is accompanied by a slight decrease in the motion of the transverse mode. This indicates that these two modes can interact through a two-to-one type internal resonance.

Figure 10.22 presents the nonlinear response of system 4 with larger detuning. The natural frequency of the rotational mode is 62.00 Hz. The initial conditions of the systems are identical to that in Figure 10.21. It is seen that a typical beat phenomenon occurs for rotational mode. Note that the maximum response amplitude of rotational mode is less than in Figure 10.21 and the amplitude of transverse mode remains nearly constant. This is because the faster beat rate resulting from greater detuning shortens the time that energy is passed into rotational mode. As a result, a smaller amount of energy is passed to rotational mode.

The forced responses of system 4 with zero detuning parameter are shown in Figure 10.23. A dynamic moment with amplitude 0.3 Nm and frequency 64.06 Hz is imposed at pulley 4. The initial conditions of the systems are the same as that in Figure 21. Modal damping for rotational mode is set at 2% and for transverse mode is set at 0.1%. The response of rotational mode grows quickly and reaches its steady state amplitude. The response of span 3 grows exponentially with time indicating that the system is unstable.

The numerical simulation of system 4 demonstrates that transverse motion of span 3 may be parametrically excited through two-to-one internal resonance. The internal and the external detuning parameters have significant effect on the nonlinear response. Reducing the level of the excitation and moving the excitation frequency away from the rotational mode frequency helps to avoid parametric resonance in serpentine belt systems.

Similar to the one-to-one internal resonance, two possibilities arise in the steady state responses of two-to-one internal resonance, that is 1) $\alpha_m = 0, \alpha_n \neq 0$ and 2) $\alpha_m \neq 0, \alpha_n \neq 0$. In the case of $\alpha_m = 0$, the governing equations for α_n and ζ_2 are identical to equations (10.173) and (10.174). The internal detuning parameter σ_1 does not appear in these two equations.

Figure 10.24 shows the amplitude curves of system 5 versus σ_2 for different modal damping in the case of $\alpha_m = 0$. It can be seen from Figure 10.24 that bifurcation occurs as σ_2 is within 0.5114 1/s and 0.8061 1/s. The dominance of cubic nonlinearity is evident from the hardening behavior due to the large response amplitude. It is noted that no bifurcation occurs when the modal damping is not equal to zero. This conclusion is identical to that for one-to-one internal

resonance. Figure 10.25 shows the region where there exist multi-valued amplitudes.

Similarly, for the steady state response of two-to-one internal resonance, in the case of $\alpha_m \neq 0$, equations (10.156) – (10.159) can be rewritten as

$$\frac{\operatorname{Re}(\Theta_1)}{8}\alpha_n^3 + \frac{\operatorname{Re}(\Theta_2)}{8}\alpha_n\alpha_m^2 - \frac{\operatorname{Re}(p_1)\cos\zeta_1 - \operatorname{Im}(p_1)\sin\zeta_1}{2}\alpha_m^2 - F_d\sin\zeta_2 + \hat{\zeta}_n\omega_n\alpha_n = 0 \quad (10.179)$$

$$\frac{\operatorname{Im}(\Theta_1)}{8}\alpha_n^3 + \frac{\operatorname{Im}(\Theta_2)}{8}\alpha_n\alpha_m^2 - \frac{\operatorname{Im}(p_1)\cos\zeta_1 + \operatorname{Re}(p_1)\sin\zeta_1}{2}\alpha_m^2 + F_d\cos\zeta_2 + \alpha_n\sigma_2 = 0 \quad (10.180)$$

$$\frac{\operatorname{Re}(\Theta_6)}{8}\alpha_m^2 + \frac{\operatorname{Re}(\Theta_5)}{8}\alpha_n^2 - \frac{\operatorname{Re}(p_2)\cos\zeta_1 + \operatorname{Im}(p_2)\sin\zeta_1}{2}\alpha_n + \hat{\zeta}_m\lambda_m = 0 \quad (10.181)$$

$$\frac{\operatorname{Im}(\Theta_6)}{8}\alpha_m^2 + \frac{\operatorname{Im}(\Theta_5)}{8}\alpha_n^2 - \frac{\operatorname{Im}(p_2)\cos\zeta_1 - \operatorname{Re}(p_2)\sin\zeta_1}{2}\alpha_n + \alpha_m \frac{\sigma_1 + \sigma_2}{2} = 0 \quad (10.182)$$

In Figure 10.26, the solution curves for α_n and α_m of system 5 are shown with σ_2 as the parameter on the x -axis. The modal damping for rotational mode is 1% and for transverse mode is 0.3%. It is seen that three branch curves exist for α_n , which is different from one-to-one internal resonance. The results obtained in this study qualitatively agree with the experimental results by Beikmann *et al.* (1996). Two steady state solutions are possible for α_m , one being stable and the other unstable in a certain range of σ_2 values. From Figure 10.26, it is observed that quadratic nonlinearity dominates at low amplitude. As the amplitude level increases, the cubic nonlinearity term controls the response.

Figure 10.27 shows a Hopf bifurcation which leads to oscillating amplitudes and phases. It is seen from Figure 10.27 that there is a branch of solutions or periodic orbits emanating from the

rest state. The frequency of the periodic solutions as a function of detuning parameter σ_2 is shown in Figure 10.28. The frequency of the periodic solutions does not change with σ_2 , which is different from one-to-one resonance. The periodic solutions for α_n , α_m , ζ_1 , and ζ_2 are shown in Figure 10.29 for $\sigma_2 = 1.135$ 1/s at which the amplitudes and phases become periodic. Phase plane curves of α_n and α_m versus ζ_1 and ζ_2 in Figure 10.30 reflect their limit cycle behavior.

The effect of the amplitude of excitation on dynamic response of system 5 is illustrated in Figure 10.31. The external detuning parameter σ_2 is set at 10.00 1/s and the internal detuning parameter σ_1 is set at 7.4838 1/s. Figure 10.32 shows the effect of the internal detuning parameter σ_1 on dynamic response of system 5. The external detuning parameter σ_2 is set at 10.00 1/s and the excitation amplitude is set at 0.5. There is no non-trivial solution for α_m when σ_1 is outside – 18.86 1/s and 24.19 1/s. Two possible solutions exist for α_m when σ_1 is within –0.8984 1/s and 24.19 1/s. One solution is stable and the other is unstable.

10.8 SUMMARY AND CONCLUSIONS

In this chapter, the discretization multiple scales method is employed to the treatment of elastic serpentine belt drive systems. The hybrid nonlinear equations of motion are discretized using the eigenfunctions of corresponding linear problems. The method of multiple scales is then applied to the resulting ordinary differential equations. The interaction between subsystem 1 and subsystem 2 is investigated. Transverse motion of subsystem 1 may be parametrically excited

through the linear component of the dynamic tension while subsystems 2 is also excited by the nonlinear components of the dynamic tension which is due to transverse vibrations of subsystem 1. Due to the existence of the quadratic and cubic nonlinearities, both one-to-one and two-to-one internal resonance may occur.

The effect of the internal detuning parameter has been investigated through the variation of the mass attached at the end of the tensioner arm. For large values of detuning parameter σ_1 , the system is far from resonance and there is only one solution. When the system is near or at exact one-to-one internal or two-to-one resonances, the response becomes very large and shows a typical multi-valued nonlinear phenomenon.

The excitation frequency has a significant effect on the system response. Moving the excitation frequency away from the rotational mode frequency significantly increases the excitation level necessary to produce parametric resonance. Multiple limit cycles exist when the excitation is above threshold levels.

The results presented in this chapter indicate the possibility of complicated bifurcations in serpentine belt drive systems. For certain range of detuning parameter σ_2 , the steady state solutions for the amplitudes and phases of serpentine belt drive system undergo Hopf bifurcation. The resulting system response could be amplitude-modulated motion. The period doubling bifurcation also occurs.

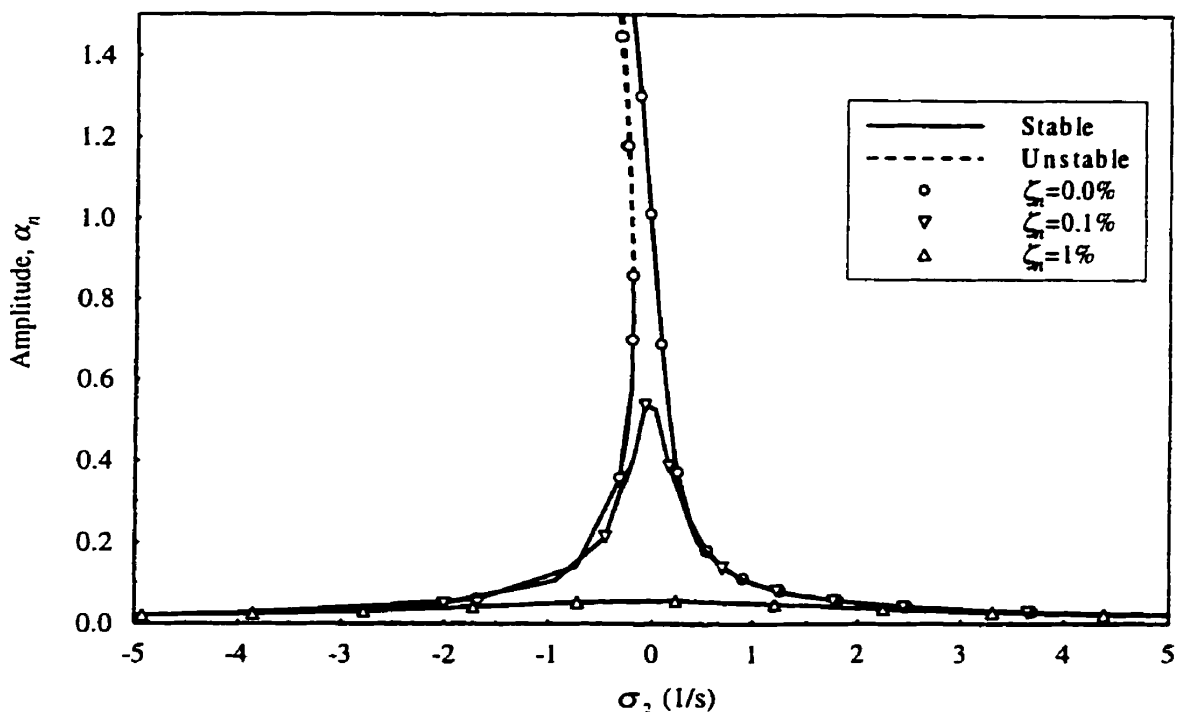


Figure 10.1: Response-frequency curves of system 1 for $\alpha_m=0.0$

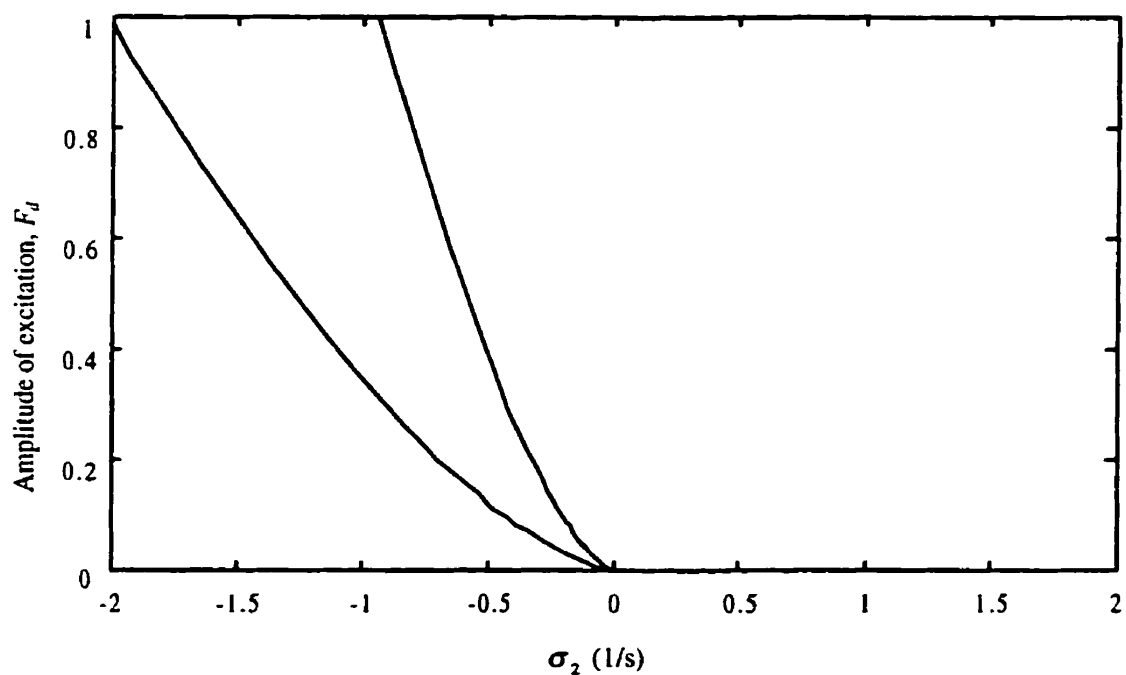


Figure 10.2: Multi-valued region of system 1 for $\alpha_m = 0.0$

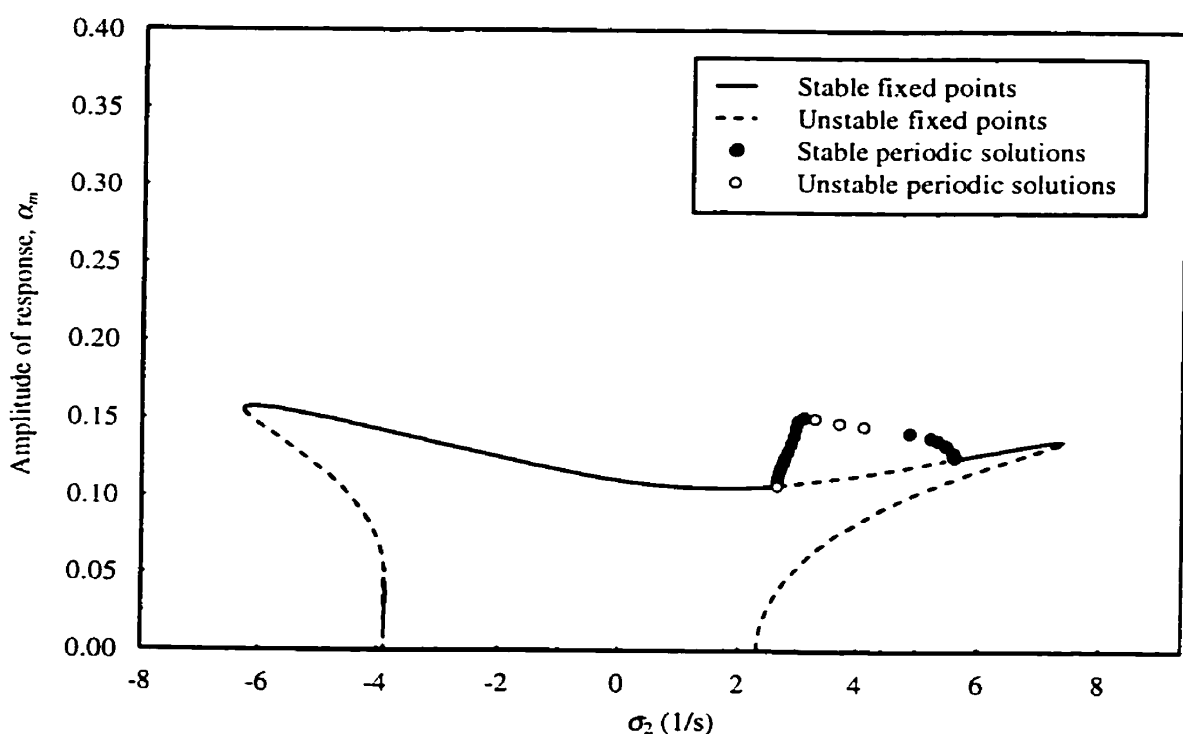
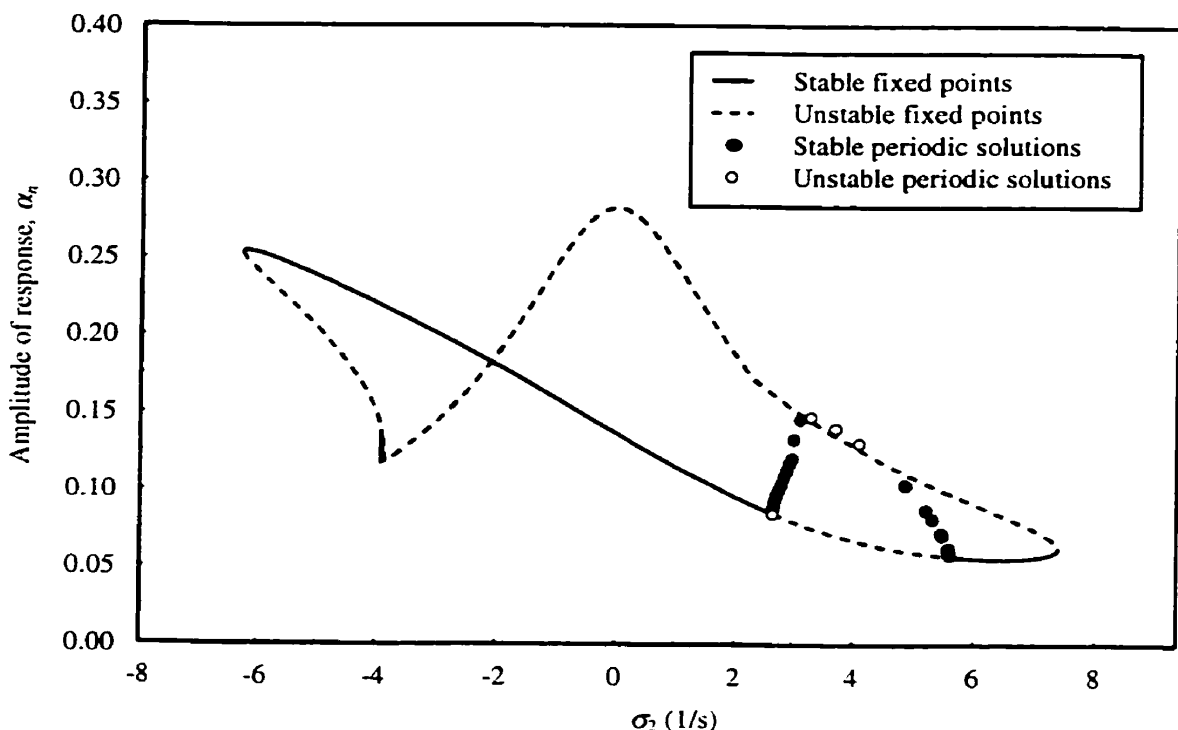


Figure 10.3: Response-frequency curves of system 1 for $\zeta_n = 1\%$, $\zeta_m = 0.3\%$

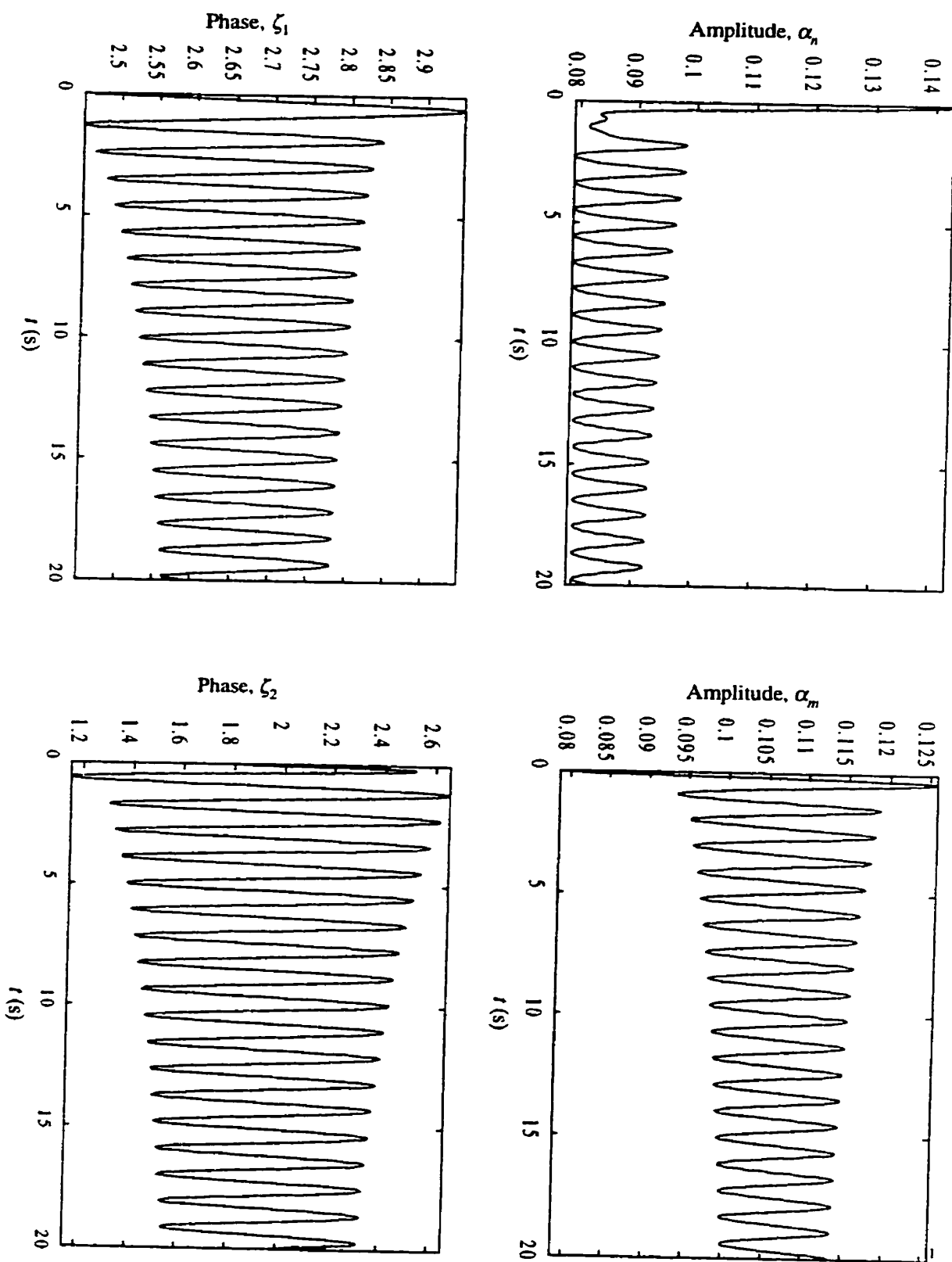


Figure 10.4: Periodic solutions of system 1

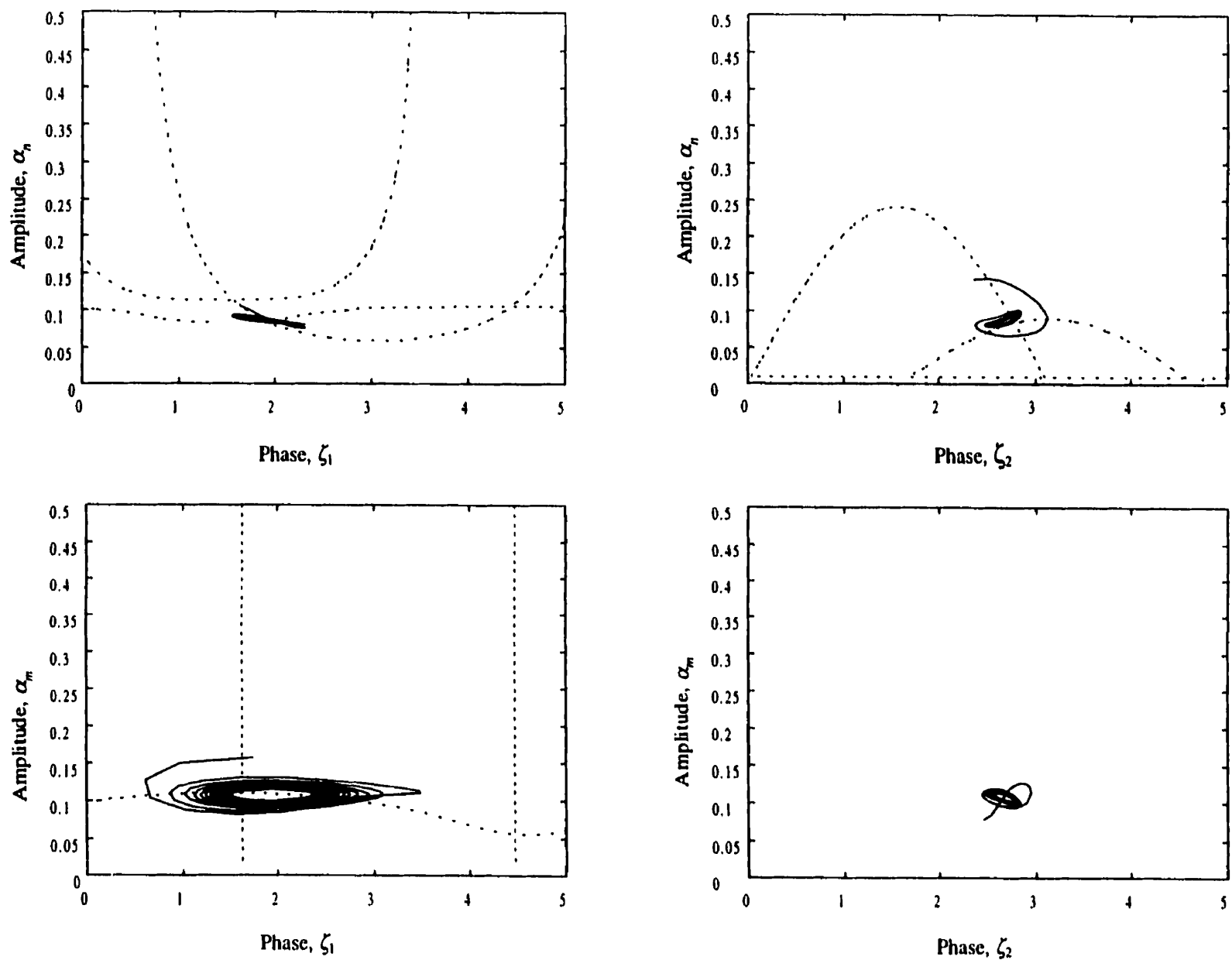


Figure 10.5: Phase plane curves of system 1 (dotted lines represent the nullclines)

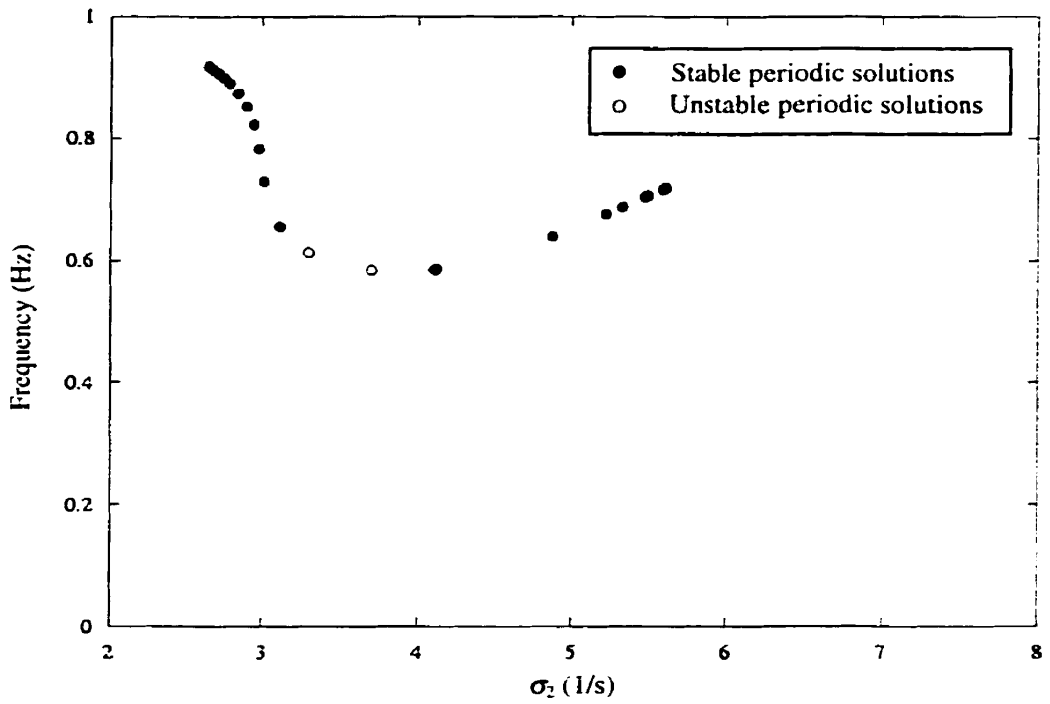


Figure 10.6: Relation between frequencies of periodic solutions and σ_2 for system 1

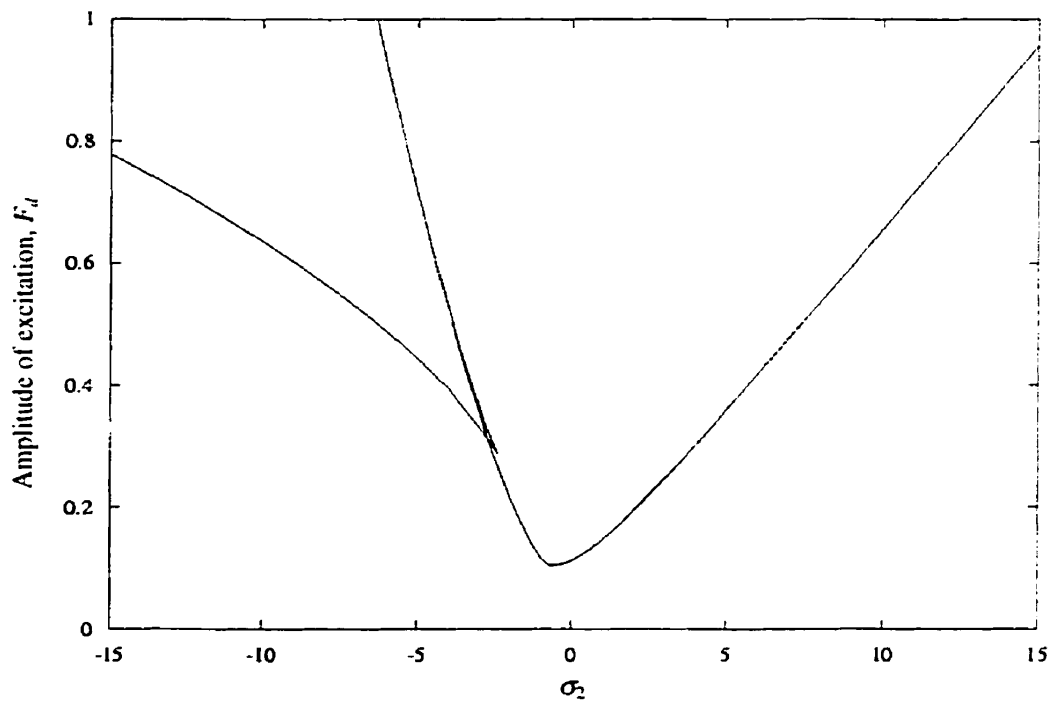


Figure 10.7: Region of nontrivial limit cycles of system 1

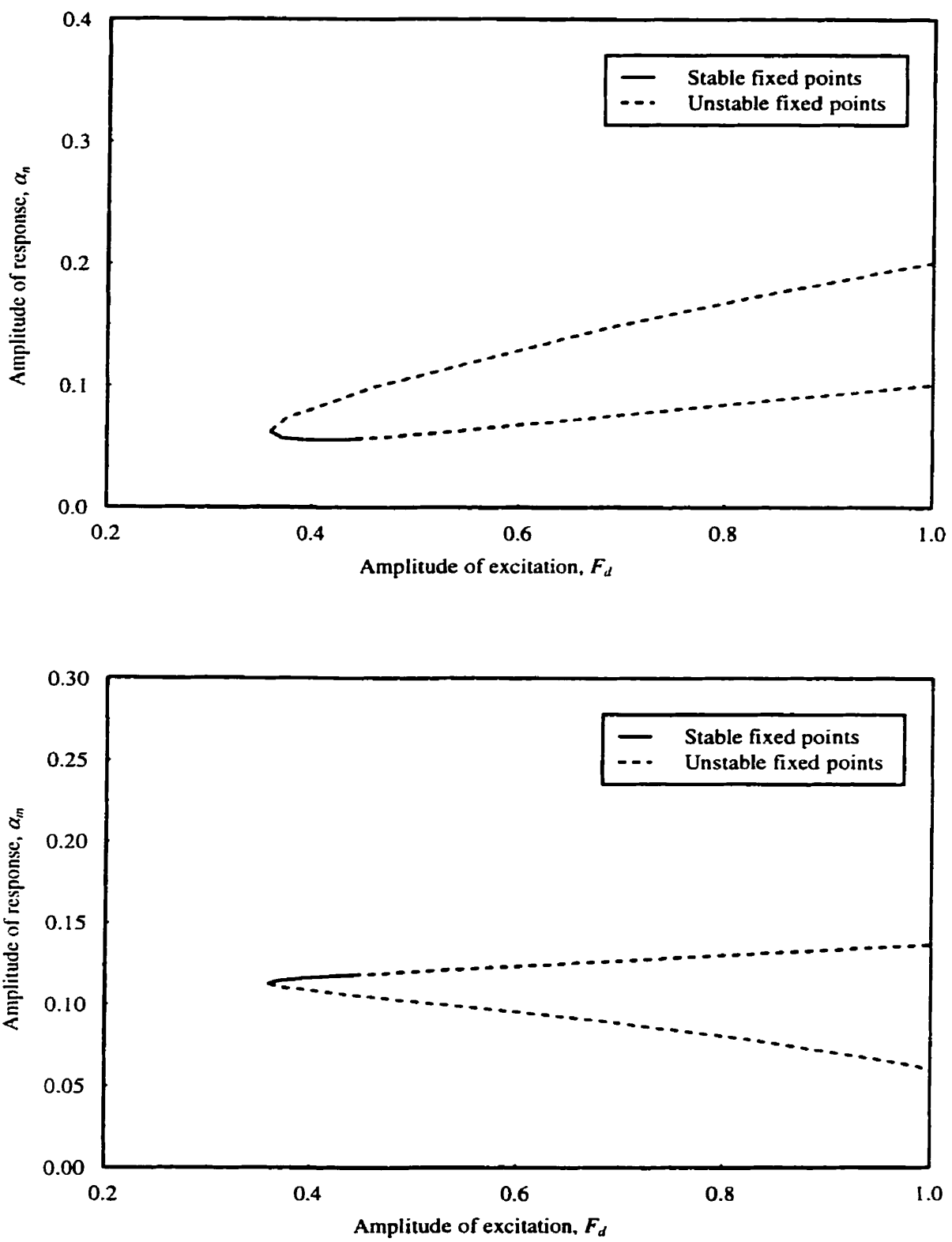


Figure 10.8: Response-excitation curves of system 1 for $\hat{\zeta}_n = 1\%$, $\hat{\zeta}_m = 0.3\%$
 $(\sigma_1=0.529594 \text{ 1/s and } \sigma_2=5.0 \text{ 1/s})$

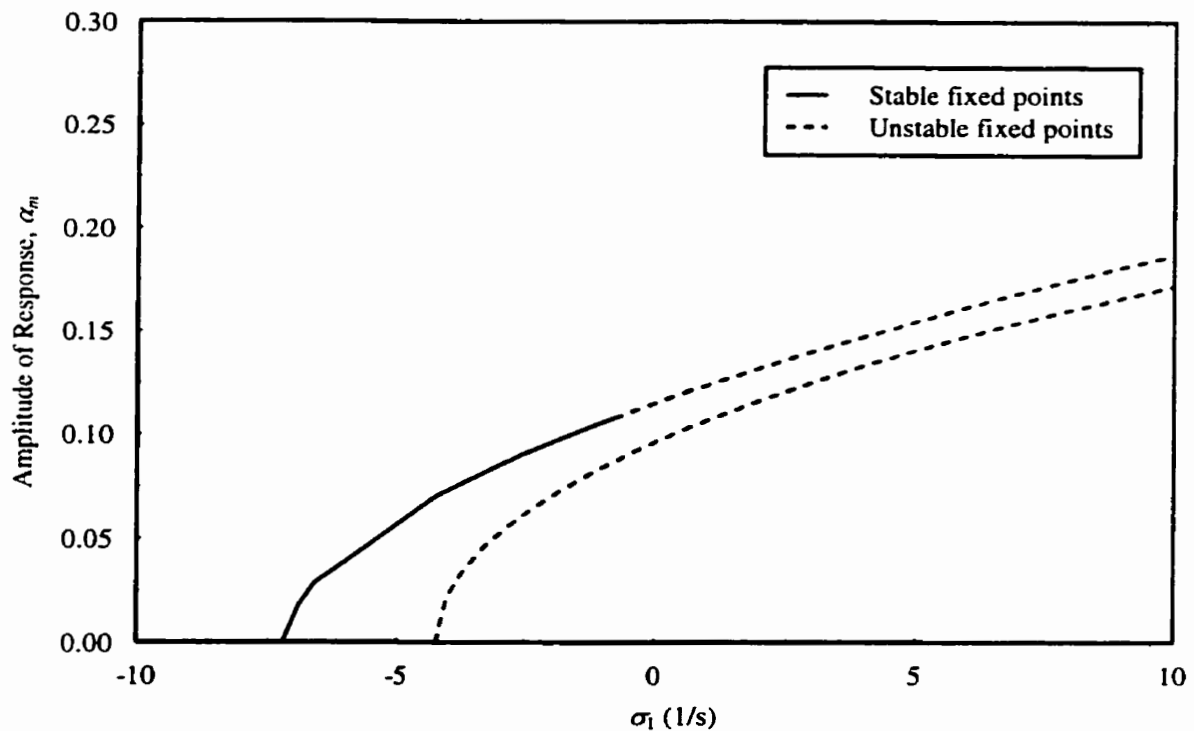
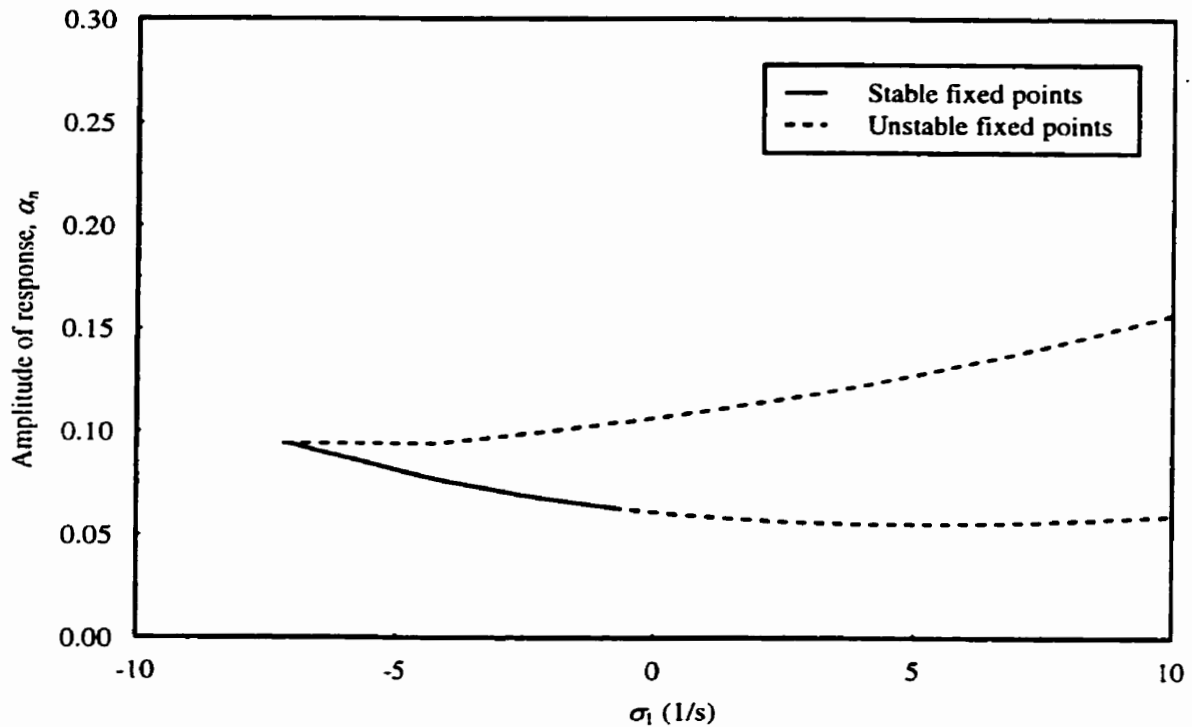


Figure 10.9: Relation between responses of system 1 and internal detuning parameter σ_1
 $(\sigma_2=5.0 \text{ } 1/\text{s} \text{ and } F_d=0.5)$

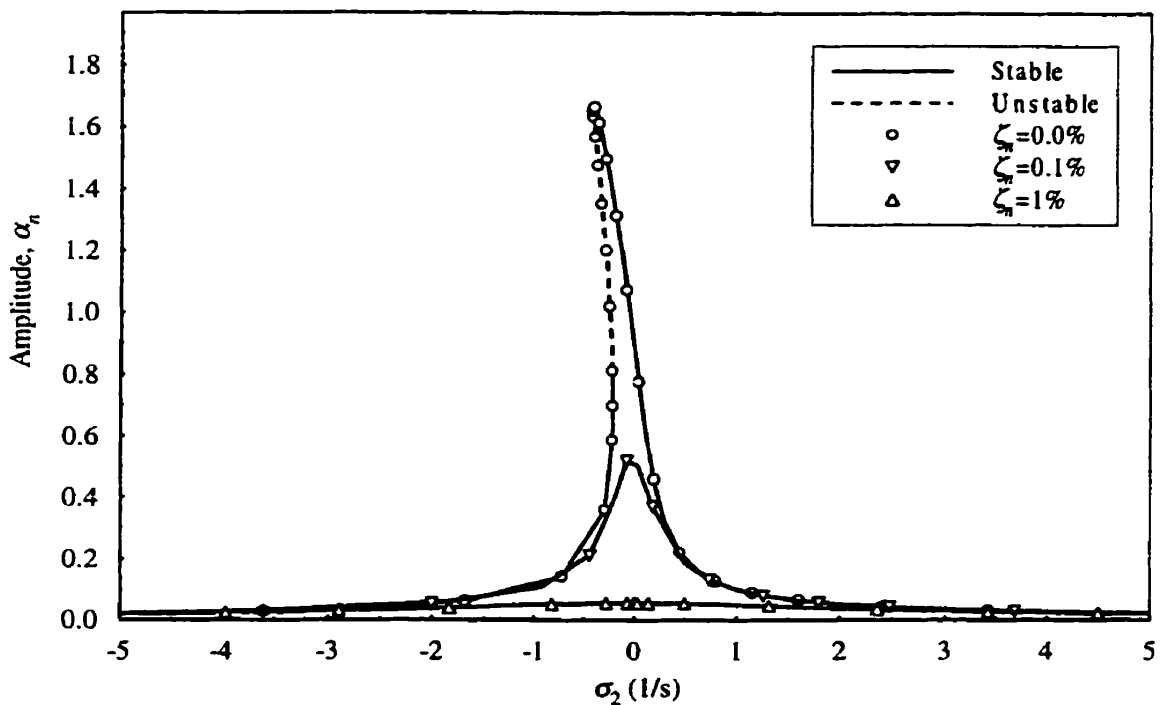


Figure 10.10: Response-frequency curves of system 2 for $\alpha_m=0$

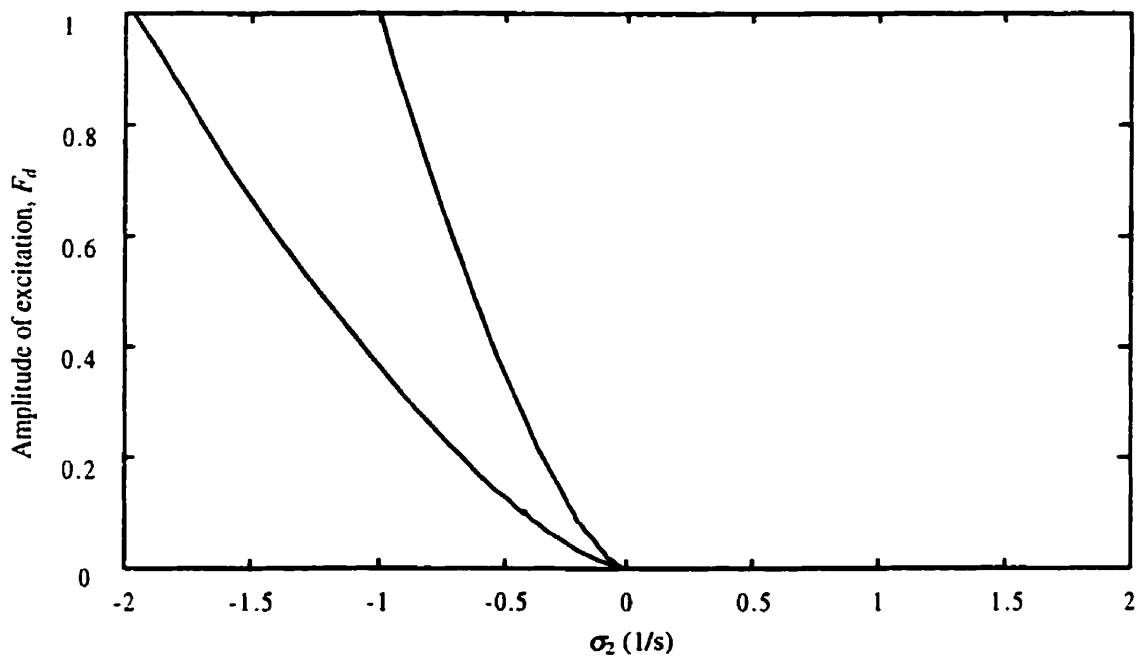


Figure 10.11: Multi-valued region of system 2 for $\alpha_m = 0.0$

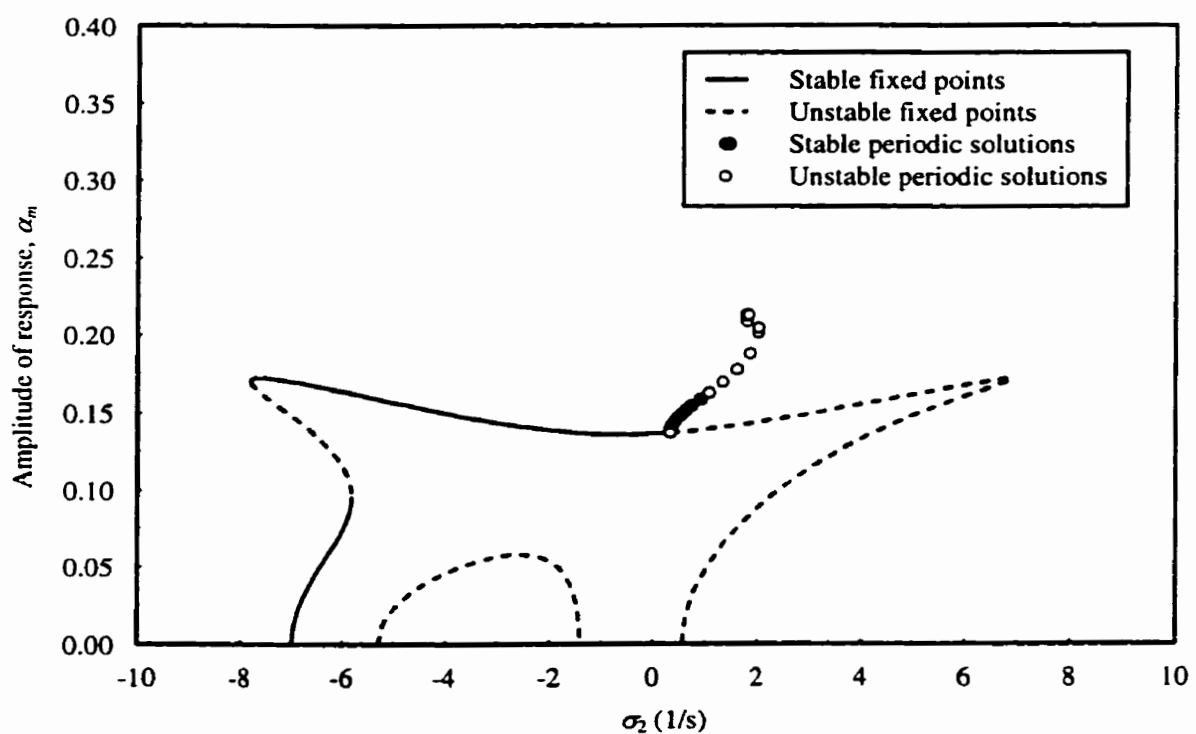
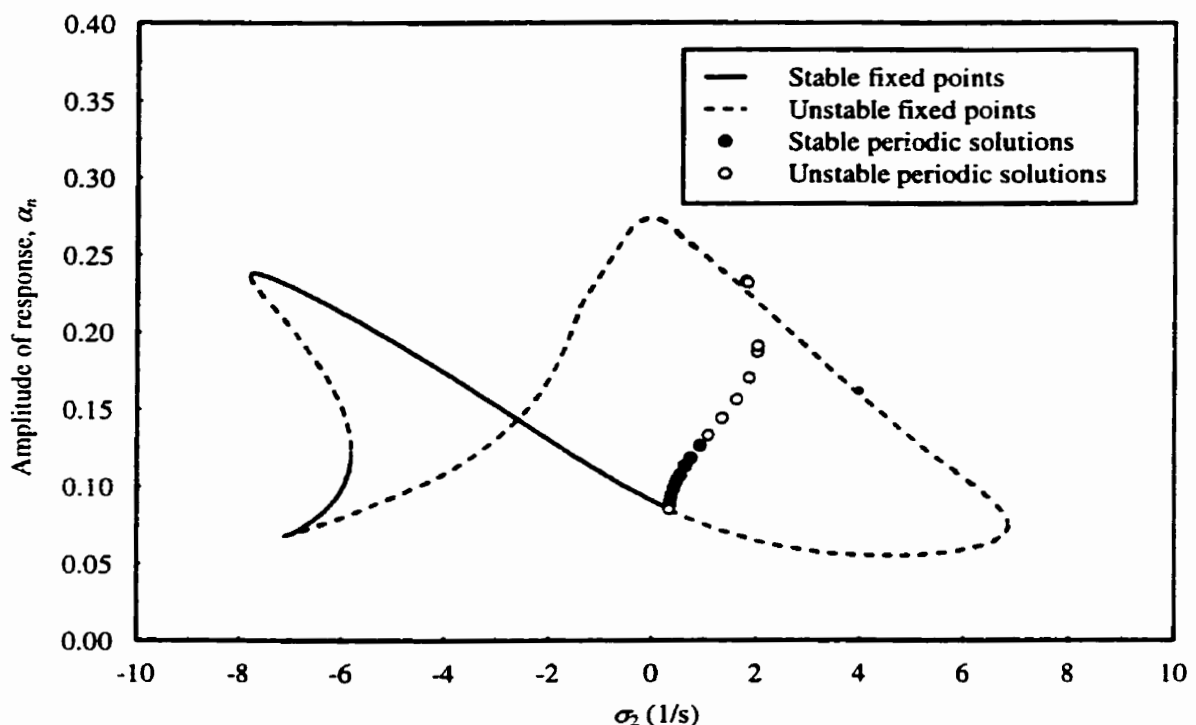


Figure 10.12: Response-frequency curves of system 2 for $\hat{\zeta}_n = 1\%$, $\hat{\zeta}_m = 0.3\%$

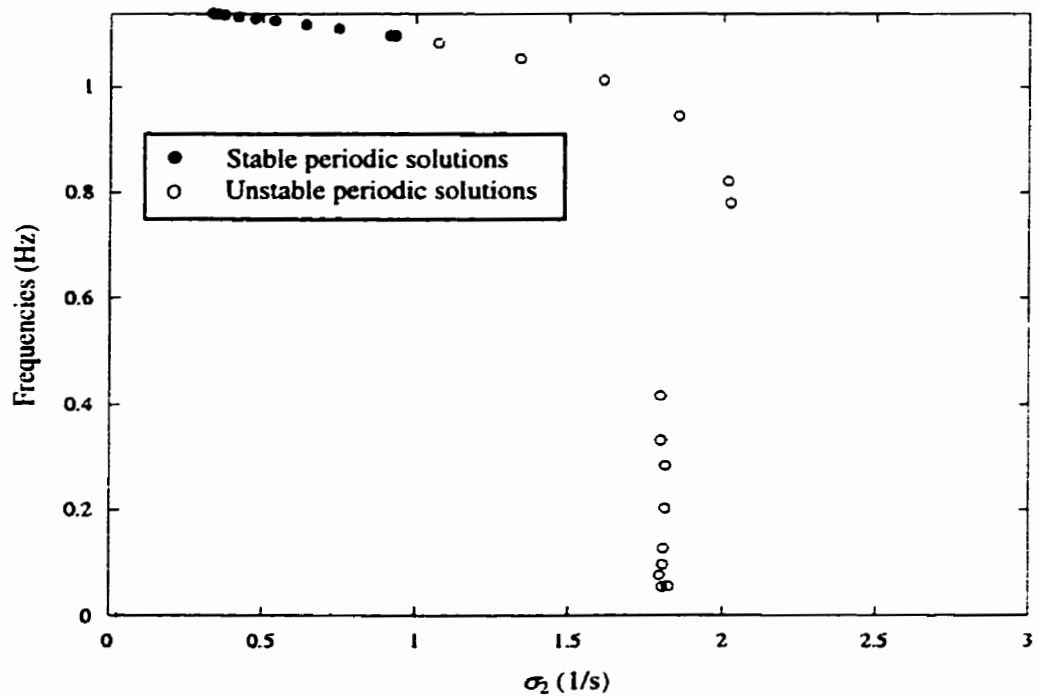


Figure 10.13: Relation between frequencies of periodic solutions and σ_2 for system 2

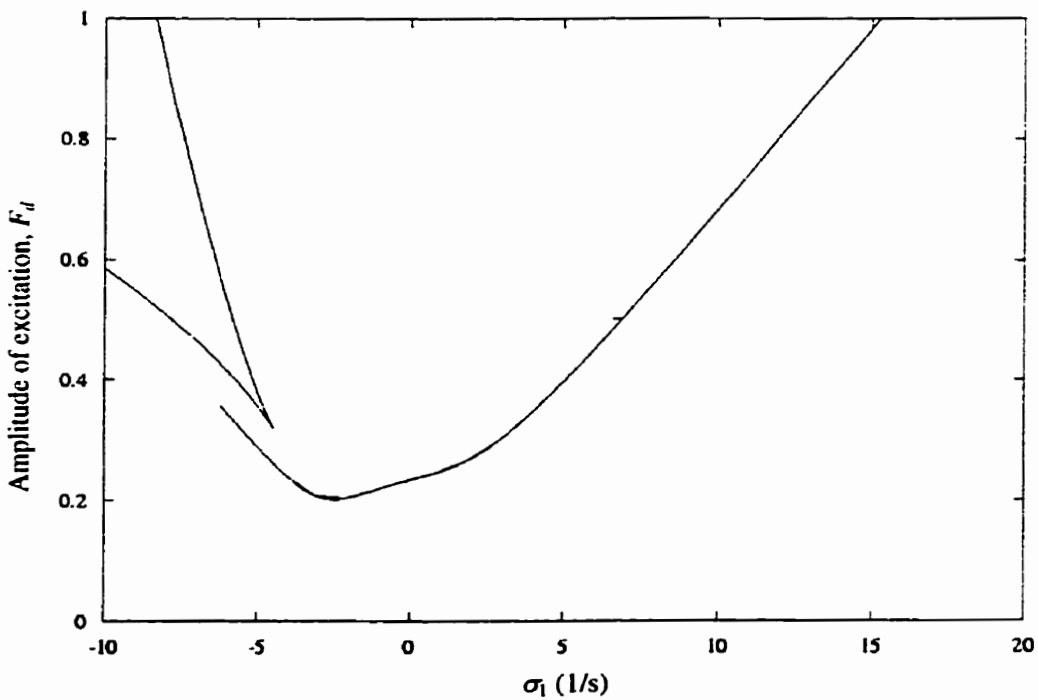


Figure 10.14: Region of nontrivial limit cycles of system 2

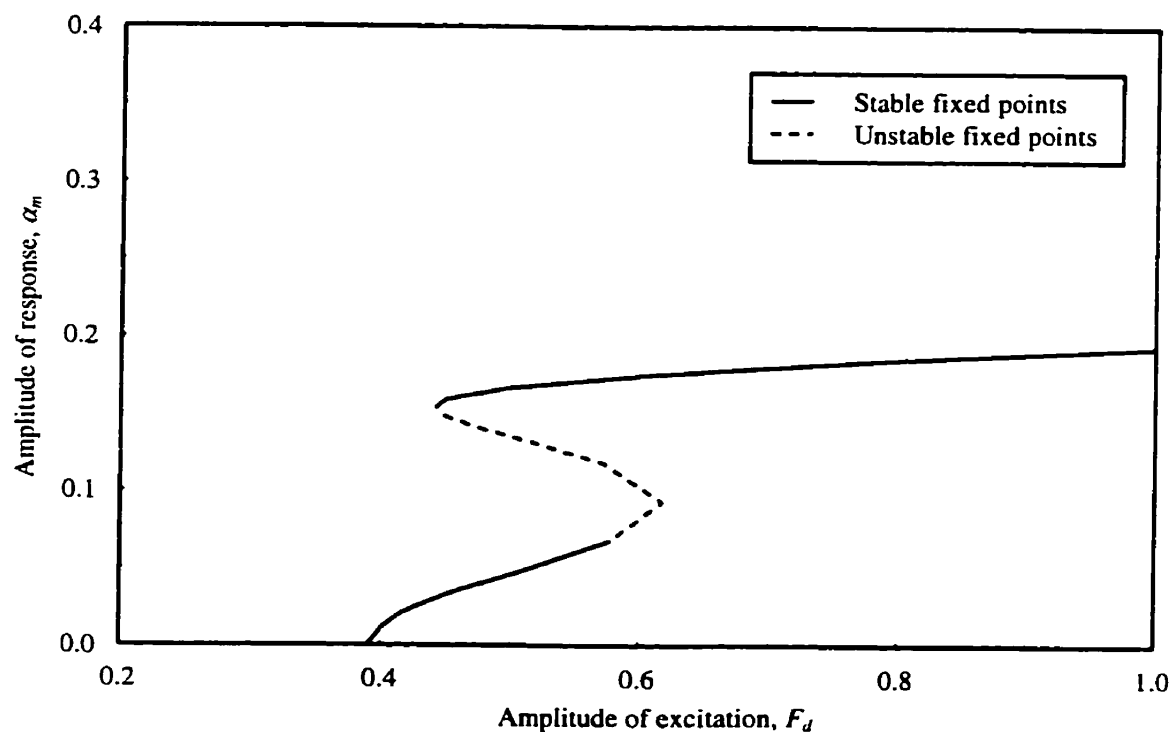
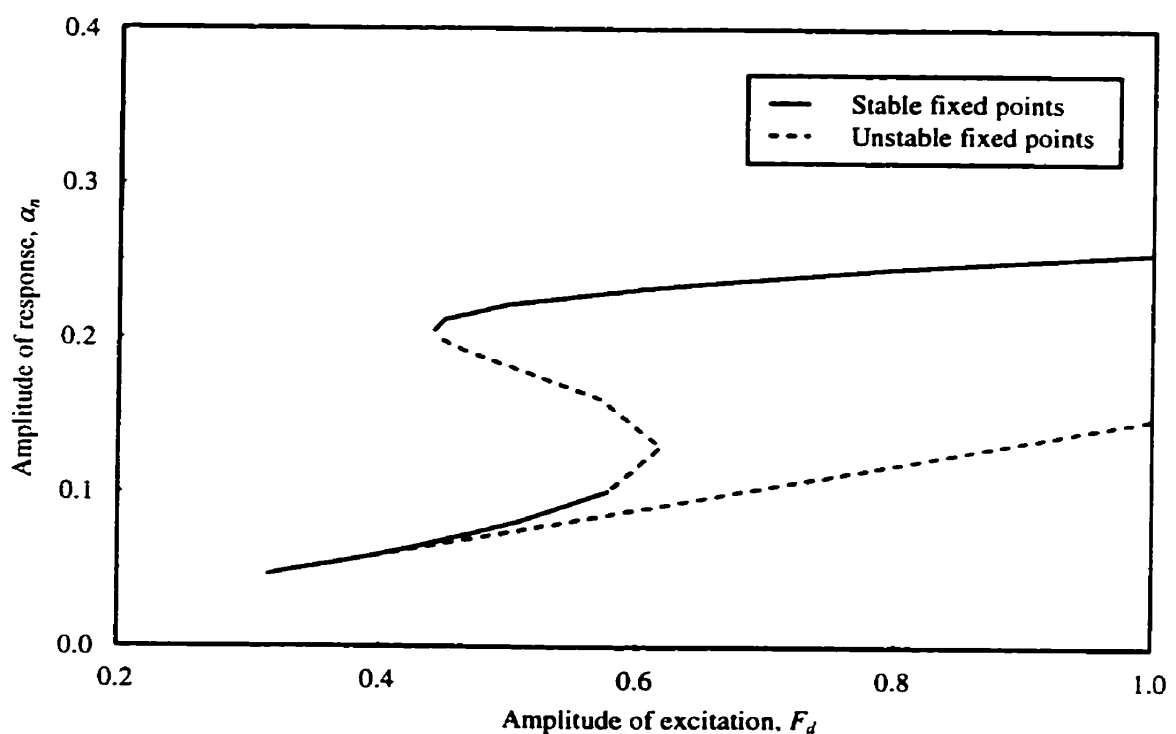


Figure 10.15: Response-excitation curves of system 2 for $\hat{\zeta}_n = 1\%$, $\hat{\zeta}_m = 0.3\%$
 $(\sigma_1 = 5.95989 \text{ 1/s and } \sigma_2 = -6.5 \text{ 1/s})$

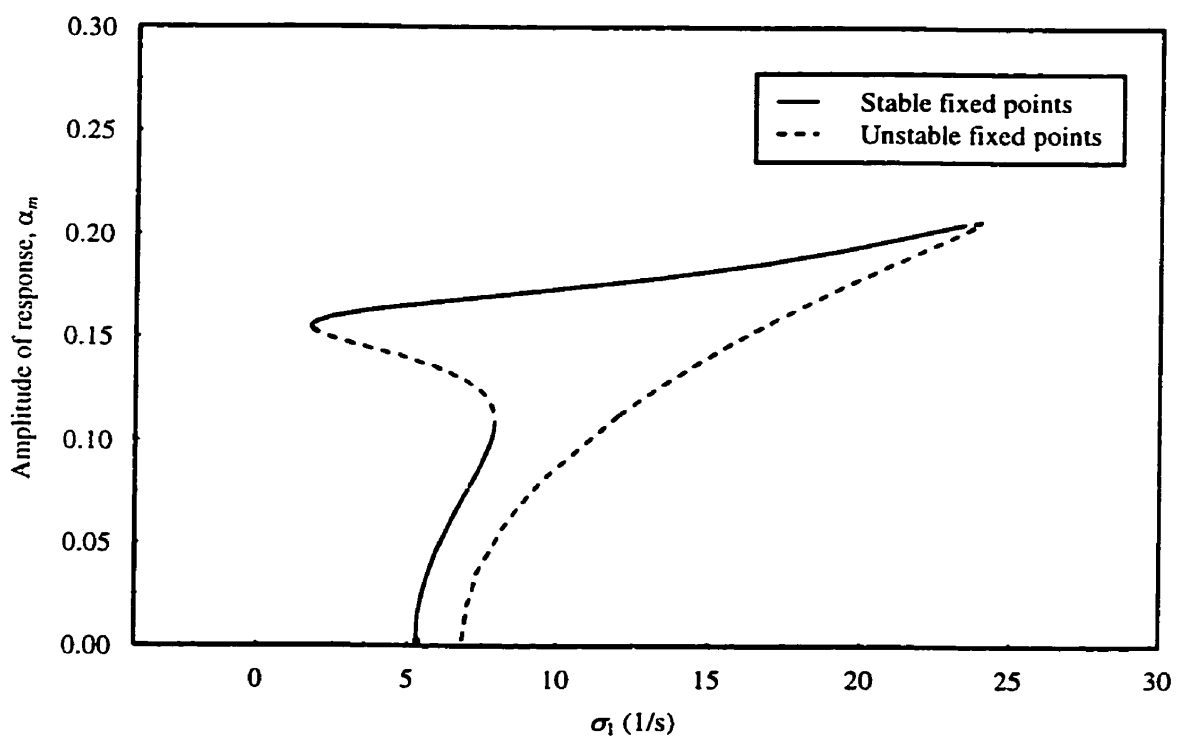
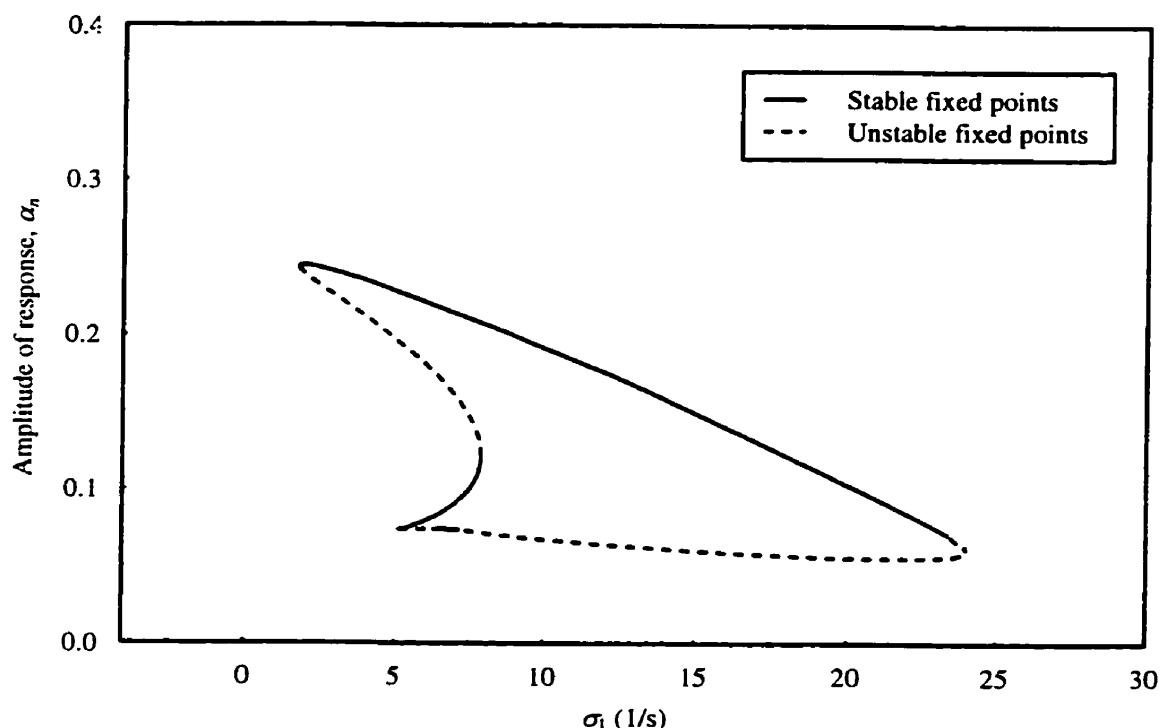


Figure 10.16: Relation between responses of system 2 and internal detuning parameter σ_1
($\sigma_2=5.0$ 1/s and $F_d=0.5$)

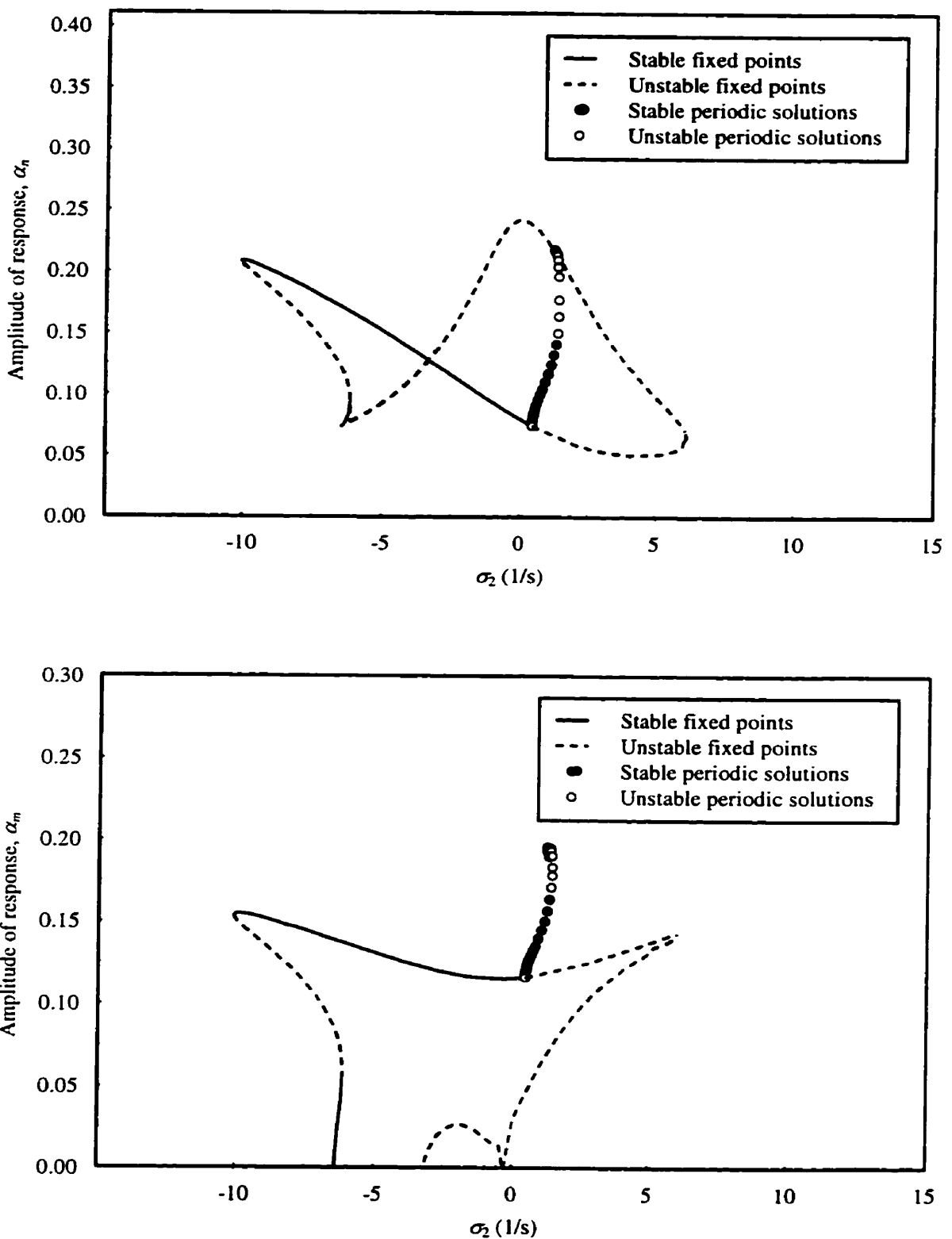


Figure 10.17: Response-frequency curves of system 3 for $\hat{\zeta}_n = 1\%$, $\hat{\zeta}_m = 0.3\%$

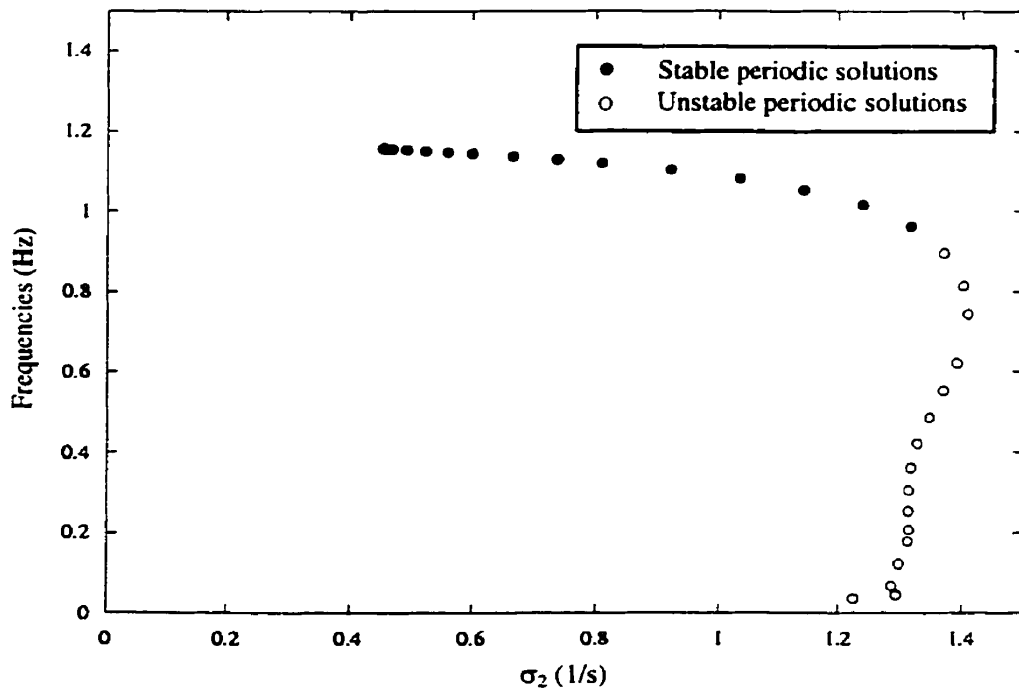


Figure 10.18: Relation between frequencies of periodic solutions and σ_2 for system 3

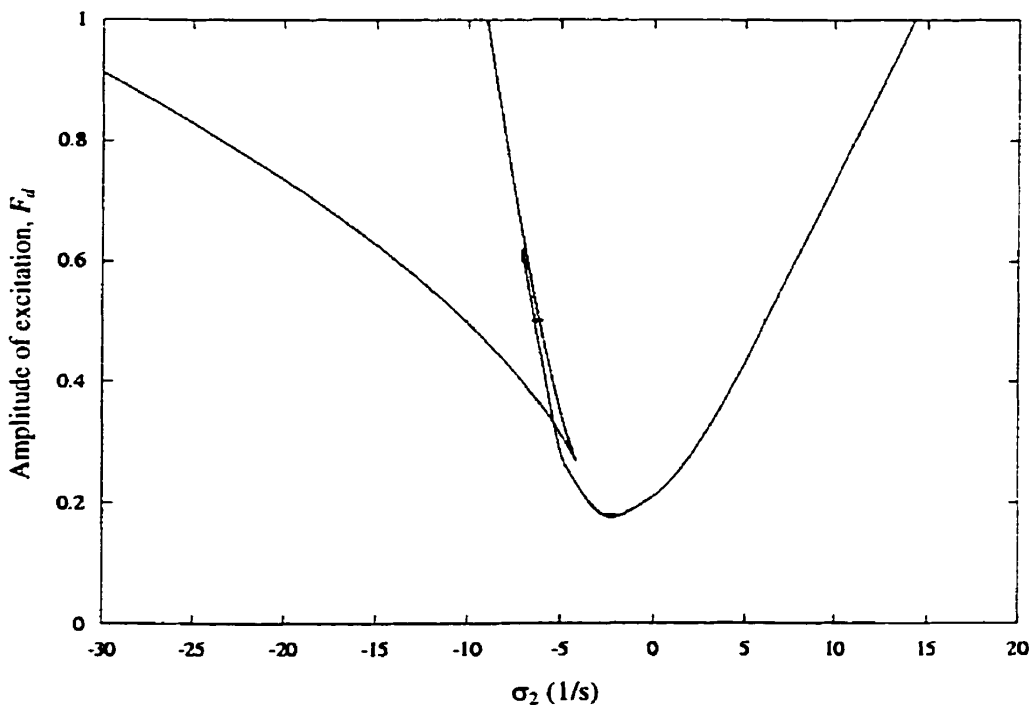


Figure 10.19: Region of nontrivial limit cycles of system 3

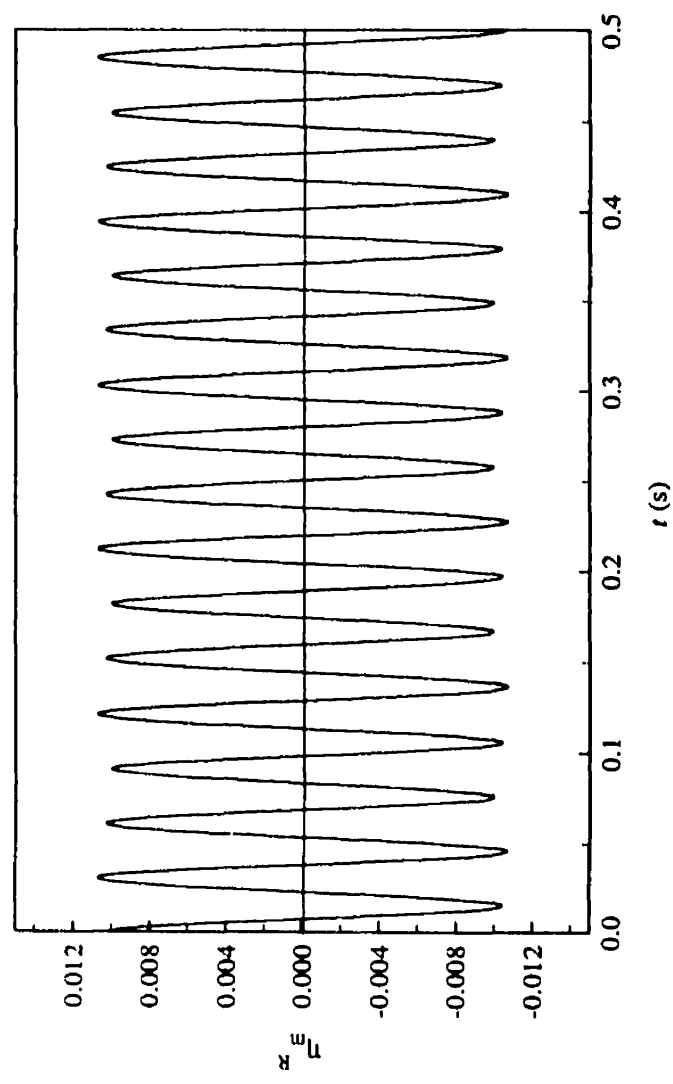
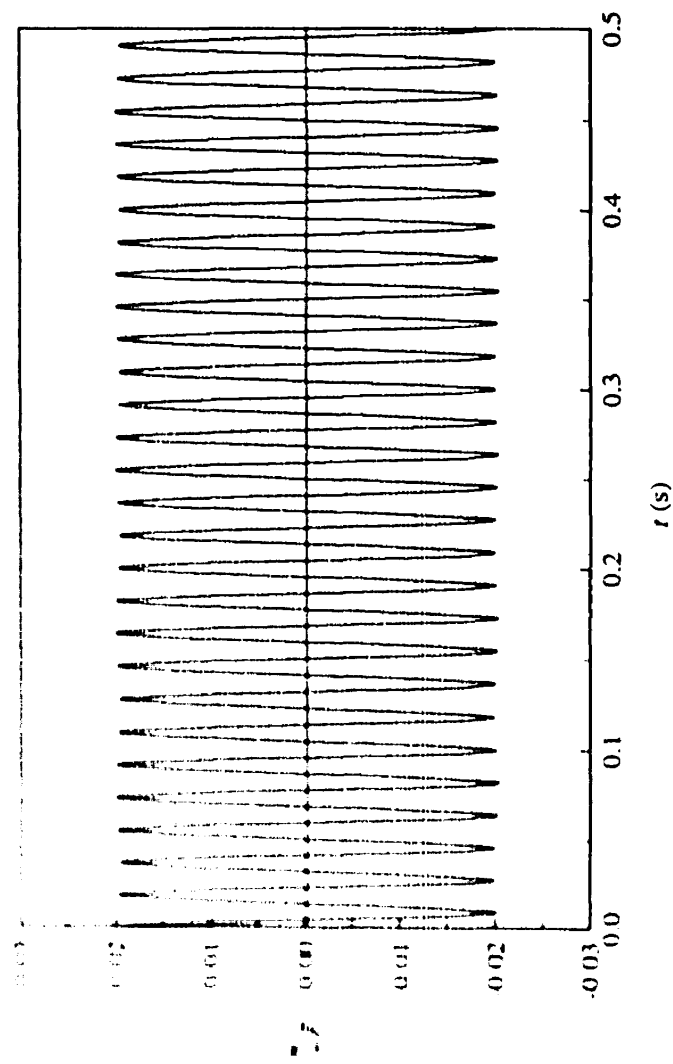


Figure 10.20: Free responses of rotationally dominant mode and transversely dominant mode for system 4 in the case of no internal resonance

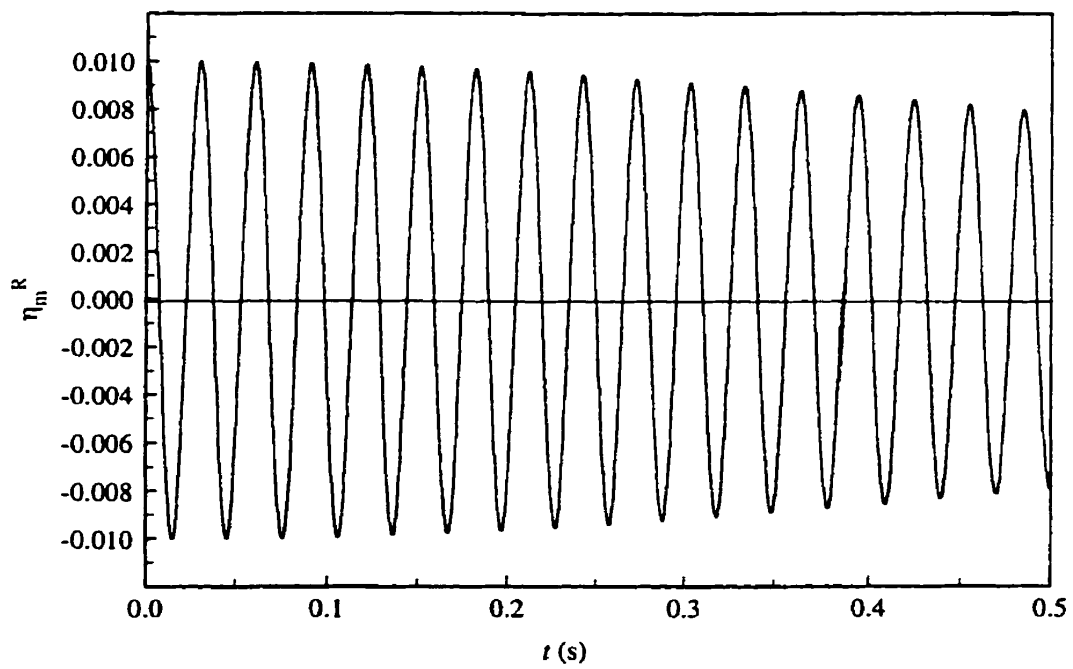
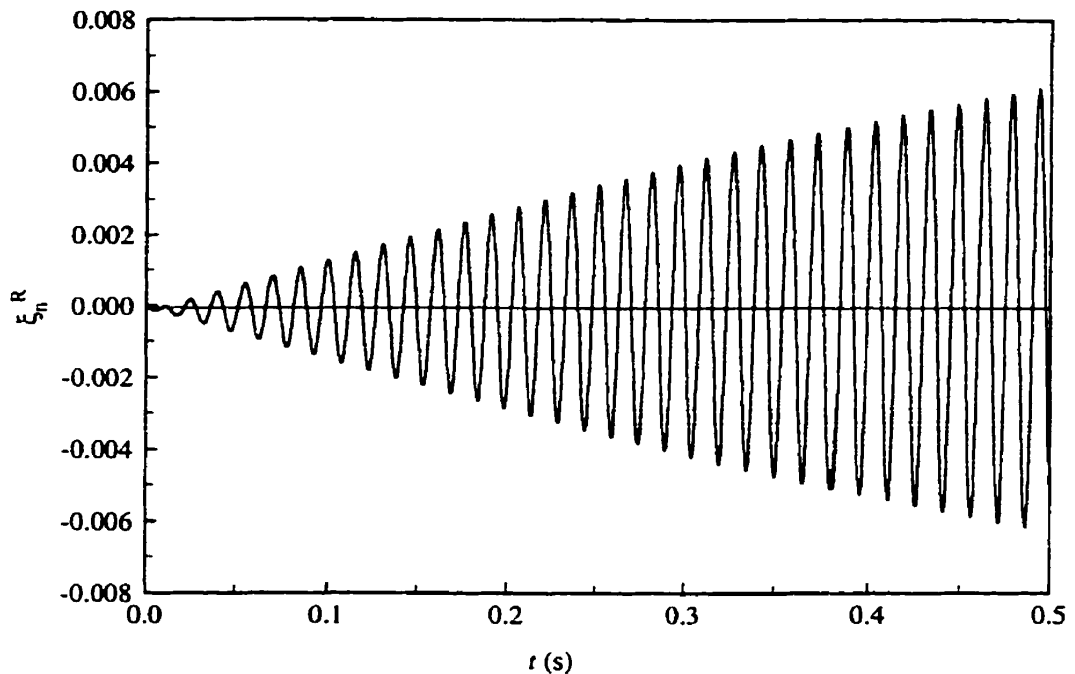


Figure 10.21: Free responses of rotationally dominant mode and transversely dominant mode for system 4 in the case of internal resonance

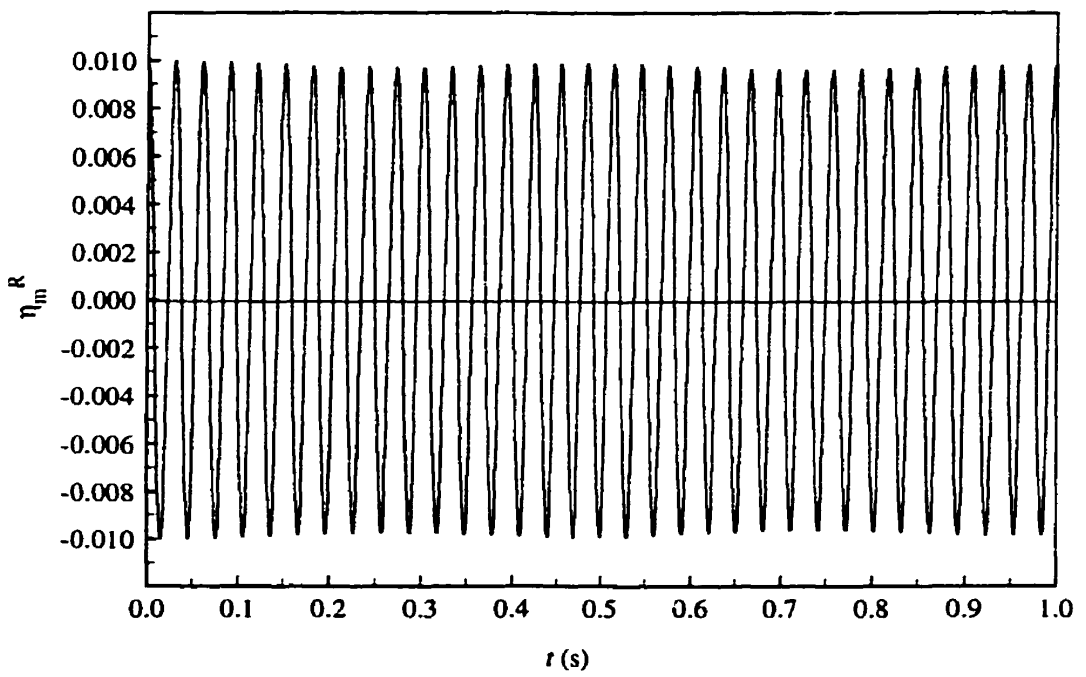
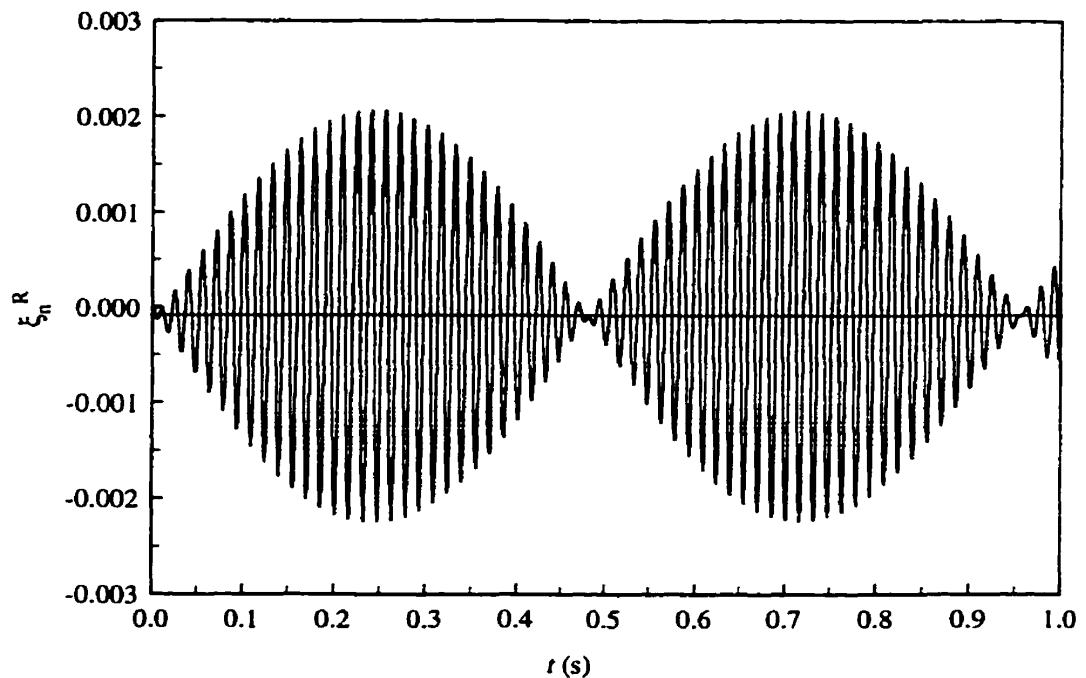


Figure 10.22: Free responses of rotationally dominant mode and transversely dominant mode for system 4 in the case of internal resonance (3.1% detuning)

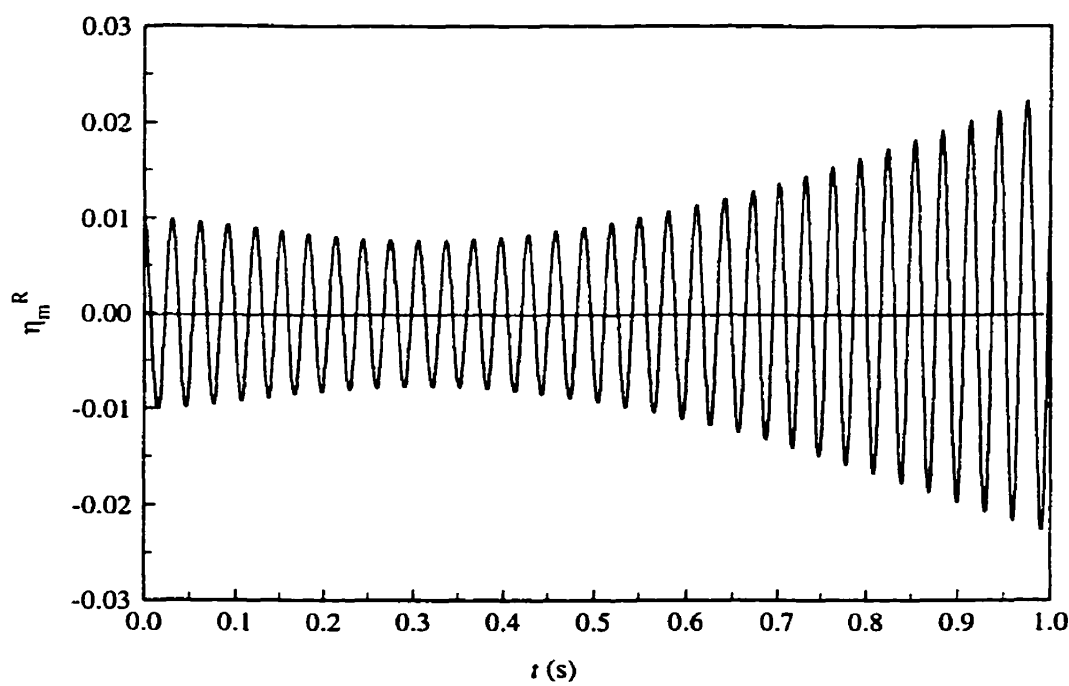
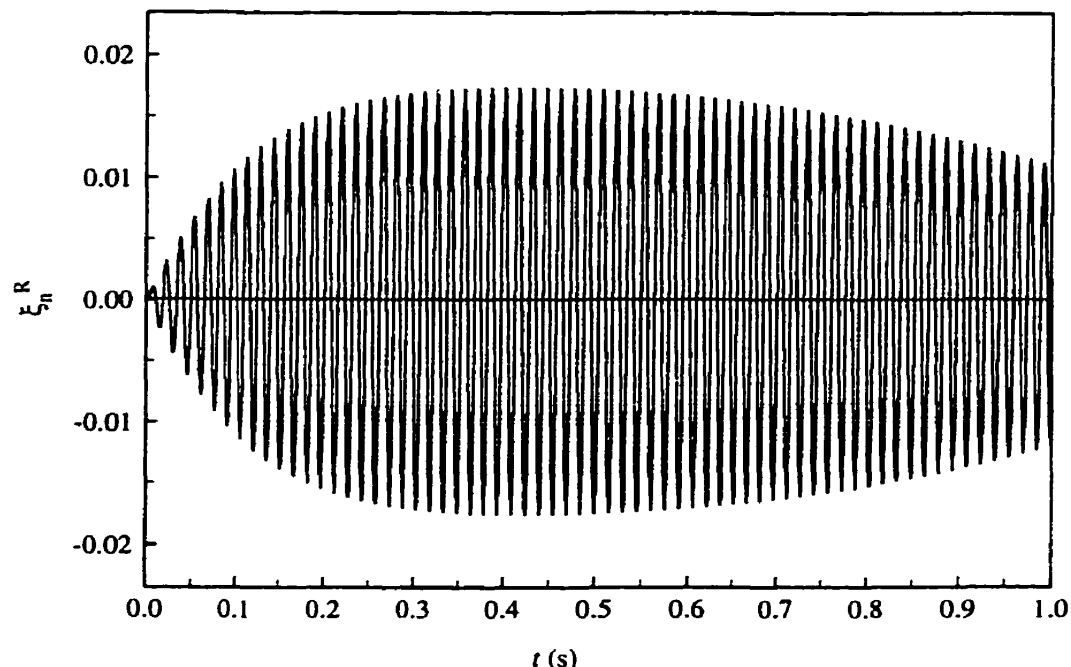


Figure 10.23: Forced, damped responses of rotationally dominant mode and transversely dominant mode ($\zeta_n = 1\%$, $\zeta_m = 0.1\%$) for system 4

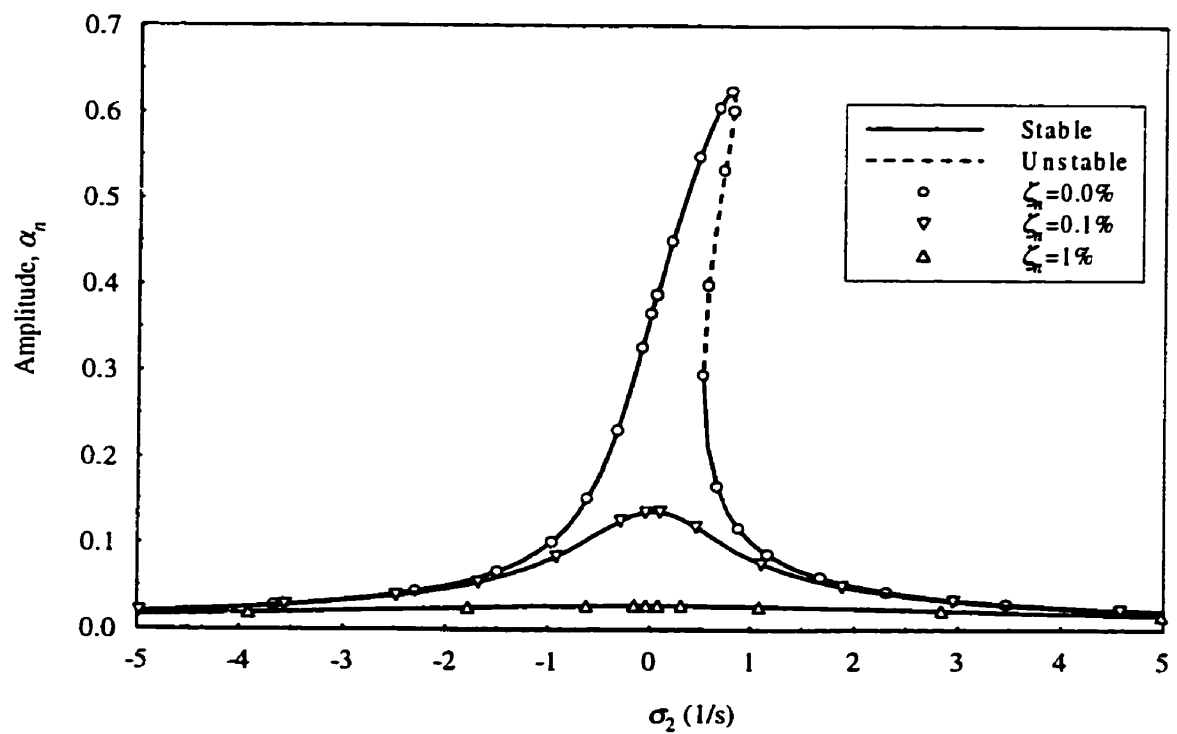


Figure 10.24: Response-frequency curves of system 5 for $\alpha_m=0.0$

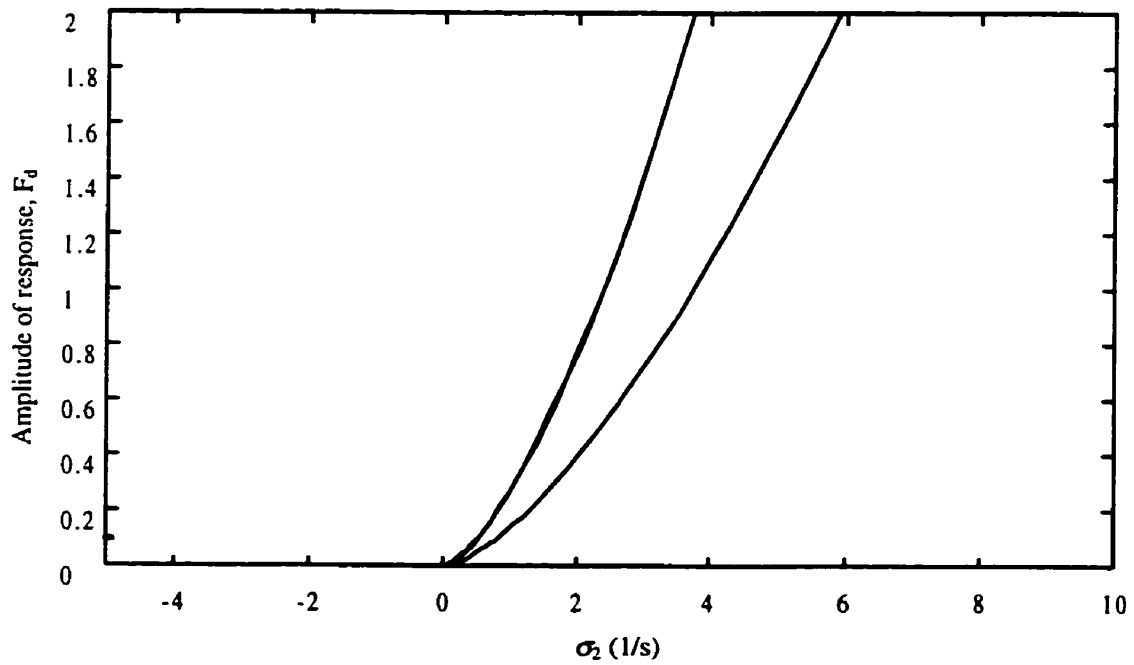


Figure 10.25: Multiple-valued region of system 5 for $\alpha_m=0.0$

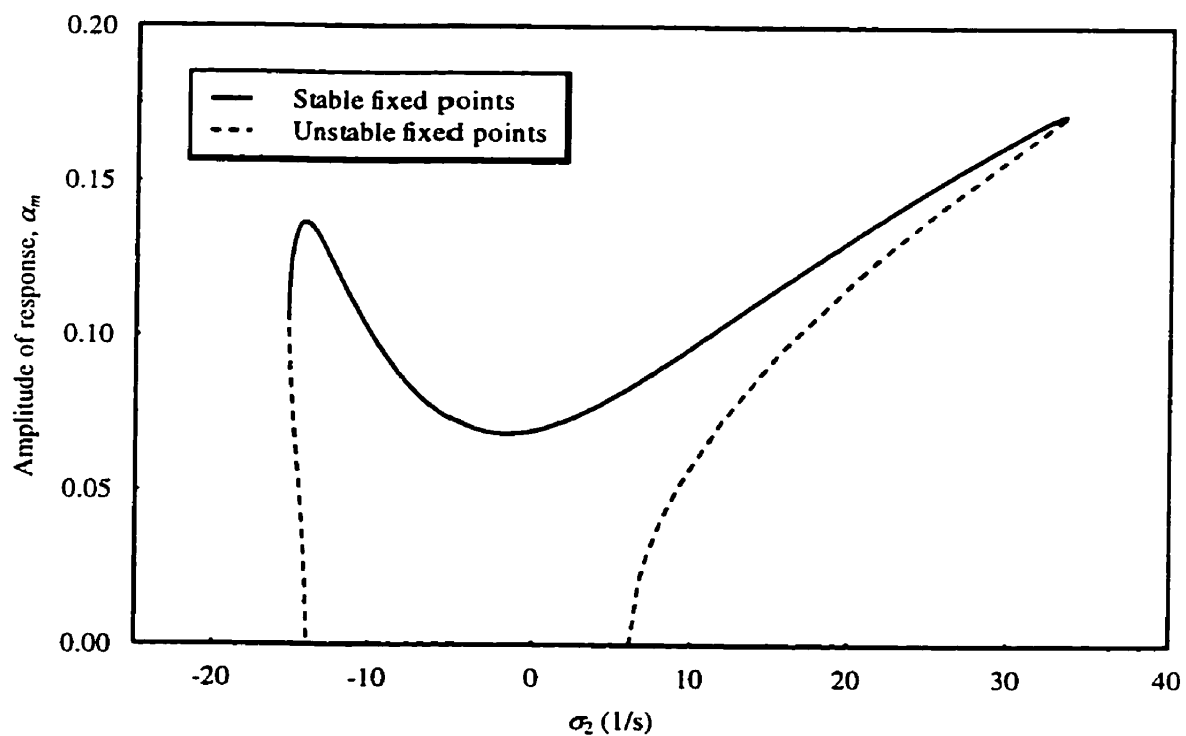
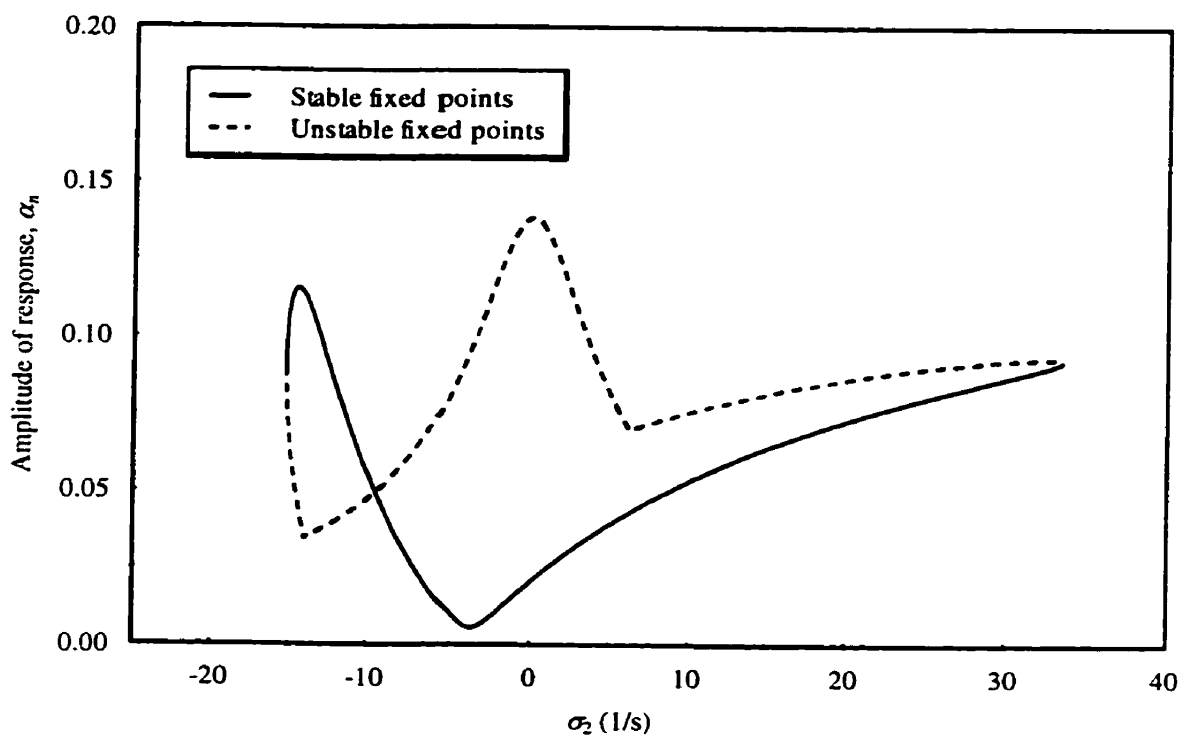


Figure 10.26: Response-frequency curves of system 5 for $\hat{\zeta}_n = 1\%$, $\hat{\zeta}_m = 0.3\%$

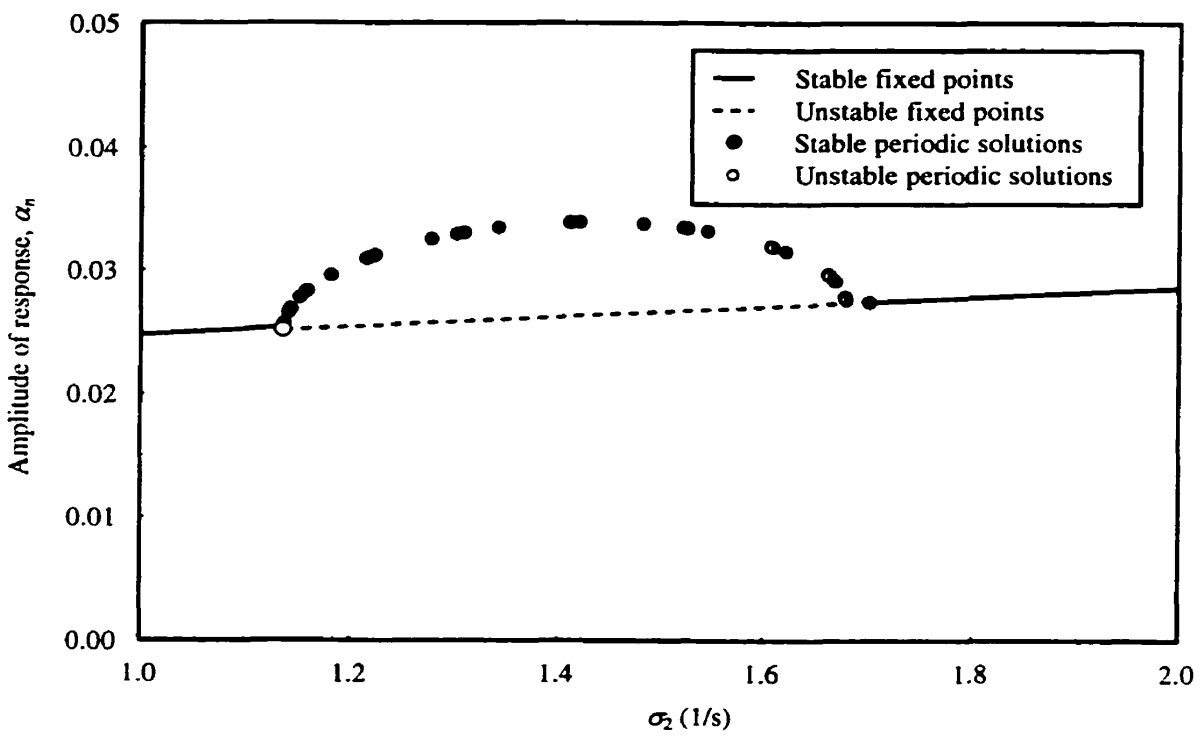


Figure 10.27: Periodic solutions of the amplitude α_n for system 5

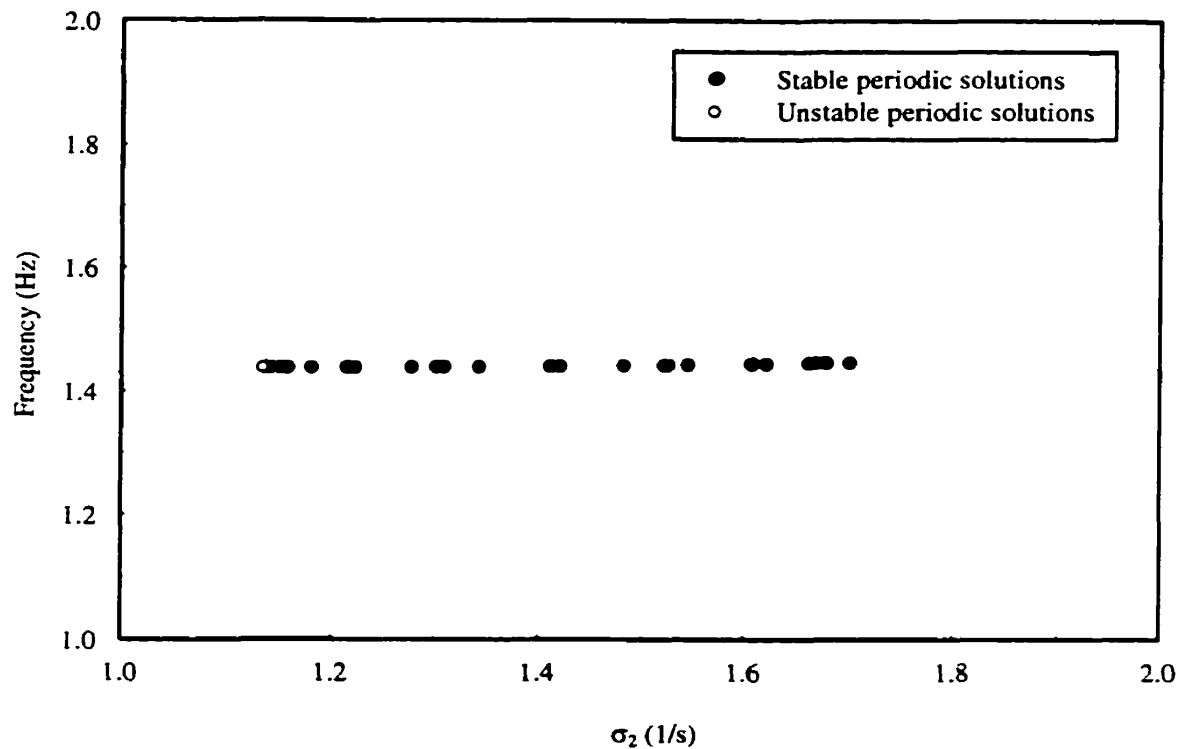


Figure 10.28: Relation between frequencies of periodic solutions and σ_2 for system 5

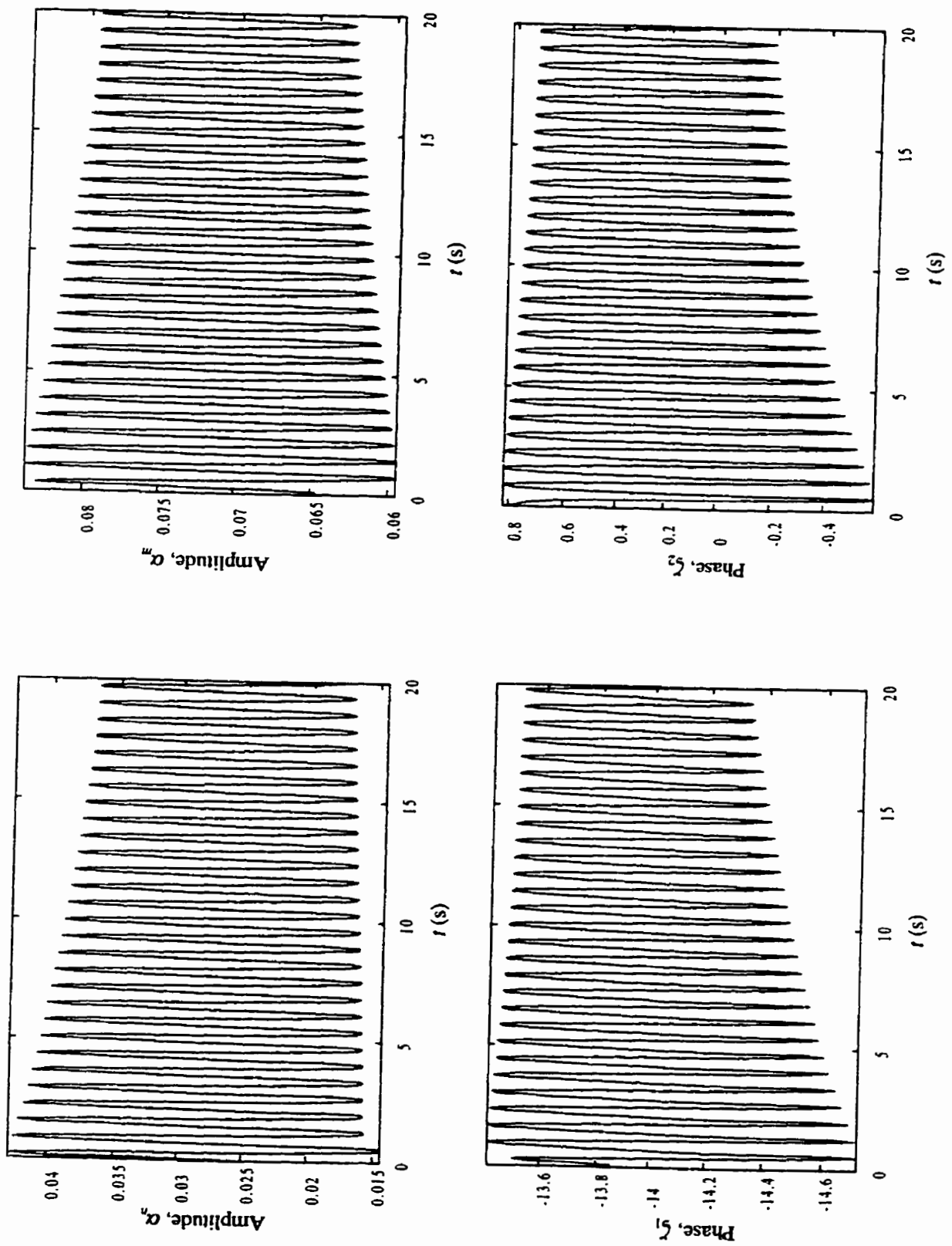


Figure 10.29: Periodic solutions of system 5

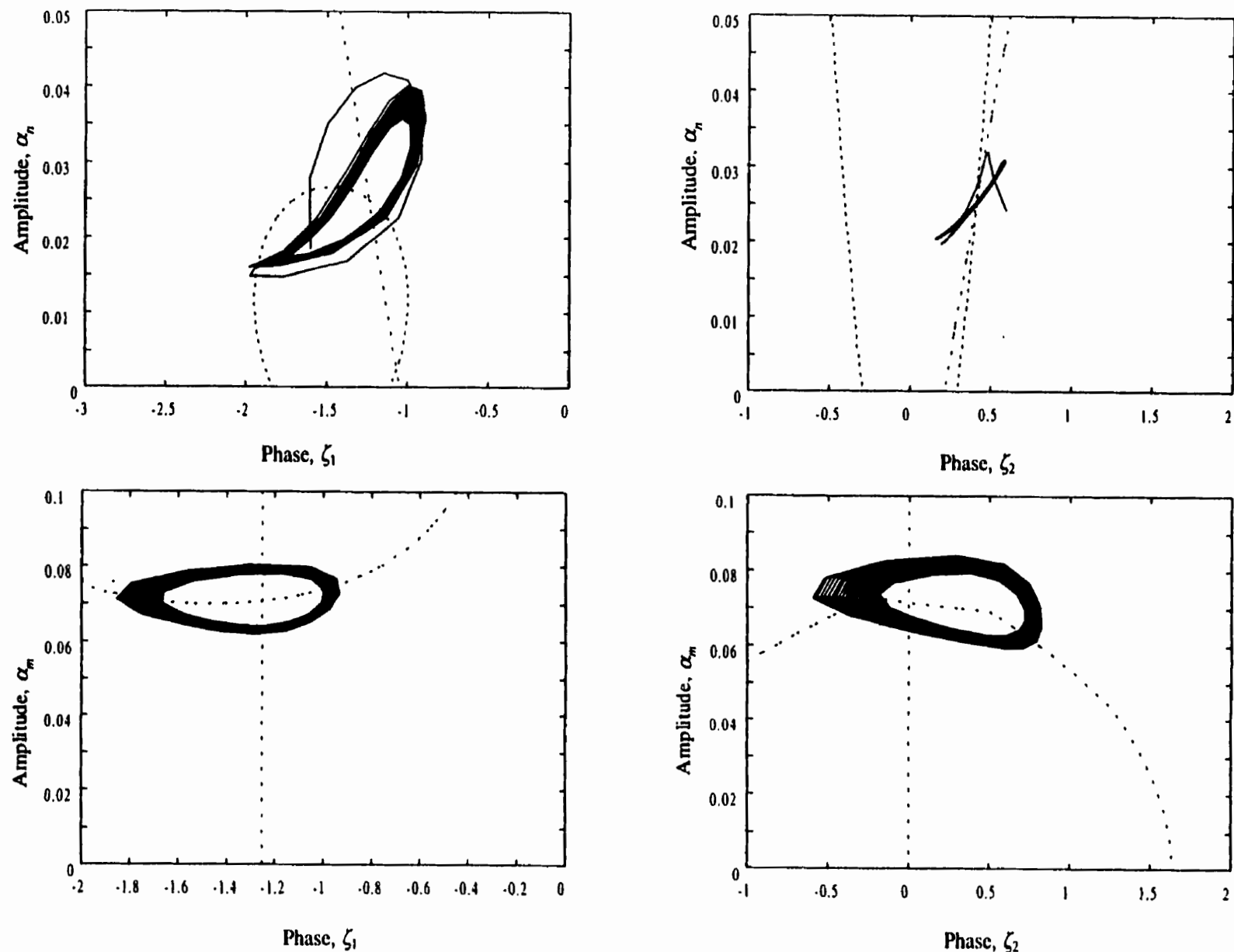


Figure 10.30: Phase plane curves of system 5 (dotted lines represent the nullclines)

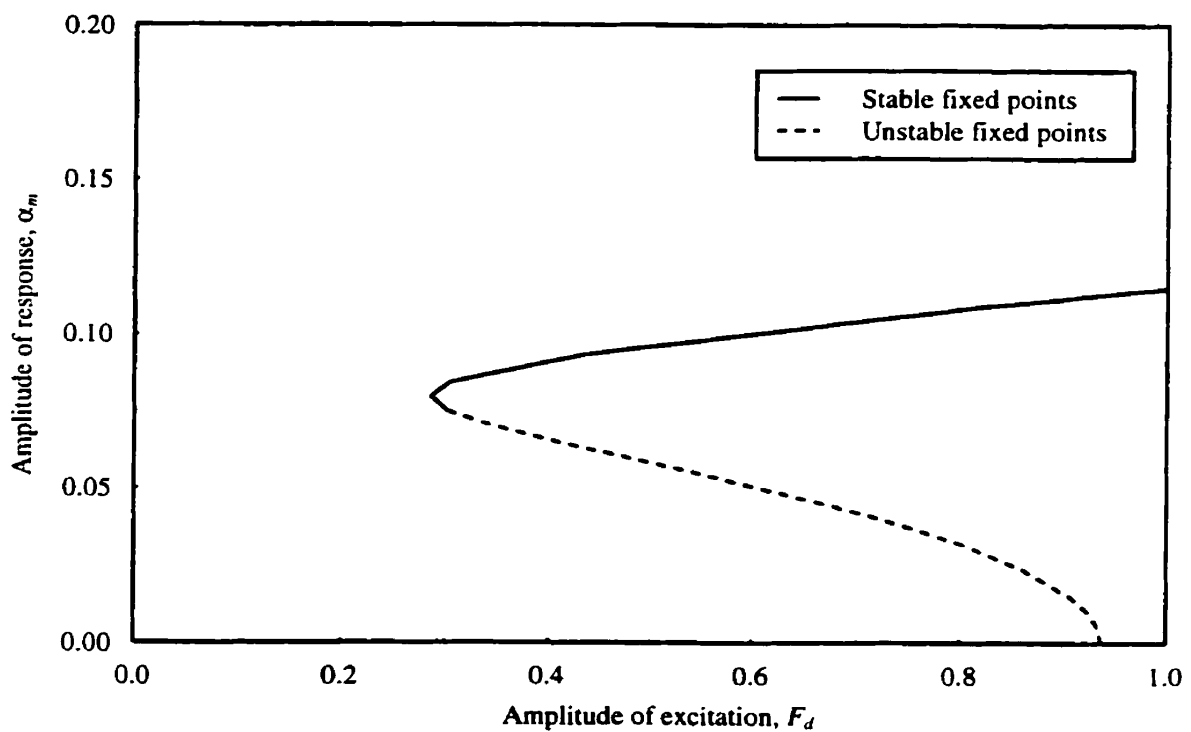
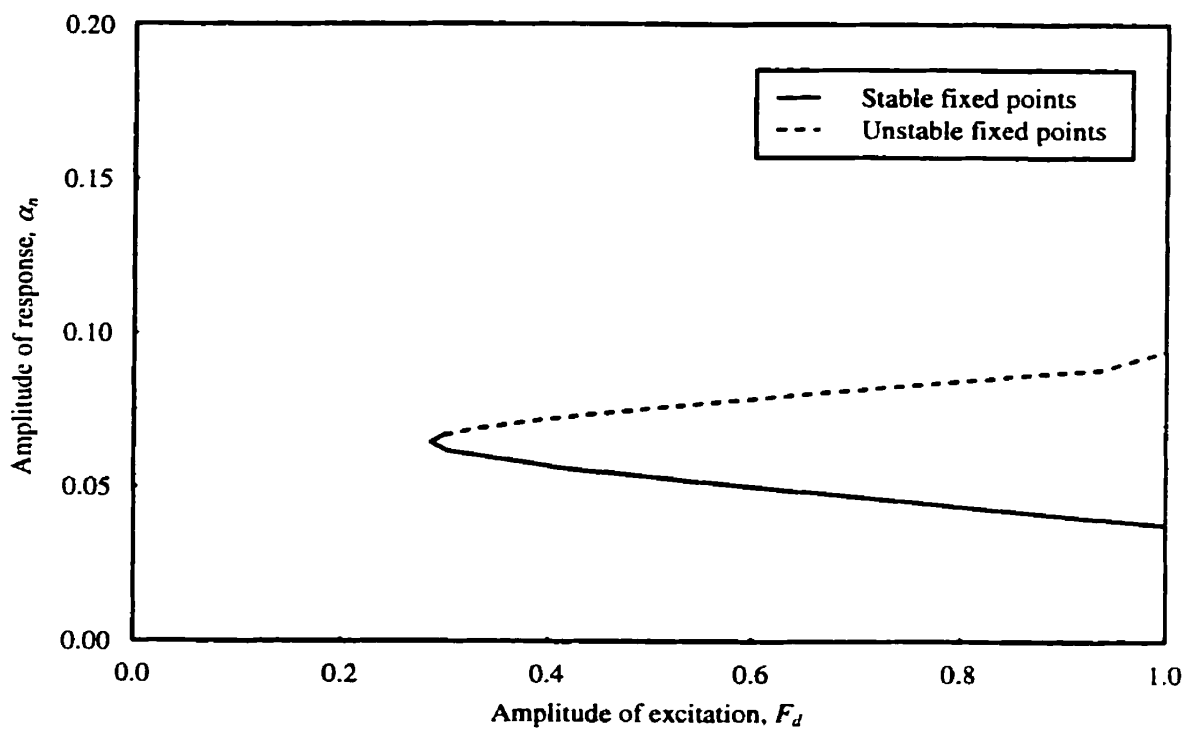


Figure 10.31: Response-excitation curves of system 5 for $\hat{\zeta}_n = 1\%$, $\hat{\zeta}_m = 0.3\%$
 $(\sigma_1=7.48379 \text{ 1/s and } \sigma_2=10.0 \text{ 1/s})$

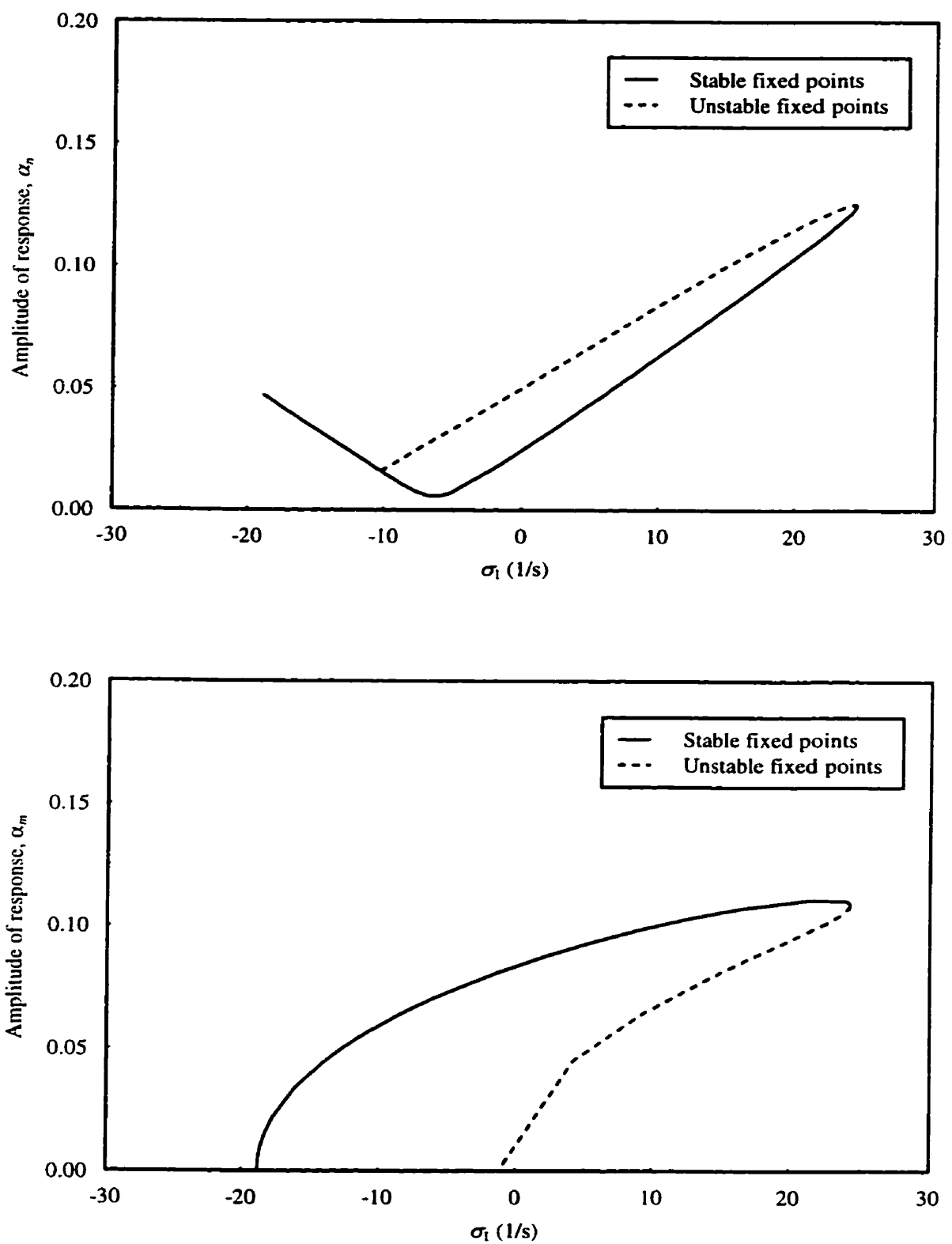


Figure 10.32: Relation between responses of system 5 and internal detuning parameter σ_1
 $(\sigma_2=10.0 \text{ } 1/\text{s} \text{ and } F_d=0.5)$

CHAPTER 11

NONLINEAR VIBRATION ANALYSIS OF ELASTIC SERPENTINE BELT DRIVE SYSTEMS: DIRECT MULTIPLE SCALES METHOD

In Chapter 10, the coupled nonlinear equations of motion of serpentine belt drive systems are solved using the discretization multiple scales method. By assuming the eigenfunctions of the linear problem to be the spatial solutions at all levels of approximations, the governing partial-differential equations and boundary conditions are reduced to ordinary-differential equations in time. The usual multiple scales is then applied to the ordinary-differential equations.

In the present chapter, the multiple scales method is applied directly to the original partial different equations. This direct treatment does not involve an *a priori* assumption regarding the spatial solutions. Nayfeh *et al.* (1992) were the first to show that direct perturbation methods yield better results for finite mode truncations and for systems having quadratic and cubic nonlinearities. Pakdemirli *et al.* (1995) compared the results of both direct perturbation method and discretization method for a nonlinear cable vibration problem. It is concluded from his study that the bifurcation and stability analysis might differ for both methods, with the direct perturbation method better representing the behavior of the real system.

In this study, it is also demonstrated that there exist discrepancies between the direct multiple scales method and the discretization multiple scales method for the nonlinear analysis of serpentine belt drive systems. The discretization multiple scales method might yield incomplete spatial distributions of the displacements. The cases of both one-to-one internal resonance and two-to-one internal resonance combined with a primary external resonance are investigated. The amplitude and phase modulation equations are obtained and the steady state responses are derived. Effects of excitation frequencies, excitation amplitudes and internal detuning parameter are investigated.

11.1 DIRECT MULTIPLE SCALES METHOD

A solution uniformly valid up to the third order for equations (10.1) and (10.4) is presented by assuming an expansion of the form

$$\mathbf{W} = \epsilon \mathbf{W}_1(T_0, T_1, T_2) + \epsilon^2 \mathbf{W}_2(T_0, T_1, T_2) + \epsilon^3 \mathbf{W}_3(T_0, T_1, T_2) + \dots \quad (11.1)$$

$$w_3 = \epsilon w_{31}(T_0, T_1, T_2) + \epsilon^2 w_{32}(T_0, T_1, T_2) + \epsilon^3 w_{33}(T_0, T_1, T_2) + \dots \quad (11.2)$$

where \mathbf{W}_i and w_{3i} are $O(1)$.

The external excitations F_{d1} , F_{d4} , damping coefficient C_3 of span 3, and damping matrix \mathbf{C} of system 2 are reordered so that their effects balance the effect of nonlinearity; that is

$$F_{d1} = \epsilon^3 \hat{F}_{d1} \quad F_{d4} = \epsilon^3 \hat{F}_{d4} \quad (11.3)$$

$$\mathbf{D} = \epsilon^2 \hat{\mathbf{D}} \quad D_3 = \epsilon^2 \hat{D}_3 \quad (11.4)$$

The time derivatives can be written in terms of the T_n as follows

$$\frac{\partial}{\partial t} = \frac{\partial}{\partial T_0} + \varepsilon \frac{\partial}{\partial T_1} + \varepsilon^2 \frac{\partial}{\partial T_2} + \dots \quad (11.5)$$

$$\frac{\partial^2}{\partial t^2} = \frac{\partial^2}{\partial T_0^2} + 2\varepsilon \frac{\partial^2}{\partial T_0 \partial T_1} + \varepsilon^2 \left(\frac{\partial^2}{\partial T_1^2} + 2 \frac{\partial^2}{\partial T_0 \partial T_2} \right) + \dots \quad (11.6)$$

11.1.1 Direct Approach

Substituting equations (11.1) – (11.6) into equations (10.1) and (10.4) and equating coefficient of like powers of ε yield

First order, subsystem 1

$$M_3 \frac{\partial^2 w_{31}}{\partial T_0^2} + G_3 \frac{\partial w_{31}}{\partial T_0} + K_3 w_{31} = 0 \quad (11.7)$$

$$w_{31}(0, t) = 0 \quad w_{31}(l_3, t) = 0 \quad (11.8)$$

First order, subsystem 2

$$M \frac{\partial^2 W_1}{\partial T_0^2} + G \frac{\partial W_1}{\partial T_0} + K W_1 = 0 \quad (11.9)$$

$$w_{11}(0, t) = 0 \quad w_{11}(l_1, t) = \chi_{31}(t) \sin \psi_1 \quad (11.10)$$

$$w_{21}(0, t) = \chi_{31}(t) \sin \psi_2 \quad w_{21}(l_2, t) = 0 \quad (11.11)$$

Second order, subsystems 1

$$M_3 \frac{\partial^2 w_{32}}{\partial T_0^2} + G_3 \frac{\partial w_{32}}{\partial T_0} + K_3 w_{32} = -2M_3 \frac{\partial^2 w_{31}}{\partial T_0 \partial T_1} - G_3 \frac{\partial w_{31}}{\partial T_1} + N_{23} \quad (11.12)$$

$$w_{32}(0, t) = 0 \quad w_{32}(l_3, t) = 0 \quad (11.13)$$

where

$$N_{Q3} = k_3(\chi_{11} - \chi_{41})w_{31,xx} \quad (11.14)$$

Second order, subsystems 2

$$\mathbf{M} \frac{\partial^2 \mathbf{W}_2}{\partial T_0^2} + \mathbf{G} \frac{\partial \mathbf{W}_2}{\partial T_0} + \mathbf{K} \mathbf{W}_2 = -2\mathbf{M} \frac{\partial^2 \mathbf{W}_1}{\partial T_0 \partial T_1} - \mathbf{G} \frac{\partial \mathbf{W}_1}{\partial T_1} + \mathbf{N}_Q \quad (11.15)$$

$$w_{12}(0,t) = 0 \quad w_{12}(l_1,t) = \chi_{32}(t) \sin \psi_1 \quad (11.16)$$

$$w_{22}(0,t) = \chi_{32}(t) \sin \psi_2 \quad w_{22}(l_2,t) = 0 \quad (11.17)$$

where

$$\mathbf{N}_Q = \left\{ \begin{array}{l} k_1(\chi_{31} \cos \psi_1 + \chi_{21} - \chi_{11})w_{11,xx} \\ k_2(\chi_{31} \cos \psi_2 + \chi_{41} - \chi_{21})w_{21,xx} \\ \frac{EA}{2l_1} \int_0^{l_1} w_{11,x}^2 dx - \frac{EA}{2l_3} \int_0^{l_3} w_{31,x}^2 dx \\ \frac{EA}{2l_2} \int_0^{l_2} w_{21,x}^2 dx - \frac{EA}{2l_1} \int_0^{l_1} w_{11,x}^2 dx \\ -\frac{EA}{2l_2} \int_0^{l_2} w_{21,x}^2 dx \cos \psi_2 - \frac{EA}{2l_1} \int_0^{l_1} w_{11,x}^2 dx \cos \psi_1 \\ \frac{EA}{2l_3} \int_0^{l_3} w_{31,x}^2 dx - \frac{EA}{2l_2} \int_0^{l_2} w_{21,x}^2 dx \end{array} \right\} \quad (11.18)$$

Third order, subsystem 1

$$\begin{aligned} M_3 \frac{\partial^2 w_{33}}{\partial T_0^2} + G_3 \frac{\partial w_{33}}{\partial T_0} + K_3 w_{33} &= -M_3 \left(2 \frac{\partial^2 w_{31}}{\partial T_0 \partial T_2} + \frac{\partial^2 w_{31}}{\partial T_1^2} + 2 \frac{\partial^2 w_{32}}{\partial T_0 \partial T_1} \right) \\ &\quad - G_3 \left(\frac{\partial w_{31}}{\partial T_2} + \frac{\partial w_{32}}{\partial T_1} \right) - \hat{D}_3 \frac{\partial w_{31}}{\partial T_0} + N_{C3} \end{aligned} \quad (11.19)$$

$$w_{33}(0,t) = 0 \quad w_{33}(l_3,t) = 0 \quad (11.20)$$

where

$$N_{C3} = k_3(\chi_{11} - \chi_{41})w_{32,xx} + k_3(\chi_{12} - \chi_{42})w_{31,xx} + \frac{EA}{2l_3} \int_0^{l_3} w_{31,x}^2 dx w_{31,xx} \quad (11.21)$$

Consider the case in which subsystem 2 is excited by a primary extremal resonance and subsystem 1 is excited indirectly by internal resonance. Hence, the solutions of equations (11.7)

11.1.2 The First Order Solutions and Nonlinear Terms of the Second Order Equations

$$\left\{ \begin{aligned}
 N^c = & \left[\begin{array}{l}
 \frac{EA}{l_3} \int_0^{l_2} w_{31,x} w_{32,x} dx - \frac{EA}{l_2} \int_0^{l_3} w_{21,x} w_{22,x} dx \\
 - \frac{EA}{l_2} \int_0^{l_3} w_{21,x} w_{22,x} dx \cos \psi_2 - \frac{EA}{l_1} \int_0^{l_2} w_{11,x} w_{12,x} dx \cos \psi_1 \\
 \frac{EA}{l_2} \int_0^{l_3} w_{21,x} w_{22,x} dx - \frac{EA}{l_1} \int_0^{l_2} w_{11,x} w_{12,x} dx \\
 \frac{EA}{l_1} \int_0^{l_2} w_{11,x} w_{12,x} dx - \frac{EA}{l_3} \int_0^{l_2} w_{31,x} w_{32,x} dx \\
 + \frac{2l_2}{EA} \int_0^{l_2} w_{21,x} dw_{21,x} \\
 k_2 (\chi_{31} \cos \psi_2 + \chi_{41} - \chi_{21}) w_{22,x} + k_2 (\chi_{32} \cos \psi_2 + \chi_{42} - \chi_{22}) w_{21,x} \\
 + \frac{2l_1}{EA} \int_0^{l_2} w_{11,x} dw_{11,x} \\
 k_1 (\chi_{31} \cos \psi_1 + \chi_{21} - \chi_{11}) w_{12,x} + k_1 (\chi_{32} \cos \psi_1 + \chi_{22} - \chi_{12}) w_{11,x}
 \end{array} \right] \\
 (11.26)
 \end{aligned} \right.$$

$$F^a = \begin{bmatrix} 0 & 0 & F_{d1} & 0 & 0 & F_{d2} \end{bmatrix} \quad (11.25)$$

where

$$w_{23}(0,t) = \chi_{33}(t) \sin \psi_2 \quad w_{23}(l_2,t) = 0 \quad (11.24)$$

$$w_{13}(0,t) = 0 \quad w_{13}(l_1,t) = \chi_{33}(t) \sin \psi_1 \quad (11.23)$$

$$\left\{ \begin{aligned}
 M \frac{\partial^2 W^3}{\partial T^2} + G \frac{\partial W^3}{\partial T^0} + KW^3 = -M \left(2 \frac{\partial T^0}{\partial W^1} \frac{\partial T^2}{\partial W^1} + \frac{\partial T^1}{\partial W^1} + 2 \frac{\partial T^0}{\partial W^2} \frac{\partial T^2}{\partial W^2} \right. \\
 \left. - G \left(\frac{\partial T^2}{\partial W^1} + \frac{\partial T^2}{\partial W^2} \right) - D \frac{\partial T^0}{\partial W^1} + F^a + N^c \right)
 \end{aligned} \right. \quad (11.22)$$

Third order, subsystem 2

and (11.9) are sought in the form

$$w_{31} = \varphi_m B_m(T_1, T_2) e^{i\lambda_m T_0} + cc \quad (11.27)$$

$$\mathbf{W}_1 = \phi_n A_n(T_1, T_2) e^{i\omega_n T_0} + cc \quad (11.28)$$

where *cc* stands for the complex conjugate of the preceding terms, λ_m and ω_n are the eigenvalues associated with subsystem 1 and subsystem 2, respectively, ϕ_n and φ_m are the corresponding eigenfunctions, and A_n and B_m are complex functions yet to be determined.

Substituting equations (11.27) and (11.28) into (11.14) and (11.18) with algebraic manipulation yields

$$N_{Q3} = \left(k_3 (\hat{\chi}_{1n} - \hat{\chi}_{4n}) \frac{\partial^2 \phi_m}{\partial x^2} A_n B_m e^{i(\omega_n + \lambda_m) T_0} + cc \right) + \left(k_3 (\hat{\chi}_{1n} - \hat{\chi}_{4n}) \frac{\partial^2 \bar{\phi}_m}{\partial x^2} A_n \bar{B}_m e^{i(\omega_n - \lambda_m) T_0} + cc \right) \quad (11.29)$$

$$\mathbf{N}_Q = (\mathbf{F}_{p1} A_n^2 e^{2i\omega_n T_0} + cc) + \mathbf{F}_{p2} A_n \bar{A}_n + (\mathbf{F}_{p3} B_m^2 e^{2i\lambda_m T_0} + cc) + \mathbf{F}_{p4} B_m \bar{B}_m \quad (11.30)$$

where

$$\mathbf{F}_{p1} = \left\{ \begin{array}{l} k_1 (\hat{\chi}_{3n} \cos \psi_1 + \hat{\chi}_{2n} - \hat{\chi}_1) \frac{\partial^2 \phi_{1n}}{\partial x^2} \\ k_2 (\hat{\chi}_{3n} \cos \psi_2 + \hat{\chi}_{4n} - \hat{\chi}_{2n}) \frac{\partial^2 \phi_{2n}}{\partial x^2} \\ \frac{EA}{2l_1} \int_0^{l_1} \left(\frac{\partial \phi_{1n}}{\partial x} \right)^2 dx \\ \frac{EA}{2l_2} \int_0^{l_2} \left(\frac{\partial \phi_{2n}}{\partial x} \right)^2 dx - \frac{EA}{2l_1} \int_0^{l_1} \left(\frac{\partial \phi_{1n}}{\partial x} \right)^2 dx \\ - \frac{EA}{2l_2} \int_0^{l_2} \left(\frac{\partial \phi_{2n}}{\partial x} \right)^2 dx \cos \psi_2 - \frac{EA}{2l_1} \int_0^{l_1} \left(\frac{\partial \phi_{1n}}{\partial x} \right)^2 dx \cos \psi_1 \\ - \frac{EA}{2l_2} \int_0^{l_2} \left(\frac{\partial \phi_{2n}}{\partial x} \right)^2 dx \end{array} \right\} \quad (11.31)$$

$$\mathbf{F}_{p2} = \left\{ \begin{array}{l} k_1 (\hat{\chi}_{3n} \cos \psi_1 + \hat{\chi}_{2n} - \hat{\chi}_{1n}) \left(\frac{\partial^2 \phi_{1n}}{\partial x^2} + \frac{\partial^2 \bar{\phi}_{1n}}{\partial x^2} \right) \\ k_2 (\hat{\chi}_{3n} \cos \psi_2 + \hat{\chi}_{4n} - \hat{\chi}_{2n}) \left(\frac{\partial^2 \phi_{2n}}{\partial x^2} + \frac{\partial^2 \bar{\phi}_{2n}}{\partial x^2} \right) \\ \frac{EA}{l_1} \int_0^{l_1} \frac{\partial \phi_{1n}}{\partial x} \frac{\partial \bar{\phi}_{1n}}{\partial x} dx \\ \frac{EA}{l_2} \int_0^{l_2} \frac{\partial \phi_{2n}}{\partial x} \frac{\partial \bar{\phi}_{2n}}{\partial x} dx - \frac{EA}{l_1} \int_0^{l_1} \frac{\partial \phi_{1n}}{\partial x} \frac{\partial \bar{\phi}_{1n}}{\partial x} dx \\ - \frac{EA}{l_2} \int_0^{l_2} \frac{\partial \phi_{2n}}{\partial x} \frac{\partial \bar{\phi}_{2n}}{\partial x} dx \cos \psi_2 - \frac{EA}{l_1} \int_0^{l_1} \frac{\partial \phi_{1n}}{\partial x} \frac{\partial \bar{\phi}_{1n}}{\partial x} dx \cos \psi_1 \\ - \frac{EA}{l_2} \int_0^{l_2} \frac{\partial \phi_{2n}}{\partial x} \frac{\partial \bar{\phi}_{2n}}{\partial x} dx \end{array} \right\} \quad (11.32)$$

$$\mathbf{F}_{p3} = \left\{ \begin{array}{l} 0 \\ 0 \\ - \frac{EA}{2l_3} \int_0^{l_3} \left(\frac{\partial \varphi_m}{\partial x} \right)^2 dx \\ 0 \\ 0 \\ \frac{EA}{2l_3} \int_0^{l_3} \left(\frac{\partial \varphi_m}{\partial x} \right)^2 dx \end{array} \right\} \quad \mathbf{F}_{p4} = \left\{ \begin{array}{l} 0 \\ 0 \\ - \frac{EA}{l_3} \int_0^{l_3} \frac{\partial \varphi_m}{\partial x} \frac{\partial \bar{\varphi}_m}{\partial x} dx \\ 0 \\ 0 \\ \frac{EA}{l_3} \int_0^{l_3} \frac{\partial \varphi_m}{\partial x} \frac{\partial \bar{\varphi}_m}{\partial x} dx \end{array} \right\} \quad (11.33)$$

11.2 ONE-TO-ONE INTERNAL RESONANCE

To quantitatively describe a primary external resonance and a one-to-one internal resonance, introducing two detuning parameters σ_1 and σ_2 defined by

$$\omega_n = \lambda_m + \varepsilon^2 \sigma_1 \quad (11.34)$$

$$\Omega = \omega_n + \varepsilon^2 \sigma_2 \quad (11.35)$$

where Ω is the frequency of external excitation.

11.2.1 Solvability Condition of the Second Order Equations

Substituting equations (11.34) and (11.35) into (11.29) and (11.30), it is noted that for one-to-one internal resonance, there is no secular terms arising from N_Q and N_{Q3} . Therefore, the solvability conditions for equations (11.12) and (11.15) are

$$\langle -(2i\omega_n M \phi_n + G \phi_n), \phi_n \rangle \frac{\partial A_n}{\partial T_1} = 0 \quad (11.36)$$

$$\langle -(2i\lambda_m M_3 \varphi_m + G_3 \varphi_m), \varphi_m \rangle \frac{\partial B_m}{\partial T_1} = 0 \quad (11.37)$$

Inserting the expressions of ϕ_n and φ_m from Chapter 8 into equations (11.36) and (11.37) results in

$$\frac{\partial A_n}{\partial T_1} = 0 \quad (11.38)$$

$$\frac{\partial B_m}{\partial T_1} = 0 \quad (11.39)$$

Therefore, $A_n = A_n(T_2)$ and $B_m = B_m(T_2)$ only. This shows that for one-to-one internal resonance, there is no $T_1 = \varepsilon t$ dependence. This conclusion is the same as that drawn from the discretization multiple scales method.

11.2.2 Spatial Distribution Functions Using Modal Expansions

In discretization multiple scales method, the spatial distribution functions of the second order solution is the same as that of the first order solutions. In direct multiple scales method, the spatial distributions are obtained by solving the corresponding boundary value problem.

After eliminating the secular terms, the solutions of equations (11.12) and (11.15) can be assumed of the form

$$\mathbf{W}_2 = (\gamma_1 A_n^2 e^{2i\omega_n T_0} + cc) + \gamma_2 A_n \bar{A}_n + (\gamma_3 B_m^2 e^{2i\lambda_m T_0} + cc) + \gamma_4 B_m \bar{B}_m \quad (11.40)$$

$$w_{32} = \gamma_{51}(x) A_n B_m e^{i(\omega_n + \lambda_m) T_0} + \gamma_{61}(x) A_n \bar{B}_m e^{i(\omega_n - \lambda_m) T_0} + cc \quad (11.41)$$

where

$$\gamma_1 = \begin{Bmatrix} \gamma_{11}(x) \\ \gamma_{12}(x) \\ \gamma_{13} \\ \gamma_{14} \\ \gamma_{15} \\ \gamma_{16} \end{Bmatrix}, \quad \gamma_2 = \begin{Bmatrix} \gamma_{21}(x) \\ \gamma_{22}(x) \\ \gamma_{23} \\ \gamma_{24} \\ \gamma_{25} \\ \gamma_{26} \end{Bmatrix}, \quad \gamma_3 = \begin{Bmatrix} \gamma_{31}(x) \\ \gamma_{32}(x) \\ \gamma_{33} \\ \gamma_{34} \\ \gamma_{35} \\ \gamma_{36} \end{Bmatrix}, \quad \gamma_4 = \begin{Bmatrix} \gamma_{41}(x) \\ \gamma_{42}(x) \\ \gamma_{43} \\ \gamma_{44} \\ \gamma_{45} \\ \gamma_{46} \end{Bmatrix} \quad (11.42)$$

and the γ_{ij} capture the spatial dependence of the motion. Substituting equations (11.40) and (11.41) into (11.12) and (11.15), the closed-form expressions for γ_{ij} can be obtained by using modal analysis method

$$\gamma_j = \sum_{k=1}^{\infty} \xi_{kj}^R \phi_k^R + \xi_{kj}^I \phi_k^I \quad (j = 1, 4) \quad (11.43)$$

$$\gamma_{51}(x) = \sum_{k=1}^{\infty} \eta_{k5}^R \varphi_k^R + \eta_{k5}^I \varphi_k^I \quad (11.44)$$

$$\gamma_{61}(x) = \sum_{k=1}^{\infty} \eta_{k6}^R \varphi_k^R + \eta_{k6}^I \varphi_k^I \quad (11.45)$$

where

$$\xi_{kl}^R = \frac{2i\omega_n q_{kl}^R + \omega_k q_{kl}^I}{\omega_k^2 - 4\omega_n^2} \quad (11.46)$$

$$\xi'_{k1} = \frac{2i\omega_n q'_{k1} - \omega_k q^R_{k1}}{\omega_k^2 - 4\omega_n^2} \quad (11.47)$$

$$\xi^R_{k2} = \frac{q'_{k2}}{\omega_k} \quad (11.48)$$

$$\xi'_k = -\frac{q^R_{k2}}{\omega_k} \quad (11.49)$$

$$\xi^R_{k3} = \frac{2i\lambda_m q^R_{k3} + \omega_k q'^R_{k3}}{\omega_k^2 - 4\lambda_m^2} \quad (11.50)$$

$$\xi'_k = \frac{2i\lambda_m q'_{k3} - \omega_k q^R_{k3}}{\omega_k^2 - 4\lambda_m^2} \quad (11.51)$$

$$\xi^R_{k4} = \frac{q'_{k4}}{\omega_k} \quad (11.52)$$

$$\xi'_k = 0 \quad (11.53)$$

$$\eta^R_{k5} = \frac{\lambda_k q'_{k5} + i(\omega_n + \lambda_m) q^R_{k5}}{\lambda_k^2 - (\omega_n + \lambda_m)^2} \quad (11.54)$$

$$\eta'_k = \frac{-\lambda_k q^R_{k6} + i(\omega_n + \lambda_m) q'^R_{k6}}{\lambda_k^2 - (\omega_n + \lambda_m)^2} \quad (11.55)$$

$$\eta^R_{k6} = \frac{\lambda_k q'_{k6} + i(\omega_n - \lambda_m) q^R_{k6}}{\lambda_k^2 - (\omega_n - \lambda_m)^2} \quad (11.56)$$

$$\eta'_k = \frac{-\lambda_k q^R_{k6} + i(\omega_n - \lambda_m) q'^R_{k6}}{\lambda_k^2 - (\omega_n - \lambda_m)^2} \quad (11.57)$$

$$q^R_{kj} = -\omega_k \int_0^{t_1} F_{pj}(1) \phi'_{kk} dx - \omega_k \int_0^{t_2} F_{pj}(2) \phi'_{2k} dx \quad (j=1,4) \quad (11.58)$$

$$q'_{kj} = \omega_k \int_0^{t_1} F_{pj}(1) \phi^R_{kk} dx + \omega_k \int_0^{t_2} F_{pj}(2) \phi^R_{2k} dx + \\ \omega_k \left(\hat{\chi}_{1k} F_{pj}(3) + \hat{\chi}_{2k} F_{pj}(4) + \hat{\chi}_{3k} F_{pj}(5) + \hat{\chi}_{4k} F_{pj}(6) \right) \quad (j=1,4) \quad (11.59)$$

$$q_{k5}^R = -\lambda_k \int_0^{l_3} \varphi_k' k_3 (\hat{\chi}_{1n} - \hat{\chi}_{4n}) \frac{\partial^2 \varphi_m}{\partial x^2} dx \quad (11.60)$$

$$q_{k5}' = \lambda_k \int_0^{l_3} \varphi_k^R k_3 (\hat{\chi}_{1n} - \hat{\chi}_{4n}) \frac{\partial^2 \varphi_m}{\partial x^2} dx \quad (11.61)$$

$$q_{k6}^R = -\lambda_k \int_0^{l_3} \varphi_k' k_3 (\hat{\chi}_{1n} - \hat{\chi}_{4n}) \frac{\partial^2 \bar{\varphi}_m}{\partial x^2} dx \quad (11.62)$$

$$q_{k6}' = \lambda_k \int_0^{l_3} \varphi_k^R k_3 (\hat{\chi}_{1n} - \hat{\chi}_{4n}) \frac{\partial^2 \bar{\varphi}_m}{\partial x^2} dx \quad (11.63)$$

11.2.3 Spatial Distribution Functions Using the Exact Method

An alternative approach to obtain the spatial variation γ_{ij} is to substitute equations (11.40) and (11.41) into (11.12) and (11.15) and separate variables. The resulting two-point boundary value problems can then be solved by the algorithms proposed in Chapter 8. Some of the closed-form solutions are shown in the follows:

Determination of $\{\gamma_{11}(x) \quad \gamma_{12}(x) \quad \gamma_{13} \quad \gamma_{14} \quad \gamma_{15} \quad \gamma_{16}\}^T$

$$\gamma_{11}(x) = e^{2i\omega_n x/c'_1} [a_{11} \sin(2\omega_n x/c'_1) + b_{11} \cos(2\omega_n x/c'_1)] + \hat{\gamma}_{11}(x) \quad (11.64)$$

$$\gamma_{12}(x) = e^{2i\omega_n x/c'_2} [a_{12} \sin(2\omega_n x/c'_2) + b_{12} \cos(2\omega_n x/c'_2)] + \hat{\gamma}_{12}(x) \quad (11.65)$$

$$(\mathbf{K}_{DD} - \mathbf{M}_{DD} (4\omega_n^2)) \begin{Bmatrix} \gamma_{13} \\ \gamma_{14} \\ \gamma_{15} \\ \gamma_{16} \end{Bmatrix} = \begin{Bmatrix} F_{p1}(3) \\ F_{p1}(4) \\ F_{p1}(5) + f_{17} \sin \psi_1 - f_{18} \sin \psi_2 \\ F_{p1}(6) \end{Bmatrix} \quad (11.66)$$

where

$$\hat{\gamma}_{11}(x) = c_{11} e^{i\omega_n ((x-l_1)/c'_1 + x/c'_1)} + d_{11} e^{i\omega_n ((x-l_1)/c'_1 - x/c'_1)} \quad (11.67)$$

$$\hat{\gamma}_{12}(x) = c_{12} e^{i\omega_n(x/c'_b + (l_2-x)/c'_2)} + d_{12} e^{i\omega_n(x/c'_b - (l_2-x)/c'_2)} \quad (11.68)$$

$$a_{11} = \frac{[\gamma_{15} \sin \psi_1 - \hat{\gamma}_{11}(l_1)] e^{-2i\omega_n l_1 / c'_1} + \hat{\gamma}_{11}(0) \cos(2\omega_n l_1 / c'_1)}{\sin(2\omega_n l_1 / c'_1)} \quad (11.69)$$

$$b_{11} = -\hat{\gamma}_{11}(0) \quad (11.70)$$

$$a_{12} = -\gamma_{15} \sin \psi_2 \cot(2\omega_n l_2 / c'_2) + \cot(2\omega_n l_2 / c'_2) \hat{\gamma}_{12}(0) - \frac{e^{-2i\omega_n l_2 / c'_2} \hat{\gamma}_{12}(l_2)}{\sin(2\omega_n l_2 / c'_2)} \quad (11.71)$$

$$b_{12} = \gamma_{15} \sin \psi_2 - \hat{\gamma}_{12}(0) \quad (11.72)$$

$$c_{11} = -\frac{k_1 (\hat{\chi}_{3n} \cos \psi_1 + \hat{\chi}_{2n} - \hat{\chi}_{1n}) \hat{a}_{1n} h_{11}^2}{2i(P_{11} h_{11}^2 - 4mch_{11} - 4m)} \quad (11.73)$$

$$d_{11} = \frac{k_1 (\hat{\chi}_{3n} \cos \psi_1 + \hat{\chi}_{2n} - \hat{\chi}_{1n}) \hat{a}_{1n} h_{12}^2}{2i(P_{11} h_{12}^2 - 4mch_{12} - 4m)} \quad (11.74)$$

$$c_{12} = -\frac{k_2 (\hat{\chi}_{3n} \cos \psi_2 + \hat{\chi}_{4n} - \hat{\chi}_{2n}) \hat{a}_{2n} h_{22}^2}{2i(P_{12} h_{22}^2 - 4mch_{22} - 4m)} \quad (11.75)$$

$$d_{12} = \frac{k_2 (\hat{\chi}_{3n} \cos \psi_2 + \hat{\chi}_{4n} - \hat{\chi}_{2n}) \hat{a}_{2n} h_{21}^2}{2i(P_{12} h_{21}^2 - 4mch_{21} - 4m)} \quad (11.76)$$

$$\mathbf{K}_{DD} = \begin{bmatrix} k_1 + k_3 & -k_1 & -k_1 \cos \psi_1 & -k_3 \\ -k_1 & k_1 + k_2 & k_1 \cos \psi_1 - k_2 \cos \psi_2 & -k_2 \\ -k_1 \cos \psi_1 & k_1 \cos \psi_1 - k_2 \cos \psi_2 & k_{33} & k_2 \cos \psi_2 \\ -k_3 & -k_2 & k_2 \cos \psi_2 & k_2 + k_3 \end{bmatrix} \quad (11.77)$$

$$k_{33} = k_1 \cos^2 \psi_1 + k_2 \cos^2 \psi_2 + k_4 + P_{11} \sin^2 \psi_1 \cot\left(\frac{2\omega_n l_1}{c'_1}\right) \frac{2\omega_n}{c'_1} + P_{12} \sin^2 \psi_2 \cot\left(\frac{2\omega_n l_2}{c'_2}\right) \frac{2\omega_n}{c'_2} \quad (11.78)$$

$$\mathbf{M}_{DD} = \begin{bmatrix} m_1 & 0 & 0 & 0 \\ 0 & m_2 & 0 & 0 \\ 0 & 0 & m_3 & 0 \\ 0 & 0 & 0 & m_4 \end{bmatrix} \quad (11.79)$$

$$f_{17} = -\frac{2\omega_n P_{i1} e^{2i\omega_n l_1/c'_1} \hat{\gamma}_{11}(0)}{c'_1 \sin(2\omega_n l_1/c'_1)} + \left(2i\omega_n m c + P_{i1} \cot\left(\frac{2\omega_n l_1}{c'_1}\right) \frac{2\omega_n}{c'_1} \right) \hat{\gamma}_{11}(l_1) - P_{i1} \hat{\gamma}'_{11}(l_1) \quad (11.80)$$

$$f_{18} = \frac{2\omega_n P_{i2} e^{-2i\omega_n l_2/c'_2} \hat{\gamma}_{12}(0)}{c'_2 \sin(2\omega_n l_2/c'_2)} + \left(2i\omega_n m c - P_{i2} \cot\left(\frac{2\omega_n l_2}{c'_2}\right) \frac{2\omega_n}{c'_2} \right) \hat{\gamma}_{12}(0) - P_{i2} \hat{\gamma}'_{12}(0) \quad (11.81)$$

Determination of $\{\gamma_{31}(x) \ \ \gamma_{32}(x) \ \ \gamma_{33} \ \ \gamma_{34} \ \ \gamma_{35} \ \ \gamma_{36}\}^T$

$$\gamma_{31}(x) = e^{2i\lambda_m x/c'_3} [a_{31} \sin(2\lambda_m x/c'_1) + b_{31} \cos(2\lambda_m x/c'_1)] \quad (11.82)$$

$$\gamma_{32}(x) = e^{2i\lambda_m x/c'_3} [a_{32} \sin(2\lambda_m x/c'_2) + b_{32} \cos(2\lambda_m x/c'_2)] \quad (11.83)$$

$$(\mathbf{K}_{DD} - \mathbf{M}_{DD} (4\lambda_m^2)) \begin{bmatrix} \gamma_{33} \\ \gamma_{34} \\ \gamma_{35} \\ \gamma_{36} \end{bmatrix} = \begin{bmatrix} F_{\rho_3}(3) \\ 0 \\ 0 \\ F_{\rho_3}(6) \end{bmatrix} \quad (11.84)$$

where

$$a_{31} = \frac{\gamma_{35} \sin \psi_1 e^{-2i\lambda_m l_1/c'_3}}{\sin(2\lambda_m l_1/c'_1)} \quad (11.85)$$

$$b_{31} = 0 \quad (11.86)$$

$$a_{32} = -\gamma_{35} \sin \psi_2 \cot(2\lambda_m l_2/c'_2) \quad (11.87)$$

$$b_{32} = \gamma_{35} \sin \psi_2 \quad (11.88)$$

$$k_{33} = k_1 \cos^2 \psi_1 + k_2 \cos^2 \psi_2 + k_3 + P_{i1} \sin^2 \psi_1 \cot\left(\frac{2\lambda_m l_1}{c'_1}\right) \frac{2\lambda_m}{c'_1} + P_{i2} \sin^2 \psi_2 \cot\left(\frac{2\lambda_m l_2}{c'_2}\right) \frac{2\lambda_m}{c'_2} \quad (11.89)$$

Determination of $\gamma_{51}(x)$

$$\gamma_{51}(x) = e^{i(\omega_n + \lambda_m)x/c'_c} [a_{51} \sin((\omega_n + \lambda_m)x/c'_3) + b_{51} \cos((\omega_n + \lambda_m)x/c'_3)] + \hat{\gamma}_{51}(x) \quad (11.90)$$

where

$$\hat{\gamma}_{51}(x) = c_{51} e^{i\lambda_m((x-l_3)/c'_c + x/c'_3)} + d_{51} e^{i\lambda_m((x-l_3)/c'_c - x/c'_3)} \quad (11.91)$$

$$a_{51} = \frac{-\hat{\gamma}_{51}(l_3) e^{-i(\omega_n + \lambda_m)l_3/c'_c} + \hat{\gamma}_{51}(0) \cos((\omega_n + \lambda_m)l_3/c'_3)}{\sin((\omega_n + \lambda_m)l_3/c'_3)} \quad (11.92)$$

$$b_{51} = -\hat{\gamma}_{51}(0) \quad (11.93)$$

$$c_{51} = -\frac{k_3(\hat{\chi}_{1n} - \hat{\chi}_{4n})\hat{a}_m\lambda_m^2 h_{31}^2}{2i(-m(\omega_n + \lambda_m)^2 - 2mc\lambda_m(\omega_n + \lambda_m)h_{31} + P_{t1}\lambda_m^2 h_{31}^2)} \quad (11.94)$$

$$d_{51} = \frac{k_3(\hat{\chi}_{1n} - \hat{\chi}_{4n})\hat{a}_m\lambda_m^2 h_{32}^2}{2i(-m(\omega_n + \lambda_m)^2 - 2mc\lambda_m(\omega_n + \lambda_m)h_{32} + P_{t1}\lambda_m^2 h_{32}^2)} \quad (11.95)$$

Determination of $\gamma_{61}(x)$

$$\gamma_{61}(x) = e^{i(\omega_n - \lambda_m)x/c'_c} [a_{61} \sin((\omega_n - \lambda_m)x/c'_3) + b_{61} \cos((\omega_n - \lambda_m)x/c'_3)] + \hat{\gamma}_{61}(x) \quad (11.96)$$

where

$$\hat{\gamma}_{61}(x) = c_{61} e^{-i\lambda_m((x-l_3)/c'_c + x/c'_3)} + d_{61} e^{-i\lambda_m((x-l_3)/c'_c - x/c'_3)} \quad (11.97)$$

$$a_{61} = \frac{-\hat{\gamma}_{61}(l_3) e^{-i(\omega_n - \lambda_m)l_3/c'_c} + \hat{\gamma}_{61}(0) \cos((\omega_n - \lambda_m)l_3/c'_3)}{\sin((\omega_n - \lambda_m)l_3/c'_3)} \quad (11.98)$$

$$b_{61} = -\hat{\gamma}_{61}(0) \quad (11.99)$$

$$c_{61} = \frac{k_3(\hat{\chi}_{1n} - \hat{\chi}_{4n})\hat{a}_m\lambda_m^2 h_{31}^2}{2i(-m(\omega_n - \lambda_m)^2 + 2mc\lambda_m(\omega_n - \lambda_m)h_{31} + P_{t3}\lambda_m^2 h_{31}^2)} \quad (11.100)$$

$$d_{61} = -\frac{k_3(\hat{\chi}_{1n} - \hat{\chi}_{4n})\hat{a}_m\lambda_m^2 h_{32}^2}{2i(-m(\omega_n - \lambda_m)^2 + 2mc\lambda_m(\omega_n - \lambda_m)h_{32} + P_{t3}\lambda_m^2 h_{32}^2)} \quad (11.101)$$

From equations (11.40) and (11.41), it is noted that the spatial variations of the second order solution include eigenfunctions of all linear modes while the spatial variations of the arbitrary

order solution in discretization multiple scales involve only eigenfunctions of resonance modes. Hence, the spatial variations in discretization multiple scales are incomplete. This would lead to the discrepancy of the modulation equations governing the first order amplitudes and phases of the motion, which are determined from the third order equations. Therefore, the two approaches predict qualitatively different motions for serpentine belt drive systems.

11.2.4 Solvability Condition of the Third Order Equations

Substituting equations (11.27), (11.28), (11.40) and (11.41) into (11.21) and (11.26) leads to

$$\mathbf{N}_C = \left\{ \begin{pmatrix} \Gamma_{11} \\ \Gamma_{12} \\ \Gamma_{13} \\ \Gamma_{14} \\ \Gamma_{15} \\ \Gamma_{16} \end{pmatrix} A_n^2 \bar{A}_n + \begin{pmatrix} \Gamma_{21} \\ \Gamma_{22} \\ \Gamma_{23} \\ \Gamma_{24} \\ \Gamma_{25} \\ \Gamma_{26} \end{pmatrix} A_n B_m \bar{B}_m + \begin{pmatrix} \Gamma_{31} \\ \Gamma_{32} \\ \Gamma_{33} \\ \Gamma_{34} \\ \Gamma_{35} \\ \Gamma_{36} \end{pmatrix} \bar{A}_n B_m^2 e^{-2i\sigma_1 T_2} \right\} e^{i\omega_n T_0} + \mathbf{NST} \quad (11.102)$$

$$N_{C3} = (\Gamma_{41} A_n^2 \bar{B}_m e^{2i\sigma_1 T_2} + \Gamma_{51} A_n \bar{A}_n B_m + \Gamma_{61} B_m^2 \bar{B}_m) e^{i\lambda_n T_0} + NST3 \quad (11.103)$$

where **NST** and **NST3** denote non-secular terms and

$$\begin{aligned} \Gamma_{11} &= k_1 (\hat{\chi}_{3n} \cos \psi_1 + \hat{\chi}_{2n} - \hat{\chi}_{1n}) \left(\frac{\partial^2 \gamma_{21}}{\partial x^2} + \frac{\partial^2 \gamma_{11}}{\partial x^2} \right) + k_1 (\gamma_{15} \cos \psi_1 + \gamma_{14} - \gamma_{13}) \frac{\partial^2 \bar{\phi}_{1n}}{\partial x^2} + \\ &\quad k_1 (\gamma_{25} \cos \psi_1 + \gamma_{24} - \gamma_{23}) \frac{\partial^2 \phi_{1n}}{\partial x^2} + \frac{EA}{2l_1} \left[\int_0^{l_1} \left(\frac{\partial \phi_{1n}}{\partial x} \right)^2 dx \frac{\partial^2 \bar{\phi}_{1n}}{\partial x^2} + \int_0^{l_1} 2 \frac{\partial \phi_{1n}}{\partial x} \frac{\partial \bar{\phi}_{1n}}{\partial x} dx \frac{\partial^2 \phi_{1n}}{\partial x^2} \right] \end{aligned} \quad (11.104)$$

$$\begin{aligned} \Gamma_{12} &= k_2 (\hat{\chi}_{3n} \cos \psi_2 + \hat{\chi}_{4n} - \hat{\chi}_{2n}) \left(\frac{\partial^2 \gamma_{22}}{\partial x^2} + \frac{\partial^2 \gamma_{12}}{\partial x^2} \right) + k_2 (\gamma_{15} \cos \psi_2 + \gamma_{16} - \gamma_{14}) \frac{\partial^2 \bar{\phi}_{2n}}{\partial x^2} + \\ &\quad k_2 (\gamma_{25} \cos \psi_2 + \gamma_{26} - \gamma_{24}) \frac{\partial^2 \phi_{2n}}{\partial x^2} + \frac{EA}{2l_2} \left[\int_0^{l_2} \left(\frac{\partial \phi_{2n}}{\partial x} \right)^2 dx \frac{\partial^2 \bar{\phi}_{2n}}{\partial x^2} + \int_0^{l_2} 2 \frac{\partial \phi_{2n}}{\partial x} \frac{\partial \bar{\phi}_{2n}}{\partial x} dx \frac{\partial^2 \phi_{2n}}{\partial x^2} \right] \end{aligned} \quad (11.105)$$

$$\Gamma_{13} = \frac{EA}{l_1} \int_0^{l_1} \left(\frac{\partial \phi_{1n}}{\partial x} \frac{\partial \gamma_{21}}{\partial x} + \frac{\partial \bar{\phi}_{1n}}{\partial x} \frac{\partial \gamma_{11}}{\partial x} \right) dx \quad (11.106)$$

$$\Gamma_{14} = \frac{EA}{l_2} \int_0^{l_2} \left(\frac{\partial \phi_{2n}}{\partial x} \frac{\partial \gamma_{22}}{\partial x} + \frac{\partial \bar{\phi}_{2n}}{\partial x} \frac{\partial \gamma_{12}}{\partial x} \right) dx - \frac{EA}{l_1} \int_0^{l_1} \left(\frac{\partial \phi_{1n}}{\partial x} \frac{\partial \gamma_{21}}{\partial x} + \frac{\partial \bar{\phi}_{1n}}{\partial x} \frac{\partial \gamma_{11}}{\partial x} \right) dx \quad (11.107)$$

$$\Gamma_{15} = -\frac{EA}{l_2} \int_0^{l_2} \left(\frac{\partial \phi_{2n}}{\partial x} \frac{\partial \gamma_{22}}{\partial x} + \frac{\partial \bar{\phi}_{2n}}{\partial x} \frac{\partial \gamma_{12}}{\partial x} \right) dx \cos \psi_2 - \frac{EA}{l_1} \int_0^{l_1} \left(\frac{\partial \phi_{1n}}{\partial x} \frac{\partial \gamma_{21}}{\partial x} + \frac{\partial \bar{\phi}_{1n}}{\partial x} \frac{\partial \gamma_{11}}{\partial x} \right) dx \cos \psi_1 \quad (11.108)$$

$$\Gamma_{16} = -\frac{EA}{l_2} \int_0^{l_2} \left(\frac{\partial \phi_{2n}}{\partial x} \frac{\partial \gamma_{22}}{\partial x} + \frac{\partial \bar{\phi}_{2n}}{\partial x} \frac{\partial \gamma_{12}}{\partial x} \right) dx \quad (11.109)$$

$$\Gamma_{21} = k_1 (\gamma_{45} \cos \psi_1 + \gamma_{44} - \gamma_{43}) \frac{\partial^2 \phi_{1n}}{\partial x^2} \quad (11.110)$$

$$\Gamma_{22} = k_2 (\gamma_{45} \cos \psi_2 + \gamma_{46} - \gamma_{44}) \frac{\partial^2 \phi_{2n}}{\partial x^2} \quad (11.111)$$

$$\Gamma_{23} = \frac{EA}{l_1} \int_0^{l_1} \left(\frac{\partial \phi_{1n}}{\partial x} \frac{\partial \gamma_{41}}{\partial x} \right) dx - \frac{EA}{l_3} \int_0^{l_3} \left(\frac{\partial \phi_m}{\partial x} \frac{\partial \gamma_{61}}{\partial x} + \frac{\partial \bar{\phi}_m}{\partial x} \frac{\partial \gamma_{51}}{\partial x} \right) dx \quad (11.112)$$

$$\Gamma_{24} = \frac{EA}{l_2} \int_0^{l_2} \left(\frac{\partial \phi_{2n}}{\partial x} \frac{\partial \gamma_{42}}{\partial x} \right) dx - \frac{EA}{l_1} \int_0^{l_1} \left(\frac{\partial \phi_{1n}}{\partial x} \frac{\partial \gamma_{41}}{\partial x} \right) dx \quad (11.113)$$

$$\Gamma_{25} = -\frac{EA}{l_2} \int_0^{l_2} \left(\frac{\partial \phi_{2n}}{\partial x} \frac{\partial \gamma_{42}}{\partial x} \right) dx \cos \psi_2 - \frac{EA}{l_1} \int_0^{l_1} \left(\frac{\partial \phi_{1n}}{\partial x} \frac{\partial \gamma_{41}}{\partial x} \right) dx \cos \psi_1 \quad (11.114)$$

$$\Gamma_{26} = \frac{EA}{l_3} \int_0^{l_3} \left(\frac{\partial \phi_m}{\partial x} \frac{\partial \gamma_{61}}{\partial x} + \frac{\partial \bar{\phi}_m}{\partial x} \frac{\partial \gamma_{51}}{\partial x} \right) dx - \frac{EA}{l_2} \int_0^{l_2} \left(\frac{\partial \phi_{2n}}{\partial x} \frac{\partial \gamma_{42}}{\partial x} \right) dx \quad (11.115)$$

$$\Gamma_{31} = k_1 (\hat{x}_{3n} \cos \psi_1 + \hat{x}_{4n} - \hat{x}_{2n}) \frac{\partial^2 \gamma_{31}}{\partial x^2} + k_1 (\gamma_{35} \cos \psi_1 + \gamma_{34} - \gamma_{33}) \frac{\partial^2 \bar{\phi}_{1n}}{\partial x^2} \quad (11.116)$$

$$\Gamma_{32} = k_2 (\hat{x}_{3n} \cos \psi_2 + \hat{x}_{4n} - \hat{x}_{2n}) \frac{\partial^2 \gamma_{32}}{\partial x^2} + k_2 (\gamma_{35} \cos \psi_2 + \gamma_{36} - \gamma_{34}) \frac{\partial^2 \bar{\phi}_{2n}}{\partial x^2} \quad (11.117)$$

$$\Gamma_{33} = \frac{EA}{l_1} \int_0^{l_1} \left(\frac{\partial \bar{\phi}_{1n}}{\partial x} \frac{\partial \gamma_{31}}{\partial x} \right) dx - \frac{EA}{l_3} \int_0^{l_3} \left(\frac{\partial \phi_m}{\partial x} \frac{\partial \bar{\gamma}_{61}}{\partial x} \right) dx \quad (11.118)$$

$$\Gamma_{34} = \frac{EA}{l_2} \int_0^{l_2} \left(\frac{\partial \bar{\phi}_{2n}}{\partial x} \frac{\partial \gamma_{32}}{\partial x} \right) dx - \frac{EA}{l_1} \int_0^{l_1} \left(\frac{\partial \bar{\phi}_{1n}}{\partial x} \frac{\partial \gamma_{31}}{\partial x} \right) dx \quad (11.119)$$

$$\Gamma_{35} = -\frac{EA}{l_2} \int_0^{l_2} \left(\frac{\partial \bar{\phi}_{2n}}{\partial x} \frac{\partial \gamma_{32}}{\partial x} \right) dx \cos \psi_2 - \frac{EA}{l_1} \int_0^{l_1} \left(\frac{\partial \bar{\phi}_{1n}}{\partial x} \frac{\partial \gamma_{31}}{\partial x} \right) dx \cos \psi_1 \quad (11.120)$$

$$\Gamma_{36} = \frac{EA}{l_3} \int_0^{l_3} \left(\frac{\partial \varphi_m}{\partial x} \frac{\partial \bar{\gamma}_{61}}{\partial x} \right) dx - \frac{EA}{l_2} \int_0^{l_2} \left(\frac{\partial \bar{\phi}_{2n}}{\partial x} \frac{\partial \gamma_{32}}{\partial x} \right) dx \quad (11.121)$$

$$\Gamma_{41} = k_3 (\hat{x}_{1n} - \hat{x}_{4n}) \frac{\partial^2 \gamma_{61}}{\partial x^2} + k_3 (\hat{x}_{1n} - \hat{x}_{4n}) \frac{\partial^2 \bar{\gamma}_{51}}{\partial x^2} + k_3 (\gamma_{13} - \gamma_{16}) \frac{\partial^2 \bar{\varphi}_m}{\partial x^2} \quad (11.122)$$

$$\Gamma_{51} = k_3 (\hat{x}_{1n} - \hat{x}_{4n}) \frac{\partial^2 \gamma_{61}}{\partial x^2} + k_3 (\hat{x}_{1n} - \hat{x}_{4n}) \frac{\partial^2 \gamma_{51}}{\partial x^2} + k_3 (\gamma_{23} - \gamma_{26}) \frac{\partial^2 \bar{\varphi}_m}{\partial x^2} \quad (11.123)$$

$$\begin{aligned} \Gamma_{61} &= k_3 (\gamma_{33} - \gamma_{36}) \frac{\partial^2 \bar{\varphi}_m}{\partial x^2} + k_3 (\gamma_{43} - \gamma_{46}) \frac{\partial^2 \varphi_m}{\partial x^2} + \\ &\quad \frac{EA}{2l_3} \left[\int_0^{l_3} \left(\frac{\partial \varphi_m}{\partial x} \right)^2 dx \frac{\partial^2 \bar{\varphi}_m}{\partial x^2} + \int_0^{l_3} 2 \frac{\partial \varphi_m}{\partial x} \frac{\partial \bar{\varphi}_m}{\partial x} dx \frac{\partial^2 \varphi_m}{\partial x^2} \right] \end{aligned} \quad (11.124)$$

The solvability conditions for equations (11.19) and (11.22) are found to be as follows:

$$-M_G \frac{\partial A_n}{\partial T_2} + A_n^2 \bar{A}_n \Theta_1 + A_n B_m \bar{B}_m \Theta_2 + \bar{A}_n B_m^2 e^{-2i\sigma_1 T_2} \Theta_3 + (\hat{F}_{d1} \hat{x}_{1n} + \hat{F}_{d4} \hat{x}_{4n}) e^{i\sigma_1 T_2} - 2i\zeta_n A_n = 0 \quad (11.125)$$

$$-M_{3G} \frac{\partial B_m}{\partial T_2} + A_n^2 \bar{B}_m e^{2i\sigma_1 T_2} \Theta_4 + A_n \bar{A}_n B_m \Theta_5 + B_m^2 \bar{B}_m \Theta_6 - 2i\zeta_m B_m = 0 \quad (11.126)$$

where ζ_n and ζ_m are modal damping and

$$M_G = (2i\omega_n \langle M\phi_n, \phi_n \rangle + \langle G\phi_n, \phi_n \rangle) \quad (11.127)$$

$$M_{3G} = (2i\lambda_m \langle M_3 \varphi_m, \varphi_m \rangle + \langle G_3 \varphi_m, \varphi_m \rangle) \quad (11.128)$$

$$\Theta_1 = \int_0^{l_1} \Gamma_{11} \bar{\phi}_{1n} dx + \int_0^{l_2} \Gamma_{12} \bar{\phi}_{2n} dx + \Gamma_{13} \hat{x}_{1n} + \Gamma_{14} \hat{x}_{2n} + \Gamma_{15} \hat{x}_{3n} + \Gamma_{16} \hat{x}_{4n} \quad (11.129)$$

$$\Theta_2 = \int_0^{l_1} \Gamma_{21} \bar{\phi}_{1n} dx + \int_0^{l_2} \Gamma_{22} \bar{\phi}_{2n} dx + \Gamma_{23} \hat{x}_{1n} + \Gamma_{24} \hat{x}_{2n} + \Gamma_{25} \hat{x}_{3n} + \Gamma_{26} \hat{x}_{4n} \quad (11.130)$$

$$\Theta_3 = \int_0^{l_1} \Gamma_{31} \bar{\phi}_{1n} dx + \int_0^{l_2} \Gamma_{32} \bar{\phi}_{2n} dx + \Gamma_{33} \hat{x}_{1n} + \Gamma_{34} \hat{x}_{2n} + \Gamma_{35} \hat{x}_{3n} + \Gamma_{36} \hat{x}_{4n} \quad (11.131)$$

$$\Theta_4 = \int_0^{l_3} \Gamma_{41} \bar{\phi}_m dx \quad (11.132)$$

$$\Theta_5 = \int_0^{l_3} \Gamma_{51} \bar{\phi}_m dx \quad (11.133)$$

$$\Theta_6 = \int_0^{l_3} \Gamma_{61} \bar{\phi}_m dx \quad (11.134)$$

Using the normalized eigenfunctions of serpentine belt drive systems, the expressions M_G and M_{3G} can be simplified as:

$$M_G = \frac{2i}{\omega_n} \quad M_{3G} = \frac{2i}{\lambda_m} \quad (11.135)$$

Equations (11.125) and (11.126) govern the time evolution of the amplitudes and phases of the response. The terms Θ_i defined in equations (11.129) – (11.134) are composed of integrals of the spatial solutions determined at the first and second orders. Thus the spatial solutions have strong influence on the evolution of the complex amplitudes A_n and B_m . Since the spatial variation of the second order is different from that of the first order, there exist discrepancies between the direct approach and the discretization approach.

11.2.5 Modulation Equations and Steady State Solutions

Substituting polar form of A_n and B_m into equations (11.125) and (11.126), and separating the result into real and imaginary parts, the first order differential equations for the amplitudes and

phases are obtained as follows

$$\begin{aligned} \frac{\partial \alpha_n}{\partial T_2} - \omega_n \frac{\text{Im}(\Theta_1)}{8} \alpha_n^3 - \omega_n \frac{\text{Im}(\Theta_2)}{8} \alpha_n \alpha_m^2 \\ - \omega_n \frac{\text{Im}(\Theta_3) \cos \zeta_1 - \text{Re}(\Theta_3) \sin \zeta_1}{8} \alpha_n \alpha_m^2 - F_d \sin \zeta_2 + \omega_n \zeta_n \alpha_n = 0 \end{aligned} \quad (11.136)$$

$$\begin{aligned} \alpha_n \left(\sigma_2 - \frac{\partial \zeta_2}{\partial T_2} \right) + \omega_n \frac{\text{Re}(\Theta_1)}{8} \alpha_n^3 + \omega_n \frac{\text{Re}(\Theta_2)}{8} \alpha_n \alpha_m^2 + \\ \omega_n \frac{\text{Re}(\Theta_3) \cos \zeta_1 + \text{Im}(\Theta_3) \sin \zeta_1}{8} \alpha_n \alpha_m^2 + F_d \cos \zeta_2 = 0 \end{aligned} \quad (11.137)$$

$$\begin{aligned} \frac{\partial \alpha_m}{\partial T_2} - \lambda_m \frac{\text{Im}(\Theta_6)}{8} \alpha_m^3 - \lambda_m \frac{\text{Im}(\Theta_5)}{8} \alpha_n^2 \alpha_m - \\ \lambda_m \frac{\text{Im}(\Theta_4) \cos \zeta_1 + \text{Re}(\Theta_4) \sin \zeta_1}{8} \alpha_n^2 \alpha_m + \lambda_m \zeta_m \alpha_m = 0 \end{aligned} \quad (11.138)$$

$$\begin{aligned} \alpha_m \left(\sigma_1 + \sigma_2 - \frac{1}{2} \frac{\partial \zeta_1}{\partial T_2} - \frac{\partial \zeta_2}{\partial T_2} \right) + \lambda_m \frac{\text{Re}(\Theta_6)}{8} \alpha_m^3 + \lambda_m \frac{\text{Re}(\Theta_5)}{8} \alpha_n^2 \alpha_m \\ + \lambda_m \frac{\text{Re}(\Theta_4) \cos \zeta_1 - \text{Im}(\Theta_4) \sin \zeta_1}{8} \alpha_n^2 \alpha_m = 0 \end{aligned} \quad (11.139)$$

where

$$\zeta_1 = 2(\beta_n - \beta_m + \sigma_1 T_2) \quad (11.140)$$

$$\zeta_2 = \sigma_2 T_2 - \beta_n \quad (11.141)$$

$$F_d = \omega_n (\hat{\chi}_{1n} \hat{F}_{d1} + \hat{\chi}_{4n} \hat{F}_{d4}) \quad (11.142)$$

For the steady-state response, the amplitude α_n and α_m and the new phase angle ζ_1 and ζ_2 in equations (11.136) – (11.139) should be constant. Thus, the amplitude and phase of the response can be determined from the following algebraic equations,

$$\begin{aligned} -\omega_n \frac{\text{Im}(\Theta_1)}{8} \alpha_n^3 - \omega_n \frac{\text{Im}(\Theta_2)}{8} \alpha_n \alpha_m^2 \\ - \omega_n \frac{\text{Im}(\Theta_3) \cos \zeta_1 - \text{Re}(\Theta_3) \sin \zeta_1}{8} \alpha_n \alpha_m^2 - F_d \sin \zeta_2 + \omega_n \zeta_n \alpha_n = 0 \end{aligned} \quad (11.143)$$

$$\alpha_n \sigma_2 + \omega_n \frac{\operatorname{Re}(\Theta_1)}{8} \alpha_n^3 + \omega_n \frac{\operatorname{Re}(\Theta_2)}{8} \alpha_n \alpha_m^2 + \omega_n \frac{\operatorname{Re}(\Theta_3) \cos \zeta_1 + \operatorname{Im}(\Theta_3) \sin \zeta_1}{8} \alpha_n \alpha_m^2 + F_d \cos \zeta_2 = 0 \quad (11.144)$$

$$-\lambda_m \frac{\operatorname{Im}(\Theta_6)}{8} \alpha_m^3 - \lambda_m \frac{\operatorname{Im}(\Theta_5)}{8} \alpha_n^2 \alpha_m - \lambda_m \frac{\operatorname{Im}(\Theta_4) \cos \zeta_1 + \operatorname{Re}(\Theta_4) \sin \zeta_1}{8} \alpha_n^2 \alpha_m + \lambda_m \zeta_m \alpha_m = 0 \quad (11.145)$$

$$\alpha_m (\sigma_1 + \sigma_2) + \lambda_m \frac{\operatorname{Re}(\Theta_6)}{8} \alpha_m^3 + \lambda_m \frac{\operatorname{Re}(\Theta_5)}{8} \alpha_n^2 \alpha_m + \lambda_m \frac{\operatorname{Re}(\Theta_4) \cos \zeta_1 - \operatorname{Im}(\Theta_4) \sin \zeta_1}{8} \alpha_n^2 \alpha_m = 0 \quad (11.146)$$

11.3 TWO-TO-ONE INTERNAL RESONANCE

To quantitatively describe a primary external resonance and a two-to-one internal resonance, introducing two detuning parameters σ_1 and σ_2 defined by

$$\omega_n = 2\lambda_m + \epsilon \sigma_1 \quad (11.147)$$

$$\Omega = \omega_n + \epsilon^2 \sigma_2 \quad (11.148)$$

11.3.1 The Second Order Solution

Substituting equations (11.147) and (11.148) into equations (11.12) and (11.15) and eliminating the secular terms result in the solvability conditions

$$-M_C \frac{\partial A_n}{\partial T_1} + (\hat{x}_{n+} - \hat{x}_{n-}) \frac{EA}{2l_3} \int_0^{l_3} \left(\frac{\partial \phi_m}{\partial x} \right)^2 dx e^{-i\sigma_1 T_1} B_m^2 = 0 \quad (11.149)$$

$$-M_{3G} \frac{\partial B_m}{\partial T_1} + k_3 (\hat{\chi}_{1n} - \hat{\chi}_{4n}) \int_0^{l_3} \frac{\partial^2 \bar{\varphi}_m}{\partial x^2} \bar{\varphi}_m dx A_n \bar{B}_m e^{i\sigma_1 T_1} = 0 \quad (11.150)$$

Therefore, $\frac{\partial A_n}{\partial T_1}$ and $\frac{\partial B_m}{\partial T_1}$ can be expressed as

$$\frac{\partial A_n}{\partial T_1} = p_1 e^{-i\sigma_1 T_1} B_m^2 \quad (11.151)$$

$$\frac{\partial B_m}{\partial T_1} = p_2 e^{i\sigma_1 T_1} A_n \bar{B}_m \quad (11.152)$$

where

$$p_1 = \frac{(\hat{\chi}_{4n} - \hat{\chi}_{1n}) \frac{EA}{2l_3} \int_0^{l_3} \left(\frac{\partial \varphi_m}{\partial x} \right)^2 dx}{M_G} \quad (11.153)$$

$$p_2 = \frac{k_3 (\hat{\chi}_{1n} - \hat{\chi}_{4n}) \int_0^{l_3} \frac{\partial^2 \bar{\varphi}_m}{\partial x^2} \bar{\varphi}_m dx}{M_{3G}} \quad (11.154)$$

It is noted that for two-to-one resonance, the complex amplitudes A_n and B_m are dependent on T_2 while there is no dependence for one-to-one resonance. Differentiating equations (11.151) and (11.152) with respect to T_1 yields

$$\frac{\partial^2 A_n}{\partial T_1^2} = p_1 (-i\sigma_1 e^{-i\sigma_1 T_1} B_m^2 + 2p_2 A_n B_m \bar{B}_m) \quad (11.155)$$

$$\frac{\partial^2 B_m}{\partial T_1^2} = p_2 (i\sigma_1 e^{i\sigma_1 T_1} A_n \bar{B}_m + p_1 B_m^2 \bar{B}_m + \bar{p}_2 A_n \bar{A}_n B_m) \quad (11.156)$$

After eliminating the secular terms, at order ϵ^2 , the solutions of equations (11.12) and (11.15) can be obtained by solving the corresponding linear bound value problems

$$W_2 = (\gamma_1 A_n^2 e^{2i\omega_n T_0} + CC) + \gamma_2 A_n \bar{A}_n + \gamma_4 B_m \bar{B}_m \quad (11.157)$$

$$W_{32} = \gamma_{51}(x) A_n B_m e^{i(\omega_n + \lambda_n) T_0} + CC \quad (11.158)$$

where γ_1 , γ_2 , γ_4 and $\gamma_{51}(x)$ are identical to those determined in Section 2.

11.3.2 Solvability Condition of the Third Order Equations

Substituting the solutions of the first order and the second order equations into (11.21) and (11.26) leads to

$$\mathbf{N}_C = \left(\begin{bmatrix} \Gamma_{11} \\ \Gamma_{12} \\ \Gamma_{13} \\ \Gamma_{14} \\ \Gamma_{15} \\ \Gamma_{16} \end{bmatrix}, \begin{bmatrix} \Gamma_{21} \\ \Gamma_{22} \\ \Gamma_{23} \\ \Gamma_{24} \\ \Gamma_{25} \\ \Gamma_{26} \end{bmatrix}, A_n^2 \bar{A}_n + \begin{bmatrix} \Gamma_{23} \\ \Gamma_{24} \end{bmatrix} A_n B_m \bar{B}_m \right) e^{i\omega_n T_0} + \text{NST} \quad (11.159)$$

$$N_{C3} = (I_{51} A_n \bar{A}_n B_m + I_{61} B_m^2 \bar{B}_m) e^{i\omega_n T_0} + \text{NST3} \quad (11.160)$$

where and Γ_{ij} are the same as those defined in Section 11.2.4 except for the following terms

$$\Gamma_{23} = \frac{EA}{l_1} \int_0^{l_1} \left(\frac{\partial \phi_{1n}}{\partial x} \frac{\partial \gamma_{41}}{\partial x} \right) dx - \frac{EA}{l_3} \int_0^{l_3} \left(\frac{\partial \bar{\varphi}_m}{\partial x} \frac{\partial \gamma_{51}}{\partial x} \right) dx \quad (11.161)$$

$$\Gamma_{26} = \frac{EA}{l_3} \int_0^{l_3} \left(\frac{\partial \bar{\varphi}_m}{\partial x} \frac{\partial \gamma_{51}}{\partial x} \right) dx - \frac{EA}{l_2} \int_0^{l_2} \left(\frac{\partial \phi_{2n}}{\partial x} \frac{\partial \gamma_{42}}{\partial x} \right) dx \quad (11.162)$$

$$\Gamma_{51} = k_3 (\hat{x}_{1n} - \hat{x}_{4n}) \frac{\partial^2 \gamma_{51}}{\partial x^2} + k_3 (\gamma_{23} - \gamma_{26}) \frac{\partial^2 \varphi_m}{\partial x^2} \quad (11.163)$$

$$\Gamma_{61} = k_3 (\gamma_{43} - \gamma_{46}) \frac{\partial^2 \varphi_m}{\partial x^2} + \frac{EA}{2l_3} \left[\int_0^{l_3} \left(\frac{\partial \varphi_m}{\partial x} \right)^2 dx \frac{\partial^2 \bar{\varphi}_m}{\partial x^2} + \int_0^{l_1} 2 \frac{\partial \varphi_m}{\partial x} \frac{\partial \bar{\varphi}_m}{\partial x} dx \frac{\partial^2 \varphi_m}{\partial x^2} \right] \quad (11.164)$$

Substituting equations (11.159) and (11.160) into (11.19) and (11.22) and eliminating the secular terms, the solvability conditions for equations (11.19) and (11.22) are found to be as follows

$$-M_G \frac{\partial A_n}{\partial T_2} - \langle \mathbf{M}\phi_n, \phi_n \rangle \frac{\partial^2 A_n}{\partial T_1^2} + A_n^2 \bar{A}_n \Theta_1 + A_n B_m \bar{B}_m \Theta_2 + (\hat{F}_{d1} \hat{\chi}_{1n} + \hat{F}_{d4} \hat{\chi}_{4n}) e^{i\sigma_2 T_2} - 2i \hat{\zeta}_n A_n = 0 \quad (11.165)$$

$$-M_{3G} \frac{\partial B_m}{\partial T_2} - \langle \mathbf{M}_3 \varphi_m, \varphi_m \rangle \frac{\partial^2 B_m}{\partial T_1^2} + A_n \bar{A}_n B_m \Theta_5 + B_m^2 \bar{B}_m \Theta_6 - 2i \hat{\zeta}_m B_m = 0 \quad (11.166)$$

where Θ_i are identical to those defined in Section 11.2.4, which are composed of integrals of the spatial solutions determined at the first and second orders.

Inserting equations (11.155) and (11.156) into (11.165) and (11.166) leads to the explicit expression for $\frac{\partial A_n}{\partial T_2}$ and $\frac{\partial B_m}{\partial T_2}$ as

$$\frac{\partial A_n}{\partial T_2} = p_3 A_n^2 \bar{A}_n + p_4 A_n B_m \bar{B}_m + p_5 e^{-i\sigma_1 T_1} B_m^2 + p_6 e^{i\sigma_2 T_2} - \hat{\zeta}_n \omega_n A_n \quad (11.167)$$

$$\frac{\partial B_m}{\partial T_2} = p_7 A_n \bar{A}_n B_m + p_8 e^{i\sigma_1 T_1} A_n \bar{B}_m + p_9 B_m^2 \bar{B}_m - \hat{\zeta}_m \lambda_m B_m \quad (11.168)$$

where

$$p_3 = \frac{\Theta_1}{M_G} \quad (11.169)$$

$$p_4 = \frac{-2 \langle \mathbf{M}\phi_n, \phi_n \rangle p_1 p_2 + \Theta_2}{M_G} \quad (11.170)$$

$$p_5 = \frac{\langle \mathbf{M}\phi_n, \phi_n \rangle p_1 \sigma_1 i}{M_G} \quad (11.171)$$

$$p_6 = -\frac{F_d i}{2} \quad (11.172)$$

$$p_7 = \frac{-\langle M_3 \phi_m, \phi_m \rangle p_2 \bar{p}_2 + \Theta_5}{M_{3G}} \quad (11.173)$$

$$p_8 = -\frac{\langle M_3 \phi_m, \phi_m \rangle p_2 \sigma_1 i}{M_{3G}} \quad (11.174)$$

$$p_9 = \frac{-\langle M_3 \phi_m, \phi_m \rangle p_2 p_1 + \Theta_6}{M_{3G}} \quad (11.175)$$

From equations (11.67) and (11.168), it is noted that even though the space distributions of the second order solution were the same as those of the first order solution, the final modulation equations derived from the two approaches should be different. This is because there is an additional term $\langle M \phi_n, \phi_n \rangle \frac{\partial^2 A_n}{\partial T_1^2}$ arising as a secular term in direct multiple scales method. There is no equivalent term in the discretization multiple scales method. This kind of discrepancy occurs only for the two-to-one internal resonance of gyroscopic systems.

11.3.3 Modulation Equations and Steady State Solutions

Noting that A_n and B_m are independent of T_0 , equations (11.151), (11.152), (11.167) and (11.168) can be combined to form the equations of motion for the slow evaluation of A_n and B_m in time t

$$\frac{dA_n}{dt} = (\epsilon p_1 + \epsilon^2 p_5) e^{-i\sigma_1 T_1} B_m^2 + \epsilon^2 (p_3 A_n^2 \bar{A}_n + p_4 A_n B_m \bar{B}_m + p_6 e^{i\sigma_2 T_2} - \zeta_n \omega_n A_n) \quad (11.176)$$

$$\frac{dB_m}{dt} = (\epsilon p_2 + \epsilon^2 p_8) e^{i\sigma_1 t} A_n \bar{B}_m + \epsilon^2 (p_7 A_n \bar{A}_n B_m + p_9 B_m^2 \bar{B}_m - \zeta_m \lambda_m B_m) \quad (11.177)$$

Expressing the complex amplitudes A_n and B_m in the polar form, substituting this polar form into equations (11.176) and (11.177), and separating the resulting equations into real and imaginary parts, the first order differential equations for the amplitudes and phases are obtained as follows

$$\begin{aligned} \frac{d\alpha_n}{dt} &= \epsilon^2 \frac{\operatorname{Re}(p_3)}{4} \alpha_n^3 + \epsilon^2 \frac{\operatorname{Re}(p_4)}{4} \alpha_n \alpha_m^2 + 2\epsilon^2 (\operatorname{Re}(p_6) \cos \zeta_2 - \operatorname{Im}(p_6) \sin \zeta_2) \\ &\quad + \epsilon \frac{\operatorname{Re}(p_1 + \epsilon p_5) \cos \zeta_1 - \operatorname{Im}(p_1 + \epsilon p_5) \sin \zeta_1}{2} \alpha_m^2 - \epsilon^2 \zeta_n \omega_n \alpha_n \end{aligned} \quad (11.178)$$

$$\begin{aligned} \alpha_n \left(-\frac{d\zeta_2}{dt} + \epsilon^2 \sigma_2 \right) &= \epsilon^2 \frac{\operatorname{Im}(p_3)}{4} \alpha_n^3 + \epsilon^2 \frac{\operatorname{Im}(p_4)}{4} \alpha_n \alpha_m^2 + 2\epsilon^2 (\operatorname{Im}(p_6) \cos \zeta_2 + \operatorname{Re}(p_6) \sin \zeta_2) \\ &\quad + \epsilon \frac{\operatorname{Im}(p_1 + \epsilon p_5) \cos \zeta_1 + \operatorname{Re}(p_1 + \epsilon p_5) \sin \zeta_1}{2} \alpha_m^2 \end{aligned} \quad (11.179)$$

$$\begin{aligned} \frac{d\alpha_m}{dt} &= \epsilon^2 \frac{\operatorname{Re}(p_9)}{4} \alpha_m^3 + \epsilon^2 \frac{\operatorname{Re}(p_7)}{4} \alpha_n^2 \alpha_m \\ &\quad + \epsilon \frac{\operatorname{Re}(p_2 + \epsilon p_8) \cos \zeta_1 + \operatorname{Im}(p_2 + \epsilon p_8) \sin \zeta_1}{2} \alpha_n \alpha_m - \epsilon^2 \zeta_m \lambda_m \alpha_m \end{aligned} \quad (11.180)$$

$$\begin{aligned} \alpha_m \frac{\zeta'_1 - \zeta'_2 + \epsilon \sigma_1 + \epsilon^2 \sigma_2}{2} &= \epsilon^2 \frac{\operatorname{Im}(p_9)}{4} \alpha_m^3 + \epsilon^2 \frac{\operatorname{Im}(p_7)}{4} \alpha_n^2 \alpha_m + \\ &\quad \epsilon \frac{\operatorname{Im}(p_2 + \epsilon p_8) \cos \zeta_1 - \operatorname{Re}(p_2 + \epsilon p_8) \sin \zeta_1}{2} \alpha_n \alpha_m \end{aligned} \quad (11.181)$$

where

$$\zeta_1 = 2\beta_m - \beta_n - \epsilon \sigma_1 t \quad (11.182)$$

$$\zeta_2 = -\beta_n + \epsilon^2 \sigma_2 t \quad (11.183)$$

The amplitude and phase of the steady-state response can be determined from equations (11.178) – (11.181) by setting $\epsilon = 1$ and $d\alpha_n/dt = d\alpha_m/dt = d\zeta_1/dt = d\zeta_2/dt = 0$:

$$\begin{aligned} & \frac{\operatorname{Re}(p_3)}{4} \alpha_n^3 + \frac{\operatorname{Re}(p_4)}{4} \alpha_n \alpha_m^2 + 2(\operatorname{Re}(p_6) \cos \zeta_2 - \operatorname{Im}(p_6) \sin \zeta_2) \\ & + \frac{\operatorname{Re}(p_1 + p_5) \cos \zeta_1 - \operatorname{Im}(p_1 + p_5) \sin \zeta_1}{2} \alpha_m^2 - \zeta_n \omega_n \alpha_n = 0 \end{aligned} \quad (11.184)$$

$$\begin{aligned} & \frac{\operatorname{Im}(p_3)}{4} \alpha_n^3 + \frac{\operatorname{Im}(p_4)}{4} \alpha_n \alpha_m^2 + 2(\operatorname{Im}(p_6) \cos \zeta_2 + \operatorname{Re}(p_6) \sin \zeta_2) \\ & + \frac{\operatorname{Im}(p_1 + p_5) \cos \zeta_1 + \operatorname{Re}(p_1 + p_5) \sin \zeta_1}{2} \alpha_m^2 - \alpha_n \sigma_2 = 0 \end{aligned} \quad (11.185)$$

$$\frac{\operatorname{Re}(p_9)}{4} \alpha_m^3 + \frac{\operatorname{Re}(p_7)}{4} \alpha_n^2 \alpha_m + \frac{\operatorname{Re}(p_2 + p_8) \cos \zeta_1 + \operatorname{Im}(p_2 + p_8) \sin \zeta_1}{2} \alpha_n \alpha_m - \hat{\zeta}_m \lambda_m \alpha_m = 0 \quad (11.186)$$

$$\frac{\operatorname{Im}(p_9)}{4} \alpha_m^3 + \frac{\operatorname{Im}(p_7)}{4} \alpha_n^2 \alpha_m + \frac{\operatorname{Im}(p_2 + p_8) \cos \zeta_1 - \operatorname{Re}(p_2 + p_8) \sin \zeta_1}{2} \alpha_n \alpha_m - \alpha_m \frac{\sigma_1 + \sigma_2}{2} = 0 \quad (11.187)$$

11.4 NUMERICAL RESULTS AND DISCUSSIONS

In this section, the equations of steady state responses with one-to-one and two-to-one internal resonances are solved using program AUTO. The results are then compared with those obtained in discretization multiple scales method. Effects of excitation amplitude, excitation frequency and the internal resonance parameter are investigated.

11.4.1 One-to-one Internal Resonance

A comparison is made between the direct multiple scales method and the discretization multiple scales method. Focus will be on system 2 used in Chapter 10 with an addition of 2.15 kg mass being added to the tensioner arm, at the tensioner pulley axis. The operating speed is 2000 RPM. The frequency of the first transverse mode of span 3 is calculated as 28.1104 Hz and the

frequency of the first rotationally dominant mode is calculated as 29.0590 Hz.

In the case of $\alpha_m = 0$, the amplitude curves of α_n versus σ_2 of system 2 for different modal damping are shown in Figure 11.1. It is seen that bifurcation occurs when modal damping is equal to zero and the system shows a typical multi-valued nonlinear phenomenon. No bifurcation occurs when damping is not equal to zero, which indicates that damping has a significant effect on the nonlinear response of serpentine belt systems. Figure 11.2 shows the region where there exists multi-valued amplitude for zero damping. Within the region bounded by the two curves, there are three rest states and outside of the two curves there is only one steady state solution.

Comparison between the results for $\alpha_m = 0$ obtained by the direct multiple scales method and those obtained by the discretization multiple scales method shows that the two approaches yield qualitatively different predictions of the system response. For discretization multiple scales method, the dominance of quadratic nonlinearity is evident from the softening behavior shown in Figure 10.10. For direct multiple scales method, the dominance of the cubic nonlinearity leads to a hardening behavior shown in Figure 11.1. The steady state responses of direct multiple scales appear to be more reasonable since the one-to-one internal resonance results from the cubic nonlinearity.

In the case of $\alpha_m \neq 0$, the solution curves for α_n and α_m of system 2 are shown in Figure 11.3. The modal damping for rotational mode is 1% and for transverse mode is 0.3%. It is seen that three branch curves exist for α_n within certain range of detuning parameter σ_2 . The highest

branch corresponds to the case $\alpha_m = 0$. The presence of cubic nonlinearity causes distortion and asymmetry in these curves. There always exist two steady state solutions for α_n within the range where non-trivial solutions exist. The difference between the two steady state solutions for α_n approaches to zero as σ_2 becomes smaller. Two steady state solutions are possible for α_m within a certain range of σ_2 values. There are two sets of Hopf bifurcation emanating from the steady state solutions, which lead to oscillating amplitudes and phases. Filled circles represent stable periodic orbits and open circles are unstable.

It is evident that the responses for α_n and α_m obtained from the direct multiple scales method are quite different from those obtained from the discretization multiple scales method. For the discretization multiple scales method (see Figure 10.12), two branch curves exist for α_n and α_m on both sides of $\sigma_2 = 0$, which is typical of a coupled system with quadratic nonlinearity. For the direct multiple scales method, the distortion and asymmetry caused by the cubic nonlinearity seems to be more dominant.

The frequency of the periodic solutions as a function of detuning parameter σ_2 is presented in Figure 11.4. Note that multi-valued phenomenon exists within certain ranges of σ_2 . The periodic solutions for α_n , α_m , ζ_1 , and ζ_2 are shown in Figures 11.5 for $\sigma_2 = 2.844$ 1/s at which the amplitudes and phases become periodic. Phase plane curves of α_n and α_m versus ζ_1 and ζ_2 , shown in Figures 11.6, reflect their limit cycle behavior.

The effect of the amplitude of excitation on the dynamic response of system 2 is illustrated in Figure 11.7. The external detuning parameter σ_2 is chosen as 10 1/s and the internal detuning parameter σ_1 is 5.95989 1/s. As the excitation level is increased from low levels, the steady state response is initially zero. When the excitation reaches a certain level, the response jumps to high amplitude.

Figure 11.8 shows the effect of the internal detuning parameter σ_1 on the dynamic response of system 2. The external detuning parameter σ_2 is set at 10 1/s and the excitation amplitude is set at 0.5. The results are also different from those obtained from discretization multiple scales method.

The numerical solutions for one-to-one internal resonance show that the discrepancy between the two approaches are particularly large. The reason is that the one-to-one internal resonance is due to the cubic nonlinearity and the belt drive system involves quadratic and cubic nonlinearities. The space variation used in the discretization multiple scales method is incomplete since components of the nonlinearity in the original system that are orthogonal to the linear mode shapes are discarded during the discretization.

11.4.2 Two-to-one Internal Resonance

The prototypical system simulated in this example is system 5 that is used in Chapter 10. An addition of 0.39 kg mass is added to the tensioner arm. The operating speed for the system is

2000 RPM. The frequency of the first transverse mode of span 3 is 28.1104 Hz and the frequency of the first rotationally dominant mode is 57.4120 Hz.

In the case of $\alpha_m = 0$, Figure 11.9 shows the amplitude curves of α_n versus σ_2 for different modal damping. Figure 11.10 shows the region where there exists multi-valued amplitude. It is observed that the direct multiple scales method and the discretization multiple scales method predict different responses of the belt system. However, the difference is not so large as that of one-to-one internal resonance. The trend of responses obtained by the two approaches is the same.

In the case of $\alpha_m \neq 0$, the steady state solution curves of system 5 for α_n and α_m of the system are shown in Figure 11.11. The two Hopf bifurcations, which lead to oscillating amplitudes and phases, are also presented. The results obtained in this study qualitatively agree with the experimental results by Beikmann *et al.* (1996). For the discretization multiple scales method, there is only one Hopf bifurcation point and the existence range for Hopf bifurcations is smaller. The frequency of the periodic solutions for system 5 as a function of detuning parameter σ_2 is shown in Figure 11.12. It is different from one-to-one resonance that the frequency of the periodic solutions almost does not change with σ_2 . The periodic solutions for α_n , α_m , ζ_1 , and ζ_2 are shown in Figure 11.13 for $\sigma_2 = 1.135$ 1/s at which the amplitudes and phases become periodic. Phase plane curves of α_n and α_m versus ζ_1 and ζ_2 in Figure 11.14 reflect their limit cycle behavior.

The effect of the amplitude of excitation on nonlinear response of system 5 is illustrated in Figure 11.15. The external detuning parameter σ_2 is chosen as 10 1/s and the internal detuning parameter σ_1 is 7.48379 1/s. Figure 11.16 shows the effect of the internal detuning parameter σ_1 on the response of system 5. The external detuning parameter σ_2 is set at 10 1/s and the excitation amplitude is set at 0.5.

The numerical solutions for two-to-one internal resonance show that the discrepancy between the two approaches exists but not large. This is because that the two-to-one internal resonance is due to the quadratic nonlinearity. The resonance modes dominate the response. Therefore, nonlinearity being discarded during the discretization does not cause large error.

11.5 SUMMARY AND CONCLUSIONS

In this chapter, the multiple scales method is used to solve the governing partial differential equations of the serpentine belt drive system directly. It is found that transverse motion of subsystem 1 may be parametrically excited under one-to-one and two-to-one resonance conditions. The effects of excitation amplitude, external detuning parameter σ_2 and the internal detuning parameter σ_1 have been investigated. For large values of detuning parameter σ_1 and σ_2 , the system is far from resonance and there is only one solution. When the system is near or at exact one-to-one or two-to-one internal resonances, the response becomes very large and shows a typical multi-valued nonlinear phenomenon. Moving the excitation frequency away from the rotation mode frequency significantly increases the excitation level necessary to produce

parametric resonance. Reduce the excitation level is also an effective way to avoid parametric resonance.

It is found that spatial solutions at the second order are different from the linear eigenfunctions of the system. These spatial solutions have a strong influence on the modulation equations governing the first order amplitudes and phase of the motion, which are determined from the third order equations. Therefore there exist discrepancies between the direct multiple scales method and the discretization multiple scales method.

The discrepancy for one-to-one internal resonance between the two approaches is particularly large. The quadratic nonlinearity dominates for discretization multiple scales method while the cubic nonlinearity dominates for direct multiple scales method in the case of $\alpha_m = 0$. The Hopf bifurcation, the relation between response and excitation amplitude, and the relation between response and excitation frequency for the two approaches are different. The discrepancy for two-to-one internal resonance between the two approaches is small. The trend of responses obtained by the two approaches is the same.

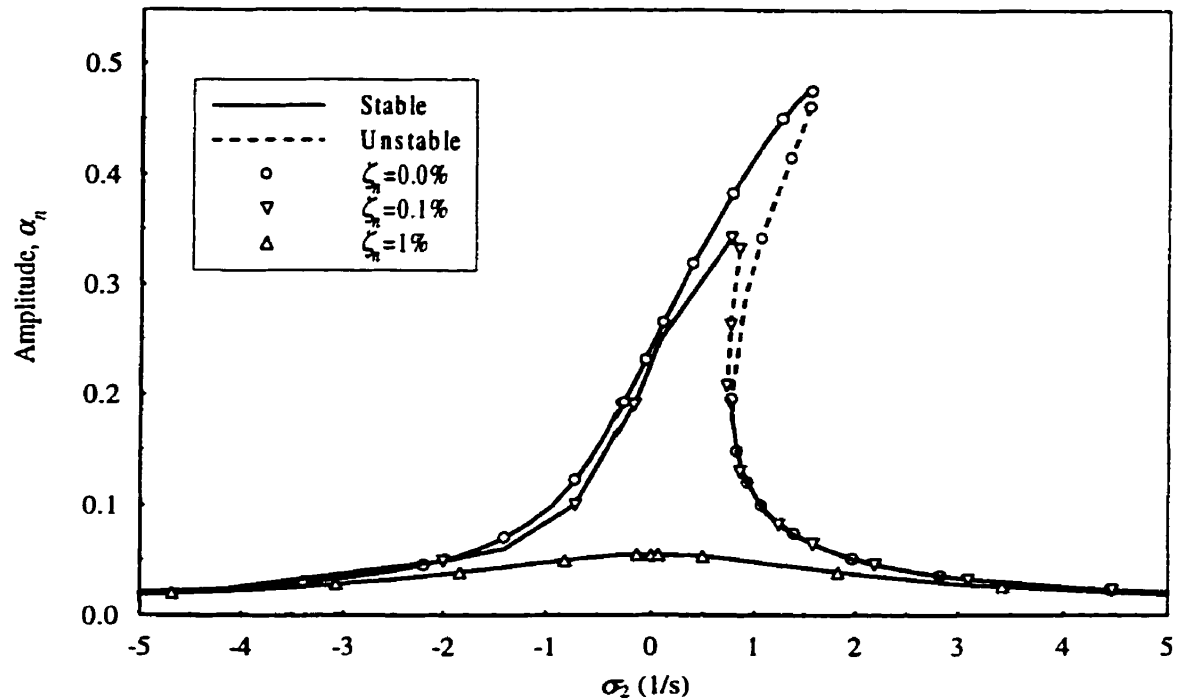


Figure 11.1: Response-frequency curves of system 2 for $\alpha_m=0$

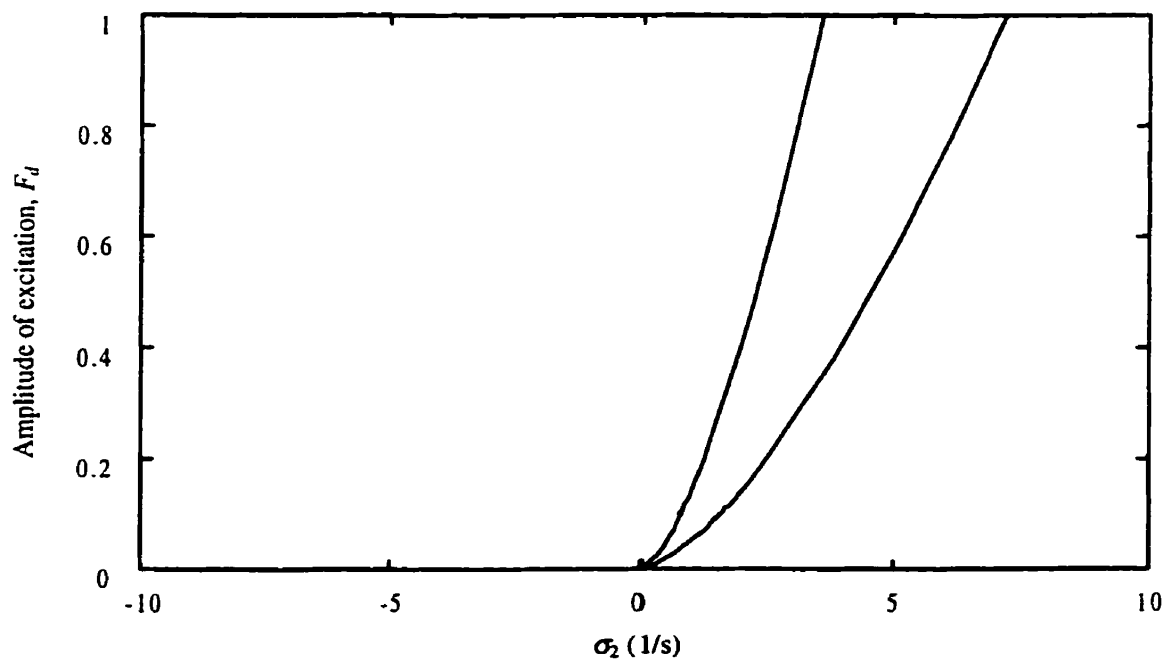


Figure 11.2: Multi-valued region of system 2 for $\alpha_m = 0.0$

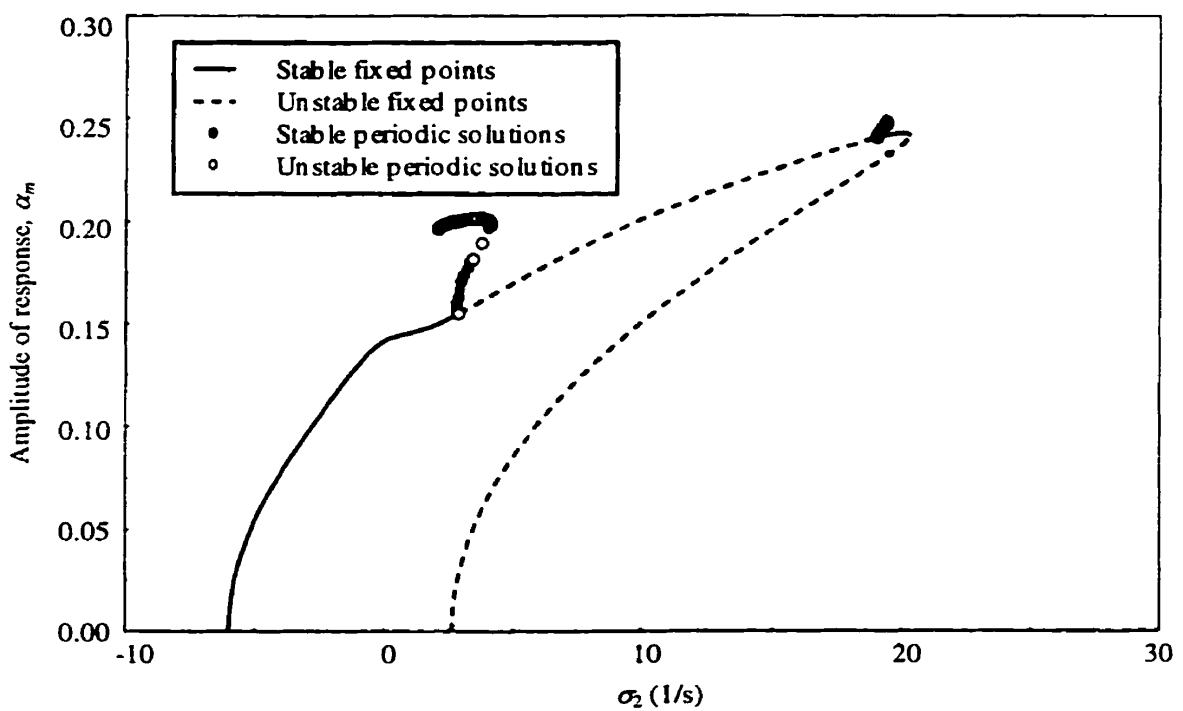
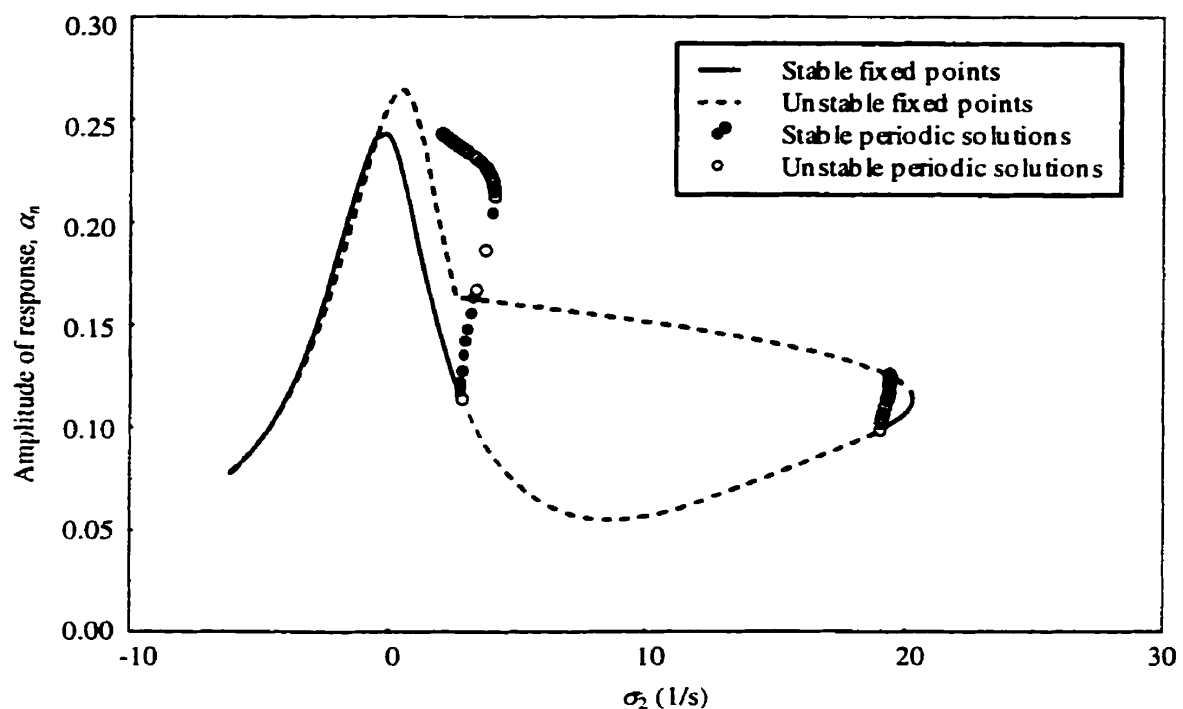


Figure 11.3: Response-frequency curves of system 2 for $\hat{\zeta}_n = 1\%$, $\hat{\zeta}_m = 0.3\%$

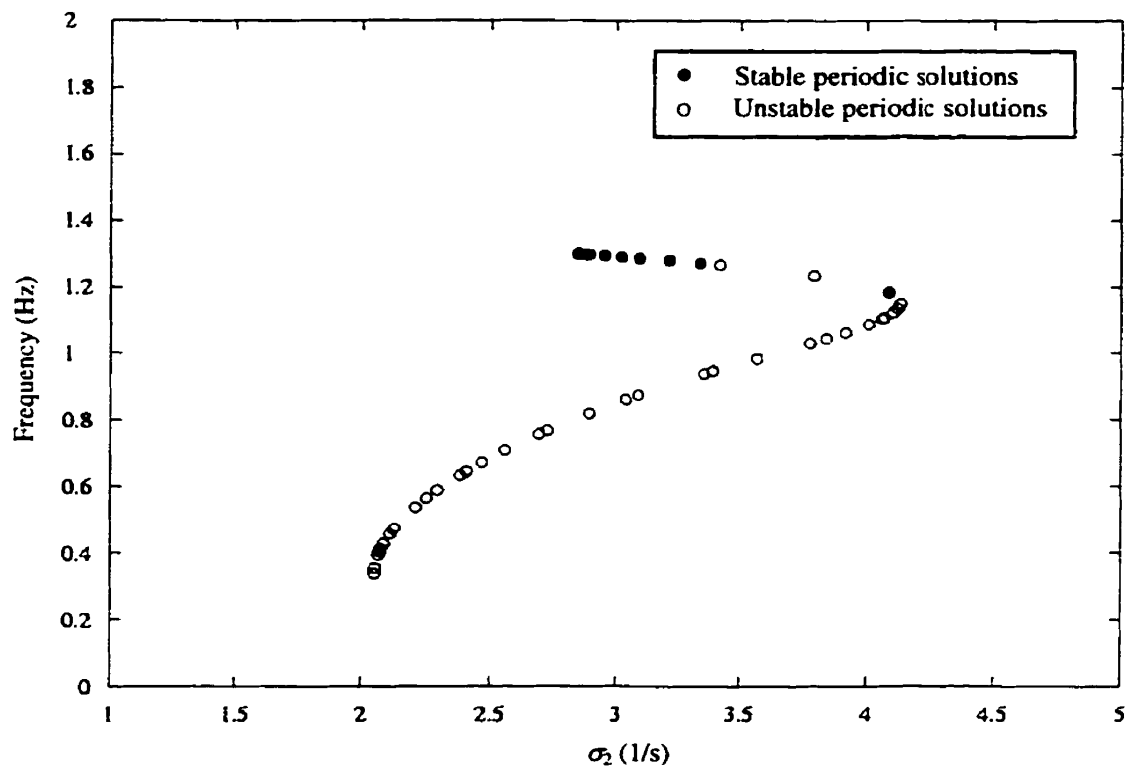


Figure 11.4: Relation between frequencies of periodic solutions and σ_2 for system 2

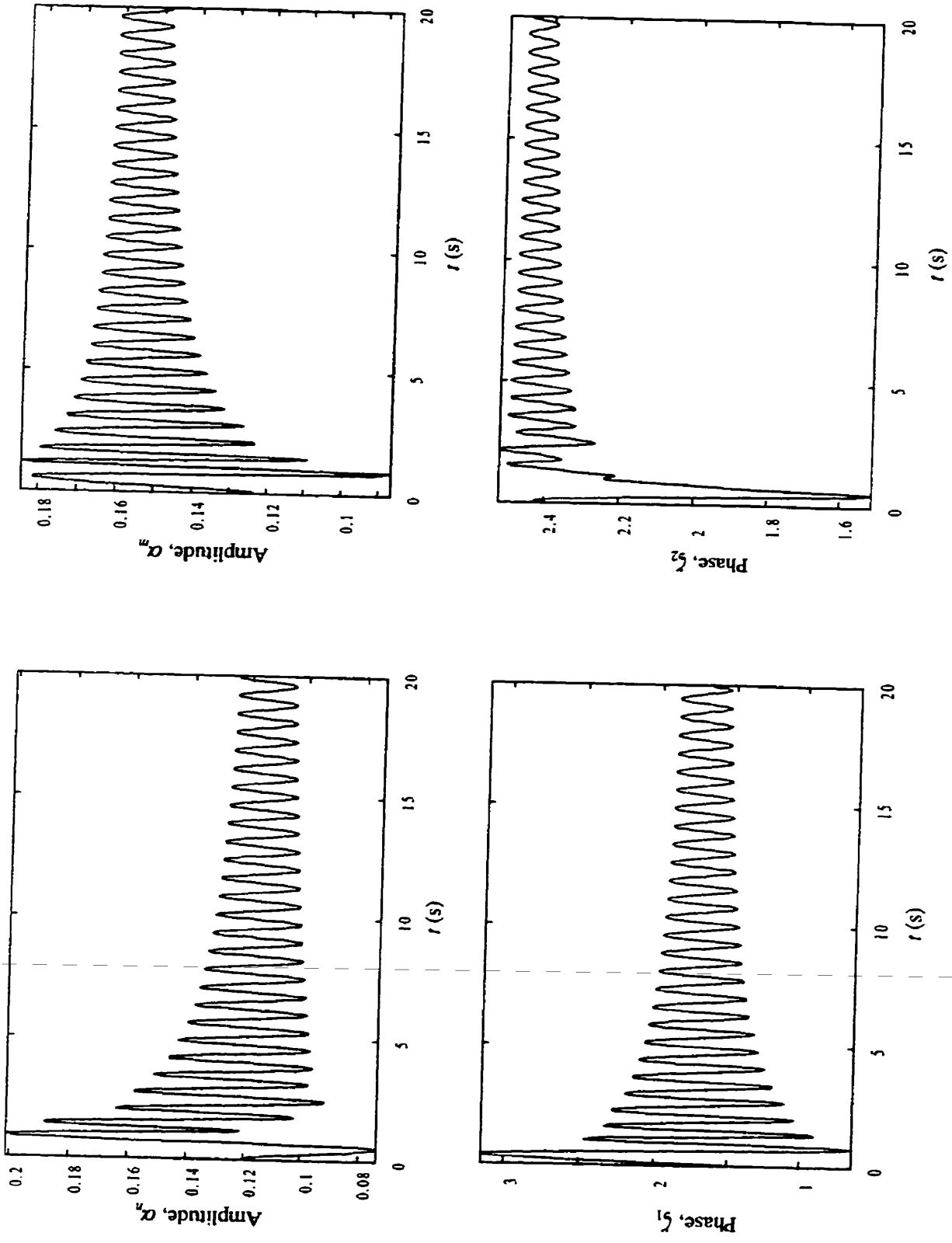


Figure 11.5: Periodic solutions of system 2

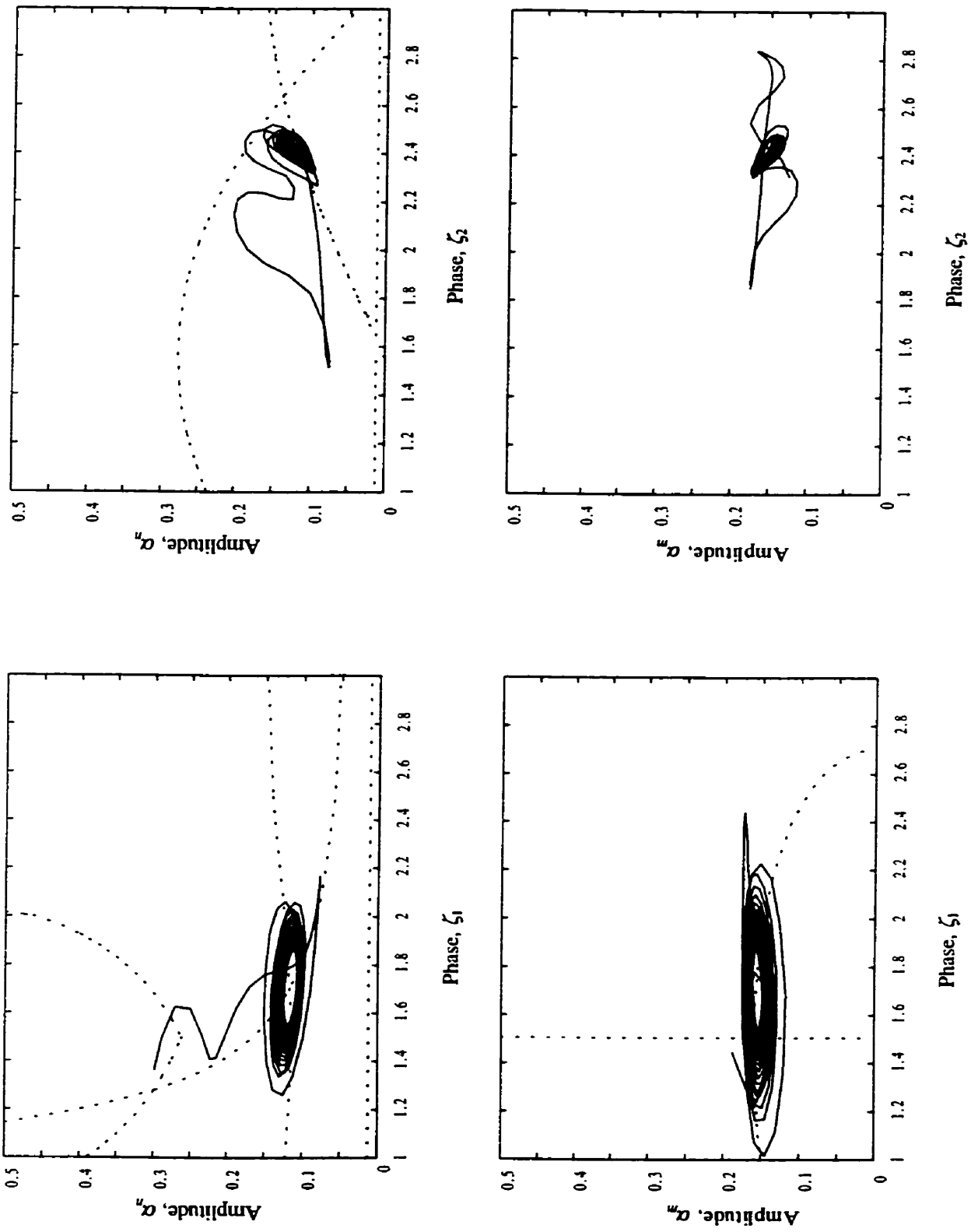


Figure 11.6: Phase plane curves of system 2 (dotted lines represent the nullclines)

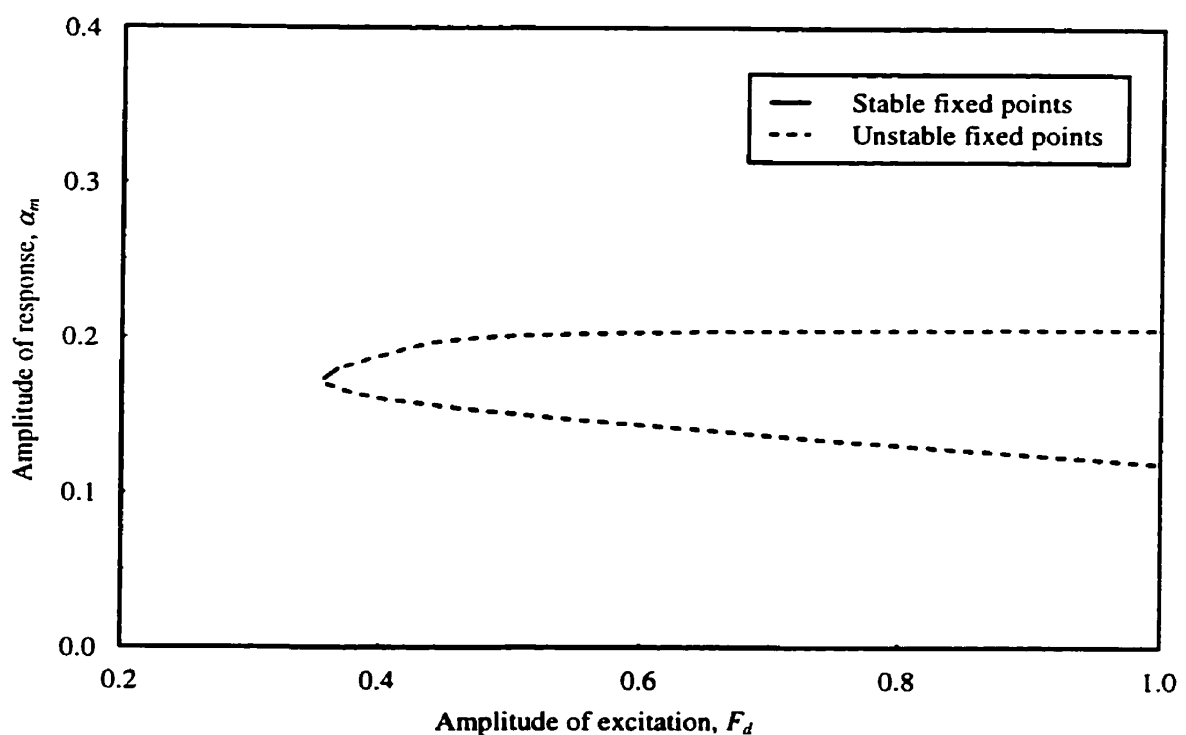
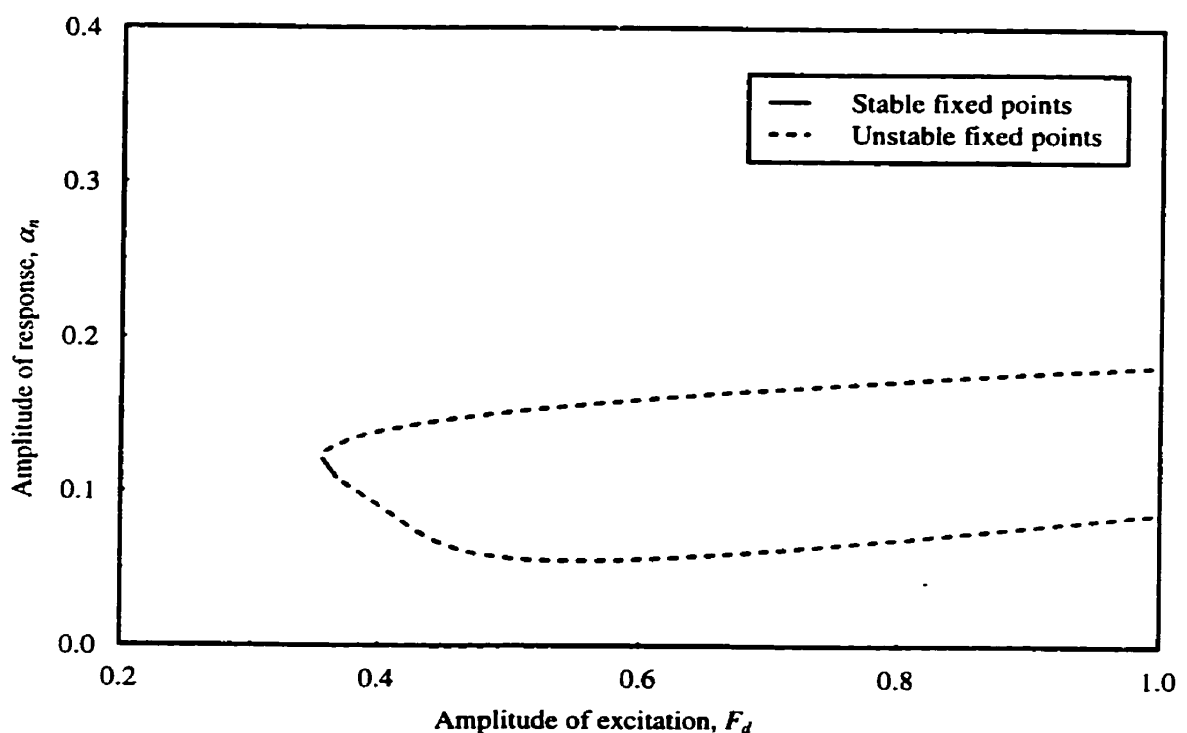


Figure 11.7: Response-excitation curves of system 2 for $\hat{\zeta}_n = 1\%$, $\hat{\zeta}_m = 0.3\%$
 $(\sigma_1=5.95989 \text{ 1/s and } \sigma_2=10.0 \text{ 1/s})$

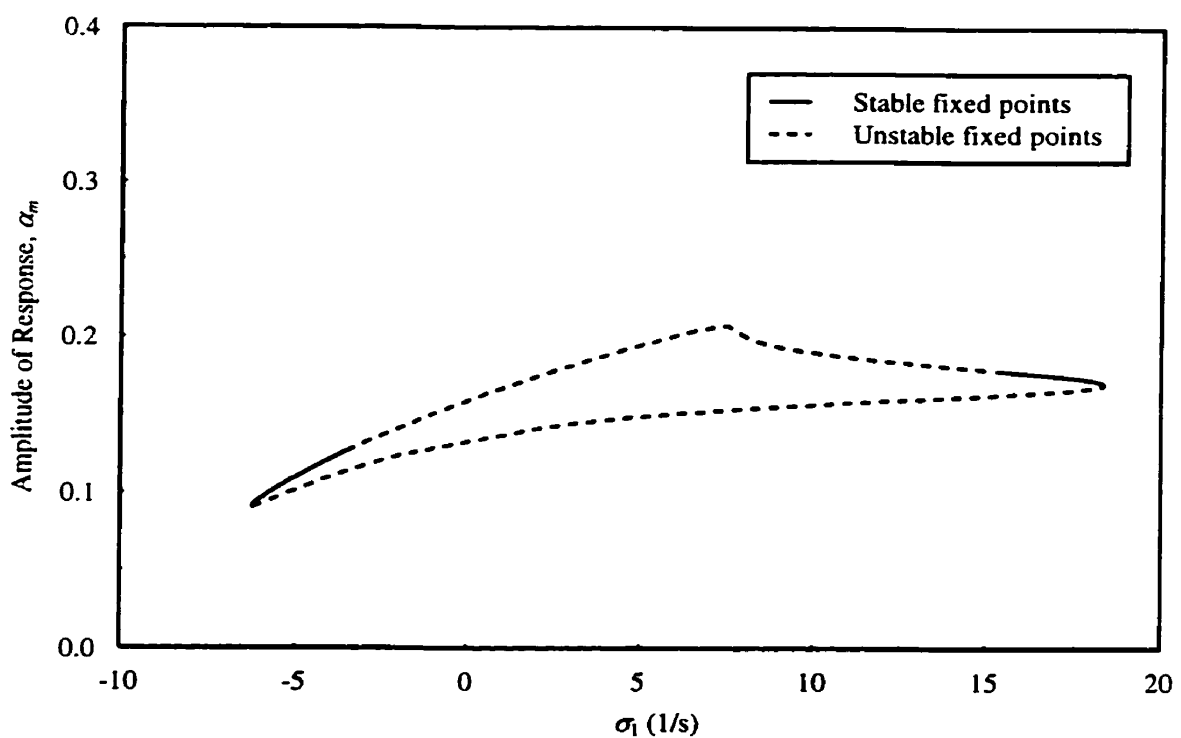
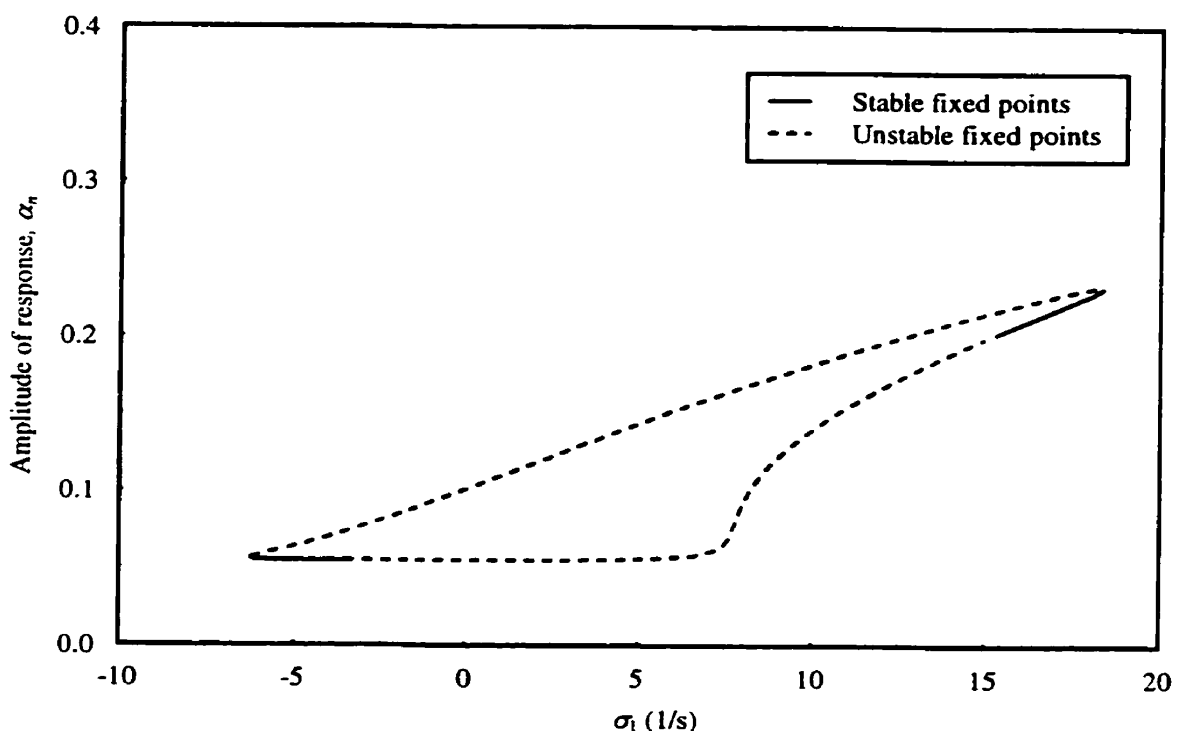


Figure 11.8: Relation between responses of system 2 and internal detuning parameter σ_1
 $(\sigma_2=10.0 \text{ 1/s and } F_d=0.5)$

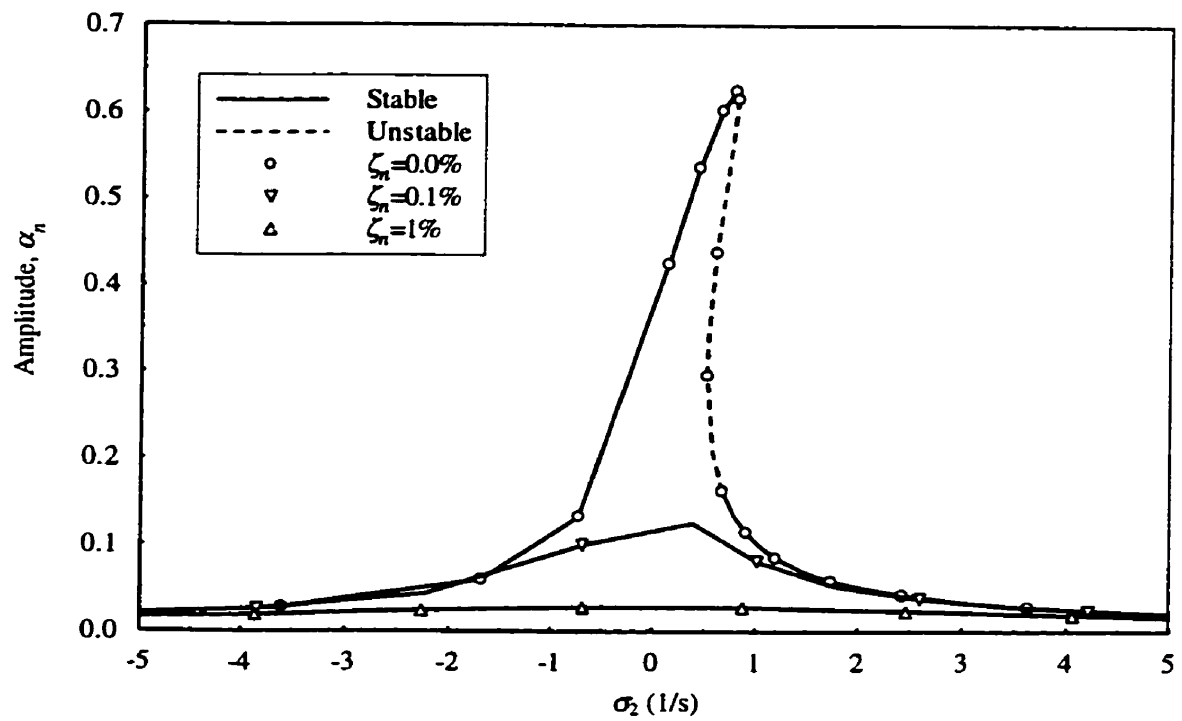


Figure 11.9: Response-frequency curves of system 5 for $\alpha_m=0$

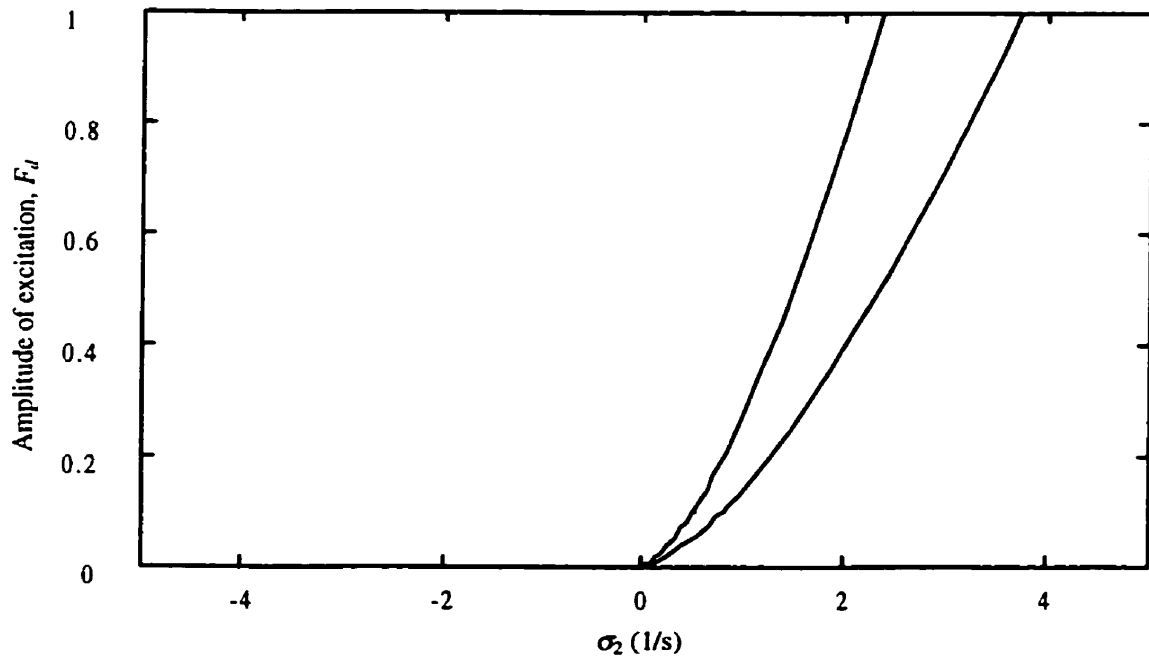


Figure 11.10: Multi-valued region of system 5 for $\alpha_m = 0.0$

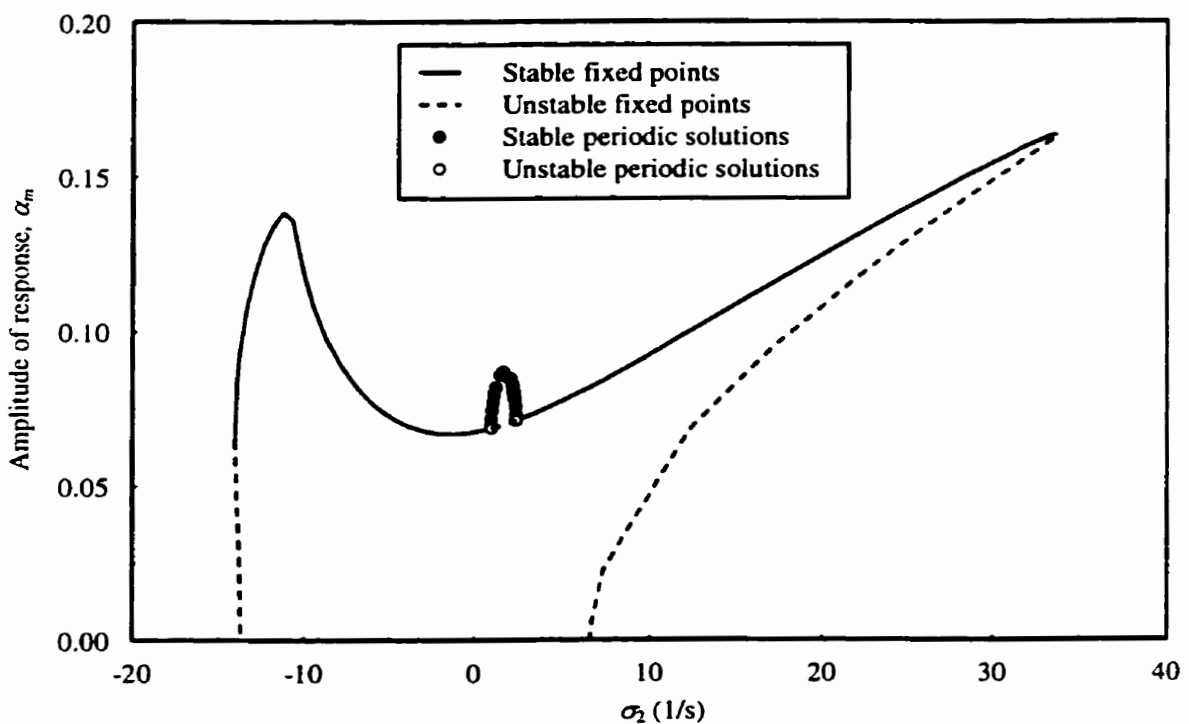
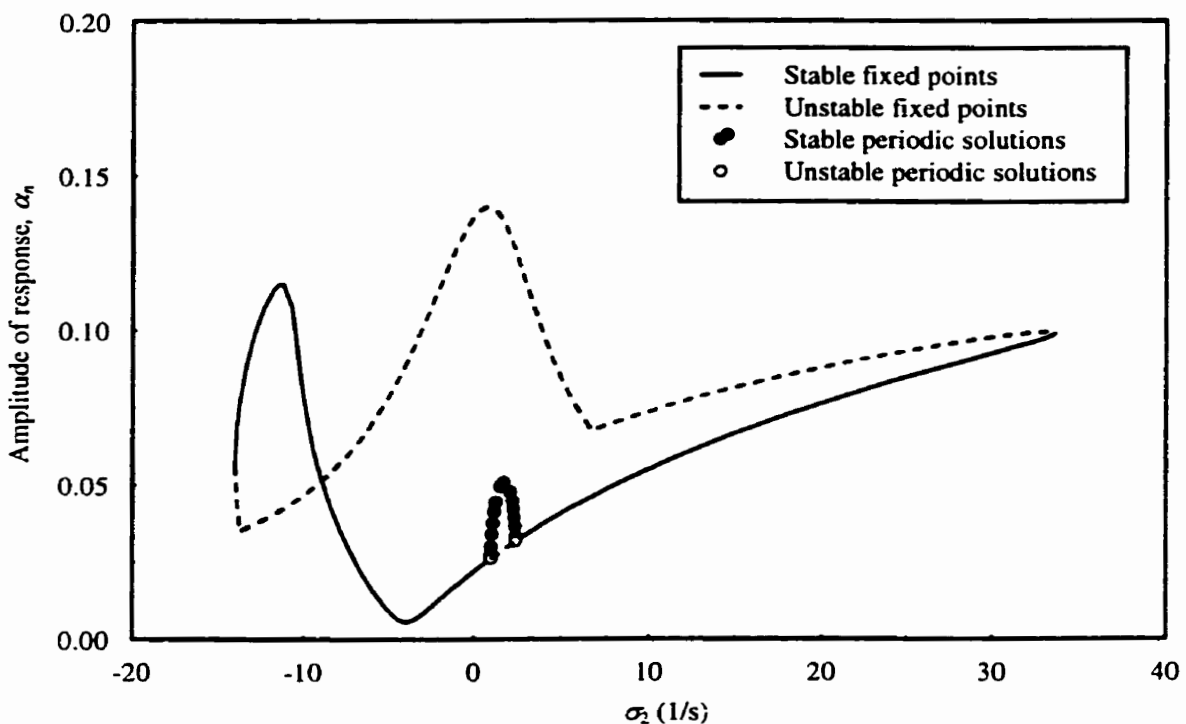


Figure 11.11: Response-frequency curves of system 5 for $\zeta_n = 1\%$, $\zeta_m = 0.3\%$

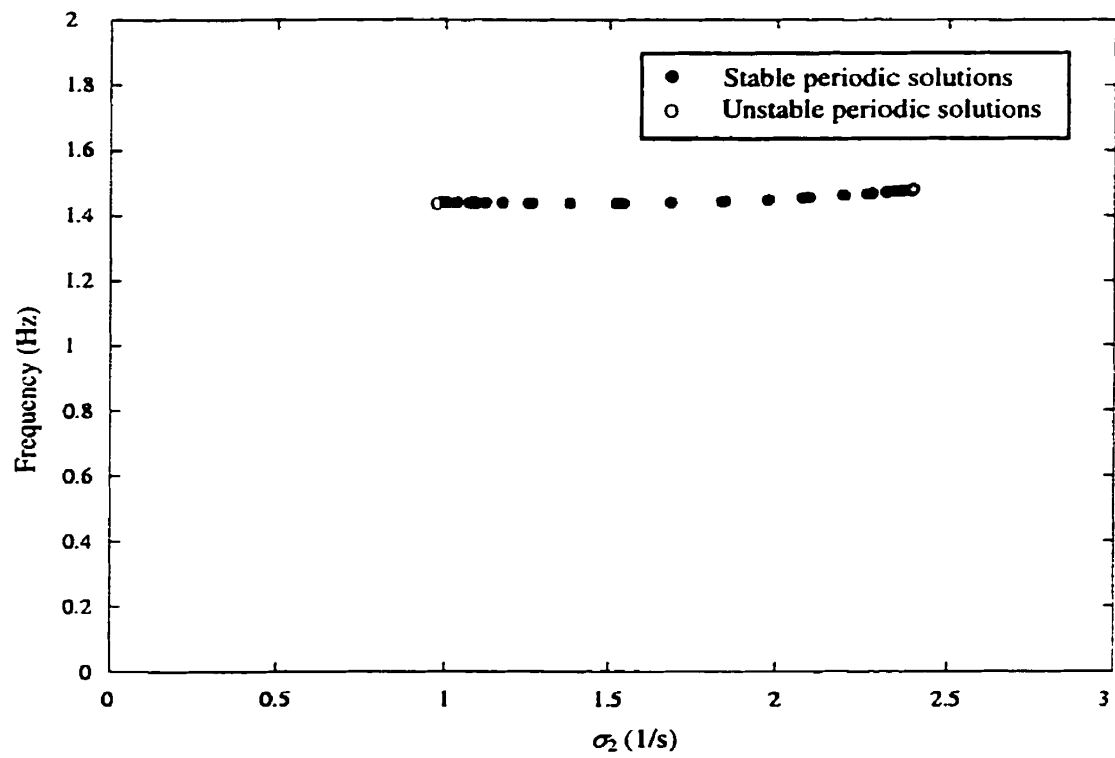


Figure 11.12: Relation between frequencies of periodic solutions and σ_2 for system 5

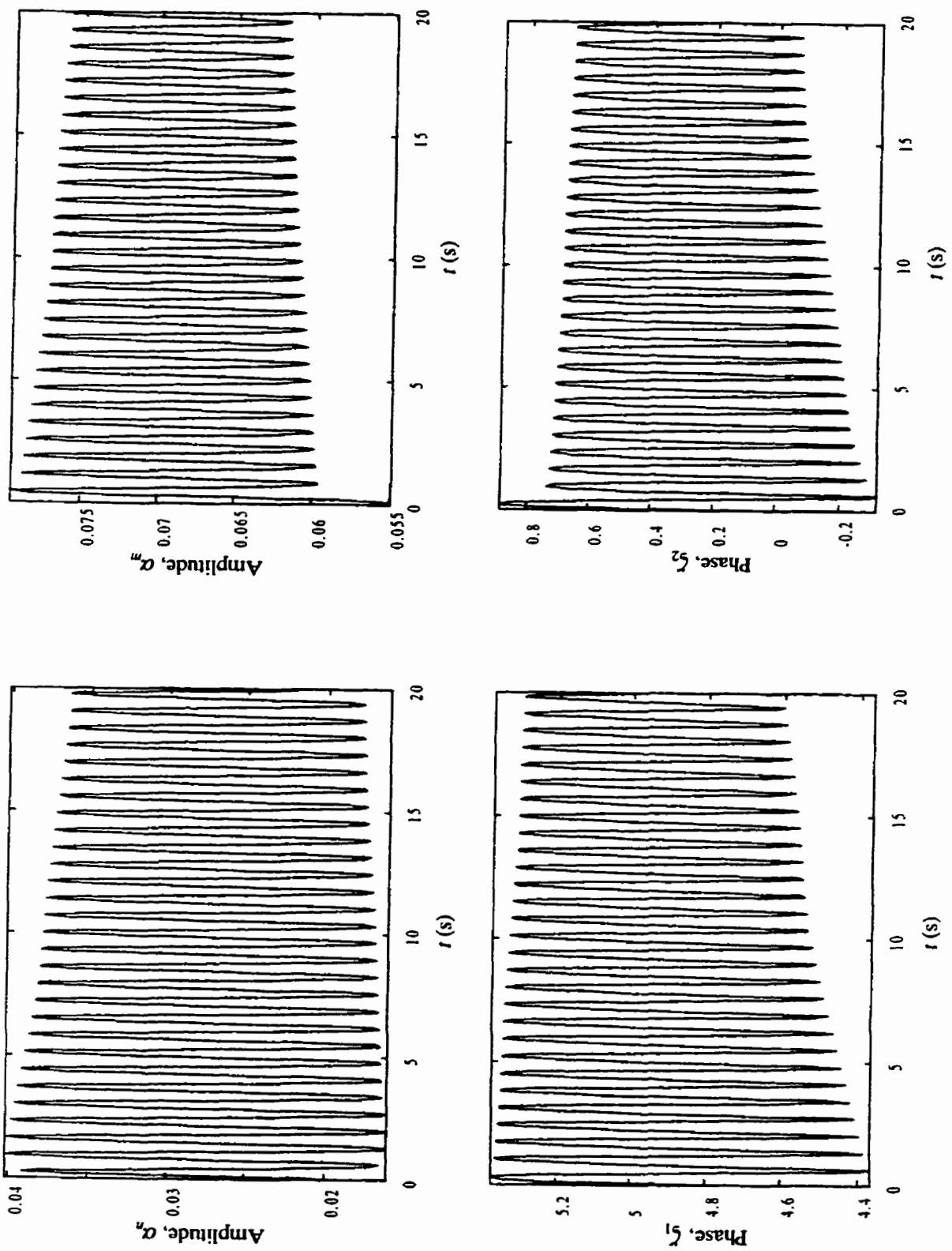


Figure 11.13: Periodic solutions of system 5

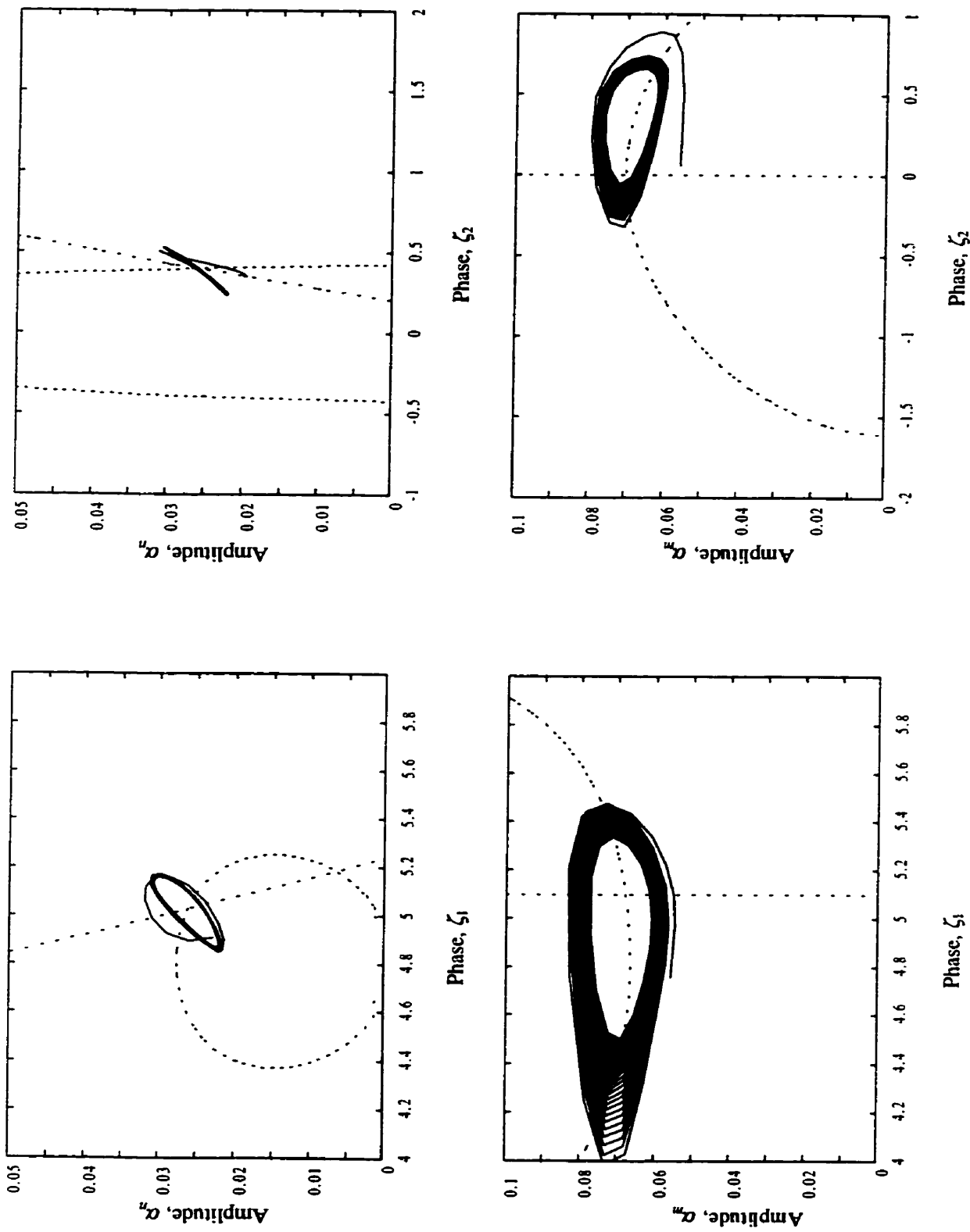


Figure 11.14: Phase plane curves of system S (dotted lines represent the nullclines)

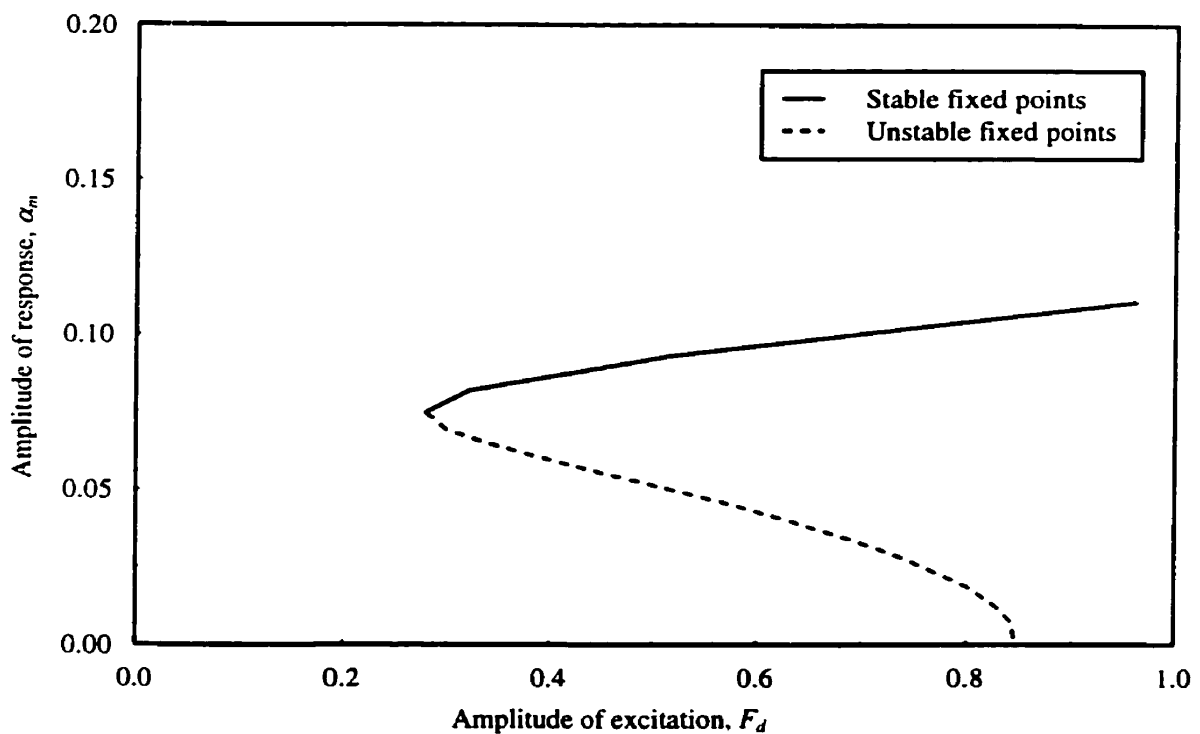
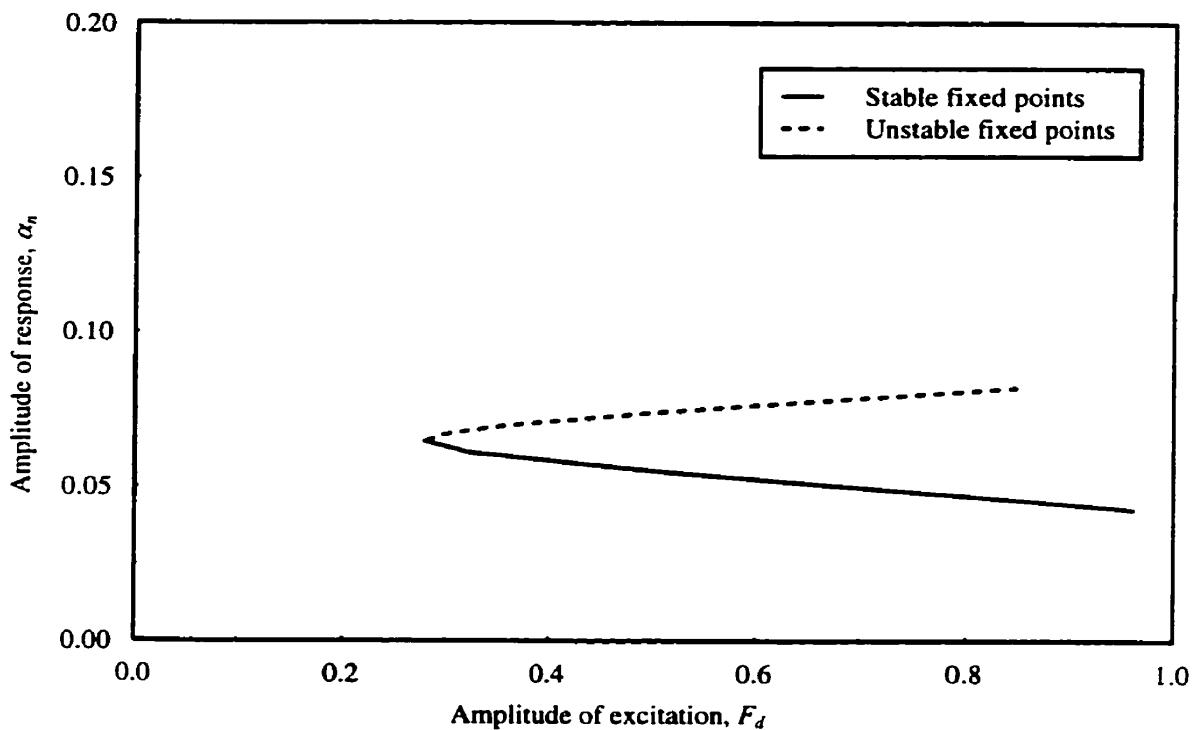


Figure 11.15: Response-excitation curves of system 5 for $\hat{\zeta}_n = 1\%$, $\hat{\zeta}_m = 0.3\%$
 $(\sigma_1=7.48379 \text{ 1/s and } \sigma_2=10.0 \text{ 1/s})$

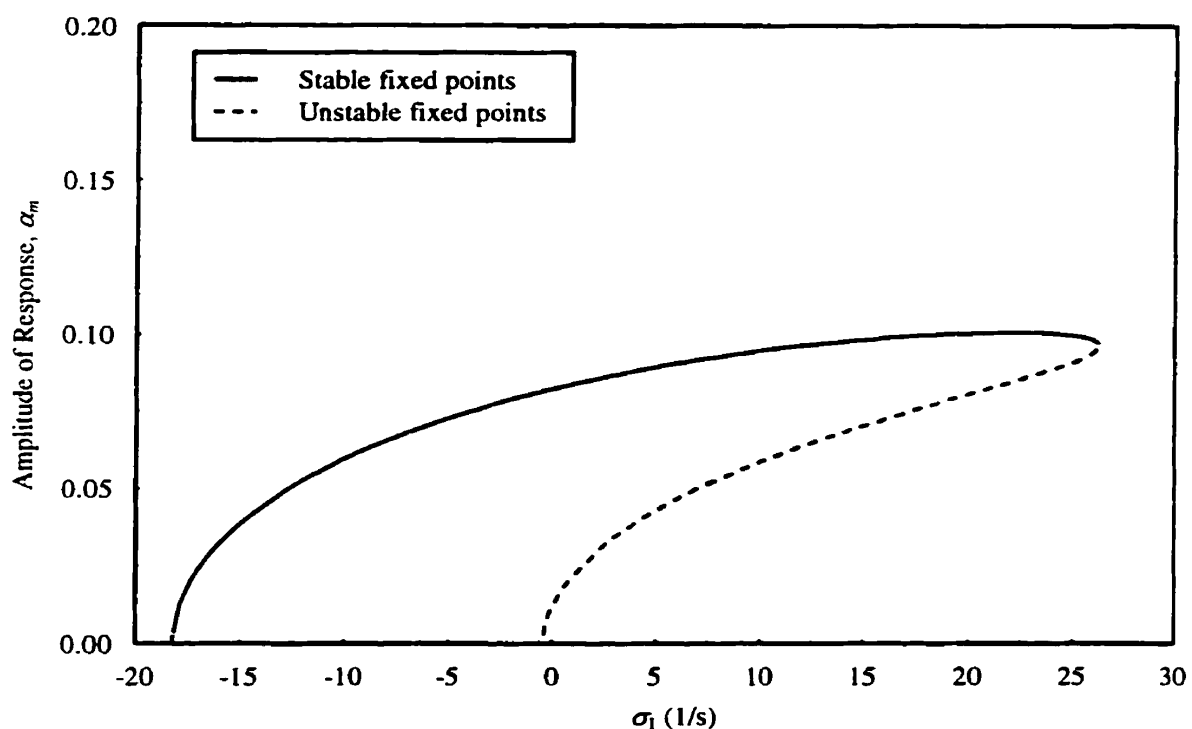
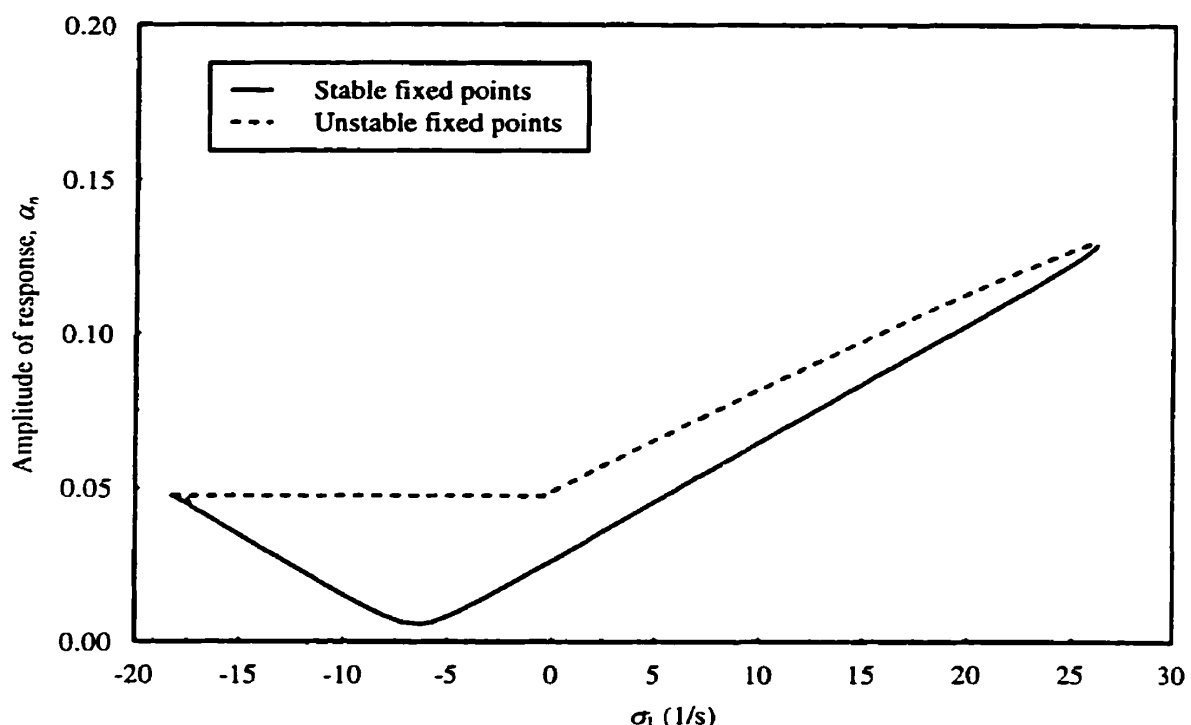


Figure 11.16: Relation between responses of system 5 and internal detuning parameter σ_1 ($\sigma_2=10.0$ 1/s and $F_d=0.5$)

CHAPTER 12

NONLINEAR VIBRATION ANALYSIS OF VISCOELASTIC SERPENTINE BELT DRIVE SYSTEMS

In Chapter 10 and Chapter 11, vibration of *elastic* serpentine belt drive systems is investigated. Modal damping is introduced without reference to damping mechanisms. This chapter discusses the nonlinear vibration of *viscoelastic* serpentine belt drive systems. The Kelvin viscoelastic model is employed to characterize the damping behavior of belt materials. The discretization multiple scales method is then used to determine the dynamic response of belt drive systems. Although the direct multiple scales method seems to be more accurate than the discretization multiple scales method, it is too complicated to apply the direct approach in the nonlinear analysis of viscoelastic systems. Both one-to-one and two-to-one internal resonances combined with a primary external resonance are considered. The effect of damping on dynamic responses is studied.

12.1 EQUATIONS OF MOTION

A prototypical serpentine belt drive system shown in Figure 7.1 is used in the present study. The Kelvin viscoelastic constitutive law is adopted to represent the material property of belts. The entire system is divided into two subsystems: subsystem 1 which includes span 3 only and subsystem 2 which includes all the other components of the whole system. The equations of

motion for subsystem 1 and subsystem 2 are derived in Chapter 7. For subsystem 1, the equation of motion can be compactly written in the operator form as

$$M_3 \ddot{w}_3 + G_3 \dot{w}_3 + K_3 w_3 = P_{d3} w_{3,xx} \quad (12.1)$$

with boundary conditions

$$w_3(0, t) = 0 \quad w_3(l_3, t) = 0 \quad (12.2)$$

For subsystem 2, the equations of motion can be rewritten in the operator form as

$$M \ddot{\mathbf{W}} + G \dot{\mathbf{W}} + K \mathbf{W} = \mathbf{F} - D \dot{\mathbf{W}} \quad (12.3)$$

with boundary conditions

$$w_1(0, t) = 0 \quad w_1(l_1, t) = \chi_3(t) \sin \psi_1 \quad (12.4)$$

$$w_2(0, t) = \chi_3(t) \sin \psi_2 \quad w_2(l_2, t) = 0 \quad (12.5)$$

where D is the damping matrix defined in Chapter 9 and the vector \mathbf{F} includes all non-homogeneous and nonlinear terms:

$$\mathbf{F} = \begin{Bmatrix} P_{d1} w_{1,xx} \\ P_{d2} w_{2,xx} \\ P_{d1NL} - P_{d3NL} + F_{d1} \\ P_{d2NL} - P_{d1NL} \\ -P_{d2NL} \cos \psi_2 - P_{d1NL} \cos \psi_1 \\ P_{d3NL} - P_{d2NL} + F_{d4} \end{Bmatrix} \quad (12.6)$$

The total dynamic tension P_{di} in each span can be separated into the linear component P_{diL} and the nonlinear component P_{diNL}

$$P_{di} = P_{diL} + P_{diNL} \quad (12.7)$$

$$P_{d1L} = k_1(\chi_3 \cos \psi_1 + \chi_2 - \chi_1) + d_1(\dot{\chi}_3 \cos \psi_1 + \dot{\chi}_2 - \dot{\chi}_1) \quad (12.8)$$

$$P_{d2L} = k_2(\chi_3 \cos \psi_2 + \chi_4 - \chi_2) + d_2(\dot{\chi}_3 \cos \psi_2 + \dot{\chi}_4 - \dot{\chi}_2) \quad (12.9)$$

$$P_{d3L} = k_3(\chi_1 - \chi_4) + d_3(\dot{\chi}_1 - \dot{\chi}_4) \quad (12.10)$$

$$P_{diNL} = \frac{EA}{2l_i} \int_0^{l_i} w_{i,x}^2 dx + \frac{\eta A}{l_i} \int_0^{l_i} w_{i,x} \dot{w}_{i,x} dx \quad (12.11)$$

Note that damping terms are added to the linear dynamic tension and the nonlinear dynamic tension. Equations (12.1) and (12.3) provide the basis for the perturbation analysis.

12.2 DISCRETIZATION MULTIPLE SCALES METHOD

To apply the discretization multiple scales method, equations (12.1) and (12.3) must be discretized first using appropriate eigenfunctions. The eigenvalues and eigenfunctions of linear damped serpentine belt drive systems are derived in Chapter 9. However, since the eigenvalue is not pure imaginary, it is difficult to use the eigenfunctions of damped systems as the base functions of modal expansions for the perturbation analysis. Therefore, eigenfunctions for undamped systems used in Chapter 10 are employed in the present chapter and only the eigenfunctions of those modes involving internal resonances are adopted in the expressions of solutions, that is,

$$w_3 = \eta_m^R \phi_m^R + \eta_m' \phi_m' \quad (12.12)$$

$$\mathbf{W} = \xi_n^R \phi_n^R + \xi_n' \phi_n' \quad (12.13)$$

Substituting equations (12.12) and (12.13) into (12.1) and (12.3), taking the inner product with vectors $(\phi_m^R, \phi_m')^T$ and $(\phi_n^R, \phi_n')^T$, respectively, and applying the orthogonal conditions yield

$$\dot{\xi}_n^R - \omega_n \xi_n' = q_n^R \quad (12.14)$$

$$\dot{\xi}_n' + \omega_n \xi_n^R = q_n' - d_n \xi_n' \quad (12.15)$$

$$\dot{\eta}_m^R - \lambda_m \eta_m' = q_{m3}^R \quad (12.16)$$

$$\dot{\eta}_m' + \lambda_m \eta_m^R = q_{m3}' \quad (12.17)$$

where

$$d_n = \omega_n^2 \langle \hat{\chi}_n, D\hat{\chi}_n \rangle \quad (12.18)$$

$$\hat{\chi}_n = (\hat{\chi}_{1n} \quad \hat{\chi}_{2n} \quad \hat{\chi}_{3n} \quad \hat{\chi}_{4n})^T \quad (12.19)$$

$$q_n^R = g_1 (\xi_n^R)^2 + g_2 \xi_n^R \xi_n' + g_{17} (\xi_n')^2 + g_3 (\xi_n^R)^3 + g_4 (\xi_n^R)^2 \xi_n' + g_5 \xi_n^R (\xi_n')^2 + g_6 (\xi_n')^3 \quad (12.20)$$

$$\begin{aligned} q_n' = & g_7 (\xi_n^R)^2 + g_8 \xi_n^R \xi_n' + g_9 (\xi_n')^2 + g_{10} (\eta_m^R)^2 + g_{11} \eta_m^R \eta_m' + g_{12} (\eta_m')^2 \\ & + g_{13} (\xi_n^R)^3 + g_{14} (\xi_n^R)^2 \xi_n' + g_{15} \xi_n^R (\xi_n')^2 + g_{16} (\xi_n')^3 + \omega_n (F_{d1} \hat{\chi}_{1n} + F_{d4} \hat{\chi}_{4n}) \end{aligned} \quad (12.21)$$

$$\begin{aligned} q_{m3}^R = & h_1 \xi_n^R \eta_m^R + h_2 \xi_n^R \eta_m' + h_{13} \xi_n' \eta_m^R + h_{14} \xi_n' \eta_m' \\ & + h_3 (\eta_m^R)^3 + h_4 (\eta_m^R)^2 \eta_m' + h_5 \eta_m^R (\eta_m')^2 + h_6 (\eta_m')^3 \end{aligned} \quad (12.22)$$

$$\begin{aligned} q_{m3}' = & h_7 \xi_n^R \eta_m^R + h_8 \xi_n^R \eta_m' + h_{15} \xi_n' \eta_m^R + h_{16} \xi_n' \eta_m' \\ & + h_9 (\eta_m^R)^3 + h_{10} (\eta_m^R)^2 \eta_m' + h_{11} \eta_m^R (\eta_m')^2 + h_{12} (\eta_m')^3 \end{aligned} \quad (12.23)$$

Note that there are no linear damping terms in equations (12.16) and (12.17) for the Kelvin viscoelastic model. This is because the expression of strain for subsystem I is a nonlinear function of the transverse displacement. From equations (12.20) – (12.23), it is seen that there are additional terms $g_{17} (\xi_n')^2$, $h_{13} \xi_n' \eta_m^R$, $h_{14} \xi_n' \eta_m'$, $h_{15} \xi_n' \eta_m^R$ and $h_{16} \xi_n' \eta_m'$ for viscoelastic belts drive systems. The definitions of g_i and h_i for viscoelastic systems, which are shown in Appendices A and B, are also different from those for elastic systems.

The multiple scales method can then be used to treat the ordinary differential equations (12.14) – (12.17). Using the same procedure as in Chapter 10, the dynamic response for both one-to-one

and two-to-one internal resonance can be obtained. The equations of amplitude and phase of steady state response for viscoelastic systems are identical to equations for elastic system. However, the expressions of s_i , t_i , $\hat{\Theta}_i$, and $\tilde{\Theta}_i$ for viscoelastic systems (see Appendices C and D), are different from those of elastic systems.

12.3 NUMERICAL RESULTS AND DISCUSSIONS

In this section, example results are presented to highlight the significant effect of damping introduced by the viscoelastic constitutive relation. The steady state responses under different belt damping ratio are compared. Both one-to-one and two-to-one internal resonances are studied.

12.3.1 One-to-one Internal Resonance

The damping constant d_i ($i=1,3$) introduced by the Kelvin viscoelastic model may be linked with spring constant k_i ($i=1,3$) through an experimentally determined damping constant δ :

$$d_i = \delta k_i \quad (12.24)$$

where δ for a typical production belt can range from 0.00001 to 0.01 (Kraver *et al.*, 1996). A comparison is made between two different values of δ , $\delta = 0.0001$ and $\delta = 0.0005$. The damping constant, d_4 , which results from viscous and coulomb damping, is set at 24.02 N s/m.

System 2 introduced in Section 10.7.1 is used in this simulation. The operating speed is 2000 RPM. The natural frequency of the first transverse mode of span 3 is calculated as 28.1104 Hz

and the natural frequency of the first rotationally dominant mode is 29.0590 Hz.

In the case of $\alpha_m \neq 0$, the solution curves for α_n and α_m versus σ_2 are shown in Figure 12.1. The damping constant δ is chosen as 0.0001. It is seen that two branch curves exist for α_n within certain range of detuning parameter σ_2 . There always exist two steady state solutions for α_n within the range where non-trivial solutions exist. Two steady state solutions are possible for α_m within a certain range of σ_2 values. There is one set of Hopf bifurcation emanating from the steady state solutions, which lead to oscillating amplitudes and phases. Comparing Figure 12.1 for the viscoelastic system and Figure 10.12 for the elastic system shows that the solutions of α_n for both systems are similar while the solutions of α_m are different. For viscoelastic systems, cubic nonlinearity appears to dominate the steady state response.

Figure 12.2 shows the effect of the internal detuning parameter σ_1 on the dynamic responses of system 2. The external detuning parameter σ_2 is set at 6.0 1/s and the excitation amplitude is set at 0.5. It is seen that the curve α_m versus σ_1 is very similar to the curve α_m versus σ_2 . There exist two steady state solutions α_m within a certain range of σ_1 values. With the increase of σ_1 , the two steady state solutions α_m grow. It is clear that the amplitude α_m of transverse vibration of subsystem 1 is greater than α_n of rotational vibration of subsystem 2. This is because no damping terms are introduced to the equations of motion for subsystem 1.

The influence of the amplitude of excitation on the dynamic response of system 2 is illustrated in

Figure 12.3. The external detuning parameter σ_2 is chosen as 6.0 1/s and the internal detuning parameter σ_1 is 5.95989 1/s. As the excitation level is increased from low levels, the steady state response is initially zero. When the excitation reaches a certain level, two possible steady state response may exist. The two response amplitudes increase with the growth of excitation amplitude.

The numerical results with damping constant $\delta = 0.0005$ are presented in Figures 12.4 – 12.6. It is seen that no Hopf bifurcation exists for higher damping constant. Comparison between the results with $\delta = 0.0001$ and $\delta = 0.0005$ shows that the damping introduced by viscoelasticity has a great influence on system response. With the increase of damping constant, the steady state response decreases significantly. Moreover, the region where non-trivial solutions exist narrows with the growth of damping. These results indicate that by increasing the damping constant, an unstable belt drive system can be stabilized.

12.3.2 Two-to-one Internal Resonance

System 5 introduced in Section 10.7.2 is used in this simulation. The operating speed for the system is 2000 RPM. The frequency of the first transverse mode of span 3 is 28.1104 Hz and the frequency of the first rotationally dominant mode is 57.4120 Hz. Two different values of δ , $\delta = 0.00005$ and $\delta = 0.0001$, are chosen to study the influence of damping. d_4 is set at 5.31 Ns/m.

The steady state responses with $\delta = 0.00005$ are shown in Figures 12.7 – 12.9 and the steady

state solutions with. $\delta = 0.0001$ are illustrated in Figures 12.10 – 12.12. It is evident that no Hopf bifurcation occurs for the two damping constants. Curves of α_n and α_m versus σ_2 with $\delta = 0.00005$ are similar to that of the corresponding elastic system while the curves with $\delta = 0.0001$ are quite different from those of the elastic system. The steady state response decreases with the growth of damping constant. The results of the viscoelastic model appear to agree with the experimental results better than the results of the elastic model.

12.4 SUMMARY AND CONCLUSIONS

In this chapter, the discretization multiple scales method is employed for the analysis of nonlinear vibration of viscoelastic serpentine belt drive systems. The Kelvin model is used to represent the elastic and damping behavior of belt materials. The nonlinear equations of motion are discretized using the eigenfunctions of linear undamped problems.

The damping introduced by the Kelvin viscoelastic model plays an important role in the dynamic response of serpentine belt drive systems. It is possible to predict a desirable damping value that can significantly reduce the vibration level and stabilize an unstable belt drive system. The viscoelastic model can be used to accurately represent the damping mechanism of belt materials. The numerical results of viscoelastic systems agree much better with the experimental results (Beikmann *et al.*, 1996) than those of elastic systems.

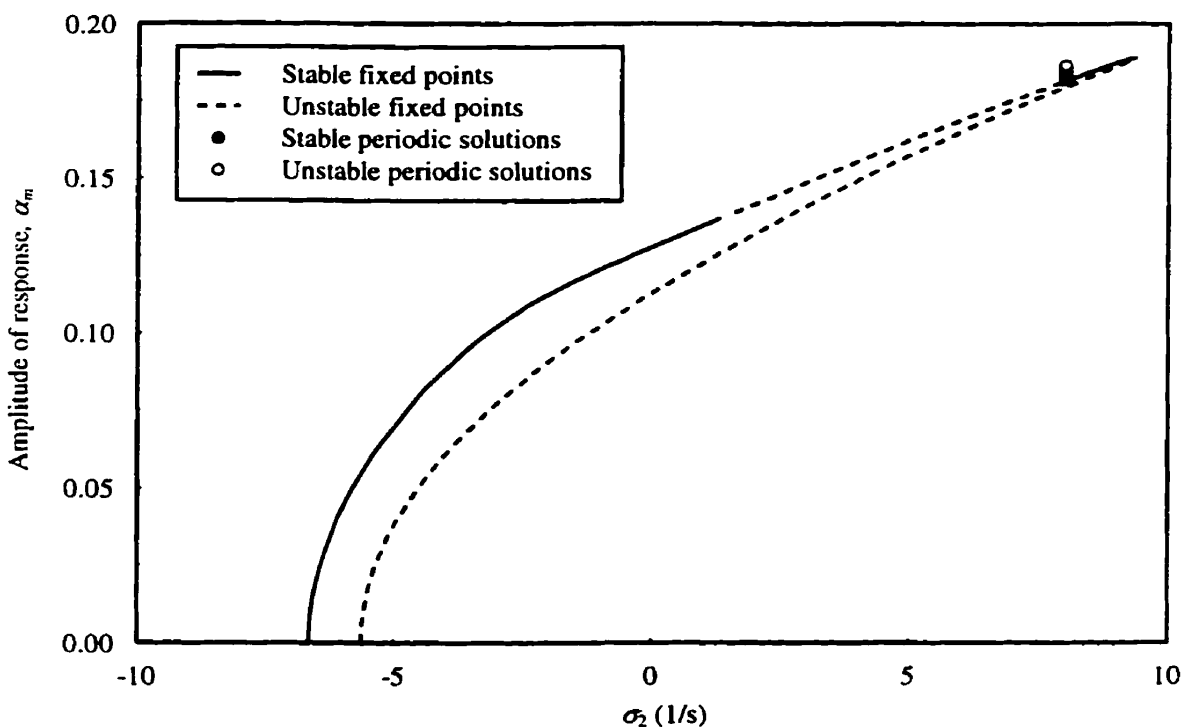
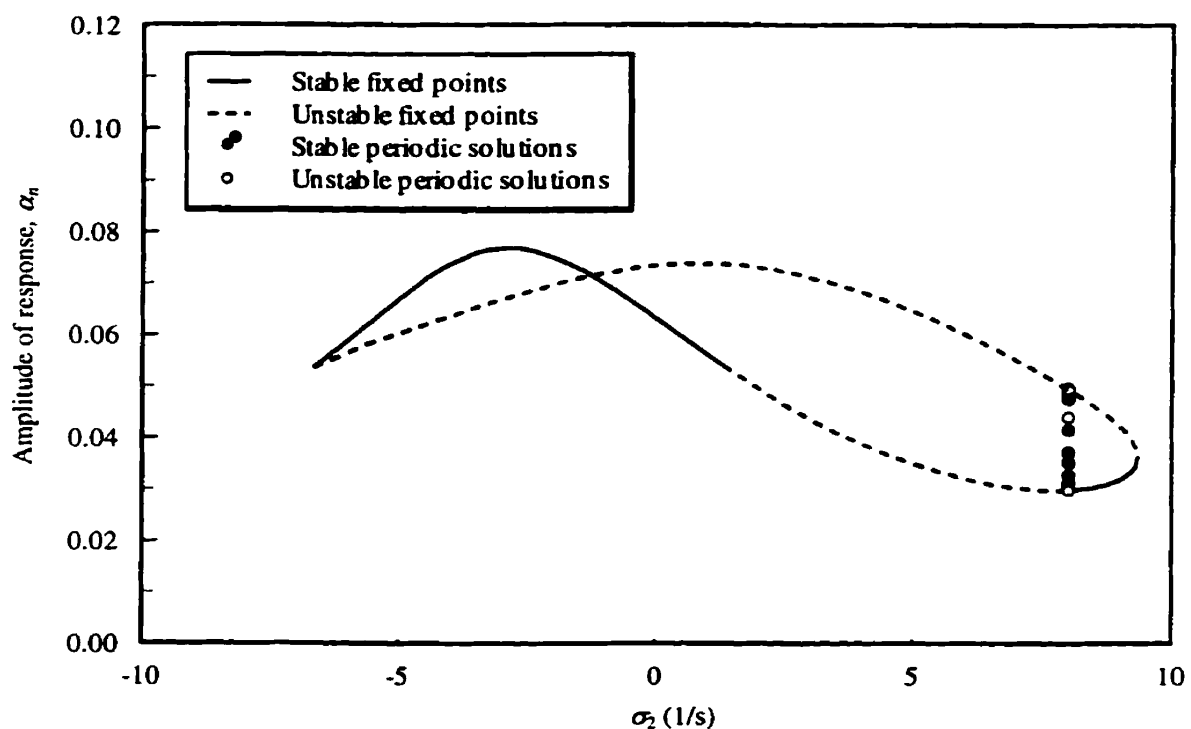


Figure 12.1: Response-frequency curves of system 2 for $\delta = 0.0001$

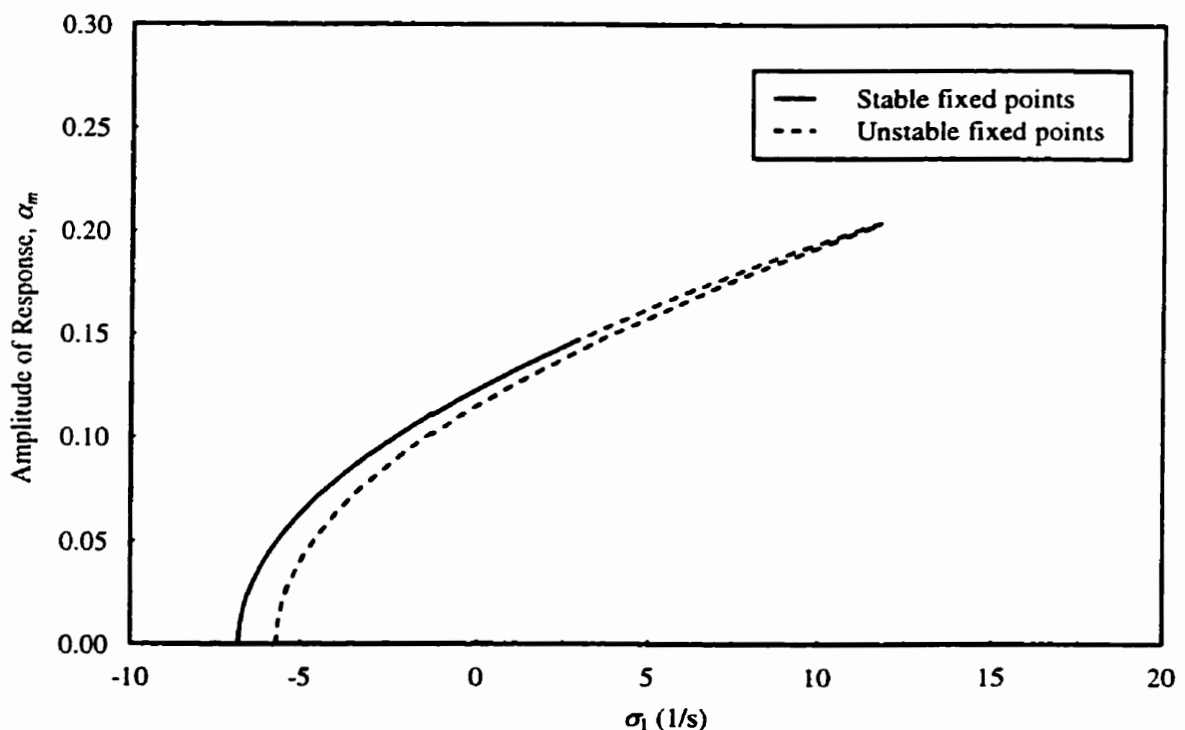
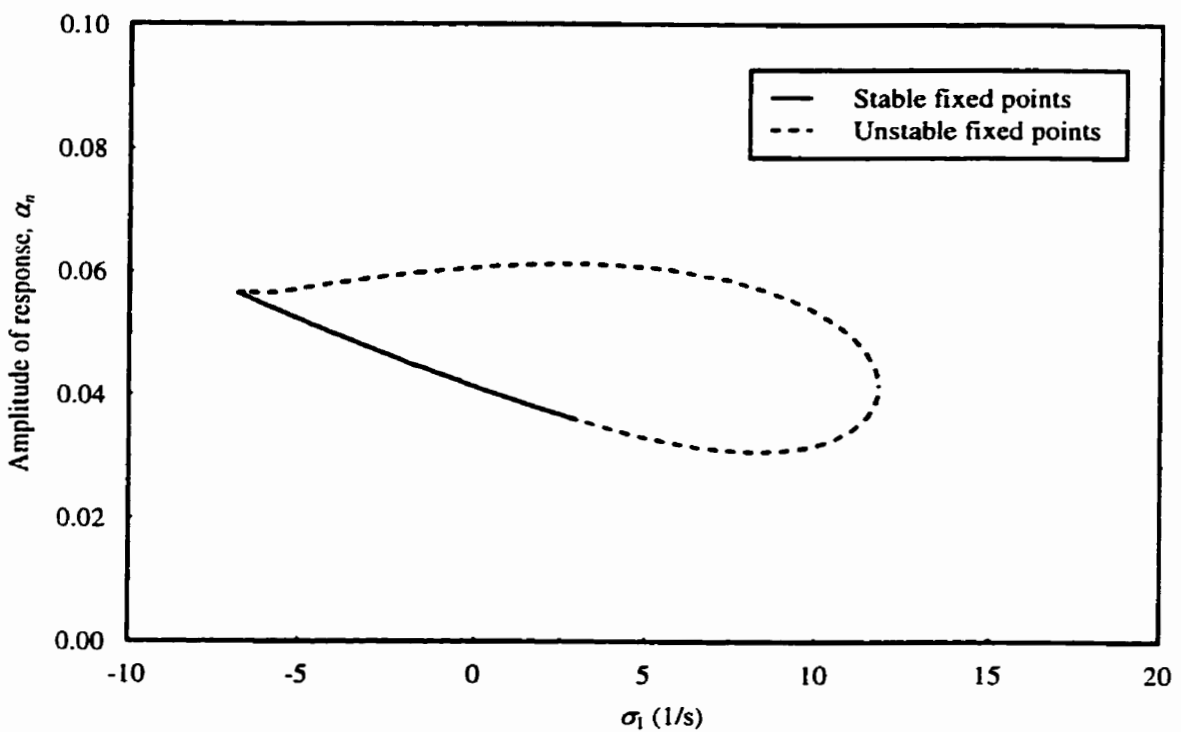


Figure 12.2: Relation between responses of system 2 and parameter σ_1 for $\delta = 0.0001$
 $(\sigma_2=6.0 \text{ 1/s and } F_d=0.5)$

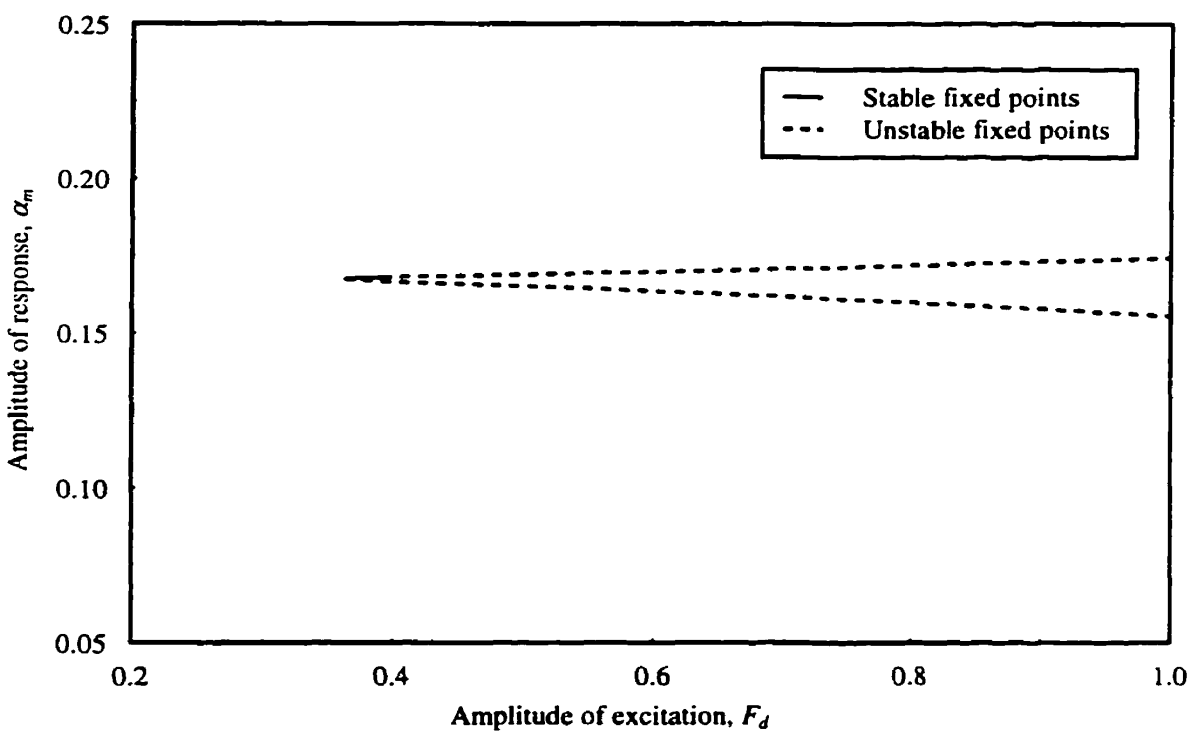
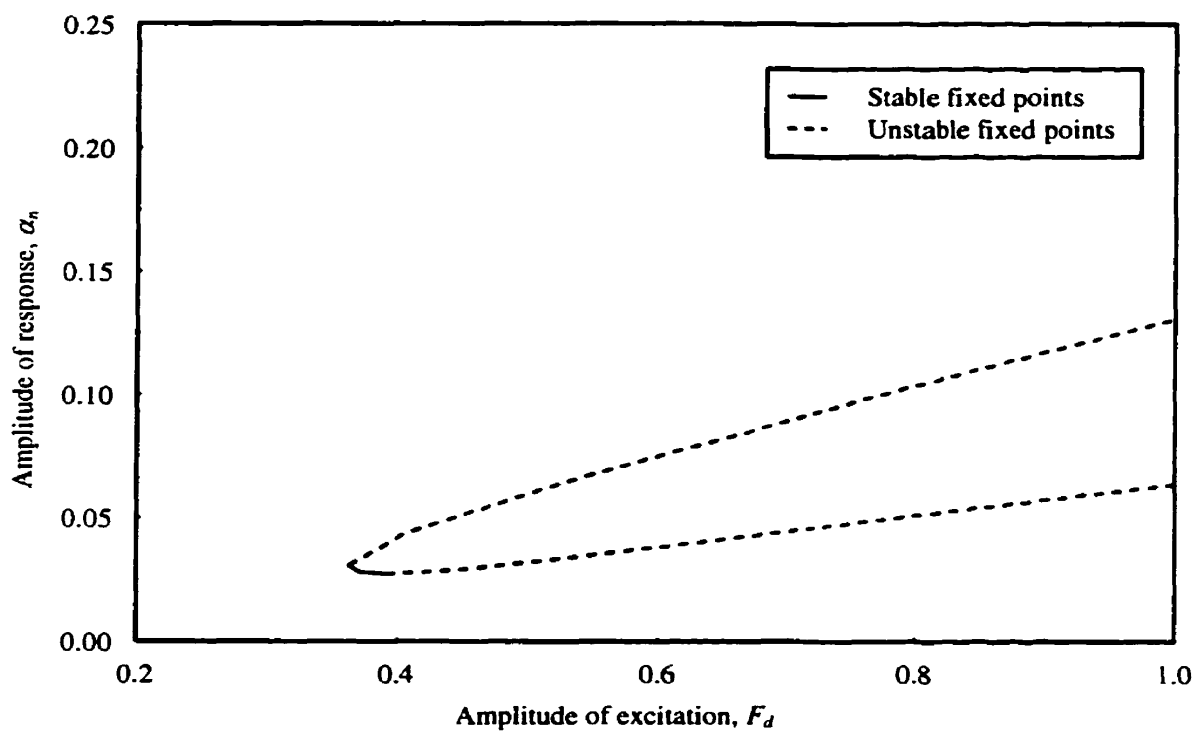


Figure 12.3: Response-excitation curves of system 2 for $\delta = 0.0001$
 $(\sigma_1=5.95989 \text{ l/s and } \sigma_2=6.0 \text{ l/s})$

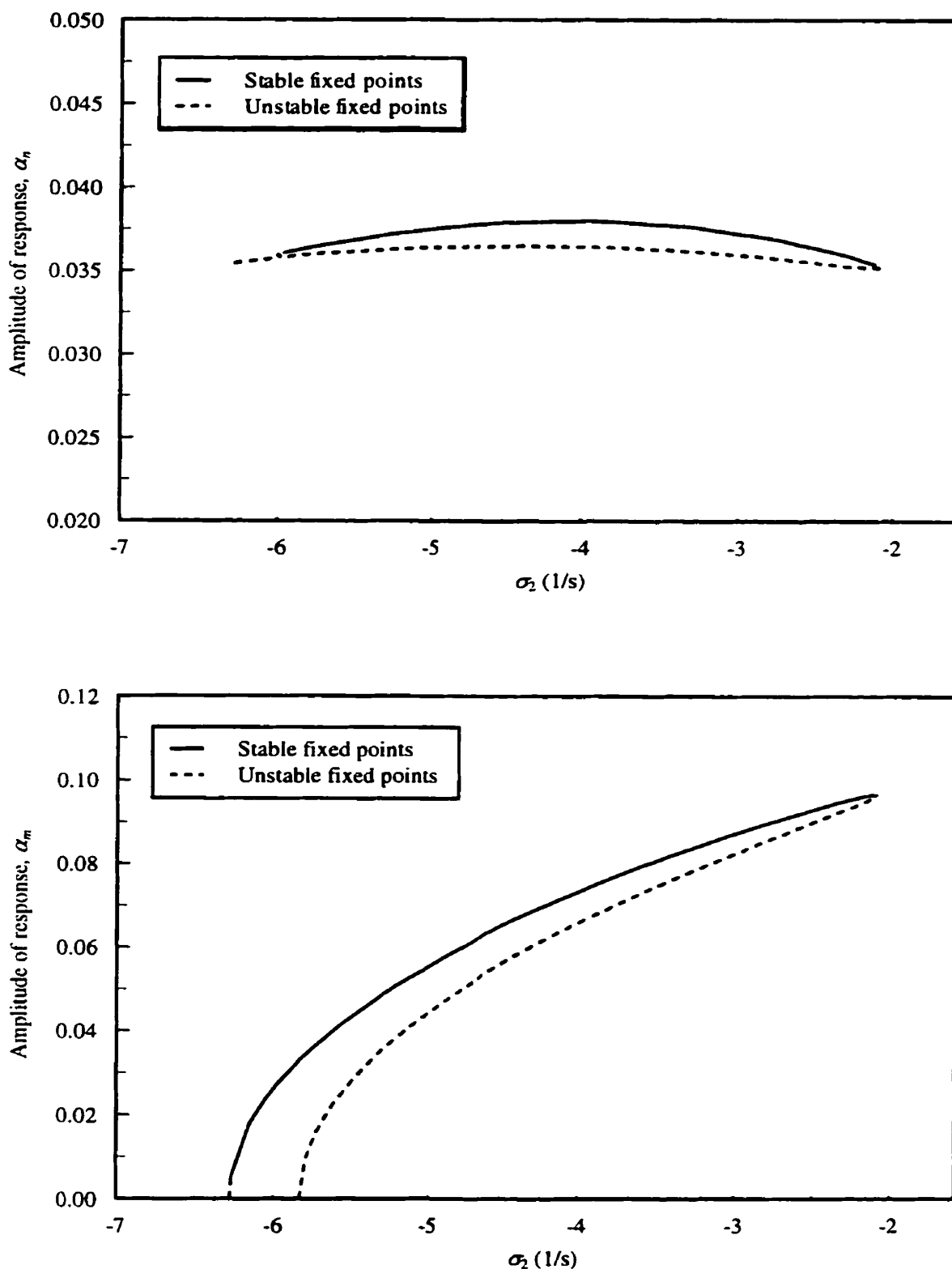


Figure 12.4: Response-frequency curves of system 2 for $\delta = 0.0005$

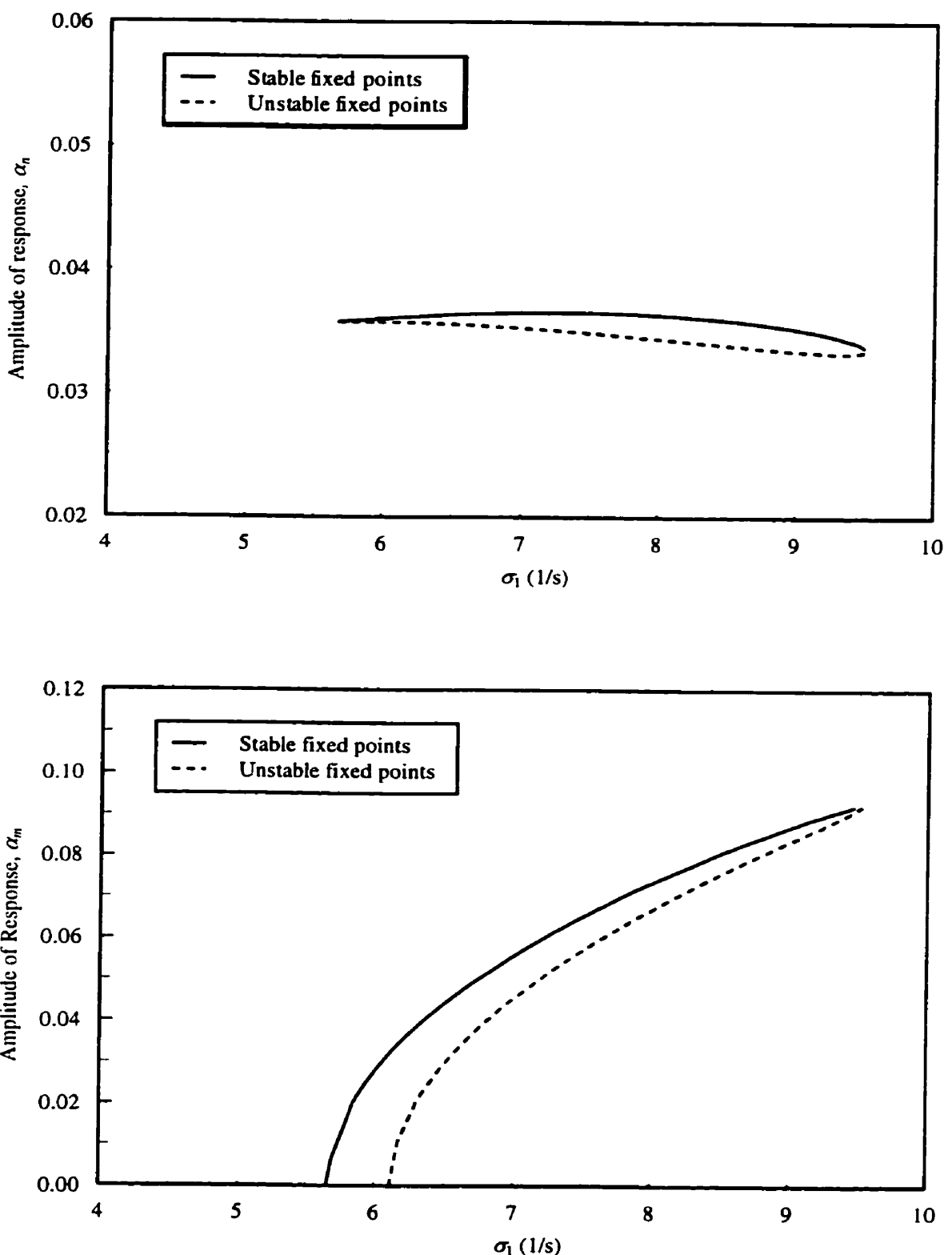


Figure 12.5: Relation between responses of system 2 and parameter σ_1 for $\delta = 0.0005$
 $(\sigma_2 = -6.0 \text{ } 1/\text{s} \text{ and } F_s = 0.5)$

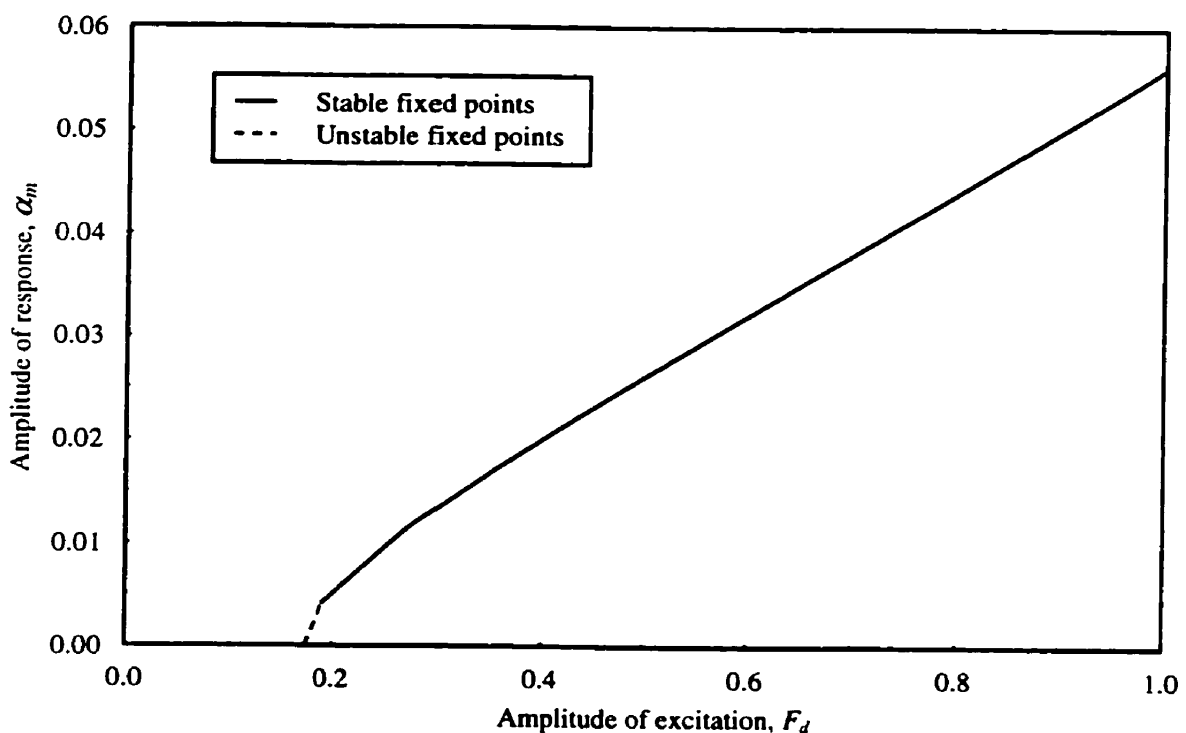
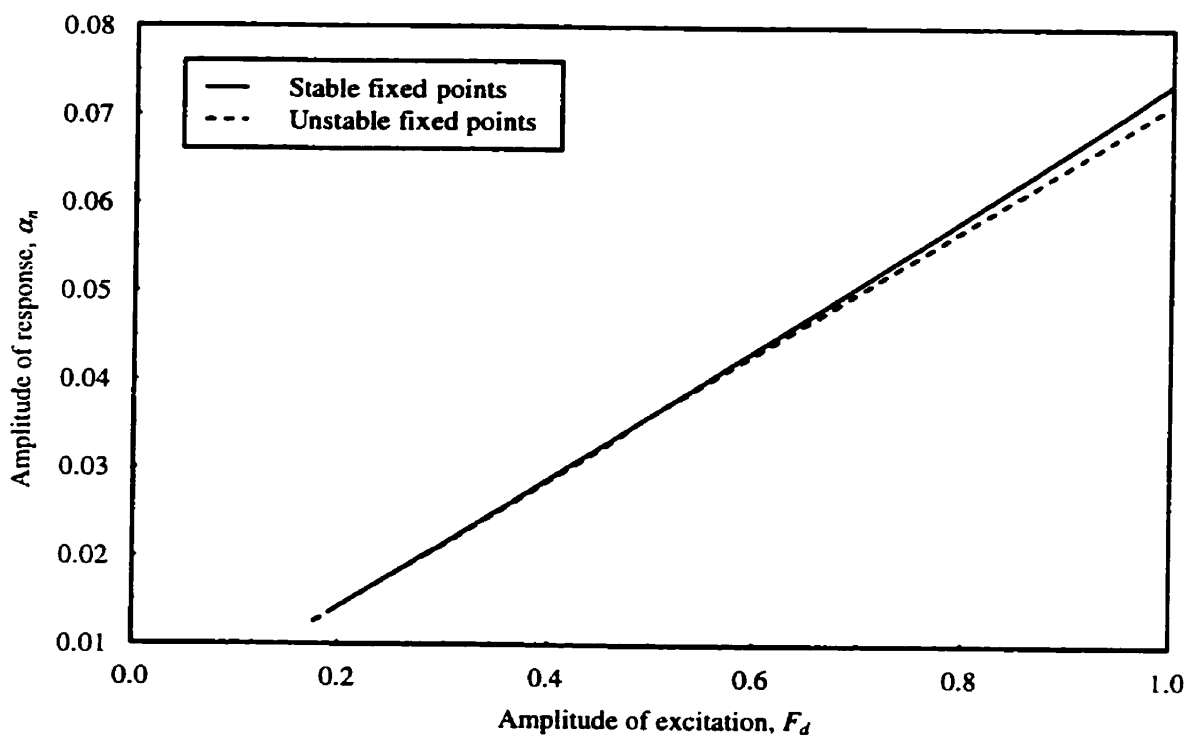


Figure 12.6: Response-excitation curves of system 2 for $\delta = 0.0005$

($\sigma_1=5.95989 \text{ 1/s}$ and $\sigma_2=-6.0 \text{ 1/s}$)

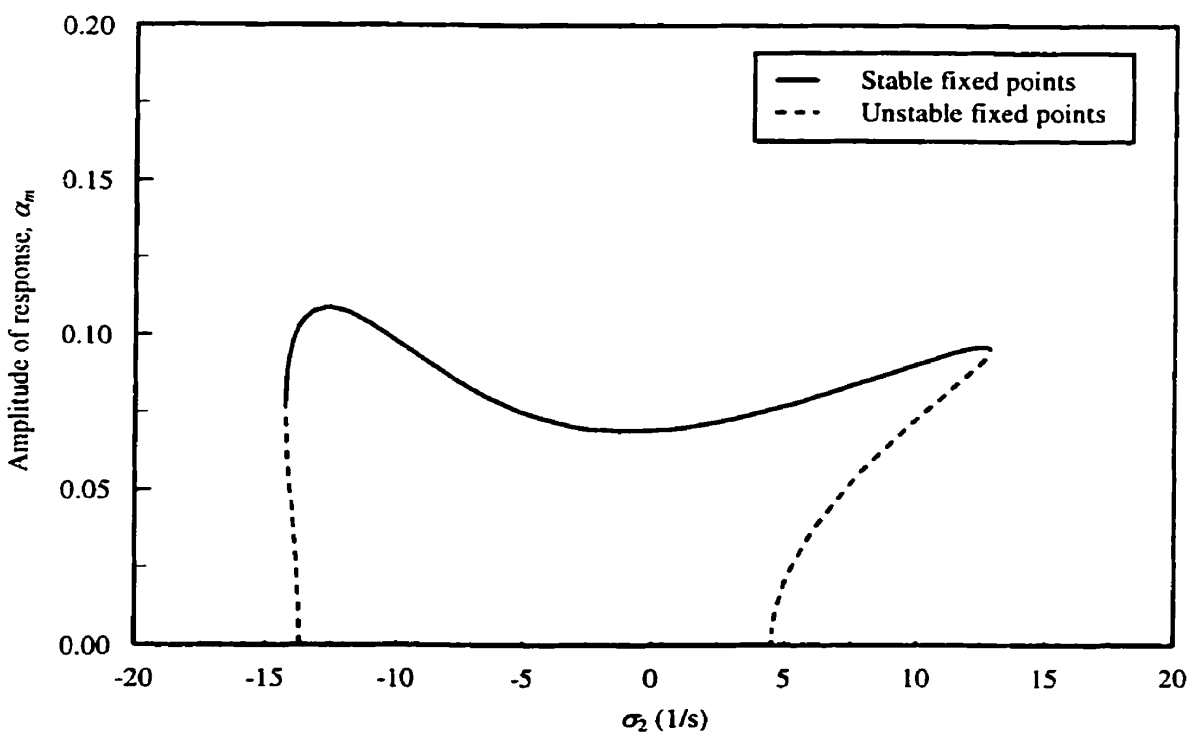
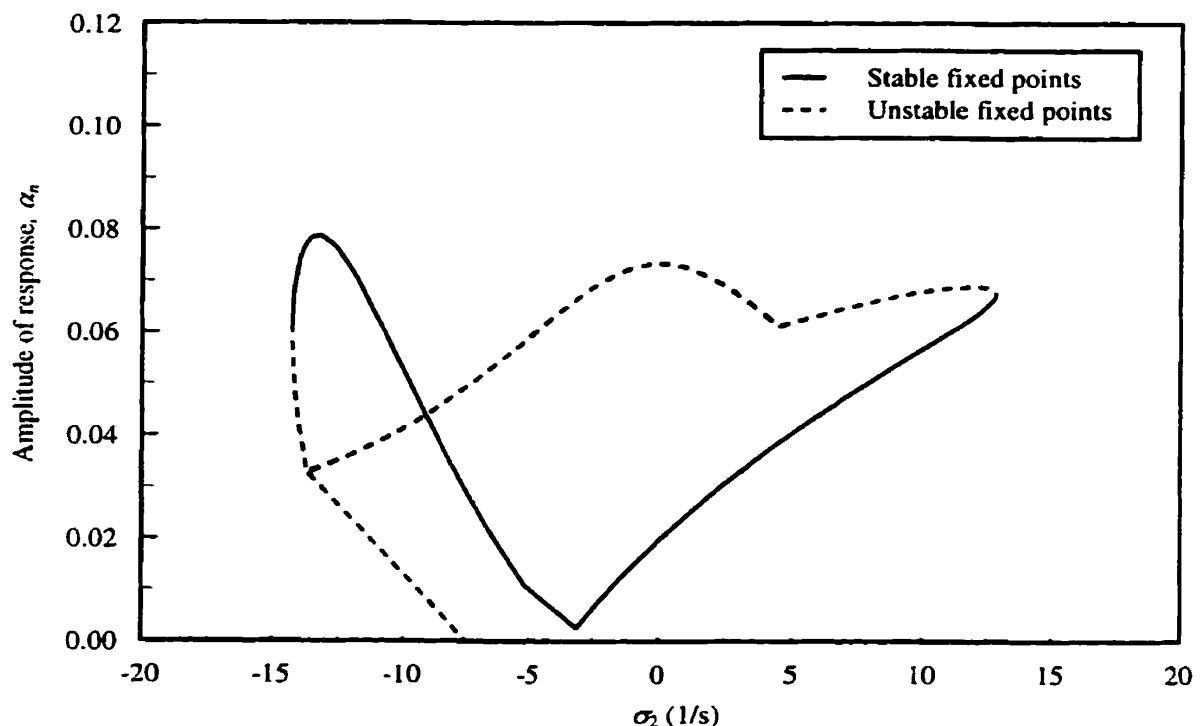


Figure 12.7: Response-frequency curves of system 5 for $\delta = 0.00005$

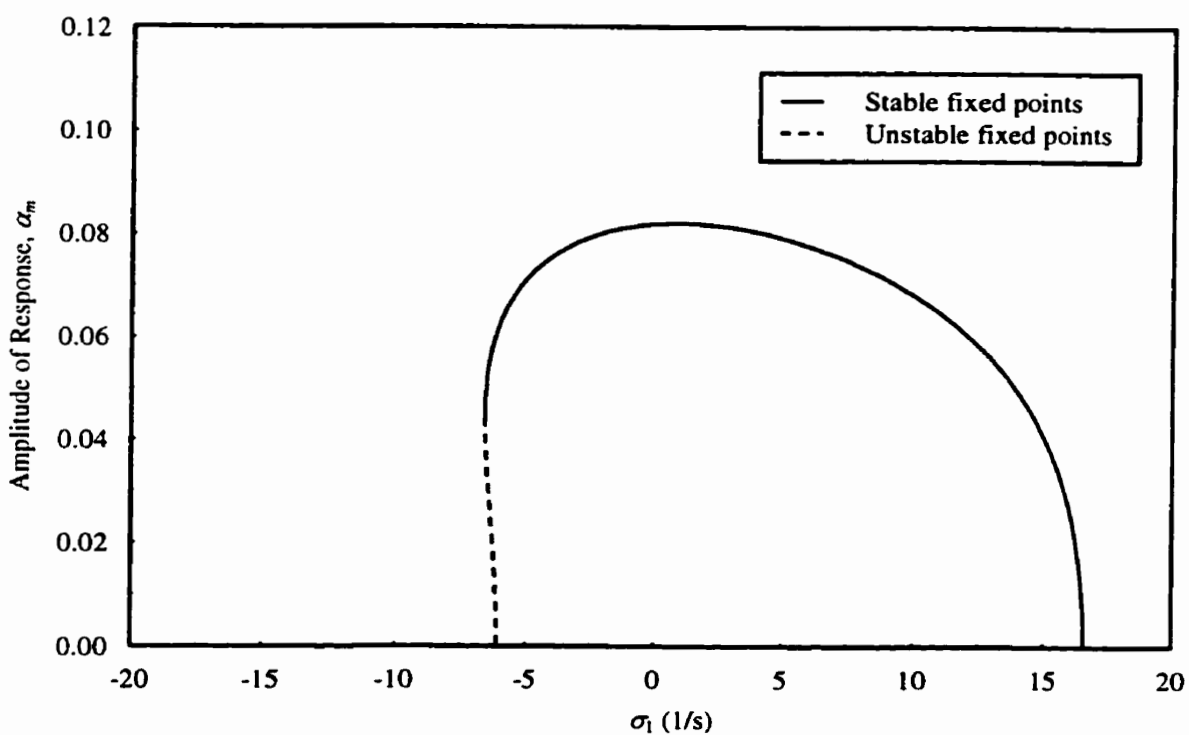
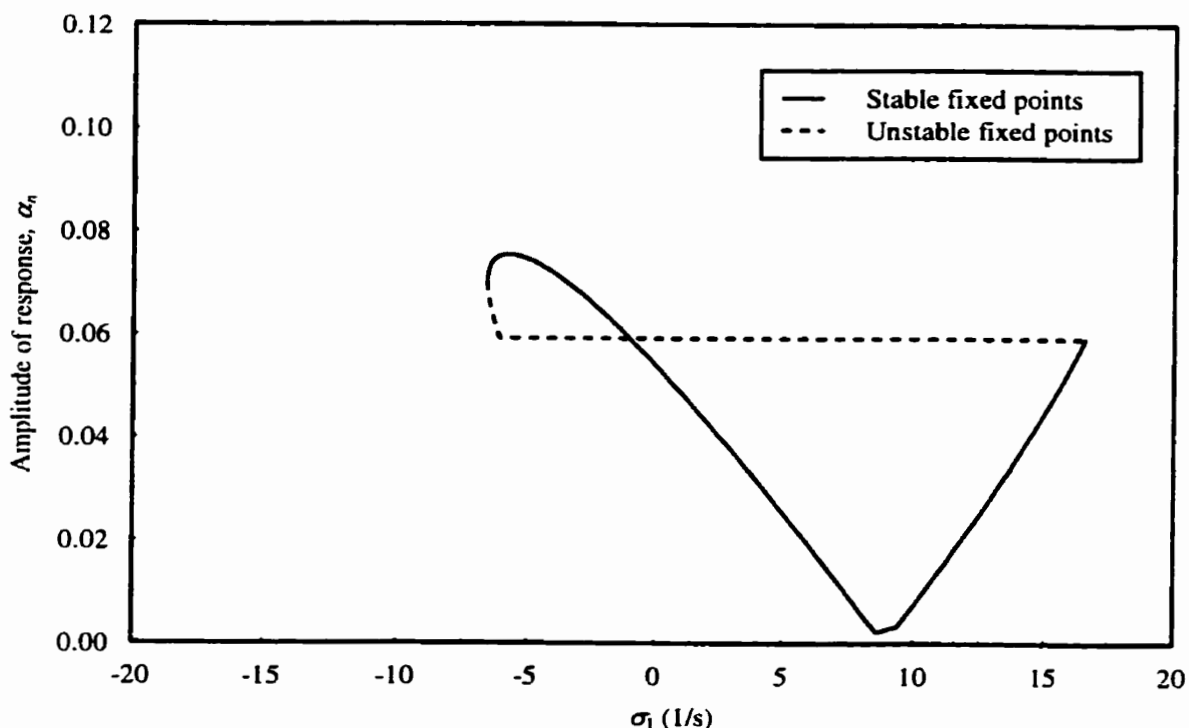


Figure 12.8: Relation between responses of system 5 and parameter σ_1 for $\delta = 0.00005$
 $(\sigma_2 = -5.0 \text{ 1/s} \text{ and } F_d = 0.5)$

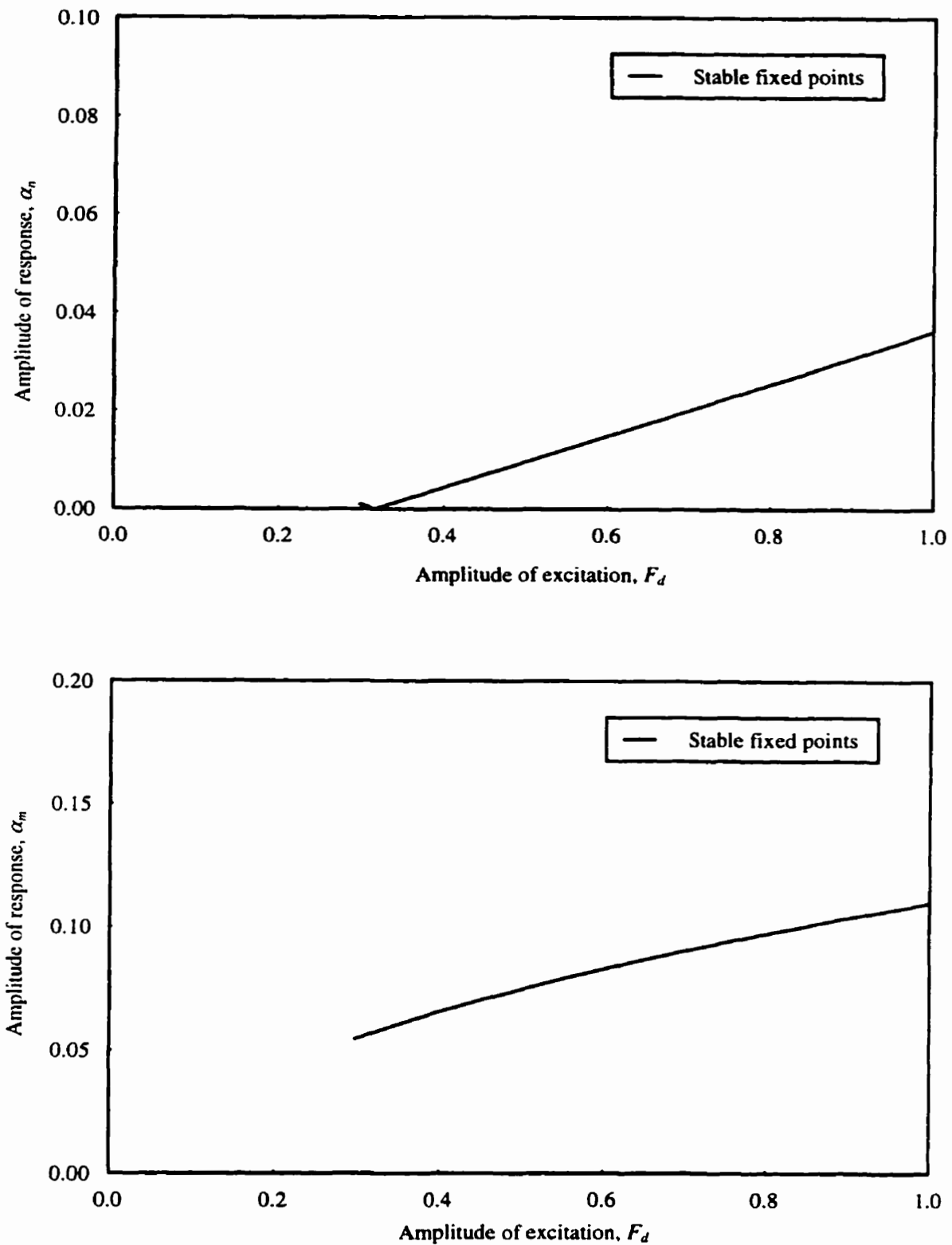


Figure 12.9: Response-excitation curves of system 5 for $\delta = 0.00005$
 $(\sigma_1=7.48379 \text{ l/s and } \sigma_2=-5.0 \text{ l/s})$

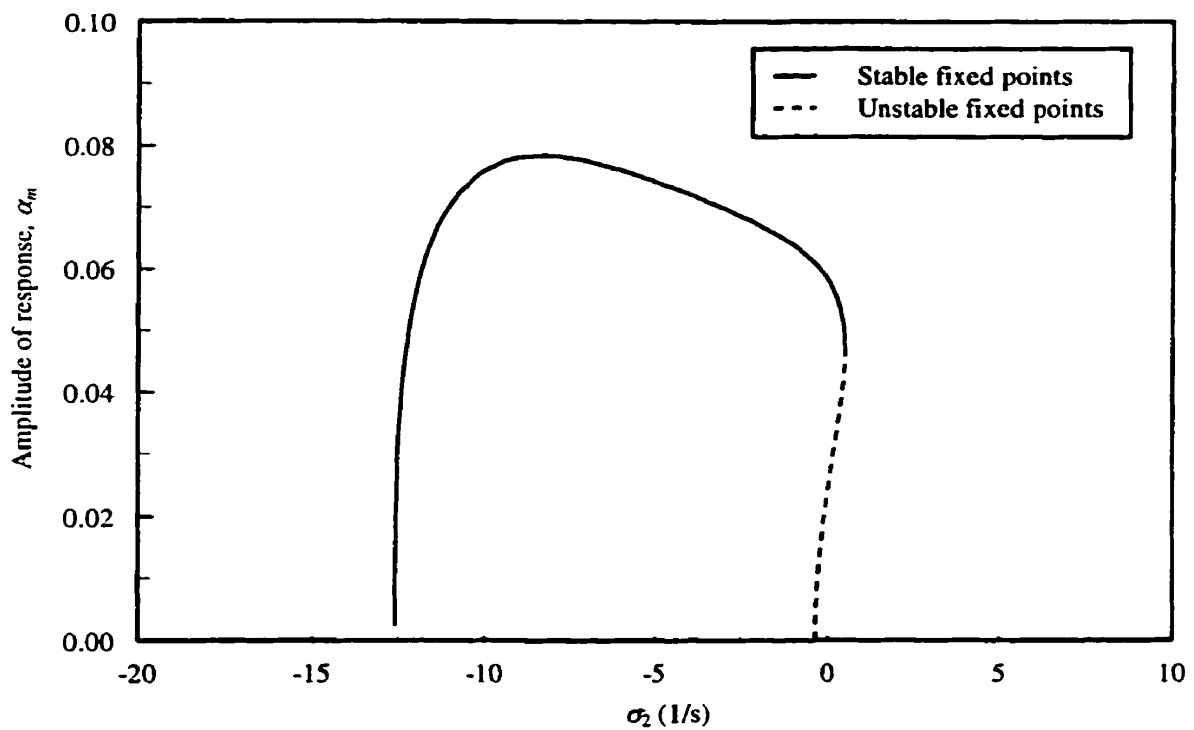
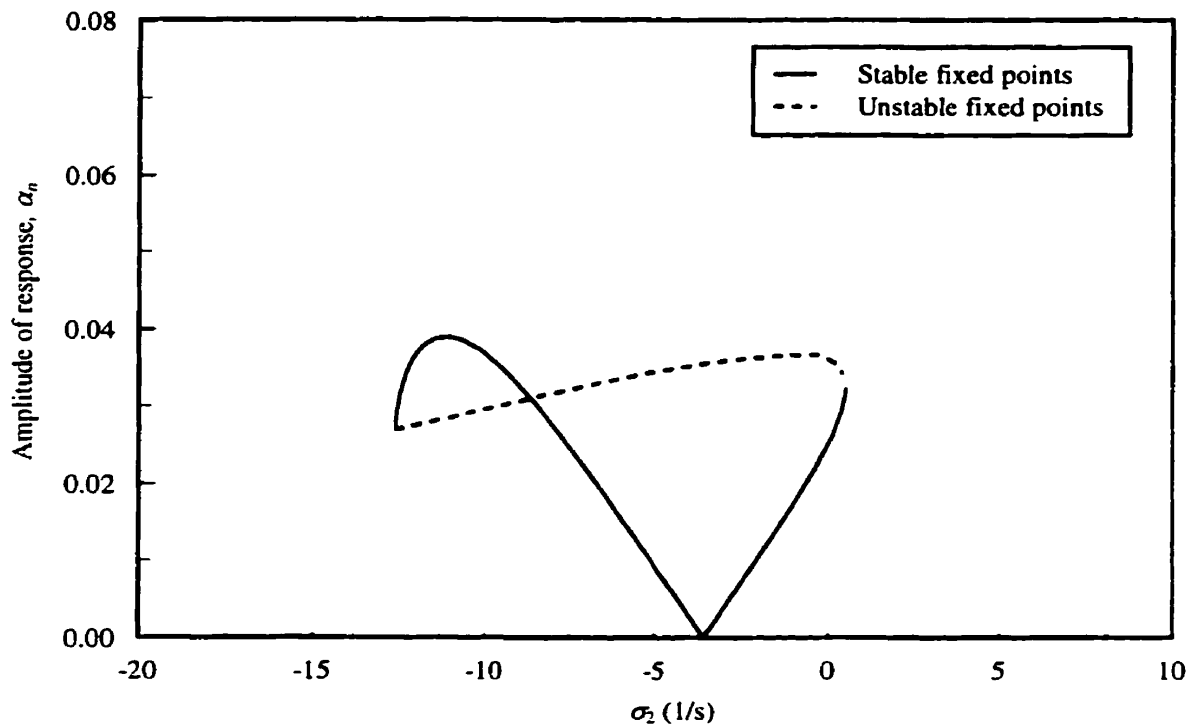


Figure 12.10: Response-frequency curves of system 5 for $\delta = 0.0001$

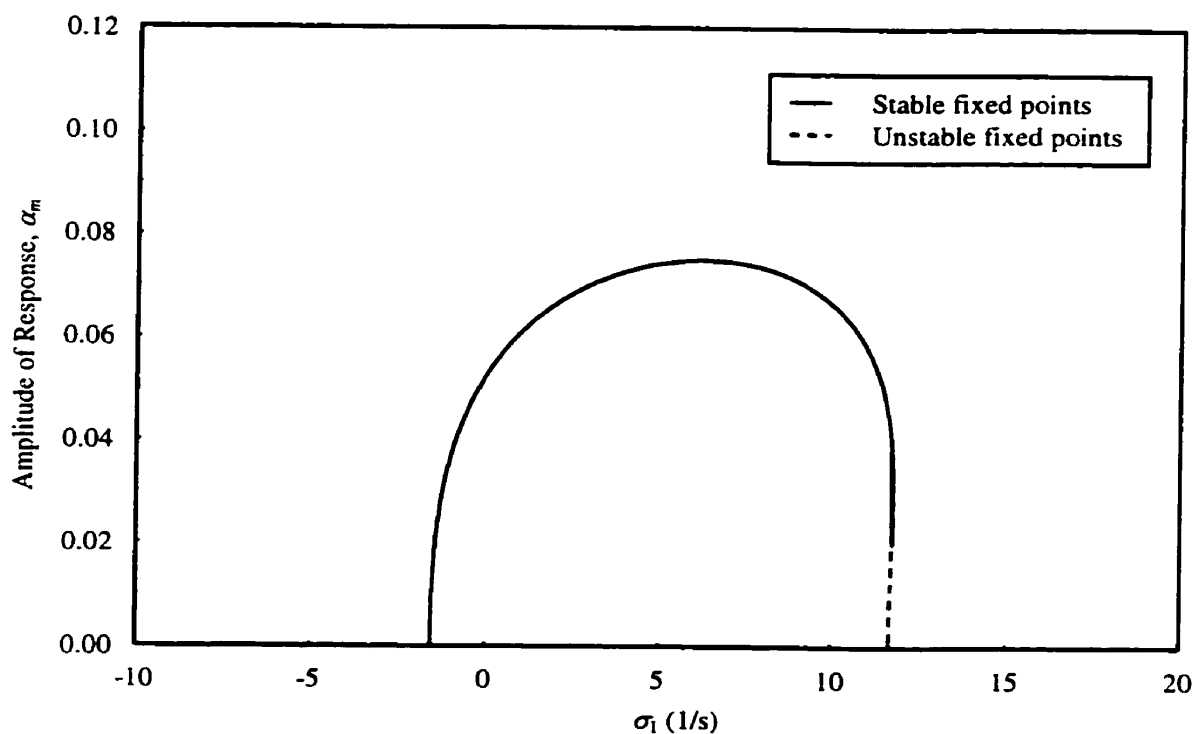
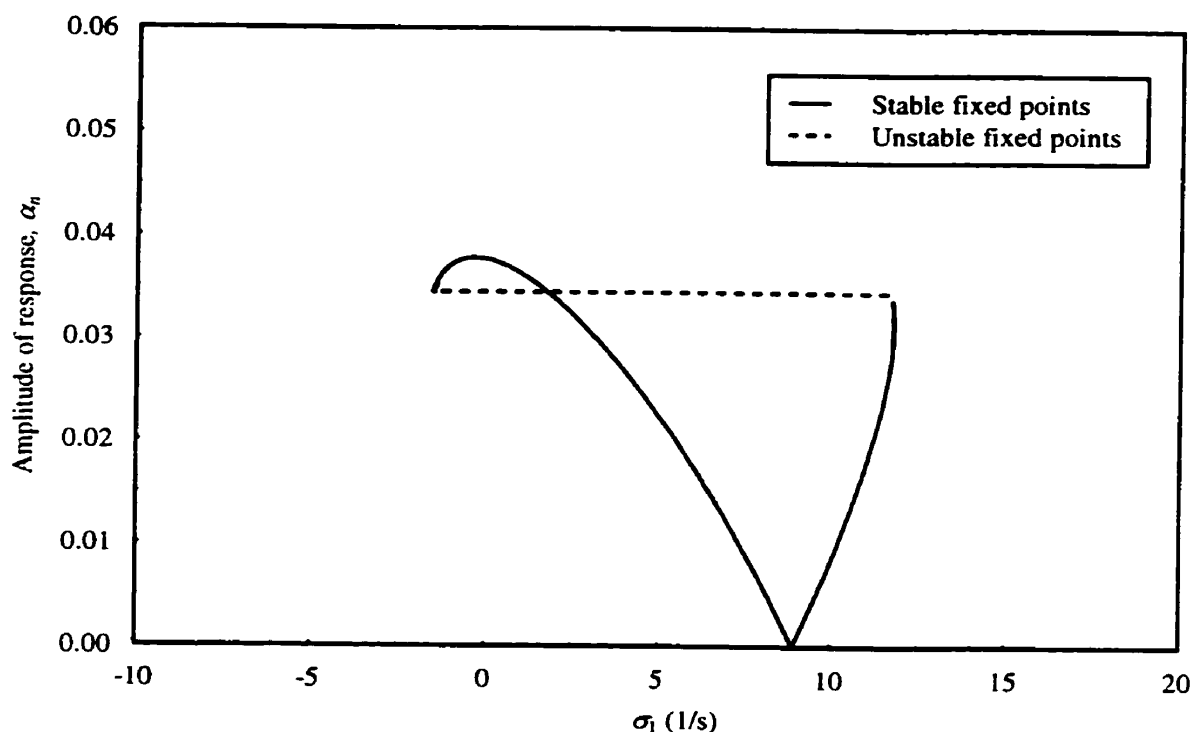
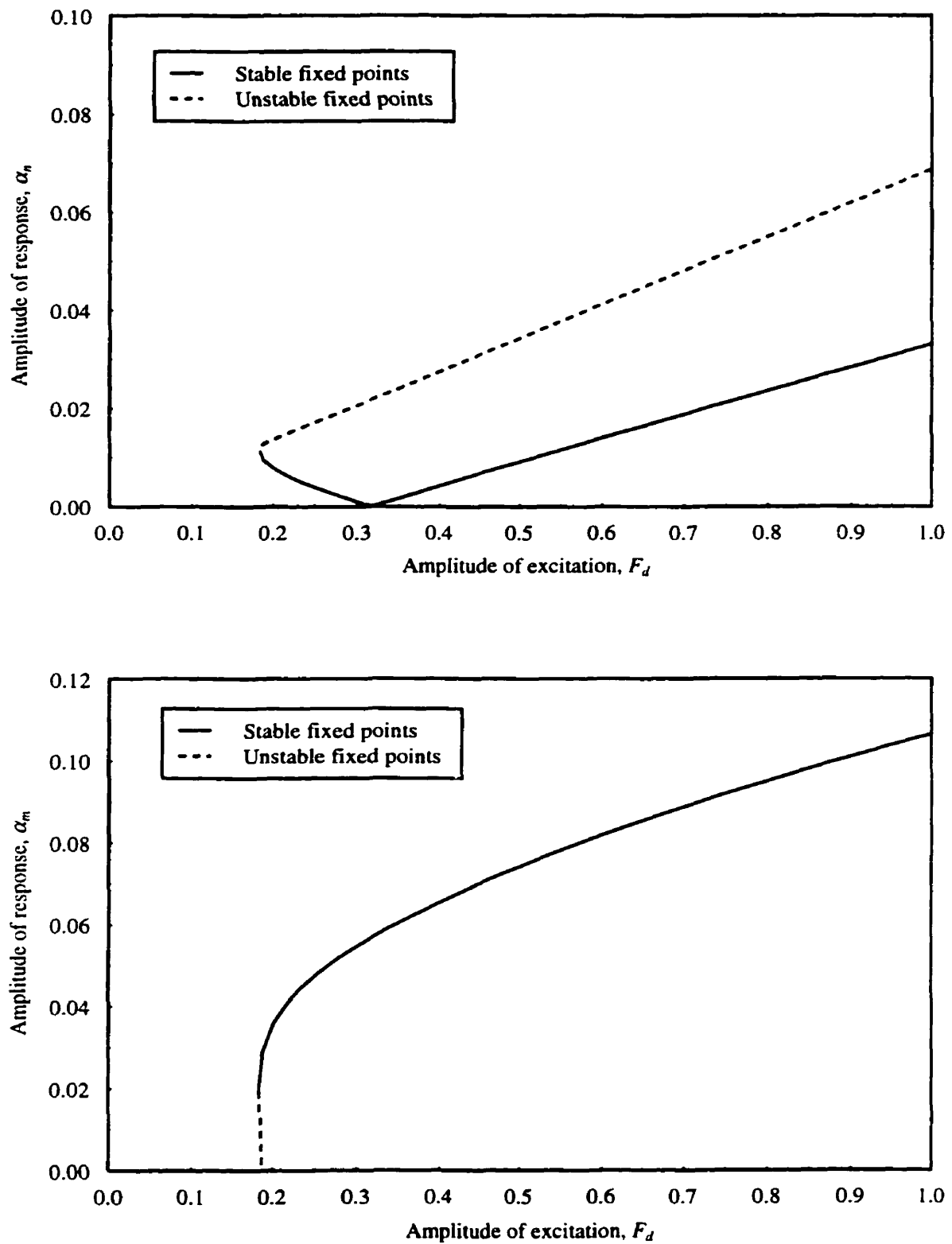


Figure 12.11: Relation between responses of system 5 and parameter σ_1 for $\delta = 0.0001$
 $(\sigma_2 = -5.0 \text{ } 1/\text{s} \text{ and } F_d = 0.5)$



**Figure 12.12: Response-excitation curves of system 5 for $\delta = 0.0001$
 $(\sigma_1=7.48379 \text{ 1/s and } \sigma_2=-5.0 \text{ 1/s})$**

CHAPTER 13

SUMMARY, CONCLUSIONS, RECOMMENDATIONS FOR DESIGN WORK, AND FUTURE WORK

The present chapter summarizes the research of this thesis, proposes general recommendations for design work of serpentine belt drives, and suggest future work in the dynamic study of serpentine belt drive systems.

13.1 SUMMARY AND CONCLUSIONS

The free and forced vibrations of viscoelastic moving belts are studied in Chapter 2 and Chapter 3. Viscoelastic models are proposed to describe the damping mechanism of belt materials. The nonlinear natural frequencies and near-modal nonlinear response for free vibration of viscoelastic elastic moving belts are obtained by using the direct multiple scales method. The amplitude of near- and exact-resonant response is predicted for viscoelastic moving belts excited by the eccentricity of pulleys. The proposed direct multiple scales method does not involve a prior assumption regarding the spatial dependence of the motion. The damping introduced by the viscoelastic model reduces amplitude of response significantly while it has no significant effect on nonlinear natural frequencies of the system. The relation of nonlinear natural frequencies and nonlinear response versus moving speed agrees well with experimental measurements.

The parametric resonance problem is solved in Chapter 4 and Chapter 5. Closed-form expressions are found for the response and existence conditions of the summation parametric resonance. Stability boundaries of the trivial limit cycle for general summation and difference parametric resonance are obtained analytically. The first non-trivial limit cycle is always stable for both viscoelastic and elastic parametric resonance. The second non-trivial limit cycle is unstable for both viscoelastic parametric resonance and for elastic parametric resonance. A major conclusion of this study is that there exists an upper existence boundary for the viscoelastic model and this upper boundary of existence for non-trivial limit cycles is determined by the viscoelastic property E_v . This suggests that viscoelasticity narrows the stable region of the first limit cycle and the unstable region of the second limit cycle. For elastic moving belts, the lower boundary of existence for non-trivial limit cycles is identical to the stability boundary of the trivial solution, which indicates that the non-trivial limit cycles of the summation parametric resonance bifurcate from the trivial limit cycle at the boundary of the trivial limit cycle. For viscoelastic systems, however, the existence boundary of non-trivial limit cycles is different from the stability boundary of the trivial limit cycle.

The transient response of viscoelastic moving belts with general constitutive law is calculated numerically in Chapter 6. The viscoelastic integral constitutive law is appropriate to characterize complicated physical properties of some belt materials. The convergence of travelling eigenfunctions proposed in Chapter 6 is superior to the convergence of stationary eigenfunctions. The block-by-block method used to solve the resulting differential-integral equations is demonstrated to be more accurate, convenient and efficient than the finite difference method. The parametric resonance occurs at both frequencies ω_n and $2\omega_n$ for harmonic variation of the

axially moving velocity. The damping introduced by the viscoelasticity leads to the decrease of vibration frequencies.

The dynamic model derived in Chapter 7 describes the serpentine belt drive systems as a hybrid (continuous and discrete elements), gyroscopic, and non-conservative system. Viscoelastic constitutive law is proposed to represent the internal damping property of belt materials. Viscous damping and coulomb damping of tensioner arm are considered. The resulting equations of motion form the basis for the linear and nonlinear vibration analysis.

The modal analysis of the linear undamped serpentine belt drive system is performed in Chapter 8. The explicit exact characteristic equation for eigenvalues is derived without using the iteration approach, which provides insight concerning effect of the design parameters on natural frequencies. The response of serpentine belt drive system subjected to arbitrary excitations is represented as a superposition of orthogonal eigenfunctions. When the excitations are non-resonance harmonic, the explicit exact solution without using eigenfunction expansion is derived. The natural frequency of transversely dominant modes decreases with the increase of the translating speed. The natural frequency spectrum of rotationally dominant modes is speed-independent. The tensioner arm orientation influences natural frequency of rotationally dominant modes greatly. At lower translating speed, the effect of the tensioner arm on transversely dominant modes is small. With the increase of the translating speed, this effect also becomes more significant.

The linear vibration problem of non-self-adjoint hybrid serpentine belt drive systems is solved in

Chapter 9. The eigenfunctions of the adjoint system are found to be the modal shapes of an auxiliary system, which is the same as the original system but with its transport speed in the opposite direction. This relationship illustrates the physical meaning of the adjoint eigenfunctions and makes it easy to determine the adjoint eigenfunctions. The eigenvalue of non-self-adjoint systems is not pure imaginary, which is different from undamped serpentine belt drive systems. The state space eigenfunctions of original system and the corresponding adjoint system are in the bi-orthogonality relations. The dynamic response of a non-self-adjoint system subjected to arbitrary disturbances and initial conditions are obtained in the modal expansion expression.

Nonlinear vibrations of *elastic* serpentine belt drives are analyzed in Chapter 10 using the *discretization multiple scales method*. The hybrid nonlinear equations of motion are discretized using the eigenfunctions of corresponding linear problems. The method of multiple scales is then applied to the resulting ordinary differential equations. This perturbation analysis provides a basic understanding of parametric excitation threshold levels and the existence of multiple limit cycles. Numerical results show that subsystem 1 may be parametrically excited through the linear component of the dynamic tension while subsystems 2 is also excited by the nonlinear components of the dynamic tension. For large values of internal detuning parameter σ_1 , the system is far from resonance and there is only one solution. When the system is near or at exact two-to-one internal or one-to-one resonance, the response becomes very large and shows a typical multi-valued nonlinear phenomenon. The excitation frequency has a significant effect on the system response. The results also indicate the possibility of complicated bifurcations in serpentine belt drive systems. For certain range of excitation frequencies, the steady state solutions for the amplitudes and phases undergo Hopf bifurcation. The resulting response could

be amplitude-modulated motion. The period doubling bifurcation also occurs.

Nonlinear vibrations of *elastic* serpentine belt drives are analyzed in Chapter 11 using the *direct multiple scales method*. It is found that there exist discrepancies between the direct multiple scales method and the discretization multiple scales method. Numerical results show that the discrepancy between the two approaches for one-to-one internal resonance is large. The quadratic nonlinearity dominates for discretization multiple scales method while the cubic nonlinearity dominates for direct multiple scales method in the case of $\alpha_m = 0$. The Hopf bifurcation, the relation between response and excitation amplitude, and the relation between response and excitation frequency for the two approaches are also quite different. The discrepancy between the two approaches for two-to-one internal resonance is small. The trend of responses obtained by the two approaches is the same.

Nonlinear vibration analysis of *viscoelastic* serpentine belt drives is performed in Chapter 12. The Kelvin model is employed to describe the mechanical behavior of belt materials. It is found that the damping introduced by the Kelvin viscoelastic model is very important in determine dynamics of serpentine belt drive systems. It is possible to significantly reduce the vibration level and stabilize an unstable belt drive system by increasing the belt damping level.

The viscoelastic moving continua model and the hybrid viscoelastic belt drive model proposed in this research encompass diverse mechanical systems such as high-speed magnetic tapes, translating sheets and webs, aerial cable tramways, band saws, pipes that contain flowing fluid, and power transmission chains. The method of solution can be applied to a wide range of

gyroscopic systems (for instance, disks, shafts, and rotors) without being restricted to serpentine belt drives. The direct multiple scales method and the discretization multiple scales method are readily extended to systems with more complicated nonlinearity and damping mechanism.

13.2 RECOMMENDATIONS FOR DESIGN WORK

Based on this research, the following general recommendations are proposed for the design work of serpentine belt drives:

- 1) The viscoelastic moving belt model and the discrete spring-mass model are recommended for preliminary design work. The hybrid viscoelastic serpentine belt drive model is recommended for final design work.
- 2) Increasing the belt damping and the tensioner damping can greatly reduce the vibration amplitude and stabilize an unstable belt drive system. Belt damping has a more significant effect on rotational vibration amplitude than tensioner damping.
- 3) Increasing the modulus of elasticity can lead to higher natural frequencies and lower vibration response.
- 4) Selecting a tensioner with a low spring constant could keep the resonance frequencies below the operating speed range. A low tensioner spring constant also acts to increase the belt critical speed and reduce the magnitude of belt tension variations.
- 5) Adjusting the tensioner orientation properly can reduce the coupling between the rotational vibration and transverse vibration and thus reduce the opportunity of internal resonances.
- 6) Increasing the belt tension and shortening belt length can reduce vibration amplitudes.
- 7) Adjusting the translating speed of belt property can narrow the instability region. For primary

internal resonance, the instability region reaches maximum when the translating speed approaches zero.

- 8) Detuning the rotation mode natural frequency away from the excitation frequency significantly increases the excitation level necessary to produce parametric resonance.
- 9) Moving the rotation mode natural frequency away from the transverse mode natural frequency or its integer times can reduce the dynamic tensions for a given excitation.
- 10) Avoiding unbalance of belts or pulleys and uneven torque loading can reduce vibration amplitude.

13.3 FUTURE WORK

This thesis has provided a basic understanding of dynamic behavior of serpentine belt drive systems. Based on this research, the following future work is suggested to improve the prediction of the analysis and to provide a more powerful tool for determining the location, size, rigidity, and damping characteristic of the tensioner that will minimize belt vibrations.

- 1) Measure viscoelastic properties of belt materials by experiment. It has been shown that viscoelastic parameters have a significant influence on the dynamic response of serpentine drives. However, the experimental data of belt materials, especially about damping, relaxation and creep properties, is very limited. All the material constants used in this study are from previous published papers.
- 2) Verify the dynamic response of serpentine belt drives through experimental study. The dynamic behavior of serpentine drives has been analyzed theoretically and tested by

simulation in this thesis. The models used in the analysis are based on assumptions such as negligible bending stiffness, negligible bearing compliance, and so on. Experimental study is needed to identify effects of all these assumptions.

- 3) Develop an analytical approach for the response of serpentine belt drives based on more complicated viscoelastic models. This would provide a deep insight concerning the effect of different viscoelastic model on dynamic response and help accessory drive engineers choose the appropriate viscoelastic model.
- 4) Include the material nonlinearity in the prototypical model. In this thesis, only geometric nonlinearity is considered. However, the constitutive relation of belt materials might be nonlinear if the transverse vibration of belt spans is large. This would provide another nonlinear coupling mechanism that may lead to parametric resonances.
- 5) Include creep in the analysis. Creep can cause excessive slip of belts, which leads to temperature increase.
- 6) Include belt bending stiffness in the analysis. This would provide better estimates of modal frequencies, which is very important in predicting response of parametric resonance.

REFERENCES

1. Abrate, S., 1992, "Vibrations of Belts and Belt Drives", *Mechanisms and Machine Theory*, Vol. 27, pp. 645-659.
2. Aiken, J., 1878, "An Account of Some Experiment on Rigidity Produced by Centrifugal Force", *Philosophical Magazine and Journal of Science*, Vol. 5, pp. 81-105.
3. Archibald, F.R. and Emslie, A.G., 1958, "The Vibration of a String Having a Uniform Motion along Its Length", *ASME Journal of Applied Mechanics*, Vol. 25, pp. 347-348.
4. Bapat, V.A. and Srinivasan, P. 1967, "Non-linear Transverse Oscillation in Traveling Strings by the Method of Harmonic Balance", *ASME Journal of Applied Mechanics*, Vol. 34, pp. 775-777.
5. Barker, C.R., Oliver, L.R., and Breig, W.F., 1991, "Dynamic Analysis of Belt Drive Tension Forces During Rapid Engine Acceleration", *SAE Conference*, Detroit, Michigan, pp. 239-254.
6. Beikmann, R.S., Perkins, N.C., and Ulsoy, A.G., 1996, "Free Vibration of Serpentine Belt Drive Systems", *ASME Journal of Vibration and Acoustics*, Vol. 118, pp. 406-413.
7. Beikmann, R.S., Perkins, N.C., and Ulsoy, A.G., 1996, "Nonlinear Coupled Vibration Response of Serpentine Belt Drive Systems", *ASME Journal of Vibration and Acoustics*, Vol. 118, pp. 567-574.
8. Christensen, R.M., 1982, *Theory of Viscoelasticity*, Second Edition, Academic Press, New York.
9. Chen, C.F., 1971, "Hurwitz Stability Criterion and Fuller's Aperiodicity Criterion in Non-linear System Analysis", *International Journal of Electronics*, Vol. 31, pp. 609-619.

10. Chen, T.M., 1995, "The Hybrid Laplace Transform/Finite Element Method Applied to the Quasi-static and Dynamic Analysis of Viscoelastic Timoshenko Beams", *International Journal for Numerical Method in Engineering*, Vol. 38, pp. 509-522.
11. Coleman, B.D. and Noll, W., 1960, "An Approximation Theorem for Functional with Application in Continuum Mechanics", *Archive for Rational Mechanics and Analysis*, Vol. 6, pp. 355-370.
12. Doedel, E.J., 1986, *Auto- Software for Continuation and Bifurcation Problems in Ordinary Differential Equations*, California Institute of Technology, Pasadena, California.
13. Findley, W.N., Lai, J.S., and Onarna, K., 1976, *Creep and Relaxation of Nonlinear Viscoelastic Materials*, North-Holland, New York.
14. Flügge, W., 1975, *Viscoelasticity*, Second Edition, Springer-Verlag, Berlin.
15. Fung, R.F., Huang, J.S., and Chen, W.H., 1996, "Dynamic Stability of a Viscoelastic Beam Subjected to Harmonic and Parametric Excitations Simultaneously", *Journal of Sound and Vibration*, Vol. 198, No. 1, pp. 1-6.
16. Fung, R. F., Huang, J.S., and Chen, Y.C., 1997, "The Transient Amplitude of the Viscoelastic Traveling String: an Integral Constitutive Law", *Journal of Sound and Vibration*, Vol. 201, No. 2., pp. 153-167.
17. Hawker, L.E., 1991, "A Vibration Analysis of Automotive Serpentine Accessory Drive Systems", *Ph.D. Dissertation*, University of Windsor, Ontario, Canada.
18. Huang, J.S., Fung, R.F., and Lin, C.H., 1995, "Dynamic Stability of a Moving String Undergoing Three-dimensional Vibration", *International Journal of Mechanical Sciences*. Vol. 37, pp. 145-160.
19. Hwang, S.J., Perkins, N.C., Ulsoy, A.G., and Meckstroth, R.J., 1994, "Rotational Response

- and Slip Prediction of Serpentine Belt Drive Systems", ASME *Journal of Vibration and Acoustics*, Vol. 116, No. 1, pp. 71-78.
20. Keller, H.B., 1977, "Numerical Solutions of Bifurcation and Nonlinear Eigenvalue Problems", in *Application of Bifurcation Theory*, Rabinowitz, P.H. ed., Academic Press, New York.
21. Korde, K.R., 1985, "On Non-linear Oscillation of Moving String", ASME *Journal of Applied Mechanics*, Vol. 52, pp. 493-494.
22. Kraver, T.C., Fan, G.W., and Shah, J.J., 1996, "Complex Modal Analysis of a Flat Belt Pulley System with Belt Damping and Coulomb-Damped Tensioner", ASME *Journal of Mechanical Design*, Vol. 118, pp. 306-311.
23. Lee, E.H. and Rogers, T.G., 1963, "Solution of Viscoelastic Stress Analysis Problem Using Measured Creep or Relations Functions", ASME *Journal of Applied Mechanics*, Vol. 30, pp. 127-135.
24. Linz, P., 1985, *Analytical and Numerical Methods for Volterra Equations*, SIAM, Philadelphia.
25. Mahalingam, S., 1957, "Transverse Vibration of Power Transmission Chains," *British Journal of Applied Physics*, Vol. 8, pp. 145-148.
26. Meirovitch, L., 1974, "A New Method of Solution of the Eigenvalue Problem for Gyroscopic Systems", *American Institute of Aeronautics and Astronautics Journal*, Vol. 12, pp. 1337-1342.
27. Meirovitch, L., 1975, "A Modal Analysis for the Response of Linear Gyroscopic Systems", ASME *Journal of Applied Mechanics*, Vol. 42, pp. 446-450.
28. Meirovitch, L., 1986, *Elements of Vibration Analysis*, Second Edition, MacGraw Hill Inc.,

New York.

29. Mockensturm, E.M., Perkins, N.C., and Ulsoy, A.G., 1996, "Stability and Limit Cycles of Parametrically Excited Axially Moving Strings", *ASME Journal of Vibration and Acoustics*, Vol. 118, pp. 346-351.
30. Moon, J. and Wickert, J.A., 1997, "Non-linear Vibration of Power Transmission Belts". *Journal of Sound and Vibration*, Vol. 200, No. 4, pp. 419-431.
31. Mote, Jr., C.D., 1966, "On the Non-linear Oscillation of an Axially Moving String", *ASME Journal of Applied Mechanics*, Vol. 33, pp. 463-464.
32. Mote, Jr., C. D., 1968, "Parametric Excitation of an Axially Moving String", *ASME Journal of Applied Mechanics*, Vol. 35, pp. 171-175.
33. Mote, Jr., C.D., 1972, "Dynamic Stability of Axially Moving Materials", *Shock and Vibration Digest*, Vol. 4, No. 4, pp. 2-11.
34. Naguleswaran, S. and Williams, C. J. H., 1968, "Lateral Vibrations of Band-Saw Blade. Pulley Belts and the Like," *International Journal of Mechanics Science*, Vol. 10, pp. 239-250.
35. Nayfeh, A.H., Nayfeh, J.F., and Mook, D.T., 1992, "On Methods for Continuous Systems with Quadratic and Cubic Nonlinearities", *Nonlinear Dynamics*, Vol. 3, pp. 145-162.
36. Nayfeh, A.H. and Nayfeh, S.A., 1994, "On Nonlinear Modes of Continuous Systems". *Journal of Vibration and Acoustics*, Vol. 116, pp. 129-136.
37. Nayfeh, A.H. and Balachandran B., 1995, *Applied Nonlinear Dynamics: Analytical, Computational, and Experimental Methods*, John Wiley & Sons Inc., New York.
38. Pakdemirli, M., Ulsoy, A.G., and Cerenoglu, A., 1994, "Transverse Vibration of an Axially Accelerating String", *Journal of Sound and Vibration*, Vol. 169, pp. 179-196.

39. Pakdemirli, M., Nayfeh, S. A., and Nayfeh, A.H., 1995, "Analysis of One-to-one Autoparametric Resonances in Cables-Discretization vs. Direct Treatment", *Nonlinear Dynamics*, Vol. 8, pp. 65-83.
40. Pakdemirli, M. and Ulsoy A. G., 1997, "Stability Analysis of an Axially Acceleration String", *Journal of Sound and Vibration*, Vol. 203, pp. 815-832.
41. Palmgren, H., 1986, *The V-belt Handbook*, Sweden Studentliteratur.
42. Pesterev, A.V. and Bergman, L.A., 1998, "Response of a Nonconservative Continuous System to a Moving Concentrated Load", *ASME Journal of Applied Mechanics*, Vol. 65, pp. 436-444.
43. Rahman, Z. and Burton, T.D., 1989, "On Higher Order Methods of Multiple Scales in Nonlinear Oscillations-periodic Steady State Response", *Journal of Sound and Vibration*, Vol. 133, pp. 369-379.
44. Rao, G.V. and Iyengar, R.N., 1991, "Internal Resonance and Nonlinear Response of a Cable Under Periodic Excitation", *Journal of Sound and Vibration*, Vol. 149, pp. 25-41.
45. Rao, J.S., 1992, *Advanced Theory of Vibration*, Wiley, New York.
46. Rao, S.S., 1986, *Mechanical Vibrations*, Addison-Wesley, New York.
47. Roach, G.F., 1982, *Green's Functions*, Second Edition, Cambridge University Press, New York.
48. Sack, R.A., 1954, "Transverse Oscillations in Travelling Strings", *British Journal of Applied Physics*, Vol. 5, pp. 224-226.
49. Skutch, R., 1897, "Über die Bewegung Eines Gespannten Fadens, Weicher Gezwungen ist, Durch Zwei Feste Punkte, mit Einer Constanten Geschwindigkeit zu gehen, und Zwischen denselben in Transversal-Schwingungen von Gerlinger Amplitude Versetzt Wird", *Annalen*

- der Physik und Chemie*, Vol. 61, pp. 190-195.
50. Thurman, A.L. and Mote, Jr., C.D., 1969, "Free, Periodic, Non-linear Oscillation of an Axially Moving Strip", *ASME Journal of Applied Mechanics*, Vol. 36, pp. 83-91.
51. Ulsoy, A.G., Whitsell, J.E., and Hooven, M.D., 1985, "Design of Belt-Tensioner Systems for Dynamic Stability", *ASME Journal of Vibrations, Acoustics, Stress, and Reliability in Design*, Vol. 107, No. 3, pp. 282-290.
52. Wanda, S., 1990, *The Behavior of Nonlinear System*, Kluwer Academic Publishers, The Netherlands.
53. Wang, K.W., 1992, "On the Stability of Chain Drive Systems Under Periodic Sprocket Oscillation", *ASME Journal of Vibration and Acoustics*, Vol. 114, pp. 119-126.
54. Wickert, J.A., 1992, "Non-linear Vibration of a Traveling Tensioned Beam", *International Journal of Non-linear Mechanics*, Vol. 27, No. 3, pp. 503-517.
55. Wickert, J.A. and Mote, Jr., C.D., 1990, "Classical Vibration Analysis of Axially Moving Continua", *ASME Journal of Applied Mechanics*, Vol. 57, pp. 738-744.
56. Wickert, J.A. and Mote, Jr., C.D., 1991, "Response and Discretization Methods for Axially-Moving Materials", *ASME Applied Mechanics Reviews*, Vol. 44, pp. 279-284.
57. Yang, B., 1996, "Integral Formulas for Non-self-adjoint Distributed Dynamic Systems". *American Institute of Aeronautics and Astronautics Journal*, Vol. 34, pp. 2132-2139.
58. Zhang, L. and Zu, J.W., 1998, "Nonlinear Vibrations of Viscoelastic Moving Belts, Part I: Free Vibration Analysis", *Journal of Sound and Vibration*, Vol. 216, pp. 75-91.
59. Zhang, L. and Zu, J.W., 1998, "Nonlinear Vibrations of Viscoelastic Moving Belts, Part 2: Forced Vibration Analysis", *Journal of Sound and Vibration*, Vol. 216, pp. 93-105.
60. Zhang, L. and Zu, J.W., 1999, "Modal Analysis of Serpentine Belt Drive Systems", *Journal*

of Sound and Vibration, Vol. 222, pp. 259-279.

61. Zhang, L. and Zu, J.W., 1999, "Nonlinear Vibration of Parametrically Excited Viscoelastic Moving Belts, Part 1: Dynamic Response", *ASME Journal of Applied Mechanics*, Vol. 66, pp. 396-402.
62. Zhang, L. and Zu, J.W., 1999, "Nonlinear Vibration of Parametrically Excited Viscoelastic Moving Belts, Part 2: Stability Analysis", *ASME Journal of Applied Mechanics*, Vol. 66, pp. 403-409.
63. Zhang, L. and Zu, J.W., "Nonlinear Vibration Analysis of Serpentine Belt Drive Systems", submitted to: *International Journal of Nonlinear Mechanics*, 1998.
64. Zu, J.W. and Zhang, L., "Two-to-one Internal Resonance in Serpentine Belt Drive Systems", submitted to: *ASME Journal of Applied Mechanics*, 1998.

APPENDIX A

EXPRESSIONS OF g_i FOR VISCOELASTIC SYSTEMS

$$g_1 = -\omega_n k_1 e_1 \int_0^{l_1} \phi_{1n}' \frac{\partial^2 \phi_{1n}^R}{\partial x^2} dx - \omega_n k_2 e_2 \int_0^{l_2} \phi_{2n}' \frac{\partial^2 \phi_{2n}^R}{\partial x^2} dx \quad (\text{A.1})$$

$$\begin{aligned} g_2 = & -\omega_n k_1 e_1 \int_0^{l_1} \phi_{1n}' \frac{\partial^2 \phi_{1n}^R}{\partial x^2} dx - \omega_n^2 d_1 e_1 \int_0^{l_1} \phi_{1n}' \frac{\partial^2 \phi_{1n}^R}{\partial x^2} dx \\ & - \omega_n k_2 e_2 \int_0^{l_2} \phi_{2n}' \frac{\partial^2 \phi_{2n}^R}{\partial x^2} dx - \omega_n^2 d_2 e_2 \int_0^{l_2} \phi_{2n}' \frac{\partial^2 \phi_{2n}^R}{\partial x^2} dx \end{aligned} \quad (\text{A.2})$$

$$\begin{aligned} g_3 = & -\omega_n \frac{EA}{2l_1} \int_0^{l_1} \left(\frac{\partial \phi_{1n}^R}{\partial x} \right)^2 dx \int_0^{l_1} \phi_{1n}' \frac{\partial^2 \phi_{1n}^R}{\partial x^2} dx + \omega_n^2 d_1 \int_0^{l_1} \frac{\partial \phi_{1n}^R}{\partial x} \frac{\partial \phi_{1n}'}{\partial x} dx \int_0^{l_1} \phi_{1n}' \frac{\partial^2 \phi_{1n}^R}{\partial x^2} dx \\ & - \omega_n \frac{EA}{2l_2} \int_0^{l_2} \left(\frac{\partial \phi_{2n}^R}{\partial x} \right)^2 dx \int_0^{l_2} \phi_{2n}' \frac{\partial^2 \phi_{2n}^R}{\partial x^2} dx + \omega_n^2 d_2 \int_0^{l_2} \frac{\partial \phi_{2n}^R}{\partial x} \frac{\partial \phi_{2n}'}{\partial x} dx \int_0^{l_2} \phi_{2n}' \frac{\partial^2 \phi_{2n}^R}{\partial x^2} dx \end{aligned} \quad (\text{A.3})$$

$$\begin{aligned} g_4 = & - \left(\omega_n \frac{EA}{2l_1} \int_0^{l_1} \left(\frac{\partial \phi_{1n}^R}{\partial x} \right)^2 dx - \omega_n^2 d_1 \int_0^{l_1} \frac{\partial \phi_{1n}^R}{\partial x} \frac{\partial \phi_{1n}'}{\partial x} dx \right) \int_0^{l_1} \phi_{1n}' \frac{\partial^2 \phi_{1n}^R}{\partial x^2} dx \\ & - \left(\omega_n \frac{EA}{2l_1} \int_0^{l_1} 2 \frac{\partial \phi_{1n}^R}{\partial x} \frac{\partial \phi_{1n}'}{\partial x} dx + \omega_n^2 d_1 \left(\int_0^{l_1} \left(\frac{\partial \phi_{1n}^R}{\partial x} \right)^2 dx - \int_0^{l_1} \left(\frac{\partial \phi_{1n}'}{\partial x} \right)^2 dx \right) \right) \int_0^{l_1} \phi_{1n}' \frac{\partial^2 \phi_{1n}^R}{\partial x^2} dx \\ & - \left(\omega_n \frac{EA}{2l_2} \int_0^{l_2} \left(\frac{\partial \phi_{2n}^R}{\partial x} \right)^2 dx - \omega_n^2 d_2 \int_0^{l_2} \frac{\partial \phi_{2n}^R}{\partial x} \frac{\partial \phi_{2n}'}{\partial x} dx \right) \int_0^{l_2} \phi_{2n}' \frac{\partial^2 \phi_{2n}^R}{\partial x^2} dx \\ & - \left(\omega_n \frac{EA}{2l_2} \int_0^{l_2} 2 \frac{\partial \phi_{2n}^R}{\partial x} \frac{\partial \phi_{2n}'}{\partial x} dx + \omega_n^2 d_2 \left(\int_0^{l_2} \left(\frac{\partial \phi_{2n}^R}{\partial x} \right)^2 dx - \int_0^{l_2} \left(\frac{\partial \phi_{2n}'}{\partial x} \right)^2 dx \right) \right) \int_0^{l_2} \phi_{2n}' \frac{\partial^2 \phi_{2n}^R}{\partial x^2} dx \end{aligned} \quad (\text{A.4})$$

$$\begin{aligned}
g_5 = & - \left(\omega_n \frac{EA}{2l_1} \int_0^{l_1} \left(\frac{\partial \phi_{1n}'}{\partial x} \right)^2 dx + \omega_n^2 d_1 \int_0^{l_1} \frac{\partial \phi_{1n}^R}{\partial x} \frac{\partial \phi_{1n}'}{\partial x} dx \right) \int_0^{l_1} \phi_{1n}' \frac{\partial^2 \phi_{1n}^R}{\partial x^2} dx \\
& - \left(\omega_n \frac{EA}{2l_1} \int_0^{l_1} 2 \frac{\partial \phi_{1n}^R}{\partial x} \frac{\partial \phi_{1n}'}{\partial x} dx + \omega_n^2 d_1 \left(\int_0^{l_1} \left(\frac{\partial \phi_{1n}^R}{\partial x} \right)^2 dx - \int_0^{l_1} \left(\frac{\partial \phi_{1n}'}{\partial x} \right)^2 dx \right) \right) \int_0^{l_1} \phi_{1n}' \frac{\partial^2 \phi_{1n}'}{\partial x^2} dx \\
& - \left(\omega_n \frac{EA}{2l_2} \int_0^{l_2} \left(\frac{\partial \phi_{2n}^R}{\partial x} \right)^2 dx + \omega_n^2 d_2 \int_0^{l_2} \frac{\partial \phi_{2n}^R}{\partial x} \frac{\partial \phi_{2n}'}{\partial x} dx \right) \int_0^{l_2} \phi_{2n}' \frac{\partial^2 \phi_{2n}^R}{\partial x^2} dx \\
& - \left(\omega_n \frac{EA}{2l_2} \int_0^{l_2} 2 \frac{\partial \phi_{2n}^R}{\partial x} \frac{\partial \phi_{2n}'}{\partial x} dx + \omega_n^2 d_2 \left(\int_0^{l_2} \left(\frac{\partial \phi_{2n}^R}{\partial x} \right)^2 dx - \int_0^{l_2} \left(\frac{\partial \phi_{2n}'}{\partial x} \right)^2 dx \right) \right) \int_0^{l_2} \phi_{2n}' \frac{\partial^2 \phi_{2n}'}{\partial x^2} dx
\end{aligned} \tag{A.5}$$

$$\begin{aligned}
g_6 = & -\omega_n \frac{EA}{2l_1} \int_0^{l_1} \left(\frac{\partial \phi_{1n}'}{\partial x} \right)^2 dx \int_0^{l_1} \phi_{1n}' \frac{\partial^2 \phi_{1n}'}{\partial x^2} dx - \omega_n^2 d_1 \int_0^{l_1} \frac{\partial \phi_{1n}^R}{\partial x} \frac{\partial \phi_{1n}'}{\partial x} dx \int_0^{l_1} \phi_{1n}' \frac{\partial^2 \phi_{1n}^R}{\partial x^2} dx \\
& - \omega_n \frac{EA}{2l_2} \int_0^{l_2} \left(\frac{\partial \phi_{2n}'}{\partial x} \right)^2 dx \int_0^{l_2} \phi_{2n}' \frac{\partial^2 \phi_{2n}'}{\partial x^2} dx - \omega_n^2 d_2 \int_0^{l_2} \frac{\partial \phi_{2n}^R}{\partial x} \frac{\partial \phi_{2n}'}{\partial x} dx \int_0^{l_2} \phi_{2n}' \frac{\partial^2 \phi_{2n}^R}{\partial x^2} dx
\end{aligned} \tag{A.6}$$

$$\begin{aligned}
g_7 = & \omega_n e_1 \left(k_1 \int_0^{l_1} \phi_{1n}^R \frac{\partial^2 \phi_{1n}^R}{\partial x^2} dx - \frac{EA}{2l_1} \int_0^{l_1} \left(\frac{\partial \phi_{1n}^R}{\partial x} \right)^2 dx + \omega_n d_1 \int_0^{l_1} \frac{\partial \phi_{1n}^R}{\partial x} \frac{\partial \phi_{1n}'}{\partial x} dx \right) \\
& + \omega_n e_2 \left(k_2 \int_0^{l_2} \phi_{2n}^R \frac{\partial^2 \phi_{2n}^R}{\partial x^2} dx - \frac{EA}{2l_2} \int_0^{l_2} \left(\frac{\partial \phi_{2n}^R}{\partial x} \right)^2 dx + \omega_n d_2 \int_0^{l_2} \frac{\partial \phi_{2n}^R}{\partial x} \frac{\partial \phi_{2n}'}{\partial x} dx \right)
\end{aligned} \tag{A.7}$$

$$\begin{aligned}
g_8 = & \omega_n e_1 \left(k_1 \int_0^{l_1} \phi_{1n}^R \frac{\partial^2 \phi_{1n}'}{\partial x^2} dx - \frac{EA}{2l_1} \int_0^{l_1} 2 \frac{\partial \phi_{1n}^R}{\partial x} \frac{\partial \phi_{1n}'}{\partial x} dx \right) \\
& + \omega_n^2 e_1 d_1 \left(\int_0^{l_1} \phi_{1n}^R \frac{\partial^2 \phi_{1n}^R}{\partial x^2} dx - \left(\int_0^{l_1} \left(\frac{\partial \phi_{1n}^R}{\partial x} \right)^2 dx - \int_0^{l_1} \left(\frac{\partial \phi_{1n}'}{\partial x} \right)^2 dx \right) \right) \\
& + \omega_n e_2 \left(k_2 \int_0^{l_2} \phi_{2n}^R \frac{\partial^2 \phi_{2n}'}{\partial x^2} dx - \frac{EA}{2l_2} \int_0^{l_2} 2 \frac{\partial \phi_{2n}^R}{\partial x} \frac{\partial \phi_{2n}'}{\partial x} dx \right) \\
& + \omega_n^2 e_2 d_2 \left(\int_0^{l_2} \phi_{2n}^R \frac{\partial^2 \phi_{2n}^R}{\partial x^2} dx - \left(\int_0^{l_2} \left(\frac{\partial \phi_{2n}^R}{\partial x} \right)^2 dx - \int_0^{l_2} \left(\frac{\partial \phi_{2n}'}{\partial x} \right)^2 dx \right) \right)
\end{aligned} \tag{A.8}$$

$$g_9 = -\omega_n e_1 \frac{EA}{2l_1} \int_0^{l_1} \left(\frac{\partial \phi_{1n}^R}{\partial x} \right)^2 dx - \omega_n^2 e_1 d_1 \left(\int_0^{l_1} \frac{\partial \phi_{1n}^R}{\partial x} \frac{\partial \phi_{1n}'^I}{\partial x} dx - \int_0^{l_2} \phi_{2n}^I \frac{\partial^2 \phi_{2n}^I}{\partial x^2} dx \right) \quad (\text{A.9})$$

$$- \omega_n e_2 \frac{EA}{2l_2} \int_0^{l_2} \left(\frac{\partial \phi_{2n}^I}{\partial x} \right)^2 dx - \omega_n^2 e_2 d_2 \left(\int_0^{l_2} \frac{\partial \phi_{2n}^R}{\partial x} \frac{\partial \phi_{2n}'^I}{\partial x} dx - \int_0^{l_2} \phi_{2n}'^I \frac{\partial^2 \phi_{2n}^I}{\partial x^2} dx \right)$$

$$g_{10} = \omega_n e_3 \frac{EA}{2l_3} \int_0^{l_3} \left(\frac{\partial \phi_m^R}{\partial x} \right)^2 dx - \omega_n \lambda_m e_3 d_3 \int_0^{l_3} \frac{\partial \phi_m^R}{\partial x} \frac{\partial \phi_m'^I}{\partial x} dx \quad (\text{A.10})$$

$$g_{11} = \omega_n e_3 \frac{EA}{2l_3} \int_0^{l_3} 2 \frac{\partial \phi_m^R}{\partial x} \frac{\partial \phi_m'^I}{\partial x} dx + \omega_n \lambda_m e_3 d_3 \left(\int_0^{l_3} \left(\frac{\partial \phi_m^R}{\partial x} \right)^2 dx - \int_0^{l_3} \left(\frac{\partial \phi_m'^I}{\partial x} \right)^2 dx \right) \quad (\text{A.11})$$

$$g_{12} = \omega_n e_3 \frac{EA}{2l_3} \int_0^{l_3} \left(\frac{\partial \phi_m'^I}{\partial x} \right)^2 dx + \omega_n \lambda_m e_3 d_3 \int_0^{l_3} \frac{\partial \phi_m^R}{\partial x} \frac{\partial \phi_m'^I}{\partial x} dx \quad (\text{A.12})$$

$$g_{13} = \omega_n \frac{EA}{2l_1} \int_0^{l_1} \left(\frac{\partial \phi_{1n}^R}{\partial x} \right)^2 dx \int_0^{l_1} \phi_{1n}^R \frac{\partial^2 \phi_{1n}^R}{\partial x^2} dx - \omega_n^2 d_1 \int_0^{l_1} \frac{\partial \phi_{1n}^R}{\partial x} \frac{\partial \phi_{1n}'^I}{\partial x} dx \int_0^{l_1} \phi_{1n}^R \frac{\partial^2 \phi_{1n}^R}{\partial x^2} dx \\ + \omega_n \frac{EA}{2l_2} \int_0^{l_2} \left(\frac{\partial \phi_{2n}^R}{\partial x} \right)^2 dx \int_0^{l_2} \phi_{2n}^R \frac{\partial^2 \phi_{2n}^R}{\partial x^2} dx - \omega_n^2 d_2 \int_0^{l_2} \frac{\partial \phi_{2n}^R}{\partial x} \frac{\partial \phi_{2n}'^I}{\partial x} dx \int_0^{l_2} \phi_{2n}^R \frac{\partial^2 \phi_{2n}^R}{\partial x^2} dx \quad (\text{A.13})$$

$$g_{14} = \left(\omega_n \frac{EA}{2l_1} \int_0^{l_1} \left(\frac{\partial \phi_{1n}^R}{\partial x} \right)^2 dx - \omega_n^2 d_1 \int_0^{l_1} \frac{\partial \phi_{1n}^R}{\partial x} \frac{\partial \phi_{1n}'^I}{\partial x} dx \right) \int_0^{l_1} \phi_{1n}^R \frac{\partial^2 \phi_{1n}^R}{\partial x^2} dx \\ + \left(\omega_n \frac{EA}{2l_1} \int_0^{l_1} 2 \frac{\partial \phi_{1n}^R}{\partial x} \frac{\partial \phi_{1n}'^I}{\partial x} dx + \omega_n^2 d_1 \left(\int_0^{l_1} \left(\frac{\partial \phi_{1n}^R}{\partial x} \right)^2 dx - \int_0^{l_1} \left(\frac{\partial \phi_{1n}'^I}{\partial x} \right)^2 dx \right) \right) \int_0^{l_1} \phi_{1n}^R \frac{\partial^2 \phi_{1n}^R}{\partial x^2} dx \\ + \left(\omega_n \frac{EA}{2l_2} \int_0^{l_2} \left(\frac{\partial \phi_{2n}^R}{\partial x} \right)^2 dx - \omega_n^2 d_2 \int_0^{l_2} \frac{\partial \phi_{2n}^R}{\partial x} \frac{\partial \phi_{2n}'^I}{\partial x} dx \right) \int_0^{l_2} \phi_{2n}^R \frac{\partial^2 \phi_{2n}^R}{\partial x^2} dx \\ + \left(\omega_n \frac{EA}{2l_2} \int_0^{l_2} 2 \frac{\partial \phi_{2n}^R}{\partial x} \frac{\partial \phi_{2n}'^I}{\partial x} dx + \omega_n^2 d_2 \left(\int_0^{l_2} \left(\frac{\partial \phi_{2n}^R}{\partial x} \right)^2 dx - \int_0^{l_2} \left(\frac{\partial \phi_{2n}'^I}{\partial x} \right)^2 dx \right) \right) \int_0^{l_2} \phi_{2n}^R \frac{\partial^2 \phi_{2n}^R}{\partial x^2} dx \quad (\text{A.14})$$

$$\begin{aligned}
g_{15} = & \left(\omega_n \frac{EA}{2l_1} \int_0^{l_1} \left(\frac{\partial \phi_{1n}'}{\partial x} \right)^2 dx + \omega_n^2 d_1 \int_0^{l_1} \frac{\partial \phi_{1n}^R}{\partial x} \frac{\partial \phi_{1n}'}{\partial x} dx \right) \int_0^{l_1} \phi_{1n}^R \frac{\partial^2 \phi_{1n}^R}{\partial x^2} dx \\
& + \left(\omega_n \frac{EA}{2l_1} \int_0^{l_1} 2 \frac{\partial \phi_{1n}^R}{\partial x} \frac{\partial \phi_{1n}'}{\partial x} dx + \omega_n^2 d_1 \left(\int_0^{l_1} \left(\frac{\partial \phi_{1n}^R}{\partial x} \right)^2 dx - \int_0^{l_1} \left(\frac{\partial \phi_{1n}'}{\partial x} \right)^2 dx \right) \right) \int_0^{l_1} \phi_{1n}^R \frac{\partial^2 \phi_{1n}'}{\partial x^2} dx \\
& + \left(\omega_n \frac{EA}{2l_2} \int_0^{l_2} \left(\frac{\partial \phi_{2n}^R}{\partial x} \right)^2 dx + \omega_n^2 d_2 \int_0^{l_2} \frac{\partial \phi_{2n}^R}{\partial x} \frac{\partial \phi_{2n}'}{\partial x} dx \right) \int_0^{l_2} \phi_{2n}^R \frac{\partial^2 \phi_{2n}^R}{\partial x^2} dx \\
& + \left(\omega_n \frac{EA}{2l_2} \int_0^{l_2} 2 \frac{\partial \phi_{2n}^R}{\partial x} \frac{\partial \phi_{2n}'}{\partial x} dx + \omega_n^2 d_2 \left(\int_0^{l_2} \left(\frac{\partial \phi_{2n}^R}{\partial x} \right)^2 dx - \int_0^{l_2} \left(\frac{\partial \phi_{2n}'}{\partial x} \right)^2 dx \right) \right) \int_0^{l_2} \phi_{2n}^R \frac{\partial^2 \phi_{2n}'}{\partial x^2} dx
\end{aligned} \tag{A.15}$$

$$\begin{aligned}
g_{16} = & \omega_n \frac{EA}{2l_1} \int_0^{l_1} \left(\frac{\partial \phi_{1n}'}{\partial x} \right)^2 dx \int_0^{l_1} \phi_{1n}^R \frac{\partial^2 \phi_{1n}'}{\partial x^2} dx + \omega_n^2 d_1 \int_0^{l_1} \frac{\partial \phi_{1n}^R}{\partial x} \frac{\partial \phi_{1n}'}{\partial x} dx \int_0^{l_1} \phi_{1n}^R \frac{\partial^2 \phi_{1n}'}{\partial x^2} dx \\
& \omega_n \frac{EA}{2l_2} \int_0^{l_2} \left(\frac{\partial \phi_{2n}'}{\partial x} \right)^2 dx \int_0^{l_2} \phi_{2n}^R \frac{\partial^2 \phi_{2n}'}{\partial x^2} dx + \omega_n^2 d_2 \int_0^{l_2} \frac{\partial \phi_{2n}^R}{\partial x} \frac{\partial \phi_{2n}'}{\partial x} dx \int_0^{l_2} \phi_{2n}^R \frac{\partial^2 \phi_{2n}'}{\partial x^2} dx
\end{aligned} \tag{A.16}$$

$$g_{17} = -\omega_n^2 d_1 e_1 \int_0^{l_1} \phi_{1n}' \frac{\partial^2 \phi_{1n}^R}{\partial x^2} dx - \omega_n^2 d_2 e_2 \int_0^{l_2} \phi_{2n}' \frac{\partial^2 \phi_{2n}^R}{\partial x^2} dx \tag{A.17}$$

$$e_1 = \hat{\chi}_{3n} \cos \psi_1 + \hat{\chi}_{2n} - \hat{\chi}_{1n} \tag{A.18}$$

$$e_2 = \hat{\chi}_{3n} \cos \psi_2 + \hat{\chi}_{4n} - \hat{\chi}_{2n} \tag{A.19}$$

$$e_3 = \hat{\chi}_{4n} - \hat{\chi}_{1n} \tag{A.20}$$

APPENDIX B

EXPRESSIONS OF h_i FOR VISCOELASTIC SYSTEMS

$$h_1 = \lambda_m k_3 e_3 \int_0^{l_3} \varphi'_m \frac{\partial^2 \varphi_m^R}{\partial x^2} dx \quad (B.1)$$

$$h_2 = \lambda_m k_3 e_3 \int_0^{l_3} \varphi'_m \frac{\partial^2 \varphi'_m}{\partial x^2} dx \quad (B.2)$$

$$h_3 = - \left(\lambda_m \frac{EA}{2l_3} \int_0^{l_3} \left(\frac{\partial \varphi_m^R}{\partial x} \right)^2 dx - \lambda_m^2 d_3 \int_0^{l_3} \frac{\partial \varphi_m^R}{\partial x} \frac{\partial \varphi'_m}{\partial x} dx \right) \int_0^{l_3} \varphi'_m \frac{\partial^2 \varphi_m^R}{\partial x^2} dx \quad (B.3)$$

$$\begin{aligned} h_4 = & - \left(\lambda_m \frac{EA}{2l_3} \int_0^{l_3} \left(\frac{\partial \varphi'_m}{\partial x} \right)^2 dx + \lambda_m^2 d_3 \int_0^{l_3} \frac{\partial \varphi_m^R}{\partial x} \frac{\partial \varphi'_m}{\partial x} dx \right) \int_0^{l_3} \varphi'_m \frac{\partial^2 \varphi'_m}{\partial x^2} dx \\ & - \left(\lambda_m \frac{EA}{l_3} \int_0^{l_3} \frac{\partial \varphi_m^R}{\partial x} \frac{\partial \varphi'_m}{\partial x} dx + \lambda_m^2 d_3 \left(\int_0^{l_3} \left(\frac{\partial \varphi_m^R}{\partial x} \right)^2 dx - \int_0^{l_3} \left(\frac{\partial \varphi'_m}{\partial x} \right)^2 dx \right) \right) \int_0^{l_3} \varphi'_m \frac{\partial^2 \varphi_m^R}{\partial x^2} dx \end{aligned} \quad (B.4)$$

$$\begin{aligned} h_5 = & - \left(\lambda_m \frac{EA}{2l_3} \int_0^{l_3} \left(\frac{\partial \varphi'_m}{\partial x} \right)^2 dx + \lambda_m^2 d_3 \int_0^{l_3} \frac{\partial \varphi_m^R}{\partial x} \frac{\partial \varphi'_m}{\partial x} dx \right) \int_0^{l_3} \varphi'_m \frac{\partial^2 \varphi_m^R}{\partial x^2} dx \\ & - \left(\lambda_m \frac{EA}{l_3} \int_0^{l_3} \frac{\partial \varphi_m^R}{\partial x} \frac{\partial \varphi'_m}{\partial x} dx + \lambda_m^2 d_3 \left(\int_0^{l_3} \left(\frac{\partial \varphi_m^R}{\partial x} \right)^2 dx - \int_0^{l_3} \left(\frac{\partial \varphi'_m}{\partial x} \right)^2 dx \right) \right) \int_0^{l_3} \varphi'_m \frac{\partial^2 \varphi'_m}{\partial x^2} dx \end{aligned} \quad (B.5)$$

$$h_6 = - \left(\lambda_m \frac{EA}{2l_3} \int_0^{l_3} \left(\frac{\partial \varphi'_m}{\partial x} \right)^2 dx + \lambda_m^2 d_3 \int_0^{l_3} \frac{\partial \varphi_m^R}{\partial x} \frac{\partial \varphi'_m}{\partial x} dx \right) \int_0^{l_3} \varphi'_m \frac{\partial^2 \varphi'_m}{\partial x^2} dx \quad (B.6)$$

$$h_7 = - \lambda_m k_3 e_3 \int_0^{l_3} \varphi_m^R \frac{\partial^2 \varphi_m^R}{\partial x^2} dx \quad (B.7)$$

$$h_8 = - \lambda_m k_3 e_3 \int_0^{l_3} \varphi_m^R \frac{\partial^2 \varphi'_m}{\partial x^2} dx \quad (B.8)$$

$$h_9 = \left(\lambda_m \frac{EA}{2l_3} \int_0^{l_3} \left(\frac{\partial \varphi_m^R}{\partial x} \right)^2 dx - \lambda_m^2 d_3 \int_0^{l_3} \frac{\partial \varphi_m^R}{\partial x} \frac{\partial \varphi_m'}{\partial x} dx \right) \int_0^{l_3} \varphi_m^R \frac{\partial^2 \varphi_m^R}{\partial x^2} dx \quad (\text{B.9})$$

$$h_{10} = \left(\lambda_m \frac{EA}{2l_3} \int_0^{l_3} \left(\frac{\partial \varphi_m^R}{\partial x} \right)^2 dx - \lambda_m^2 d_3 \int_0^{l_3} \frac{\partial \varphi_m^R}{\partial x} \frac{\partial \varphi_m'}{\partial x} dx \right) \int_0^{l_3} \varphi_m^R \frac{\partial^2 \varphi_m'}{\partial x^2} dx \\ + \left(\lambda_m \frac{EA}{l_3} \int_0^{l_3} \frac{\partial \varphi_m^R}{\partial x} \frac{\partial \varphi_m'}{\partial x} dx + \lambda_m^2 d_3 \left(\int_0^{l_3} \left(\frac{\partial \varphi_m^R}{\partial x} \right)^2 dx - \int_0^{l_3} \left(\frac{\partial \varphi_m'}{\partial x} \right)^2 dx \right) \right) \int_0^{l_3} \varphi_m^R \frac{\partial^2 \varphi_m^R}{\partial x^2} dx \quad (\text{B.10})$$

$$h_{11} = \left(\lambda_m \frac{EA}{2l_3} \int_0^{l_3} \left(\frac{\partial \varphi_m'}{\partial x} \right)^2 dx + \lambda_m^2 d_3 \int_0^{l_3} \frac{\partial \varphi_m^R}{\partial x} \frac{\partial \varphi_m'}{\partial x} dx \right) \int_0^{l_3} \varphi_m^R \frac{\partial^2 \varphi_m^R}{\partial x^2} dx \\ + \left(\lambda_m \frac{EA}{l_3} \int_0^{l_3} \frac{\partial \varphi_m^R}{\partial x} \frac{\partial \varphi_m'}{\partial x} dx + \lambda_m^2 d_3 \left(\int_0^{l_3} \left(\frac{\partial \varphi_m^R}{\partial x} \right)^2 dx - \int_0^{l_3} \left(\frac{\partial \varphi_m'}{\partial x} \right)^2 dx \right) \right) \int_0^{l_3} \varphi_m^R \frac{\partial^2 \varphi_m'}{\partial x^2} dx \quad (\text{B.11})$$

$$h_{12} = \left(\lambda_m \frac{EA}{2l_3} \int_0^{l_3} \left(\frac{\partial \varphi_m'}{\partial x} \right)^2 dx + \lambda_m^2 d_3 \int_0^{l_3} \frac{\partial \varphi_m^R}{\partial x} \frac{\partial \varphi_m'}{\partial x} dx \right) \int_0^{l_3} \varphi_m^R \frac{\partial^2 \varphi_m'}{\partial x^2} dx \quad (\text{B.12})$$

$$h_{13} = \omega_n \lambda_m d_3 e_3 \int_0^{l_3} \varphi_m^R \frac{\partial^2 \varphi_m^R}{\partial x^2} dx \quad (\text{B.13})$$

$$h_{14} = \omega_n \lambda_m d_3 e_3 \int_0^{l_3} \varphi_m' \frac{\partial^2 \varphi_m'}{\partial x^2} dx \quad (\text{B.14})$$

$$h_{15} = -\omega_n \lambda_m d_3 e_3 \int_0^{l_3} \varphi_m^R \frac{\partial^2 \varphi_m^R}{\partial x^2} dx \quad (\text{B.15})$$

$$h_{16} = -\omega_n \lambda_m d_3 e_3 \int_0^{l_3} \varphi_m' \frac{\partial^2 \varphi_m'}{\partial x^2} dx \quad (\text{B.16})$$

APPENDIX C

EXPRESSIONS OF s_i AND t_i FOR VISCOELASTIC SYSTEMS

$$s_1 = -\frac{2i(g_1 + ig_2 - g_{17}) + (g_7 + ig_8 - g_9)}{3\omega_n} \quad (C.1)$$

$$s_2 = \frac{2g_7 + 2g_9}{\omega_n} \quad (C.2)$$

$$s_3 = \frac{(g_{10} + ig_{11} - g_{12})\omega_n}{\omega_n^2 - 4\lambda_m^2} \quad (C.3)$$

$$s_4 = \frac{2g_{10} + 2g_{12}}{\omega_n} \quad (C.4)$$

$$s_5 = \frac{(g_1 + ig_2 - g_{17}) - 2i(g_7 + ig_8 - g_9)}{3\omega_n} \quad (C.5)$$

$$s_6 = -\frac{2g_1 + 2g_{17}}{\omega_n} \quad (C.6)$$

$$s_7 = \frac{2i\lambda_m(g_{10} + ig_{11} - g_{12})}{\omega_n^2 - 4\lambda_m^2} \quad (C.7)$$

$$s_8 = 0 \quad (C.8)$$

$$t_1 = \frac{i(\omega_n + \lambda_m)(h_1 + ih_2 + ih_{13} - h_{14}) + \lambda_m(h_7 + ih_8 + ih_{15} - h_{16})}{\lambda_m^2 - (\omega_n + \lambda_m)^2} \quad (C.9)$$

$$t_2 = \frac{i(\omega_n - \lambda_m)(h_1 - ih_2 + ih_{13} + h_{14}) + \lambda_m(h_7 - ih_8 + ih_{15} + h_{16})}{\lambda_m^2 - (\omega_n - \lambda_m)^2} \quad (C.10)$$

$$t_3 = \frac{i(\omega_n + \lambda_m)(h_7 + ih_8 + ih_{15} - h_{16}) - \lambda_m(h_1 + ih_2 + ih_{13} - h_{14})}{\lambda_m^2 - (\omega_n + \lambda_m)^2} \quad (C.11)$$

$$t_4 = \frac{i(\omega_n - \lambda_m)(h_7 - ih_8 + ih_{15} + h_{16}) - \lambda_m(h_1 - ih_2 + ih_3 + h_{14})}{\lambda_m^2 - (\omega_n - \lambda_m)^2} \quad (\text{C.12})$$

APPENDIX D

EXPRESSIONS OF $\hat{\theta}_i$ and $\tilde{\theta}_i$ for Viscoelastic Systems

$$\hat{\Theta}_1 = 2g_1s_1 + 2g_1s_2 + g_2s_5 + g_2s_6 - ig_2s_1 + ig_2s_2 + 3g_3 + ig_4 + g_5 + 3ig_6 + 2ig_{17}s_6 - 2ig_{17}s_5 \quad (\text{D.1})$$

$$\hat{\Theta}_2 = 2g_1s_4 + ig_2s_4 \quad (\text{D.2})$$

$$\hat{\Theta}_3 = 2g_1s_3 - ig_2s_3 + g_2s_7 - 2ig_{17}s_7 \quad (\text{D.3})$$

$$\begin{aligned} \tilde{\Theta}_1 = & 2g_7s_1 + 2g_7s_2 + g_8s_5 + g_8s_6 - ig_8s_1 + ig_8s_2 + \\ & 2ig_9s_6 - 2ig_9s_5 + 3g_{13} + ig_{14} + g_{15} + 3ig_{16} \end{aligned} \quad (\text{D.4})$$

$$\tilde{\Theta}_2 = 2g_7s_4 + ig_8s_4 + 2g_{10}t_2 + 2g_{10}t_1 + g_{11}t_4 + g_{11}t_3 + ig_{11}t_2 - ig_{11}t_1 + 2ig_{12}t_4 - 2ig_{12}t_3 \quad (\text{D.5})$$

$$\tilde{\Theta}_3 = 2g_7s_3 - ig_8s_3 + g_8s_7 - 2ig_9s_7 + 2g_{10}\bar{t}_2 + g_{11}\bar{t}_4 + ig_{11}\bar{t}_2 + 2ig_{12}\bar{t}_4 \quad (\text{D.6})$$

$$\hat{\Theta}_4 = h_1(t_2 + s_1) + h_2(t_4 - is_1) + ih_{13}t_2 + h_{13}s_5 + ih_{14}t_4 - ih_{14}s_5 \quad (\text{D.7})$$

$$\hat{\Theta}_5 = h_1(t_1 + \bar{t}_2 + s_2) + h_2(t_3 + \bar{t}_4 + is_2) + ih_{13}\bar{t}_2 - ih_{13}t_1 + h_{13}s_6 + ih_{14}\bar{t}_4 - ih_{14}t_3 + ih_{14}s_6 \quad (\text{D.8})$$

$$\hat{\Theta}_6 = 3h_3 + ih_4 + h_5 + 3ih_6 + h_1(s_3 + s_4) + h_2(-is_3 + is_4) + h_{13}s_7 - ih_{14}s_7 \quad (\text{D.9})$$

$$\tilde{\Theta}_4 = h_7(t_2 + s_1) + h_8(t_4 - is_1) + ih_{15}t_2 + h_{15}s_5 + ih_{16}t_4 - ih_{16}s_5 \quad (\text{D.10})$$

$$\tilde{\Theta}_5 = h_7(t_1 + \bar{t}_2 + s_2) + h_8(t_3 + \bar{t}_4 + is_2) + ih_{15}\bar{t}_2 - ih_{15}t_1 + h_{15}s_6 + ih_{16}\bar{t}_4 - ih_{16}t_3 + ih_{16}s_6 \quad (\text{D.11})$$

$$\tilde{\Theta}_6 = 3h_9 + ih_{10} + h_{11} + 3ih_{12} + h_7(s_3 + s_4) + h_8(-is_3 + is_4) + h_{15}s_7 - ih_{16}s_7 \quad (\text{D.12})$$